

**Synthesis and evaluation of ^{18}F -labeled inhibitors
for targeting mutant isocitrate dehydrogenase 1
(mIDH1)**

Inaugural-Dissertation

zur

Erlangung des Doktorgrades
der Mathematisch-Naturwissenschaftlichen Fakultät
der Universität zu Köln

vorgelegt von

Roberta Cologni

aus Bergamo, Italy

Jülich, 2023

Berichterstatter/in (Gutachter):

Prof. Dr. Bernd Neumaier

Prof. Dr. Ines Neundorf

Tag der mündlichen Prüfung:

20.10.2023

Abstract

PET is a fundamental imaging method used for in vivo visualization of physiological and pathophysiological processes on the molecular level. This technique relies on radiotracers, which consist of a pharmacophore addressing the biological target of interest labeled with a radionuclide to enable in vivo detection. For the design of radiotracers to target the mutant isocitrate dehydrogenase 1 enzyme (mIDH1), known scaffolds based on structures with inhibitory activity for this mutated enzyme were employed. Such mutations are prevalent in diffuse gliomas (WHO grade 2-4) setting them apart from glioblastoma (WHO grade 4). Consequently, these mutations have become crucial for differential diagnosis and prediction of patient prognosis. Unlike existing methods that require surgical sampling for detection of mIDH1, positron emission tomography (PET) with mIDH-targeting probes could offer a non-invasive alternative for determining and longitudinally assessing the mIDH status. This could lead to an early and accurate diagnosis of low-grade gliomas and facilitate to differentiate glioma recurrence from post radiation treatment effects. Furthermore, tumor heterogeneity can be determined. Thus, the application of these probes opens up new opportunities for monitoring of tumor growth and thus patient care since neither MRI nor the PET tracer [¹⁸F]fluoroethyltyrosine have these capabilities.

In the present study, specific inhibitors of mIDH1 were selected as lead structures to prepare ¹⁸F-labeled mIDH1 selective PET tracers using copper mediated radiofluorination. To this end, olutasidenib, presented in 2020, was selected as a starting scaffold. However, a first attempt to label it in position-7 failed. Therefore, a sub potent version of olutasidenib was selected as a mIDH1 selective candidate to use this compound as a proof of concept. In this case a 6-fluoro substituent was introduced into the quinolone ring system instead of the 6-chloro substituent present on the left-hand side of the original structure. The reference compound 4-(((6-fluoro-2-oxo-1,2-dihydroquinolin-3-yl)methyl)amino)-2-methoxybenzotrile was obtained in an overall yield of 13% over 5 steps starting from 4-fluoroacetanilide and tested in enzymatic assays to show an inhibitory potency of 616 nM. Two radiofluorination precursors were obtained via multi-step syntheses which consisted in the conversion of 4-bromoaniline into 6-bromo-3-formylquinolone, followed by pivaloyloxymethyl (POM) protection of the amide moiety prior to conjugation to 4-amino-2-methoxybenzotrile. For ¹⁸F-labeling by copper-mediated radiofluorination, the brominated lead structures had to be converted into boronic acid pinacol esters, to furnish the precursors 3-(((4-cyano-3-methoxyphenyl)amino)methyl)-2-oxo-6-(4,4,5,5-tetramethyl-1,3,2-dioxaborolan-2-yl)quinolin-1(2H)-yl)methyl pivalate and ((3-(((4-cyano-3-methoxyphenyl)amino)methyl)-6-(4,4,5,5-tetramethyl-1,3,2-dioxaborolan-2-yl)quinolin-2-yl)oxy)methyl pivalate in a total yield of 10% over

10 synthetic steps. For radiofluorination, [¹⁸F]fluoride was fixed on an anion exchange cartridge (AEC), eluted with 1 mg of tetraethylammonium bicarbonate (Et₄NHCO₃) in 1 mL methanol and dried. An equimolar solution of precursor and Cu(4-PhePy)₄(ClO₄)₂ (10 μmol) in 500 μL dimethylacetamide (DMA) was then added to the reactor and the mixture was stirred at 110 °C for 10 min. Subsequent deprotection with 200 μL 0.25 M NaOH in H₂O/MeOH (1:1) at 80°C for 3 min yielded the desired product with a radiochemical conversion of 26 ± 12% for the N-protected and 41 ± 20% for the O-protected precursor. After HPLC-purification, 4-(((6-[¹⁸F]fluoro-2-oxo-1,2-dihydroquinolin-3-yl)methyl)amino)-2-methoxybenzotrile ([¹⁸F]mIDH-138) was obtained in radiochemical yields of 22% for the N-protected and 29% for the O-protected precursor, respectively. The molar activity amounted to 13-540 GBq/μmol (start activities in the range of 1-4 GBq). The cellular uptake of [¹⁸F]mIDH-138 was evaluated in mIDH1 and wtIDH1 cells and revealed a statistically significant higher uptake in mIDH1 cells. The in vitro results were confirmed by in vivo experiments in a chorio allantoic membrane (CAM) model and showed negligible defluorination and high stability of the tracer over 1 hour.

After the successful proof of concept, a radiotracer based on olutasidenib (6-F-(*S*)-olutasidenib) was pursued. Moreover, the *R*- and *S*-enantiomers (6-F-olutasidenib) were prepared to confirm the importance of the spatial orientation of the methyl group on the benzylic linker. The two reference compounds were obtained starting from 6-fluoro-2-chloro-3-formylquinoline and conjugated with (*R*)-Ellman's sulfinamide to direct the methylation step in order to obtain the desired *S*-diastereoisomer as the major product. The different diastereoisomers were isolated and conjugated to 5-fluoro-1-methyl-6-oxo-1,6-dihydropyridine-2-carbonitrile, which itself was obtained via a 4 step synthesis from 5-fluoropicolinonitrile in a total yield of 13%. Enzymatic assay of 6-F-(*S*)-olutasidenib and 6-F-(*R*)-olutasidenib confirmed that the former is a more potent inhibitor with respect to the latter. The boronic acid ester precursors for the radiosynthesis of 6-[¹⁸F]fluoro-(*S*)-olutasidenib and 6-[¹⁸F]fluoro-(*R*)-olutasidenib were obtained in a similar way starting from the brominated quinolone which was POM protected after the conjugation with the N-methylpyridone and converted into boronic acid pinacol esters in a total yield of 2% and 1.5% respectively over 14 steps. Cu-mediated radiosynthesis was carried out following a similar procedure to that used for the first radiotracer and optimized (DMI, 100°C, 15 min), followed by basic cleavage of the POM group. The radiofluorination proved successful only for the O-protected precursor. No explanation could be found for the incompatibility of the N-protected precursor with radiofluorination. However, 6-[¹⁸F]fluoro-(*S*)-olutasidenib and 6-[¹⁸F]fluoro-(*R*)-olutasidenib were obtained with RCCs of 61 ± 13%, isolated radiochemical yields of 50 ± 10% and molar activities of 102-275 GBq/μmol (for starting activity of 1 GBq) and were further evaluated in cell uptake experiments. However,

unexpectedly both tracers showed negligible tracer uptake. Finally, encouraged by the results obtained with [¹⁸F]mIDH-138, a fourth radiotracer, 4-(((6-[¹⁸F]fluoro-2-oxo-1,2-dihydroquinolin-3-yl)methyl)amino)-2-(2-fluoroethoxy)benzotrile ([¹⁸F]FE-mIDH), was designed. Here the left-hand side of the molecule consisted of a POM protected 6-fluoroquinolone, identical to that of the first radiotracer. The arene on the right-hand side already present in the first tracer was modified by replacing the methoxy group with a 2-fluoroethoxy substituent, obtained in 3 synthetic steps starting from 2-hydroxy-4-nitrobenzotrile with a total yield of 70%. The reference compound was tested for its potency towards mIDH1 and revealed an IC₅₀ value in the micromolar range, despite the minor structural difference compared to the first compound. Again, due to the impossibility to debenzylate the N-protected scaffold without inducing its degradation, only the O-protected precursor could be obtained with a total yield of 10% over 8 steps. For the radiosynthesis of [¹⁸F]FE-mIDH, a mesylate leaving group was installed and exchanged against fluoride-18 by an S_N2 reaction by aliphatic radiofluorination. Fluoride-18 was trapped on an AEC cartridge and eluted with 0.5 mg of tetramethylammonium triflate (Me₄NOTf) in 0.5 mL of methanol and dried. A solution of the precursor (2 mg) in 500 μL acetonitrile was then added to the reactor and stirred at 85°C for 15 minutes followed by deprotection with 100 μL 0.1 M NaOH in ethanol at 35°C for 10 minutes. The radiotracer [¹⁸F]FE-mIDH was obtained with RCCs of 30 ± 8%, RCYs of 26 ± 8% and A_m of 14-47 GBq/μmol (start activities of 1 GBq) and further incubated in wild type and mutant cell lines. An unexpected higher uptake in wild type cells in comparison to mutant cells was observed. Recent literature demonstrated that the mechanism of selective inhibition of mIDH1 inhibitors disclosed so far is not based on a selective binding but is actually correlated to the different binding strength of the natural ligands into the active binding pocket and the dynamic nature of the dimeric interface. Conclusively, this project revealed that the radiolabeled inhibitors are not suitable for selective mIDH1 tumor imaging. However, selective targeting of mIDH to determine its status remains a desirable goal in nuclear medicine. To achieve this aim a paradigm shift in tracer development is required, and at the current moment, it is still not foreseeable what the next steps in this direction will look like.

Kurzzusammenfassung

PET ist ein klinisch wichtiges bildgebendes Verfahren, das zur in-vivo-Visualisierung physiologischer und pathophysiologischer Prozesse auf molekularer Ebene eingesetzt wird. Diese Technik basiert auf Radiotracer, die aus einem Pharmakophor, das ein molekulares Target adressiert und einem Radionuklid als signalgebendem Element bestehen. Diese radioaktiven Konstrukte, die in der Regel intravenös appliziert werden, ermöglichen nach Bindung oder Wechselwirkung mit ihrem molekularen Target dessen in-vivo-Nachweis. Für die Entwicklung von spezifischen Radiotracer für das mutierte Enzym Isocitrat-Dehydrogenase 1 (mIDH1) wurden bekannte Leitstrukturen verwendet, die auf Strukturen mit hemmender Aktivität für dieses mutierte Enzym basieren. Derartige Mutationen sind bei diffusen Gliomen (WHO-Grad 2-4) weit verbreitet und unterscheiden sie von Glioblastomen (WHO-Grad 4). Folglich sind diese Mutationen für die Differentialdiagnose und Prognose des Krankheitsverlaufs von entscheidender Bedeutung. Im Gegensatz zu den bestehenden Methoden, die eine Gewebeentnahme für den Nachweis von mIDH1 erfordern, könnte die Positronen-Emissions-Tomographie (PET) mit selektiven mIDH-Tracern eine nicht-invasive Alternative für die Bestimmung und das longitudinale Monitoring des mIDH-Status darstellen. Dies könnte zu einer frühzeitigen und genauen Diagnose von niedrig-gradigen Gliomen führen und dazu beitragen, ein Gliomrezidiv von den Folgen einer Strahlenbehandlung zu unterscheiden. Darüber hinaus kann die Heterogenität des Tumors bestimmt werden. Die Anwendung dieser Tracer eröffnet somit neue Möglichkeiten für die Differentialdiagnostik und das Monitoring des Tumorwachstums und damit für die Patientenversorgung, da dies weder mit einer MRT- noch [¹⁸F]Fluorethyltyrosin-PET-Untersuchung möglich ist.

In der vorliegenden Studie wurden mIDH1 selektive Inhibitoren als Leitstrukturen für die Herstellung von ¹⁸F-markierten mIDH1-selektiven PET-Tracern ausgewählt. Die Radiomarkierung sollte durch kupfervermittelte Radiofluorierung erfolgen. Olutasidenib, das im Jahr 2020 eingeführt wurde, wurde als Ausgangsstruktur für ¹⁸F-markierte mIDH1-selektive Tracer gewählt. Ein erster Versuch, diese Struktur in Position 7 zu markieren, schlug fehl. Daher wurde zunächst, um die Umsetzung des Konzepts zu testen, eine weniger potente Version von Olutasidenib als mIDH1-selektiver Kandidat untersucht. In diesem Fall wurde ein Fluor in Position 6 des Chinolon-Ringsystem anstelle des 6-Chlor-Substituenten auf der rechten Seite der ursprünglichen Struktur eingeführt. Die Referenzverbindung CN(C)C1=CC=C(C=C1)C(=O)N2C(=O)C=C(C=C2)C(F)3C=CC(=O)N3 4-(((6-Fluor-2-oxo-1,2-dihydrochinolin-3-yl)methyl)amino)-2-methoxybenzonnitril wurde mit einer Gesamtausbeute von 13% in fünf Schritten ausgehend von 4-Fluoracetanilid dargestellt und zeigte in enzymatischen Tests eine Inhibition von 616 nM. Zwei verschiedene Radiofluorierungsvorläufer (**39** und **40**) wurden durch mehrstufige Synthesen

gewonnen. Dabei wurde 4-Bromanilin zu 6-Brom-3-formylchinolon umgesetzt und nach Pivaloyloxymethyl (POM)-Schützung der Amideinheit mit 4-Amino-2-methoxybenzonnitril konjugiert. Für die ^{18}F -Markierung durch die kupfervermittelte Radiofluorierung mussten die bromierten Verbindungen nachfolgend in Boronsäurepinacolester umgewandelt werden. Die Vorstufen 3-(((4-Cyano-3-methoxyphenyl)amino)methyl)-2-oxo-6-(4,4,5,5-tetramethyl-1, 3,2-Dioxaborolan-2-yl)chinolin-1(2H)-yl)methylpivalat und ((3-(((4-Cyano-3-methoxyphenyl)amino)methyl)-6-(4,4,5,5-tetramethyl-1,3,2-dioxaborolan-2-yl)chinolin-2-yl)oxy)methylpivalat konnten mit einer Gesamtausbeute von 10% über 10 Syntheseschritte erhalten werden. Zur Radiofluorierung wurde [^{18}F]Fluorid auf einer Anionenaustauscherkartusche (AEC) fixiert, mit 1 mg Tetraethylammoniumbicarbonat (Et_4NHCO_3) in 1 mL Methanol eluiert und getrocknet. Anschließend wurde eine äquimolare Lösung des Vorläufers und $\text{Cu}(4\text{-PhePy})_4(\text{ClO}_4)_2$ (10 μmol) in 500 μL Dimethylacetamid in den Reaktor gegeben und das Reaktionsgemisch 10 Minuten bei 110 °C gerührt. Durch anschließende Entschützung mit 200 μL 0,25 M NaOH in $\text{H}_2\text{O}/\text{MeOH}$ (1:1) bei 80 °C für 3 min wurde das gewünschte Produkt mit einem radiochemischen Umsatz von 26 ± 12 % für den N-geschützten und 41 ± 20 % für den O-geschützten Vorläufer gewonnen. Nach HPLC-Reinigung wurde 4-(((6-[^{18}F]Fluor-2-oxo-1,2-dihydrochinolin-3-yl)methyl)amino)-2-methoxybenzonnitril ([^{18}F]mIDH-138) mit einer radiochemischen Ausbeute von 22 % für den N-geschützten und 29 % für den O-geschützten Vorläufer erhalten. Die molare Aktivität betrug 13-540 GBq/ μmol (für Ausgangsaktivitäten von 1-4 GBq). Die zelluläre Aufnahme von [^{18}F]mIDH-138 wurde in mIDH1- und wtIDH1-Zellen untersucht und ergab eine statistisch signifikant höhere Aufnahme in mIDH1-Zellen. Die in-vitro-Ergebnisse wurden durch in-vivo-Experimente in einem Chorio-Allantois-Membran (CAM)-Modell bestätigt und zeigten eine vernachlässigbare Defluorierung und hohe Stabilität des Tracers in einem Zeitraum von über einer Stunde.

Nach Bestätigung des Konzepts wurde die Entwicklung eines Radiotracers auf Grundlage von Olutasidenib (6-F-(*S*)-Olutasidenib) weiterverfolgt. Außerdem wurden die *R*- und *S*-Enantiomere (6-F-Olutasidenib) hergestellt, um die Relevanz der räumlichen Ausrichtung der Methylgruppe am benzyliischen Linker zu bestätigen. Die beiden Referenzverbindungen wurden ausgehend von 6-Fluor-2-chlor-3-formylchinolin gewonnen und mit dem (*R*)-Ellmansulfonamid konjugiert, um den Methylierungsschritt zu steuern und das gewünschte *S*-Diastereomer als Hauptprodukt zu erhalten. Die verschiedenen Diastereoisomere wurden isoliert und an 5-Fluor-1-methyl-6-oxo-1,6-dihydropyridin-2-carbonitril konjugiert, das seinerseits durch eine 4-stufige Synthese ausgehend von 5-Fluoropicolinonitril in einer Gesamtausbeute von 13% dargestellt werden konnte. Die enzymatische Untersuchung von 6-F-(*S*)-Olutasidenib und 6-F-(*R*)-Olutasidenib zeigte, dass das *S*-

Diastereomer eine höhere Inhibition von mIDH aufweist als das *R*-Diastereomer. Die Boronsäureester-Vorläufer für die Radiosynthese von 6-^[18F]Fluor-(*S*)-olutasidenib und 6-^[18F]Fluor-(*R*)-olutasidenib wurden auf ähnliche Weise gewonnen. Dafür wurde das bromierte Chinolon nach Konjugation mit *N*-Methylpyridon POM-geschützt und anschließend in 14 Schritten in die Boronsäurepinacolester mit Gesamtausbeuten von 2% bzw. 1,5% umgewandelt. Die Cu-vermittelte Radiosynthese wurde ähnlich wie für den ersten Radiotracer durchgeführt und optimiert (DMI, 100°C, 15 min). Nachfolgend wurde die POM-Gruppe des Zwischenprodukts mittels basischer Entschützung abgespalten. Die Radiofluorierung war überraschenderweise nur für den O-geschützten Vorläufer erfolgreich. Es konnte keine rationale Begründung gefunden werden, warum der N-geschützte Vorläufer keinen radiochemischen Umsatz liefert. 6-^[18F]Fluor-(*S*)-olutasidenib und 6-^[18F]Fluor-(*R*)-olutasidenib wurden mit RCCs von $61 \pm 13 \%$ und isolierten radiochemischen Ausbeuten von $50 \pm 10 \%$ und molaren Aktivitäten von 102-275 GBq/μmol (bei einer Ausgangsaktivität von 1 GBq) erhalten und in Zellaufnahmeexperimenten weiter untersucht. Beide Tracer zeigten jedoch eine vernachlässigbare Zellaufnahme. Schließlich wurde aufgrund der mit ^[18F]mIDH-138 erzielten Ergebnisse ein vierter Radiotracer, 4-(((6-^[18F]Fluor-2-oxo-1,2-dihydrochinolin-3-yl)methyl)amino)-2-(2-fluorethoxy)benzonnitril (^[18F]FE-mIDH), entwickelt. Hierbei bestand die linke Seite des Moleküls analog zum ersten Radiotracer aus einem POM-geschützten 6-Fluorchinolon. Dieses wurde modifiziert, indem die Methoxygruppe durch einen 2-Fluorethoxy-Substituenten ersetzt wurde, so dass die Zielstruktur in drei synthetischen Schritten ausgehend von 2-Hydroxy-4-nitrobenzonnitril mit einer Gesamtausbeute von 70% erhalten wurde. Die Referenzverbindung wurde auf ihre Wirksamkeit gegenüber mIDH1 getestet und ergab, trotz des geringen strukturellen Unterschieds im Vergleich zur ersten Verbindung, nur einen IC₅₀-Wert im mikromolaren Bereich. Auch hier konnte nur der O-geschützte Vorläufer mit einer Gesamtausbeute von 10% über 8 Schritte synthetisiert werden, da die Entschützung der N-geschützten Verbindung ohne deren Zersetzung nicht möglich war. Für die Radiosynthese von ^[18F]FE-mIDH wurde eine Mesylat-Abgangsgruppe eingeführt und durch eine S_N2-Reaktion mittels aliphatischer Radiofluorierung mit Fluorid-18 substituiert. Dazu wurde Fluorid-18 auf einer AEC-Kartusche fixiert, mit 0,5 mg Tetramethylammoniumtriflat (Me₄NOTf) in 0,5 mL Methanol eluiert und getrocknet. Anschließend wurde eine Lösung des Vorläufers (2 mg) in 500 μL Acetonitril zugegeben und 15 Minuten bei 85°C gerührt, bevor die Entschützung mit 100 μL 0,1 M NaOH in Ethanol bei 35°C für 10 Minuten durchgeführt wurde. Der Radiotracer ^[18F]FE-mIDH wurde mit RCCs von $30 \pm 8 \%$, RCYs von $26 \pm 8 \%$ und A_m von 14-47 GBq/μmol (bei einer Ausgangsaktivität von 1 GBq) erhalten und in Wildtyp- und mutierten Zelllinien inkubiert. Es wurde unerwarteterweise eine höhere Aufnahme in den Wildtypzellen als in den mutierten Zelllinien beobachtet. Aktuelle Literatur hat

gezeigt, dass der Mechanismus der selektiven Hemmung aller bisher bekannt gewordenen mIDH1-Inhibitoren nicht auf einer selektiven Bindung beruht, sondern mit der unterschiedlichen Bindungsstärke der natürlichen Liganden in der aktiven Bindungstasche und der dynamischen Natur der dimeren Bindungsstelle zusammenhängt. Daher war auch das Ergebnis dieser Arbeit, dass sich radioaktiv markierte mIDH-Inhibitoren nicht für die selektive Darstellung von mIDH1-Tumoren eignen. Die Bestimmung des mIDH-Status bleibt jedoch weiterhin ein wichtiges Ziel der Nuklearmedizin und radiochemischen Forschung. Um dieses Ziel letztlich zu erreichen, ist ein Paradigmenwechsel in der Tracer-Entwicklung erforderlich und zum jetzigen Zeitpunkt ist noch nicht absehbar, wie die nächsten Schritte in diese Richtung aussehen werden.

Acknowledgments

Here I would like to express my gratitude to Prof. Dr. Neumaier for granting me the opportunity to become part of his prestigious research group at INM-5. His guidance and support have been instrumental in shaping my academic and professional journey during the last three years. Additionally, I am thankful for the various occasions where I have been able to enhance my skills, such as attending conferences and engaging in enriching experiences. I also extend my thanks to my second supervisor, Prof. Dr. Neundorf, whose comments on the biological evaluation of the tracers presented in this work were enlightening. Her patient involvement in numerous progress reports throughout these years had been a source of motivation for me.

I want to extend my heartfelt gratitude to Marcus and Dirk for their unwavering support and presence during the difficult phases of my journey. Their constant encouragement was an invaluable resource as I faced various problems and obstacles that arose during my work. I am particularly grateful to Dirk and Daniela, whose patience and willingness to answer my many questions on every aspect of biological assessment greatly enriched my understanding. Thanks, in particular to Marcus, whose guidance and supervision not only made this project intriguing and challenging, but also much clearer for me. His vast experience as an organic chemist resulted in a plethora of valuable suggestions, which undoubtedly accelerated my progress. Without his insights, I might still be in the initial stages of synthesising my first tracer. Furthermore, I would like to express my heartfelt appreciation to Birte, whose patience in meticulously conducting all the NMR measurements was truly invaluable. My gratitude also extends to Annette and Melanie for their dedication in carrying out the intricate biological experiments that were an integral part of this effort. I am equally grateful to Heike and Felix for their crucial role in conducting the *in vivo* experiments. Their willingness to generously share their expertise and knowledge has been instrumental in the course of my work. They always went above and beyond, kindly answering many questions I had along the way.

I am immensely grateful for the friendship shared with all fellow PhD students who have been an integral part of this incredible journey. A special note of gratitude goes to Nils, whose easy-going and friendly nature made sharing the office an enjoyable experience. To Anna-Lena, Yannick and Benedikt goes my heartfelt appreciation for not only being friends, but for infusing humour and warmth every day. Additionally, I must acknowledge Swen's deepest gratitude for his exceptional support and invaluable assistance throughout the journey. His willingness to share insights and strategies to maintain a semblance of sanity while facing the challenges of a PhD was invaluable to say the least. I guess Benedikt will further thank him for letting me fight someone to his amusement.

During my stay in Aachen, I had the immense good fortune to cross paths with a group of extraordinary people who not only kept me company, but also helped to smile and gain a few kilos during a pandemic. I am compelled to sincerely thank Raissa and Michele, who would have to be invented if only they weren't already here. Moreover, Giuliano holds a special place in my heart as one of the closest friends I have ever had. His constant acts of kindness, including the constant supply of (delicious) food, unwavering support and laughter, were a source of deep comfort. Together, I overcame disastrous Fridays and wove a series of delightful memories through shared laughter and joy. Guys, your company has truly been a light in the darkness.

Now let's talk about Italy, which I have missed so much. I am deeply grateful to my family, who made the effort to visit me during my absence. A special acknowledgement goes to my brother Bino, who, in a moment of utmost importance, managed to retrieve the contents of my USB stick containing the only copy of my thesis, just one day before I handed it in for correction. His timely help was nothing short of miraculous. Thanks also to my sister for her heartening phone calls and entertaining stories.

To my lifelong friends, Cristina, Daniela, Valentina and Federica, goes my heartfelt appreciation. Witnessing the beautiful transformations in your lives has brought me immense joy and I have been a fervent supporter of your happiness every step of the way.

My greatest thanks go without hesitation to Sandro, who is the most supportive and loving man I have ever been lucky enough to find. Anyone who knows me knows how difficult it was not to be with you and that all this would not have been possible without you. Your emotional, culinary and technical support, especially in the last days before the delivery of this work were invaluable.

Finally, thanks to me. It took everything I had and so much more to arrive here.

Cheers!

Table of Content

ABSTRACT	5
KURZZUSAMMENFASSUNG	9
ACKNOWLEDGMENTS	13
1. INTRODUCTION	19
1.1 Radiotracers in life sciences	19
1.1.2 Development of radiotracers	22
1.2 Labelling strategies with ¹⁸F	24
1.2.1 Electrophilic Radiofluorinations	25
1.2.2 Nucleophilic Radiofluorinations	26
1.2.3 Transition metal mediated radiofluorination	31
1.2.4 Fluoride Acceptors	37
1.2.5 SuFEX	38
1.2.6 Indirect radiofluorinations	39
1.3 Development of radiotracer for neuroimaging	41
1.3.1 Prerequisites for CNS application	41
1.3.2 Radiotracer affinity and selectivity	42
1.3.3 Enzymatic inhibition	46
1.4 Mutant isocitrate dehydrogenase (mIDH)	51
1.4.1 Wild type isocitrate dehydrogenases	51
1.4.2 Mutants of isocitrate dehydrogenase	53
1.4.3 Glioma biology and classification	54
1.4.4 Diagnosis of glioma: MRI and PET	56
1.4.5 Mutated Isocitrate Dehydrogenase as a target for PET imaging of gliomas	59
1.5 Docking studies	65
1.5.1 Application of molecular docking to wild type and mutant isocitrate dehydrogenase 1	66
2. AIMS AND OBJECTIVES	69
3. RESULTS AND DISCUSSION	71
3.1 Design and docking studies of new selective tracers	71
3.2 Disubstituted quinolones	78
3.2.1 Retrosynthesis of compound 2	78
3.2.2 Preparation of a general 2-chloro-3-formylquinoline moiety	79
3.2.3 Preparative organic synthesis of compounds 2a and 2b	87
3.3 [¹⁸F]mIDH-138 [¹⁸F]30d	93
3.3.1 Preparative organic synthesis of precursor 33 and reference compound 30d	95

3.3.2 Copper mediated radiofluorination of 4-[[6-(4,4,5,5-tetramethyl-1,3,2-dioxaborolan-2-yl)quinolin-1(2H)-one methyl]amino]-2-methoxybenzotrile 33 and spiking experiment	103
3.3.3 Preparative organic synthesis of protected precursors 3-(((4-cyano-3-methoxyphenyl)amino)methyl)-2-oxo-6-(4,4,5,5-tetramethyl-1,3,2-dioxaborolan-2-yl)quinolin-1(2H)-yl)methyl pivalate 39 and ((3-(((4-cyano-3-methoxyphenyl)amino)methyl)-6-(4,4,5,5-tetramethyl-1,3,2-dioxaborolan-2-yl)quinolin-2-yl)oxy)methyl pivalate 40 and their protodeboronated analogue 2-methoxy-4-(((2-oxo-1,2-dihydroquinolin-3-yl)methyl)amino)benzotrile 30f	106
3.3.4 Copper mediated radiofluorination of (3-(((4-cyano-3-methoxyphenyl)amino)methyl)-2-oxo-6-(4,4,5,5-tetramethyl-1,3,2-dioxaborolan-2-yl)quinolin-1(2H)-yl)methyl pivalate 39 and ((3-(((4-cyano-3-methoxyphenyl)amino)methyl)-6-(4,4,5,5-tetramethyl-1,3,2-dioxaborolan-2-yl)quinolin-2-yl)oxy)methyl pivalate 40	111
3.3.5 Biological evaluation of [¹⁸ F]mIDH-138 [¹⁸ F] 30d and reference compound 30d	112
3.4 6-[¹⁸F]Fluoro-(S)-olutasidenib [¹⁸F](S)-46d and 6-[¹⁸F]Fluoro-(R)-olutasidenib [¹⁸F](R)-46d.....	122
3.4.1 Preparative organic synthesis of N-protected precursors (S)- and (R)- 49 , O-protected precursors (S)- and (R)- 50 , their protodeboronated analogues (S)- and (R)- 46f and reference compounds (S)- and (R)- 46d	123
3.4.2 Copper mediated radiofluorination of (S)- and (R)-(3-(1-(((6-cyano-1-methyl-2-oxo-1,2-dihydropyridin-3-yl)amino)ethyl)-2-oxo-6-(4,4,5,5-tetramethyl-1,3,2-dioxaborolan-2-yl)quinolin-1(2H)-yl)methyl pivalate (S) 49 and (R) 49 and (S)- and (R)-(3-(1-(((6-cyano-1-methyl-2-oxo-1,2-dihydropyridin-3-yl)amino)ethyl)-6-(4,4,5,5-tetramethyl-1,3,2-dioxaborolan-2-yl)quinolin-2-yl)oxy)methyl pivalate (S) 50 and (R) 50	134
3.4.3 Determination of absolute configuration	136
3.4.4 Biological evaluation of 6-[¹⁸ F]Fluoro-(S)-olutasidenib [¹⁸ F](S)- 46d and 6-[¹⁸ F]Fluoro-(R)-olutasidenib [¹⁸ F](R)- 46d and reference compounds (S)- 46d and (R)- 46d	137
3.5 [¹⁸F]FE-mIDH.....	144
3.5.1 Preparative organic synthesis of N-protected precursor 64 , O-protected precursor 63 and reference compound 58d	145
3.5.2 Aliphatic radiofluorination of ((3-(((4-cyano-3-(2-((methylsulfonyl)oxy)ethoxy)phenyl)amino)methyl)-6-fluoroquinolin-2-yl)oxy)methyl pivalate 63	151
3.5.3 Biological evaluation of [¹⁸ F]FE-mIDH [¹⁸ F] 58d and reference compound 58d	155
4. SUMMARY	161
5 EXPERIMENTAL PART	167
5.1 General	167
5.1.1 Solvents and reagents	167
5.1.2 Spectroscopy	167
5.1.3 Chromatography	168
5.2 Organic preparative synthesis	168
5.3 Radiochemistry	208
5.3.1 [¹⁸ F] Production	208
5.3.2 Equipment	208
5.3.3 Chromatography	208
5.3.4 Important values for the description of the radiolabeled substances	210
5.3.5 Radiosynthesis of [¹⁸ F]mIDH- 138	211
5.3.6 Radiosynthesis of 6-[¹⁸ F]Fluoro-(S)-olutasidenib and 6-[¹⁸ F]Fluoro-(S)-olutasidenib.....	216
5.3.7 Radiosynthesis of [¹⁸ F]FE-mIDH	221
5.4 Biological Evaluation	225

5.4.1 <i>In vitro</i> Stability tests in serum.....	225
5.4.2 Stability test in solution.....	225
5.4.3 Calculation of lipophilicity.....	226
6. NMR.....	229
7. ABBREVIATIONS	309
8. LITERATURE.....	315

1. Introduction

1.1 Radiotracers in life sciences

Tracer techniques employ labelled compounds to trace and investigate physiological processes like biosynthetic or metabolic processes at the molecular level.¹ While imaging techniques like magnetic resonance imaging (MRI) or computed tomography (CT) provide morphological information of the investigated organism, positron emission tomography (PET) and single photon emission computed tomography (SPECT) enable the visualization of metabolic processes, protein-protein interactions or signalling cascades. The monitoring of unusual changes in these processes can lead to early diagnosis of many diseases before an anatomical change can be observed, improving the patients' outcome.

To this end, radiotracers are used, which, according to the tracer principle, can follow or “trace” a physiological process without altering it. Their application was first introduced by Georg Charles de Hevesy, who is recognized as the “father of nuclear medicine” due to his pioneering research on radioactive indicators.

In 1923 de Hevesy used for the first time the naturally radioactive isotope ^{212}Pb to study the metabolism of *vicia faba* (broad beans) from a diluted solution of the isotope which was absorbed by the plant. The relative amounts of radioactivity in different parts of the plant were quantified from the ashes with an electroscope and de Hevesy also proved that lead was taken up in the plant in an ionizable form. Further metabolic experiments were conducted in animals with ^{210}Bi , while ^{32}P was used in 1935 for the first in vivo application. De Hevesy was awarded the Nobel prize for chemistry in 1943 “for his work on the use of isotopes as tracer elements in researches on chemical processes”.²

The tracer principle is applied in radiopharmacy, a branch of life sciences where radiopharmaceuticals are employed for both diagnosis and therapy. It consists of the development and production of radiopharmaceuticals, defined radiopharmaceutical chemistry, as well as their characterization, preclinical evaluation and clinical application, defined as radiopharmacology.

Radiotracers have two characteristics: they are easily detectable from the outside with high sensitivity despite their application in only subnanomolar amounts and they do not influence the process under investigation. These molecular targeting units, or vehicles, are composed by two subunits (Figure 1), namely a radiolabel and a pharmacophore which addresses the biological targets with high affinity and selectivity. In case of a radiometal, a chelator for complexation with a linker to connect it to the pharmacophore unit is used. Interestingly, the linker often alters the pharmacokinetic properties of the final molecule leading to unfavorable or favorable biodistribution.

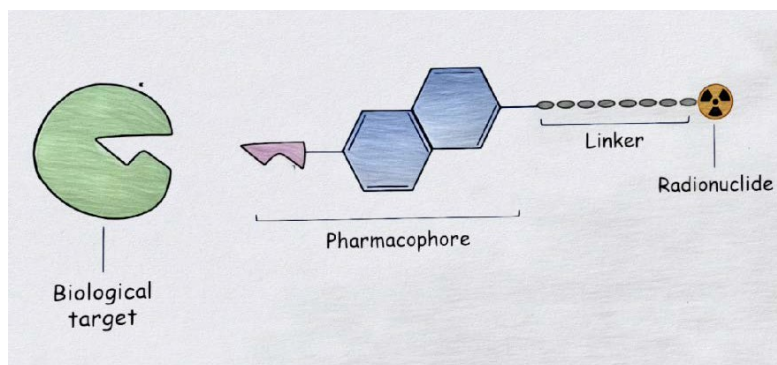


Figure 1: Composition of a radiotracer

PET or SPECT detect the radiation which is emitted after the decay of radionuclides thus providing information about the distribution of the radiotracers in an organism. The selection of a suitable PET or SPECT tracer enables imaging of specific processes due to the interaction of the tracer with its biological target. As a result, the tracer accumulates in regions where the target is mainly located. Application of radiotracers enables to detect even small alterations in the expression of the target which can be an indicator for pathological changes. Thus, tracer techniques are useful in early diagnosis of e.g. neurodegenerative diseases and tumors, as well as therapy monitoring.

1.1.1 PET Technique

Radioimaging techniques are non-invasive diagnostic methods which enable the detection of the decay products emitted from radionuclides. These are usually conjugated to a bioactive molecule which, due to specific interactions with the biological target, allows the visualisation of metabolic processes, receptor expression and other physiological processes.

The two most used radioimaging techniques are single photon emission computed tomography and positron emission tomography.

SPECT represents the 3D implementation of the planar scintigraphy and detects low energy gamma quanta (ideally ~150 keV since the probability of response is very high in this energy region) emitted by radionuclides such as ^{99m}Tc , ^{123}I or ^{67}Ga . SPECT detectors are composed of a gamma camera with a collimator to select the gamma quanta in a specific angle (90°) and a photomultiplier, which amplifies their signal. The gamma camera rotates around the patient to give several single images which are later reconstructed to show the 3D distribution of the radiotracer in the body.

PET on the other hand exploits the β^+ -decay of proton rich nuclei, located above the stable nuclei line in the chart of nuclides (Figure 2a). When the mass of these nuclei is at least equal to the mass of the daughter nuclides, the mother nuclide can decay by electron capture (ϵ). If the mass of the

daughter nuclide is additionally exceeded of at least the mass of two electrons, the mother nuclide can also decay by β^+ decay. In this case, one proton (p) is converted into a neutron (n) and an electron neutrino (ν_e) and a positron (β^+) are emitted to stabilize the mother nuclide as depicted in Formula 1.



After the emission, the positron (β^+), which is the antiparticle of an electron, is slowed down by matter and combined with an electron present in the surroundings. This process leads to the formation of a so-called positronium, which decays quickly causing the conversion of the masses of positron and electron into energy. This process of recombination of an electron with a positron is defined “annihilation”. Based on the mass-energy equivalence $E = mc^2$, the masses of the two particles are converted into two photons with an energy of 511 keV, emitted with an angle of almost 180 degrees (Figure 2b). PET detects coincidental decay events as annihilations on an imaginary straight line called line of response whose reconstruction allows the determination of the location of annihilation and quantitative determination of nuclide distribution, unfeasible with SPECT.³ High sensitivity is one advantage of PET since no collimator is needed due to the selection of only coincidental photons. PET only detects the annihilation event but not the decay, therefore, the farther the positions of the site of decay is away from the site of annihilation, the lower is the resolution of the image. Their distance depends on the energy of the emitted positron which determines the path that the positron can cover in tissues before annihilation. As a consequence, the resolution of the images depends on the nuclide used. This changes according to the density of the matter that is traversed by the positron and the range is shorter in highly dense tissues (like bone) or longer in low density tissues (like lung), respectively. For this reason, β^+ emitters with low energy positrons result in PET images with higher resolutions.

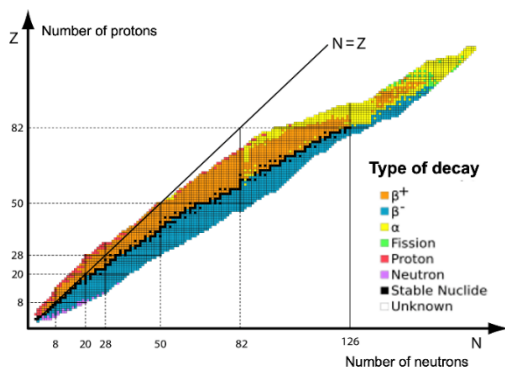


Figure 2a: Chart of nuclides
(Source: iaea.org)

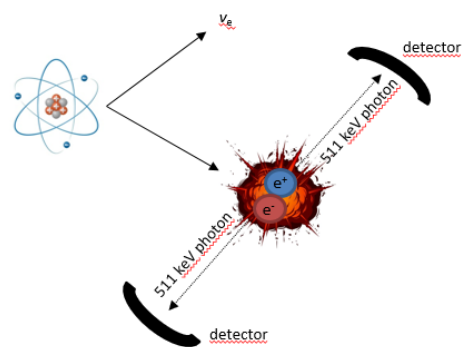


Figure 2b: Graphic description of β^+ decay (Own drawing)

1.1.2 Development of radiotracers

Radiotracers facilitate the non-invasive investigation of physiological processes and abnormal changes related to them. The initial determinant in the development process of a radiotracer is the identification of the sought information. A radiolabeled probe enables to visualize and quantify the *in vivo* distribution and pharmacokinetics of bioactive compounds. Additionally, a radiotracer with a known affinity to a biological target can provide information about the latter and potentially also about other molecules, such as drugs, which address the same target.⁴

In both cases a knowledge driven design of the radiotracer is needed and involves the design of the chemical structure of the pharmacophore, the choice of the radionuclide and the possible need for a linker. For what concerns the choice of the pharmacophore, it must grant high affinity and selectivity to the biological target but also favourable physicochemical properties and sufficient metabolic stability. The physicochemical properties are determined by, among others, molecular weight, lipophilicity and number of H-bond donors and acceptors.

The selection of an appropriate PET nuclide is fundamental. The intensity of the β^+ decay is a factor to be taken into account to avoid signal disturbance, as is the half-life, which must be compatible with the kinetics of the biological process of interest. Generally, positron emitters are produced in cyclotrons by the bombardment of targets with accelerated protons (or other light particles). β^+ -Emitters can also be obtained from radionuclide generators, making the availability of the nuclide another discriminating factor in the development of a radiotracer. The most commonly used positron emitters are shown in Table 1 with data regarding the probability of the β^+ -decay, its energy and mean positron range in water as well as the half-life. ^{11}C , ^{13}N and ^{15}O can be introduced into radiotracers without modifying the chemical properties of the biomolecule due to their high abundance in organic compounds. Unfortunately, the extremely short half-life of ^{13}N and ^{15}O severely reduces the opportunity for their usage, which is mostly limited to myocardial perfusion imaging through ^{13}N -ammonia⁵ and ^{15}O -water.⁶ ^{11}C on the other hand is introduced in a large number of natural and non-natural amino acids to produce common radiotracers such as L-[methyl- ^{11}C]methionine (^{11}C]MET) and β -[^{11}C]-L-3,4-dihydroxyphenylalanine (^{11}C]DOPA). The short half-life of this radionuclide limits its application to institutions with an on-site cyclotron.⁷

Radionuclide	Probability of β^+ decay	Half-life (minutes)	$E_{\beta^+ \text{ max}}$	Mean β^+ range in water
^{11}C	99.8%	20.38	960 keV	1.2 mm
^{13}N	100%	9.96	1198 keV	1.8 mm
^{15}O	99.9%	2.03	1735 keV	3.0 mm
^{18}F	97%	109.77	635 keV	0.6 mm
^{68}Ga	87.7%	66.70	1899 keV	3.5 mm

Table 1: Properties of β^+ -decay of the most commonly used PET nuclides

The most commonly used radionuclide in PET is fluorine-18 due to its almost ideal decay properties. Fluorine-18 is normally produced at a cyclotron via the $^{18}\text{O}(\text{p},\text{n})^{18}\text{F}$ nuclear reaction from enriched water ($[^{18}\text{O}]\text{H}_2\text{O}$) but, unlike Carbon-11, its half-life of 109.77 minutes allows a multi-step preparation and purification of radiotracers, making them available to hospitals in the proximity according to the satellite concept, thus promoting their application. Moreover, F-18 is an almost pure β^+ -emitter (97%), lacking the disturbance effect of other radiations, which permits to limit the patient's dose.

While isotopologues are easily obtained with nitrogen, oxygen and carbon, fluorine is chemically less common in natural organic molecules. However, it is often used in drug discovery as an isostere for H since their van der Waals radii are similar (1.47 vs 1.20 Å) and the length difference of C-F and C-H bonds is negligible. Consequently, the replacement of H with F does not alter the overall shape and size of the molecule making it possible to make targeted modifications in drug design while preserving the structural integrity of the molecule.⁸ However, the pharmacological properties of a fluorinated scaffold can differ significantly from those of a non-fluorinated one. The judicious introduction of fluorine into a molecule can productively influence conformation, pKa, membrane permeability, metabolic pathways, and pharmacokinetic properties. For example, fluorine exhibits poor polarizability but shows a high impact on lipophilicity, elevating it.⁹ This results in an improved ability to penetrate the lipidic membrane present on cell membrane and blood-brain barrier which has a positive effect on the drug bioavailability and efficacy. Additionally, the high electronegativity of fluorine (4 vs. 2.1 for H) leads to high polarization of the sp^3 C-F bond, increasing its strength (544 vs 414 kJ/mol) and making it less susceptible to enzymatic degradation in the body. The increased metabolic stability can result in longer physiological half-life and more sustained therapeutic effects. Similarly, incorporation of fluorine into the drugs can render them more resistant to proteolytic enzymes present in the body, allowing for better stability and prolonged reactions. Moreover, the use

of F as isostere for H interferes with hydrogen bonding, fundamental for molecular interactions, potentially altering the properties as well as the selectivity of drugs, leading to enhanced target specificity and reducing off-target effects. Beside F-18, Gallium-68 is often used as a radiometal in clinical practice. However, its high maximum energy of 1899 keV results in poor resolution of the images and represents its major disadvantage, together with its shorter half-life in respect to F-18. In addition, unlike ^{11}C and ^{18}F , introduction of gallium completely alters the structure of the target molecule as its incorporation relies on the use of chelators with great molecular weight. Nevertheless, Gallium-68 is used by clinics lacking a cyclotron, due to its practical production through a Gallium-68/Germanium-68 generator which is commercially available, transportable, of small-size and usable for 3-5 months.¹⁰

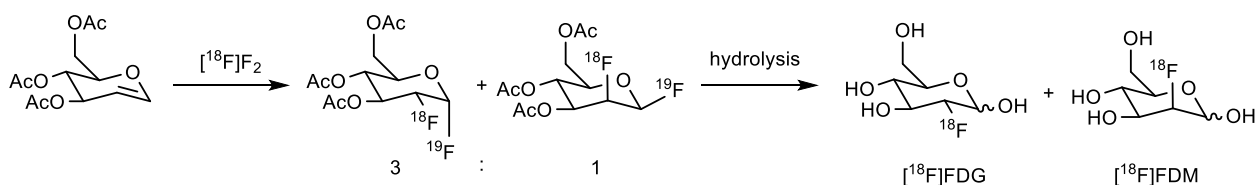
1.2 Labelling strategies with ^{18}F

The chemical organic preparation of a radioactive compound differs from that of its non-radioactive counterpart. Manipulation of relevant amounts of radioactivity necessitates the use of special equipment, personal protection and a shielded work environment. This principle also extends to chemical reactions, which in the case of radioactive substances are carried out on tiny amounts of reagents precluding the direct transfer of conventional organic methodologies to radiochemistry. Additionally, the short half-life of the radionuclide imposes a demand for fast reactions, further challenged by the low concentration of fluoride ions which influences the kinetics of the reactions. Formation of C-F bonds remains challenging, often necessitating harsh reaction conditions. Thus, in the context of PET tracers' synthesis, radiofluorination is normally performed as last step on advanced intermediates which bear complex functionalities. This procedure is called "direct" or "late-stage" radiofluorination and is normally the method of choice because of the time restrictions related to the radioactive decay. Unfortunately, certain chemical functionalities are incompatible with the harsh conditions normally required for radiofluorinations and not all the chemical reactions for fluorine-18 introduction can be carried out in short time. For this reason, "indirect" radiofluorination are also a matter of research and they involve the integration of fluorine into a so called "prosthetic group", subsequently conjugated to a more complex molecule under milder conditions. From the chemical point of view, introduction of fluorine-18 can be established via electrophilic or nucleophilic substitution using either gaseous $[^{18}\text{F}]\text{F}_2$ or aqueous $[^{18}\text{F}]\text{F}^-$.

1.2.1 Electrophilic Radiofluorinations

Gaseous fluorine is produced in a cyclotron via the $^{20}\text{Ne}(\text{d},\alpha)^{18}\text{F}$ reaction.¹¹ Here fluoride is produced and exhibits an extremely high reactivity which results in partial adsorption on the target walls and therefore becomes difficult to extract. For this reason, elemental fluorine F_2 (around $200\mu\text{mol}$) is added as carrier and gaseous $[^{18}\text{F}]\text{F}_2$ formed via isotopic exchange, allowing the extraction of the reagent.¹² Due to the carrier's addition, electrophilic radiofluorinations can achieve 50% of the maximum theoretical molar activity, due to the competing reaction between ^{18}F and ^{19}F . This also applies to the maximum achievable yield because only one between $[^{18}\text{F}]$ and $[^{19}\text{F}]$ can be transferred with essentially equal probability.

Additionally, F_2 is highly reactive and associated with low selectivity, concerning both enantioselectivity and regioselectivity. This leads to the formation of mixtures of products with high structural similarity, which are difficult to isolate. A significant example is the production of $[^{18}\text{F}]\text{FDG}$ from 3,4,6-tri-O-acetyl-D-glucal (Scheme 1). Here the electrophilic addition to the unsaturated bond produces a 3:1 mixture of the 1,2-difluorinated glucose isomer and the 1,2-difluorinated mannose isomer.¹³ After hydrolysis under acidic or basic conditions, 2- $[^{18}\text{F}]$ fluoro-2-deoxy-glucose ($[^{18}\text{F}]\text{FDG}$) and 2- $[^{18}\text{F}]$ fluoro-2-deoxy-mannose ($[^{18}\text{F}]\text{FDM}$) are obtained. Moreover, the presence of ^{19}F as carrier leads also to the formation of $[^{19}\text{F}]\text{FDG}$ and $[^{19}\text{F}]\text{FDM}$.



Scheme 1: Preparation of 2- $[^{18}\text{F}]$ fluoro-2-deoxy-glucose via electrophilic radiofluorination

In order to decrease the high reactivity of $[^{18}\text{F}]\text{F}_2$, secondary electrophilic reagents have been proposed such as $[^{18}\text{F}]\text{XeF}_2$, acetyl $[^{18}\text{F}]$ hypofluorite or $[^{18}\text{F}]\text{Selectfluor}$ bistriflate. However since all these reagents are still based on carrier added $[^{18}\text{F}]\text{F}_2$, limitations concerning the molar activity remain.¹⁴ Additionally, to increase the regioselectivity of electrophilic aromatic radiofluorination metal-organic leaving groups are preferably used, such as $\text{Sn}(\text{Me})_3$, $\text{Ge}(\text{Me})_3$ or $\text{Si}(\text{Me})_3$, with acetyl $[^{18}\text{F}]$ hypofluorite.

1.2.2 Nucleophilic Radiofluorinations

No-carrier-added (n.c.a.) fluoride [^{18}F] F^- can be produced in a cyclotron via the $^{18}\text{O}(\text{p},\text{n})^{18}\text{F}$ nuclear reaction¹⁵ by proton bombardment¹⁶ of enriched water ($[^{18}\text{O}]\text{H}_2\text{O}$) in high yields, high activity concentration and high molar activity of 4×10^4 GBq/ μmol .¹⁷ Consequently, the n.c.a. [^{18}F] F^- is obtained from the cyclotron in aqueous solution, incompatible with radiofluorinations due to the high solvation of the anion diminishing the nucleophilicity of [^{18}F] F^- . To subsequently increase the reactivity, [^{18}F] F^- is trapped on an anion exchange cartridge (AEC), separated from the enriched water, which can be recycled, and is eluted with an organic-aqueous solution containing a base and a phase transfer catalyst. The mixture of organic solvent and water is then azeotropically dried under inert gas at reduced pressure using multiple acetonitrile additions until the so-called “naked” ^{18}F -fluoride is obtained. Usually, K_2CO_3 is used in combination with the cryptand Kryptofix® (commonly abbreviated as $\text{K}_{2.2.2}$) which encapsulates the potassium cation forming a fluoride complex ($\text{K}\subset 2.2.2$) with high reactivity and solubility (Figure 3). This procedure, although defined as “conventional”, is time consuming and can lead to by-products, hence chemical impurities, due to the high basicity of carbonate. However, mildly basic conditions are required in radiofluorinations in order to avoid the protonation of [^{18}F] F^- in presence of acidic groups, such as -OH or -COOH, and its subsequent conversion into the volatile and less reactive [^{18}F] HF .

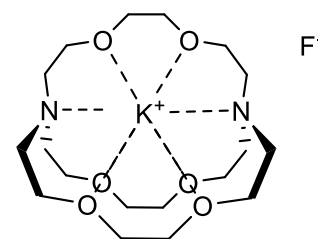


Figure 3: $\text{K}\subset 2.2.2$ complex

Many efforts have been made in order to develop fluoride-18 preprocessing that avoids the azeotropic drying and provides milder fluorination conditions, compatible with a wider range of substituents. To this extent, bases with large soft cations, such as the bulky alkali metal ions Cs^+ , Rb^+ , or tetraalkylammonium (R_4N^+) cations can be used as alternative to $\text{K}_{2.2.2}/\text{K}_2\text{CO}_3$ without the need of a cryptand. Moreover, in 2014, Richarz et al reported the “minimalist approach” which avoids the time-consuming azeotropic drying step and does not require base or additives.¹⁸ They suggested that onium salts, namely iodonium and trialkyl ammonium salts, in alcoholic solutions could be used to elute the fluoride-18 from the anion exchange cartridge. A methanolic solution is preferable since it guarantees $^{18}\text{F}^-$ recoveries of 90- 98% and can be quickly evaporated at reduced pressure before addition of the desired solvent for radiofluorination. Additionally, due to the controllable basicity via their counter anions and the high solubility of the precursors in organic solvents, no bases or other additives are required for this radiofluorination method. Moreover, this approach suggests that the ^{18}F -fluoride can be fixed from one side of the cartridge and eluted from the opposite one, hence avoiding

that $^{18}\text{F}]\text{F}^-$ travels through the whole volume of the QMA and therefore less base is needed to elute the it.⁵⁰

A “minimalist-like” approach could also be applied to non-ionic precursors by use of a tetraalkylammonium salt (e.g. tetraethylammonium bicarbonate¹⁹, tetrabutylammonium bicarbonate²⁰) in methanolic solution to elute $^{18}\text{F}^-$. Afterwards, methanol can be evaporated and a solution of the precursor in the desired solvent added to the reactor, again avoiding the time-consuming azeotropic drying.²¹

An advantage of the preprocessing by anion exchange cartridge is that long-lived radiometals, formed during the irradiation from the target material (e.g. ^{48}V in a titanium target or ^{56}Co in a Havar foil)²², are retained, thereby reducing the risk of radionuclidic impurities in the final product.

Radiofluorinations via nucleophilic substitution reactions show the same requirements as macroscopic organic nucleophilic substitutions, namely the use of a polar aprotic solvent, the presence of a nucleophile and of a leaving group. Concerning the solvents, polar aprotic solvents such as acetonitrile (ACN), dimethylsulfoxide (DMSO) and dimethylformamide (DMF) are used. These are in the ideal polarity range to form dissociated ion pairs with fluoride, making it nucleophilic, but are not sufficiently polar to solvate the fluoride themselves, due to lack of hydrogen-bond donor/acceptor moieties.

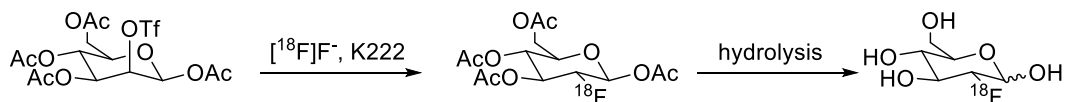
Finally, according to the position of the leaving group, ^{18}F substitution can occur in an aliphatic or an aromatic position.

1.2.2.1 Aliphatic radiofluorination

Aliphatic radiofluorinations are used to introduce fluorine-18 into a variety of molecules via $\text{S}_{\text{N}}2$ mechanism, namely a concerted backside attack of the nucleophile upon the leaving group with inversion of the stereocenter (Walden inversion). A prerequisite for the success of the reaction is presence of a good leaving group such as triflate, tosylate, mesylate and others. Additionally, all protic functional groups (e.g. COOH , OH , NH , SH) in the precursor must be protected before and deprotected after the radiofluorination, since, after the drying step, fluoride represents a powerful nucleophile with a strongly basic character.

One of the best known examples of aliphatic radiofluorination is the preparation of 2- ^{18}F fluoro-2-deoxy-glucose (^{18}F]FDG) from tetraacetyl mannose triflate (Scheme 2).²³ ^{18}F]FDG is the most frequently used radiotracer in nuclear medicine for the imaging of neurological, cardiovascular and oncological diseases. The reaction is carried out on a protected mannose, followed by hydrolysis

under acidic or basic conditions. Afterwards, the final desired radiotracer is purified using a series of ion exchange, normal and reversed phase cartridges and obtained in isolated radiochemical yields up to 70%.



Scheme 2: Radiosynthesis of 2-[¹⁸F]fluoro-2-deoxy-glucose

Like glucose, [¹⁸F]FDG is taken up by the transport protein GLUT-1 in tumors and brain tissues and is phosphorylated by the enzyme hexokinase. The substitution of fluorine at position C-2 prevents further metabolism and induces the accumulation of [¹⁸F]FDG in cells,²⁴ a process known as metabolic trapping.²⁵ Additionally, the altered metabolism of cancer cells leads to an increased glucose uptake in order to promote their growth and proliferation. This is defined as Warburg effect²⁶ and, in combination with the metabolic trapping, makes [¹⁸F]FDG a suitable tracer for tumor imaging.

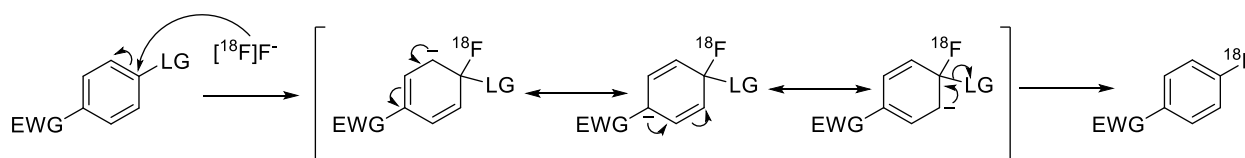
Typical side reactions during S_N reactions using precursors with good leaving groups are elimination and hydrolysis. Consequently, the amount of base and the precursor/base ratio are important factors with regard to the RCY. While [¹⁸F]FDG is a good example of the conditions which are typically applied, many tracers suffer of base-sensitivity. This is the case for example of [¹⁸F]FET whose acetyl protected mesylethoxy precursor undergoes elimination which leads to final RCYs of 25% when the reaction is carried out with the conventional approach.²⁷

Different elution approaches have been investigated to obviate this problem and conduct aliphatic radiofluorinations at low basicity. It needs to be reminded that AEC cartridges are predominantly used in the carbonate form (e.g. QMA), thus contain a basic, non-nucleophilic counter ion to capture [¹⁸F]F⁻. A certain, non-quantified amount of the carbonate is inevitably added to the reactions, due to ion exchange processes with the anion from the elution salt. For this reason, Lee et al. used non basic mesylate anions to precondition the QMA carbonate cartridge, thus exchanging carbonate as the counter ion with mesylate and elute [¹⁸F]F⁻ followed by addition of a defined amount of base directly to the eluate.²⁸ This strategy allowed improvement of RCY when applied to different base-sensitive tracers but a high adsorption of fluoride on the glass walls of the reaction vessel was also observed. A subsequent strategy of using non-basic anions for elution and preconditioning ions as the only source of basicity resulted in higher and more robust RCYs. Similarly, Krasikova's group presented the use of tetrabutylammonium tosylate as non-basic salt for the elution of fluoride in combination

with ethanol for the synthesis of [^{18}F]fluoroethyltyrosine ([^{18}F]FET) reporting a RCY of 40% within 35 minutes in comparison to 25% using the conventional Kryptofix conditions.²⁹ The same group optimized this protocol by decreasing the amount of tosylate salt from 4 to 1 mg and the amount of precursor from 2 to 0.6 mg while retaining the same RCY and synthesis time for the preparation of [^{18}F]FET using an automated TRACERLab radiofluorination device.³⁰

1.2.2.2 Aromatic radiofluorination

A direct introduction of $^{18}\text{F}^-$ into aromatic scaffolds is of great interest, since many natural products and pharmaceuticals contain aromatic moieties. Additionally, the sp^2 C-F bond is much stronger than the sp^3 C-F which can potentially increase the tracer's stability in vivo. Aromatic substitutions ($\text{S}_{\text{N}}\text{Ar}$) proceed through a carbanion intermediate (Meisenheimer complex) with suitable leaving groups, such as nitro- (NO_2^-), trimethylammonium (Me_3N^-) groups or halogens (Scheme 3).³¹



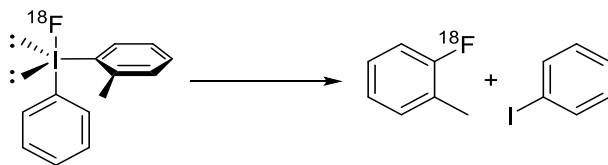
Scheme 3: Mechanism of nucleophilic aromatic substitution

Generally, $\text{S}_{\text{N}}\text{Ar}$ s are facilitated by the presence of electron-withdrawing groups in *ortho*- and *para*-positions to the leaving group since they help stabilizing the negative charge of the intermediate. This represents a major limitation considering that many leading structures of interest are actually electron-rich. For these compounds, electron-withdrawing substituents should be introduced on the aromatic ring to activate the substrate towards radiofluorination and subsequently be removed. This would result in a time-consuming multi-step synthesis which is not amenable to radiofluorinations. A good example is phenol, which cannot be directly radiofluorinated even in presence of a protective group or harsh conditions. Instead, more complex syntheses have to be used. One approach is the radiofluorination of an activated aldehyde precursor to obtain [^{18}F]fluorobenzaldehyde. The latter can be converted via Bayer-Villiger oxidation with carefully tuned reaction conditions into the formic acid phenolate which, after hydrolysis, yields [^{18}F]fluorophenol.

To obviate this limitation, different classes of precursors have been developed.

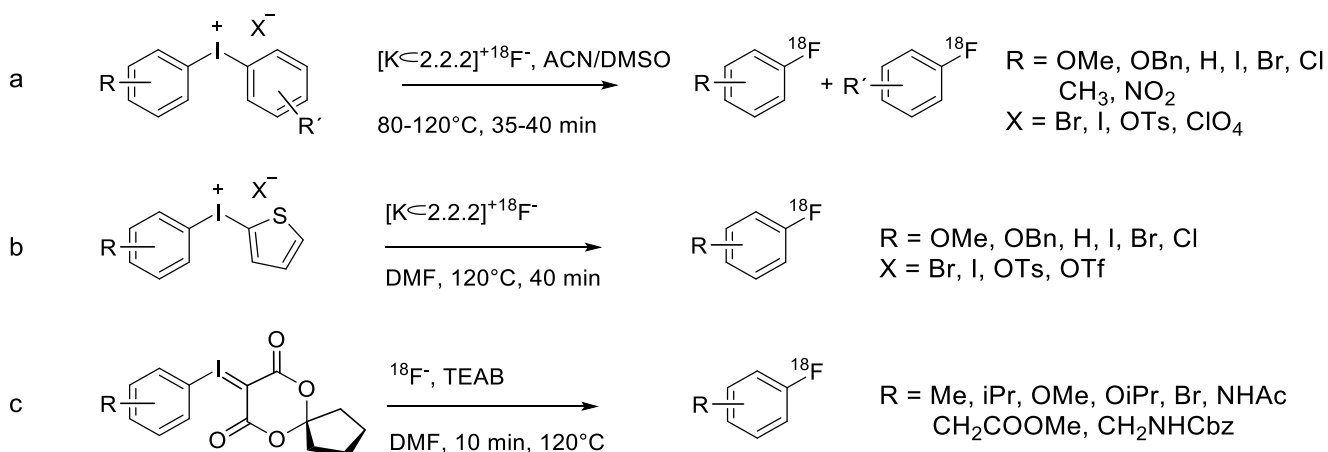
Based on the pioneering work of Gruschin et al. in 1957,³² Pike and Aigbirhio presented in 1995 the use of aryl iodonium salts as precursors for radiofluorinations (Scheme 5a).³³ In the case of asymmetrical iodonium salts though, both arenes can be radiofluorinated and the $^{18}\text{F}^-$ introduction is

driven by electronic and steric effects. Fluoride-18 is introduced preferentially at the arene with lower electron density because of the stabilization of the negative charge. Additionally, arenes with a substituent in *ortho* position are preferentially labelled due to the so called “ortho effect”.



Scheme 4: Graphical representation of “ortho effect”

Here the steric hindrance imposed by the *ortho*- substituent forces the arene to be placed in equatorial position to the two free electron pairs, driving the nucleophilic attack on the substituted arene (Scheme 4). The main disadvantage of this procedure is that the radiofluorination takes place preferably at the more electron-deficient ring. To overcome this limitation, Ross et al. in 2007 proposed the use of aryl(2-thienyl)iodonium salts.³⁴ The thienyl group was used as a highly electron-rich heteroaromatic activator for the radiofluorination of a less but still electron-rich arene such as anisole (Scheme 5b). In particular the classical labelling procedure with 2-methoxyphenyl(2-thienyl)iodonium bromide was tested, exploiting the ortho effect, thereby obtaining the electron-rich 2- ^{18}F fluoroanisole in 61% radiochemical conversion. However, the application of these compounds is limited due to the difficulty of their preparation and their low stability. Aryl iodonium ylides (Scheme 5c) on the other hand have a carbanionic character and the nucleophilic attack takes place selectively on the aromatic ring of the aryl group due to the distribution of the charge density.³⁵ Additionally, these precursors are relatively stable and lack a counterion which can compete with $^{18}\text{F}^-$ for the role of nucleophile. With spiroiodine (III)-based precursors, a wide range of deactivated arenes with different substitution patterns, including steric hindering *ortho*-substituents, could be regioselectively radiofluorinated.³⁶



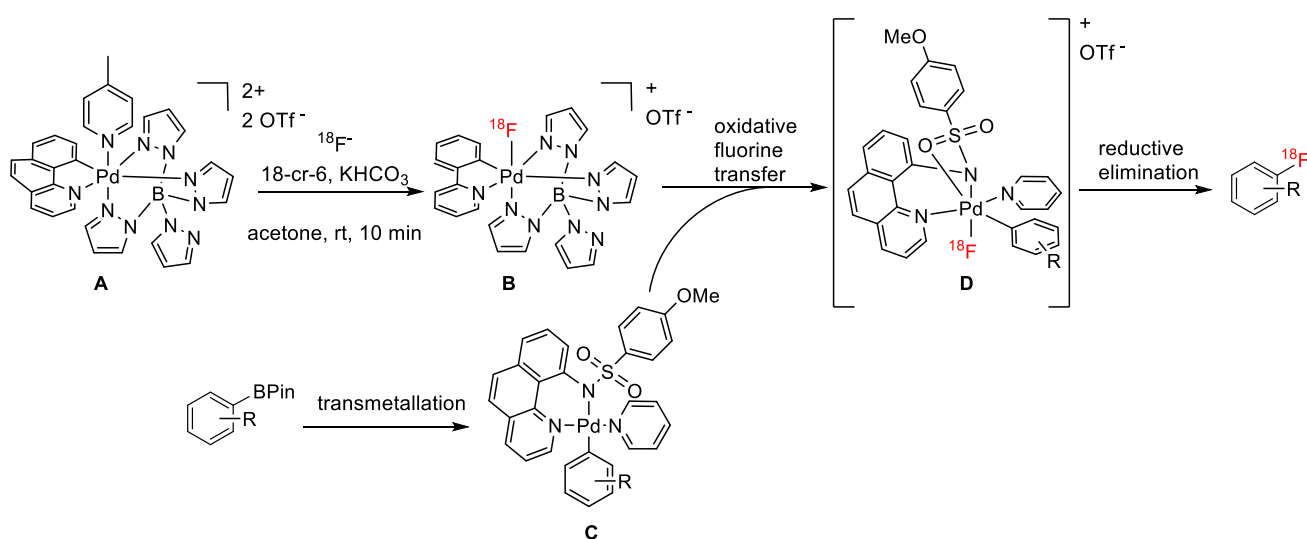
Scheme 5: Radiofluorination of iodonium salts with n.c.a [18F]KF

Given the challenge represented by the radiofluorination of electron-rich arenes, the use of transition metals as mediators for radiofluorination with [18F]KF was seen as an appealing opportunity to enhance selectivity and reactivity.

1.2.3 Transition metal mediated radiofluorination

The use of transition metal allows radiofluorination by mean of polarity inversion, defined “Umpolung”. In this process, nucleophilic fluoride is converted into an electrophilic species which allows radiofluorination of a wider range of aromatic and heteroaromatic compounds.

In 2011, Lee et al. developed an electrophilic radiofluorination from a high-valent Pd(IV) fluoride complex (Scheme 6).³⁷

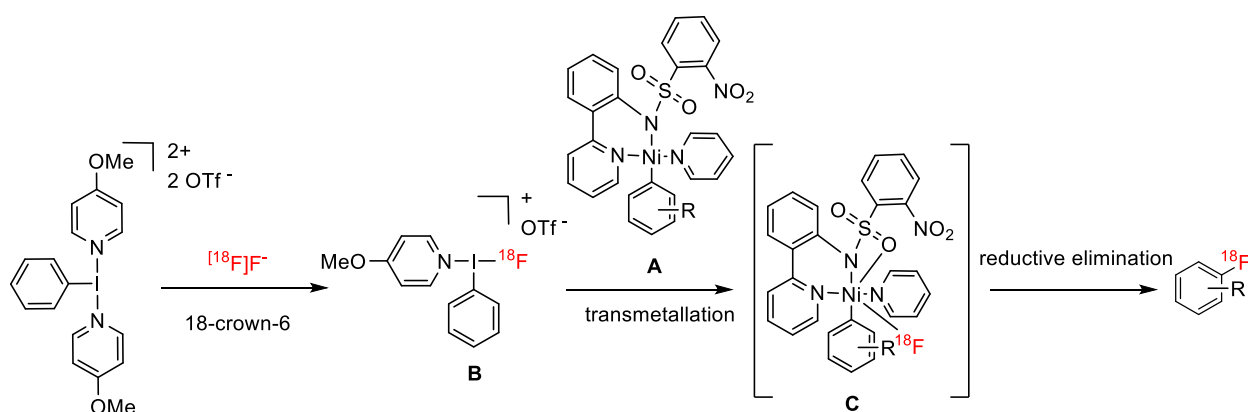


Scheme 6: Pd-mediated radiofluorination according to Lee et al.

[¹⁸F]Fluoride binds to a cationic Pd(IV) species (A) to form the radiofluorinating agent (B). A second Pd(II) complex (C) is synthesised *via* transmetallation from an aryl boronic pinacol ester and undergoes an oxidative fluorine transfer to give an arylpalladium (IV)-[¹⁸F]fluoride intermediate (D). The latter undergoes reductive elimination to form the final ¹⁸F-fluorinated product.

In 2013, Mazzotti et al. published another Pd-mediated fluorination method.³⁸ They were able to isolate a Pd(III) intermediate and could therefore conclude that the Pd-mediated mechanism proceeds via single-electron transfer. However, the two-step procedure increases the reaction time, requires azeotropic drying and the palladium complex in high oxidation states are of difficult accessibility as well as not stable in air, limiting the method's applicability for practical use.

One year later, the same group reported the use of aryl nickel complexes (Scheme 7) as metal mediator for radiofluorinations in presence of a hypervalent iodine compound as oxidant.³⁹ In this case, an aryl Ni(II) complex (A), previously synthesised by oxidative addition from Ni(0), is oxidized with the aid of the radiofluorinated hypervalent iodine compound (B) to the Ni(IV) complex (C). After this critical step, the highly oxidized Ni(IV) complex undergoes reductive elimination to yield the ¹⁸F-fluorinated arene.

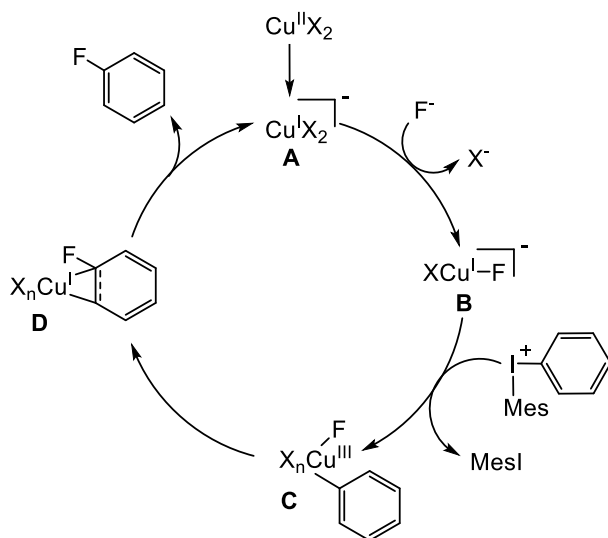


Scheme 7: Ni-mediated radiofluorination according to Lee et al.

Nickel aryl complexes were used in small amounts of 1 μ mol and the radiofluorination carried out at room temperature in acetonitrile for 1 minute. Despite the possibility to obtain radiofluorinated small molecules, the sensitivity of hypervalent iodine scaffolds towards hydrolysis impaired the use of this procedure for the production of PET tracers on an automated scale.

1.2.3.1 Copper mediated radiofluorination

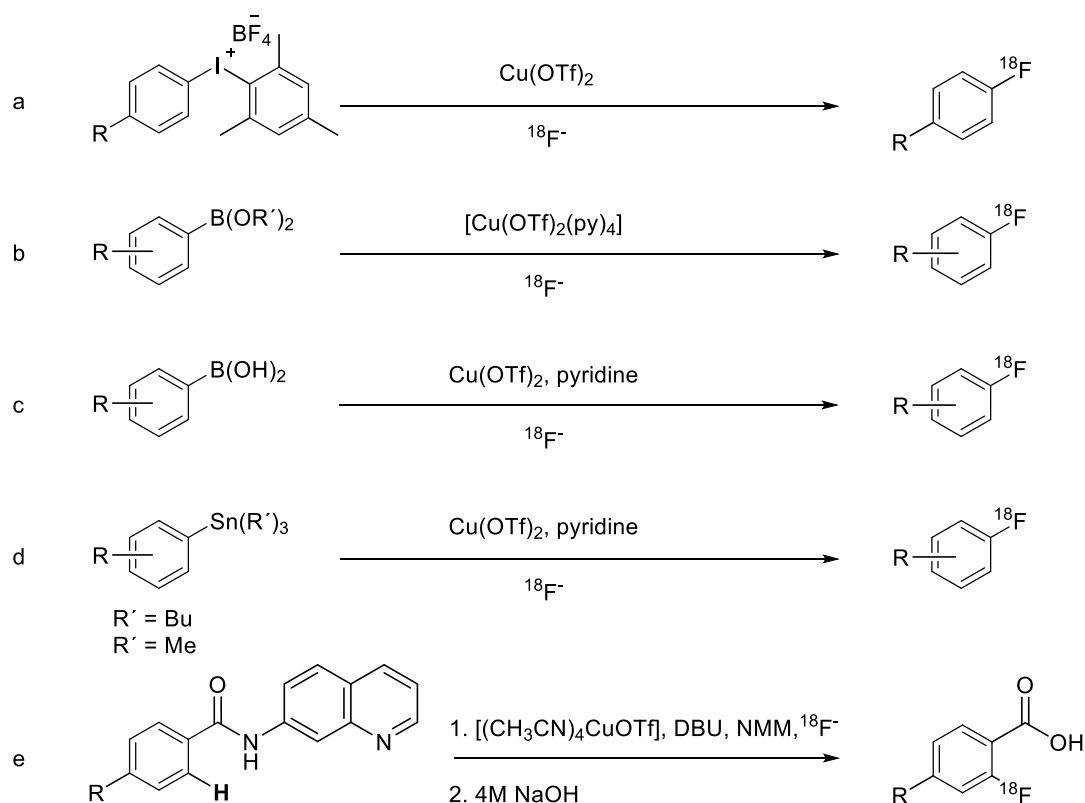
The strategies to overcome the limitations concerning the ^{18}F -introduction in electron-rich arenes can be summarised as the radiofluorination of iodonium salts and the use of transition metals as mediators. In this regard, Ichiishi et al (Scheme 9a) presented in 2014 a procedure which involves the use of both the aforementioned methods by radiofluorinating (mesityl)(aryl)iodonium salts with the aid of $\text{Cu}(\text{OTf})_2$ as mediator.⁴⁰ The reaction proceeds under mild conditions with the mesityl group directing the radiofluorination to the less sterically hindered arene, regardless of its electronic properties, thereby inverting the *ortho*-effect observed in the classical, non-copper mediated radiofluorination of iodonium salts. The same group postulated that the reaction proceeds via a $\text{Cu}^{\text{I}}/\text{Cu}^{\text{III}}$ catalytic cycle (Scheme 8) starting from a $\text{Cu}(\text{II})$ mediator, which is reduced *in situ* to furnish the $\text{Cu}(\text{I})$ complex (A).⁴¹ From this, the active species (B) is formed, followed by oxidative addition of the diaryliodonium salt to furnish a $\text{Cu}(\text{III})$ -F-aryl intermediate (C). Afterwards an intermediate (D) is formed via interaction of the arene with copper which undergoes reductive elimination to furnish the fluorinated arene. The reaction proceeds with both $\text{Cu}(\text{I})$ and $\text{Cu}(\text{II})$ mediators, although the *in situ* reduction of the latter potentially explains the slower rate of the reaction when $\text{Cu}(\text{II})$ is used.



Scheme 8: Proposed mechanism for the $\text{Cu}^{\text{I}}/\text{Cu}^{\text{III}}$ catalytic cycle for radiofluorination of (mesityl)(aryl)iodonium salts

A large number of electron-rich, -neutral and -poor substrates were radiofluorinated with high selectivity and high radiochemical conversions with less than 2% of ^{18}F fluoromesitylene formation. This procedure was implemented for the synthesis of few PET tracers, but although successful on a

small scale, it proved not to be well suited for large scale production of tracers due to the high hygroscopicity of $\text{Cu}(\text{OTf})_2$. Encouraged by the use of copper mediators, Tredwell (Scheme 9b) proposed in 2014 the radiofluorination of boronic esters with $[\text{}^{18}\text{F}]\text{KF}$, mediated by the commercially available $\text{Cu}(\text{OTf})_2(\text{py})_4$ complex, much less sensitive to water than $\text{Cu}(\text{OTf})_2$.⁴² Boronic esters are bench stable and easily prepared. Additionally, the reaction can be carried out under air, has a broad substrate scope and high functional group tolerance. Tredwell carried out the radiofluorinations with high yields by using aliquots of the $[\text{}^{18}\text{F}]\text{fluoride}$, previously preprocessed with potassium carbonate/ $\text{K}_{2,2,2}$. However, when the reaction was carried out one-pot, a severe loss of yield was observed, probably due to the instability of the aforementioned copper complexes under basic conditions, which represented the main limitation of this procedure.⁴³ Mossine et al. broadened the scope of this method to boronic acids⁴⁴ (Scheme 9c) and stannanes⁴⁵ (Scheme 9d) with use of $\text{Cu}(\text{OTf})_2$ in combination with pyridine, whose role as co-ligand was proven beneficial. In all the aforementioned approaches, copper mediated radiofluorinations are carried out in DMF or DMA at 100-110°C. Additionally, the conventional azeotropic drying step is required and base and other additives (pyridine, $\text{K}_{2,2,2}$, KOTf and K_2CO_3), although necessary, led to loss of RCY⁴⁶.



Scheme 9: Copper mediated radiofluorinations

Finally, in 2019 Lee et al. proposed a quinoline-directed copper mediated radiofluorination (Scheme 9e).⁴⁷ This method allows the formation of a sp^2 C-F bond from a sp^2 C-H bond due to the mere presence of aminoquinoline in *ortho*-position. The quinoline is afterwards hydrolysed under basic conditions. However, the reaction gives only moderate yields and lacks *ortho*-position selectivity, therefore it is restricted to either symmetric compounds or those which have only one unsubstituted *ortho* position.

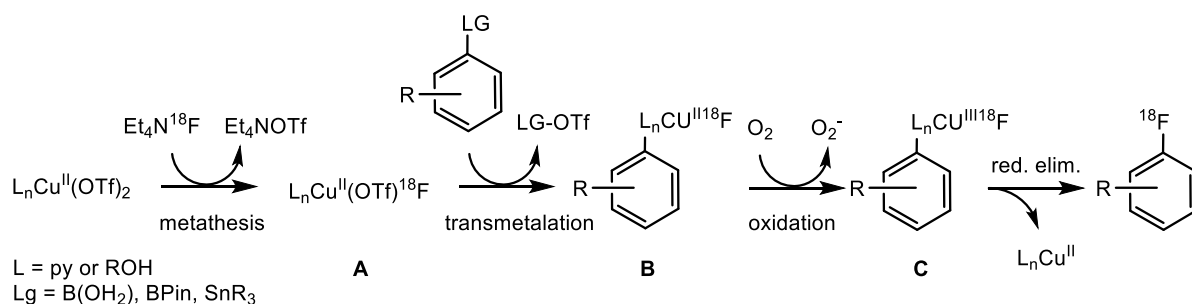
1.2.3.2 Optimisation of the copper mediated radiofluorination procedures

Aromatic radiofluorinations have been widely studied in the past 20 years and much progress has been made. Specifically, the utilization of copper mediated radiofluorination of iodonium salts allowed preparation of electron-rich, -neutral and -poor ^{18}F -labeled arenes with high RCC but the difficult preparation of the precursors and their limited shelf-life represented a major limitation to their applicability. For this reason, further optimization of copper mediated radiofluorinations of boronic precursors were carried out.

A modification of the “minimalist” approach proposed by Zischler et al.⁴⁸ called “alcohol enhanced protocol” allowed to avoid the azeotropic drying step in Cu-mediated radiofluorinations of boronic acids and esters by use of alcohols as co-solvents. Here an eluting salt can be selected in order to regulate the basicity of the radiofluorination and dissolved in an alcoholic solution to be used as eluting agent. For this purpose, ^{18}F fluoride is fixed on a QMA and eluted in the reactor with a tetraalkylammonium salt (e.g. TEAB) in alcoholic solution, followed by addition of a solution with the boronic precursor and the copper mediator of choice. The influence of primary and secondary alcohol as co-solvents was investigated and *n*-BuOH proved to be the best compromise between elution efficiency and radiochemical conversion. *n*-BuOH can indeed be eluted directly in the reactor and used as co-solvent with DMA or DMF in a ratio of 1:2 due to the fact that it can solvate ^{18}F fluoride anions reducing their basicity without hampering their nucleophilicity.⁴⁹

This hypothesis supports an alternative mechanism for the copper mediated radiofluorination of boronic acids, esters and stannanes which was proposed by Zarrad et al.⁵⁰. In this case the reaction proceeds via a $\text{Cu}^{\text{II}}/\text{Cu}^{\text{III}}$ catalytic cycle (Scheme 10) which starts with the anion metathesis to form the Cu^{II} active species (A). The latter transmetalates (B) with the precursors before being oxidized by air to furnish the ^{18}F -aryl(III)cuprate (C), stabilized by pyridine and alcohol. Finally, reductive elimination yields the desired radiofluorinated arene. Additionally, it can be speculated that alcohols can stabilize the transition state of the transmetalation step through the formation of hydrogen bonds between the hydroxyl hydrogens of the alcohols and the oxygen of the boronic acids or esters. This

explanation would also clarify the reason for the lack of beneficial effect on stannanes, for which no increase of RCC was observed in alcoholic reaction medium due to their inability to form hydrogen bonds.



Scheme 10: Proposed mechanism for the CuII/CuIII catalytic cycle for radiofluorination of aryl pinacol boronates, boronic acids and stannanes proposed by Zarrad et al.

The practical value of the method was confirmed by the preparation of clinically relevant PET tracers, namely 6-[¹⁸F]FDA and 6-[¹⁸F]FDOPA with RCCs over 85%. The main drawback of the alcohol enhanced Cu-mediated radiofluorination resides in the high amounts of solvent, copper mediator and precursor needed (30 and 60 μmol). To solve this problem, alternative preprocessing methods that avoid the drying step have been investigated. In 2019 the elution of the fixed ¹⁸F- from a non-carbonated cartridge with a solution of Cu(OTf)₂ in DMA was presented.⁵¹ For this procedure high amounts of copper mediator (48 μmol) were needed to ensure a good elution efficiency. This represented a major limitation to the applicability of the method, in addition to the only moderate yields obtained for the preparation of several PET radiotracers. In the same year, Antuganov et al. showed the practicality of using pyridinium sulfonates in DMA as phase transfer catalyst in organic solvents and as source of pyridine to increase the efficiency of the copper catalyst during the radiofluorination of boronic esters.⁵² Similarly, they described that the use of the non-basic tetrabutylammonium *p*-toluenesulfonate (TBAOTs) in *i*-PrOH is advantageous for radiofluorination of boronic esters with high elution efficiencies and radiochemical conversions.⁵³ Compared with the seminal “alcohol enhanced” procedure, this method allows to use decreased amounts of precursor (15 vs. 60 μmol) and copper mediator (7.5 vs. 30 μmol). Lately, a “minimalist-like” approach is preferred, where the elution is carried out with methanolic solution of an auxiliary tetraalkyl ammonium salt instead of an -onium precursor, followed by evaporation of the methanol. Finally, in 2022, Hoffmann et al. performed a systematic investigation on copper mediators with the aim to improve the yields for the radiofluorination of various substrates bearing -B(OH)₂ or -Bpin groups.⁵⁴ A series of Cu(II) complexes resulted from the combination of 15 ligands and 9 counterions was evaluated for the alcohol-mediated radiofluorinations and Cu(4-PhPy)₄(ClO₄)₂, Cu(3,4-Me₂-Py)₄(OTf)₂ and Cu(3,4-

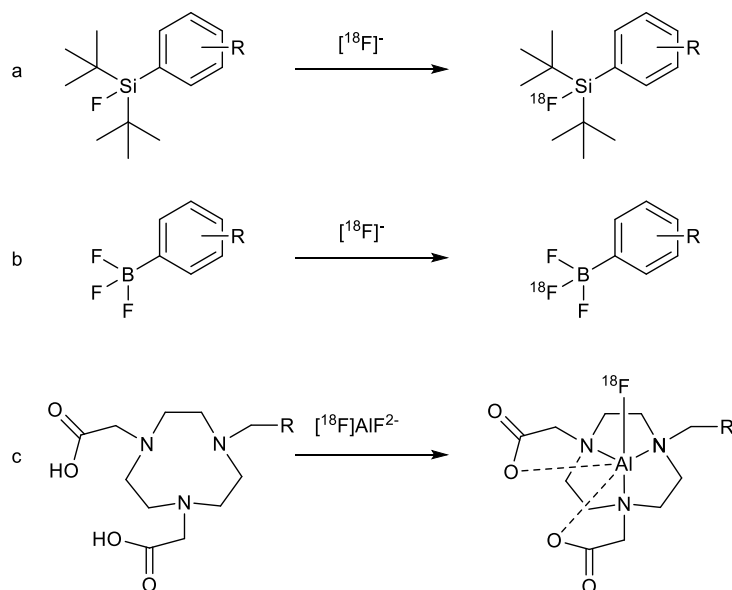
$\text{Me}_2\text{-Py}_4(\text{ClO}_4)_2$ provided the best results. Additionally, the authors demonstrated that DMI is typically superior to DMA as co-solvent for the radiofluorination of this class of precursors using the alcohol enhanced approach.

1.2.4 Fluoride Acceptors

As a consequence of the harsh conditions normally used, peptides, unlike small molecules, are unsuitable for radiofluorination reactions carried out at high temperatures, in presence of aprotic solvents and basic conditions. Additionally, the presence of amino acids bearing protic groups and the need of a selective fluoride introduction represent a significant obstacle. Fluoride acceptors represent an attractive alternative to obtain radiofluorinated peptides from nucleophilic $^{18}\text{F}^-$. Fluoride acceptors are elements like aluminium, boron and silicon, that can form bonds with fluorine with a low activation energy and a high dissociation energy.⁵⁵ Therefore, the radiofluorination is simplified once these elements are incorporated in the molecules as an acceptor group.

An early example of a silicon based radiolabelled fluoride acceptor is ^{18}F trimethylsilyl fluoride, however it was found to be prone to *in vivo* hydrolysis and was therefore replaced with the more sterically hindered di-*tert*-butylphenyl ^{18}F fluorosilane (Scheme 11a).^{56,57} This could be obtained by isotopic exchange which allowed use of mild conditions at the expense of decreased molar activity. Boron is another element that can form strong bonds with fluorine.⁵⁸ Its use in radiochemistry was pioneered by Perrin et al. who showed that boronic acids and esters readily react with $^{18}\text{F}[\text{KHF}_2]$ to the corresponding trifluoroborates.⁵⁹ Alternatively, trifluoroborates can be used directly as precursors for the labelling with $^{18}\text{F}^-$ via isotopic exchange (Scheme 11b).⁶⁰ The main disadvantage of trifluoroborates resides in their limited stability towards hydrolysis *in vivo*⁶¹ which leads to defluorination.⁶² Wade et al. reported the use of zwitterionic trifluoroborates to increase their hydrolytic stability.⁶³ In particular they showed that a proximal cationic moiety, such as a phosphonium unit⁶⁴ or an ammonium group⁶⁵, leads to an increase in the stability of the trifluoroborates enough for *in vivo* imaging. Aluminium also forms strong bonds with F but not with C. For this reason, aqueous ^{18}F fluoride is reacted with AlCl_3 to furnish $^{18}\text{F}[\text{AlF}_2^-]$, which can be introduced in the molecules of interest via complexation with a suitable chelator, for example 1,4,7-triazacyclononane-1,4,7-triacetic acid (NOTA) (Scheme 11c).⁶⁶ A careful control of pH is fundamental since $\text{Al}-^{18}\text{F}$ results stable around pH 4-5, while at higher values aluminium hydroxide complexes are formed and at lower values $^{18}\text{F}^-$ is converted into the $^{18}\text{F}[\text{HF}]$ form. An addition of carrier is not required, therefore high molar activities are normally achieved. A major

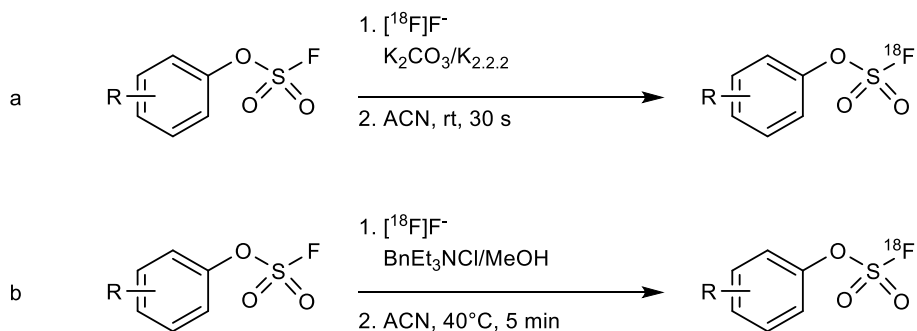
limitation is however represented by the need of high temperatures (100°C). Finally, despite the high impact of the chelator on the physico-chemical properties of a peptide, its selectivity is often retained.



Scheme 11: Nucleophilic radiofluorination by means of fluoride acceptors

1.2.5 SuFEX

In addition to the previously mentioned boron, aluminium and silicon, fluoride shows a high affinity to different heteroatoms, such as sulphur. The Sulphur-Fluoride-Exchange (SuFEX) click chemistry was recently applied to radiochemistry and allowed the synthesis of novel PET tracers by isotopic $^{19}\text{F}/^{18}\text{F}$ exchange. Zheng et al.⁶⁷ used the conventional eluting procedure followed by radiofluorination in acetonitrile at room temperature for 30 seconds (Scheme 12a). However, major discrepancies between the RCC (80-99%) and isolated RCY (20-40%) were reported. An optimized version was published by Walter et al. in 2022 (Scheme 12b).⁶⁸ This more robust method allows radiofluorination of nanomolar amounts of arylfluorosulfates in low concentrations (20 μg , 1 mL) without need of azeotropic drying or base addition. The reaction can be carried out in 5 minutes and the final products are isolated by means of solid phase extraction, without need of HPLC. Additionally, based on the fact that $-\text{OSO}_2\text{F}$ can be used as isostere for $-\text{OCH}_2\text{CH}_2\text{F}$, a large number of radiotracers can be synthesised in 20-25 minutes with high activity yields and high purity.

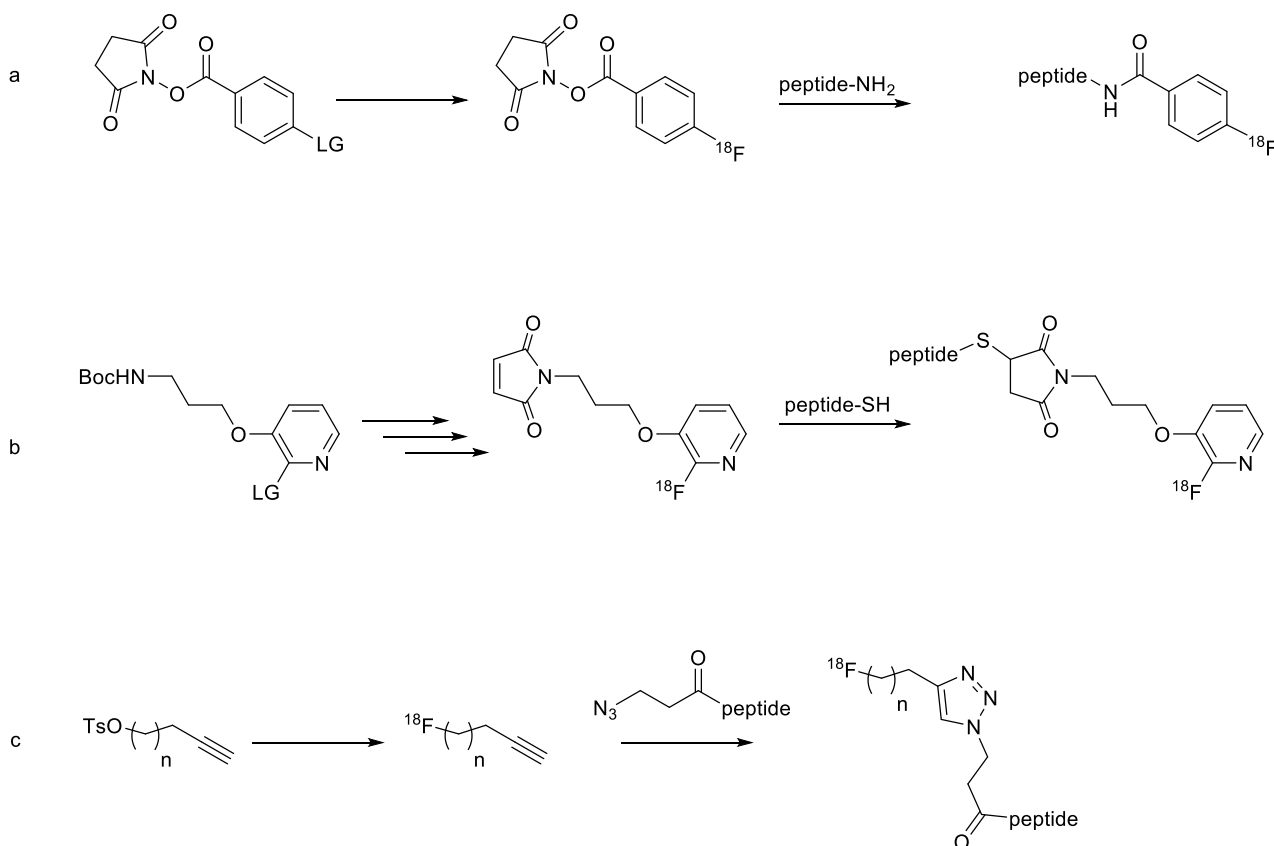


Scheme 12: Radiofluorination via SuFEX-click chemistry

1.2.6 Indirect radiofluorinations

Late-stage radiofluorinations are the most desirable labeling procedures when it comes to radiotracers preparation due to the time constraints imposed by the nuclide decay. Given the harsh conditions and the basicity used to carry out radiofluorinations though, indirect methods have also gained importance to permit the labeling of highly functionalised or heat-sensitive molecules such as peptides or oligonucleotides. Indirect radiofluorinations comprise the combination of direct fluorination of a small bifunctional molecule and its conjugation to the molecule of interest under mild reaction conditions in order to obtain the radiotracer. These small molecules are defined indistinctly prosthetic groups or synthons. While in radiochemistry these two definitions coincide, they actually differ in organic chemistry, where a prosthetic group represents an auxiliary group that is added, for example, to a protein while a synthon is to be interpreted in a retrosynthetic way as a building block which can be used in build-up synthesis to furnish the target compound. In radiofluorinations, versatile prosthetic groups/synthons are for example $[^{18}\text{F}]$ fluoroethyltosylate, $[^{18}\text{F}]$ fluorobenzaldehyde and $[^{18}\text{F}]$ fluronitrobenzene. Moreover, N-succinimidyl 4- $[^{18}\text{F}]$ fluorobenzoate ($[^{18}\text{F}]$ SFB) (Scheme 13a) can be introduced for example by facile acylation of the side chain amino group of lysines to allow the radiofluorination of unmodified peptides or antibodies.⁶⁹ Similarly maleimides show a selective reaction with thiols, which are present as the side chain residue of cysteine in peptides. Compared to amines, which are common in peptides and proteins by the obligatory N-terminus and the high abundance of lysine residues, cysteinyl groups and therefore thiols are less common, making maleimide-thiol conjugation potentially more regioselective. (1-[3-(2- $[^{18}\text{F}]$ fluoropyridin-3-yloxy)propyl]pyrrole-2,5-dione, $[^{18}\text{F}]$ FPyME, for example was presented by de Bruine et al.⁷⁰ for the radiolabelling of unmodified peptides and proteins (Scheme 13b). Additionally, similar to the importance of the azide-alkyne cycloaddition as a conjugation reaction in biochemistry, use of F-18 fluorinated azides or alkynes has gained more and more importance in radiochemistry due to the

possibility to perform the 1,3-cycloaddition under the “click-chemistry” criteria. These include high yields, high regioselectivity, facile purification of the final products and use of mild conditions. For example, the N-terminus of peptides can be converted into an azide and afterwards clicked to a [^{18}F]fluorinated alkyne to furnish the desired 1,4-triazole (Scheme 13c).⁷¹ More recent approaches overcome the use of potentially biotoxic copper catalysts, for example through the use of strained cycloalkynes to obtain a selective addition.⁷²



Scheme 13: Indirect radiofluorination of unmodified (a, b) or modified (c) peptides

1.3 Development of radiotracer for neuroimaging

Unlike the development of drugs, which follows the lead discovery and optimization progress, the development of radiotracers should always start with a profound knowledge of the biological target.⁷³ Most importantly, a biological question has to be clearly defined at the very beginning to justify the expensive and time-consuming process of tracer development. The question can arise from an unmet clinical need or from clinical brain research, for example to clarify or confirm neurophysiological concepts. It is of utmost importance to choose one clinical target of the several that are normally correlated with one biological question. There exist, for example, various PET tracers to address different biological targets of cancer, whose use varies accordingly to the tumor in question.⁷⁴ [¹⁸F]FDG exploits the hypermetabolism of tumor cells,⁷⁵ [¹⁸F]FMISO gives an indication of hypoxia,⁷⁶ a lack of oxygen shared by most of the malignant tumors,⁷⁷ [¹⁸F]FET⁷⁸ accumulation derives by the over expression of the amino acid transporter (LAT1) on tumors. Another strategy consists in addressing the markers which are specific for one kind of tumor, for example PSMA⁷⁹ in case of prostate cancer, or an enzymatic mutation as it will be presented in this work. It has to be kept in consideration that the low mass dose of the radiotracer requires a high brain to plasma ratio and a high specific binding as well as adequate accumulation and washout times. For this reason, labelling of therapeutic agents or known ligands can be misleading and is often replaced by the longer *de novo* approach. Even when developing a library of compounds, it is highly recommended to synthesize molecules with even small changes in the structure. As it will be shown, the introduction of a methyl group can have a substantial impact on stability or affinity. Ideally, the structure should be amenable to late-stage modification.

Finally, it is essential to run *in vitro* experiments as soon as possible during the development process because they represent a valuable guide for the *in vivo* characteristics of the tracer.

1.3.1 Prerequisites for CNS application

While all tracers share the basic prerequisites of high selectivity, high molar activity and high *in vivo* stability, the ones used for CNS applications are more complex.

The first and most important prerequisite is the ability to cross the blood brain barrier (BBB) which represents a physical and chemical barrier that regulates the movement of molecules, ions and cells and protects the cerebral system from toxins and pathogens.⁸⁰ It is composed of non-fenestrated vessels which allow the passive diffusion of small lipophilic molecules and the active transport of various nutrients.⁸¹

One of the criteria for passive diffusion concerns the molecular weight, which must be less than circa 500 kDa as the heavier compounds normally show no or slow accumulation in the brain.⁸²

Lipophilicity, defined by the partition coefficient between octanol and buffer at physiological pH, also plays an important role for the drugs or tracer whose goal is to penetrate the BBB via passive diffusion. For molecules with a high hydrophilicity ($\text{Log}D_{7.4}$ close or lower than 1), it is difficult to cross the lipid membrane unless there is active transport, on the other hand if this parameter is too high (higher than 5) the tracer will tend to remain in the lipid layer decreasing the bioavailability. Additionally, charge and polarity highly influence the lipophilicity and are correlated with increased susceptibility to efflux transport.⁸³ These transporters drive the compounds from the brain back into the blood stream, impairing the accumulation and are therefore responsible for inactivity of a large portion of drugs.⁸⁴

Moreover, new radiotracers are evaluated with regard to their target-binding and pharmacokinetic properties which define the administration, distribution and metabolism of the compound in the body and its excretion from it. Tracers are intravenously administered therefore their bioavailability is 100% since they overcome the first-pass effect.⁸⁵ Information about the distribution of the tracers are of fundamental importance to predict their clinical radiological safety and can be established with a full-body PET scan and with dosimetry measurement in animal experiments⁸⁶. Despite the non-toxicity of the tracers themselves, low dosimetry is sought in all organs that are not involved in the pathological search. As for the drugs, also for radiotracers it is important to acknowledge the in vivo metabolism which in many cases concerns the phenomenon of defluorination, where loss of fluoride from the tracer, leads to its accumulation in bones.⁸⁷

1.3.2 Radiotracer affinity and selectivity

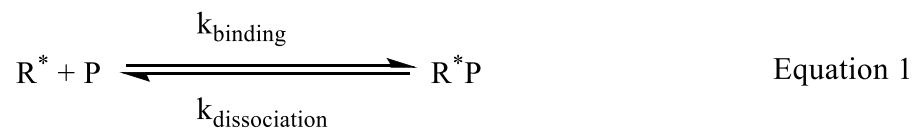
Common biological targets for CNS radiotracers include receptors,⁸⁸ transporters,⁸⁹ ion channels,⁹⁰ enzymes⁹¹ and aggregated proteins (such as β -amyloids⁹² and Tau⁹³).

The design of the tracer is driven by the need of high selectivity and high affinity towards the targets but often nonspecific binding represents a collateral result derived by the interaction of the tracer with targets other than the desired one.

Selectivity is the ability of a drug to show a high binding affinity for one subtype or isoform of a receptor or an enzyme. This parameter is therefore experimentally measured in a pure system, where one subtype at a time is present. Specificity on the other hand refers to the ability of the drug to discriminate between negative and positive interactions, namely it should bind to the receptor or enzyme of interest with high affinity while having no cross reactivity with others.⁹⁴

Formation of Van der Waals interaction and hydrogen bonds between ligand and binding site influences both specificity and affinity. In particular, the quality of the bonds has an impact on the affinity while their number has an impact on specificity: strong bonds result in high affinity while many bonds result in high specificity.

The use of a radiotracer to image the expression of a receptor and its measurement with binding equations are based on the assumption that the radiotracer (R^*) binds reversibly to the target protein (P) to form a complex (R^*P) and follows the law of mass-action (Equation 1).⁹⁵



The association reaction (k_{binding}) involves two reagents and is therefore a second order rate constant having units $\text{nM}^{-1}\text{min}^{-1}$, while the dissociation constant ($k_{\text{dissociation}}$) on the other hand is a first order rate constant having unit min^{-1} . At equilibrium, the rate of association is equal to the rate of dissociation and the equilibrium constant (K_{eq}) can be defined as the ratio between the two rate constants resulting in M^{-1} (Equation 2).

$$K_{\text{eq}} = \frac{k_{\text{binding}}}{k_{\text{dissociation}}} = \frac{[R^*][P]}{[R^*P]} \quad \text{Equation 2}$$

This is a thermodynamic parameter which is directly correlated to the Gibbs free energy: the bigger the K_{eq} , the more favoured the reaction is (highly negative ΔG). The dissociation equilibrium constant (K_D) is the reciprocal of the equilibrium constant, has unit of M and can normally be directly correlated to affinity. Since normally the k_{binding} has a negligible value, the $k_{\text{dissociation}}$ can be directly correlated to the affinity. This means that the lower the K_D value, the higher the affinity for a specific combination of ligand and protein.

Considering that the total amount of target protein (total P) is given by the amount of free (P) and bound (R^*P) protein, the law of mass action predicts the fraction occupancy as a function of the ligand concentration (Equation 3).

$$\text{Fraction occupancy} = \frac{[R^*P]}{[R^*P] + [P]} \quad \text{Equation 3}$$

Additionally, the specific binding is a function of the fraction occupancy multiplied by the number of receptors expressed in the same unit (sites per cell), defined as B_{\max} . Finally, the specific binding can be narrowed down to equation 4.

$$\text{Specific binding} = \frac{[R^*]}{[R^*] + K_D} \quad \text{Equation 4}$$

It can therefore be deduced that when the concentration of the radioligand R^* is 0, the occupancy is 0 while when the concentration is very high (around 100 times K_D), the occupancy approaches saturation point, namely 1.

Experimentally, the affinity can be measured with two different approaches: kinetic or equilibrium experiments. Kinetic experiments consist in determining the rate of the association and dissociation reactions as a function of the concentration of the radioligand in time to obtain the values of k_{binding} and $k_{\text{dissociation}}$ which can then be used to calculate the K_D . As Pollard et al. reported, this method is the most precise but not very often used because it requires the use of the pre-steady state kinetic information, more complex to obtain.

In most cases, competition experiments are the procedure of choice and are based on the assumption that binding follows the law of mass action and it reaches equilibrium. In competition binding assays, the total binding of the radiotracer R^* is measured, followed by a measurement of the unspecific binding which, subtracted to the total, yields the specific binding of the radiotracer and therefore its K_D . To measure the total binding, the target protein P is present in a biological matrix such as tissue homogenate,⁹⁶ isolated membranes⁹⁷ or overexpressed on intact cells⁹⁸. The radioligand R^* is incubated at different concentrations in the medium and the percentage of bound radiotracer R^*P is measured experimentally and plotted in a graph with the concentration of free R^* . Experimentally, nonspecific binding can be obtained in presence of a saturated concentration (around 100-1000 folds excess in respect to K_D) of a non labeled ligand which can bind to the same target.

The unlabelled ligand can be either the non-radioactive reference compound or a chemically distinct ligand and has to be present in a concentration sufficient to saturate the binding sites of the receptor, so that the radioligand can only bind to the non-specific ones. Finally, subtraction of the unspecific binding from the total binding, calculated at the same radiotracer concentration, can show the specific radioligand binding to the receptor (Figure 4). When specific binding is plotted, K_D can be visualised as the concentration of radioligand that occupies half of the maximum number of receptors. It is

important to remember that the success of the analysis requires the ability to separate the bound and free species.

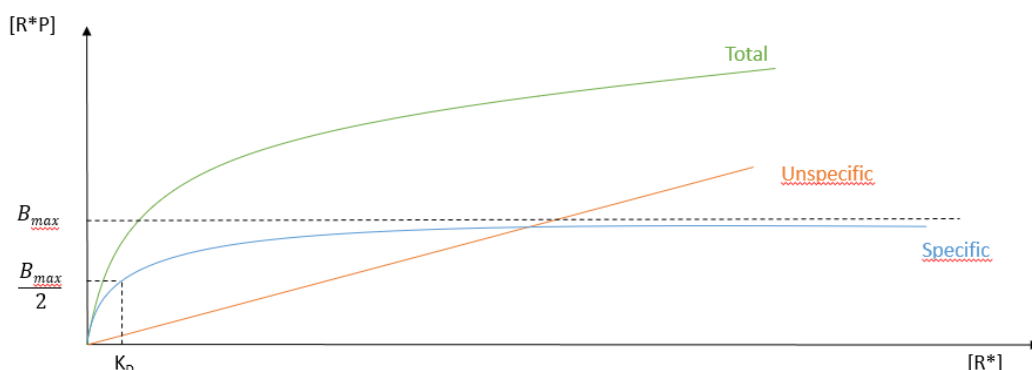


Figure 4: Saturation binding experiment for a radiotracer R^*

According to Clark's theory,⁹⁹ the effect of a drug is proportional to the fraction of occupied receptors and the maximum effect can be reached when all receptors are bound.

Often the radiotracers' structures are designed based on the inhibitors' structures for a specific receptor. For this reason, it is interesting to measure the inhibitory constant (K_i) and the half maximum inhibitory concentration (IC_{50}).

The K_i can be measured similarly to the K_D : a fixed concentration of the radioligand is incubated with an increasing concentration of a known inhibitor with the target protein. The inhibitor will compete with the radiotracer for occupation of the target protein resulting in a reduced portion of receptor available for bind with the radiotracer. The concentration of the inhibitor which displaces half of the radiolabelled ligand is known as the IC_{50} of the drug. The inhibitory constant K_i can be further derived from the IC_{50} through the Cheng and Prusoff equation (Equation 5).¹⁰⁰

$$K_i = \frac{IC_{50}}{1 + ([R^*] / K_D)} \quad \text{Equation 5}$$

It is important to notice that IC_{50} and K_i are equal only for concentrations of radiotracer significantly smaller than the K_D and that in the ideal case of absence of unspecific binding K_D would be equal to K_i .

1.3.3 Enzymatic inhibition

When developing a tracer to image enzymes, its structure can be based on that of a ligand or an inhibitor, reversible or irreversible.¹⁰¹

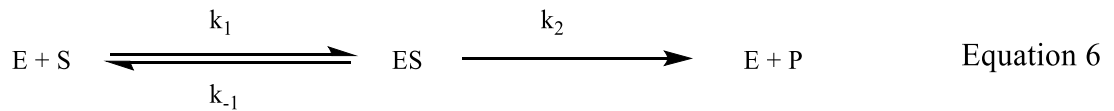
Ligand based radiotracers bind in the active binding pocket. Their design can be challenging because often natural ligands do not have the proper pharmacokinetic properties and an extensive change in their structure may cause a dramatic loss of selectivity. Additionally, often the natural ligand is shared by all the subtypes or isomers of a class of enzymes.

Radiotracers which act as reversible inhibitor bind non-covalently to the enzyme with high affinity (in the range of nM). This approach has several advantages, for example the hypothetically low background uptake due to the quick washout from areas with low concentration of the enzyme. Another advantage is the binding at unique “allosteric sites”, which makes it more probable for the tracer to be selective for one isomer over the others belonging to the same class of enzyme.¹⁰² The design of this class of radiotracers can be inspired by the inhibitors designed as therapeutics but also by the ones which were discarded due to their rapid metabolism or side effects, since none of these parameters are important to the development of a radiotracers.

It is important to note that the tracer images the enzymatic expression and not the enzymatic activity since it binds in a one to one ratio with the enzyme regardless the activation state of the enzyme.^{103,104}

Finally, radiotracers can be based on the structure of irreversible inhibitors which activate the enzyme and are transformed in a reactive intermediate that is covalently bound to the enzyme, inhibiting it permanently. These compounds rely on the activity of the enzyme, unlike the reversible ones, and are bound irreversibly, therefore they image the enzyme activity in a one to one ratio. The disadvantage of this class of compounds is that one molecule of radiotracer can image one unit of enzyme and no more while with reversible binding the enzyme can bind multiple time the same molecule of radiotracer according to its turnover.

While receptor binding can be described using equilibrium binding equations, enzymatic inhibition can be mathematically described by using kinetic equations such as the Michalis-Menten¹⁰⁵ equation. This equation describes the reversible reaction between an enzyme (E) and a substrate (S) which form the so called “Michaelis complex” (ES) which is then irreversibly converted into the product (P) as depicted in Equation 6.



E and S represent the free enzyme and substrate respectively while ES represents the bound enzyme-substrate complex which is formed with a rate proportional to the association constant (k_1) and consumed by formation of the product (k_2) and equilibrium with the free reagents (k_{-1}).

Analogously to the binding equations, the dissociation constant can be described as the ratio between the constants of degradation and association of the ES complex (Equation 7).

$$K_D = \frac{k_{-1}}{k_1} = \frac{[E][S]}{[ES]} \quad \text{Equation 7}$$

For the steady state assumption, rate of degradation of the ES complex has to be equal to the rate of its formation at any time, therefore the sum of v_{-1} and v_2 equals v_1 and equation 8 is obtained.

$$k_{-1} [ES] + k_2 [ES] = k_1 [E][S] \quad \text{Equation 8}$$

Since the total amount of enzyme (E total) is given by the sum of free (E) and bound enzyme (ES), the rate of the process can be described by equation 9, where the maximum velocity (v_{\max}) reached by the system is limited by k_2 (rate determining step) multiplied by the total amount of bound enzyme.

$$v = \frac{v_{\max} [S]}{K_m + [S]} \quad v_{\max} = k_2 [ES] \quad \text{Equation 9}$$

Finally, K_m is the Michaelis constant and is described as the ratio between the sum of the constants of the degradation processes and the association process (Equation 10).

$$K_m = \frac{k_2 + k_{-1}}{k_1} \quad \text{Equation 10}$$

This parameter indicates the concentration of substrate needed to reach half the maximum rate and represents the affinity of the substrate for the Michaelis complex. Although conceptually it is the same as the K_D for the receptor binding equations, it has to be noted that here there are two

degradation processes, therefore K_m equals K_D only in the limiting case where the formation of the product doesn't take place ($k_2 = 0$).

When an inhibitor is introduced in the enzyme-substrate system, the parameters for the in vitro enzymatic assay of three classes of radiotracers differ greatly, although all based on the Michaelis Menten equation. In this work a reversible inhibitor was used as model for the development of the radiotracers, therefore only the kinetic properties related to this process will be further discussed.

For reversible inhibition, a more complex model must be applied to describe the system. This includes the introduction of an inhibitor (I) which reversibly binds to the enzyme interfering with its activity. This class of inhibitors is composed by competitive, uncompetitive and mixed inhibitors, defined by the parameter of the Michaelis Menten equation they affect (Figures 5 and 6)¹⁰⁶.

Competitive¹⁰⁷ inhibitors compete with the substrate for binding in the same active pocket, forming the EI complex and increasing the amount of substrate to reach the half of the maximum velocity (increase K_m , v_{max} unaffected).¹⁰⁸

Uncompetitive inhibitors bind to the ES complex therefore not only they do not interfere with the substrate binding to the enzymatic pocket but they actually need it in order to inhibit the product formation.¹⁰⁹

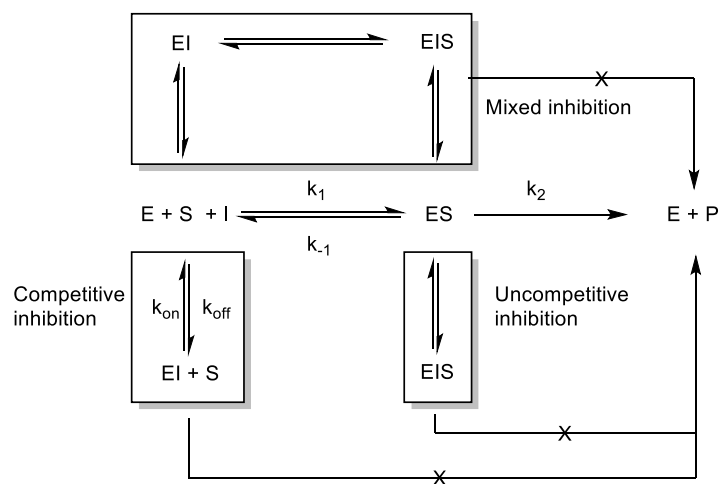


Figure 5: Graphical description of the effect of a reversible inhibitor on an enzyme-substrate system

Additionally, binding of the inhibitor to the enzyme induces conformational changes which make it more difficult for the ligand to unbind from the enzyme, decreasing k_{-1} (reduced K_m). Since part of the Michaelis complex cannot be converted into the product, the v_{max} is also decreased. While the effect of competitive inhibitors can be reduced or eliminated by increasing the concentration of the substrate, uncompetitive inhibitors are not affected by it. Finally, non-competitive inhibitors, also called mixed, are a combination of the two previously described. They can bind to both the enzyme and the enzyme-substrate complex and do not affect the rate of conversions but only the concentration of the ES complex (v_{max} reduced).¹¹⁰

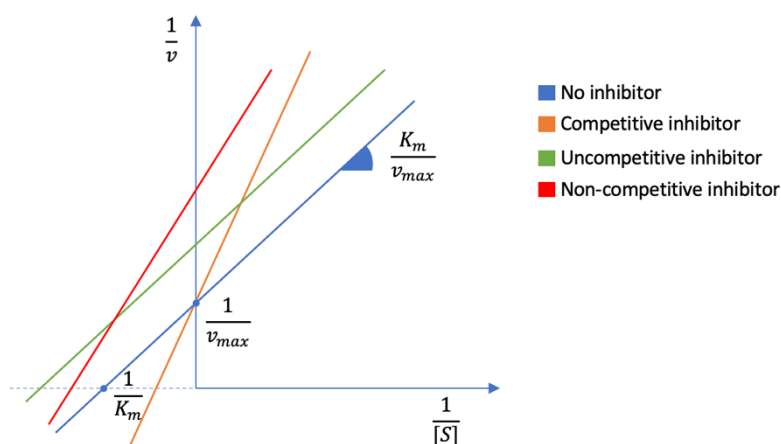


Figure 6: Graph depicting competitive, uncompetitive and non-competitive inhibition.

Most often, the radiotracers for PET imaging of enzymes are designed as competitive inhibitors, normally starting from the structure of the natural substrate, product or transition state.

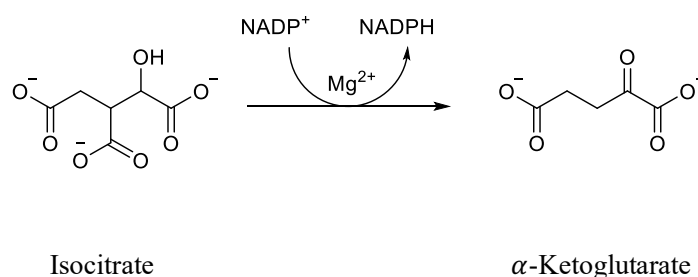
While tracers based on ligands should be analyzed by K_m mean, for reversible inhibitors it is important to measure either the K_i or the IC_{50} . The first one is the equilibrium constant for the formation of the enzyme-inhibitor complex, defined as the ratio between the k_{off} and the k_{on} . IC_{50} on the other hand is the concentration of the inhibitor which impairs 50% of the enzyme activity. While K_i is independent of substrate and enzyme concentrations, IC_{50} values are dependent on assay conditions and are therefore more difficult to compare between different laboratories. For radiotracers purpose, inhibition of the enzyme is not relevant *per se* but still a low K_i or IC_{50} values are highly desirable because correlated with the concentration of the tracer at the site of interest.

1.4 Mutant isocitrate dehydrogenase (mIDH)

Isocitrate dehydrogenases (IDH) are a class of enzymes which reside in mitochondria and cytoplasm and play a role in the Krebs cycle (Figure 7a).¹¹¹

1.4.1 Wild type isocitrate dehydrogenases

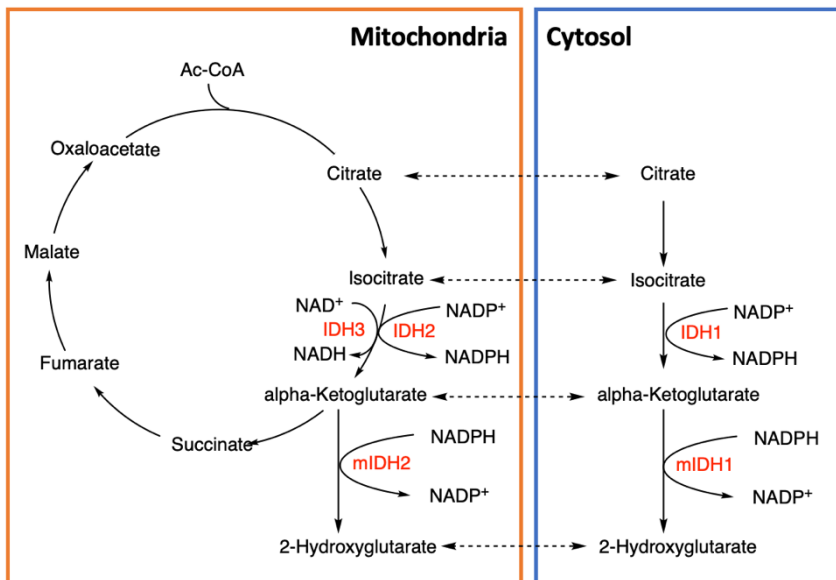
The wild type enzyme has three isoforms: IDH1, which resides in cytoplasm, and IDH2 and 3, which reside in mitochondria. All the isoforms show high affinity for NADP⁺ and a divalent metal cation, normally Mg²⁺ or Mn²⁺, and catalyse the oxidative decarboxylation of isocitrate (ICT) with formation of one equivalent of NADPH and α -ketoglutarate (α KG) (Scheme 14).^{112,113} Additionally, the production of one equivalent of NADPH for both mitochondrial and cytosolic IDHs makes them fundamental for cellular defence against oxidative damage.¹¹⁴



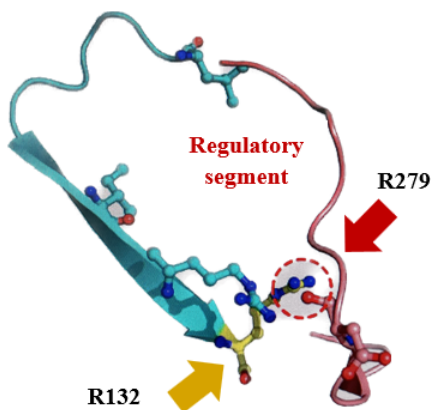
Scheme 14: Enzymatic reaction catalyzed by Isocitrate dehydrogenase

Isocitrate dehydrogenase is an asymmetric homodimer composed by three domains: one large (residues 1-103 and 286-414), one small (residues 104-136 and 186-285), and one clasp domain (residues 137-185).¹¹⁵ The latter joints the two subunits and contributes to formation of the active site where amino acid residues from both subunits are present, suggesting that the enzymatic activity is thrived by the homodimeric conformation. The active site is hydrophilic and accessible to solvent, substrate and cofactor, as well as metal ion which is coordinated by one α -carboxylate oxygen and the hydroxyl oxygen of isocitrate together with several amino acids. NADP⁺ interacts almost with the same amino acids in both active sites, despite their slight difference. In this structure, the residues 271-286, defined by Xu as “regulatory segment” and more commonly referred to as α 10⁷⁵, regulate the conversion between the inactive and the active conformation. This segment protrudes into the isocitrate binding site in the open, inactive conformation blocking the access with a combination of steric hindrance and electrostatic repulsion. In particular, Asp279 occupies the exact position of ICT

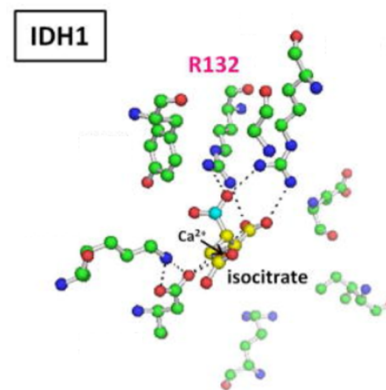
and interacts with Arg132 and Gln277 on the two small domains to keep the regulatory segment in place (Figure 7b). When a certain concentration of ICT and metal ion is reached, the substrate displaces the hydrogen bonding interactions of Asp279 and binds at the active site in the closed, active form (Figure 7c). Additionally, Arg132 establishes hydrogen bond connections with the α -carboxyl and β -carboxyl sites of isocitrate increasing the affinity of ICT for the wild type enzyme.¹¹⁶



a



b

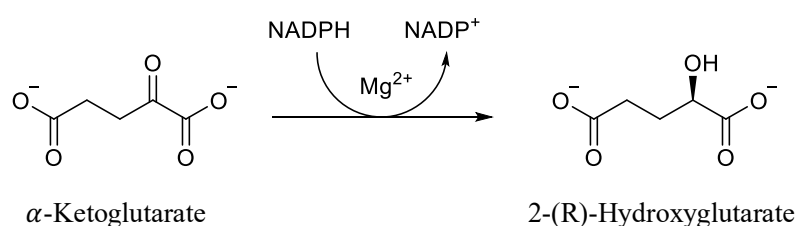


c

Figure 7: a: Krebs cycle and intracellular activity of cytosolic and mitochondrial IDHs; b: Interactions between R132 and D279 on the regulatory segment (modified from Neumaier et al. 2023); c: Graphic explanation of high affinity of wtIDH1 for ICT: interactions between R132 and α -carboxyl and β -carboxyl sites of isocitrate (modified).

1.4.2 Mutants of isocitrate dehydrogenase

Mutants of IDH have been correlated to different cancer types, such as myeloid malignancies and solid tumors.¹¹⁷ When Arginine 132 on IDH1 and 140 on IDH2 are replaced with less polar amino acids, the enzymes gain the neomorphic ability to convert α -ketoglutarate into 2-(R)-hydroxyglutarate (2HG) with consumption of one equivalent of NADPH (Scheme 15).¹¹⁸ 2HG is a competitive inhibitor for α KG-dependent enzymes resulting in silencing the tumor suppressor gene TET2¹¹⁹ and impairment of normal cellular differentiation¹²⁰ while leading to hypermethylation of histones,¹²¹ known to be associated with cancer development.



Scheme 15: Enzymatic reaction catalyzed by mutant Isocitrate dehydrogenasas

In particular, mutant isocitrate dehydrogenase 1 (mIDH1) has been found in around 80% of low-grade gliomas (LGG)^{122,123} and secondary glioblastomas¹²⁴, while mIDH2 is often involved in acute myeloid leukemia (AML)^{125,126}. Around 95-97% of gliomas present mutation at the codon 132 on IDH1: in 90% of the cases, arginine is replaced with histidine (R132H) while the remaining 5-7% with serine (R132S), leucine (R132L), glycine (R132G), cysteine (R132C) or valine (R132V).^{127,128,129} Finally, mutations of IDH2 cover 3-5% of the cases but cause the same pathological conditions.¹³⁰

Being R132H by far the most common one, it will be the only mutation addressed in this work.

It has to be noted that mutant IDHs are heterodimers, containing a wild type monomer which guarantees α KG production, as well as a mutant monomer which converts the latter into the oncometabolite 2HG. Biological studies have shown that a homodimer formed by two mutant monomers would be catalytically inactive (Figure 8a).¹³¹

The loss of natural enzymatic activity and the gain of the neomorphic one by the mutant monomer of IDH1 can be explained by the difference in interactions caused by the replacement of Arginine 132 with other less polar amino acids.

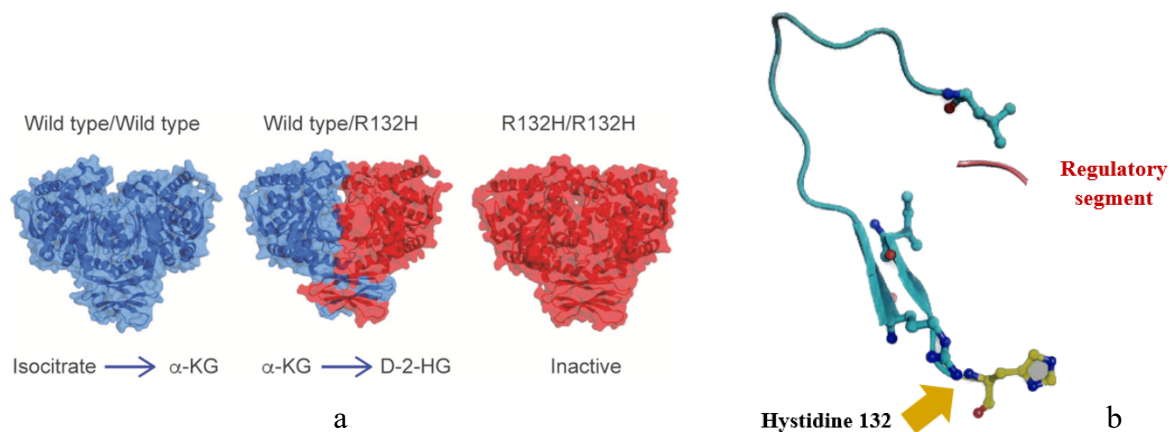


Figure 8: a: Homodimeric structure of wtIDH and heterodimeric structure of mIDH (unmodified from Han et al. 2020); b: Loss of interactions between R132 and D279 on the regulatory segment (modified from Neumaier et al. 2023).

As explained in 1.4.1, the ICT-Mg²⁺ complex binds to the NADP-bound inactive conformation of wild type IDH1 with high affinity. Two complexes are bound per each wild type homodimer. The mutant heterodimer retains the ICT-Mg²⁺ bound to the active site on the wild type monomer but not on the mutant one. Here, the replacement of Arginine 132 with different amino acids impairs the R132-D279 interactions causing a disruption of the active site by displacement of the regulatory segment (Figure 8b). Additionally, ICT and Mg²⁺ can bind to the mutant monomer only as two separated entities and it has been demonstrated that each of them has a reduced affinity for the mutant monomer: Mg²⁺ shows a Km around 300 times higher¹³² while ICT cannot be stabilized by the hydrogen bonds with R132. This causes a loss of affinity to a lower value than the one of α-KG which allows the latter to become the new preferred ligand.

1.4.3 Glioma biology and classification

Gliomas are aggressive brain tumors with an annual incidence rate of 5-7 per 100.000¹³³ and represent about 33% of all brain tumors. They originate from glial cells, including astrocytes, oligodendrocytes and microglia (Figure 9), that surround neurons in the brain.

Their occurrence is in most cases totally incidental, but some genetically transmissible tumors, such as tuberous sclerosis and Turcot syndrome, are associated with gliomagenesis.

The median survival for grade IV gliomas (glioblastoma), the most aggressive ones, is one year and the treatment involves surgical resection followed by radiotherapy which has been correlated to prolonged survival.¹³⁴

Characterized by high mortality rate, high recurrence risk and the huge burden on families, glioma represents one of the deadliest and most devastating malignant tumors known.¹³⁵ To date, there are no known prevention methods for the development of these aggressive brain tumors.

Grade I gliomas are more common in children and young adults and are normally well-circumscribed therefore their resection often leads to long-term survival. Low-grade and high-grade gliomas are, on the other hand, more common in adults and are slightly more common in male than in females.¹³⁶ Grade II gliomas acquire genetic defects that result in malignant transformation to higher grades¹³⁷ which seems to be not preventable even by a very early intervention.¹³⁸ Nevertheless, it has been shown that complete surgical resection could keep the symptoms under control even though the overall survival rate is not improved.¹³⁹

As explained, the vast majority of low-grade gliomas bear a mutation on IDH1 or IDH2 which has been shown to be correlated with an improved prognosis in terms of better treatment response and longer disease-free survival.^{140,141} Another important event in tumorigenesis is the 1p19q gene codeletion which occurs in 40-70% of tumors and makes them more responsive to therapy.¹⁴² 1p19q deletion, along with TP53 mutation, has been correlated to mutant IDHs and a study of their timing reveals that mutations on isocitrate dehydrogenase normally precede them. For this reason, the assessment of the IDH status has been proposed as a standard procedure in the characterisation of brain cancers.¹⁴³

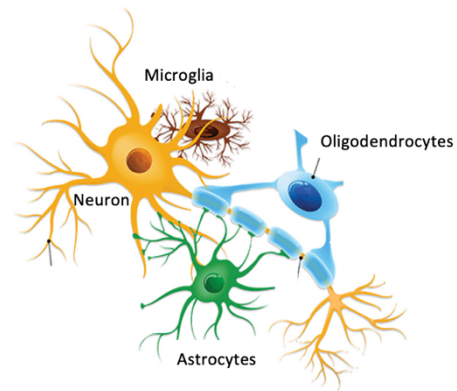


Figure 9: Different types of glial cells (modified from ScienceNewsExplores)

The classification of gliomas was historically performed based on the cells of origin (Astrocytoma, Oligodendroglioma) and they were graded according to different histological and morphological features as low-grade gliomas (WHO grade I and II) or high-grade gliomas (WHO grade III and IV). Additionally, glioblastomas were divided into “primary and secondary glioblastomas”, where the first ones are grown “de novo” without sign of a previously existing low-grade tumor, while the latter ones originate from low-grade gliomas. The inconsistency between the presence of mIDH in high-grade (HGG) tumors and longer survival, led in 2016 to a new classification of gliomas

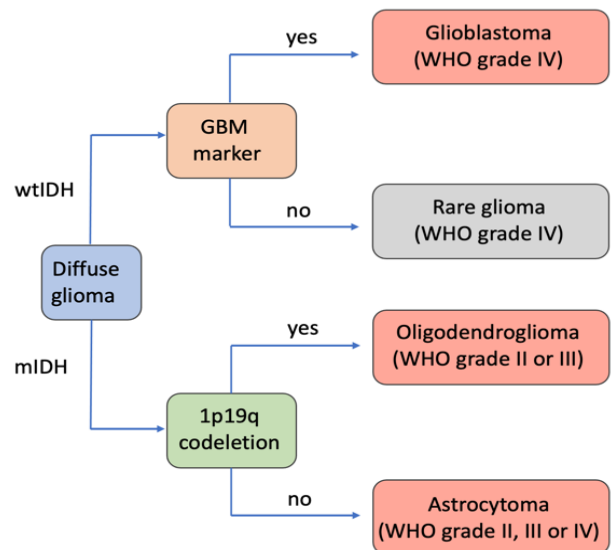


Figure 10: Graphic visualization of the characterization of glioma according to the EANO guidelines of 2021 (modified from Weller et al., 2021)

based on the assessment of the IDH status.¹⁴⁴ The subsequent edition, in 2021, suggested the classification of astrocytomas and oligodendrogliomas based on the presence and absence, respectively, of the 1p19q gene codeletion, and the distinction between glioblastomas and rare WHO grade IV gliomas based on the presence of the GBM biomarker (Figure 10).¹⁴⁵

1.4.4 Diagnosis of glioma: MRI and PET

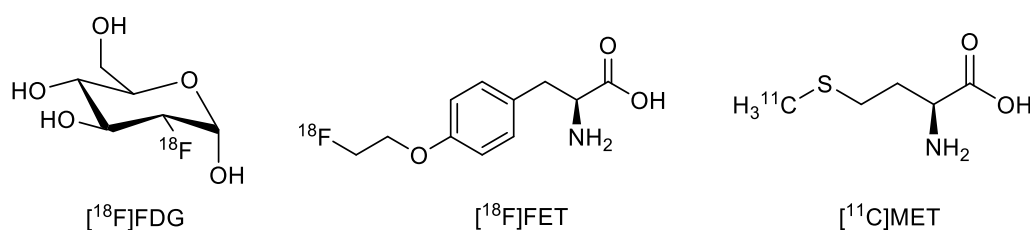
Magnetic Resonance Imaging (MRI) with and without gadolinium-based contrast imaging is the gold standard for diagnosis and therapeutic monitoring of gliomas. This technique gives high resolution anatomical information but lacks biological specificity, further challenged by the irregular shape and heterogeneous composition of gliomas. One additional limitation to the use of MRI for non invasive and precise diagnosis of glioma is the significant portion of WHO grade II and III gliomas which show no enhancement with Gadolinium administration, making the quantification of tumor burdens very challenging.¹⁴⁶ Moreover, the degree and heterogeneity of contrast enhancement have been associated with high tumor grades¹⁴⁷ but the lack of enhancement of many malignant WHO grade II and III gliomas as well as the frequent overlap of imaging characteristics of different groups limit the role of MRI as definitive tool for tumor grading. Different grades and subtypes of gliomas cannot only be classified by imaging techniques but normally an invasive biopsy of the tumor tissues is required. Nevertheless, the sampling of the tissues can and is guided by imaging given the importance

of maximal safe surgical resection. MRI does not represent a reliable technique for detection of the margins of the active tumor given the limited correlation between the contrast enhancement and heterogeneity. This could lead to an undersampling of the most biologically malignant part of the tumor (malignant foci) which is fundamental for patient's prognosis and treatment.^{148,149}

Additionally, the poor specificity of MRI makes the analysis of treatment response often inconclusive. This technique lacks in ability to differentiate between glioma recurrence or progression and the so called "pseudoprogression" which after radiotherapy often consists in transient blood-brain barrier alteration that enhances upon gadolinium administration, resembling neoplastic lesion.^{150,151}

It is of fundamental importance to distinguish between mutant and wild type IDH bearing gliomas and diagnose them as soon as possible to really have influence on the patient's prognosis. Given the MRI limitations in grading and the low enhancement of low-grade Glioma (LGG) upon gadolinium administration, Positron Emission Tomography (PET) imaging has been suggested as a more reliable technique for the initial evaluation of gliomas.^{152,153,154}

Molecular imaging, rather than the anatomical one, can give more insights into the biological processes and be used for the non-invasive grading, analysis of tumor heterogeneity, delineation of tumor burden as well as support for the surgical removal or radiotherapeutic planning. Here a short comparison between 2-deoxy-2-¹⁸F-fluoroglucose (¹⁸F]FDG) and two amino acid tracers, L-¹⁸F]fluoroethyltyrosine (¹⁸F]FET) and L-[methyl-¹¹C]methionine (¹¹C]MET) (Scheme 16), will be presented according to their utility as PET ligands for the characterization of these complex tumors (Figure 11).



Scheme 16: Chemical structures of 2-deoxy-2-¹⁸F]fluoroglucose, L-¹⁸F]fluoroethyltyrosine and L-[methyl-¹¹C]methionine

Despite ¹⁸F]FDG being the most used radiotracer in PET imaging, its use is limited for CNS tumors purposes since the brain has a physiologically high rate of glucose metabolism, hence the high background uptake of the grey matter makes it more difficult to identify low-grade gliomas.^{155, 156,}

^{157,158}

Amino acid PET improves sensitivity, specificity and accuracy in cases of diagnostic uncertainty. For example, amino acids have significantly higher uptake in WHO grades III and IV compared to grade II gliomas.^{159,160} In HGG, [¹⁸F]FET and [¹¹C]MET uptakes are similar and have shown a wider contrast-enhancing volume in comparison to MRI (around 2-3.5 cm difference).¹⁶¹ Unfortunately, different grades often show an overlap¹⁶² and around 30% of grade II and III gliomas are [¹⁸F]FET negative.¹⁶³ Nevertheless, the accuracy of non-invasive grading can be improved with kinetic experiments using [¹⁸F]FET. WHO grade II gliomas are characterized by a slight but steady increase in uptake from 5 to 60 minutes while higher grade gliomas show a higher uptake around 10-20 minutes post injection, followed by a rapid decrease.¹⁶⁴ The higher early uptake typical of HGG can be explained by their hypervascularization and the consequent facilitated amino acid transportation¹⁶⁵ while the mechanism of wash-out is not clear.¹⁶⁶

Additionally, amino acids not only succeed in more accurately defining tumor burdens but their metabolic information can detect tumor heterogeneity as well as tumor areas with different biological and/or clinical behavior.¹⁶⁷

As explained, glioma characterization commonly implies a biopsy followed by surgical removal of the tumor and radiotherapy. Integration of amino acid PET enables a more precise identification of the malignant foci¹⁶⁸ and therefore a more comprehensive biopsy¹⁶⁹ of the tumor heterogeneity as well as a decreased risk of incomplete resection of cancerous tissues.¹⁷⁰

A major MRI limitation is the poor differentiation between glioma recurrence or progression and non-neoplastic lesions, such as post radiation treatment effect or necrosis. On the contrary, several studies have shown that reduced uptake of amino acid PET is a highly sensitive and specific sign of treatment response associated with long term outcome.¹⁷¹

To date, the prognostic value of [¹⁸F]FDG or amino acid radiotracers for gliomas is controversial and needs more detailed study.

<p>MRI:</p> <ul style="list-style-type: none"> <input type="checkbox"/> High resolution <input type="checkbox"/> No biological specificity <input type="checkbox"/> Poor quantification of tumor burden <input type="checkbox"/> Not reliable for tumor grading <input type="checkbox"/> Not efficient localization of malignant foci <input type="checkbox"/> Poor differentiation between progression and pseudo progression.
<p>FDG:</p> <ul style="list-style-type: none"> <input type="checkbox"/> High background uptake <input type="checkbox"/> Difficult identification of low-grade gliomas <input type="checkbox"/> Poor tumor burden delineation <input type="checkbox"/> Low specificity in distinguishing gliomas from other non-neoplastic lesions
<p>Amino acid PET:</p> <ul style="list-style-type: none"> <input type="checkbox"/> Low background uptake <input type="checkbox"/> Kinetic experiments for highly accurate grading <input type="checkbox"/> Improved tumor burden delineation and tumor heterogeneity <input type="checkbox"/> High specificity in distinguishing gliomas from other non-neoplastic lesions

Figure 11: List of advantages and disadvantage of different imaging techniques and agents.

1.4.5 Mutated Isocitrate Dehydrogenase as a target for PET imaging of gliomas

After the assessment of the IDH status was introduced as a standard procedure for characterization and diagnosis of glioma, several research groups have focused on finding an approach to non-invasively determine it. Some approaches exploit the use of MRI to quantify the concentration of 2HG in tumors¹⁷² while others report the use of selective PET tracers claiming that they could be used for direct detection of the mutation.^{173,174,175} This approach is far from being confirmed but could allow a more precise tumor burden delineation and could be used to monitor the efficiency of treatment, as well as to guide biopsies and differentiate the tumor progression from treatment-related lesions. For the design of the radiotracers, known inhibitors of mutant IDH have served as inspiration and have been modified to meet the tracers' prerequisites.

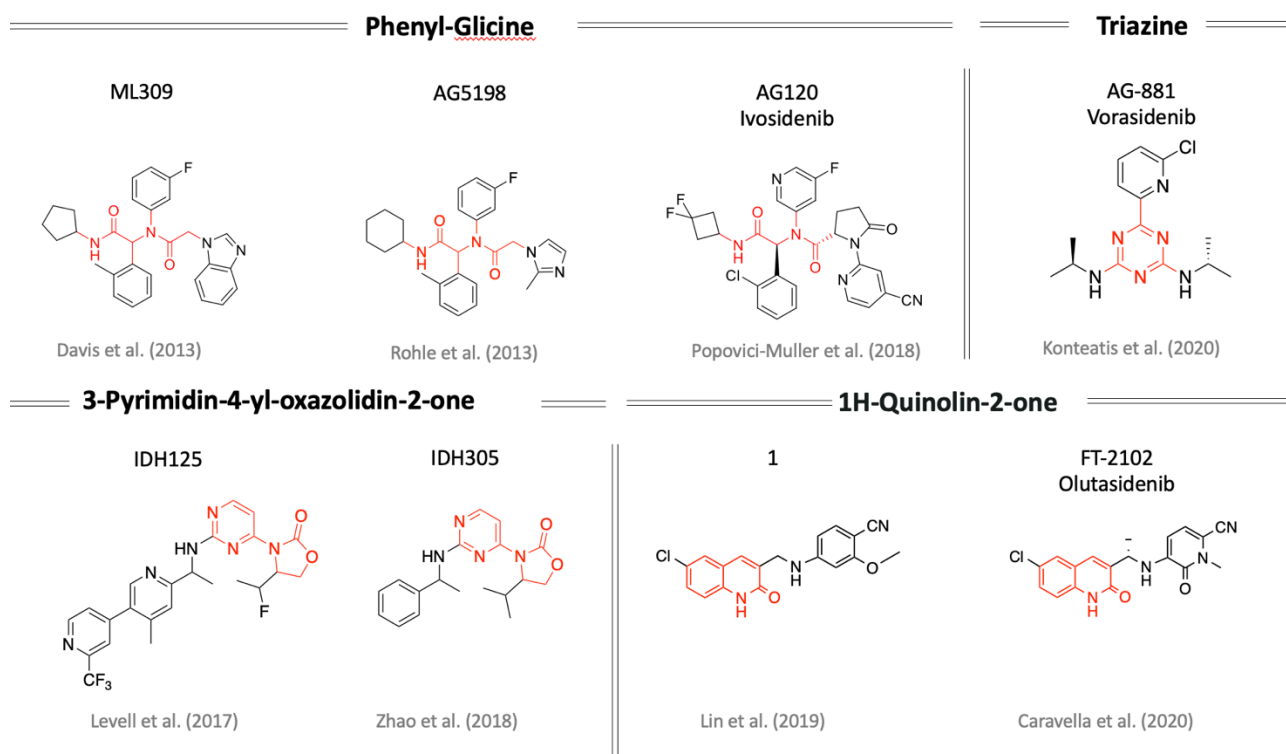
1.4.5.1 mIDH inhibitors: state of the art until 2020

In the last 15 years, a plethora of compounds (Scheme 17) has been produced to specifically inhibit mIDH1 or 2 in the attempt to decrease the 2HG concentration and, consequently, its effect as tumor-enhancer. Few attempts have been made to synthesize competitive inhibitors that bind to the orthosteric binding site given the incompatibility between the extreme hydrophilicity of the natural ligand (ICT) and the penetration of the BBB by passive diffusion.^{176,177,178}

Second-class inhibitors bind to an allosteric pocket and have shown efficient inhibitory activity upon conformational change of various amino acids such as histidine 132.

It has been shown that all the inhibitors presented so far bind to the same allosteric pocket situated at the dimer intersection. When they bind to one face of the regulatory segment, they induce a conformational change that involves the active site. Given the low affinity of Mg^{2+} and αKG towards the mutant active site, the conformational changes weaken their binding to the active pocket to an extent that the reduction of αKG to 2HG cannot take place. In 2013, Popovici-Muller et al¹⁷⁹ proposed the first selective inhibitor for mIDH1 after optimization of a compound¹⁸⁰ resulted from a high throughput screen of a library of compounds against the mutant homodimer. **ML309**, composed of a phenyl-glycine backbone, showed good selectivity between wild type and mutant enzyme, an IC_{50} value of 96 nM, good solubility and in vivo stability but no accumulation of BBB. In the same year, Rohle et al. attempted an optimization and proposed **AGI-5198**¹⁸¹ with the same backbone that, with an IC_{50} of 70 nM, showed efficient inhibition of 2HG production in a dose-dependent manner.¹⁸² Unfortunately, the rapid metabolization and clearance from the body, along with the poor drugability limited its further clinical applications. The same company, Agios, developed the highly selective **AG-120**¹⁸³ that inhibited mIDH1 with high potency ($IC_{50} = 3.5$ nM), which, along with low blood clearance and high stability, made it reach clinical trials III as a drug for the treatment of AML under the name Ivosidenib.¹⁸⁴ Upon 50 mg/kg administration, the compound showed a 4.1% BBB penetration in rats which suggests that its administration in patients with disrupted BBB may allow significant accumulation of the drug in the brain. In this regard, a clinical study (NCT03343197) is being carried out on 49 patients. Shortly thereafter Caferro et al. reported the use of a 3-Pyrimidin-4-yl-oxazolidin-2-one for mIDH related pathologies, Levell et al¹⁸⁵ designed **IDH125** in 2017 which shared the same backbone and showed good selectivity but had a poor inhibition rate. In the same year, Novartis¹⁸⁶ disclosed a similar compound, with a more complex structure, named **IDH305** with high potency towards mIDH1 ($IC_{50} = 18$ nM) and around 200-fold specificity for mutant rather than wild type IDH1. Preclinical tests showed its efficacy in reducing 2HG concentration in tumors, consequently the first clinical trial started in 2016 (NCT02381886). Two years later Zhao et al showed

that the clearance of the compound is not ideal, therefore Novartis has been working ever since on improving its clearance rate and metabolic stability without affecting the other properties.¹⁸⁷ In 2020, Agios presented the first dual mIDH1 and 2 inhibitor, named **AG-881**.¹⁸⁸ The drug (Vorasidenib) shows high potency towards the most common mutants (R132H, R132C, R132L and R132S) and, thanks also to its high brain penetration, is in clinical trials phase I for the cure of AML (NCT02481154), tested over 93 patients.



Scheme 17: Selection of drug candidates for inhibition of mutant IDHs

Few days later, Caravella et al.¹⁸⁹ presented **FT-2102** under the name olutasidenib as an optimized version of the previously disclosed **1**.¹⁹⁰ Both the compounds shared a quinolone backbone and compound **1** shows good cell permeability and ADME properties but poor solubility. The optimized **FT-2102** showed slightly higher potency ($IC_{50} = 21.2$ nM vs 127nM) and that was cleared as orally active inhibitor to be used to treat AML¹⁹¹ (NCT02719574) and is currently in clinical trials phase II for the treatment of glioma and glioblastoma (NCT03684811). When the present project started in 2020, the first discriminating factor for the selection of a known inhibitor was novelty and given the two recently published **FT-2102** and vorasidenib, the choice was between one of them. Both resulted from an optimization process from **AG-221** and from **compound 1** (Scheme 17) but, in the first case a radiotracer with the same backbone had already been developed and showed severe defluorination (Chitneni 2018). Additionally, despite vorasidenib having been reported to function as a potent dual

inhibitor for IDH1 and IDH2 (6 nM against IDH1-R132H and 118 nM against IDH2-R140Q), a more careful analysis revealed its low specificity over the wild type IDHs (190 nM against wtIDH1 and 374 nM against wtIDH2). **FT-2102**, on the other hand, showed high selectivity (21 nM against IDH1-R132H versus >100 μ M against IDH2-R140Q) and specificity (22 000 nM against wtIDH1) which, along with its chemical accessibility, led us to choose the latter over Vorasidenib as target. Interestingly, no more mIDH1 selective inhibitors have been published ever since.

1.4.5.2 mIDH selective tracers: state of the art until 2023

Inhibitors that can bind to an allosteric pocket of the mutant IDH1 enzyme have represented an inspiration for the development of selective radiotracers.

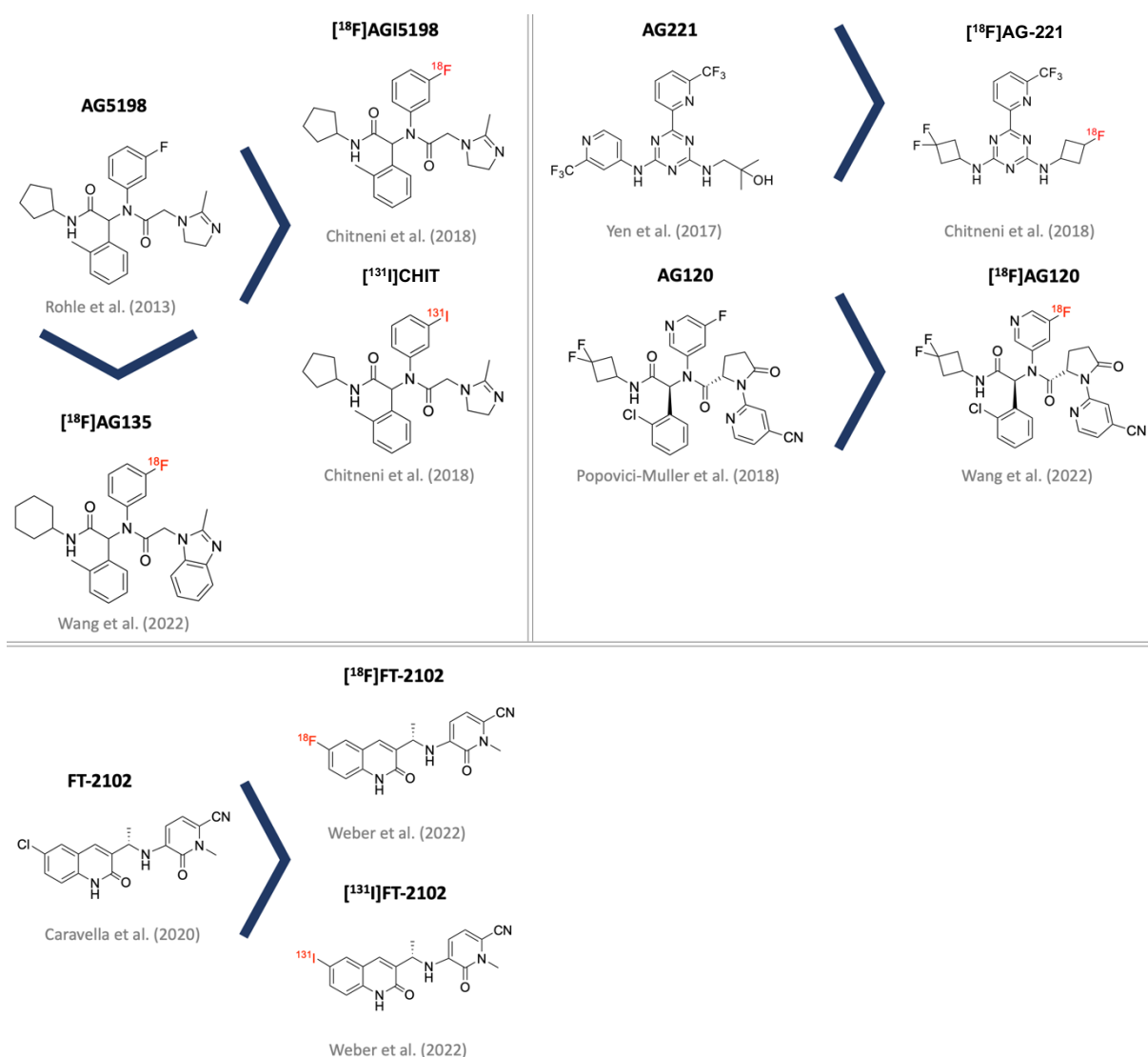
During drug development, drug efficacy is the key factor in discriminating promising drugs from those that are not. In contrast, during the development of an imaging tracer, efficacy, in this case enzyme inhibition, is irrelevant given the extremely small amounts of substance administered. In contrast, the binding affinity between the tracer and the enzyme becomes the key property for judging the quality of the tracer. In all the available literature, drug potency data were reported but never correlated to K_D values therefore all research groups that attempted a similar radiotracer development selected the starting inhibitors on the assumption that IC_{50} would highly correlate with the affinity of binding.

In 2018 Chitneni et al.¹⁹² proposed three different radiotracers (Scheme 18). Two of their structures derived from the inhibitor **AGI-5198** which was first radioiodinated ($[^{131}I]CHIT$) and subsequently radiofluorinated ($[^{18}F]AGI-5198$). Cell experiments showed a slightly higher uptake in mutant rather than wild type enzyme for both compounds. On the other hand, in vivo experiments showed a higher tumor-to-background ratio for $[^{131}I]CHIT$ in respect to $[^{18}F]AGI-5198$ but there was no difference in uptake between the mutant and wild type IDH bearing tumors. The lack of selective uptake suggested that AGI-5198 analogues were not a promising base for further optimization of radiotracers, therefore Chitneni selected **AG-221 (Enasidenib)**, proposed by Yen et al. in 2017,¹⁹³ to design a second mIDH1 selective radiotracer $[^{18}F]AG-221$.

In this case he opted for an isotopic exchange to introduce the radioactive label, modifying therefore the chemical structure of the compound (Scheme 18). The ligand showed a 7-fold higher uptake for mutant IDH1 cells than wild type IDH1 but in vivo experiments in rodents showed severe defluorination and consequent high bone uptake.

During the course of this PhD project, Wang et al.¹⁹⁴ proposed two new radiotracers on the bases of the inhibitors **AG-120** (Ivosidenib) and **AG-135**. Both radiotracers showed a significantly higher

uptake in mutant IDH1-R132H cells of 10 and 24-fold respectively, supported by experimental K_D values of 28.46 ± 1.25 nM and 45.33 ± 1.20 nM, respectively.



Scheme 18: Disclosed tracers selective for mIDHs

Additionally, when tested in healthy mice, rapid clearance and low dosimetry was registered in both cases as well as low bone uptake, suggesting absence of defluorination. However, when tested in vivo in tumor-bearing mice, [¹⁸F]AG135 did not show any uptake, most likely due to its suboptimal logP of 5.9. On the contrary, [¹⁸F]AG120 showed high affinity and high specificity against mutant rather than wild type IDH1 enzyme, despite previous enzymatic experiments, conducted by Popovici-Muller et al., showed that AG120 was highly selective for the IDH1 isoform over IDH2 but not specific for mutant rather than wild type enzyme (mIDH1 IC₅₀ = 12 nM, wtIDH1 IC₅₀ = 71 nM). Additionally, the lack of BBB penetration of [¹⁸F]AG120 made it unsuitable for the non-invasive

assessment of the IDH status in glioma and glioblastoma, therefore the need for a selective and brain penetrant tracer remained unmet.

During the same year, Weber et al.¹⁹⁵ presented radioiodinated ($[^{131}\text{I}]\text{FT-2102}$) and radiofluorinated ($[^{18}\text{F}]\text{FT-2102}$) analogs of FT-2102. While the first radiolabeling reaction was successful, with a yield of $85 \pm 10\%$ and a molar activity of $35\text{ GBq}/\mu\text{mol}$, the latter produced $[^{18}\text{F}]\text{FT-2102}$ in low yield of $7 \pm 2\%$ and molar activity of $3\text{ GBq}/\mu\text{mol}$. These results did not allow further biological evaluation, therefore the project presented in this work was carried on in order to test the radiotracers in vitro and in vivo.

1.5 Docking studies

Biological effects are the result of a multitude of interactions between two complementary molecules. This process is defined as molecular recognition and involves several chemical interactions, including hydrogen bonding, van der Waals interactions, metal coordination and several others. Experimentally, the design of new drugs or radiotracers is often carried out by drawing inspiration from the natural ligands of specific receptors or enzymes or through the time-consuming and expensive process of high-throughput screening of large libraries. Computationally, the chemical and geometrical complementarity between ligand and protein can be predicted with molecular docking, which allows the virtual screening of larger libraries in affordable time and costs and has become of more and more importance in the last decades¹⁹⁶. This chapter describes the computational technique of Molecular Docking applied to the mutant IDH1 and wild type IDH1 enzymes to assist in the development of novel tracers for the early assessment of the mIDH status in grade II and III gliomas. Molecular docking is a technique that predicts the preferred orientation of one molecule to a second, for instance, a target receptor and a ligand when a complex is formed¹⁹⁷.

The 3D structure of the protein of interest is required so that a conformational space can be screened and the predominant binding modes of a ligand predicted. Afterwards, they are ranked according to their spatial and electronic compatibility with the binding pocket and scored according to the most energetically favourable conformation. The molecular docking performed in this work, models the protein as rigid while the ligands are allowed different conformations and orientations. Specifically, Maestro was used, which was developed by Schroedinger (Maestro, Schrödinger, LLC, New York, NY, 2023^[MOU1]). Each binding pose in the pocket is rated by the so-called gscore¹⁹⁸. This is a scoring function derived by the Glide (Grid-based Ligand Docking with Energetics) search for favourable interactions between ligand and protein. The product is a plethora of combinations of the ligand conformation with its position and orientation, defined as ligand pose. The different poses are filtered and finally ranked with a score that is supposed to correlate with the binding free-energy¹⁹⁹.

Practically, the docking protocol used here consists of four steps:

- Protein preparation: this includes the removal of water molecules in the proximity of the ligand and generation of the so-called “het status” at pH values 7-3 which furnishes the amino acids in different protonation-deprotonation statuses.
- Receptor grid generation: indication of the position of the binding sites, if known, otherwise search for possible binding pockets.
- Ligand preparation: a 2D structure is furnished to the program which proceeds to create all possible enantiomers or diastereoisomers.
- Searching algorithms: finds the poses that the flexible ligand could use to approach the binding site in order to have the highest affinity and generates glide scores (gscore). The biggest negative value correlates with the best pose and gscores below -10 are defined as bad matches.

1.5.1 Application of molecular docking to wild type and mutant isocitrate dehydrogenase 1

Lin et al¹⁹⁰. carried out docking studies combined with experiments on a homodimeric mutant IDH1 structure (6O2Y), crystallized with nicotinamide adenine dinucleotide phosphate (NADP+), isocitrate (ICT) and 4-(((6-fluoro-2-oxo-1,2-dihydroquinolin-3-yl)methyl)amino)-2-methoxybenzonitrile **1** (Figure 12a), to characterise the binding to the protein and perform rational structure-based optimization of this quinolone-based scaffold. In the obtained binding pose of **1**, the carbonyl moiety of the quinolone is fundamental for inhibition (quinoline shows loss of inhibition in the μM range).

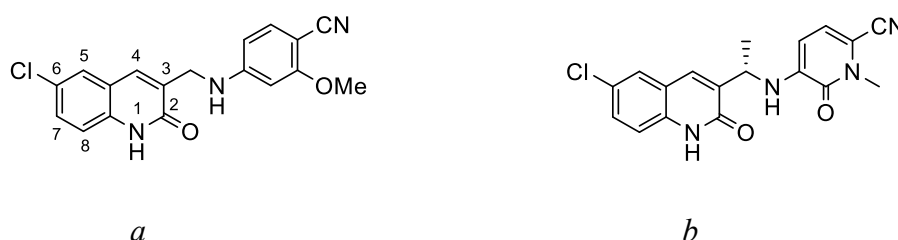


Figure 12: a) Chemical structure of **1**; b) Chemical structure of **FT-2102**

Specifically, the carboxyl group and the amino group of the amide form hydrogen bonds with Arg109 and Arg 279, respectively (Figure 14a). Chloro substituent in position 6 guarantees the highest inhibition with respect to -H, -CH₃ and -OCH₃. Also, they showed that sterically demanding

substituents, like -Br, -*t*Bu, -CF₃, are well accommodated in the hydrophobic site created by Trp267, Ala258, Ile130 and Ile128 (Figure 13a). Additionally, the metabolic stability of the ligand increases with introduction of electron-withdrawing groups in position 6, therefore -Cl was selected as the best option and used to further optimize the structure. Interestingly, despite its small size, replacement of -Cl with -F retained the potency (IC₅₀ = 0.138 μM vs. 0.127). Different aromatic rings have been tested but all retained a cyano substituent in para position. This substituent can form a hydrogen bond with the backbone NH of Leu120, proven fundamental by the dramatic decrease of inhibition registered in its absence (Figure 13a). Finally, it was hypothesized that addition of a substituent on the alpha position of the benzylic aniline linker could constrain it into the bioactive conformation. In particular, introduction of a (*S*)-methyl group imposes a conformational constraint which keeps the bioactive conformation to an energetic minimum, resulting in a 5-fold increase in potency. On the other hand, (*R*)-methyl imposes a conformation that differs from the bioactive one, doesn't represent an energetic minimum, and results in a 100-fold loss in potency. Unexpectedly, a racemic mixture shows a slight decrease in potency but guarantees a dramatic increase in metabolic stability. Caravella¹⁸⁹ et al. continued the docking studies on 6U4J, crystallized with NADP⁺ and ICT and replaced the aromatic ring with a pyridone, whose carbonyl oxygen binds to the NH of Ile128 (Figure 13b). Their final proposed compound, **FT-2102** (Figure 12b) resulted in a stable and potent selective inhibitor for mIDH1.

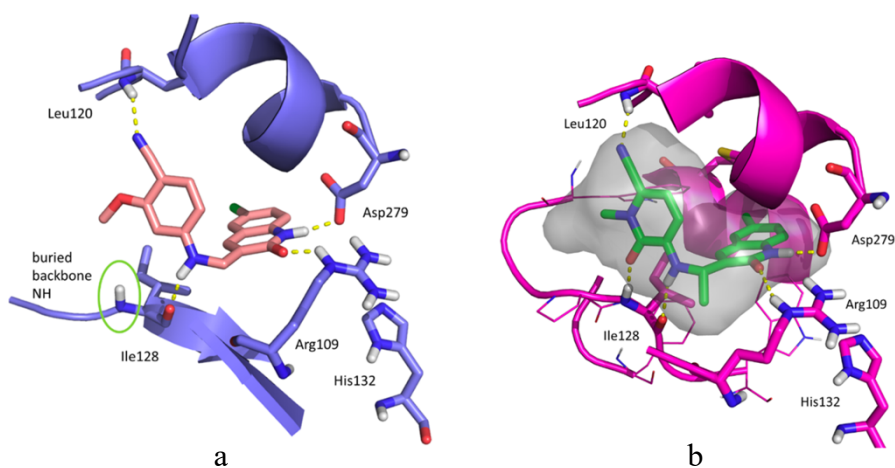


Figure 13: a) Crystal structure of compound **1** (salmon), in complex with mIDH1 (purple);
b) Crystal structure of **FT-2102** (green), in complex with mIDH1 (pink)

Another recent study²⁰⁰, published in 2022, confirmed with molecular dynamics simulations that **FT-2102** is bound to an allosteric binding pocket of the mutant enzyme with stable hydrogen bonds, van der Waals and Pi-Pi stacked interactions to the key residues Arg109, Ile128 and Val281. Different

computational studies showed that despite homodimers mIDH1 and mIDH2 only have a 68.50% identity, **FT-2102** can potentially bind also mIDH2. Interestingly the predicted binding pose of **FT-2102** on mIDH2 shows interaction with Tyr311, Asp174, Arg172 and Val147, none of which belongs to the portion of conserved residues. The high selectivity of inhibition of **FT-2102** against mIDH1 over mIDH2 experimentally confirmed by Caravella was explained by the long retention of the binding to the key amino acids during the MD simulations. On the contrary, the molecular origin of the selective inhibition showed by **FT-2102** on mutant IDH1 over the wild type enzyme has not yet been fully disclosed.

2. Aims and objectives

Isocitrate dehydrogenase (IDH) is a homodimeric enzyme that catalyses the reversible NADP⁺- and Mg²⁺-dependent decarboxylation of isocitrate (ICT) to α -ketoglutarate (α -KG). In human cancers (glioma, acute myeloid leukaemia, chondrosarcoma, and intrahepatic cholangiocarcinoma) these metabolic enzymes are commonly mutated. These mutated variants of IDH (mIDH) are heterozygous missense mutations at codon R132 of IDH1 (>90%) which acquire a neomorphic activity, namely, conversion of α -ketoglutarate to the oncometabolite 2-(*R*)-hydroxyglutarate (2-HG). Thus, mIDHs have emerged as highly promising therapeutic targets and several mIDH specific inhibitors have been developed. Therefore, PET imaging using appropriate radiolabeled mIDH inhibitors should be suitable for the non-invasive assessment of the mIDH status in gliomas. Moreover, the evaluation of mIDH status, currently performed by biopsy, is essential for patient stratification, treatment and follow-up.

The aim of the present project is therefore the design and development of a radiotracer for PET that can non-invasively and specifically assess the mIDH status. Moreover, uptake in low grade gliomas would enable the detection of glioma recurrence with high accuracy. For this purpose, from a series of enzyme inhibitors, selective mIDH1 inhibitors with inactivity towards wtIDH1 have to be selected to serve as a starting point for F-18 labeled mIDH1 selective agents. The identification of chemically accessible positions for the introduction of fluorine-18 will be carried out with the aid of docking analyses in collaboration with the Institute of Neuroscience and Medicine INM-9: Computational Biomedicine at the Forschungszentrum Jülich. Additionally, this screening should identify appropriate molecules which fulfil the main requirements of selective inhibition and the ability to penetrate the blood brain barrier.

These results should provide the basis to proof the concept of principle study and to guide the synthetic preparation of better suited radiotracers bearing a quinolone motif (Figure 14). All this work includes the preparation of reference compounds and precursors which should be chemically modified according to the radiofluorination method. Moreover, the lead compound olutasidenib should be deployed as a starting point for further developments. Olutasidenib exhibits enhanced stability and potency ascribed to an additional *S*-methyl group on the benzylic linker.

Since a quinolone moiety is involved, the ¹⁸F-radiolabel should be introduced in different positions of the aromatic system. Usually appropriate B(OH)₂ or BPin substituents

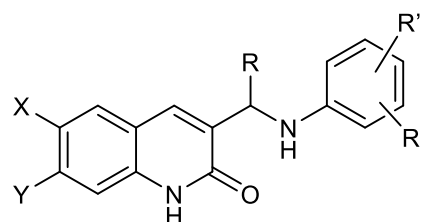


Figure 14: General structure of quinolone-based inhibitors on the base of olutasidenib

should be introduced as leaving groups to enable the application of copper mediated radiofluorination. The radiosyntheses should be optimized with regard to different reaction parameters (solvent, precursor amount, temperature, salt for elution, basic deprotection).

Additionally, other conventional ^{18}F -labeling techniques should be applied for the radiosyntheses of mIDH selective ligands. For the biological evaluation, the non-radioactive reference compounds should be tested in vitro in enzymatic assays and the results compared with data from the literature. Moreover, their physicochemical properties should be experimentally determined to obtain indications about their ability to cross the blood-brain-barrier. Since the in vivo stability is an important criterion for clinical applications, the metabolic stability of all the radiotracers should be studied. Moreover, their specificity should be evaluated in mutant and wild type cell lines. Finally, the radiotracers should be evaluated in in vivo systems like tumor bearing chorio allantoic chicken egg or tumor xenografted mice models.

3. Results and discussion

3.1 Design and docking studies of new selective tracers

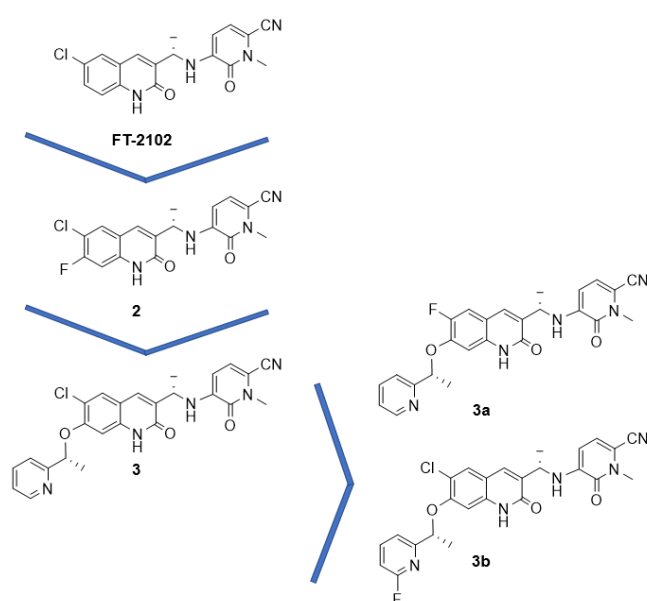
Caravella selected FT-2102¹⁸⁹ as the most promising drug candidate of a series of quinolonebased structures due to its high potency, high selectivity and specificity, good stability in human liver microsomes and adequate solubility. Other quinolone analogues with different decorations were discarded for therapeutic purposes but can represent good candidates for the development of selective PET tracers.

Structure-activity relationship have shown that decoration of position 7 (Scheme 19, compounds 2 and 3) of the quinolone ring can improve potency against the mutant enzyme. In particular, introduction of a fluorine showed retention of potency and HLM stability over 30 minutes but decreased solubility, which doesn't represent an obstacle for its use as radiotracer. Additionally, introduction of a (*R*)-7-[1-(pyridin-2-yl)methoxy] substituent (compound 3) produced the most potent inhibitor ($IC_{50} = 8$ nM) due to the R-methyl group which constrains the linker so that the pyridine adopts a fixed orientation towards the pocket, close to His132.

The first goal of the project was therefore to identify the most promising scaffold to begin the organic synthesis with in order to produce mIDH selective PET tracers.

Unlike compound 2, compound 3 doesn't have a fluorine atom in its structure, necessary for the development of the radiotracer. Position 6 of the quinolone (compound 3a) and the ortho position of the pyridine ring (compound 3b) appeared to be the chemically most accessible ones for the introduction of ¹⁸F. Therefore docking studies were carried out to understand if the modifications in the structure were detrimental or beneficial for the ligand-protein interaction.

Docking studies were performed on protein 6U4J¹⁸⁹, a homodimeric IDH1-R132H mutant, whose structure was deposited on the protein database by Caravella who use it for the simulations.



Scheme 19: Candidates for the development of a new selective tracer

First step was to validate our docking method by docking FT-2102 in the protein and check similarities with the result previously obtained by Caravella. It was possible to identify the two binding pockets, here called 503 and 504, and the docked molecule showed perfect superimposition to the crystallized one with a gscore of around -14 for both the *S*- and *R*-enantiomers in both pockets (Figure 17a). From this result it was also possible to confirm that the ligand-protein interactions are indeed as reported in literature. Once the technique was validated, it was possible to dock compound **3a** and **3b** in the pockets and compare the binding score between them and with the original **FT-2102**. Unlike **FT-2102**, whose both enantiomers showed a good binding pose, the *S,R*-diastereoisomer of compound **3a** (Scheme 19) demonstrated to be by far the preferred pose in pocket 503 (gscore -15.75) but only slightly in pocket 504 (gscore -16.031), where both couples of diastereoisomers showed good binding ability (gscore around -13, -14). For both compounds **3a** and **3b**, the binding pose of the quinolone scaffold showed almost complete superimposition to the one of FT-2102, while different spatial orientation of the substituent in position 7 played the major role in defining the best fitting (Figure 17b). Same results were obtained for ligand **3b** whose diastereoisomers showed good binding poses for both pockets (Figure 17c).

To keep the screen quick, docking experiments are normally carried out with a rigid receptor and a flexible ligand but this represents a poor approximation of the real molecular recognition mechanism. Therefore, a simulation analysis of the protein in aqueous solution with ligands during time was run and hundreds of different conformations were obtained in the first 2.5 ns. Two conformations with big RMSD in respect to the original protein were chosen to run further docking experiments and confirm the quality of the molecular recognition, namely 0.66 ns and 2.2 ns (Figure 15).

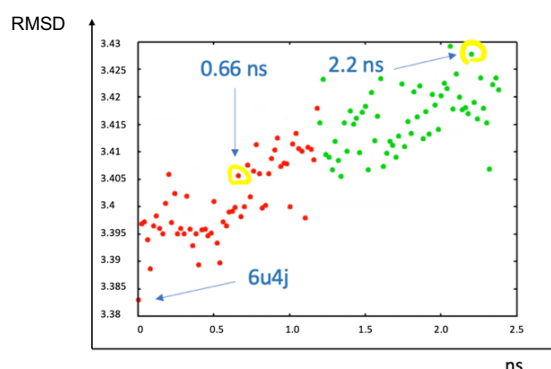


Figure 15: Molecular dynamic simulation of 6U4J in water for 2.5 ns

Search for binding sites did not result in pockets 503 and 504 and docking **FT-2102** in those binding sites gave poor results in terms of gscore (max -6). Superimposition of the binding sites between the 3 different conformations of the protein showed that the binding pocket closes during time, spoiling its binding to FT-2102 (Figure 16).

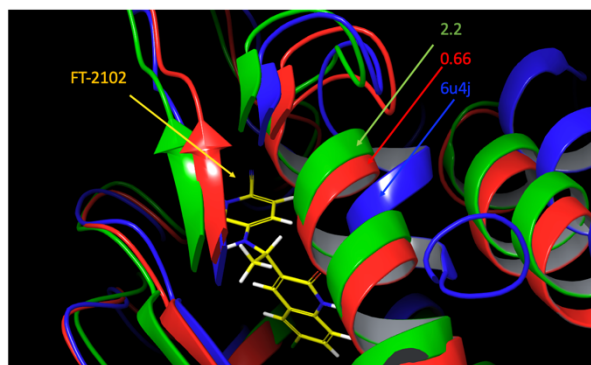
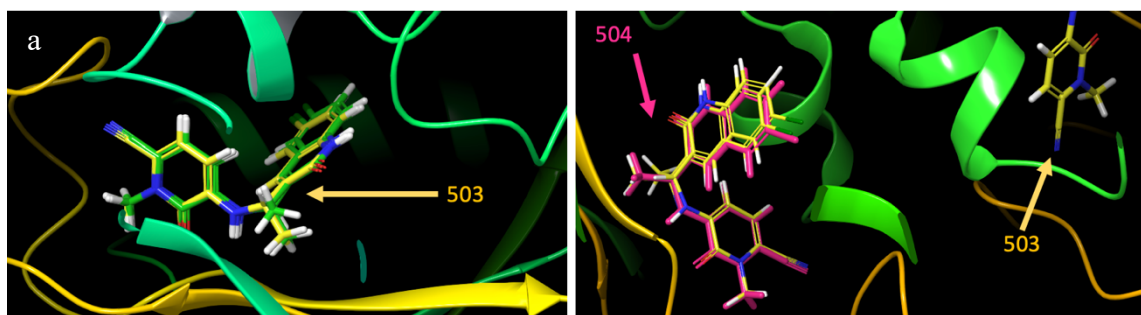
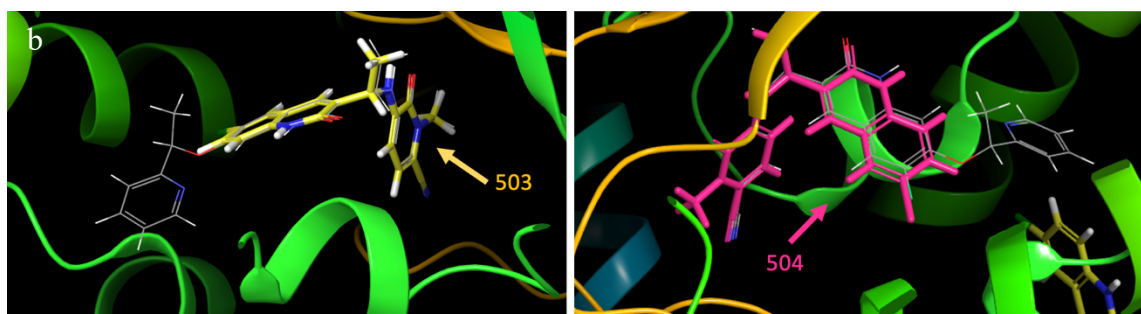


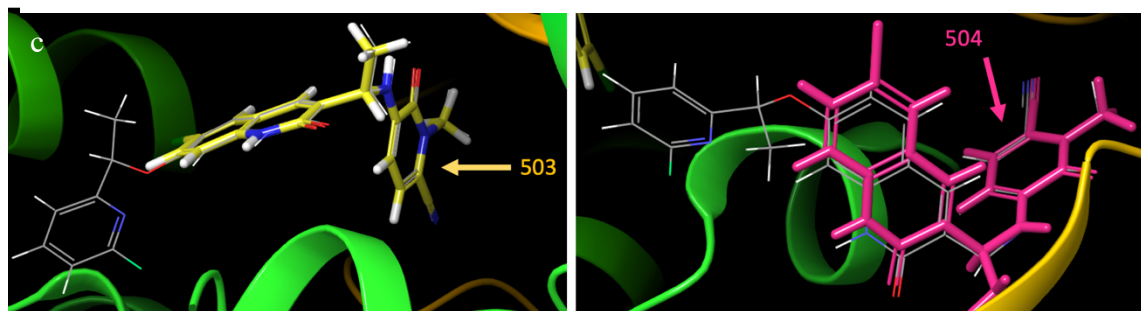
Figure 16: Superimposition of binding site of different protein conformations



Ligand	Pocket 503	Pocket 504
(S)-2	-14.355	-14.038
(R)-2	-14.000	-14.603



Ligand	Pocket 503	Pocket 504
(S,R)-3a	-15.756	-16.031
(R,S)-3a	X	-13.191
(S,S)-3a	X	-13.606
(R,R)-3a	X	-13.240



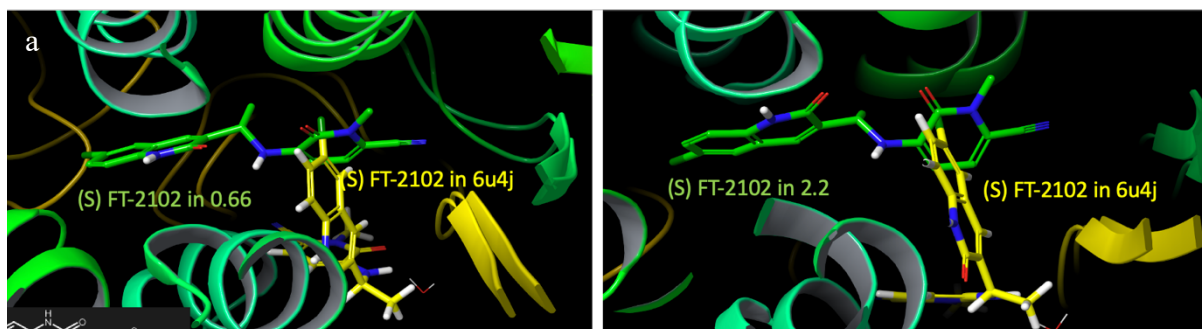
Ligand	Pocket 503	Pocket 504
(S,R)-3a	-15.952	-16.167
(R,S)-3a	-14.897	-15.476
(S,S)-3a	-15.585	-7.946
(R,R)-3a	-15.324	-12.908

Figure 17: a: Superimposition of docked **FT-2102** (in yellow on the left and in green on the right) with the crystallized **FT-2102** in 504 (pink) and 503 (yellow); b: superimposition of (S,R)-diastereoisomer **3a** to the crystallized one in 503 (left) and 504 (right); c: superimposition of (S,R)-diastereoisomer **3b** to the crystallized one in 503 (left) and 504 (right).

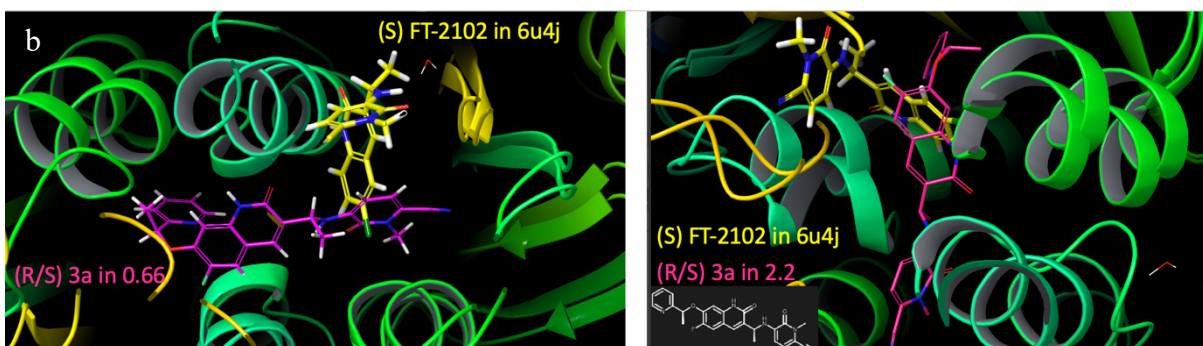
Provided that docking wasn't suitable for this investigation, induced fit docking was further applied to predict the binding modes and structural changes of the receptor at the same time. Induced fit docking of both enantiomers of **FT-2102** resulted in several poses but superimposition of the best ones with crystallized **FT-2102** in 6U4J showed that the binding site actually shifts during time (Figure 17a). The same results were shown by induced fit docking of compounds **3a** and **3b** in both conformations (Figures 17b and c).

In conclusion, the docking studies confirmed that **(S)-FT-2102** is the preferred enantiomer as well as the *(R,S)*-diastereoisomers for both compounds **3a** and **3b**. Unexpectedly, the binding site closes during time, therefore imposition of the docking of the structures in conformations that differ from 6U4J does not give good results while induced fit docking showed that the binding pocket shifts during time. It can be deduced that the mechanism of molecular recognition works by induced docking but a more complex simulation would allow the backbones' movement and permit a deeper analysis.

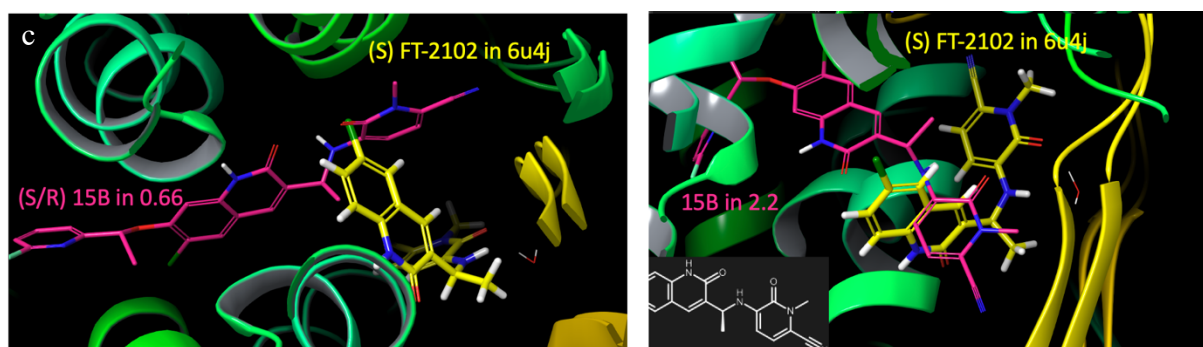
Since the docking didn't provide useful information about compounds **3a** and **3b**, it was decided to start the synthesis of compound **2**.



Ligand	Pocket 503	Pocket 504	Protein conformation
(S)-FT-2102	-16.2	n.d.	0.66
	-14.9	n.d.	2.22
(R)-FT-2102	-15.2	n.d.	0.66
	-14.9	n.d.	2.2



Ligand	Pocket 503	Pocket 504	Protein conformation
(S,R)-3a	-9.3	n.d.	0.66
	X	n.d.	2.2
(R,S)-3a	-12.6	n.d.	0.66
	-13.4	n.d.	2.2
(R,R)-3a	X	n.d.	0.66
	X	n.d.	2.2
(S,S)-3a	-7.8	n.d.	0.66
	-13.8	n.d.	2.2



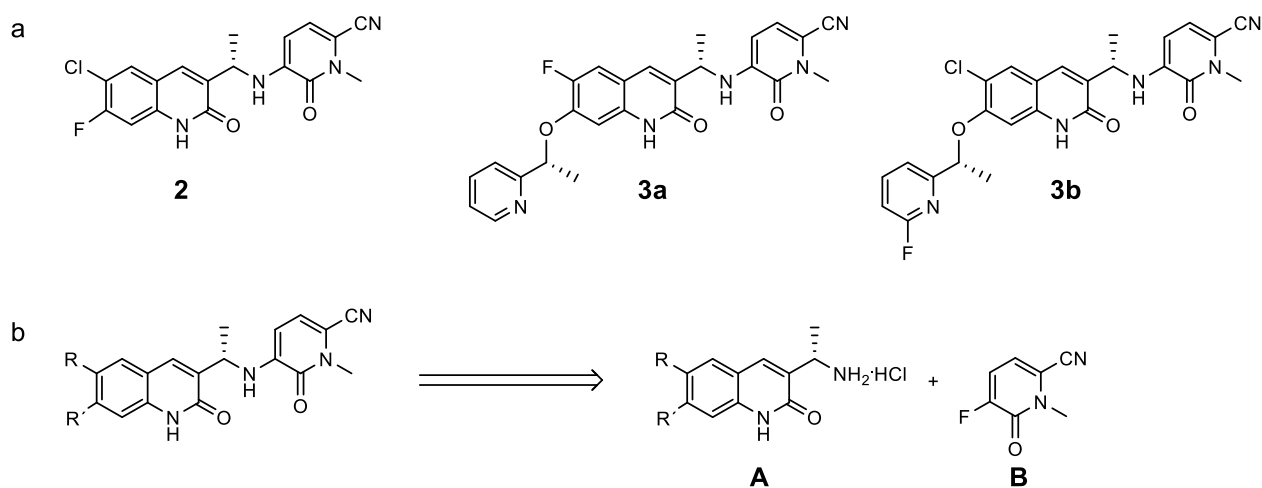
Ligand	Pocket 503	Pocket 504	Protein conformation
(S,R)-3b	n.d.	-14.5	0.66
	n.d.	-8.5	2.2
(R,S)-3b	n.d.	-11.0	0.66
	n.d.	-8.5	2.2
(R,R)-3b	n.d.	X	0.66
	n.d.	-8.3	2.2
(S,S)-3b	n.d.	-14.2	0.66
	n.d.	-14.0	2.2

Figure 18: a: Superimposition of **FT-2102** docked in conformation at 0.66 ns with the crystallized **FT-2102** in 6U4J (pocket 503 on the left, 504 on the right); b: superimposition of **(R,S)-3a** in 0.66 (left) and 2.2 (right) to the crystallized one in pocket 503 of 6U4J; c: superimposition of **(S,R)-3a** in 0.66 (left) and 2.2 (right) to the crystallized one in pocket 504 of 6U4J.

3.2 Disubstituted quinolones

The present study involves the selection of potential candidates, namely compounds **2**, **3a** and **3b** (Scheme 20a) for the purpose of developing mDH1 selective radiotracers, intended for the early diagnosis of gliomas.

These compounds share a common quinolonic feature (A) which is conjugated to an aromatic ring (B) through a benzylic aniline linker bearing a (*S*)-methyl group. The incorporation of the methyl group is aimed at enhancing the metabolic stability of the inhibitor (Scheme 20b). Its spatial orientation, on the other hand, provides a stronger binding to the enzyme, which results in improved potency.



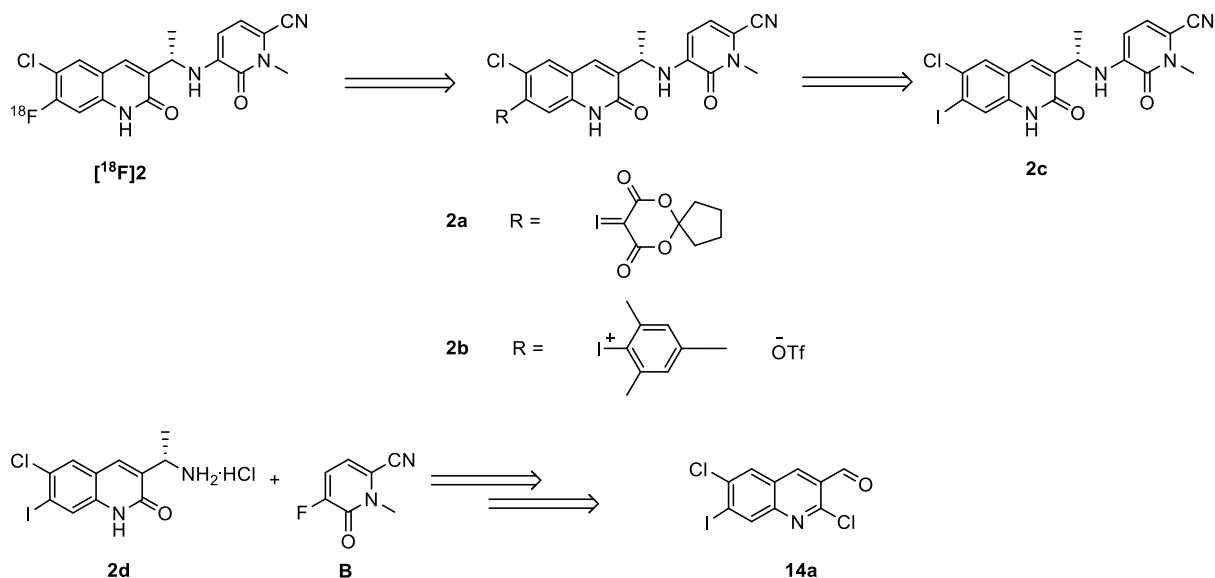
Scheme 20: a) Selection of inhibitors to be converted into radiotracers; b) Retrosynthetic approach for their synthesis

3.2.1 Retrosynthesis of compound **2**

The direct introduction of F-18 on compound **2** in order to obtain the radiotracer [¹⁸F]**2** (Scheme 21) is not feasible due to the absence of activation at position 7 of the quinolone moiety.

As alternative strategy it was hypothesised to use the corresponding iodonium ylide (**2a**) or mesityl iodonium salt (**2b**) as precursors. These are suitable leaving groups for radiofluorinations carried out with the so called “minimalist approach”, namely the use of -onium salts in an alcoholic solution to elute the [¹⁸F]fluoride from an anion exchange cartridge without addition of base or additives. Both of these species can be prepared from the corresponding aryl iodide (**2c**), obtained by conjugation of

the two building blocks **2d** and **B**. Specifically, **2d** derives from the 2,6-dichloro-7-iodio-3-formylquinoline **14a** which was synthesized first.



Scheme 21: Retrosynthetic approach for the introduction of F-18 in position 7 of the quinolone

3.2.2 Preparation of a general 2-chloro-3-formylquinoline moiety

Quinolones and quinolines are an essential class of heterocyclic compounds, serving diverse roles in various applications. They find utility for example as solvents for resins and terpenes or as versatile chelating agents in their hydroxyl form while the 2- and 4-methyl derivatives are precursors for cyanine dyes.²⁰¹ In addition to their industrial use, these compounds exhibit significant pharmacological importance. Antimicrobial²⁰², antimalarial²⁰³, antitumoral²⁰⁴ and anti-inflammatory²⁰⁵ activities have been associated with 2-chloro-3-formylquinolines showing their significant application in the field of pharmacology.

The synthesis of quinolones is normally carried out with the Vilsmeier-Haack reagent (**VHR**), a chloromethyleneiminium salt formed by the reaction between DMF and an oxychloride.

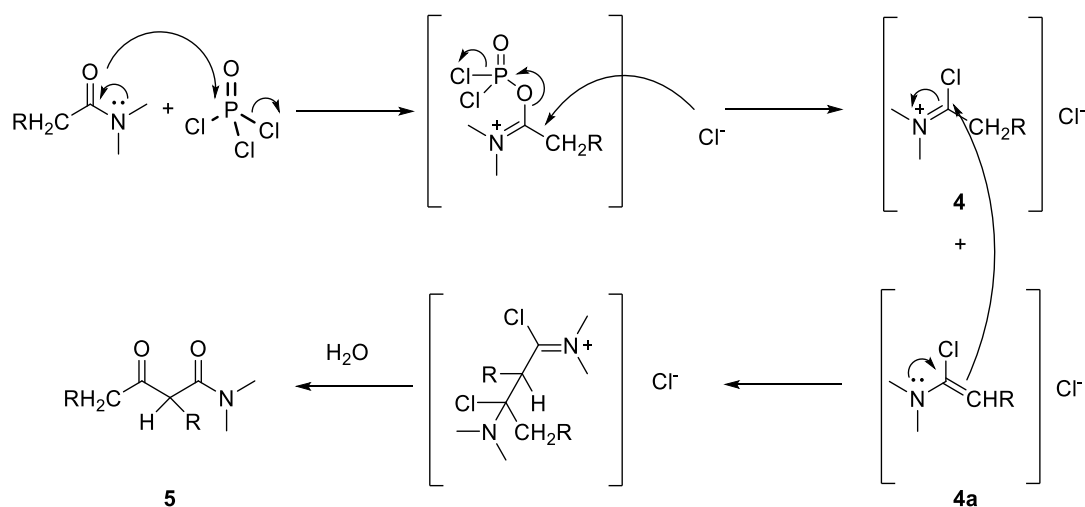
3.2.2.1 Imidoyl halogens and the Vilsmeier-Haack reagent

The synthesis of imidoyl chlorides involves a reaction between N-substituted amides and chlorinating agents, such as phosphoryl oxychloride, oxalyl chloride or thionyl chloride.

In this reaction (Scheme 22), the carboxylic oxygen atom of the amide undergoes a nucleophilic attack on the phosphorus atom of the chlorinating agent, conventionally POCl₃. This results in the

displacement of a chloride anion which afterwards attacks the iminium salt forming the desired imidoyl chloride (**4**) and releasing one equivalent of phosphorus (V) oxychloride.

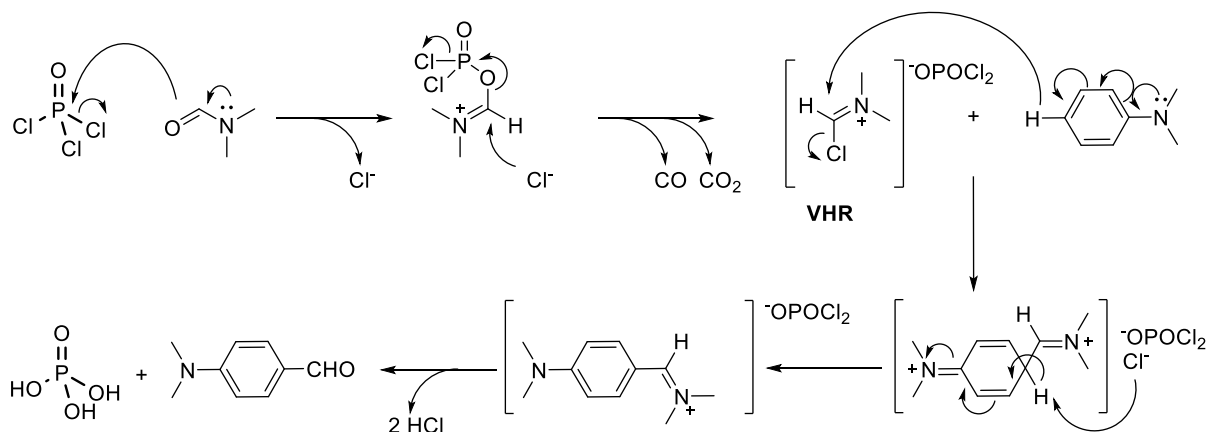
These compounds possess a highly electrophilic nature making them prone to readily react with activated methylene or nucleophilic olefins in order to stabilize the positive charge on the carbon atom. An example of this reaction is represented by the self-condensation of imidoyl chlorides, already disclosed in 1960 by Eilingsfel et al. (Scheme 22).²⁰⁶ Here, due to the presence of a labile α -hydrogen attached to the iminium bond, the ion is rapidly converted into its enamine tautomeric form (**4a**) which then acts as a nucleophile in a subsequent attack to the starting iminium chloride (**4**). The attack does not occur on the nitrogen but rather on the carbon, which yields a β -keto amide (**5**) after aqueous work-up.²⁰⁷



Scheme 22: *In situ* formation of the imidoyl chloride **4** and its self-condensation

The self-condensation can be minimized by using compounds that lack a labile α -hydrogen, such as DMF. In these cases, the imidoyl chloride reacts with a variety of substrates. One example is the Vilsmeier-Haack formylation where the imidoyl chloride is used as a mild, economic and efficient reagent for the formylation of aromatic and heteroaromatic substrates (Scheme 23).²⁰⁸

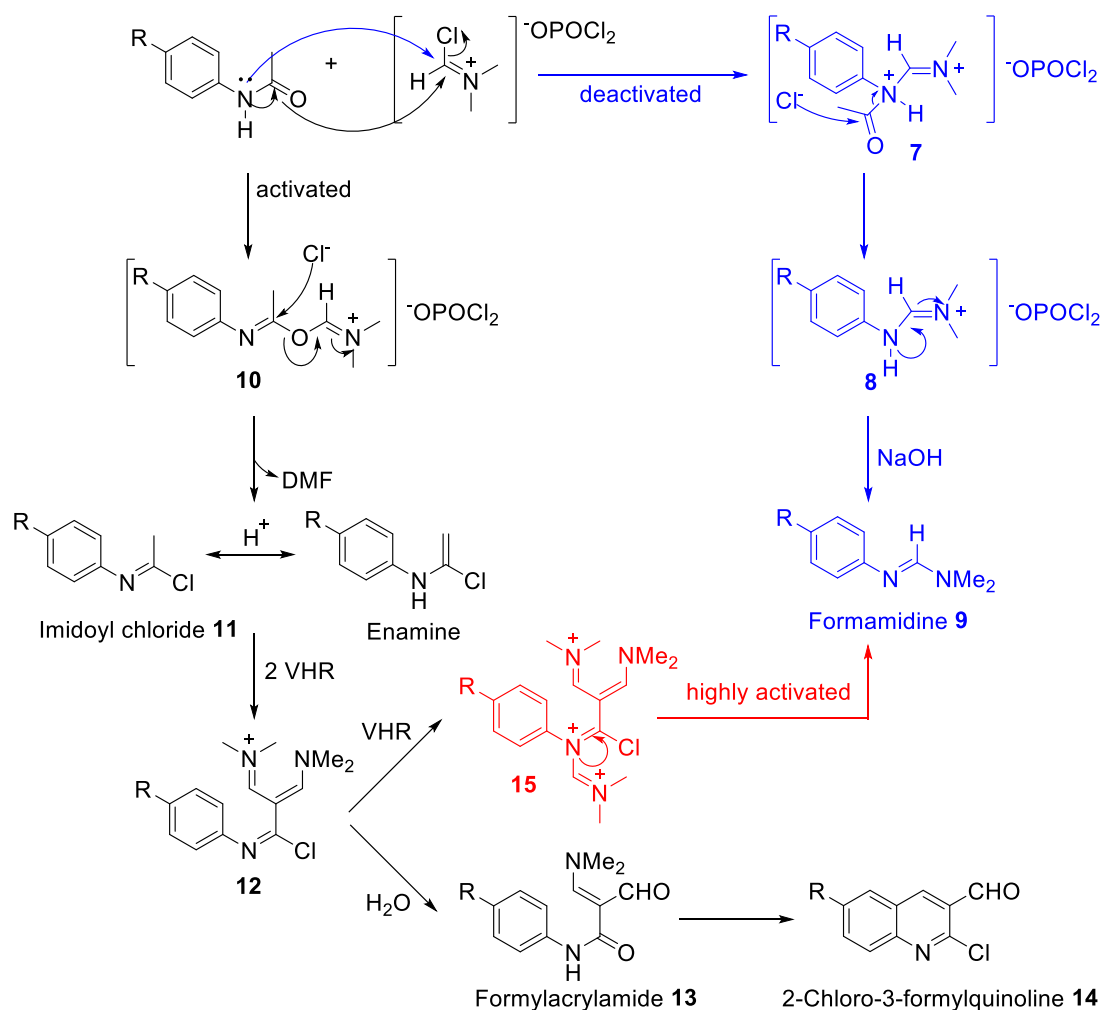
The reagent, known as Vilsmeier Haack reagent (**VHR**) is prepared from the reaction between DMF and a chlorinating agent. Here the carboxylic oxygen of the amide attacks the electrophilic position of the phosphoryl chloride, resulting in the displacement of a chloride anion which then attacks the iminium ion forming the Vilsmeier Haack reagent (**VHR**) along with one equivalent of CO and CO₂. In presence of a nucleophile, an intermediate iminium chloride is formed upon S_N2 reaction and is hydrolysed to the corresponding aldehyde.



Scheme 23: In situ formation of the VHR and its use as formylating agent

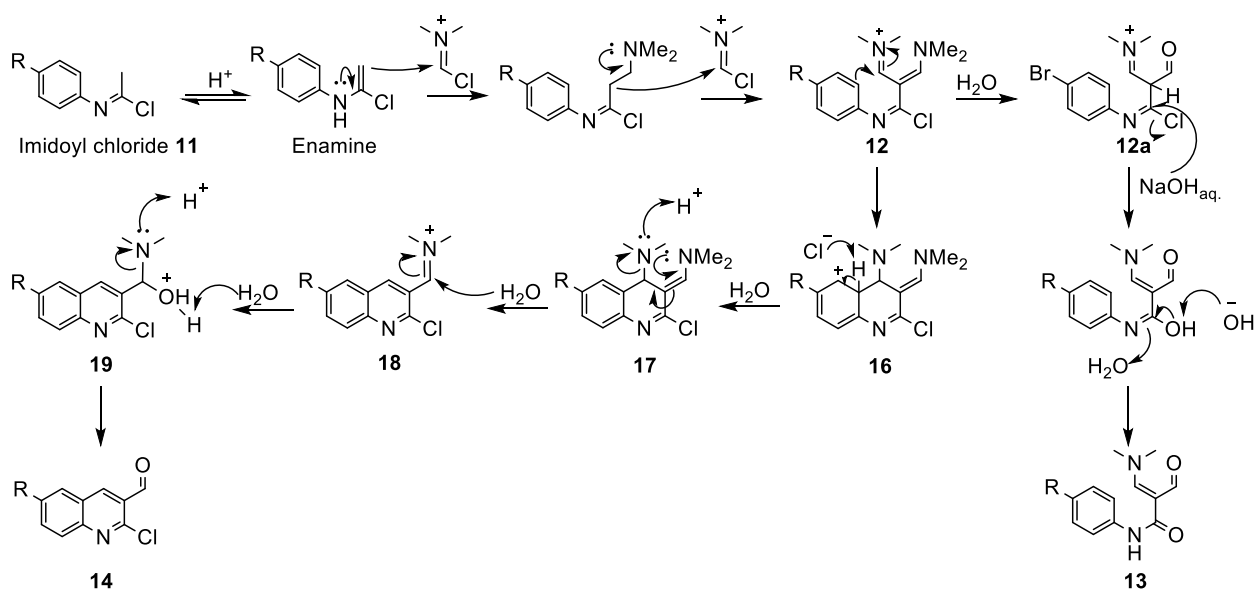
3.2.2.2 Meth-Cohn's synthesis of quinolines through the Vilsmeier-Haack formylation

Meth-Cohn's approach to synthesizing quinolines from acetanilides employs the Vilsmeier-Haack formylating agent, which originates from the reaction of DMF with phosphorus oxychloride. Reaction of substituted acetanilides (**6**) with the imidoyl chloride is a mildly electrophilic process which begins with the formation of a diformylated intermediate. This undergoes cyclization which ultimately leads to the formation of the 2-chloro-3-formylquinoline. The process involves a series of equilibria which, through different mechanisms, ultimately lead to formation of three products **9**, **13** and **14** whose ratio depends on the degree of activation of the nucleophilic aromatic ring (Scheme 24). In presence of electron-withdrawing groups, N-formylation is the favoured pathway. The initial attack of chlorine on the acetyl group of **7** results in formation of intermediate **8**, which is deprotonated upon base addition, leading to formation of the unreactive formamidine **9**.



Scheme 24: Proposed mechanism for the formation of formylacrylamide **13**, formamidine **9** and 2-chloro-3-formylquinoline **14**

On the other hand, in activated aromatic systems where an electron-donating group in *ortho* or *para* position is present, the lone electron pair of nitrogen can be delocalised onto the oxygen end. The latter attacks the C-end of the VHR, leading to expulsion of a chlorine anion (**10**) which further attacks the intermediate at the carbon and expels DMF, yielding the imidoyl chloride **11**. Here, the acid catalysed tautomerism of the imidoyl chloride²⁰⁹ to the corresponding enamine allows C-addition of 2 equivalents of the VHR resulting in the iminium salt **12** (Scheme 25). At this point, electron rich aromatic rings can, to some extent, attack the C-end of the imine (**16**) to allow cyclisation (**17**) and restoration of the aromaticity due to the expulsion of one equivalent of dimethylamine (**18**). Before the aqueous work-up, the reaction mixture consists of the unreactive formamidine **9**, intermediate **16** and the amount of **12** that could not proceed through cyclisation. Addition of water and ice, followed by 30 minutes of stirring, induces formation of intermediate **19** to yield the desired quinoline (**14**), readily obtained by filtration.



Scheme 25: Proposed mechanism of cyclization and further conversion to the corresponding 2-chloro-3-formylquinoline 14

The imine of the diformylated intermediate (**12**) is hydrolysed due to the aqueous acidic environment while the enamine can be found in its protonated form (**12a**). After filtration of the quinoline, addition of 40% NaOH_{aq.} restores the enamine moiety while the imidoyl chloride is attacked by sodium hydroxide, yielding the final acrylamide **13**. The mixture of **9** and **13** can be extracted with chloroform and formylacrylamides can be isolated via trituration due to their poor solubility in petroleum ether, unlike formamidines which are readily dissolved.

Finally, Alonso et al. demonstrated in 1993²¹⁰ that extremely high activation of the aromatic system (i.e. 4-methyl-2,5-dimethoxy acetanilide) could lead to the N-addition of a third VHR (**15**) to intermediate **12**, and subsequent formation of a triformylated compound **15**. Elimination of the diformylated side chain would follow, resulting in formamide **9**.

Meth-Cohn dedicated many years to the study of this reaction in order to gain an in-depth understanding of the underlying mechanism governing the reaction and to investigate potential strategies to manipulate the product ratios.

His initial effort was to verify if it was possible to reverse the formation of formamide, but addition of acetyl chloride or acetic acid to the reaction, did not decrease the amount of unreactive formamide. This, however, led to the realisation that the tautomerism between the imidoyl chloride and the enamine is acid catalysed and actually self-catalytic considering that one equivalent of HCl is formed at each formylation. In an attempt to fully understand the role of acid catalysis, the

formylation of *para*-chloroacetanilide under different conditions was studied (Table 2). The starting conditions of 3 eq. DMF and 7 eq. POCl₃ at 100°C in a sealed tube produced 13% quinoline and less than 25% acrylamide with 50% formamidine (entry c). Formylation of 2- and 3-chloroacetanilides yielded 0% (entry a) and 35% (entry b) quinoline and 95 and 54% formamidine, respectively, demonstrating that the +M effect of halogens favours the reactivity. The addition of one equivalent of HCl with a slightly shorter reaction time improved the acrylamide yield, showing that diformylation is indeed acid catalysed (entry d).

Entry	T (°C)	Time (h)	HCl (eq.)	9	13	14	
a	2-Cl	100	1.25	0	95	< 25	0*
b	3-Cl	100	1.25	0	54	n.d.	35**
c	4-Cl	100	2	0	50	n.d.	13
d	4-Cl	100	1.2	1	n.d.	60	2
e	4-Cl	100	3	1	n.d.	62	2
f	4-Cl	140	2.2	1	70	0	23
g	4-Cl	75	1	0	n.d.	73	1
h	4-Cl	75	1.5	0	n.d.	69	2
i	4-Cl	75	3	1	n.d.	66	4
l	4-Cl	60	3	0	n.d.	0	0
m	2-NO ₂	75	1.5	0	95	0	0***
n	2-NO ₂	20	18	0	n.d.	14	0***
o	2-NO ₂	20	48	0	95	0	0***

* 8-chloro quinoline ** 7-chloro quinoline *** 8-nitroquinoline

Table 2: Formylation of mono-substituted acetanilides under different conditions

Extending the reaction time had no effect (entry e), while increase of temperature facilitated cyclization (entry f). The absence of acrylamide could probably be explained by the fact that the fraction of intermediate **12** that did not undergo cyclization underwent a third N-alkylation (**15**) and was converted into formamidine **9**, which represented 70% of the total yield.

The use of milder conditions was further investigated. Treatment with 2.5 equivalents of DMF proved adequate and the lower temperatures allowed the use of an open flask. While the cyclization decreased to 1%, the formation of acrylamide increased to 73% with a reaction time of 1 hour (entry g) and 69% with a slightly longer reaction time (entry h). The addition of HCl at the milder temperature of 75°C proved unnecessary (entry i), as the equivalents produced during each addition of VHR remain in solution. Attempts to further decrease the temperature (entry l) failed to produce both acrylamide and quinoline even though it was not reported if the reason resided in the absence of reactivity below 75°C or in a full conversion to formamidine. A similar study was performed on 2-nitroacetanilide which showed almost full conversion to formamidine at 75°C (entry m) but partial formation of acrylamide was reported at 20 °C (entry n) suggesting that the reaction could start, even though formation of formamidine was not investigated. Surprisingly, longer reaction times showed 95% formation of formamidine supporting Alonso's theory that the acrylamide formed could be fully converted into formamidine within prolonged reaction time (entry o).

At the end of the study, he could conclude that the harsh initial conditions led to higher amount of quinolines with aromatic compounds bearing halogens, while the milder ones favoured it in the presence of electron-donating substituents (Table 3).

Acetanilide	Time (h)	Quinoline 14	Acrylamide 13	Formamidine 9	Conditions
	2.25	74 %	n.d.	n.d.	1
4-Me	16	70 %	10 %	6 %	2
	1.25	10 %	n.d.	n.d.	1
4-OMe	16	56 %	n.d.	27 %	2
	2	13 %	n.d.	50 %	1
4-Cl	1.5	2 %	69 %	n.d.	2
	2	30 %	n.d.	50 %	1
4-Br	16.5	23 %	32 %	45	2
	1.25	0 %	n.d.	72 %	1
4-NO ₂	1.5	0 %	53 %	45 %	2

Conditions 1: 3 eq. DMF, 7eq. POCl₃, 100°C, sealed tube
Conditions 2: 2.5 eq. DMF, 7eq. POCl₃, 75°C, open flask

Table 3: Comparison of yields of para-substituted acetanilides under harsh and mild formylating conditions

It was also observed that the formylation is extremely regioselective and, in the case of *meta*-substituted acetanilides (Table 4, Entry a), the cyclisation occurred only at the least sterically hindered *ortho* position, without any trace of 5-methoxyquinoline. The same result was obtained with the disubstituted 3,4-dimethoxyacetanilide where 6,7-dimethoxyquinoline was obtained in 72% yield as the only product after filtration (entry b). The highly activated 3,4,5-trimethoxyacetanilide (entry c) was obtained in 92% yield, confirming that electron-rich aromatic systems are the best scaffolds for formylation. These results have been confirmed by different research groups^{211,212,213}.

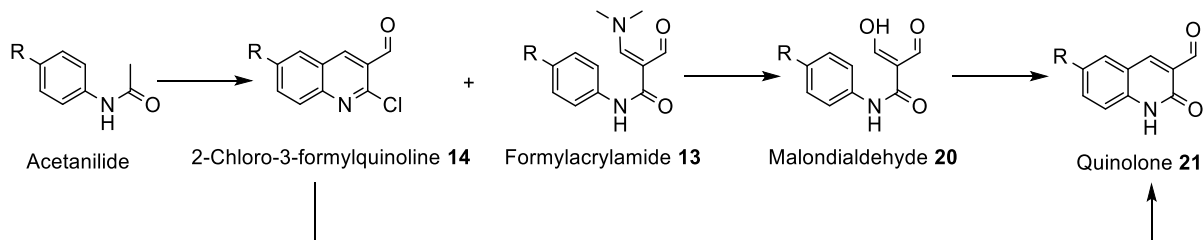


Entry	Acetanilide			Quinoline			
	R ₃	R ₄	R ₅	R' ₅	R' ₆	R' ₇	y (%)
a	OMe	H	H	H	H	OMe	89 %
b	OMe	OMe	H	H	OMe	OMe	72 %
c	OMe	OMe	OMe	OMe	OMe	OMe	92 %

Table 4: Formylation of asymmetric and multi-substituted acetanilides

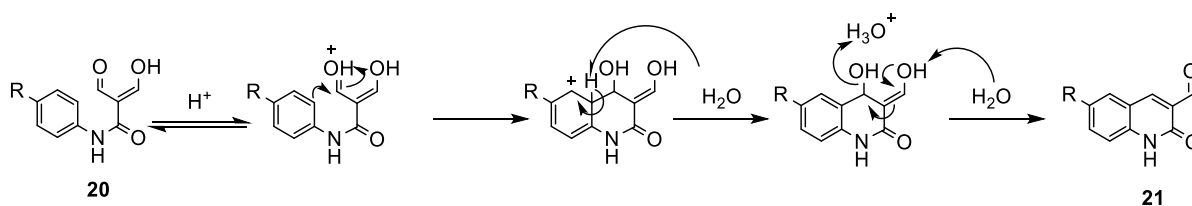
3.2.2.3 Preparation of 3-formyl-2(1H)-quinolones

Meth-Cohn proposed the preparation of 3-formylquinolones from the corresponding quinolines upon treatment with concentrated HCl at reflux and aqueous work-up. However, in response to the low yields obtained for quinolines starting from electron-poor acetanilides, an alternative multi-step approach to obtain quinolones was introduced (Scheme 26). After treatment of acetanilides with DMF and POCl₃, the traces of quinolines can be filtered off and the mixture of acrylamide **13** and formamidine **9** extracted. The isolated products can be then treated with 20% sodium hydroxide in ethanol. The addition of concentrated HCl to the mixture induces the precipitation of malondialdehyde **20** which can be obtained pure after about 3 hours upon filtration and washing with water.



Scheme 26: Preparation of quinolones through further conversion of acetanilide's formylation products

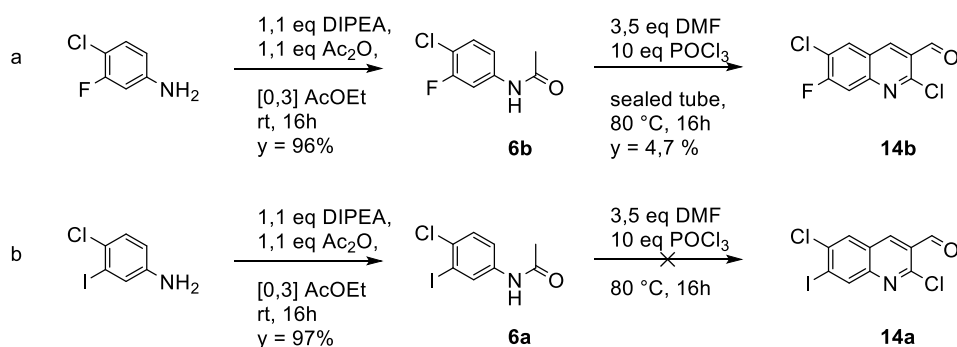
Finally, treatment of the latter with polyphosphoric acid at 150°C for 15 minutes induces ring closure and formation of the final quinolone **21** in quantitative yields. Meth-Cohn confirmed that addition of acid has no impact on the cyclization of the diformylated acrylamide **12**, because the iminium ion is already formed and that presence of a second ion cannot advance the reaction. On the contrary, addition of acid to the malondialdehyde **20** induces protonation of the aldehyde, increasing the polarization of the C=O bond and activating it towards nucleophilic addition (Scheme 27).



*Scheme 27: Mechanism of ring closure from malondialdehyde **20** to quinolone **21***

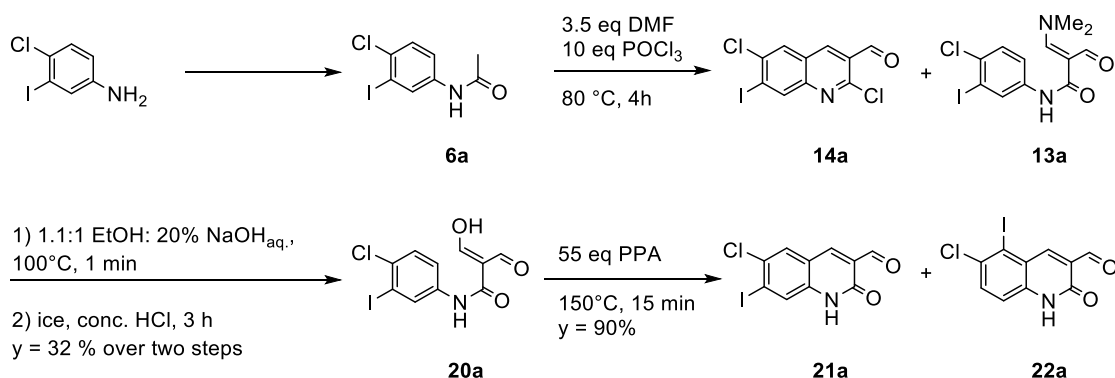
3.2.3 Preparative organic synthesis of compounds **2a** and **2b**

As depicted in scheme 20, both compounds **2a** and **2b** are derived from the 2,6-dichloro-7-iodo-3-formylquinoline **14a**. The first attempt to prepare the latter was made on the example of the 7-fluorinated analogue (**14b**), obtained by Caravella in 4.7% yield (Scheme 28) using conditions similar to those proposed by Meth-Cohn. Unfortunately, when the same conditions were applied to 4-chloro-3-iodoacetanilide **6a**, no quinoline precipitated upon aqueous work-up.



Scheme 28: Synthesis of 2,6-dichloro-7-iodoquinoline **14a** (b) reproducing Caravella's procedure (a)

Suspecting a full conversion of acrylamide into formamidine, the reaction was repeated and quenched after 4 hours, when TLC analysis showed complete consumption of the starting material. Unfortunately, absence of quinoline was observed. Aware of the possibility to convert quinolones into their corresponding quinolines^{214,215}, the alternative multi-step preparation of 6-chloro-7-iodoquinolone was attempted. The mother liquor obtained upon aqueous work-up of the formylation reaction was made basic and extraction with chloroform yielded a mixture of the corresponding formamidine **9a** and acrylamide **13a** (Scheme 29), which could not be obtained pure upon trituration with hexane or petroleum ether. The crude mixture was then converted into intermediate **20a**, obtained pure in 32% yield over two steps. Further treatment with PPA and subsequent aqueous quench produced a precipitate that was isolated in 90% yield.



Scheme 29: Synthesis of 6-chloro-7-iodoquinoline **14a** and its corresponding 3-formyl quinolone **21a**

NMR analysis showed presence of 2 geometric isomers obtained upon ring closure on both the available ortho positions. In particular, the undesired 6-chloro-5-iodoquinolone **22a** was obtained as the major product while 6-chloro-7-iodoquinolone **21a** as the minor in a ratio of 1 to 0.6 (Figure 18).

This outcome was unexpected but actually predictable. Ring closure on diformylated acrylamide **12** occurs in fact only at the least sterically hindered position due to the presence of imine and enamine. For this reason, the electronic nature of the substituents on the arene only defines the amount of **12** that can be converted into quinoline but does not play a role in directing it. On the contrary, in the malondialdehyde **20**, this moiety is replaced by an enol and an aldehyde, whose reduced steric hindrance makes the attack on both the ortho positions possible. Here therefore, the nature of the substituents plays a role only in directing the attack but not in defining the activation towards the reaction which, due to the harsh conditions, can reach 100% yield even for poorly activated aromatic rings.

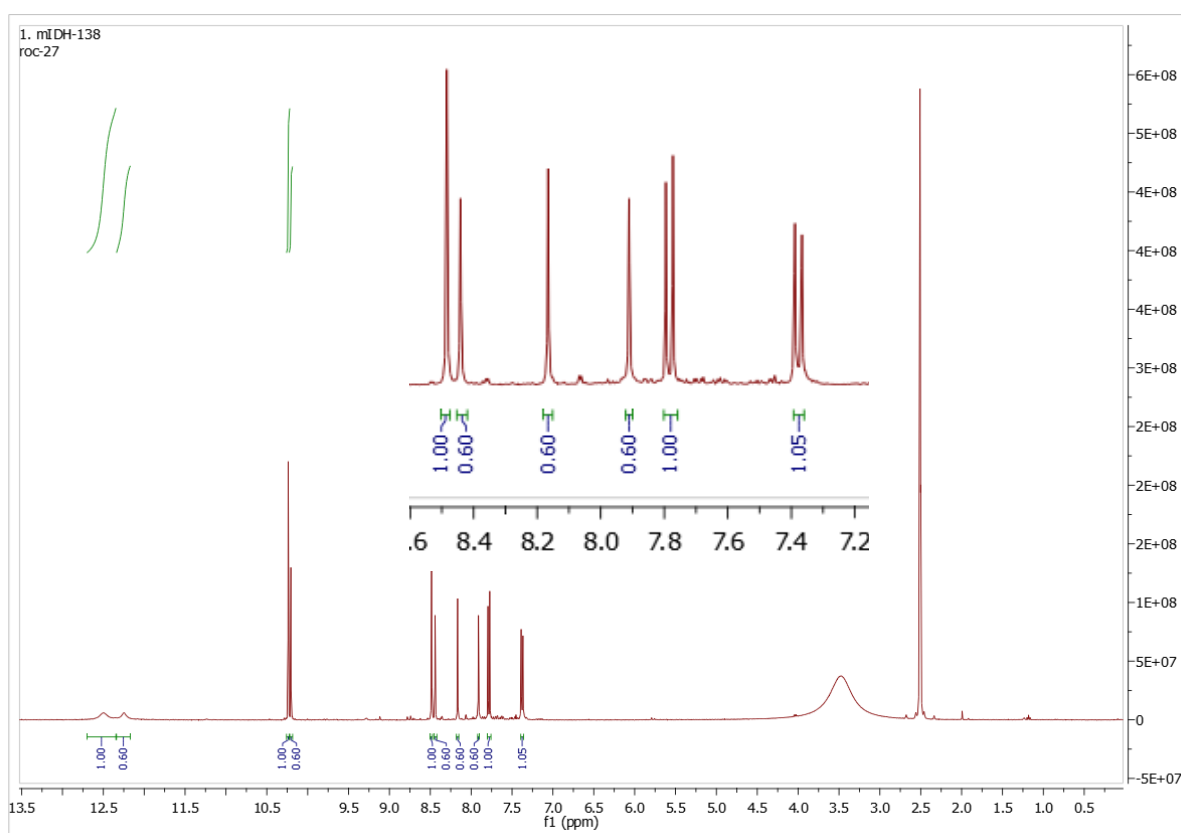


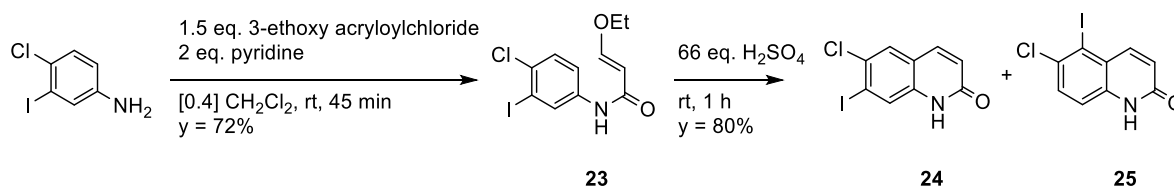
Figure 18: $^1\text{H-NMR}$ of **21a-22a** mixture

A deeper study of the effect of the substituents on the activation of the arene could therefore clarify the reasons behind the ratio of compounds **21a** and **22a**. On acetanilide **6a**, -Cl, -I and -NH-CHO, contribute to the reactivity of the aromatic ring towards electrophilic aromatic substitution and direct the site of attack. The amide moiety is the most activating group, both by inductive (+I) and mesomeric (+M) effects, and directs the attack at the two ortho positions (2 and 6). Halogens, on the other hand, contribute with a positive mesomeric effect (+M), due to the electron pair that can be

donated to the ring. This effect is partially cancelled out by the negative inductive effect (-I) resulted by their electronegativity. In terms of halogens, fluorine is the most activating one due to the similar energy of the 2p orbitals of C and F which results in a favourable overlap, hence a good electron density donation. For chlorine, the 3p orbital results in a lower ability to donate the available electron pair and this trends throughout the seventh group, attributing an even lower +M character to bromine and iodine. In these cases, though, the minor electronegativity of Br and I in respect to Cl confers them a minor -I effect, resulting in a higher *ortho-para* activating effect.

Additionally, the *ortho* and the *para* position in respect to -Cl are occupied (positions 3 and 1) while attack on the only available *ortho* position (5) would produce a 7-membered ring which is less favoured in respect to a 6-membered one. Finally, iodine activates the two *ortho* positions (2 and 6) ideal for the ring closure. Considering that in this particular reaction, steric hindrance did not play a role, it can be concluded that position 2 must be electronically more activated in respect to 6, which is less sterically hindered. While it is known that mesomeric effect does not increase with decreasing distance, therefore 2 and 6 are equally activated, the inductive effect decreases with increasing distance, therefore the -I effect should be stronger on position 2 rather than position 6, making the latter more activated. Since this theoretical explanation was contradicted by experimental evidence, it was thought to test a different procedure with a more sterically hindered scaffold, such as an ethoxy group.

4-Chloro-3-iodoaniline was reacted with 3-ethoxy acryloylchloride to form intermediate **23** which was treated with sulfuric acid to induce cyclization (Scheme 30)²¹⁶.



Scheme 30: Synthesis of 6-chloro-7-iodoquinolone **24**

Again, 6-chloro-7-iodoquinolone **24** was obtained as the minor product and 6-iodo-5-chloroquinolone **25** as the major in a ratio of 0.6 to 1 (Figure 19). This confirms that steric hindrance does not play a role in directing the attack.

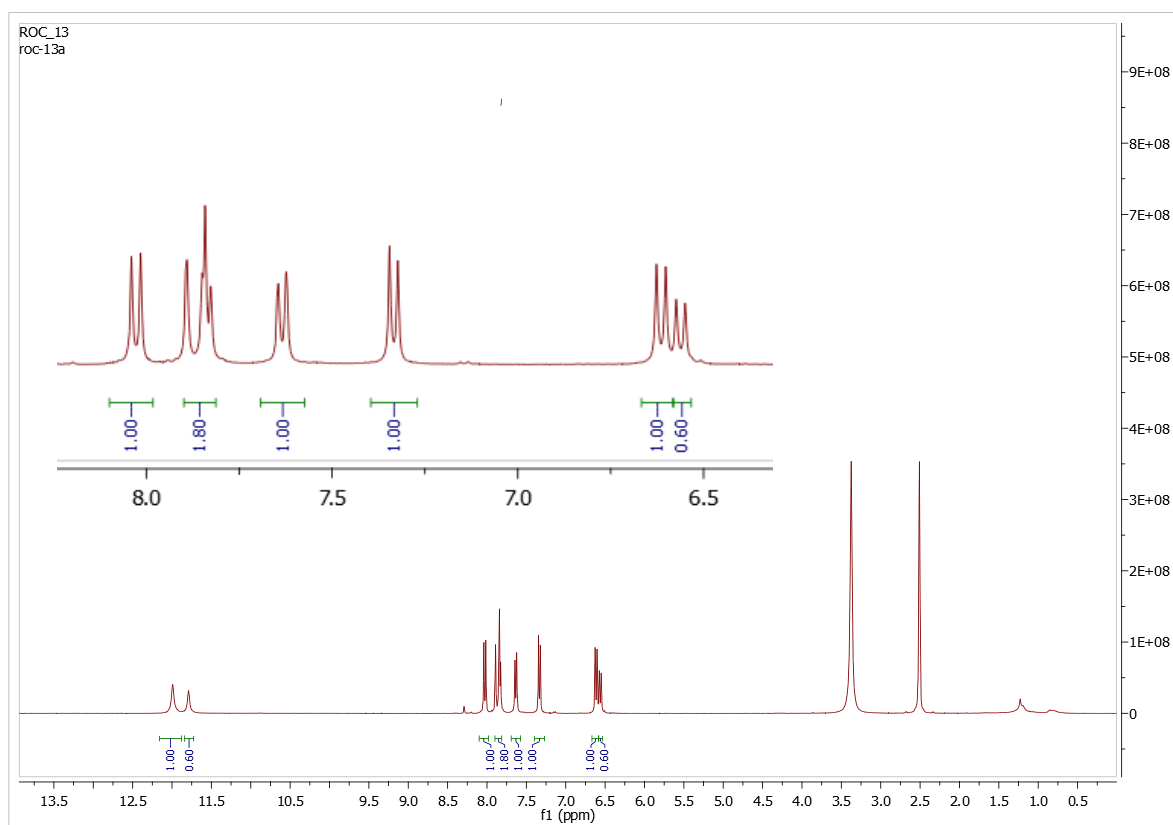
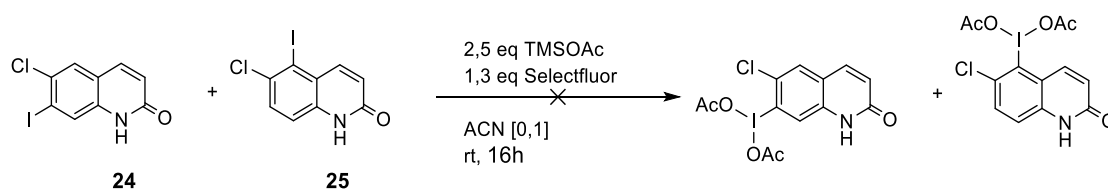


Figure 19: $^1\text{H-NMR}$ of the mixture of **24** and **25**

In addition to the fact that the desired compound was produced in less than 30% yield, both couples of products, **21a-22a** and **24-25**, could not be separated though column chromatography due to their high polar similarity in different eluents. It was hypothesized that introduction of a sterically demanding functional group would introduce a difference in the molecules' geometry, hence a bigger difference in their polarity, facilitating their separation. In an attempt to carry on the synthesis of the precursors, the mixture of **24** and **25** was treated with trimethylsilyl acetate and Selectfluor but the oxidation to diacetoxy iodine was not successful (Scheme 31).



Scheme 31: Acetylation of iodine

Due to the high chemical complexity of the preparation of these scaffolds, it was decided to prepare a chemically more accessible molecule and use it as a proof of concept. In particular, the feasibility

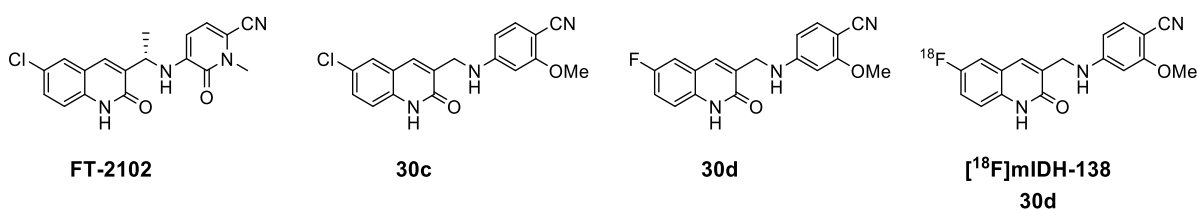
of the radiofluorination, the inhibitory constant and ultimately the selective imaging of the mutant IDH cells were to be investigated in the shortest time before more effort was invested in the synthesis optimization.

3.3 [^{18}F]mIDH-138 [^{18}F]30d

In a sought to prepare a chemically more accessible analogue of compound **FT-2102**, presented by Caravella et al., a suboptimal inhibitor (**30c**) was selected as candidate for the development of mIDH1 selective tracer (Scheme 32). The selection of this compound was guided by criteria to simplify the synthetic process and enhance chemical accessibility. This compound, **30c**, features in fact a single *para*-substituted quinolone structure that can be prepared via ring closure without formation of undesired products. Additionally, the aromatic ring on the right-hand side can be readily obtained via one step synthesis using a commercially available starting material.

Lin presented compound **30c** in 2019 as a suboptimal inhibitor, with an inhibitory constant of 127 nM towards mIDH1 and a low solubility. While high solubility is not a prerequisite for tracer development due to their use in tiny amounts, the reported inhibitory constant of 100 μM towards the wild type mIDH1 confirmed the retained selectivity towards the mutant enzyme. This selectivity is crucial for enabling the distinct visualisation of tumors bearing the mIDH1 enzyme.

As explained in the introduction, when preparing a radiotracer it is always sought to replace one element of the structure with its own radioisotope in order not to change its biochemical properties. In this case, however, neither **FT-2102** nor **30c** presented a fluorine in their structure, essential for the preparation of a radiofluorinated tracer. However, an analogue of **30c**, with a fluorine in position 6 had been previously tested by Lin et al. and a potency against mIDH1 similar to that of **30c** had been confirmed. For this reason, the introduction of radiofluorine was designed to take place at position 6.



Scheme 32: Candidates for the preparation of a selective tracer

Similarly to **FT-2102**, compound **30c** binds to the allosteric binding site and retains most of the interactions of the first with the enzyme (Figure 20). The carbonyl and the amide moieties of the quinolone interact with Arg109 and Asp279 respectively while the amine of the benzylic linker is bound to Ile128 through a hydrogen bond. While the chlorine in position 6 fills a hydrophobic pocket, positions 7 and 8 are the only ones exposed. This consideration led to the introductions of different

substituents and ultimately to compounds **2** and **3**, showed in paragraph 3.2. Concerning the aromatic ring, the 2-methoxy group occupies a hydrophobic cleft while the cyano moiety forms a hydrogen bond with Leu120. Loss of interaction between the carbonyl of the pyridone of FT-2102 and Ile128 allows enhanced conformational mobility and results in the decreased IC_{50} registered for **30c** in respect to FT-2102.

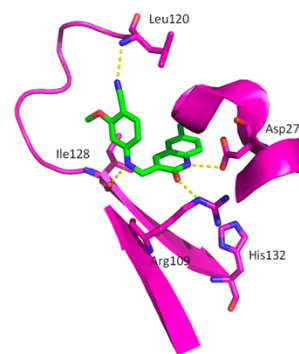
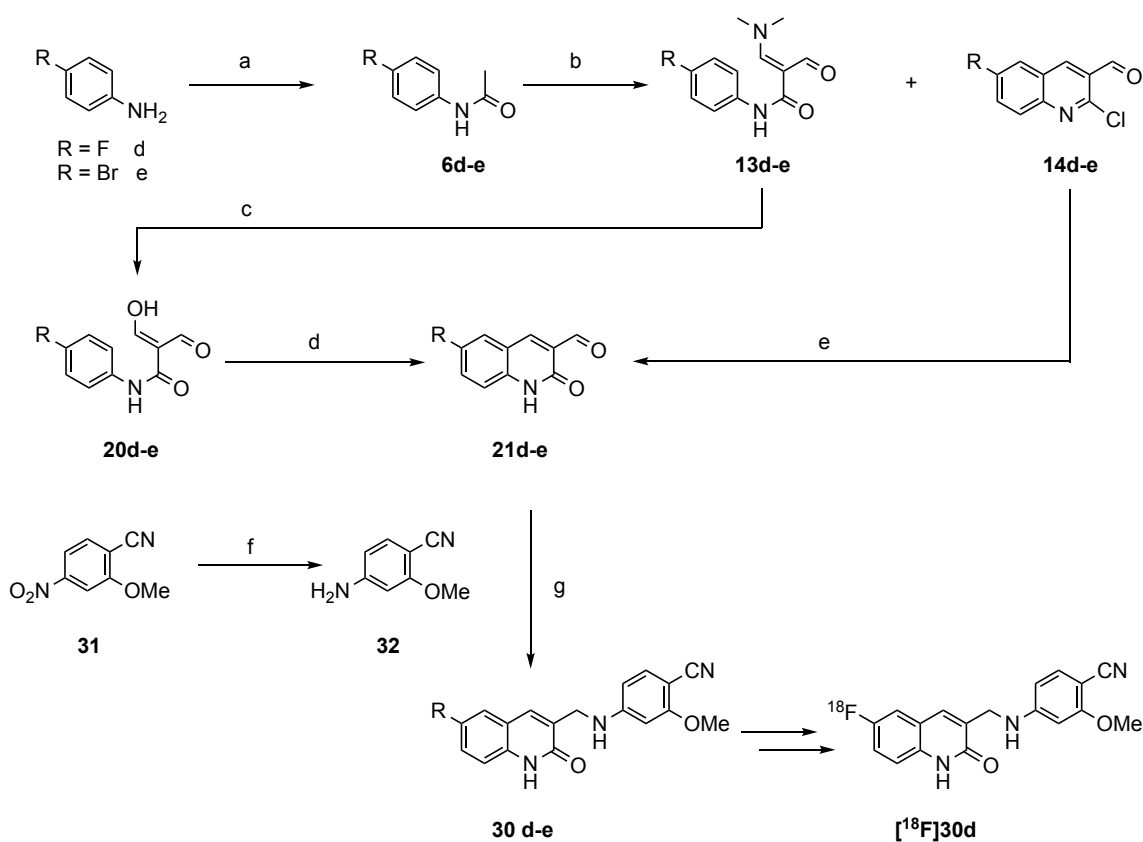


*Figure 20: Interactions of **30c** with the allosteric binding pocket in mIDH1*

3.3.1 Preparative organic synthesis of precursor **33** and reference compound **30d**

For the development of the radiotracer [^{18}F]**30d**, the precursors **33** and the non-radioactive reference compound **30d** were synthesized starting from the synthetic pathway published by Lin et al. During the course of the project, several steps have been modified (Scheme 33) either because the detailed procedures were protected by patent or because their reproduction was unsuccessful. Additionally, Lin produced few milligrams of a library of compounds in order to test them in cells, therefore the syntheses were performed on a small scale and often starting from commercially available reagents, unlike the syntheses described in the next chapters.

All compounds were obtained by conjugating the desired quinolone **21** to 3-methoxybenzonitrile **32**.



Scheme 33: Synthetic pathway for the development of compounds **30d** and **30e**

Procedures: a) 1.1 eq. Ac_2O , 1.1 eq. DMAP, [0.2] AcOEt , rt, 16h; b) 1) 2.5 eq. DMF, 7 eq. POCl_3 , 75 °C; 2) 40% NaOH_{aq} , 30 min; c) [0,1] 1:1 20% NaOH_{aq} : EtOH , 80°C, 1min. HCl , rt, 3h; d) PPA, 150°C, 15'; e) HCl , reflux, 16h; f) 3 eq. Zn powder, 3 eq. NH_4Cl , 1:1 EtOH : AcOEt , [0.3], 40°C, 2 h, $y = \text{quantitative}$; g) 3 eq AcOH , 2 eq $\text{NaBH}(\text{OAc})_3$, [0,2] CH_2Cl_2 , rt, 16h.

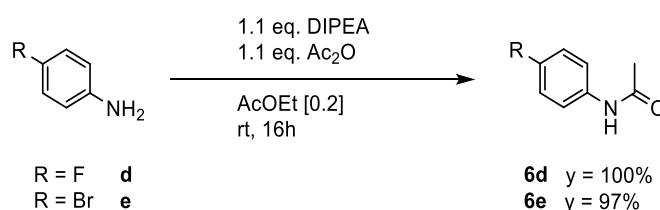
For the introduction of fluorine, a good leaving group is required at the site of attack due to the low activation of position 6 of the quinolone. Boronic acid pinacol ester was selected as leaving group for

a copper mediated radiofluorination. As shown by Tredwell⁴² in 2014, introduction of radioactive fluorine can be carried out with the commercially available $\text{Cu}(\text{OTf})_2(\text{py})_4$ complex in air and with high yields. Additionally, boronic esters are easily prepared, non-toxic, bench stable and the reaction conditions are well tolerated by most functional groups.

The most efficient method for the introduction of a pinacol ester is to perform a Miyaura reaction on the brominated analogue, therefore the synthesis of 6-bromo-3-formylquinolone **21e** will be here discussed in detail.

3.3.1.1 Organic preparation of the 6-halogenated quinolone moieties **21d** and **21e**

As described in paragraph 3.2.2.2, Otto Meth Cohn's procedure was used for the formylation of substituted acetanilides. These were obtained in quantitative yields upon acetylation of *para*-substituted anilines with slight excess of DIPEA and acetic anhydride in ethylacetate at room temperature (Scheme 34).



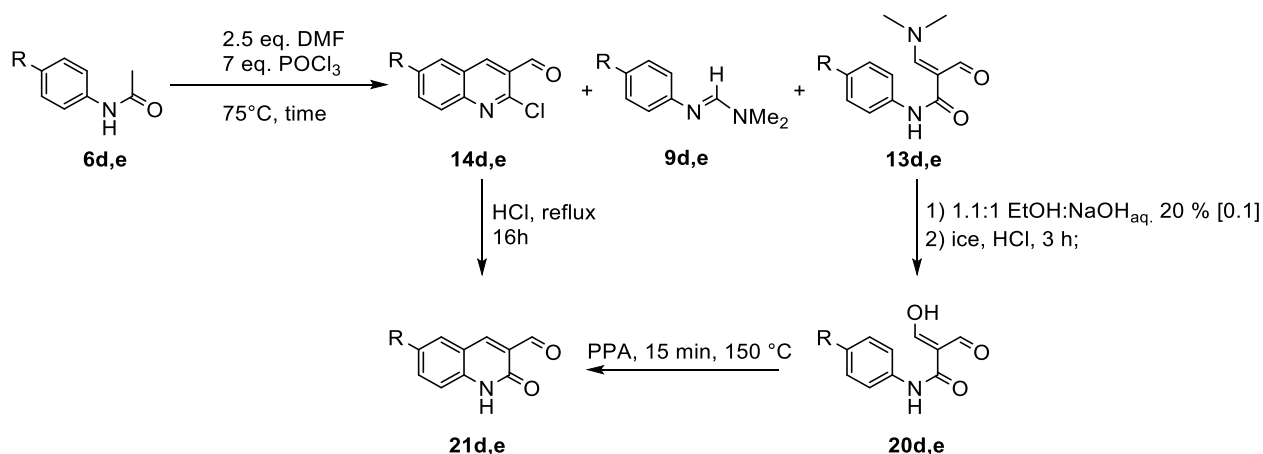
Scheme 34: Acetylation of para-substituted anilines

While phenols require a catalyst, like DMAP or pyridine, to undergo acetylation, anilines are more reactive and can carry out the nucleophilic attack on the acetic anhydride. The protonated acetanilide is afterwards deprotonated by the acetate anion. In order to avoid the final acidic condition, Hünig's base can be added in slight excess to deprotonate the intermediate and quench the acetate in solution. Addition of water and extraction with ethylacetate provide pure products, which were used without need of further purification.

Subsequently, the two *para*-halogenated acetanilides **6d** and **6e** were treated with 2.5 equivalents of DMF and 7 equivalents of phosphoryl chloride as indicated by Meth Cohn (Scheme 35). Formation of the Vilsmeier-Haack reagent took place in strictly dry conditions by dropwise addition of POCl_3 to DMF at 0°C . The clear transparent solution was allowed to reach room temperature before addition of the starting material, followed by heating at 75°C . The open-flask procedure was preferred in comparison to the one in the sealed tube since evidence showed that the former tends to give the

highest acrylamide formation with inactivated acetanilides while the latter favours formation of the quinoline (paragraph 3.1).

The preparation of 6-bromo-3-formylquinolone **21e** was reported in literature on a 46.69 mmol (10 grams) scale and was therefore reproduced on a multigram scale. For this purpose, 5 grams of acetanilide **6e** were stirred under inert atmosphere at 75°C overnight and poured onto ice after 16 hours (table 5, entries a and b).



*Scheme 35: Preparation of 6-halogenated quinolones **21d** and **21e***

No precipitate appeared and further conversion into malondialdehyde **20e** failed. In an attempt to understand whether the success resulted from the scale or the reaction time, the same conditions were applied to 3.40 mmol (< 1 g) of starting material (entry c) and resulted in 18% formation of malondialdehyde **20e**. Shorter reaction time of 2 hours was tested on increasing scales starting from 3.40 mmol (entries d and e) up to 21.02 mmols (entries f, g and h). Encouraged by the obtained increasing yields, the same test was repeated with the shorter time of 1.4 hours. For this test, a minimum amount of 8.00 mmoles (2 grams) of starting material was reacted, since the product of this reaction represents one of the initial compounds for the preparation of the radiofluorination precursor, of which a conspicuous amount is necessary (items i, l, m and n). Higher yields were obtained with the reduced time even though no correlation with the scale was found.

Entry	Scale	Time	Quinoline 14e	Malondialdehyde 20e
a	23.35 mmol	16 h	0%	0%
b	23.35 mmol	16 h	0%	0%
c	3.40 mmol	16 h	0%	18%
d	3.40 mmol	2 h	0%	77%
e	3.40 mmol	2 h	0%	20%
f	4.60 mmol	2 h	4%	18%
g	8.90 mmol	2 h	0%	24%
h	21.02 mmol	2 h	0%	56%
i	8.00 mmol	1.4 h	2%	40%
l	9.34 mmol	1.4 h	3%	65%
m	17.42 mmol	1.4 h	0%	41%
n	23.35 mmol	1.4 h	2%	22%
o	9.34 mmol	1.4 h	3%	37%
p	9.34 mmol	1.4 h	2%	50%
q	9.34 mmol	1.4 h	2%	34%
r	9.34 mmol	1.4 h	2%	14%
s	9.34 mmol	1.4 h	3%	22%
t	9.34 mmol	1.4 h	2%	20%

Table 5: Formylation of 4-bromoacetanilide with different reaction conditions

In order to investigate the consistency of the method, the same reaction was repeated 6 times on 9.34 mmol of 4-bromoacetanilide for 1.4 hours (entries o, p, q, r, s and t) confirming the irreproducibility of the reaction.

When the same procedure was applied to 4-fluoroacetanilide with different scales and reaction times, no traces of the corresponding quinoline were isolated (Table 6).

Entry	Scale	Time	Quinoline 14d	Malondialdehyde 20d
a	3.40 mmol	3.5 h	0%	49%
b	6.60 mmol	3.5 h	0%	37%
c	4.60 mmol	3.5 h	0%	20%
d	3.40 mmol	1.5 h	0%	10%
e	6.60 mmol	1.5 h	0%	25%

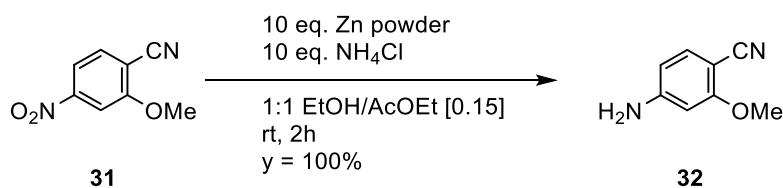
Table 6: Formylation of 4-fluoroacetanilide with different reaction conditions

Moreover, reaction on 3.40 mmols of 4-fluoroacetanilide for 3.5 hours furnished the subsequent malondialdehyde in 49% yield (entry a), while attempts to reproduce the reaction on larger scales resulted in loss of yield (entries b and c). Finally, shorter reaction times resulted in lower yields even though TLC analysis showed complete consumption of starting material already after 1.5 hours. Although the reaction was proven to be irreproducible, only few milligrams of the reference compound are sufficient for its purpose therefore no further studies were conducted for the preparation of the 4-fluoromalondialdehyde **20d** or of the final compound **21d**.

Finally, when both 4-halogenated malondialdehydes **20d** and **20e** were treated with large excess of PPA at 150°C, up to 90% yields were achieved.

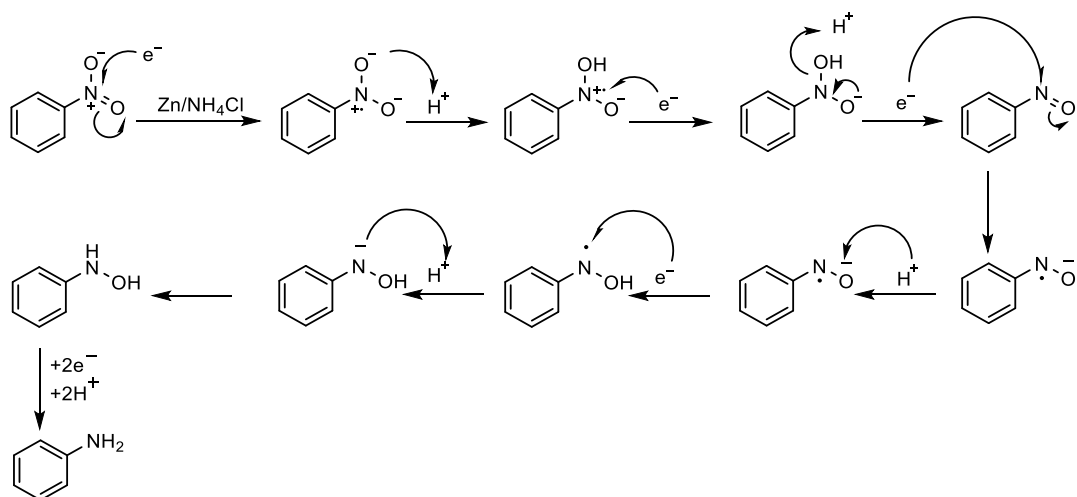
3.3.1.2 Organic preparation of the 4-amino-2-methoxybenzonitrile **32**

For the preparation of 4-amino-2-methoxybenzonitrile **32**, the corresponding nitro analogue was purchased and reduced with the aid of zinc powder and ammonium chloride (Scheme 36).



Scheme 36: reduction of nitroarenes to anilines

While the reaction is normally carried out in water, a 1 to 1 mixture of ethanol and ethylacetate was here used in order to solubilize both the salt and the starting material and obtain a homogeneous solution. The reaction exploits easily oxidisable metal ions, like iron, zinc or tin, in presence of an acid. In particular, ammonium chloride has been shown to allow formation of the arylhydroxylamine at room temperature and formation of the aniline in presence of large excess of ammonium chloride. As shown in Scheme 37, 6 electrons and 6 protons are required to allow the complete reduction of the nitro group to the corresponding -NH₂.

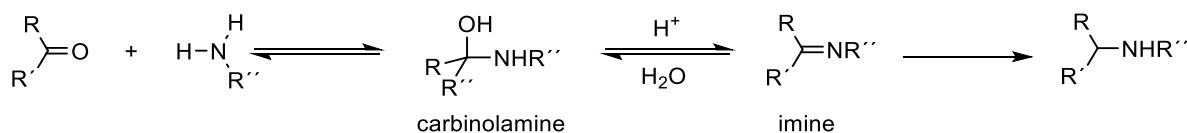


Scheme 37: Reduction of nitroarenes to anilines

The final compound **32** was obtained pure in quantitative yield after two hours at room temperature and used without need of further purification.

3.3.1.2 Reductive amination for the formation of **30d** and **30e**

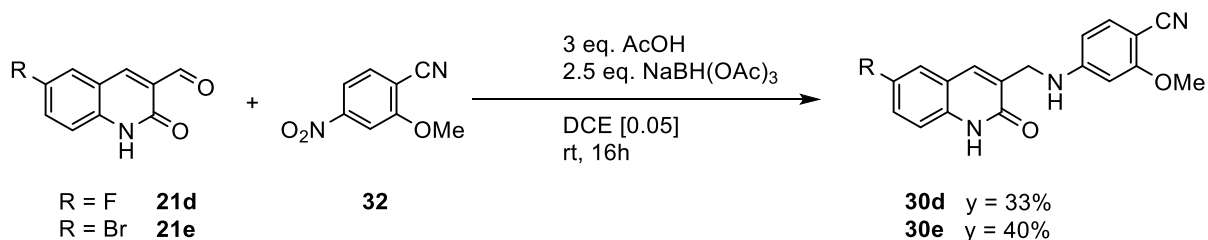
The obtained aniline **32** was further conjugated to the previously synthesized 6-halogen-3-formylquinolones **21d**, via reductive amination. In particular, this reaction involves the formation of an intermediate carbinolamine (Scheme 38), which dehydrates to form an imine (Schiff base), whose reduction produces the final product.



Scheme 38: General reductive amination pathway

Conventionally, the reaction is carried out in dichloroethane with excess of acetic acid to activate the aldehyde towards the nucleophilic attack and sodium triacetoxyborohydride as mild reducing agent. However, when this procedure was reproduced on a small scale (around 2 mmols) it proved to be only partially successful (Scheme 39). The reaction was indeed performed with highly diluted conditions (0.05M) and could not be brought to complete consumption of starting material neither with longer reaction time nor with higher reaction temperature due to the competing reduction of the aldehyde. Additionally, purification with classical chromatographic methods revealed challenging due to the low solubility of the final products and was therefore performed with a $\text{CHCl}_3:\text{AcOEt}$

mixture to yield the reference compound **30d** in 33% yield and its brominated analogue **30e** in 40% yield.



Scheme 39: Direct reductive amination

Considering that the reaction is normally performed in DCE or THF using aliphatic amines, here the insolubility of the 6-halogenated quinolones and the poor reactivity of the aniline could explain the low yield. Additionally, sodium cyanoborohydride was not tested as alternative milder reducing agent because of its toxicity and its tendency to contaminate the product with cyanide.²¹⁷

Catalytic hydrogenation, which represents the second most commonly used direct reductive amination procedure, could not be applied to this scaffold due to possible incompatibility with the nitrile.²¹⁸

Reaction optimization was therefore approached from two different angles: on the one hand, improve the formation of the intermediate imine by addition of molecular sieves to catch the formed water, on the other hand, avoid the presence of the alcoholic side product by addition of the reducing agent after complete consumption of the starting material (indirect reductive amination). A combination of the two conditions was first tested on the available 2,6-dichloro-3-formylquinolone but revealed unsuccessful because of solubility issues leading to massive recovery of starting material. The final compound could anyway be isolated in 15 % isolated yield after 12 hours, slightly higher than the 10% yield reported in literature. When reproduced on the 6-bromo-3-formylquinolone, overnight reaction did not show any advance in the intermediate formation and subsequent addition of NaBH(OAc)_3 reduced both the starting material and the intermediate yielding the final product with a 45% yield after purification via column chromatography.

3.3.1.3 Introduction of boronic acid pinacol ester for the preparation of precursor **33**

Given the objective of the proof of concept, the feasibility of the scaffold upon radiofluorination was tested before pursuing the optimization of its organic preparation. For this purpose, the brominated analogue **30e** was converted into the corresponding boronic acid pinacol ester with the Miyaura

borylation procedure,²¹⁹ a palladium-catalysed coupling reaction between bis(pinacolato)diboron and aryl or vinyl halides in presence of a base.

The mechanism (Figure 22) involves the oxidative addition of the aryl bromide to the Pd(0) complex, forming the Pd(II) complex. The base displaces the palladium halide to give an acetoxypalladium(II) species in solution, which transmetalates with the bis(pinacolato)diboron forming the acetoxo boron species and a trans Pd(II) complex. The combination of

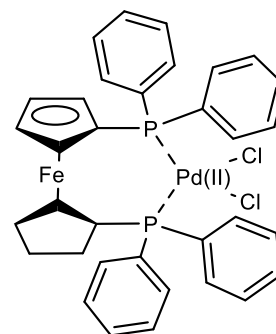


Figure 21: Pd(dppf)Cl₂

a soft acid and a hard base attributes a high reactivity to the Pd-O bond which, with the high oxophilicity of the boron centre, gives high reactivity to the oxopalladium complexes towards transmetalation. Further cis-trans isomerization and reductive elimination leads to the desired aryl boronic ester.

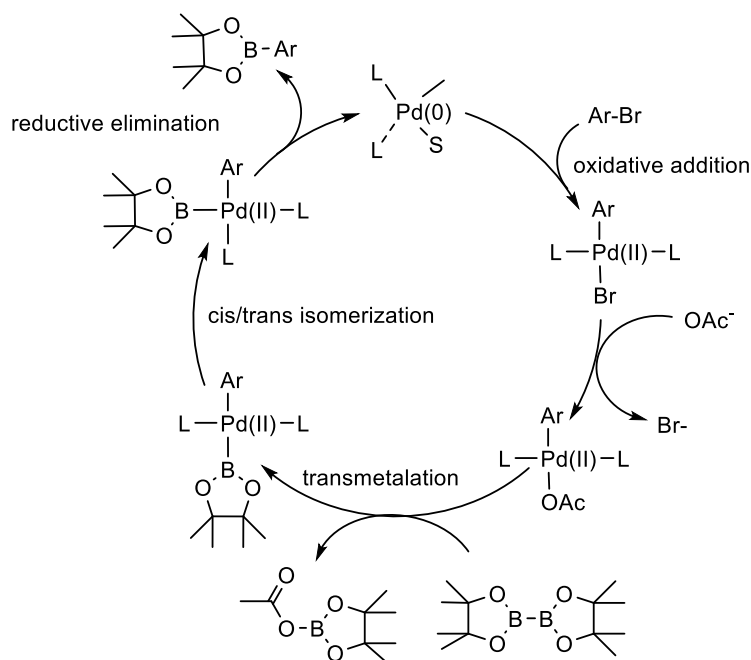
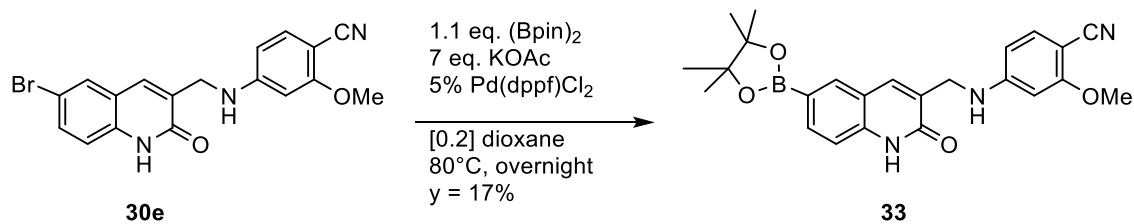


Figure 22: Catalytic cycle for production of pinacol esters

When the reaction was carried out on compound **30e**, an opaque solution was obtained, indicating the partial insolubility of the starting material.²²⁰ Additionally, the similar polarities of starting material and product made it difficult to define the end of the reaction by TLC analysis. The reaction was therefore prolonged overnight before work-up. After concentration in vacuo, the crude mixture was purified via column chromatography to yield 4-[(6-(4,4,5,5-tetramethyl-1,3,2-dioxaborolan-2-yl)quinolin-1(2H)-one) methyl]amino}-2-methoxybenzotrile **33** in 17% yield (Scheme 40).

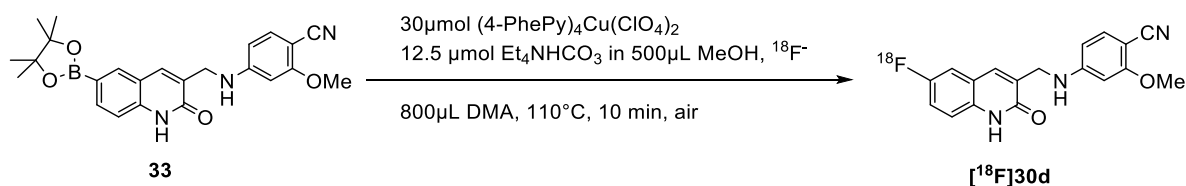


Scheme 40: Miyaura borylation of compound **30e**

3.3.2 Copper mediated radiofluorination of 4-[[[(6-(4,4,5,5-tetramethyl-1,3,2-dioxaborolan-2-yl)quinolin-1(2H)-one) methyl]amino]-2-methoxybenzonitrile **33** and spiking experiment

As mentioned in the introduction, there is a lack of radiotracers which can selectively bind to mutant IDH1 in order to assess its status in solid brain tumors, such as glioma and glioblastoma. Compound [**¹⁸F]**30d** can be used as a proof of concept to verify the feasibility of radiofluorination and test the target selectivity, in order to guide the design and development of new optimized radiotracers.**

Given the multiple benefits of nucleophilic radiofluorinations, such as easier handling and theoretically higher molar activity in respect to electrophilic methods,²²¹ the copper mediated radiofluorination procedure published by Schäfer in 2016 was applied to precursor **33**.²²² [**¹⁸F]⁻Fluoride was fixed on a QMA cartridge and rinsed with methanol and with air, to eliminate water residues and methanolic residues, respectively. Afterwards, [**¹⁸F]⁻F⁻ was eluted with a methanolic solution of tetraethylammonium bicarbonate (TEAB) and subsequently evaporated. The elution efficiency was around 99%. A different project in our institute suggested Cu(4-PhePy)₄(ClO₄)₂⁵⁴ as one of the best candidates for copper mediated radiofluorinations of aryl boronic acid pinacol esters. For this reason, an equimolar mixture of Cu(4-PhePy)₄(ClO₄)₂ and precursor **33** was dissolved in 800 μL of dimethylacetamide (DMA) and stirred at 110°C for 10 minutes, followed by mild acidification with TFA.****



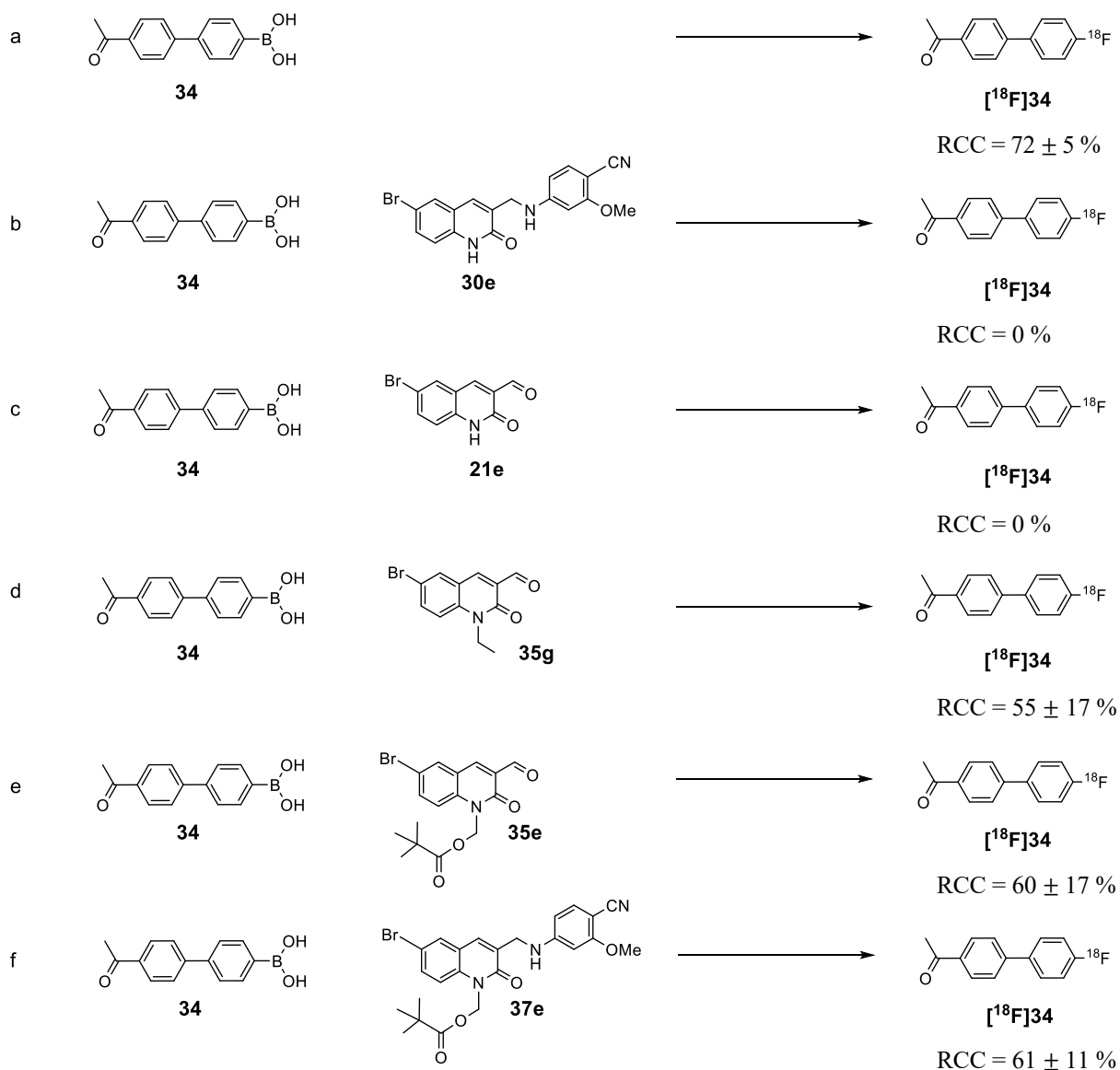
Scheme 41: Radiofluorination of **33**

Procedure: Elution of ¹⁸F⁻ with TEAB in MeOH, evaporation. Addition of Cu(4-PhePy)₄(ClO₄)₂ and **33** (30 μmol each) dissolved in 800 μL DMA, 110°C, 10 min.

An aliquot was taken and analysed via analytical HPLC and showed 10 ± 8 % radio chemical conversion (RCC) (Scheme 41). Suspecting a partial deactivation of the catalyst, a series of spiking experiments were designed to understand if the unsuccess of the synthesis was correlated to any specific moiety present on the precursor.

Radiofluorination of (4'-acetyl-[1,1'-biphenyl]-4-yl)boronic acid **34** was selected as benchmark reaction due to the similarity of the radiofluorination procedures and the high radiochemical conversion. The benchmark reaction was carried out using exactly the same conditions (time, temperature and catalyst) as the ones previously indicated and yielded 1-(4'-[^{18}F]-[1,1'-biphenyl]-4-yl)ethan-1-one [^{18}F]**34** in 72 ± 5 % RCC (Scheme 42a). Compound **30e**, analogue of **33** lacking the BPin leaving group, was subsequently added to the reaction in equimolar amount in respect to **34** and completely prevented the formation of the product (Scheme 42b). This outcome suggested that at least one of the two NH groups was interfering with the reaction mechanism. For this reason, the effect of the two moieties was tested separately. First, the unprotected brominated quinolone **21e** was spiked (Scheme 42c) causing complete impairment of reaction. This indicated that a protecting group was required to shield the proton of the amide moiety. To this end the 6-bromo-N-ethylated quinolone **35g** was synthesized and spiked in the benchmark reaction, restoring a conversion of 55 ± 17 % (Scheme 42d). This confirmed that the amide can deactivate the copper mediator, most likely by chelating to it. Subsequent replacement of the ethyl group with an easily cleavable protecting group like pivaloyloxymethyl (POM, Scheme 42e) showed 60 ± 17 % RCC and was selected as the group of choice for further investigation about the possibly detrimental effect of the amine present on the benzylic linker.

To this end, the POM protected bromo quinolone (**35e**) was conjugated to 4-amino-2-methoxybenzotrile **32** and spiked in the benchmark radiofluorination (Scheme 42g). The conversion of 61 ± 11 % in presence of the protected amide and free amine excluded the possibility of the interference of the latter with the copper mediator.



Scheme 42: Benchmark reaction and series of spiking experiment.

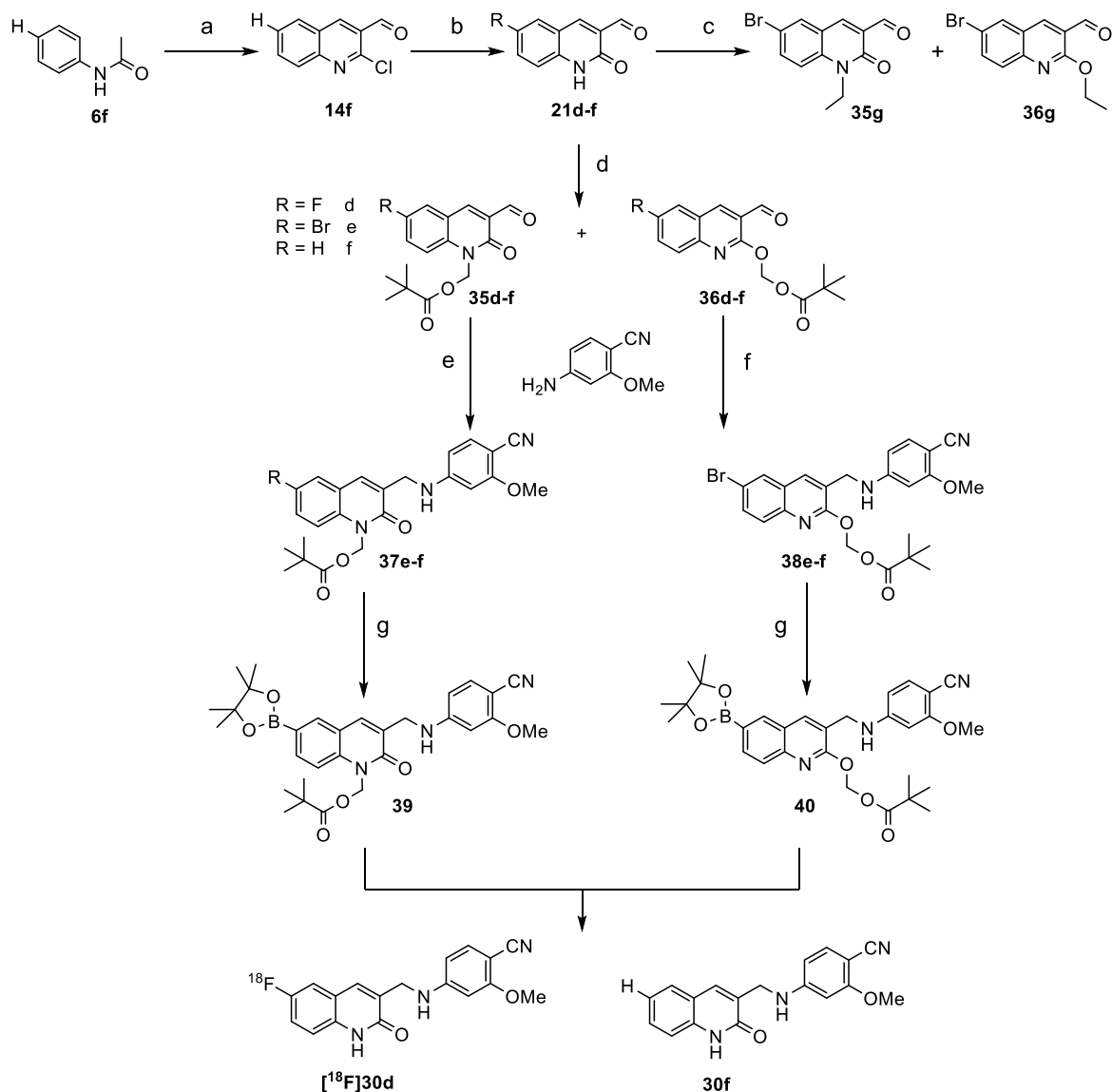
Procedure: Elution of ¹⁸F⁻ with TEAB in MeOH, evaporation. Addition of Cu(4-PhePy)₄(ClO₄)₂ and precursors (30 μmol each) dissolved in 800 μL DMA, 110°C, 10 min.

Hence, the pivaloyloxymethyl group was selected as the protecting group due to its straightforward introduction and cleavage upon base addition. For this reason, the synthesis of compounds **35g**, **35e** and **37e** is further discussed in detail in the next paragraph.

3.3.3 Preparative organic synthesis of protected precursors 3-(((4-cyano-3-methoxyphenyl)amino)methyl)-2-oxo-6-(4,4,5,5-tetramethyl-1,3,2-dioxaborolan-2-yl)quinolin-1(2H)-yl)methyl pivalate **39** and ((3-(((4-cyano-3-methoxyphenyl)amino)methyl)-6-(4,4,5,5-tetramethyl-1,3,2-dioxaborolan-2-yl)quinolin-2-yl)oxy)methyl pivalate **40** and their protodeboronated analogue 2-methoxy-4-(((2-oxo-1,2-dihydroquinolin-3-yl)methyl)amino)benzonitrile **30f**

The protonated precursors **39** and **40** were prepared as depicted in Scheme 43 starting from their acetanilides as already depicted in scheme 33.

Given the feasibility of the synthesis and the improved yields, the same procedure was applied to acetanilide **6f** in order to prepare **30f** as a reference compound for the protodeboronated impurity formed during the radiosynthesis. The introduction of the protecting group, either ethyl or POM, was carried out at the quinolone stage for both 6-fluoro- and 6-bromo-3-formylquinolones **21d, e** and 3-formylquinolone **21f**, obtained from the corresponding quinoline **14f**.



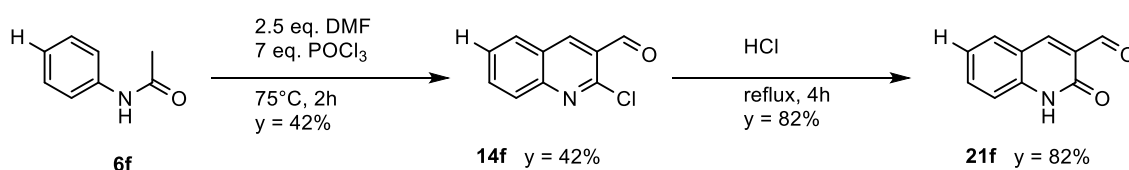
Scheme 43: Synthetic pathway for the development of protected precursors 39 and 40, their protodeboronated analogue

Procedure: a) 2.5 eq. DMF, 7 e.q. POCl₃, 75 °C, 2h then 40% NaOH_{aq.}, 30 min, y = 42%; b) HCl, reflux, 16h, y = 82% c) 1.5 eq. EtBr, 1.5 eq. Na₂CO₃, DMF, [1.5], 60°C, 2h, y = 85%; d) 1.5 eq. POM-Cl, 1.5 eq. Na₂CO₃, DMF, [0.2], 60°C, 2h; e) 1 eq. 32, 2.5 eq. TMS-Cl, 1 eq. NaBH₄, DMF [0.5], 0°C, 15 min; f) 1 eq. 32, 2.5 eq. TMS-OTf, 1 eq. NaBH₄, DMF [0.5], 0°C, 1 h, g) 1.2 eq. (Bpin)₂, 7 eq. KOAc, 5% Pd(dppf)Cl₂, dioxane, [0.1], 80°C, 16h.

3.3.3.1 Organic preparation of N-protected 6-halogenated quinolones

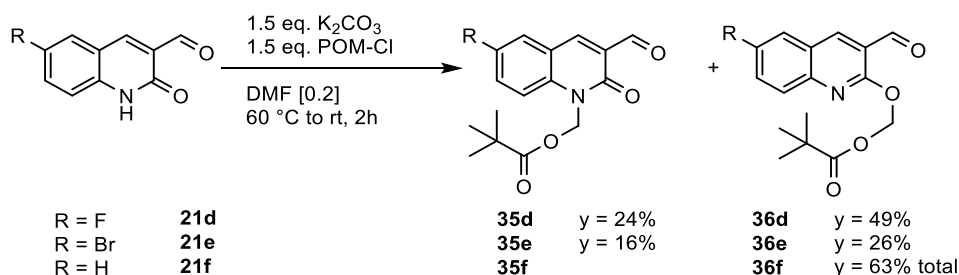
Protection of the amide moiety was carried out on 6-bromo-3-formylquinolone **21e**, previously prepared from 4-bromoacetanilide, as described in paragraph 3.3.2. As indicated by Laali et al.²²³, the quinolone scaffold was dissolved in DMF with potassium carbonate, followed by addition of bromoethane. After work-up, NMR analysis showed presence of both the N-ethylated **35g** and the O-

ethylated **36g** analogues in a ratio of 0.55:1. The crude mixture was purified via column chromatography and the protected compounds were isolated with a total yield of 85% (Experimental part). The same procedure was applied to quinolones **21d**, **21e** and **21f** with pivaloyloxymethyl chloride as nucleophile with the aim to introduce a labile protecting group. In particular, quinolone **21f** (Scheme 44) was prepared by treating 1.5 grams of acetanilide **6f** with phosphorus (V) oxychloride and dimethylformamide to obtain the corresponding quinoline **14f** as major product in 42% yield, confirming Meth Cohn's studies. This was further dissolved in concentrated HCl and refluxed for 4 hours, followed by aqueous work up. Quinolone **21f** precipitated and was obtained pure in 82% yield after filtration.



Scheme 44: Preparation of 3-formylquinolone 21f

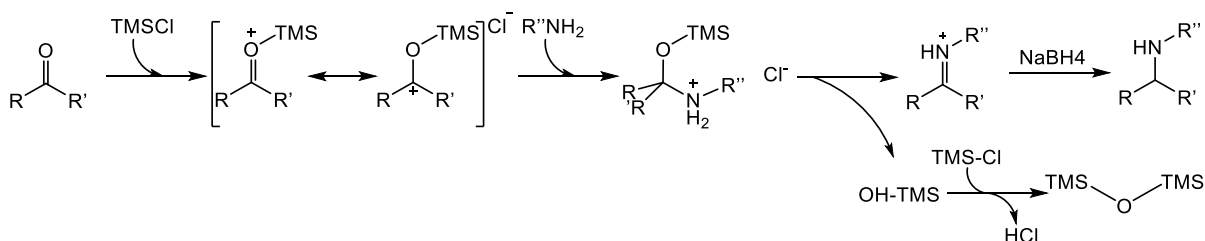
When **21d**, **21e** and **21f** were treated with POM-Cl, the O-alkylated isomer was found to be the major product (Scheme 45) in all cases. This is due to the stability given by the restoration of aromaticity after the nitrogen deprotection. Interestingly, the ratio of O- to N- protected compounds was found to be 1:0.7, 1:0.6 and 1:0.45 respectively for 6-H-, 6-Br and 6-F-quinolones respectively. In all cases it was possible to isolate the compounds in 55 to 75% yield by column chromatography. It is possible that the suboptimal yields were caused by the direct attack at the carbonyl group of the POM chloride resulting in the production of the acetylated N- and O-quinolone analogues.



Scheme 45: formation of two POM protected isomers of 3-formylquinolones 35d-f and 36d-f

3.3.3.2 Reductive amination for the formation of **39** and **40**

Attempts to carry out the reductive amination on the protected scaffolds **35e,f** and **36e,f** using the conditions previously reported revealed unsuccessful. Despite their perfect solubility in DCE, the steric hindrance provided by the protecting group slowed down the imine formation and induced several side reactions. Replacement of acetic acid with pyrrolidine²²⁴ furnished the N protected compound **37e** in 13% yield, still insufficient for the purpose of the brominated compound. Attempt to invert the protection and the conjugation steps yielded **37e** in an improved yield of 26%, still far away from the required result. Finally, the method described by Pletz et al.²²⁵ with TMS-Cl proved to be the best option. Here the coordination of the aldehyde to the silyl group guarantees a strong activation of the carbon atom towards nucleophilic attack thus enabling the formation of the imine with 4-amino-2-methoxybenzonitrile. TMS was described by the authors as the most effective replacement for AcOH given the absence of common by-products as well as its high availability and low price. Procedure involves use of a high substrate concentration in DMF at around 1.5 M at 0°C in order for the reaction to be concluded in 15 minutes. However, when reproduced on scaffolds **35d-f** and **36d-f**, a maximum concentration of 1 M was always applied to ensure sufficient dissolution of the starting materials. In the proposed mechanism (Scheme 46) trimethylsilyl chloride plays a dual role as activator for the carbonyl substrate and as dehydrating agent. This shifts the equilibrium towards the imine formation and allows displacement of TMS-OH, whose decomposition by TMS-Cl provides the acidic species required for the formation of the iminium ion, further reduced by NaBH₄.

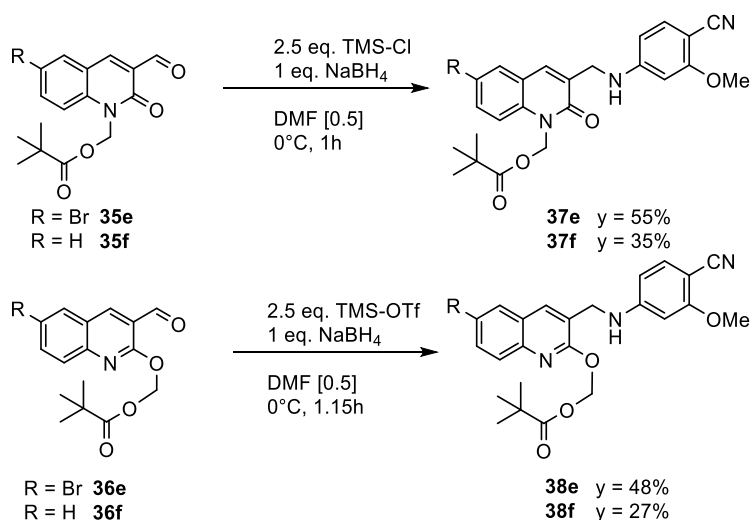


Scheme 46: Mechanism of the reductive amination with TMS-Cl proposed by Pletz et al.

When equimolar amounts of 6-bromo-3-formyl-1-(pivaloyloxy)methylquinol-2-one **35e** and aniline **32** were reacted with large excess of trimethylsilyl chloride and 1 equivalent of sodium borohydride in DMF, the desired product **37d** was obtained in 55% yield after column chromatography (Scheme 47). Interestingly, the same procedure revealed to be ineffective for the O protected analogue **36e** due to the steric hindrance of POM group close to the site of attack. The need of a stronger activator was

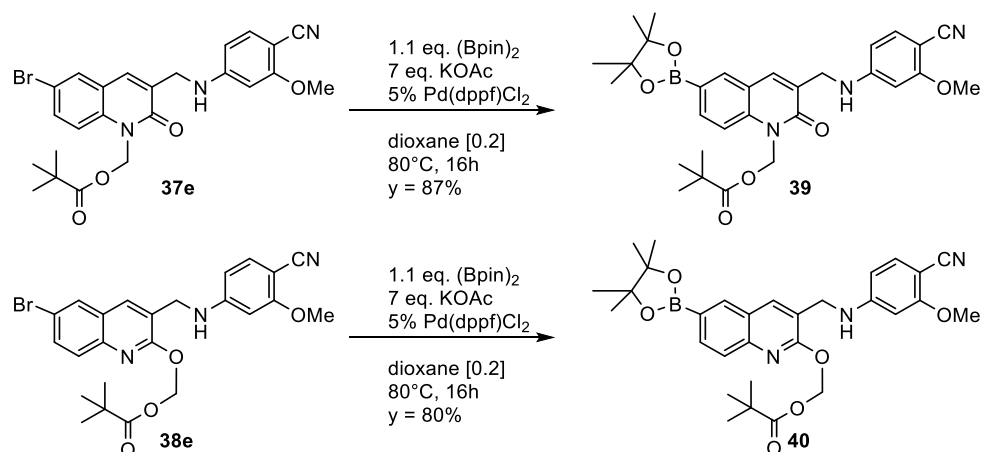
met by using excess of trimethylsilyl triflate for the conjugation of ((6-bromo-3-((4-cyano-3-methoxyphenyl)amino)methyl)quinolin-2-yl)oxy)methyl pivalate **36e** and **32**. Compound **38e** was obtained in 48% yield after column chromatography.

The same procedure was applied to the mixture of unsubstituted analogues **35f** and **36f** and yielded **37f** and **38f** in a total yield of 63%.



Scheme 47: Reductive amination for the formation of **37d-f** and **38d-f**.

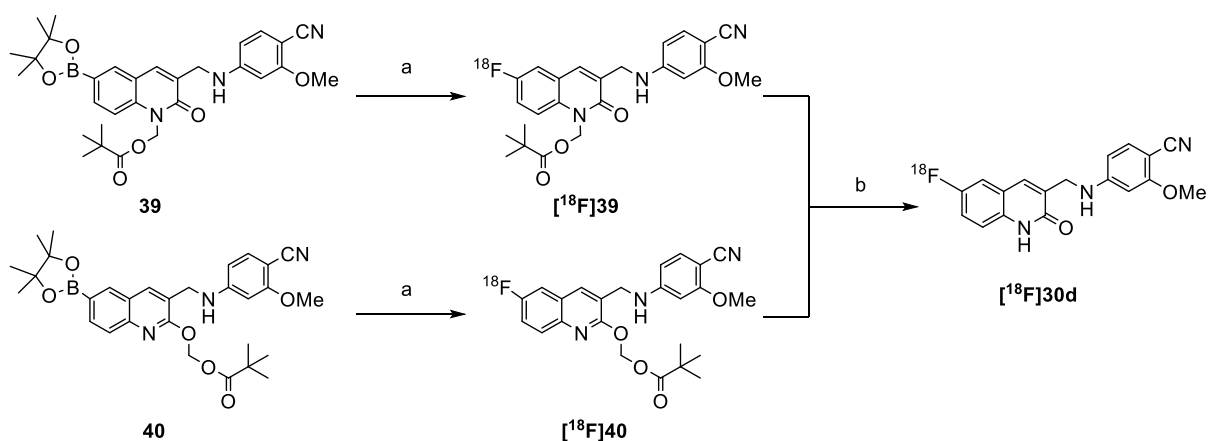
Finally, given the improved solubility of **37e** and **38e**, both underwent a Miyaura borylation until consumption of the starting material to afford compounds **39** and **40** in 87% and 80% yield respectively (Scheme 48).



Scheme 48: introduction of a boronic acid pinacol ester as leaving group for radiofluorination

3.3.4 Copper mediated radiofluorination of (3-(((4-cyano-3-methoxyphenyl)amino)methyl)-2-oxo-6-(4,4,5,5-tetramethyl-1,3,2-dioxaborolan-2-yl)quinolin-1(2H)-yl)methyl pivalate **39** and ((3-(((4-cyano-3-methoxyphenyl)amino)methyl)-6-(4,4,5,5-tetramethyl-1,3,2-dioxaborolan-2-yl)quinolin-2-yl)oxy)methyl pivalate **40**

Radiolabeling of boronic acid pinacol esters **39** and **40** was carried out using the copper mediated radiofluorination protocol previously described in paragraph 3.3.2,²⁷ followed by deprotection of the POM group under basic conditions to afford [¹⁸F]**30d** (Scheme 49).



*Scheme 49: Radiosynthesis of [¹⁸F]**30d***

Procedure: a) Elution of ¹⁸F⁻ with TEAB in MeOH, evaporation. Addition of Cu(4-PhePy)₄(ClO₄)₂ and **39** or **40** (10 μmol each) dissolved in 500 μL DMA, 110°C, 10 min; b) NaOH_{aq} 0.25M in MeOH 200 μL, 80°C, 3 min followed by quench with 5% TFA in ACN 200 μL.

In particular, after treating compounds **39** or **40** with the Cu-mediator in DMA at 110°C for 10 minutes, 200 μL of 0.25M NaOH_{aq} in methanol were added and the mixture stirred at 80°C for 3 minutes, followed by acidification with 5% TFA in acetonitrile (200 μL). Before injection into the semi-preparative HPLC, the mixture was diluted with 2 mL of water and purified via solid phase extraction (SPE) in order to remove solvent and large part of the copper mediator. The HLB cartridge was rinsed with 6 mL of water to remove the unreacted [¹⁸F]fluoride and the product eluted with 1.5 mL of an ACN:water mixture (1:2) with an elution efficiency of about 95%. The product was finally applied to a semi-preparative HPLC and eluted with a retention time of 42-47 minutes. Given the long elution time and therefore large elution volume, the collected fraction was diluted with a volume of water around three times the volume of the eluate, fixed on a second HLB cartridge and further eluted with 1 mL of ethanol which was evaporated in order to formulate the tracer ready for injection.

When performed on precursor **39**, [¹⁸F]**30d** was obtained with a radiochemical conversion of $26 \pm 12\%$ (n = 15), a radiochemical yield of $22 \pm 11\%$ (n = 11), a molar activity of 13-180 GBq/μmol (start activities in the range of 1-4 GBq) (n = 7) and a radiochemical purity >99%.

When performed on precursor **40**, [¹⁸F]**30d** was obtained with a radiochemical conversion of $41 \pm 20\%$ (n = 38), a radiochemical yield of $29 \pm 11\%$ (n = 30), a molar activity of 13-540 GBq/μmol (start activities in the range of 1-4 GBq) (n = 18) and a radiochemical purity >99%.

Due to the low solubility of the radiotracer, the pure dried compound was formulated with 1% Tween 80 and phosphate buffer (PBS) before biological evaluation. Contents of residual solvents or copper were below the limit of detection.

Attempts to reduce the precursors amount to 4 or 2 μmoles proved unsuccessful and resulted in loss of conversion up to 50%. Deprotection conditions were carefully designed to be sufficiently basic in order to cleave the protective group in a few minutes but not to completely degrade the precursor. Boronic acid pinacol esters are indeed known to be easily hydrolysed to boronic acids under basic conditions. Furthermore, the C-B bond is labile under both acidic and basic conditions and is replaced by a C-H bond, producing a protodeboronated compound. Due to the similarity between H and F, the protodeboronated compound has very similar polarity to that of the radiotracer, constituting a potential impurity in the final product. However, 2-methoxy-4-(((2-oxo-1,2-dihydroquinolin-3-yl)methyl)amino)benzotrile **30f** could be separated from the desired radiotracer via semi-preparative HPLC (Experimental part)

3.3.5 Biological evaluation of [¹⁸F]mIDH-138 [¹⁸F]**30d** and reference compound **30d**

PET provides information on the annihilation site of the radionuclide, which in the case of fluorine is about 1 mm from the decay site, due to the low energy of the emitted positrons. Apart from the information that the fluorine-18 is still attached to the probe molecule at the time of decay (otherwise it would accumulate in the bone), PET is unable to measure if and how the tracer molecule is metabolized by the enzymes of the body.

For this reason, it is fundamental to test the stability of the radiotracer in solution and in vivo before more complex biological evaluations are carried out. It is interesting to notice that in some cases the radiotracer and the reference compound, although chemically identical, can show slightly different stabilities.

3.3.5.1 Stability of [^{18}F]mIDH-138 in rat blood serum

Radiotracer [^{18}F]30d was formulated in PBS/Tween and an aliquot was added to 500 μL rat blood serum, preheated at 37°C. After 5, 15, 30 and 60 minutes, equal aliquots were taken and added to a fixed volume of acetonitrile, used to denature the blood proteins. For each time slot, the organic solution was analysed in triplicate with radio-TLC and compared with the reference compound (Figure 23). No defluorination or formation of radiometabolites could be observed over one hour. Additionally, the recovery of radioactivity in organic solution could be measured by separating the supernatant from the plasma proteins (solid phase) and was always found to be around 85-90%.

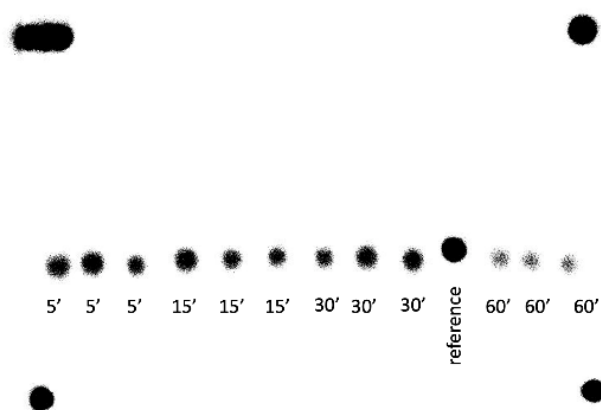


Figure 23: Radio TLC of [^{18}F]30d incubated in rat serum at 37°C for the indicated times (three lanes for each incubation time) and reference compound for comparison. TLC developed with 70% ethylacetate in hexane

3.3.5.2 Stability of [^{18}F]mIDH-138 and 30d in solution

A small aliquot of radiotracer [^{18}F]30d dissolved in DMSO was added to 500 μL of PBS buffer and left at room temperature for a maximum of 2 hours.

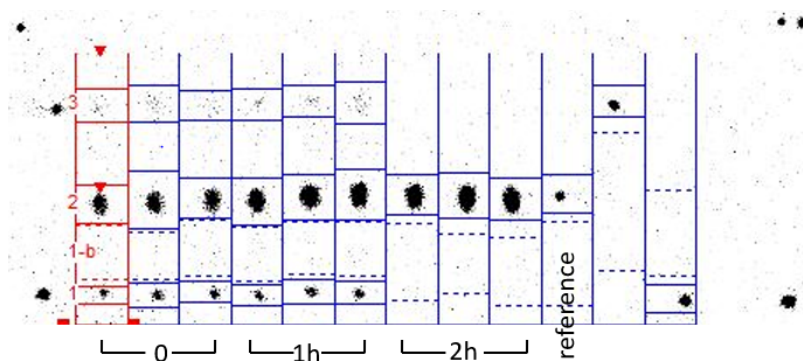


Figure 24: Radio TLC of [^{18}F]30d in PBS solution for the indicated times and reference compound for comparison. TLC developed with 70% ethylacetate in hexane

At the starting point and at each hour, the same aliquot was taken and spotted on a TLC with the reference compound, aniline **32** ($R_f = 0.8$) and quinolone **21d** ($R_f = 0.0$). Partial defluorination could be observed at $t = 0$ and 1h, probably due to silica degradation. This hypothesis is supported by the absence of degradation at 2 hours, sign that the defluorination did not occur in solution but rather on the silica plate (Figure 24).

3.3.5.3 Stability of reference compound **30d** in organic solution

A 1 mg/mL solution of the reference compound was prepared in DMSO and injected in the analytical HPLC every few hours for a total amount of 28 hours.

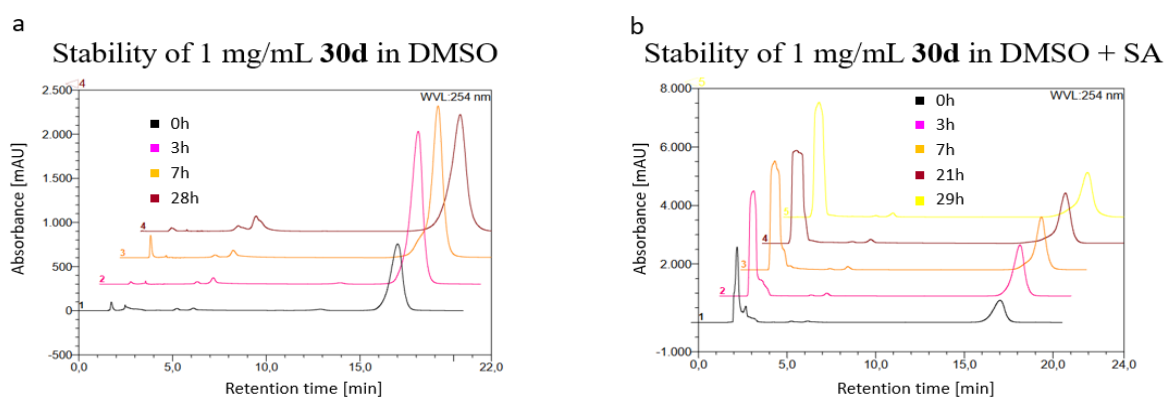
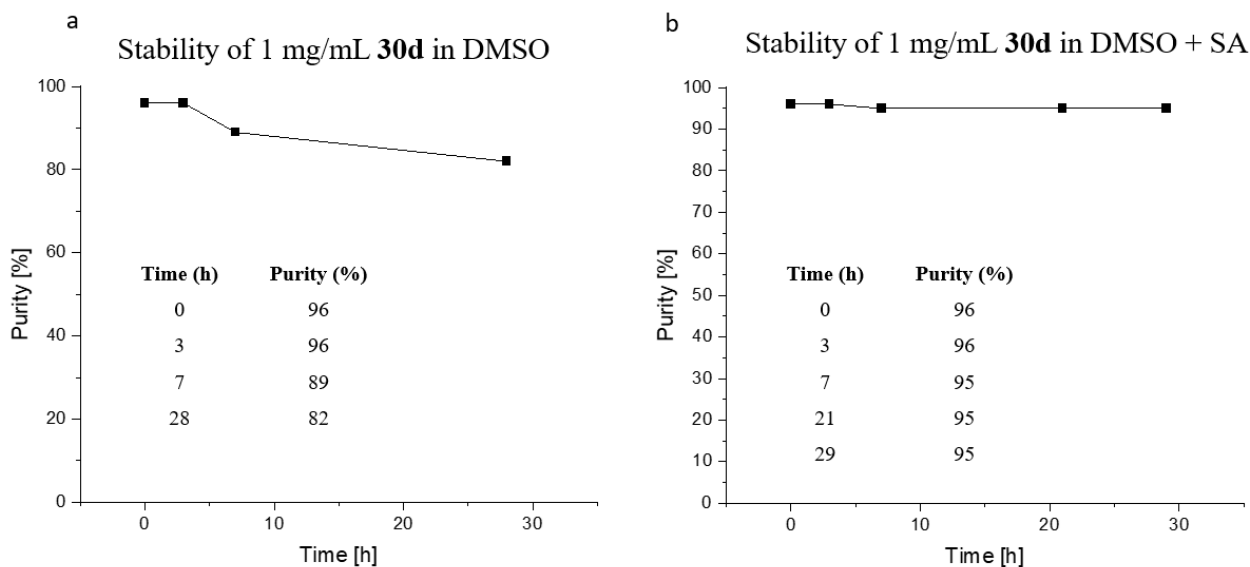


Figure 25: Stacked chromatograms of a solution of **30d** during time (max 29 h) without (a) and with (b) addition of sodium ascorbate

All UV active peaks were integrated and the area of the reference compound divided by the total area of the peaks to give a percentage of purity during time. The latter was plotted in Graph 1a to show the rate of degradation (Figure 25a). The compound, which was 96% pure at the beginning of the experiment, showed a loss of purity of 14% during 28 hours. The degradation products were identified to be the 6-fluoro-3-formylquinolone **21d** and aniline **32**, probably due to oxidization and subsequent cleavage of the C-N bond on the benzylic linker by radicals. To confirm this hypothesis, sodium ascorbate (SA) was added as radical scavenger to a freshly prepared 1 mg/mL solution of the reference compound and the degradation pattern was not repeated, showing only 1% degradation over 29 hours (Figure 25b). This confirmed the role of radicals in the degradation of the reference compound in solution.



Graph 1: Stability of **30d** in concentrated solution of 1 mg/mL of DMSO without (a) and with (b) addition of sodium ascorbate as radical scavenger

3.3.5.4 LogD

A small aliquot of [^{18}F]**30d** dissolved in organic solvent was added to a 1:1 mixture of n-octanol and aqueous solution and vortexed for two minutes, followed by separation of the two phases upon centrifugation. Equal amounts of organic and aqueous solutions were taken and separately analysed with a low gamma counter. The logarithmic ratio between the activity in organic and aqueous phase is defined as partition coefficient. When PBS buffer was used as aqueous solution, the final value was referred to as $\log D_{7.4}$ while when water was used, the final value was defined $\log P$.

The experimentally found $\log D_{7.4}$ value of 2.67 ± 0.04 was coherent with the one calculated using the ADMETlab platform of 2.75. The experimental $\log P$ value was 2.50 ± 0.03 , indicating no ionization of the molecule. Both values indicated a lipophilicity in the range of values considered optimal for BBB penetration.

3.3.5.4 Inhibitory constant (IC_{50})

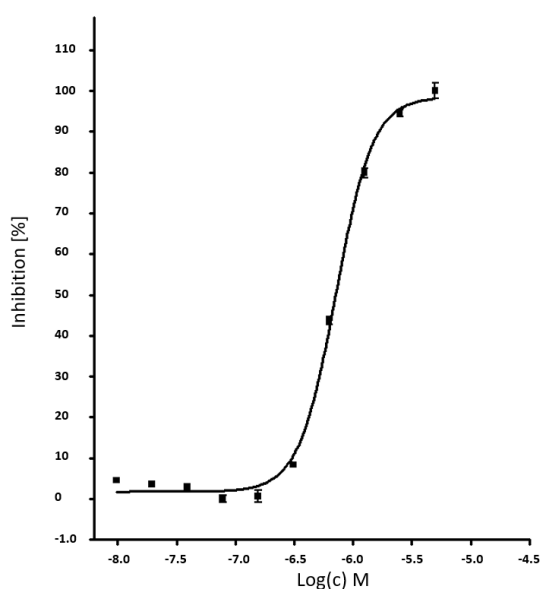
*All experiments were designed and carried out by Dr. D. Bier and Dr. D. Schneider

The inhibitory efficiency of the synthesized non radioactive analogue **30d** against mutant IDH1 was evaluated in our lab and compared to the results presented by Lin et al. The reactions catalysed by dehydrogenases have $NADP^+/NADPH$ as a cofactor, which is stoichiometrically correlated to the enzymatic reaction. For this reason, the advancement of both wt-IDH1 and R132H-IDH1 enzymatic reactions could be observed spectroscopically by measuring the increase or decrease, respectively, of the NADPH absorption.

Lin et al. measured the IC_{50} values for 4-(((6-chloro-2-oxo-1,2-dihydroquinolin-3-yl)methyl)amino)-2-methoxybenzotrile **30c** (Scheme 25) and the 6-fluorinated analogue **30d** and observed a negligible difference in the inhibition potency of the two inhibitors. Compound **30d** was measured with the commercially available assay kit (1IDH1 (R132H) from BPS Bioscience, San Diego, USA). The value was found in line with the literature (Table 7) and confirmed that the potency is not affected by the replacement of chlorine with fluorine at position 6.

IC_{50} (nM)	Lin et al.		This work
	30c (nM)	30d (nM)	30d (nM)
Wt-IDH1	100,000	Not reported	Non detectable
R132H-IDH1	127	138	616

Table 7: IC_{50} evaluation of **30c** and **30d**



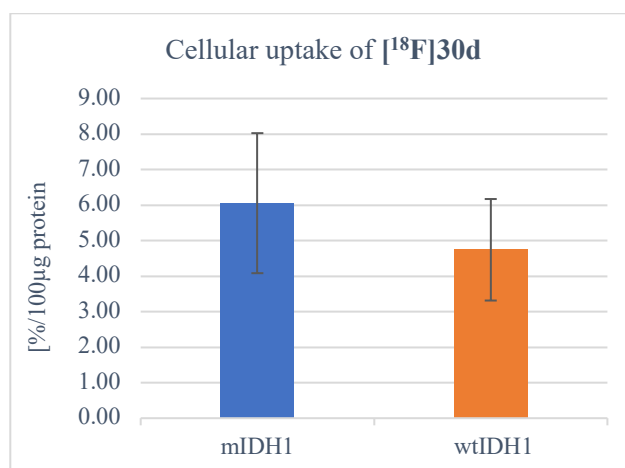
Graph 2: Inhibitory constant of **30d**: concentration of **30d** plotted against the percentage of inhibition towards mIDH1 enzyme

3.3.5.6 Cellular uptake and fractionation

*All experiments were designed and carried out by Dr. D. Bier, Dr. D. Schneider and A. Schulze

The cell uptake of [^{18}F]30d was tested on human cell lines U87MG-WT and U87MG-IDH1-R132H. After preparation of the cells, the radiotracer was incubated for one hour. Afterwards, the supernatant was separated and the two phases measured for radioactivity content.

The experiment was repeated six times and each measurement was performed in triplicate. An average of the results for both mutant and wild type enzymes was calculated and plotted in Graph 3, together with the standard deviation relative to the measurements. After a statistical analysis of the results, it was possible to conclude that the radiotracer has a significantly ($p = 0.03$, two-tailed t-test) higher uptake in mutant than wild type cells. Additionally, the amount of tracer internalized in the cells could be measured upon cell fractionation and was found to be around 90%, proving that the tracer can reach the cytoplasm, where the IDH1 enzymes reside.



Graph 3: Comparison of cellular uptake of radiotracer [^{18}F]30d in mutant and wild type IDH1 cells.

3.3.5.7 *In vivo* preliminary biological evaluation of [¹⁸F]mIDH-138 in Chorio Allantoic Membrane (CAM) models

*All experiments were designed and carried out by Dr. C. Stegmayr (INM-4, Forschungszentrum Jülich)

For a preliminary *in vivo* analysis of the radiotracer, the chorio allantoic membrane (CAM) chicken egg model was used.²²⁶ This consists of an extraembryonic membrane responsible for gas exchange in avian embryos.²²⁷ The membrane is highly vascularized and has a fully developed lymphatic system. The advantages of the model are the cost-effectiveness, easy handling, accessibility and rapid growth of eggs in respect to mice.²²⁸ Additionally, there is a complete access to the circulatory system which creates suitable conditions for cells incubations.²²⁹ Moreover, the system is naturally immunodeficient and does not require an animal testing license²³⁰ since the embryo does not feel pain until the estimated due date (EDD) 14²³¹ and it is not considered a living animal²³². The main disadvantage of this model is the difference with the mammalian physiology and drug metabolism.²²⁸ A first test was carried out with [¹⁸F]30d on a healthy system to confirm absence of defluorination and to follow the accumulation of the radiolabeled compound. The radiotracer was formulated as indicated in paragraph 3.3.4 and mixed with Evans blue dye to help visualisation of injection. Reconstruction of images (Figure 26) confirmed the *in vivo* stability of [¹⁸F]30d and showed minor uptake in the brain (a). The radiotracer was excreted through kidneys and the accumulation of waste products and possible radiometabolites was observed in the allantois (b) and liver (c).

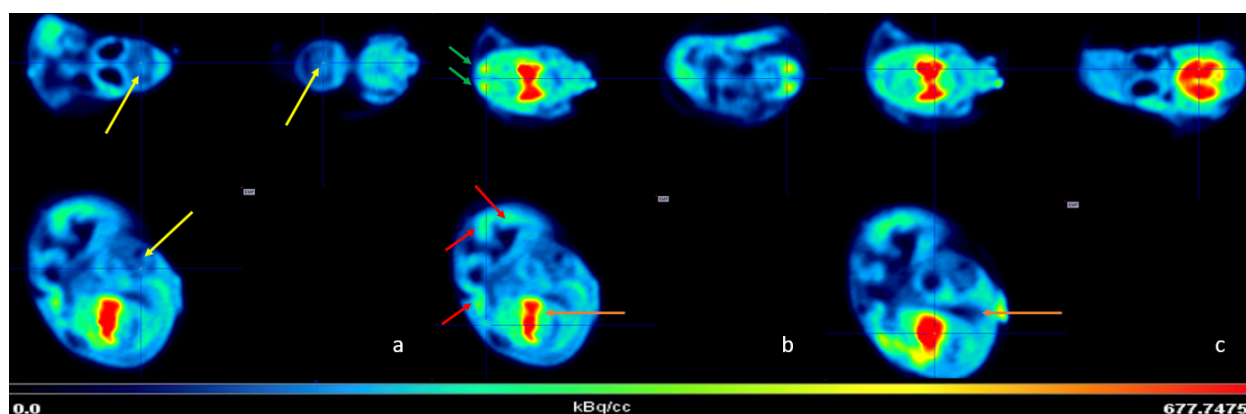


Figure 26: a) yellow arrows indicate the brain uptake; b) green arrows indicate the kidneys' uptake as they are the probable site of excretion. Red arrows indicate the subsequent accumulation in the allantois; c) accumulation in the liver and bile (orange arrow). Summed images 5-70 minutes post-injection.

After these encouraging results, a second egg was incubated and mutant and wild type U87 tumor cells were pipetted onto the CAM on EDD 9, limited by a silicone red ring (Figure 27c). The cells were applied through an opening of the egg shell and monitored daily during the incubation time, carried out in an incubator at 37°C. At EDD 19, the tumors reached a considerable size and could be analysed.

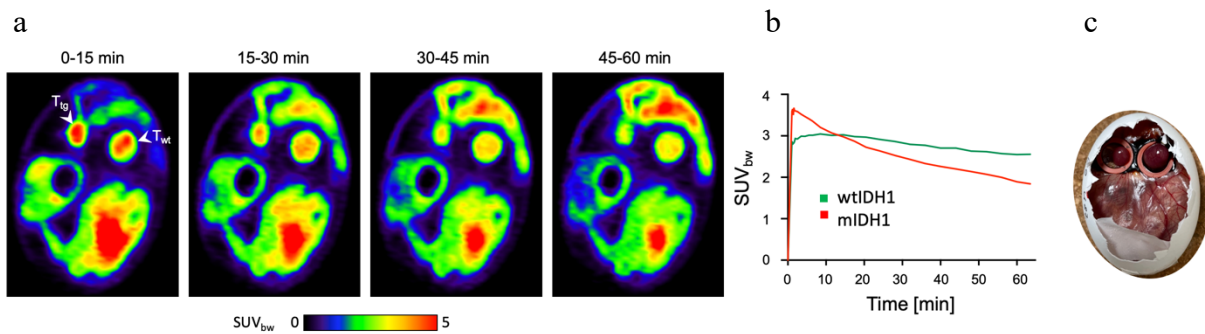


Figure 27: a) PET images of CAM uptake; b) TAC for U87-mIDH1 (red) and U87-wtIDH1 (green); c) picture of the investigated egg with the mutant (left) and (wild type) right) tumors.

It has to be noticed that the sizes differ due to the different growth rate of the mutant and wild type IDH tumors. Finally, 7 MBq of radiotracer in NaCl solution was injected with a volume of 125 μ L into a small vein on the CAM to avoid massive bleeding and the egg was immediately placed in the small animal PET scanner (Inveon, Siemens) for measurement and anesthetized with isoflurane. Reconstruction of the images (Figure 27a) showed a slightly higher uptake in the transfected IDH1 tumor in respect to the wild type one in the first 10 minutes (Figure 27b), followed by a quicker wash-out and subsequent accumulation in the allantois.

3.3.5.8 *In vivo* preliminary biological evaluation of [¹⁸F]mIDH-138 in mice

*All experiments were designed and carried out by Dr. Heike Endepols (Uni-Koeln)

While the experiments in the CAM model confirmed the absence of defluorination and uptake in the mIDH1 tumor, a similar uptake was unexpectedly registered in the wild type tumor. Unable to explain this result, the same radiotracer was applied to tumor xenografted mice.

The tracer was first formulated in PBS/Tween (125 μ L) and injected in 4 healthy mice to confirm stability and follow its absorption in different organs (Figure 28). High accumulation in liver and intestine was detected after 1h ($\text{SUV}_{\text{bw}} = 118.07 \pm 6.36$ and $\text{SUV}_{\text{bw}} = 4689.16 \pm 908.45$) and 2 h ($\text{SUV}_{\text{bw}} = 61.91 \pm 5.98$ and $\text{SUV}_{\text{bw}} = 5344.10 \pm 1465.92$).

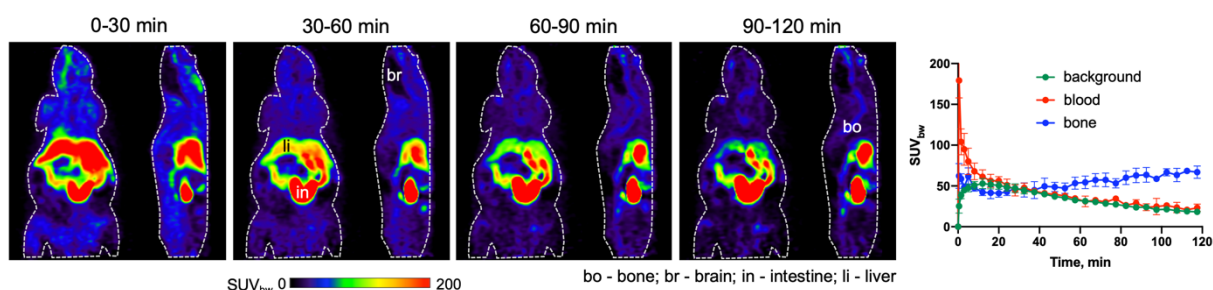


Figure 28: PET images of healthy mice ($n = 4$) at 0-120 minutes after injection of 7.5-10 MBq [¹⁸F]30d and TAC of measurement.

The PET radiotracer was afterwards analysed in tumor xenografted mice. To this end, a pair of mutant and wild type IDH tumors were incubated in each of 4 SCID mice to have immediate comparison of uptake differences. The cells were implanted subcutaneously on the shoulders in order to remove the factor of BBB penetration. A previous test with three mice has shown that the U87MG-mIDH tumor grows much faster *in vivo*, and was therefore implanted 6 days after the U87MG-WT tumor.

The PET measurement took place 8 days after the implantation of the U87MG-mIDH tumor (= 14 days after the implantation of the U87MG-WT tumor). A fixed amount of 125 μ L of formulated tracer (10 MBq per mouse) was injected and measured for 120 min at the small animal PET scanner (Focus 220, Siemens). Unexpectedly one mouse died before injection and the others within 90 minutes of measurement. A preliminary reconstruction of the images revealed a clear uptake of the radiotracer in the wild type tumor but not in the transfected one (Figure 29).

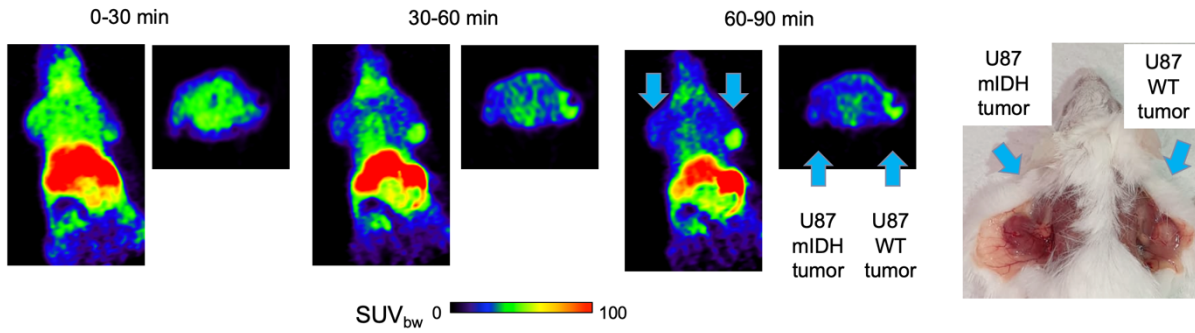
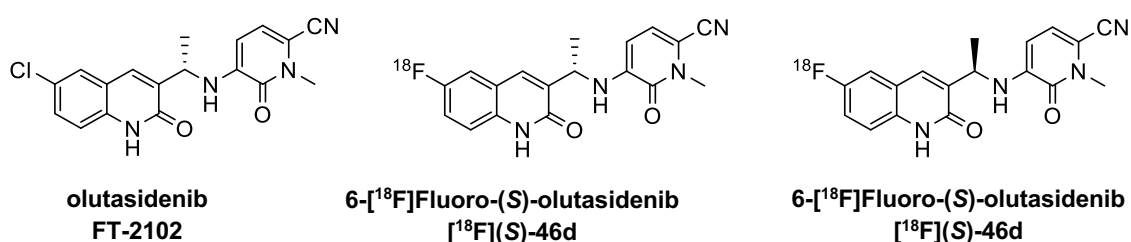


Figure 29: PET images of tumor bearing mouse at 0-90 minutes after injection of [¹⁸F]30d and picture of implanted tumors

The mice were therefore cut open at the sites of implantation and the transfected tumor resulted soft at touch. It is not possible to explain with certainty what caused the obtained results since the only difference in implantation between the mutant and wild type cell lines was the Matrigel (same manufacturer number but different batch). For this reason, further experiments should follow to confirm the low uptake in mutant IDH1 tumor.

3.4 6-¹⁸F]Fluoro-(*S*)-olutasidenib [¹⁸F](*S*)-46d and 6-¹⁸F]fluoro-(*R*)-olutasidenib [¹⁸F](*R*)-46d

Selected by Caravella et al. as the most promising candidate and accepted in 2022 by the FDA for the cure of relapsed or refractory acute myeloid leukemia (AML)²³³, olutasidenib (**FT-2102**) represented the most suitable candidate for the development of a selective tracer for the visualization of mIDH1 gliomas due to its high inhibitory potency and selectivity against mIDH1 in respect to wtIDH1. After the success of the proof of concept, carried out through synthesis and radiofluorination of [¹⁸F]mIDH-138, the first goal of the project could be pursued.



*Scheme 50: FT-2102 and the derived radiotracers 6-¹⁸F]Fluoro-(*S*)-olutasidenib and 6-¹⁸F]Fluoro-(*R*)-olutasidenib*

As shown in paragraph 3.2, introduction of fluorine-18 at position 7 through ring closure of a 3,4-substituted acetanilide could not be easily carried out. Given the minimal difference in terms of IC₅₀ between (*S*)-5-((1-(6-chloro-7-fluoro-2-oxo-1,2-dihydroquinolin-3-yl)ethyl)amino)-1-methyl-6-oxo-1,6-dihydropyridine-2-carbonitrile (**2**) and olutasidenib (**FT-2102**) (Scheme 50), introduction of fluorine-18 was performed at position 6, replacing the chlorine. Additionally, even though a 6-fluorinated version of olutasidenib was not tested by Caravella et al., it was known from previous studies that replacement of chlorine with fluorine had a negligible effect on potency.¹⁵² With these premises, 6-¹⁸F]fluoro-(*S*)-olutasidenib ([¹⁸F](*S*)-46d) was prepared and biologically evaluated (Scheme 50). Additionally, its enantiomer ([¹⁸F](*R*)-46d) was prepared and biologically tested in order to confirm any real biological advantage of the first in respect to the latter (Scheme 50).

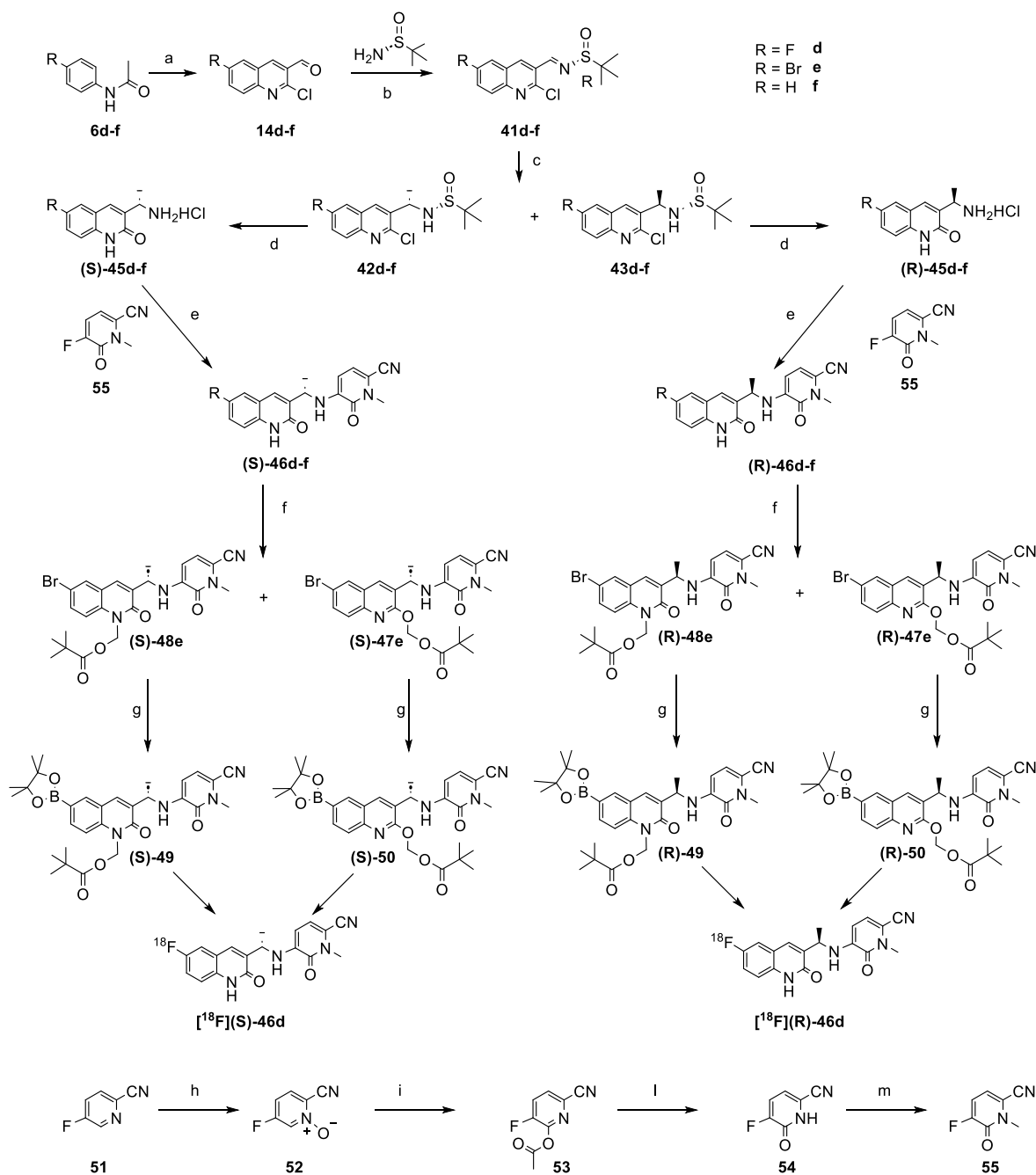
It has to be mentioned that half-way through the development of these two radiotracers, a different group published a study on 6-¹⁸F]fluoro-(*S*)-olutasidenib and 6-¹²⁵I]iodo-(*S*)-olutasidenib.¹⁹⁵

The paper reported the radioiodination and radiofluorination of a stannane precursor, mediated by palladium and copper respectively. In the second case though, radiochemical yield and molar activity of the radiofluorinated tracer were unsatisfactory and could not be used to perform any biological evaluation, that was therefore non carried out. Given the lack of biological results, it was decided to carry on the project in order to perform them.

3.4.1 Preparative organic synthesis of N-protected precursors (*S*)- and (*R*)-**49**, O-protected precursors (*S*)- and (*R*)-**50**, their protodeboronated analogues (*S*)- and (*R*)-**46f** and reference compounds (*S*)- and (*R*)-**46d**

For the preparation of the radiotracer [^{18}F](*S*)-**46d**, boronic acid pinacol esters were selected as leaving groups to undergo a copper mediated radiofluorination. A similar procedure as the one used previously described for the radiosynthesis of [^{18}F]**30d** was here carried out, therefore the POM protecting group was introduced on the precursors. For this reason, a pair of precursors, namely the N- and the O- protected, was synthesized for each enantiomer of the desired radiotracer (Scheme 51). The synthetic path was developed on the example of that proposed in literature and further modified to meet the need of consistent amounts of precursors needed to optimise the radiofluorination conditions.¹⁸⁹ The most challenging step was the production of the chloroquinolines which represented only a minor product in the Vilsmeier Haack formylation and whose production was not described by Caravella's group, who purchased them. To ensure the stereoselectivity of the methyl introduction, an Ellman's sulfinamide was used as chiral auxiliary and allowed the preparation, as well as the optimal isolation, of both the *S,R*- and *R,R*- diastereoisomers with excellent diastereomeric excess after removal of the sulfinamide.

Finally, the pyridone (**55**) on the right-hand side of the molecule was obtained with a 4 steps synthesis starting from 5-fluoropicolinonitrile and was further conjugated to the quinolone via $\text{S}_{\text{N}}2$ reaction.



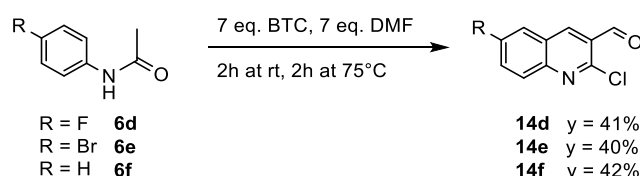
Scheme 51: Synthetic pathway for the development of protected precursors (S)- and (R)-49 and (S)- and (R)-50, their protodeboronated analogues (S)- and (R)-46f and reference compounds (S)- and (R)-46d.

Procedures: a) 7 eq. BTC, 7 eq. DMF, 75°C, 4h; b) 1.5 eq. CuSO₄, 1.5 eq. (R)-2-methylpropane-2-sulfonamide, DCE [0.5], 55°C, 16h; c) 1.5 eq. MeMgBr in Et₂O, CH₂Cl₂ [0.5], -60 °C to rt, 16h; d) 1N HCl:dioxane 1:1 [0.2], reflux, 2h; e) 1.1 eq. 55, 3 eq. DIPEA, DMSO [0.1], 110°C, 16h; f) 1.5 eq. K₂CO₃, 1.5 eq. POM-Cl, DMF [0.2], rt, 16h; g) 1.2 eq. (Bpin)₂, 7 eq KOAc, 5% Pd(dppf)Cl₂, dioxane, [0.1], 80°C, 3h; h) 2 eq. TFAA, 2 eq. UHP, CH₂Cl₂ [0.18], 16h; i) Ac₂O (10 mL per gram of 51), reflux, 16h; l) 2 eq. K₂CO₃, MeOH [0.45], rt, 2h; m) 2 eq. K₂CO₃, 1.1 eq. MeI, DMF [0.35], rt, 1 h.

3.4.1.1 Organic preparation of the (S)- and (R)-3-(1-aminoethyl)-6-halogenoquinolin-2(1H)-one hydrochlorides (S)-45d-f and (R)-45d-f

As shown in 3.3.1.1, the Vilsmeier-Haack formylation of acetamides with DMF and POCl₃ produced mainly the formylated acrylamides **13** rather than the 2-chloroquinolones **14**, except when applied to the unsubstituted acetanilide **6f**, where the corresponding quinoline **14f** was obtained in 42% yield. When applied to 4-bromo and 4-fluoroacetanilides **6e** and **6d**, the corresponding quinolines **14e** and **14d** were obtained in 2% and 0% yield. Given the high cost of these starting materials if purchased, different routes were tested in order to prepare them on gram scale.

Initially, an attempt was made to prepare the 6-halogenated-3-formylquinolones **21d-f** and further convert them into the corresponding quinolines upon treatment with POCl₃. The procedure has been reported in literature by different groups over the years but a full conversion of **21d,e** could never be reproduced in our lab.²³⁴ A second attempt involved addition of DIPEA and anisole to a solution of the 6-fluoroquinolone dissolved in POCl₃ followed by heating to 95°C.²³⁵ After 24 hours stirring, the reaction resulted in 5% quinoline and was therefore abandoned. The replacement of POCl₃ with 4,4',4-tris(carbazol-9-yl)triphenylamine (TCTA) suggested by Venkanna et al.²³⁶ was applied to 4-fluoroacetanilide **6d** but furnished no quinoline **14d**. Finally, formylation with DMF and 7 equivalents of triphosgene (BTC)²³⁷ as chlorinating agent resulted in production of quinolines in satisfactory yields (Scheme 52). Phosgene is a hazardous reagent that has to be treated with the outmost care due to its hydrolysis to carbon dioxide and hydrochloric acid in aqueous environment or if in contact with moisture. The reaction with DMF for the *in situ* preparation of the Vilsmeier-Haack (VHR) reagent proceeded smoothly at 0°C by slow dropwise addition of DMF to BTC under inert conditions. During formation of the **VHR**, two equivalents of phosgene were formed and further hydrolysed during aqueous work up. After addition of DMF, the acetanilide was added and left stirring at room temperature for two hours under inert gas stream. Finally, the mixture was heated for 2 hours at 75°C, which turned the mixture into a dense orange solution.

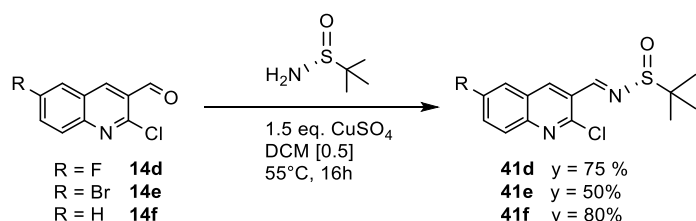


Scheme 52: Formylation of acetanilides **6d-f** with DMF-BTC for the preparation of the corresponding 2-chloroquinolines **14d-f**

After careful aqueous work-up, a precipitate appeared and could be filtered. This reaction was applied to the three acetanilides **6d-f** (500 mg to 2.5 grams) and the corresponding quinolines were obtained in around 40% yield.

Ellman's sulfinamide was then selected as chiral auxiliary to direct the methylation attack on the benzylic linker. Davis pioneered the study of *p*-toluenesulfinimines in 1974 and showed that the sulfinyl group serves as activator for the nucleophilic attack, provides optimal diastereofacial selectivity and can be cleaved upon treatment with mild acids.²³⁸ Moreover, these inexpensive reagents can be easily reacted with aldehydes in presence of a mild Lewis acid like CuSO₄ and MgSO₄ which works also as dehydrating agent to push the reaction equilibrium towards the production of the products. In 1997, Ellman and coworkers demonstrated the superiority of *tert*-butanesulfinamide in respect to *para*-toluenesulfinamides in terms of enhanced diastereofacial selectivity and reactivity of the C-N bond.²³⁹

Davis' procedure was reproduced with use of *tert*-butanesulfinamide on 6-F, 6-Br and 6-H quinolines **14d-f** dissolved in DCE, which allowed overnight mild heating at 55°C (Scheme 53).

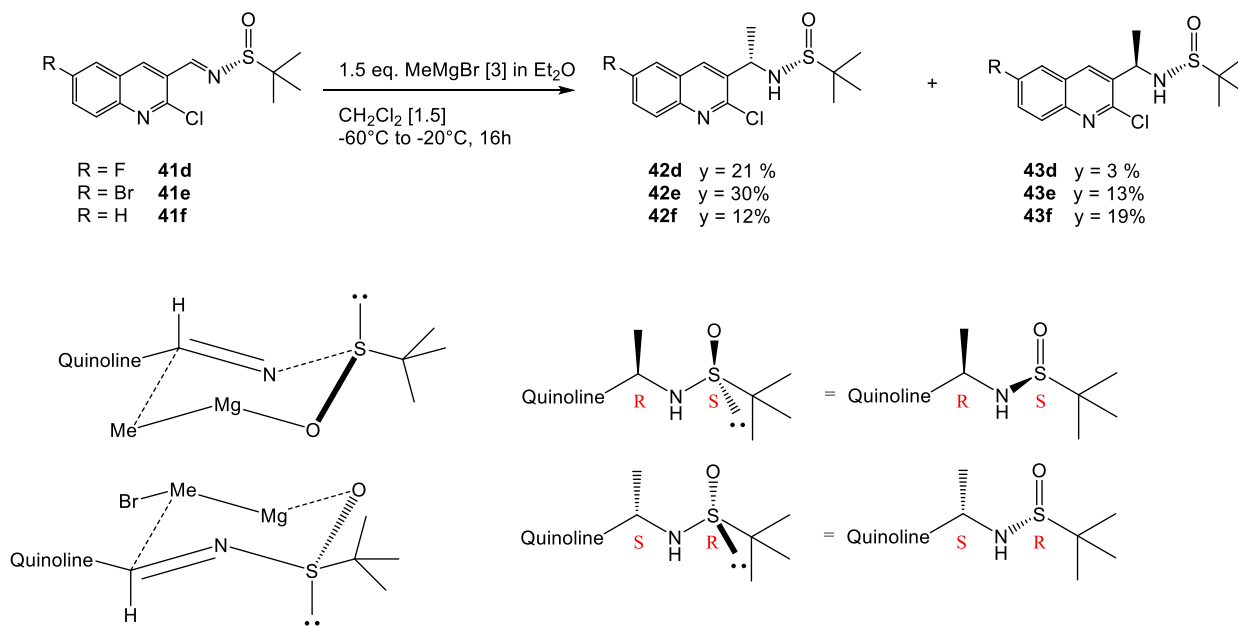


Scheme 53: Introduction of the Ellman's sulfinamide as chiral auxiliary

The complete consumption of the starting material was confirmed by TLC analysis, together with formation of a more apolar side product that was not identified. The products **41d-f** were obtained pure in a 50-80% yield after column purification.

Sulfinimines are strong electrophiles which can undergo addition with alcohols²⁴⁰, thiols²⁴¹, amines²⁴² and in general work as Michael acceptors. They can also react with nucleophiles in a highly diastereoselective manner²⁴³. Ellman reacted a series of *tert*-butanesulfinimines in CH₂Cl₂ at -48°C with different Grignard reagents and obtained the products derived from the attack on the same face (the so-called Ellman addition) as the one occupied by the auxiliary with 96-100% yield with a diastereomeric excess of 89-98%. When reproduced on ketimines, the same result was confirmed, providing a reliable method for the prediction of the stereochemical outcome.²⁴⁴ The stereochemistry of the product can be predicted by using a chair model of the six-membered transition state where the

tertbutyl group of the sulfinimine occupies the equatorial position, as the substituent of the starting aldehyde (Scheme 54).



Scheme 54: Six-membered ring transition states of the Grignard addition on chiral sulfinimines 41d-f

When tested on the three scaffolds **41d,e,f**, the methylation produced the two diastereoisomers in different ratios. Following literature indications, the major compounds were assigned as products of the Ellman addition (S,R) and the minor as products of the anti-Ellman addition (R,R). The ratio between the two products was calculated via ¹H-NMR analysis of the mixture before purification by integrating the peak of the chiral methyl group (Figure 30).

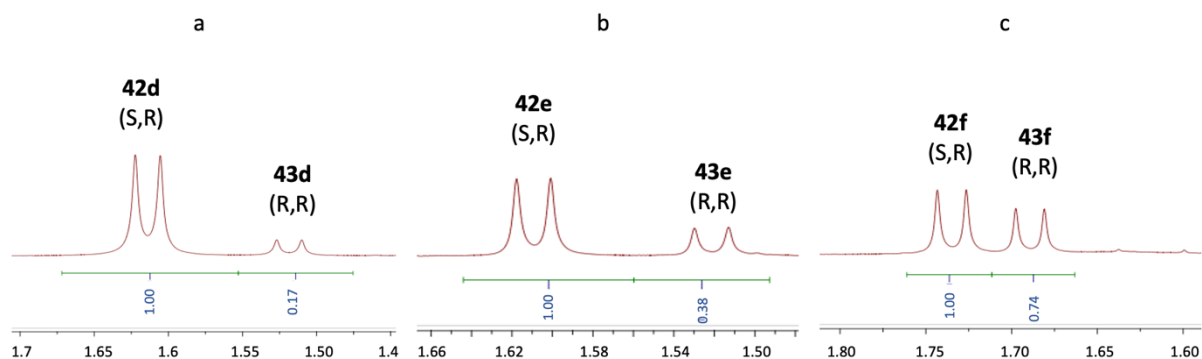
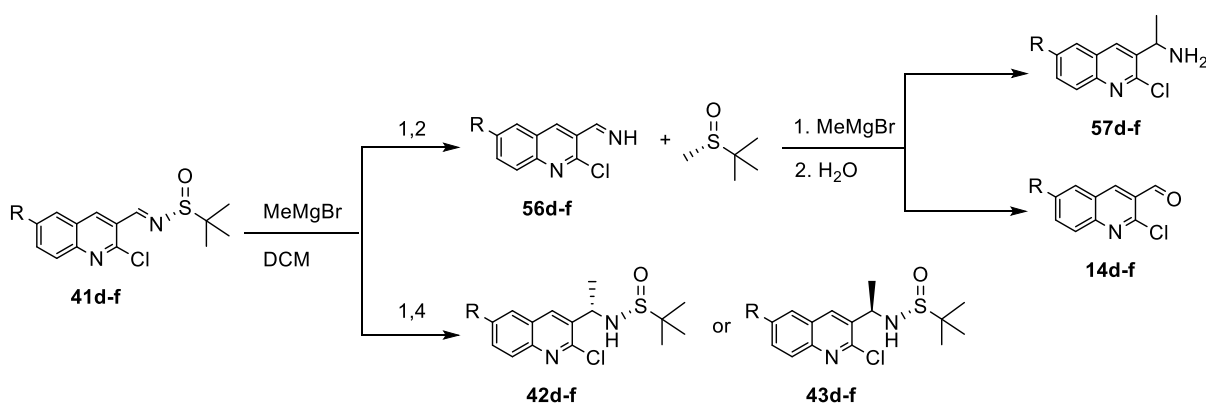


*Figure 30: ¹H-NMR integration of methyl peak to calculate the diastereomeric excess of a) 6-fluoro analogues **42d** and **43d** b) 6-bromo analogues **42e** and **43e** and c) 6-H analogues **42f** and **43f**.*

Overnight methylation of the fluorinated analogue **41d** produced both diastereoisomers in a total yield of 41% with an extremely high diastereoselectivity of 85% for the (*S,R*)-Ellman product **42d**. The high reactivity of the substrate was confirmed by the absence of unreacted starting material and the presence of an impurity resulting from the methylation of the corresponding imine **56d**, probably produced by the 1,2 addition of MeMgBr to the sulfinimine **41** (Scheme 55). The 1,2 addition was already reported by Moreau et al. as competing reaction in case of MeMgBr but not with allylmagnesium bromide or benzylmagnesium bromide. None of these results was reported by Ellman.²⁴⁵



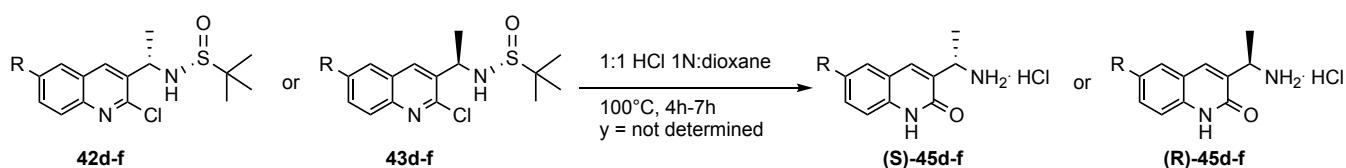
Scheme 55: Possible explanation for the side products' formation during the selective methylation of sulfinimines 41d-f.

In the case of brominated compound **41e**, the reaction was repeated several times to meet the need of large amounts of product for the synthesis of precursors. In this case, the yield oscillated between 22 and 47%. Unexpectedly, the reaction almost never reached completion and, in all cases, some sulfinimine **41e** was recovered together with the chloroquinoline **14e**, probably derived from the 1,2 methylation and further aqueous work-up. In this case, the major diastereoisomer (*S,R*)-**42e** was produced with an excess of 72% in respect to the minor (*R,R*)-**43e** (28%). Finally, when the 6-H-quinolone **41f** was treated with the Grignard reagent, a total yield of 56% was registered. The ratio between the two products was analysed by NMR and resulted to be 57:43 for (*S,R*)-**42f**, revealing the dramatic loss of stereoselectivity in respect to the halogenated compounds. Interestingly, as already observed for the fluorinated analogue, the methylated amine **57f** was the only side product produced during the reaction.

It is not clear how the substituent in position 6 of the quinoline moiety can affect the diastereoselectivity. The first hypothesis was that the steric hindrance could play a role, although minor, but this would not explain the great difference in the ratio between the 6-H and the 6-F product **42d,f** and **43d,f**. It was afterwards hypothesised that the electronic nature of the substituents could be

the discriminating factor. Considering that highest diastereoselectivities were achieved for electron withdrawing substituents, the methylation was tested on 6-methoxy sulfinimine, bearing an electron-releasing group. Here, the Ellman and anti-Ellman products were obtained in a 70:30 ratio. Given the fact that similar outcomes were obtained in presence of both electron-withdrawing and electron-releasing substituents, the role of electronic nature was ruled out as the cause of the different ratios of diastereoisomers.

After the isolation via column chromatography, the two diastereoisomers were separately dissolved in a 1:1 mixture of hydrochloric acid (1 N) and dioxane and heated to 100°C for few hours, until TLC showed complete conversion into the corresponding free amines (*S*)- and (*R*)-**45d-f** (Scheme 56). The chiral auxiliary was converted into tert-butylsulfinyl chloride upon treatment with HCl, liberating the desired compound which could be filtered off. Here, the harsh conditions guarantee the concomitant conversion of the quinolines to their corresponding quinolones. Recrystallization with diethylether or chloroform, although described in literature, was found to be unsuccessful due to low solubility. An attempt to extract the product with water after dilution with ethylacetate did not allow recovery of a clean product. Therefore, the mixture was evaporated and used without further purification. While here it was never applied, due to the low amount of Ellman's sulfinamides used, it could be possible to isolate the chiral auxiliary with high enantiomeric excess and yield. While HCl racemizes the sulfoxides and sulfinate esters,²⁴⁶ addition of a chiral alcohol, such as N-methylephedrine (NME) and triethylamine, makes it possible to capture a single diastereoisomer of the sulfinate ester in good yield after column chromatography. Subsequent treatment with LiNH₂/NH₃ cleaves the ester bond thus liberating the enantiopure auxiliary.²⁴⁷

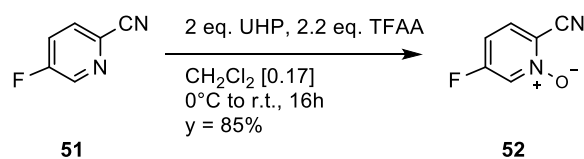


Scheme 56: Acidic cleavage of sulfinamides

3.4.1.2 Organic preparation of 5-fluoro-1-methyl-6-oxo-1,6-dihydropyridine-2-carbonitrile **55**

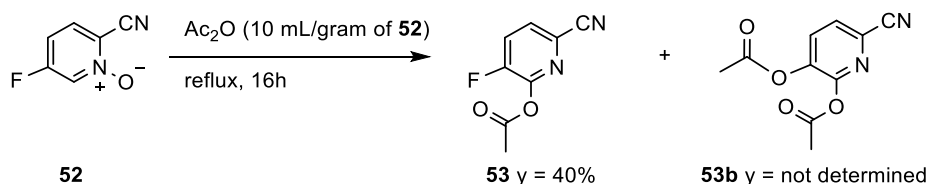
5-fluoro-1-methyl-6-oxo-1,6-dihydropyridine-2-carbonitrile **55**, which constitutes the right-hand side of the **FT-2102** analogues, was prepared via multi-step synthesis starting from the commercially available 5-fluoropicolinonitrile **51**. The latter was oxidized to the corresponding N-oxide **52** with

TFAA and the hydrogen peroxide-urea complex (UHP), which forms the highly reactive peroxytrifluoroacetic (Scheme 57).²⁴⁸



Scheme 57: Oxidation of 5-fluoropyridinonitrile with UHP/TFAA complex

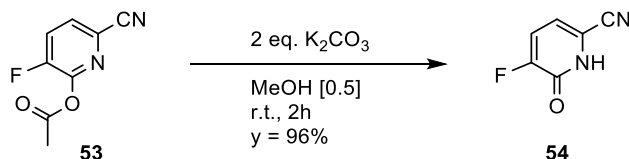
The latter was shown²⁴⁹ to be preferable to mCPBA in case of weak nucleophiles, such as the electron deficient pyridine **51**. Its preparation was normally carried out by addition of trifluoroacetic acid or anhydride to 90% hydrogen peroxide until recently the UHP-anhydride procedure was shown to be more practical and safer. The presence of the N-O bond avoids further reactions at the nitrogen and directs the substitutions to positions 2 and 4, rather than to position 3, as preferred during S_NAr . Overnight reflux of 2-cyano-5-fluoropyridine 1-oxide **52** with acetic anhydride produced 6-cyano-3-fluoropyridin-2-yl acetate **53** and the disubstituted compound **53b** as indicated by lack of fluorine signal in ^{19}F -NMR of **53b** (Scheme 58).



Scheme 58: Esterification of pyridine N-oxide 52

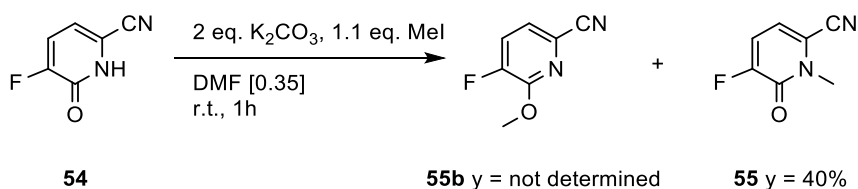
An attempt was made to avoid the formation of by-product **53b** by decreasing the reaction temperature to 90 and 100°C, which impaired the start of the reaction. The reaction was therefore carried out at reflux and meticulous analyses of the mixture each hour showed that the introductions of the two acetate groups proceed in parallel, therefore the undesired acetylation could not be avoided. The products **53** and **53b** could anyway be easily isolated via column chromatography in 40 and 13% yield respectively. The desired product **53** was further dissolved in methanol and treated with potassium carbonate at room temperature for 2 hours, when TLC confirmed its complete consumption (Scheme 59). Here potassium carbonate deprotonates the methyl group at the alpha position of the acetyl group leading to formation of the acetaldehyde and the pyridone anion. After evaporation of

methanol, addition of HCl produces 5-fluoro-6-oxo-1,6-dihydropyridine-2-carbonitrile **54**, obtained pure in 93% yield after extraction with ethyl acetate.



Scheme 59: Deacetylation of pyridine 53 to pyridone 54

Finally, methylation with methyl iodide in DMF in presence of potassium carbonate yielded the O- and N-protected compounds (**55b** and **55** respectively) in 67% total yield (Scheme 60).



Scheme 60: N- and O-methylation of 54

Unexpectedly, in contrast to the results obtained from the treatment of quinolones with POM, the N-protected 5-fluoro-1-methyl-6-oxo-1,6-dihydropyridine-2-carbonitrile **55** was obtained as the major product while the O-protected 5-fluoro-6-methoxypicolinonitrile **55b** as the minor in 1:0.13 ratio. Additionally, after the reaction was quenched and extracted, the product was left in solution overnight before concentration in vacuo. When the purification via column chromatography was performed, the two products were collected in a ratio of 1:0.38 (measured via ¹⁹F-NMR) with the O-protected **55b** compound representing 19% of the total 67% yield. It was speculated that this phenomenon could originate from the conversion of the kinetic (N-protected) product into the thermodynamic (O-protected) one. When the reaction was repeated and immediately worked up and dried, the ratio was of 1:0.8 (Figure 31), confirming the previous hypothesis.

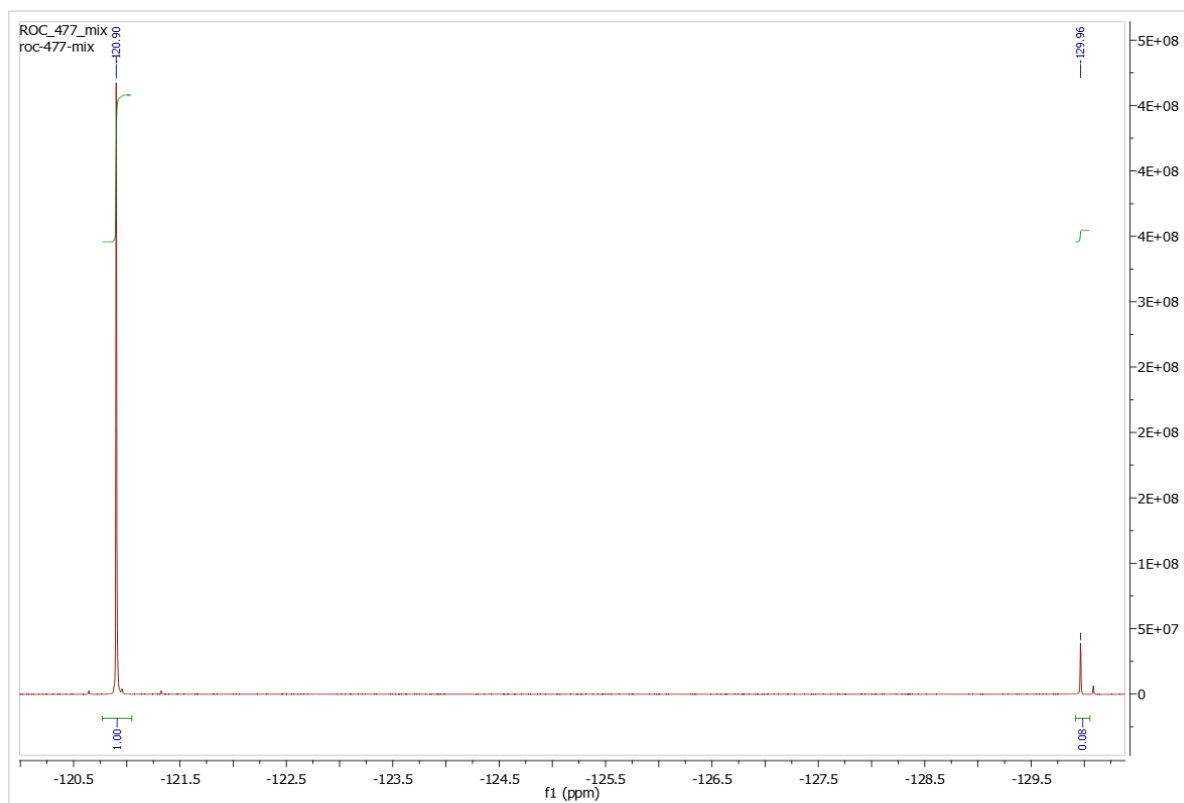
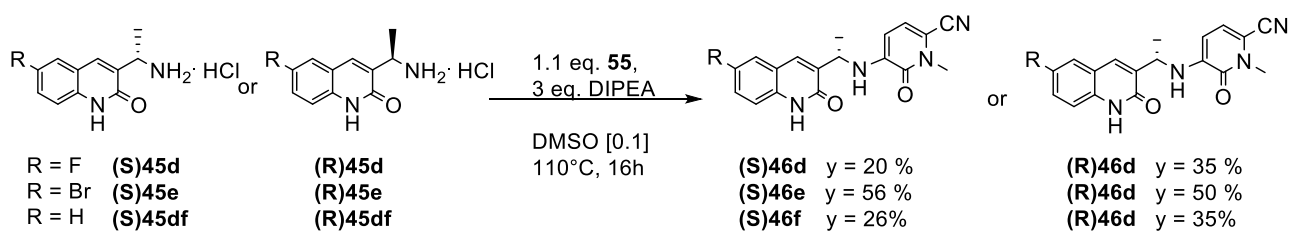


Figure 31: ^{19}F NMR integration of *N*-methylated (**55**) and *O*-methylated (**55b**) pyridones

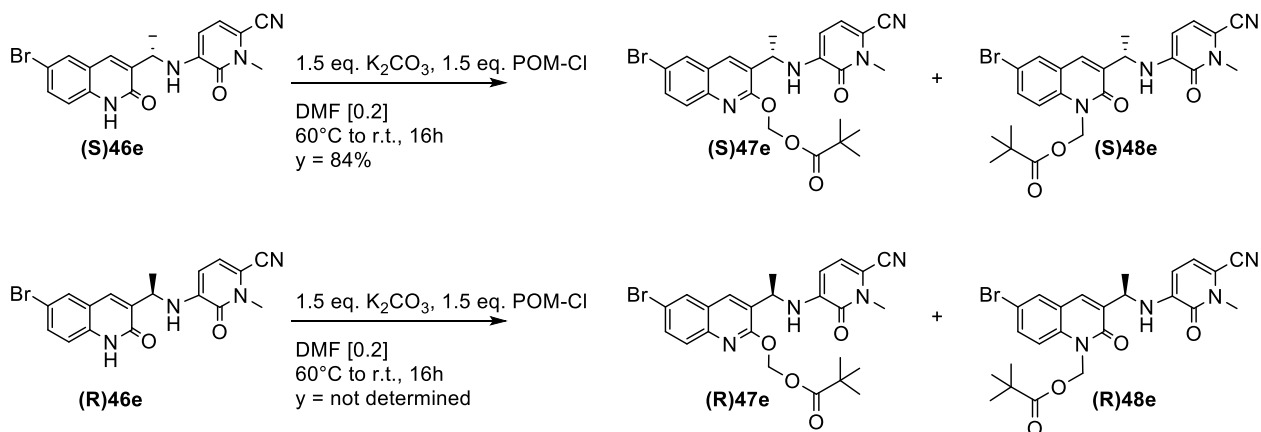
3.4.1.3 Organic preparation of *N*-protected precursors (*S*)- and (*R*)-**49**, *O*-protected precursors (*S*)- and (*R*)-**50**, their protodeboronated analogues (*S*)- and (*R*)-**46f** and reference compounds (*S*)- and (*R*)-**46d**

Conjugation between the enantiomerically pure quinolones (*S*)- and (*R*)-**45d,e,f** and the methylated pyridone **55** was carried out via $\text{S}_{\text{N}}2$ reaction with the aid of DIPEA and using DMSO as solvent (Scheme 61). The final reference compounds (*S*)- and (*R*)-**45d** were obtained in 20% and 35% isolated yield while the protodeboronated reference compounds (*S*)- and (*R*)-**45f** in 26% and 35% yield.



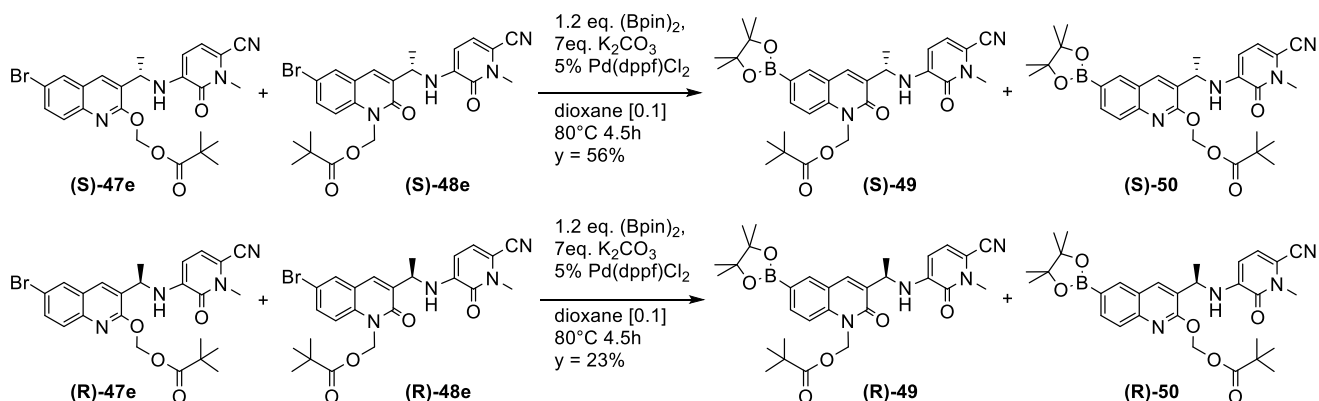
Scheme 61: Conjugation of enantiomerically pure quinolones (*S*)- and (*R*)-**45d-f** with *N*-methylated pyridone **55** via $\text{S}_{\text{N}}2$ reaction in DMSO.

The brominated analogues (**S**)- and (**R**)-**45e** were obtained in 56% and 50% yield, purified via column chromatography and further reacted with POM-Cl and potassium carbonate to introduce the protecting group on the amide moiety (Scheme 62). Given the improved solubility provided by the pyridone scaffold in respect to the previously introduced arene (chapter 3.3), the reaction reached 85% yield with a ratio of 1:0.85 for the O-protected compounds (**S**)- and (**R**)-**48e**.



Scheme 62: POM protection of (**S**)- and (**R**)-**46e**

Finally, the enantiomerically pure pairs of N- and O-protected brominated compounds (**S**)-**47e** and **48e** and (**R**)-**47e** and **48e** were converted into the corresponding boronic acid pinacol esters with a Miyaura borylation (Scheme 63). As presented in 3.3.3 the starting materials were dissolved in dioxane and treated with bis(pinacolato)diboron, potassium acetate and the palladium catalyst at 80°C for 4 hours. Pure products were obtained after column chromatography, characterized and finally used as precursors for radiofluorination.



Scheme 63: Miyaura borylation of enantiopure brominated analogues **S**)-**47e** and **48e** and (**R**)-**47e** and **48e**

3.4.2 Copper mediated radiofluorination of (*S*)- and (*R*)-(3-(1-((6-cyano-1-methyl-2-oxo-1,2-dihydropyridin-3-yl)amino)ethyl)-2-oxo-6-(4,4,5,5-tetramethyl-1,3,2-dioxaborolan-2-yl)quinolin-1(2H)-yl)methyl pivalate (**S**)**49** and (**R**)**49** and (*S*)- and (*R*)-(3-(1-((6-cyano-1-methyl-2-oxo-1,2-dihydropyridin-3-yl)amino)ethyl)-6-(4,4,5,5-tetramethyl-1,3,2-dioxaborolan-2-yl)quinolin-2-yl)oxy)methyl pivalate (**S**)**50** and (**R**)**50**

Radiolabeling of boronic acid pinacol esters (*S*)- and (*R*)-**49** and (*S*)- and (*R*)-**50** was carried out using the copper mediated radiofluorination protocol previously described in paragraph 3.3.2, followed by deprotection of the POM group under basic conditions to afford [¹⁸F](*S*)-**46d** and [¹⁸F](*R*)-**46d**. The radiosynthesis was carried out treating the four precursors separately, while the results were reported distinguishing between the N- and the O- protected compounds but not between enantiomers (Scheme 64). Given the neutrality of methyl group in regard to steric hindrance and electronic nature, it was assumed that the stereochemistry would not play a role in the fluoride-18 attack itself.

The O-protected precursors (*S*)- and (*R*)-**50** were treated with Cu(4-PhePy)₄(ClO₄)₂ at 110°C for 10 minutes before addition of 0.25 M NaOH_{aq}, but the desired radiotracers were obtained with low RCCs (Table 8, entry a).

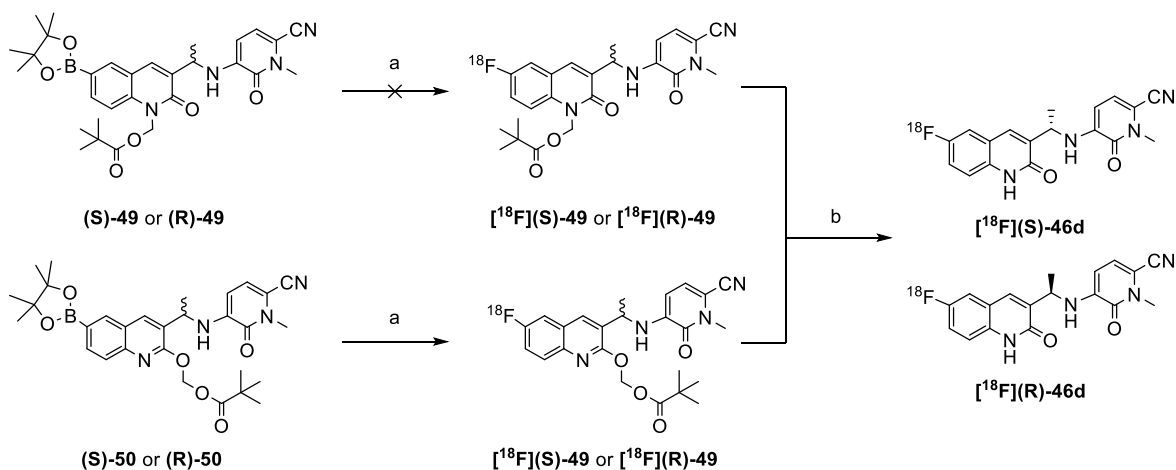
Entry	Eluting salt (1 mg/mL)	Solvent	T (°C)	Time	RCC (%)		
a	TEAB in MeOH	DMA	110	10 min	33.64	±	1.7 (n = 2)
b	TEAB in MeOH	DMA	110	15 min	13.60	±	0.5 (n = 2)
c	TEAB in MeOH	DMA	110	5 min	33.38	±	0.9 (n = 2)
d	TEAB in MeOH	DMA	100	10 min	32.24	±	5.11 (n = 2)
e	TEAB in MeOH	DMA	90	10 min	31.18	±	6.61 (n = 2)
f	TEAB in MeOH	DMA	80	10 min	21.01	±	5.08 (n = 2)
g	TEAB in MeOH	DMA	90	15 min	14.98	±	7.70 (n = 2)
h	TEAB in MeOH	DMA	100	15 min	57.39	±	3.29 (n = 2)
i	TEAB in MeOH	DMI	100	15 min	56.57	±	15.84 (n = 7)
l	TEAOTf in MeOH	DMI	100	15 min	51.93	±	13.44 (n = 3)
m	TEAB in <i>n</i> BuOH	DMI	100	15 min	21.24	±	5.67 (n = 2)
n*	TEAB in MeOH	DMI	100	15 min	10.08	±	2.50 (n = 2)

* experiment carried out on 5 μmoles of precursor

Table 8: Optimization of radiosynthesis of compounds [¹⁸F](*S*)-**46d** and [¹⁸F](*R*)-**46d** performed on the O-protected precursors (*S*)- and (*R*)-**50**

Interestingly, when the same conditions were applied to the N-protected precursors (*S*)- and (*R*)-**49** no formation of the radiotracer was observed. For this reason, the optimization of the

radiofluorination conditions was carried out on the O-protected compounds, starting with an increase (entry b) and decrease (entry c) of the reaction time, neither of which showed any improvement. Afterwards, the mixture was reacted for a fixed amount of time of 10 minutes with decreasing temperatures (entries d, e and f) which caused a decrease of the RCC. The prolonged reaction time of 15 minutes in combination with temperatures of 90°C and 100°C (entries g and h) showed the highest RCC of 57% for the latter. The alcohol enhanced protocol was afterwards applied and unexpectedly showed a highly detrimental effect (entry m). Finally, attempt to downscale the reaction by using only 5 μ moles of precursor and copper mediator showed a lowered RCC and was therefore discarded (entry n). During the course of optimization, results obtained from a different project indicated DMI as the best solvent for the radiofluorination of boronic acid pinacol esters.⁵⁴ When tested, a high RCC of 57 % was obtained (entry i). Afterwards, a non basic salt, namely TEAOTf, was used for the elution of the fixed fluoride-18, showing slight decrease in RCC (entry l). All these conditions were tested twice on the N protected precursor but no conversion was ever observed (Scheme 64). The tests were carried out on different batches of precursors which underwent several drying cycles to ensure completely dry conditions, even though not strictly required by the procedure. NMR analysis of (*S*)- and (*R*)-**49** resulted clean therefore an operator mistake was excluded. Suspecting the involvement of the unprotected amine on the benzylic linker, the precursor was spiked in a benchmark reaction as previously described (paragraph 3.3.2) but the overall RCC was not hampered. This result excluded the involvement of the NH in the reaction's impairment. In conclusions, conditions described in Table 8, entry i were found optimal for the production of [¹⁸F](*S*)-**46d** and [¹⁸F](*R*)-**46d** and were therefore applied. To this end, fluoride-18 was eluted with a TEAB methanolic solution, further dried and reacted with equimolar amounts of (*S*)- or (*R*)-**50** and Cu(4-PhePy)₄(ClO₄)₂, previously dissolved in DMI. The mixture was heated at 100°C for 15 minutes. The protecting group was cleaved with addition of 0.25M NaOH_{aq} in methanol (200 μ L) at 80°C for 3 minutes, followed by acidification with 5% TFA in acetonitrile (200 μ L). As performed for [¹⁸F]mIDH-138, the crude mixture was first fixed on a HLB cartridge, eluted with 1.5 mL of ACN:water mixture and injected in the semi preparative HPLC. The pyridone moiety confers a higher polarity to the molecule which was therefore purified with 28% ACN in water with a retention time of 35-39 minutes. The eluate was diluted with water (around 3 times the volume of the eluate) to undergo a second SPE and was eluted from the HLB cartridge with 1 mL of ethanol. When performed on the O-protected precursors (*S*)- and (*R*)-**50**, the corresponding [¹⁸F](*S*)-**46d** and [¹⁸F](*R*)-**46d** were obtained with a radiochemical conversion of 61 \pm 13% (n = 6), radiochemical yield of 50 \pm 10% (n = 4), a molar activity of 102-275 GBq/ μ mol (start activities of about 1 GBq) (n = 2) and a radiochemical purity >99%.



Scheme 64: Radiosynthesis of $[^{18}\text{F}](\text{S})\text{-46d}$ and $[^{18}\text{F}](\text{R})\text{-46d}$

Procedure: a) Elution of $^{18}\text{F}^-$ with TEAB in MeOH, evaporation. Addition of $\text{Cu}(4\text{-PhePy})_4(\text{ClO}_4)_2$ and $(\text{S})\text{-49}$ or $(\text{S})\text{-50}$ (10 μmol each) dissolved in 500 μL DMI, 100°C, 15 min; b) NaOH_{aq} 0.25M in MeOH 200 μL , 80°C, 3 min followed by quench with 5% TFA in ACN 200 μL .

The protodeboronated impurity, whose formation was confirmed via HPLC analysis via coinjection of the compound **30f**, could be separated from the desired radiotracer via semi-preparative HPLC (Experimental part) and content of residual solvents and copper were under the acceptable limit.

3.4.3 Determination of absolute configuration

The methylation of sulfinimines introduces a chiral centre, which, as known in literature, produces two diastereoisomers with a good diastereomeric excess. The major product results from the nucleophile's attack on the face occupied by the chiral auxiliary, while the minor results from the attack on the opposite face. In the methylation carried out on compounds **41d-f** it was possible to identify and isolate the two diastereoisomers: stereochemistry *S,R*- was assigned to the major product and the *R,R*- to the minor one.

This assignment was applied to all subsequent intermediates of the syntheses, to the final reference compounds **(S)-46d** and **(R)-46d** and radiofluorination precursors **(S)-**, **(R)-49** and **(S)-**, **(R)-50** due to the impossibility of verifying their absolute stereochemistry by X-ray technique and none of them being known in the literature. The optical rotation of the reference compounds and O- and N-protected precursors was analysed by polarimeter (Krüss P8000-TF), and the opposite chirality of each pair was confirmed (Experimental part). After the publication of Weber's results, it was possible to compare the NMRs of the fluorinated intermediates **42d** and **43d** with those reported in the literature.

They, in fact, had also assigned the absolute configuration via circular dichroism. The reported stereochemistry was in line with what assigned to all the intermediates and final compounds on the base of literature. After the stereochemistry of compounds **42d** and **43d** had been confidently assigned, it was possible to trace the absolute stereochemistry of the reference compounds but also of the obtained radiotracers. In particular, the latter made it possible to confidently assign the stereochemistry of the precursors, assuming that radiofluorination could not have resulted in a complete reversal of the stereochemistry at the methyl site. Indeed, by means of chiral HPLC it was possible to confirm an enantiomeric excess of 100% of the radiotracers obtained from radiofluorinations carried out on (*R*)-**50** and (*S*)-**50**. The assignment of the radiotracers stereochemistry was finally performed by co-injection with the reference compounds in chiral HPLC. The absolute configuration of the 6-H products was not assigned due to their role as reference compounds for analytical HPLC chromatography.

3.4.4 Biological evaluation of 6-[¹⁸F]Fluoro-(*S*)-olutasidenib [¹⁸F](*S*)-**46d** and 6-[¹⁸F]Fluoro-(*R*)-olutasidenib [¹⁸F](*R*)-**46d** and reference compounds (*S*)-**46d** and (*R*)-**46d**

Olutasidenib **FT-2102** has been approved for the treatment of AML and is currently undergoing clinical trials for the treatment of mIDH1 gliomas in brain. Its biological activity was tested by Caravella and found to be excellent. After synthesising the corresponding radiofluorinated tracer [¹⁸F](*S*)-**46d**, its inhibitory constant and its uptake into cells were tested in our laboratories. In addition, the same properties were also evaluated for the *R*-enantiomer, which was not tested by Caravella because aware of the fact that the orientation of (*R*)-methyl was disadvantageous for inhibition. The physico-chemical properties, such as stability in serum and solution and the lipophilicity, were tested on one of the two enantiomers indistinctly and assigned to both.

3.4.4.1 Stability of 6-[¹⁸F]Fluoro-(*S*)-olutasidenib and 6-[¹⁸F]Fluoro-(*R*)-olutasidenib in rat blood serum

Radiotracer [¹⁸F](*R*)-**46d** was formulated and an aliquot (1 μL) was added to 500μL of rat blood serum, preheated at 37°C. After 5, 15, 30 and 60 minutes, equal aliquots were taken and added to a fixed volume of acetonitrile, used to denature the blood proteins. For each time slot, the analysis was repeated in triplicate with radio-TLC and compared with the reference compound (Figure 32).

Baseline and frontline, as well as the non-radioactive reference compound, were spotted with radioactivity in order to be visualized at the phosphor imager.

No defluorination or formation of radiometabolites could be observed over one hour. Additionally, the recovery of radioactivity in organic solution could be measured by separating the acetonitrile from the plasma proteins (solid phase) and was always found to be around 85-90%.

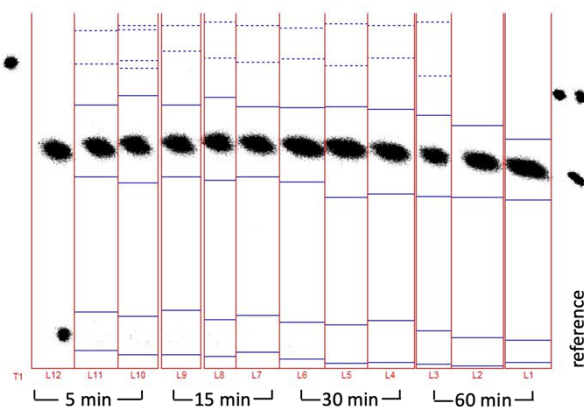


Figure 32: Radio TLC of $[^{18}\text{F}](\text{R})46\text{d}$ incubated in rat serum at 37°C for the indicated times (three lanes for each incubation time) and reference compound for comparison. TLC developed with 80% ethylacetate in hexane

3.4.4.2 Stability of 6- $[^{18}\text{F}]$ Fluoro-(S)-olutasidenib and 6- $[^{18}\text{F}]$ Fluoro-(R)-olutasidenib in solution

A small aliquot of radiotracer $[^{18}\text{F}](\text{S})-46\text{d}$ dissolved in DMSO was added to $500\mu\text{L}$ of PBS buffer and left at room temperature for a maximum of 3 hours.

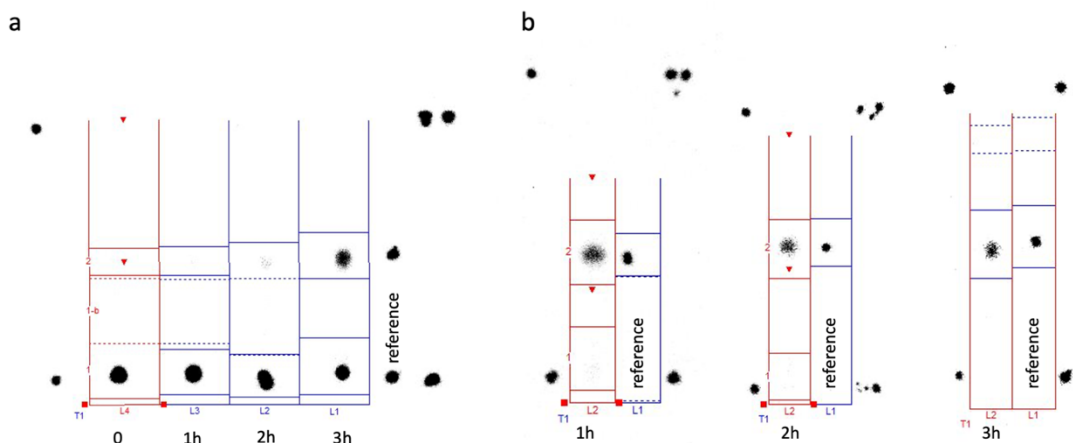


Figure 33: Radio TLC of $[^{18}\text{F}](\text{S})46\text{d}$ in PBS solution for the indicated times and reference compound for comparison. TLC developed with 80% ethylacetate in hexane

At the starting point and at each hour, the same volume of $2.5\mu\text{L}$ was taken and spotted on a TLC with the reference compound. Complete defluorination could be observed at $t = 0$ and 1h, probably due to silica degradation. Additionally, severe defluorination was observed after 2 hours and partial

after 3 hours (Figure 33a). Interestingly, the degradation was registered for the reference compound as well. For this reason, the test was repeated and the aliquots were spotted on separate TLCs after 1h, 2h and 3h and each was developed immediately, together with the reference compound (Figure 33b). With this procedure no sign of defluorination was detected, indicating full stability of the radiotracer.

3.4.4.3 Stability of reference compound (S)-46d

A 1 mg/mL solution of the reference compound (S)-46d was prepared in DMSO and injected in the analytical HPLC every few hours for a total amount of 30 hours to study the compound's stability in solution.

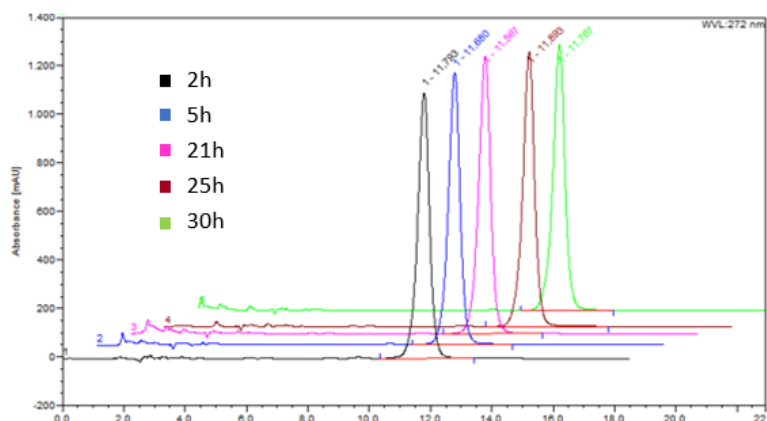
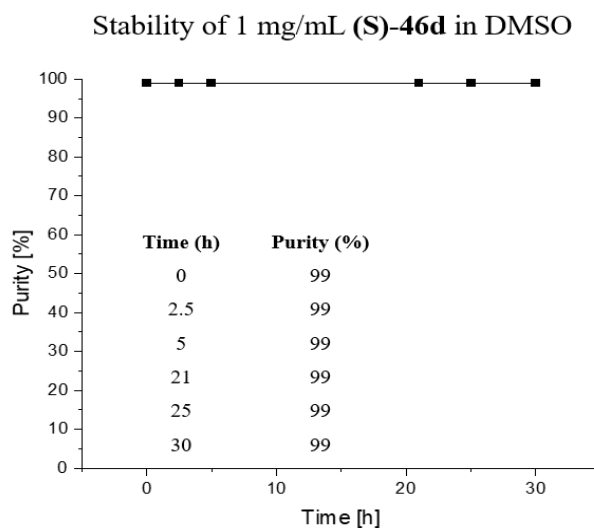


Figure 34: Stacked chromatograms of reference compound (S)-46d in DMSO solution stored at room temperature and analyzed for 30 hours

All UV active peaks were integrated and the area of the reference compound divided by the total area of the peaks to give a percentage of purity during time. As expected, 99% purity was retained between 0 and 30 hours indicating perfect stability (Figure 33, Graph 4), due to the presence of the methyl group on the benzylic linker.



Graph 4: Stability of (S)-46d in 1 mg/mL solution of DMSO

3.4.4.4 LogD

A small aliquot (0.5-1.0 μL) of [^{18}F](**R**)-**46d** dissolved in organic solvent was added to a 1:1 mixture of n-octanol and aqueous solution, vortexed for two minutes and followed by separation of the two phases upon centrifugation. Equal amounts of organic and aqueous solutions were taken and separately analysed with a low gamma counter. When PBS buffer was used as aqueous solution, the final value was referred as $\log D_{7.4}$ while when water was used, the final value was defined $\log P$.

The experimentally found $\log D_{7.4}$ value of 2.51 ± 0.11 was coherent with the one calculated using the ADMETlab platform of 2.33, in the range of values considered optimal for BBB penetration. However, the experimental $\log P$ was found to have a negative value, showing high hydrophilicity when tested in water, which indicates that one or more sites are ionized at non-physiological pH.

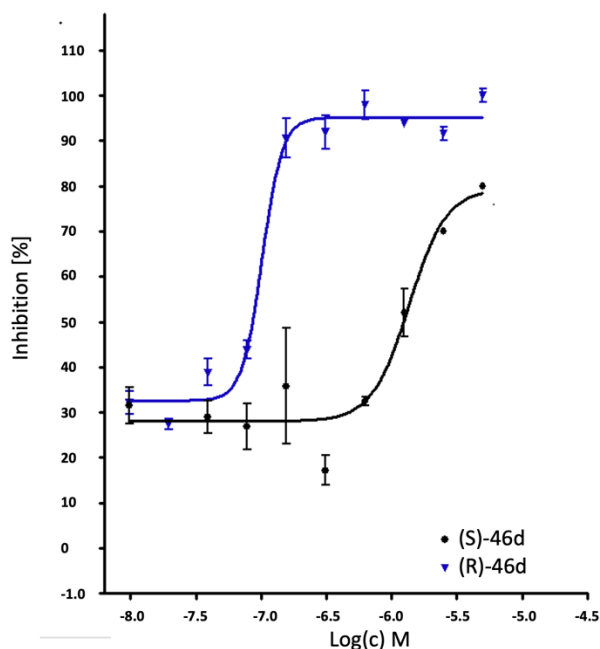
3.4.4.5 Inhibitory constant (IC_{50}) of reference compounds (**R**)-46d and (**S**)-46d

*All experiments were designed and carried out by Dr. D. Bier and Dr. D. Schneider

The non-radioactive reference compounds (**R**)-46d and (**S**)-46d (Scheme 41) were tested separately for their inhibitory potency towards the mutant R132H-IDH1 enzyme and compared to the literature known values. Caravella investigated FT-2102 but not its 6-fluorinated analogue or the *R*-enantiomer. Weber et al., on the other hand, confirmed the potency of FT-2102 previously described and experimentally determined the potency of both (**S**)-46d and (**R**)-46d, confirming the significant difference between them. Finally, we tested the two fluorinated enantiomers confirming a higher potency for the (**S**) enantiomer (Table 9).

IC_{50} (nm)	FT-2102	(S)-46d	(R)-46d
Caravella et al.	21.2 nM	Not determined	Not determined
Weber et al.	5.23 nM	22.7 nM	698 nM
This work	Not determined	103 nM	1250 nM

Table 9: IC_{50} values of (**S**)-46d and (**R**)-46d against mIDH1

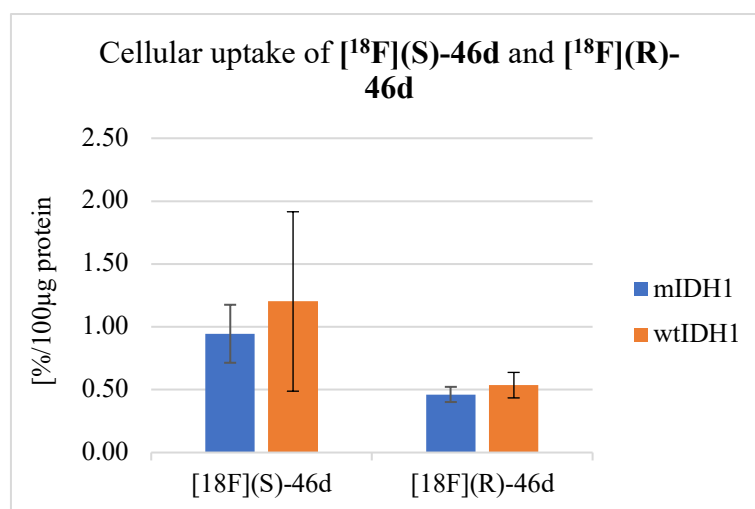


Graph 5: Inhibitory constant of (**S**)-46d and (**R**)-46d: concentration of reference compounds plotted against the percentage of inhibition towards mIDH1 enzyme

3.4.4.6 Cellular uptake and fractionation of 6-^[18F]Fluoro-(S)-olutasidenib and 6-^[18F]Fluoro-(R)-olutasidenib

*All experiments were designed and carried out by Dr. D. Bier, Dr. D. Schneider and A. Schulze

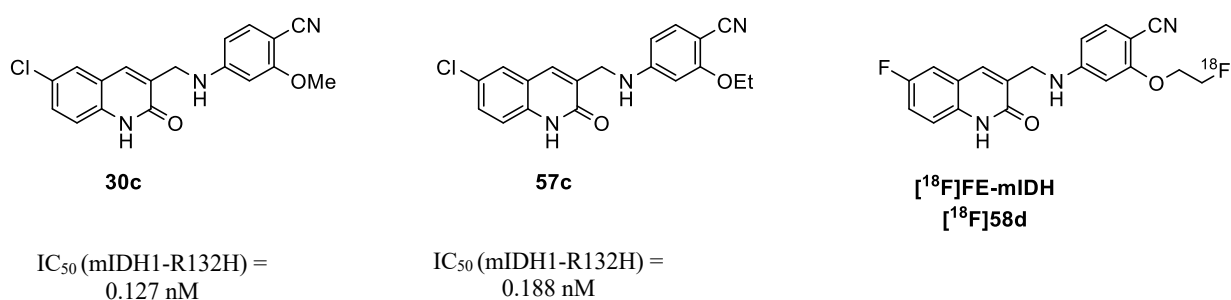
Cellular uptake experiments were performed separately on [¹⁸F](S)-46d and [¹⁸F](R)-46d with the cell lines U87MG-WT and U87MG-IDH. The experiment was repeated twice for the first radiotracer and once for the second and each measurement was performed in triplicate. An average of the results for both mutant and wild type enzymes was calculated and plotted in Graph 4. After the statistical analysis of the 6 and 3 results respectively it was possible to conclude that the radiotracer did not have a statistically significant ($p > 0.05$) higher uptake in mutant enzyme when compared to the wild type. Additionally, the amount of tracer internalized in the cells could be measured upon cell fractionation and was found to be around 90%, proving that the tracer can reach the cytoplasm, where the IDH1 enzymes reside. It needs to be noticed that 6-^[18F]Fluoro-(S)-olutasidenib [¹⁸F](S)-46d and 6-^[18F]Fluoro-(R)-olutasidenib [¹⁸F](R)-46d poorly accumulate in the cell (~ 1%) while the rest of the radioactivity is detected in the matrix. For this reason, these compounds are of scarce interest as radiotracer and no further in vivo experiments were carried out.



Graph 6: Comparison of cellular uptake of radiotracers [¹⁸F](S)-46d and [¹⁸F](R)-46d in mutant and wild type IDH1 cells.

3.5 [¹⁸F]FE-mIDH

After the encouraging results obtained from the biological evaluation of [¹⁸F]mIDH-138 in respect to 6-[¹⁸F]Fluoro-(*S*)-olutasidenib and 6-[¹⁸F]Fluoro-(*R*)-olutasidenib, the last tracer developed during this project was designed taking inspiration from the former, rather than the latter. In particular, Lin et al. investigated the introduction of an ethoxy side chain (**57c**) on the right-hand side of the molecule and demonstrated the similarity of its biological activity in respect to the methoxy bearing one (**30c**). A mesylate leaving group was installed on the ethoxy side chain of the arene and exchanged against fluoride-18 by aliphatic radiofluorination to produce [¹⁸F]FE-mIDH (Scheme 65).

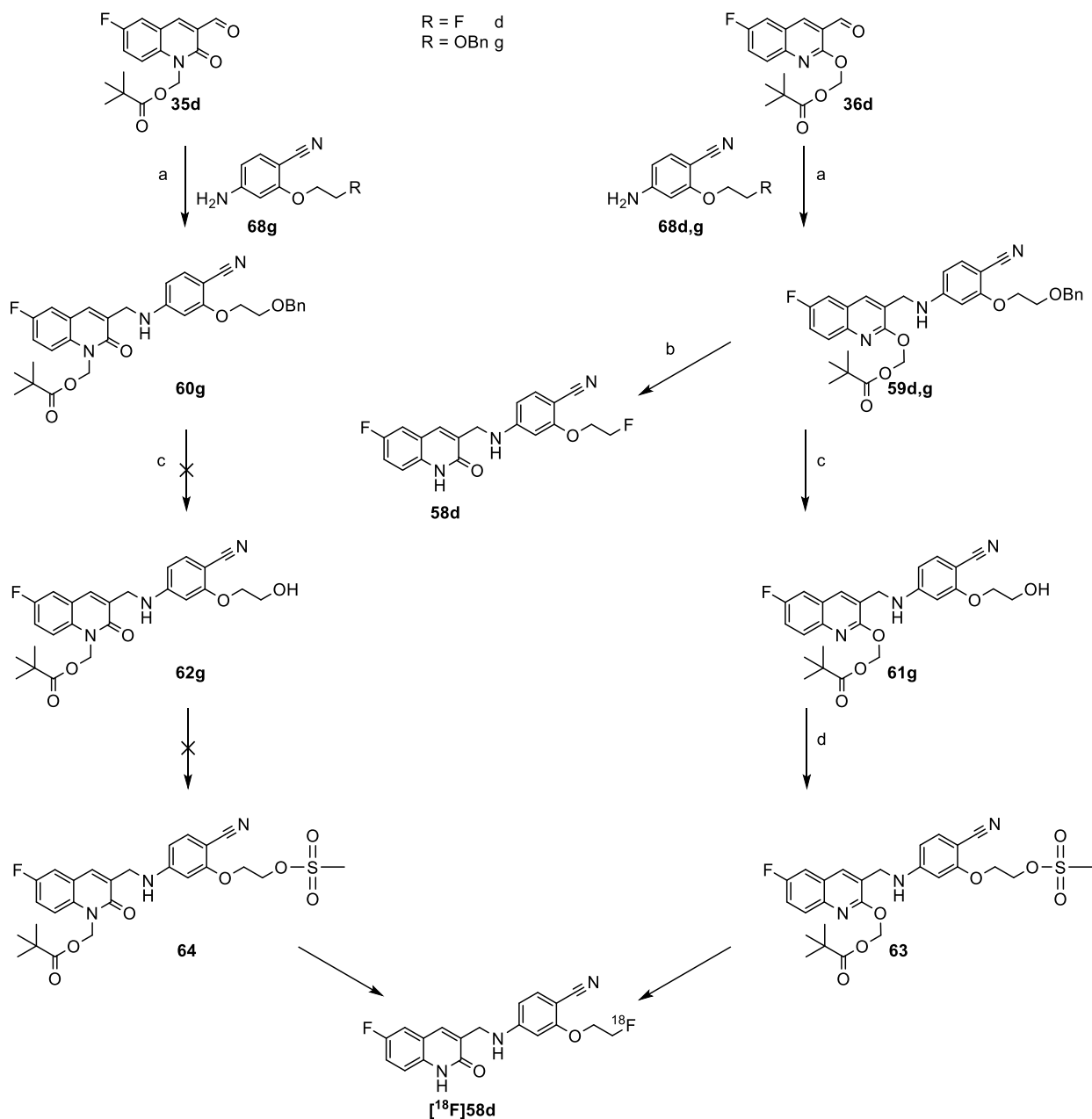


Scheme 65: Compounds 57c and 30c proposed and analyzed by Lin et al in 2019 and the proposed radiotracer [¹⁸F]FE-IDH

After the preparation of the radiotracer [¹⁸F]FE-mIDH and the non radioactive reference compound **58d**, their physico-chemical properties were experimentally measured in our labs. Additionally, **58d** was tested for its inhibitory potency towards the mutant IDH1 enzyme and the radiotracer for its selective uptake in U87 cells lines bearing both the mutant and wild type IDH1 enzymes. Finally, the obtained results were compared with the ones previously obtained.

3.5.1 Preparative organic synthesis of N-protected precursor **64**, O-protected precursor **63** and reference compound **58d**.

For the development of the radiotracer [^{18}F]**58d**, a mesyl group was selected as a leaving group due to its weakly basic nature and the delocalization of the negative charge which normally leads to its straightforward replacement (Scheme 66).

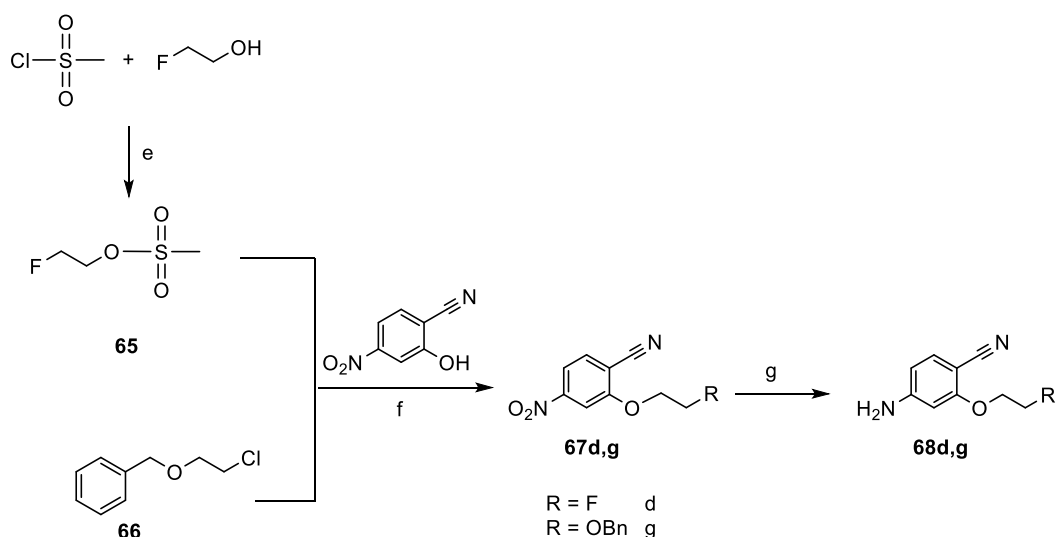


Scheme 66: Synthetic pathway for the development of precursors **63** and **64** and the non radioactive reference compound **58d**

a) 1 eq. **68g**, 2.5 eq. TMS-OTf, 1 eq. NaBH_4 , DMF [0.5], 0°C , 5 h; b) 2 mL 40% NaOH_{aq} , 2 mL MeOH, 50°C , 1h; c) 15% mass Pd/charcoal, EtOH [0.1], rt, 5h; d) 1.2 eq. Ms-Cl, 1.5 eq. NEt_3 , CH_2Cl_2 [0.2], 0°C to rt, 2.5 h.

As for the previous radiotracer [^{18}F]**30d**, the non radioactive reference compound was prepared via conjugation of the POM protected 3-formylquinolone **36d** and the aniline **68d**, followed by cleavage of the protecting group. The precursors, on the other hand, were obtained via conjugation of **35d** and **36d** and the aniline **68d** bearing a benzyl protecting group, afterwards replace by the mesyl leaving group. The benzylic group prevents that the nucleophilic attack on the intermediate imine is carried out by the hydroxyl moiety of the side chain, which, even though less reactive than the aniline, would lead to formation of a side product. Additionally, despite the fact that a copper mediator was not required for the radiosynthesis, the introduction of the POM group was carried out to both shield the acidic NH moiety and to improve the solubility of the quinolonic scaffold, hence facilitate its conjugation to the aniline.

The anilines **68d,g** were obtained via multi-step syntheses starting from 2-hydroxy-4-nitrobenzonitrile (Scheme 67).



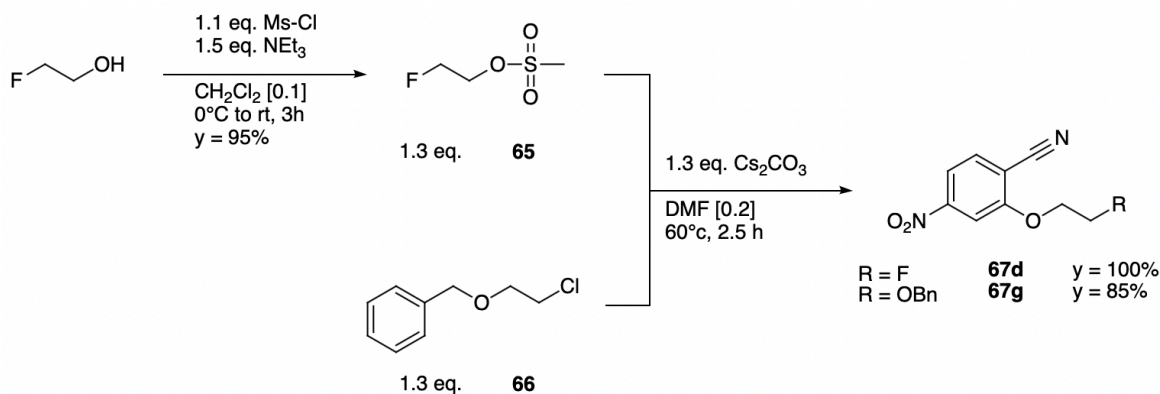
Scheme 67: Synthetic pathway for the preparation of anilines **68d** and **68g**.

Procedure: e) 1.1 eq. Ms-Cl, 1.5 eq. NEt_3 , CH_2Cl_2 [0.1], rt, 3h; f) 1.3 eq. **65** or **66**, 1.3 eq. Cs_2CO_3 , DMF [0.2], 60°C , 2.5 h; g) 10 eq. Zn powder, 10 eq. NH_4Cl , EtOH [0.2], rt.

3.5.1.1 Organic preparation of 4-amino-2-(2-fluoroethoxy)benzonitrile **68d** and 4-amino-2-(2-(benzyloxy)ethoxy)benzonitrile **68g**

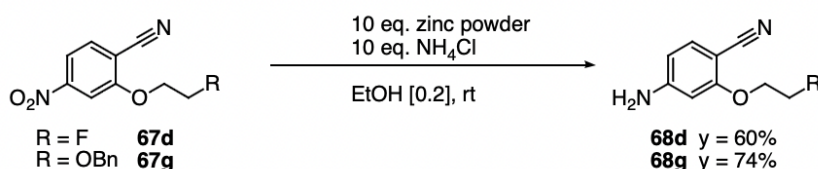
As depicted in scheme 66, the left-hand side of the final compounds, namely the 6-fluoro-3-formylquinolone, is shared by all the structures, unlike the one on the right-hand side, which can either bear the fluorine atom **68d** or the benzyl protecting group **68g**. For this purpose, 2-hydroxy-4-

nitrobenzonitrile was treated with the commercially available ((2-chloroethoxy)methyl)benzene **66** or 2-fluoroethyl methanesulfonate **65** (Scheme 68). The latter was obtained pure in 95 % yield by treatment of fluoroethyl alcohol with mesyl chloride in dichloromethane and used without need of further purification. Afterwards, 2-hydroxy-4-nitrobenzonitrile was treated with cesium carbonate and with excess of compounds **65** or **66** to obtain **67d** and **67g** in high yields after column chromatography.



*Scheme 68: Preparation of **65** and 4-nitrobenzonitriles **67d** and **67g***

Finally, the obtained scaffolds were dissolved in ethanol with excess of ammonium chloride and zinc powder to reduce the nitro group. The products, 4-amino-2-(2-fluoroethoxy)benzonitrile **68d** and 4-amino-2-(2-(benzyloxy)ethoxy)benzonitrile **68g**, were obtained in 60 and 74% yield respectively (Scheme 69).

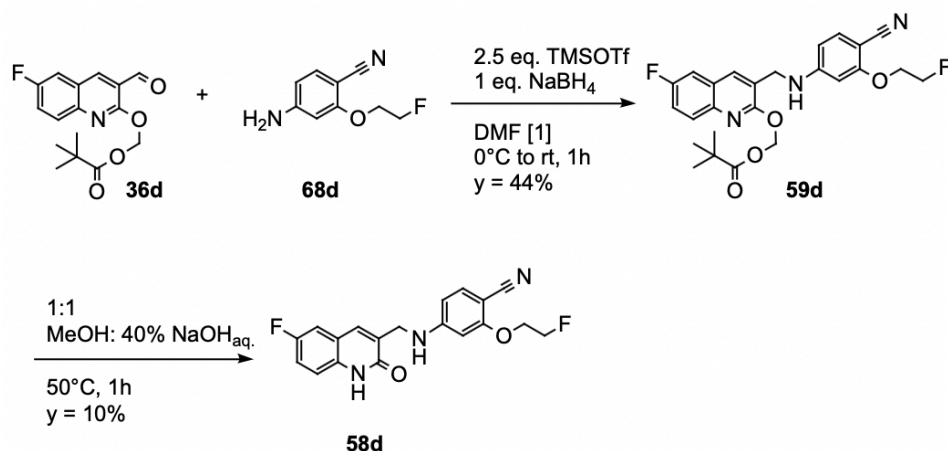


*Scheme 69: Reduction of benzonitriles **67d,g** to anilines **68d,g** with zinc and ammonium chloride*

3.5.1.2 Organic preparation of non radioactive reference compound **58d**

For the preparation of 4-(((6-fluoro-2-oxo-1,2-dihydroquinolin-3-yl)methyl)amino)-2-(2-fluoroethoxy)benzonitrile **58d**, the O-protected 6-fluoroquinolone **36d** and aniline **68d** were treated with trimethylsilyl triflate in DMF, followed by addition of NaBH₄ as reducing agent (Scheme 70). The O-protected reference compound could be isolated in 44% yield after column chromatography, before being suspended in a 1:1 mixture of methanol and 40% NaOH_{aq.}. The cleavage of the

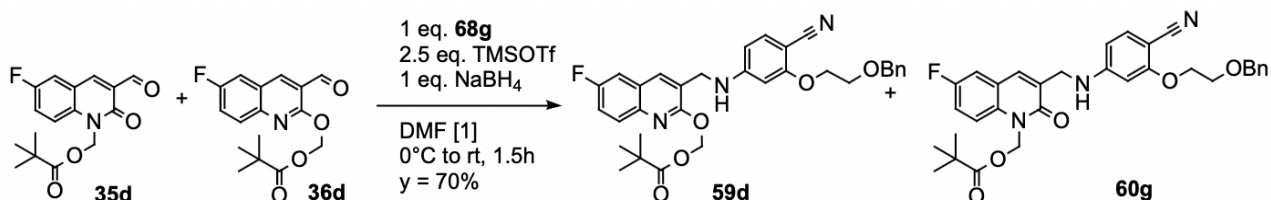
protecting group was carried out at 50°C and was completed in one hour, when the solution, initially turbid, became transparent and clear. After evaporation of methanol and addition of cold water, the pure product precipitated and could be filtered in 10% yield.



Scheme 70: Reductive amination for the preparation of **59d** and POM cleavage to furnish the non radioactive reference compound **58d**

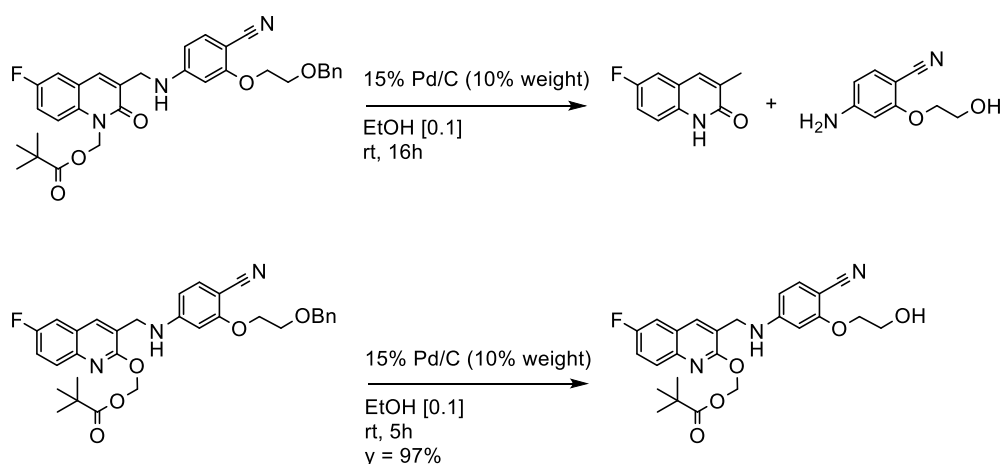
3.5.1.3 Organic preparation of precursors **63** and **64**

Compounds **59g** and **60g** were obtained via reductive amination of N- and O-protected quinolones **35d** and **36d** with 4-amino-2-(2-(benzyloxy)ethoxy)benzonitrile **68g**. The reaction was performed following the same procedure as the one used for the preparation of the non radioactive reference compound **58d**. Complete consumption of both quinolones was reached after 1.5 hours and the crude mixture was purified by column chromatography to furnish 2-(2-cyano-5-(((6-fluoro-2-((pivaloyloxy)methoxy)quinolin-3-yl)methyl)amino)phenoxy)ethyl benzoate **59g** and 2-(2-cyano-5-(((6-fluoro-2-oxo-1-((pivaloyloxy)methyl)-1,2-dihydroquinolin-3-yl)methyl)amino)phenoxy)ethyl benzoate **60g** in a total yield of 70% (Scheme 66), 44% and 27% respectively (Scheme 71).



Scheme 71: Reductive amination for the preparation of **59g** and **60g**

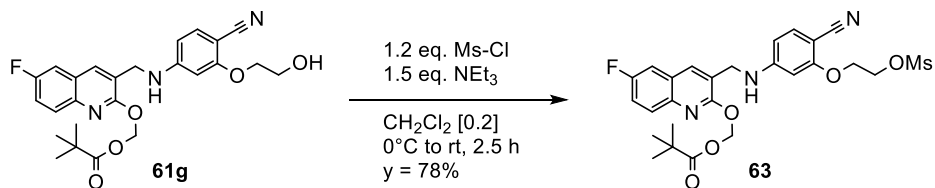
After the conjugation, the benzyl protecting group could be removed using the conventional procedure with palladium on charcoal and a hydrogen stream. To this purpose, the two compounds were dried in separate flasks and dissolved in ethanol. Finally, Pd/C was added and a hydrogen stream applied for ten minutes, followed by application of a balloon filled with H₂ and stirring for 16h. The O-protected compound was successfully debenzylated with a 97% yield upon filtration of the charcoal. However, when the same conditions were applied to the N-protected isomer, complete degradation was observed (Scheme 72).



Scheme 72: Removal of benzyl protecting group via hydrogenation

The two degradation products were identified via mass analysis as being derived from the cleavage of the benzylic linker which conjugates the quinolone scaffold to the aniline. It seems reasonable to think that while this linker is shielded completely by the POM group when the latter is attached to the oxygen of the quinolone (**59g**), the C-N bond is more susceptible to attack when the POM group is connected to the nitrogen of the quinolone (**60g**). It could be speculated that a lower amount of catalyst or a lower temperature of reaction, together with a shorter reaction time could spare the C-N bond from cleavage. However, when the reaction was repeated for 3 hours, formation of the same products was observed. When it was tested at 0°C, no consumption of starting material could be observed, while at 10°C formation of the two side products was observed from the very beginning. A final attempt was carried out using trimethylsilyl iodide as dealkylating agent.²⁵⁰ Alkyl methyl ethers react with trimethyl silyl iodides to afford mixtures of dealkylated products where the demethylated products are generally the major ones. The ethers react in a fast step to produce the silylated oxonium iodide which can then form two couples of silylated and iodinated products through a S_N1 or S_N2 mechanism. In case of excess of Me₃SiI, the silylated esters can react with iodide and form the corresponding alkyl iodide. To avoid formation of the iodinated derivative, **60g** was treated with 1

equivalent of trimethylsilyl chloride and 1 equivalent of sodium iodide in acetonitrile, to form the reagent *in situ*.²⁵¹ Start of the reaction was confirmed by immediate formation of sodium chloride but TLC analysis every two hours showed formation of multiple products where only a minor amount represented the desired one. Finally, **60g** was treated with mesyl chloride and triethylamine in dichloromethane and ((3-(((4-cyano-3-(2-((methylsulfonyl)oxy)ethoxy)phenyl)amino)methyl)-6-fluoroquinolin-2-yl)oxy)methyl pivalate **63** obtained with 78% yield (Scheme 73).

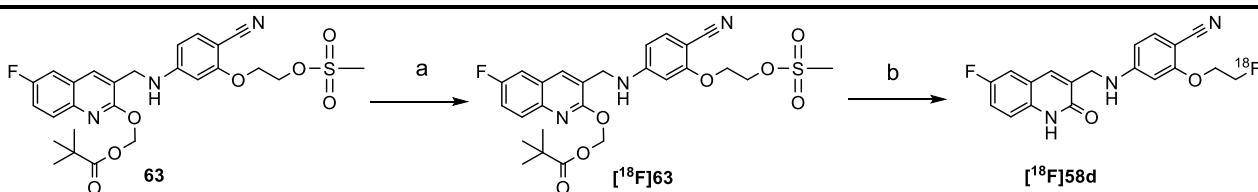


*Scheme 73: Introduction of a mesyl leaving group to obtain the radiofluorination precursor **63***

3.5.2 Aliphatic radiofluorination of ((3-(((4-cyano-3-(2-((methylsulfonyl)oxy)ethoxy)phenyl)amino)methyl)-6-fluoroquinolin-2-yl)oxy)methyl pivalate **63**

Radiofluorination of O-protected precursor **63** was carried out with the conventional protocol for aliphatic radiofluorination in acetonitrile while preprocessing of fluoride was carried out with the “minimalist-like” approach. Fluoride-18 was fixed on a QMA cartridge and eluted with a 1 mg/mL TEAB solution in methanol, as already performed for the previous tracers. After methanol evaporation, a solution of 10 μ moles of precursor **63** in acetonitrile was added to the reactor, afterwards sealed with a rubber septum, and the mixture stirred at 85°C for ten minutes. Cleavage of POM protecting group was carried out with the previously developed conditions, by addition of 200 μ L of 0.25 M NaOH_{aq.}, stirred for 3 minutes at 85°C (Table 10).

This procedure yielded the desired radiotracer in $9.67 \pm 3.20\%$ RCC without formation of active side products (Table 10, entry a). Increase of reaction time to 15 minutes showed no improvement, with a RCC of $8.30 \pm 2.99\%$ (entry b).



Entry	63 (μ mol)	Solvent	T	Time	Salt in MeOH	RCC $[^{18}\text{F}]\mathbf{58d}$ (%)
a	10 (5.4 mg)	ACN	85 °C	10 min	1 mg TEAB /mL	9.67 \pm 3.20 (n = 3)
b	10 (5.4 mg)	ACN	85°C	15 min	1 mg TEAB /mL	8.30 \pm 2.99 (n = 3)

Table 10: Radiochemical conversion of $[^{18}\text{F}]\mathbf{58d}$. Procedure: a) Elution of $^{18}\text{F}^-$ with TEAB in MeOH, evaporation. Addition of 10 μ mol of **63** dissolved in 500 μ L ACN, 85°C, 10 min; b) NaOH_{aq.} 0.25M, 200 μ L, 80°C, 3 min.

HPLC analysis of a test reaction before (without water quench) and after the deprotection showed that the amount of fluoride increased dramatically after the addition of sodium hydroxide, suggesting that the deprotection conditions could be too harsh (data not reported). Fluoroethyl substituents are indeed base sensitive and known to degrade, leading to formation of the volatile side products

[¹⁸F]fluoroethanol and [¹⁸F]vinyl fluoride, even in presence of the sole base used to preprocess [¹⁸F]fluoride.²⁵²

For this reason, the two steps of the radiosynthesis, namely introduction of [¹⁸F]fluoride and deprotection of POM group, were separately studied and optimized. Initially, the radiofluorination was carried out with 10 μmoles of precursor **63** in 500 μL of acetonitrile at 85°C for 10 minutes, followed by addition of sodium hydroxide solutions at different concentrations and temperatures (Table 11).

Entry	T	Time	Volume	NaOH _{aq.}	Impurity (4.4 min)	[¹⁸ F] 58d (12.56 min)	[¹⁸ F] 63 (21.80 min)
a	85 °C	3 min	200 μL	0.05 M in H ₂ O	6.04 %	4.00 %	2.04 %
b	rt	10 min	200 μL	0.25 M in H ₂ O	9.4 %	31.47%	0 %
c	rt	10 min	200 μL	0.25 M in H ₂ O	0 %	24.00 %	27 %
d	rt	10 min	200 μL	0.25 M in H ₂ O	2.98 %	2.45 %	2.89 %
e	rt	10 min	200 μL	0.25 M in H ₂ O	3.67 %	5.78 %	5.02 %
f	30 °C	10 min	175 μL	0.1 M in EtOH	6.33 %	14.42 %	3.26 %
g	30 °C	10 min	175 μL	0.1 M in EtOH	9.82 %	7.19 %	0 %
h	30 °C	7 min	175 μL	0.1 M in EtOH	0 %	45.99 %	4.67 %
i*	30 °C	10 min	175 μL	0.1 M in EtOH	0 %	47.40 %	0 %
l	30 °C	10 min	175 μL	0.1 M in EtOH	0 %	10.00 %	0 %
m	35 °C	5 min	200 μL	0.1 M in EtOH	0 %	30.32 %	5.40 %
n	35 °C	10 min	200 μL	0.1 M in EtOH	0 %	24.05 %	0 %

* An aliquot was taken and analyzed without previous addition of water

*Table 11: Optimization of deprotection conditions for the preparation of [¹⁸F]**58d***

Use of a diluted basic solution resulted in formation of an undefined polar impurity and a residue of the intermediate [¹⁸F]**63** (Table 11, entry a). Reduction of the reaction temperature in combination with an increase of the reaction time to 10 minutes led to higher conversions (entries b, c, d and e). However, complete deprotection of [¹⁸F]**63** could never be achieved, as well as the formation of the

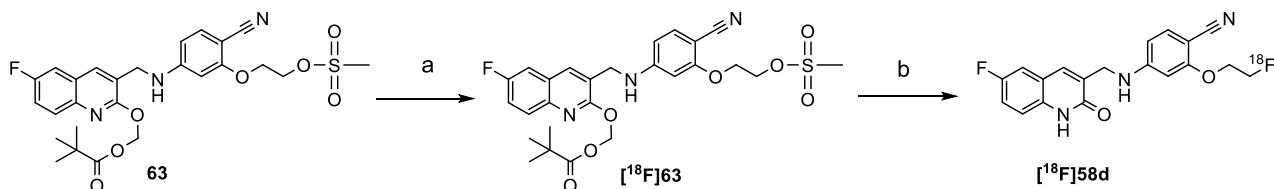
impurity could never be avoided. Finally, replacement of water with a polar solvent, like ethanol, and lower concentration of NaOH_{aq.} to 0.1 M led to improved conversions (entry f). A smaller volume of 175 μ L of 0.1M NaOH_{aq.} in ethanol was added after the radiofluorination and stirred at 30°C for 10 minutes leading to formation of the desired radiotracer as major product (f, g, h, i and l). Analysis of aliquots of the mixture after 7 and 10 minutes (entries h and i) indicated that the latter represents the minimum amount of time required to fully deprotect the intermediate [¹⁸F]**63**. Moreover, a slight increase in volume and temperature seemed reasonable to reach the complete deprotection of the intermediate since in few occasions the deprotection resulted incomplete, probably due to loss of small amounts of the basic solution on the reactor walls. Therefore, a test with 200 μ L of the solution at 35°C was carried out (entry m) but failed, confirming the need for a longer deprotection time, as confirmed by entry n. Afterwards, the radiofluorination was studied with different conditions (elution salts, solvents, temperatures and reaction times) to find the highest possible radiochemical conversion (RCC).

Entry	63 (μ mol)	Solvent	T	Time	Salt in MeOH	RCC (%)	
a	10 (5.4 mg)	ACN	85°C	10 min	1 mg TEAB /mL	5.30	\pm 4.30 (n = 3)
b	10 (5.4 mg)	ACN	85°C	10 min	0.5 mg Me ₄ NOTf / 0.5 mL	21.02	\pm 5.64 (n = 3)
c	10 (5.4 mg)	ACN	85°C	15 min	0.5 mg Me ₄ NOTf / 0.5 mL	23.51	\pm 1.48 (n = 2)
d	3.5 (2 mg)	ACN	85°C	15 min	0.5 mg Me ₄ NOTf / 0.5 mL	32.82	\pm 9.93 (n = 3)
e	1.8 (1 mg)	ACN	85°C	15 min	0.5 mg Me ₄ NOTf / 0.5 mL	24.14	\pm 4.57 (n = 2)
f	3.5 (2 mg)	DMF	100°C	15 min	0.5 mg Me ₄ NOTf / 0.5 mL	5.22	\pm 0.22 (n = 2)
g	3.5 (2 mg)	DMSO	100°C	15 min	0.5 mg Me ₄ NOTf / 0.5 mL	24.47	\pm 2.78 (n = 2)
h	3.5 (2 mg)	DMSO	120°C	15 min	0.5 mg Me ₄ NOTf / 0.5 mL	12.71	\pm 4.13 (n = 2)

Table 12: Optimization of radiofluorination conditions for the preparation of [¹⁸F]**63**

The reaction was first carried out with 10 μ moles of precursor **63** in 500 μ L of acetonitrile at 85°C for 10 minutes, followed by addition of 200 μ L of water before injection of an aliquot in the analytical

HPLC for the evaluation of the RCC. Elution with 1 mg/mL TEAB in methanol yielded the desired protected radiotracer [^{18}F]**63** in RCCs lower than 10% (Table 12, entry a) while elution with 0.5 mg/mL of the non basic Me_4NOTf rose the conversion to $20 \pm 9.90\%$ (entry b), indicating that a lower basicity leads to better conversions, probably due to partial degradation of the precursor. Increased reaction time to 15 minutes (entry c) led to a slight improvement as well as reduction of the precursor to $3.5\ \mu\text{moles}$ (entry d), but not to 1.8 (entry e). Replacement of acetonitrile to DMF (entry f) or DMSO at both $100\ ^\circ\text{C}$ (entry g) and $120\ ^\circ\text{C}$ (entry h) resulted in poor conversions and was therefore discarded, while conditions (d) were selected as optimal. The latter were finally applied to all further experiments and used to prepare the radiotracer for biological evaluations, together with the deprotection procedure previously optimized (Scheme 75).



*Scheme 75: Radiosynthesis of [^{18}F]**58d***

*Procedure: a) Elution of $^{18}\text{F}^-$ with Me_4NOTf in MeOH , evaporation. Addition of 2 mg of **63** dissolved in 500 μL ACN , 85°C , 15 min; b) NaOH_{aq} . 0.1M in ethanol 100 μL , 35°C , 10 min.*

Since the amount of precursor was decreased to 2 mg, the amount of base was decreased accordingly to 100 μL to yield the final radiotracer with a radiochemical conversion of $30 \pm 8\%$ ($n = 6$). The reaction was quenched with 400 μL of water and the total volume of 1 mL was injected in the semi-preparative HPLC, without need of previous SPE purification. After isolation, the desired radiotracer [^{18}F]**58d** was obtained with a radiochemical yield of $26 \pm 8\%$ ($n = 3$), a molar activity of 14-47 $\text{GBq}/\mu\text{mol}$ ($n = 4$) (with start activity of around 1 GBq) and a radiochemical purity $>99\%$.

Despite the mild deprotection conditions, a small amount of the precursor was deprotected, generating 2-(2-cyano-5-(((6-fluoro-2-oxo-1,2-dihydroquinolin-3-yl)methyl)amino)phenoxy)ethyl methanesulfonate **69** as chemical impurity (Figure 35). The polarities, hence the retention times, of the impurity **69** and the desired radiotracer [^{18}F]**58d**, were similar, threatening the chemical purity of the final formulation (Experimental part). However, it was possible to isolate the radiotracer in pure form with semi-preparative HPLC but only at the expense of time (Experimental part).

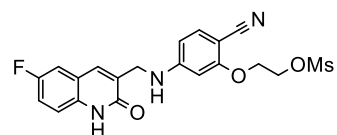


*Figure 35: Impurity **69***

3.5.3 Biological evaluation of [^{18}F]FE-mIDH [^{18}F]58d and reference compound 58d

After preparation of the radiotracer [^{18}F]58d and its non-radioactive reference compound 58d, the inhibitory constant and cellular uptake were tested, following the same procedures previously applied to [^{18}F]mIDH-138, [^{18}F](S)-46d and [^{18}F](R)-46d.

The physico-chemical properties, such as stability in serum and solution and the lipophilicity, were also experimentally calculated.

3.4.4.1 Stability of [^{18}F]58d in rat blood serum

Radiotracer [^{18}F]58d was formulated and an aliquot was added to 500 μL of rat blood serum, preheated at 37°C. After 5, 15, 30 and 60 minutes, equal aliquots were taken and added to a fixed volume of acetonitrile, used to denature the blood proteins. For each time slot, the organic solution was analysed in triplicate with radio-TLC and compared with the reference compound (Figure 36). Baseline and frontline, as well as the non-radioactive reference compound, were spotted with radioactivity in order to be visualized at the phosphor imager.

No defluorination or formation of radiometabolites could be observed over one hour. Additionally, the recovery of radioactivity in organic solution could be measured by separating the acetonitrile from the plasma proteins (solid phase) and was always found to be around 85-90%.

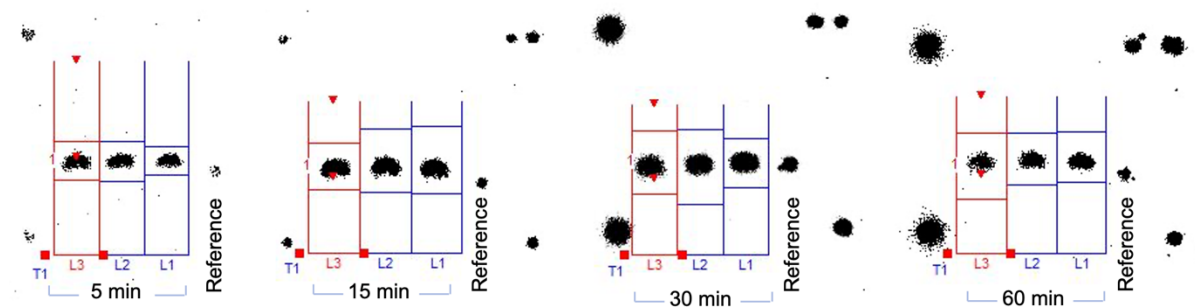


Figure 36: Radio TLC of [^{18}F]58d incubated in rat serum at 37°C for the indicated times (three lanes for each incubation time) and reference compound for comparison. TLC developed with 80% ethylacetate in hexane

3.4.4.2 Stability of [^{18}F]FE-mIDH in PBS buffer

A small aliquot of radiotracer [^{18}F]58d dissolved in DMSO (1 μL) was added to 500 μL of PBS buffer and left at room temperature for a maximum of 2 hours. At the starting point and at each hour, the same volume of 2.5 μL was taken and spotted, with the reference compound, on different TLCs, developed immediately showing full stability in buffer solution (Figure 37).

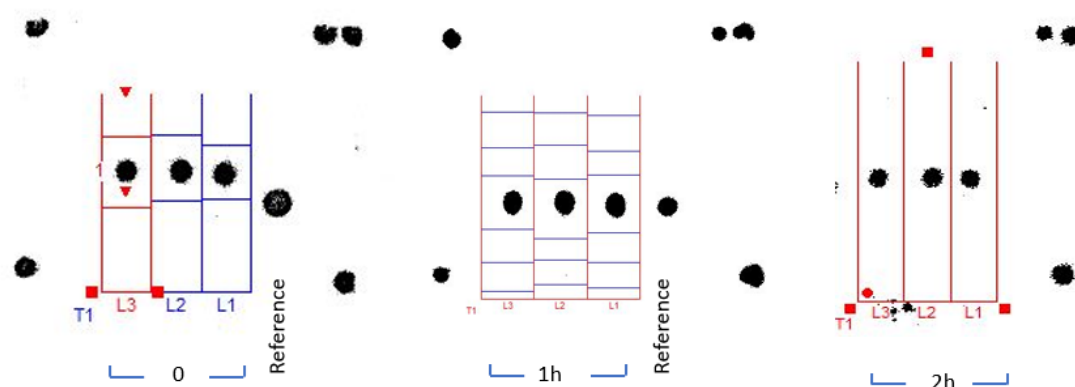


Figure 37: Radio TLC of [^{18}F]58d in PBS solution for the indicated times and reference compound for comparison. TLC developed with 80% ethylacetate in hexane

3.4.4.3 Stability of reference compound 58d in organic solution

In parallel, a 1 mg/mL solution of the reference compound (91% pure) was prepared in DMSO and injected in the analytical HPLC every few hours for a total amount of 30 hours.

Stability of 1 mg/mL 58d in DMSO

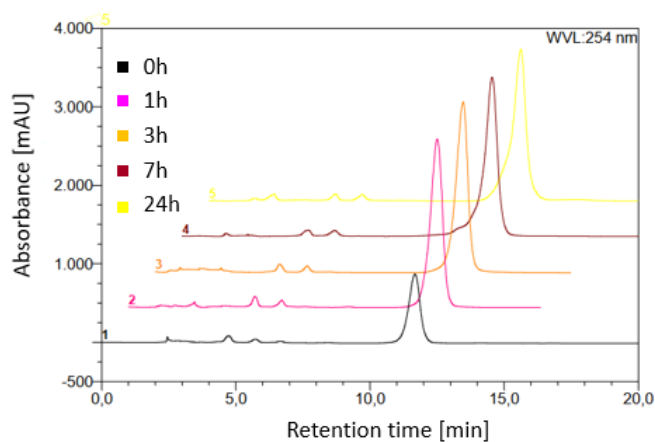
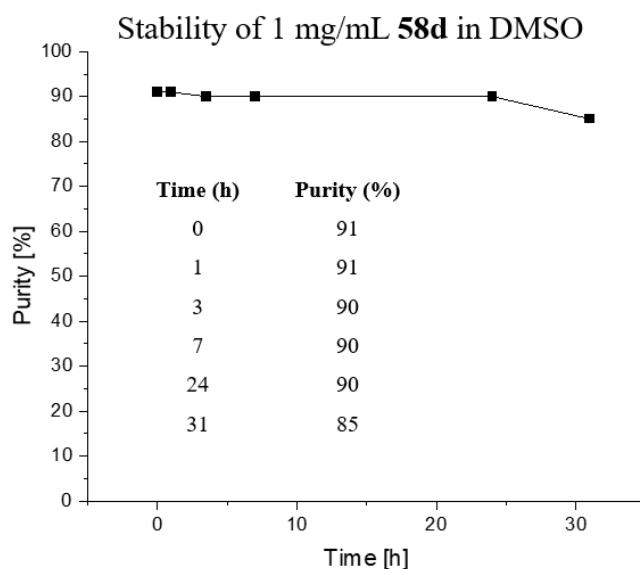


Figure 38: Stacked chromatograms of reference compound 58d in DMSO solution stored at room temperature and analyzed for 30 hours

All UV active peaks were integrated and the area of the reference compound divided by the total area of the peaks to give a percentage of purity during time. A loss of 6% purity was measured within 24 hours, indicating the same degradation pattern as for **30d**, due to the liability of the benzylic linker (Figure 38, Graph 7).



*Graph 7: Stability of **58d** in concentrated solution of 1 mg/mL of DMSO*

3.4.4.4 LogD

A small aliquot (0.5-1.0 μL) of [^{18}F]**58d** dissolved in DMSO was added to a 1:1 mixture of n-octanol and aqueous solution, vortexed for two minutes and followed by separation of the two phases upon centrifugation. Equal amounts of organic and aqueous solutions were taken and separately analysed with a low gamma counter. When PBS buffer was used as aqueous solution, the final value was referred as $\log D_{7.4}$ while when water was used, the final value was defined $\log P$.

The experimentally found $\log D_{7.4}$ value of 2.72 ± 0.06 was coherent with the one calculated using the ADMETlab platform of 2.87, while the experimental $\log P$ was found to be 2.77 ± 0.03 (ADMETlab : 2.73), confirming the suitability for CNS application.

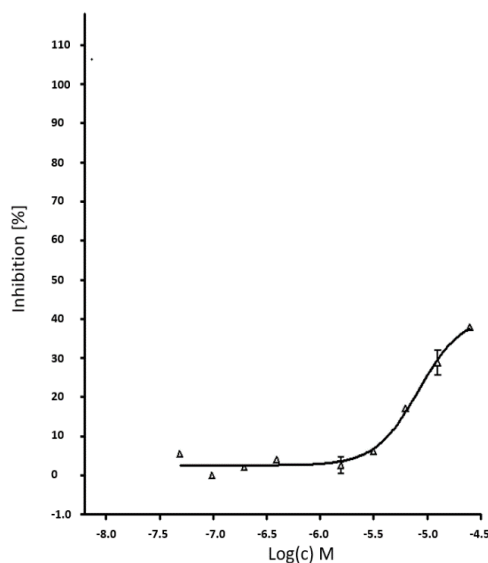
3.4.4.5 Inhibitory constant (IC_{50}) of reference compounds **58d**

*All experiments were designed and carried out by Dr. D. Bier and Dr. D. Schneider

The final compound for this project was designed by modifying a known compound, therefore no biological evaluation was available for comparison. The non-radioactive reference compounds **58d** was tested for its inhibitory potency towards the mutant R132H-IDH1 enzyme and compared to the similar compound **30d**. Interestingly, even though only a minor change had been introduced in the structure, 4-(((6-fluoro-2-oxo-1,2-dihydroquinolin-3-yl)methyl)amino)-2-(2-fluoroethoxy)benzonitrile **58d** showed inhibitory activity only in the micromolar range, showing an extremely poor biological effect.

IC_{50} 30d	IC_{50} 58d
616 nM	9100 μ M

Table 13: IC_{50} values of **30d** and **58d** against *mIDH1*

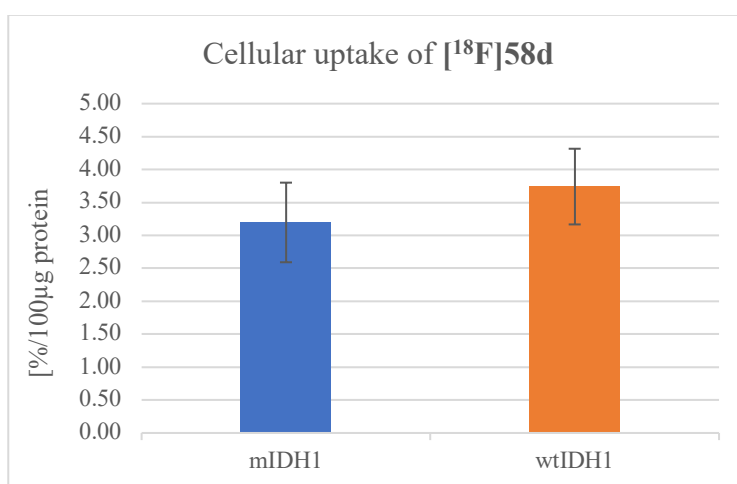


Graph 8: Inhibitory constant of **58d**: concentration of reference compounds plotted against the percentage of inhibition towards *mIDH1* enzyme

3.4.4.6 Cellular uptake and fractionation of [^{18}F]FE-mIDH

*All experiments were designed and carried out by Dr. D. Bier, Dr. D. Schneider and A. Schulze

Cellular uptake experiments were performed on [^{18}F]58d with the cell lines U87MG-WT and U87MG-IDH. The experiment was repeated four times and each measurement was performed in triplicate. An average of the results for both mutant and wild type enzymes was calculated and plotted in Graph 9 together with the standard deviation related to the measurements. After the statistical analysis of 12 results it was possible to conclude that the radiotracer had a statistically significant ($p = 0.03$) higher uptake in wild type enzyme when compared to the mutant type. Additionally, the amount of tracer internalized in the cells could be measured upon cell fractionation and was found to be around 90%, proving that the tracer can reach the cytoplasm, where the IDH1 enzymes reside.

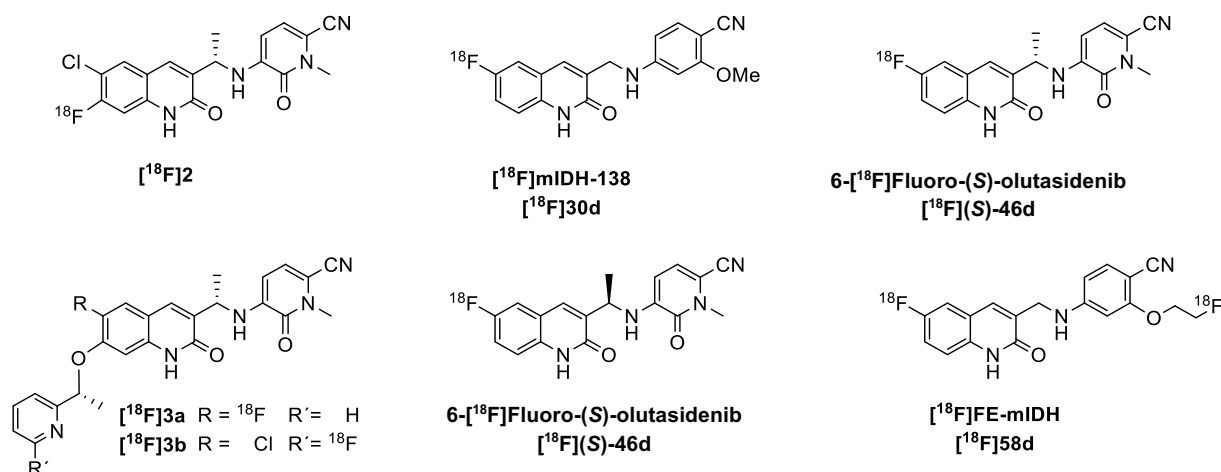


Graph 9: Cellular uptake of radiotracers [^{18}F]58d in mutant and wild type IDH1 cells.

4. Summary

Molecular imaging with PET has witnessed remarkable growth in the last decades as a powerful and non-invasive diagnostic tool. This technique is based on the detection of the γ quanta emitted after the annihilation of a positron and an electron in the surrounding medium. The positron has been previously emitted by a β^+ -emitter. Fluorine-18 is a suitable β^+ -emitter and is therefore widely used in PET imaging due to its almost ideal decay properties with regard to short half-life, high β^+ -intensity and low energy of the emitted positron. The low energy of the positron allows to obtain images with high resolution and sensitivity (the low energy of the β^+ -particle is rapidly decelerated in organs and tissues, therefore the annihilation takes place in close proximity leading to high-resolution images). The essential prerequisite for PET imaging is the development of a radiotracer, a molecule which contains a radioactive label, like F-18, and a pharmacophore, which addresses a specific biological target. In this work the molecular target was the mutated enzyme isocitrate dehydrogenase 1 (mIDH1) which is expressed in brain tumors. In this work, transition metal mediated radiofluorinations have been applied. Especially Cu-mediated radiofluorination has been widely used in the last years and this strategy allows to overcome the classical limitations related to conventional aromatic radiofluorinations. Usually, these methods require high precursor amounts or only electron deficient precursors can be labelled by conventional S_NAr radiofluorinations. Cu-mediated radiofluorination was also used in this study to prepare ^{18}F -labeled mutant isocitrate dehydrogenase inhibitors. mIDH1 is associated with gliomagenesis and expressed in 80% of low-grade gliomas (WHO grade II and III). Gliomas are usually detected with MRI or [^{18}F]fluoroethyltyrosine-PET imaging which are associated with several limitations. Thus, differentiation between gliomas expressing the mutant enzyme from those which express the wild type IDH1 enzyme is not possible. However, this information, usually obtained by biopsy, is important for the patient prognosis. Therefore, the aim of this work was to design and develop a class of selective radiotracers for the non-invasive assessment of the mIDH status. For this purpose, olutasidenib, reported in 2020 by Caravella et al., was selected as a lead due to its selective inhibition of mIDH1. Based on this structure fluorine-18 was introduced in different positions of the aromatic system, to obtain selective diagnostic tools with similar chemical and biological properties.

The first attempt to introduce F-18 in position 7 of the quinolone was not successful due to challenges during the preparation of the precursor, coming from competitive ring closure of the formylated acetanilide in the two *ortho* positions. At this point of the project it was decided to use the structure of a chemically more accessible sub potent version of olutasidenib for the development of a first radiotracer ($[^{18}F]$ mIDH-138) as a proof of concept.



The aim was to evaluate the feasibility of radiofluorination as well as to experimentally measure its physicochemical properties and to establish a suitable model for the preclinical biological evaluation. The non-radioactive reference compound **30d** was prepared, characterized and evaluated for its inhibitory potency using a commercially available enzymatic assay. An IC_{50} of 616 nM was obtained which was in line with the value of 138 nM reported in the literature. The precursor synthesis was carried out according to the literature with minor modifications. A boronic acid pinacol ester moiety was introduced in position 6 of the quinolone ring and used as a leaving group during the copper mediated radiofluorination. To this end, a pivaloyloxymethyl (POM) protecting group was introduced to protect the amide moiety, at both the N- and O-positions, in order to avoid the inactivation of the copper mediator through coordination with the quinolone moiety. Both the N- (**39**) and O-protected (**40**) precursors were radiofluorinated in dimethylacetamide (DMA) at 110°C for 10 minutes and the POM group removed by addition of 0.25M NaOH_{aq.} in MeOH (200 μ L), stirred at 85°C for 3 min. The radiotracer $[^{18}\text{F}]mIDH-138$ was obtained with RCYs of $22 \pm 11\%$ (n = 11) and $29 \pm 11\%$ (n = 30) from **39** and **40** respectively and molar activities of 13-540 GBq/ μ mol (start activities in the range of 1-4 GBq). In both cases, the formulation was carried out after HPLC purification by dissolving the isolated tracer in a mixture of PBS buffer and Tween 80. Radiochemical purities amounted to 99% were obtained and contents of residual solvents or copper were below the limit of detection. The radiotracer was found to be stable in PBS solution and in serum over 3 and 1 h respectively, without any defluorination. $\text{Log}D_{7.4}$ value was determined to 2.67 and $\text{log}P$ to 2.50. Cell uptake experiments in mIDH1 and wtIDH1 cells showed a statistically significant higher uptake in the mutated cell line in comparison to wildtype cells. Furthermore, the radiotracer was investigated in in vivo models. The chorio allantoic membrane (CAM) chicken egg model confirmed the absence of defluorination of $[^{18}\text{F}]mIDH-138$ but only a slightly higher uptake was observed in transfected in comparison to wild

type tumors in the first ten minutes, followed by a more rapid wash out. Injection of the radiotracer in 4 healthy mice showed high tracer accumulation in liver and intestine (SUV_{bw} at 2 hours = 61.91 ± 5.98 and SUV = 5344.10 ± 1465.92 respectively). Finally, metabolic stability of [¹⁸F]mIDH-138 was measured in rat serum for 1 hour at 37°C and in buffer for 3 hours at room temperature. In both cases no tracer decomposition was observed.

Encouraged by the promising results of the proof of concept study, a second radiotracer with the structure of olutasidenib (**6-[¹⁸F]fluoro-(S)-olutasidenib**) was developed by replacing the chlorine in position 6 with fluorine-18. For comparison, the *R*-enantiomer (**6-[¹⁸F]fluoro-(R)-olutasidenib**) was also prepared and tested. To this end, the precursors were prepared with the aid of a chiral auxiliary and both enantiomers could be obtained from the same starting material, isolated and converted into the (*S*)- and (*R*)-precursors with total yields of 2% and 1.5% over 17 steps. All compounds (**(S)-49**, **(R)-49**, **(S)-50** and **(R)-50**) were POM protected and boronic acid pinacol ester was used as a leaving group. Again, both *R*- and *S*- precursors were used for Cu-mediated radiofluorination in 1,3-Dimethyl-2-imidazolidinone (DMI) at 100°C for 15 minutes, followed by basification to cleave the POM protecting groups. Surprisingly, N-protected precursors did not furnish the radiolabeled products and so far the reason for no radiochemical transformation remains unclear. In contrast, the O-protected precursor yielded the desired radiotracers [¹⁸F]**(S)-46d** and [¹⁸F]**(R)-46d** in 50 ± 10% (n = 4) radiochemical yields, molar activities of 102-275 GBq/μmol (start activities in the range of 1 GBq) and radiochemical purity >99%. Both the reference compounds and the radiotracers proved to be stable in solution over 30 hours in serum and in buffer, tentatively due to the presence of the methyl group on the benzylic linker, which prevents the cleavage of the C-N bond. The reference compounds were tested for their potency towards mIDH1 and the *S*-enantiomer was 10 times more potent than the *R*-enantiomer (103 nM vs. 1250 nM). Additionally, while the log_{D7.4} was found to be in the ideal range for CNS applications (2.51), the log_P was found negative, indicating a high hydrophilicity when the aqueous phase is water. This is probably due to the fact that at least one moiety is protonated or deprotonated in water. Cellular uptake of both radiotracers showed unexpectedly poor uptake of around 1%.

Finally a fourth tracer (**[¹⁸F]FE-mIDH**) was developed mimicking the structure of the first (**[¹⁸F]mIDH-138**) with the introduction of a fluoroethoxy substituent on the arene on the right side of the molecule. Radiofluorination was carried out using the conventional aliphatic approach, therefore a mesyl group was introduced on the ethoxy side chain. The precursors were prepared by conjugating the POM protected 6-fluoroquinolones with the aniline bearing the fluoroethylmesylate substituent, obtained by debenylation and further conversion of the hydroxyl group into the mesylate leaving group in a total yield of 10% over 8 steps. The reference compound was prepared in a similar way

with a fluoroethoxy side chain, obtained in a yield of 70% over 3 synthetic steps. The reference compound showed a suitable partition coefficient both in buffer ($\log D_{7.4} = 2.72$) and water ($\log P = 2.72$). Stability tests revealed a loss of intact compound in the range of 6% over 31h (1 mg/mL compound in DMSO). Unexpectedly, **58d** showed an extremely low potency of 9100 μM against mIDH1 while the ethylated 6-chloro analogue (**57c**) developed by Caravella showed an IC_{50} similar to the methylated compound (**30c**).

The N-protected precursor **64** could not be obtained due to formation of side products during the debenzoylation. For the radiofluorination, [^{18}F]fluoride was eluted with 0.5 mg tetramethylammonium triflate (Me_4NOTf) in 0.5 mL methanol and dried. The O-protected precursor **63** was radiofluorinated in acetonitrile at 85°C for 15 minutes. Subsequent cleavage of the POM group was achieved with mildly basic conditions (200 μL 0.1 M NaOH in ethanol, 35°C, 10 min.) due to the high instability of fluoroethyl group under basic conditions. The radiotracer (^{18}F]FE-IDH) was obtained in RCYs of 26%, molar activities of 14-47 GBq/ μmol (start activities of 1 GBq) and radiochemical purity >99%. The radiotracer was stable in serum and in solution, however, cellular uptake showed a statistically significant higher uptake in wild type in comparison to mutant cell lines.

The radiotracers were developed from literature known inhibitors solely on the base of their selective inhibition towards mIDH1. Unfortunately, no affinity measurements have been reported so far.

However, a short time before the end of this project, Liu et. al.²⁵³ determined the affinity of some of the most common inhibitors using different techniques like isothermal titration calorimetry, and found that for most of them the affinity was in the range of 400 μM , except for AG120²⁵⁴, which showed comparable affinities for both the wild type and mutant enzyme (0.42 vs. 0.49 μM). These results showed that for this particular enzyme the selectivity of inhibition is not caused by a selective binding but actually by the different strength of binding between the Mg^{2+} -ICT complex and the αKG . The inhibitor can bind into the allosteric binding pockets of both the mutant and wild type enzyme, causing the disruption of the Mg^{2+} binding site, which, in the case of the Mg^{2+} -ICT does not impair the reaction, while for the separately and weakly bound Mg^{2+} and αKG precludes the reduction of the latter into 2-(*R*)-hydroxyglutarate. The authors speculate that this phenomenon arises not simply from the binding to the active site to the monomeric enzymes but actually reflects the special dimeric nature of the IDH1 enzyme. This could also explain the dynamic nature of the dimer interface region which allows such different inhibitors to work apparently by the same mechanism.

In conclusion, the assumptions that represented the base of the project, although reasonable at first and shared by several groups in the world, were ultimately wrong. This can explain the absence of similar publications and of procedures on how to carry out the biological evaluations. In particular,

for the cellular uptake experiments, several challenges were faced, probably due to the fact that the in vivo mechanisms of action of these enzymes are much more complex than what is so far known. Finally, the findings of Liu et al. served as appropriate explanation for the unexpected results obtained during this project. In the future, a different approach might be discovered to target mIDH selectively.

5 Experimental part

5.1 General

All chemical reactions were carried out in flasks under stirring. When dried conditions were applied, the flask, equipped with a magnetic stirring bar, was dried and flushed with argon for three consecutive times with a Schlenk line.

5.1.1 Solvents and reagents

Solvents were purchased commercially (MerckKGaA, Darmstadt, Germany). All chemicals used for the syntheses were commercially available (Merck, Taufkirchen, Germany; Activate Scientific, Prien, Germany; ABCR, Karlsruhe, Germany) or were prepared as described in the text.

5.1.2 Spectroscopy

^1H , ^{13}C , and ^{19}F NMR spectra were recorded at 400.13 MHz by means of a Bruker Avance Neo 400 instrument (Bruker Bio Spin GmbH, Rheinstetten, Germany), in 5% solution at 299 K. Internal reference is set to the residual solvent signal, namely 7.26 for CDCl_3 and 2.5 for DMSO for proton NMR and 77.16 and 50.32 respectively for ^{13}C NMR. In both cases the spectra are reported in a table that indicates the solvent of use and MHz of the instrument, followed by integration of protons, multiplicity and coupling constant (reported in J/Hz). Multiplicities are reported using abbreviations, here stated: s = singlet, d = doublet, t = triplet, q = quartet, p = quintet and m = multiplet.

Compound names are those generated by ChemBioDrawTM (CambridgeSoft) following IUPAC nomenclature.

Low-resolution mass spectra were obtained from analytes dissolved in methanol in electrospray ionization (ESI positive) mode with a Thermo Finnigan Surveyor mass spectrometer (Thermo Fisher Scientific GmbH, Dreieich, Germany) with a flow rate of 200 mL/min. High resolution mass spectra were performed by the University of Cologne. Reported values correspond to the m/z -values of the pseudo-ion $[\text{M}+\text{H}]^+$ for both low and high resolution mass analysis.

5.1.3 Chromatography

All reactions were monitored by mean of normal phase thin layer chromatography, visualized with the aid of a UV lamp. TLC were silica coated aluminum sheets with fluorescent indicator (SIL ALUGRAM G/UV254 Macherey-Nagel GmbH, Düren, Germany).

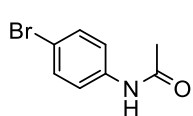
When stated that the crude mixtures were purified via column chromatography, a Grace Reveleris® iES flash chromatography system was used and the progress monitored with the RevealXTM detection, which allows for multisignal (UV/ELSD) collection. Reveleris® flash silica cartridges (size 12 to 40 mm) were employed as stationary phase while the mobile case was reported in the procedure for each purification.

5.2 Organic preparative synthesis

General procedure for the preparation of 4-halogenatedacetanilides **6d**, **6e**

Anilines (1 eq.) were placed in a round bottom flask equipped with a magnetic stirring bar, dissolved in AcOEt (0.2 M), followed by addition of acetic anhydride (1.1 eq.) and DIPEA (1.1 eq.) and stirred at room temperature.. After 16 hours TLC analysis (Hex:AcOEt 4:1) showed completion of the reaction. The mixture was extracted with water (15 mL x 2) and brine. The combined organic phases were dried over Na₂SO₄ and concentrated in vacuo after filtration to yield the final compounds **6d** and **6e** as pure solids.

4-Bromoacetanilide **6e**



4-Bromoaniline: 2.30 g (13.48 mmol)

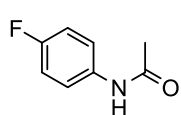
R_f: 0.2

Yield: 97% (2.80 g, 13.08 mmol)

¹H NMR (400 MHz, DMSO) δ 10.06 (s, 1H), 7.56 (d, *J* = 8.8 Hz, 2H), 7.46 (d, *J* = 8.8 Hz, 2H), 2.05 (s, 3H). ¹³C NMR (101 MHz, DMSO) δ 168.92 (s), 139.15 (s), 131.91 (s), 121.32 (s), 114.95 (s), 24.48 (s).

HRMS (ESI) calcd for C₈H₈BrNO [M + H]⁺ 214.06 found 213.9863; M.p. = 167 °C

4-Fluoroacetanilide **6d**



4-Fluoroaniline: 1.50 g (13.48 mmol)

R_f: 0.2

Yield: 100% (2.06 g, 13.45 mmol)

¹H NMR (400 MHz, DMSO-*d*₆) δ 9.97 (s, 1H), 7.74 – 7.45 (m, 2H), 7.28 – 6.99 (m, 2H), 2.03 (s, 3H). ¹⁹F NMR (376 MHz, DMSO) δ -119.82. ¹³C NMR (101 MHz, DMSO) δ 168.61 (s), 158.28 (d, *J* = 239.5 Hz), 136.19 (d, *J* = 2.4 Hz), 121.13 (d, *J* = 7.7 Hz), 115.63 (d, *J* = 22.3 Hz), 24.30 (s).

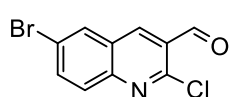
HRMS (ESI) calcd for C₈H₈FNO [M + H]⁺ 153.06 found 154.0663; M.p. = 153 °C

General procedure for the preparation of *N*-aryl-(4-halogenated)-3-dimethylamino-3-formylacrylamide **13d, e, f** and 6-halogenated-2-chloro-quinoline **14e, f**:

DMF (2.5 eq.) was placed in a flask, previously flushed with argon and equipped with a magnetic stirring bar, cooled to 0°C with the aid of an ice bath, followed by dropwise addition of POCl₃ (7 eq.). The mixture was then allowed to reach room temperature, before addition of **6d, e, f** (1 eq.), and left under vigorous stirring at room temperature for 5 minutes followed by heating at 75 °C until TLC (Hex:AcOEt 3:2) analysis showed complete consumption of the starting materials. The reactions were quenched upon ice addition which allowed precipitation of 2-chloroquinolines **14e, f**, obtained pure after filtration on paper filter.

Addition of 40% aqueous NaOH to the mother liquor gave products **9d, e, f** and **13d, e, f** which were extracted into chloroform. The organic phases were dried over Na₂SO₄, filtered and concentrated in vacuo to yield oily orange mixtures of **9d, e, f** and **13d, e, f** which were used without further purification.

6-Bromo-2-chloro-quinoline **14e**



4-Bromoacetanilide **6e**: 2.01 g (9.40 mmol)

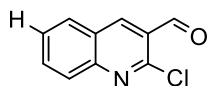
R_f: 0.89

Yield: 3% (76 mg, 0.28 mmol)

¹H NMR (400 MHz, DMSO-*d*₆) δ 10.33 (s, 1H), 8.97 (s, 1H), 8.61 (d, *J* = 2.3 Hz, 1H), 8.12 (dd, *J* = 9.0, 2.3 Hz, 1H), 8.00 (d, *J* = 9.0 Hz, 1H). ¹³C NMR (101 MHz, DMSO) δ 189.67 (s), 150.10 (s), 147.65 (s), 140.78 (s), 137.10 (s), 132.46 (s), 130.37 (s), 128.19 (s), 127.56 (s), 121.55 (s).

MS (ESI) calcd for C₁₀H₅BrClNO [M + H]⁺ 270.51 found 227.12; M.p. = 164 °C

2-Chloro-3-quinoline carboxaldehyde 14f



Acetanilide: 2.0 g (14.79 mmol)

R_f: 0.78

Yield: 29% (830.0 mg, 4.33 mmol)

¹H NMR (400 MHz, DMSO) δ 10.38 (s, 1H), 8.98 (s, 1H), 8.30 – 8.25 (m, 1H), 8.04 (ddt, *J* = 8.5, 1.4, 0.7 Hz, 1H), 7.98 (ddd, *J* = 10.1, 5.8, 2.4 Hz, 1H), 7.76 (ddd, *J* = 8.1, 6.7, 1.4 Hz, 1H).

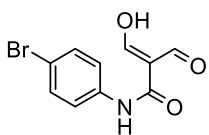
¹³C NMR (101 MHz, DMSO) δ 189.84 (s), 149.45 (s), 149.02 (s), 141.85 (s), 134.35 (s), 130.68 (s), 128.72 (s), 128.24 (s), 126.82 (s), 126.80 (s).

MS (ESI) calcd for C₁₀H₆ClNO [M + H]⁺ 191.61 found 224.17 (adduct with MeOH); M.p. = 146 °C

General procedure for the preparation of *N*-aryl-(4-bromo)-2-formyl-3-hydroxyacrylamide 20d,e:

Mixtures of **9d, e** and **13d, e** were placed in round bottom flasks (1 eq.), dissolved in a 1.1:1 mixture of EtOH and 20% aqueous NaOH (NaOH_{aq}) (0.10 M), boiled for 2 minutes and immediately poured onto ice. Concentrated HCl was added until pH 3 was reached and left under vigorous stirring for 3 hours to allow precipitation of products **20d,e**. The precipitates were filtered on a paper filter and dried to yield orange solids.

***N*-aryl-(4-bromo)-2-formyl-3-hydroxyacrylamide 20e**



Acrylamide **13e** and Formamidine **9e**

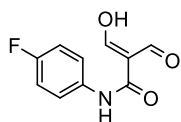
R_f: 0.0

Yield: 65% over two steps (1.67 mg, 6.17 mmol)

¹H NMR (400 MHz, DMSO-*d*₆) δ 10.70 (s, 1H), 9.02 (s, 2H), 7.62 – 7.57 (m, 2H), 7.57 – 7.52 (m, 2H). ¹³C NMR (101 MHz, DMSO) δ 188.04 – 184.91 (m), 166.20 (s), 136.86 (s), 132.26 (s), 122.98 (s), 116.77 (s), 111.32 (s).

MS (ESI) calcd for C₁₀H₈BrNO₃ [M + H]⁺ 270.08 found 227.12 (Formamidine **9e**); M.p. = 242 °C

N-aryl-(4-fluoro)-2-formyl-3-hydroxyacrylamide **20d**



Acrylamide **13d** and Formamidine **9d**

R_f : 0.0

Yield: 41% over two steps (1.13 g, 5.40 mmol)

¹H NMR (400 MHz, DMSO) δ 10.67 (s, 1H), 9.02 (s, 2H), 7.71 – 7.51 (m, 2H), 7.28 – 7.10 (m, 2H).

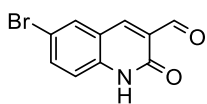
¹⁹F NMR (376 MHz, DMSO) δ -117.71 (s). ¹³C NMR (101 MHz, DMSO) δ 187.20 (s), 166.67 (s), 159.37 (d, *J* = 241.7 Hz), 133.52 (s), 123.25 (d, *J* = 8.1 Hz), 116.09 (d, *J* = 22.5 Hz), 110.79 (s).

MS (ESI) calcd for C₁₀H₈BrNO₃ [M + H]⁺ 209.18 found: no peak ; M.p. > 300 °C

General procedure for the preparation of 6-Halogenated-3-Formyl-2-quinolones 21d, e:

Compounds **20 d, e** (1 eq.) were placed in a round bottom flask with a magnetic stirring bar and polyphosphoric acid (10 g PPA for each gram of starting material) was added, heated to 150 °C (internal temperature) and stirred for 15 minutes when TLC (Hex:AcOEt 4:1) analysis confirmed complete conversion. The mixture was then poured onto ice and immediately a black precipitate was formed and filtered on a paper filter yielding the final compounds **21d** and **21e**.

6-Bromo-3-formyl-quinolone **21e**



N-aryl-(4-bromo)-2-formyl-3-hydroxyacrylamide **20e**: 1.67 g (6.17 mmol)

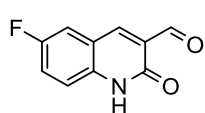
R_f : 0.0

Yield: 60% (925 mg, 3.67 mmol)

¹H NMR (400 MHz, DMSO-*d*₆) δ 12.36 (s, 1H), 10.23 (s, 1H), 8.48 (s, 1H), 8.21 (d, *J* = 2.3 Hz, 1H), 7.80 (dd, *J* = 8.8, 2.3 Hz, 1H). ¹³C NMR (101 MHz, DMSO) δ 190.13 (s), 161.66 (s), 141.65 (s), 140.57 (s), 136.43 (s), 133.05 (s), 126.88 (s), 120.27 (s), 118.06 (s), 114.57 (s).

HRMS (ESI) calcd for C₁₀H₆BrNO₂ [M + H]⁺ 252.07 found 251.9655; M.p. > 300 °C

6-Fluoro-3-formyl-quinolone **21d**



N-aryl-(4-fluoro)-2-formyl-3-hydroxyacrylamide **20d**: 1.13 g (5.40 mmol)

R_f : 0.0

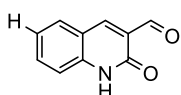
Yield: 96% (1.00 g, 5.23 mmol)

¹H NMR (400 MHz, DMSO) δ 12.31 (s, 1H), 10.24 (s, 1H), 8.49 (s, 1H), 7.81 (dd, *J* = 9.0, 2.9 Hz, 1H), 7.58 (td, *J* = 8.9, 2.9 Hz, 1H), 7.39 (dd, *J* = 9.1, 4.7 Hz, 1H). ¹⁹F NMR (376 MHz, DMSO) δ -120.11. ¹³C NMR (101 MHz, DMSO) δ 190.23 (s), 160.18 (d, *J* = 288.6 Hz), 156.37 (s), 141.93 (d, *J* = 3.6 Hz), 138.44 (s), 126.91 (s), 122.44 (d, *J* = 24.9 Hz), 119.17 (d, *J* = 9.5 Hz), 117.90 (d, *J* = 8.3 Hz), 115.50 (d, *J* = 22.8 Hz).

HRMS (ESI) calcd for C₁₀H₆BrNO₂ [M + H]⁺ 191.16 found 192.0456; M.p. > 300 °C

Synthesis of 3-Formyl-2-quinolone **21f**:

2-Chloro-3-formyl quinoline **14f** (830 mg, 4.33 mmol) was placed in a round bottom flask and suspended in HCl (12 mL). The mixture was refluxed for 16 hours followed by addition of water to allow precipitation of an orange solid which was filtered on a filter paper and dried (619.0 mg, 3.57 mmol, *y* = 82%).



¹H NMR (400 MHz, DMSO) δ 10.38 (s, 1H), 8.98 (s, 1H), 8.30 – 8.25 (m, 1H), 8.04 (ddt, *J* = 8.5, 1.4, 0.7 Hz, 1H), 7.98 (ddd, *J* = 10.1, 5.8, 2.4 Hz, 1H), 7.76 (ddd, *J* = 8.1, 6.7, 1.4 Hz, 1H). ¹³C NMR (101 MHz, DMSO) δ 189.84 (s), 149.45 (s), 149.02 (s), 141.85 (s), 134.35 (s), 130.68 (s), 128.72 (s), 128.24 (s), 126.82 (s), 126.80 (s).

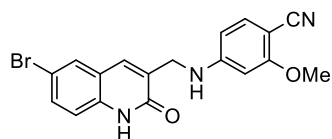
MS (ESI) calcd for C₁₀H₇NO₂ [M + H]⁺ 173.17 found 174.10 ; M.p. = 146 °C

General procedure for the preparation of 4-{{(6-Halogenated-2-oxo-1,2-dihydroquinolin-3-yl)methyl}amino}-2-methoxybenzotrile **30d, e**

Compounds **21d, e** (1 eq.) and **32** (1 eq.) were placed in a round bottomed flask, previously flushed with argon, and equipped with a magnetic stirring bar, and suspended in dry DCE (0.17M), followed by addition of acetic acid (3 eq.), which allowed complete dissolution of the reagents. The mixture was left in inert atmosphere under vigorous stirring for 16 hours and followed by addition of NaBH(OAc)₃ (2 eq.). TLC analysis (CHCl₃:AcOEt 3:7) showed no improvement over time, therefore after 6 hours the reaction was diluted with chloroform and extracted with water and saturated solution of sodium bicarbonate (x 5). The combined organic phases were dried over Na₂SO₄, concentrated in

vacuo after filtration and loaded on silica to be purified via column chromatography using a gradient of chloroform and ethyl acetate to afford the final compounds **30d, e**.

4-*{[(6-Bromo-2-oxo-1,2-dihydroquinolin-3-yl)methyl]amino}*-2-methoxybenzotrile **30e**



6-Bromo-3-formyl-quinolone **21e**: 435.50 mg (1.73 mmol)

4-amino-2-methoxybenzotrile **32**: 259.0 mg (1.73 mmol)

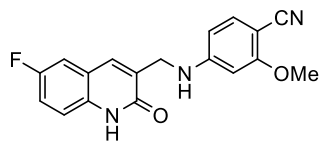
R_f: 0.6

Yield: 45% (296.80 mg, 0.77 mmol)

¹H NMR (400 MHz, DMSO) δ 12.05 (s, 1H), 7.92 (d, J = 2.0 Hz, 1H), 7.73 (s, 1H), 7.61 (dd, J = 8.7, 2.2 Hz, 1H), 7.29 (d, J = 8.6 Hz, 1H), 7.26 (d, J = 8.8 Hz, 1H), 7.16 (t, J = 5.9 Hz, 1H), 6.33 (s, 1H), 6.23 (dd, J = 8.5, 1.9 Hz, 1H), 4.25 (d, J = 4.9 Hz, 2H), 3.80 (s, 2H). ¹³C NMR (101 MHz, DMSO) δ 162.86 (s), 161.88 (s), 154.42 (s), 137.57 (s), 134.70 (s), 134.67 (s), 132.79 (s), 131.87 (s), 130.10 (s), 121.25 (s), 118.70 (s), 117.58 (s), 113.93 (s), 105.47 (s), 95.00 (s), 86.58 (s), 56.05 (s), 41.87 (s).

HRMS (ESI) calcd for C₁₈H₁₄BrN₃O₂ [M + H]⁺ 384.23 found 384.0342; M.p. > 300 °C

4-*{[(6-Fluoro-2-oxo-1,2-dihydroquinolin-3-yl)methyl]amino}*-2-methoxybenzotrile **30d**



6-Fluoro-3-formyl-quinolone **21e**: 193.00 mg (1.01 mmol)

4-amino-2-methoxybenzotrile **32**: 148.10mg (1.00 mmol)

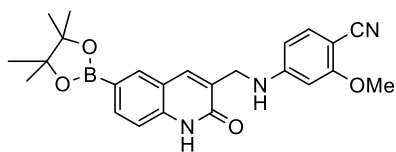
R_f: 0.6

Yield: 33% (106.70 mg, 0.33 mmol)

¹H NMR (400 MHz, DMSO) δ 12.00 (s, 1H), 7.74 (s, 1H), 7.55 (dd, J = 9.2, 2.5 Hz, 1H), 7.41 – 7.32 (m, 2H), 7.30 (d, J = 8.6 Hz, 1H), 7.17 (t, J = 6.0 Hz, 1H), 6.34 (d, J = 1.7 Hz, 1H), 6.24 (dd, J = 8.6, 1.8 Hz, 1H), 4.26 (d, J = 5.7 Hz, 2H), 3.80 (s, 3H). ¹⁹F NMR (376 MHz, DMSO) δ -121.03 (s). ¹³C NMR (101 MHz, DMSO) δ 162.29 (d, J = 115.1 Hz), 158.68 (s), 156.31 (s), 154.44 (s), 135.15 (s), 135.13 (s), 134.95 (d, J = 3.1 Hz), 134.74 (s), 131.95 (s), 120.19 (d, J = 8.8 Hz), 118.68 (s), 118.30 (d, J = 24.4 Hz), 117.14 (d, J = 8.5 Hz), 112.92 (d, J = 23.0 Hz), 105.45 (s), 95.00 (s), 86.60 (s), 60.23 (s), 56.05 (s).

HRMS (ESI) calcd for C₁₈H₁₄FN₃O₂ [M + H]⁺ 323.33 found 324.1140; M.p. = 222 °C

Synthesis of 4-*[(6-(4,4,5,5-tetramethyl-1,3,2-dioxaborolan-2-yl)quinolin-1(2H)-one)methyl]amino*}-2-methoxybenzonitrile **33**



Compound **30e** (296.80 mg, 0.77 mmol) was placed in a round bottomed flask with (Bpin)₂ (215.70 mg; 1.10 mmol), KOAc (532.0 mg; 5.40 mmol) and [Pd(Cl)₂dppf] (28.20 mg; 0.04 mmol) and the flask was filled with nitrogen. Dry dioxane (3.8 mL, 0.2M) was added and the reaction was left at 80°C under vigorous stirring for 17 hours, until TLC analysis (CHCl₃:AcOEt 1:1) showed formation of the product but no further consumption of the starting material over time.

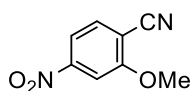
The reaction was diluted with ethyl acetate and extracted with brine (x 4), the combined organic phases were dried over sodium sulphate and concentrated in vacuo after filtration.

The crude product was loaded on silica and purified via column chromatography with a gradient of CHCl₃:AcOEt to yield the final compound (43.0 mg, 0.10 mmol) in a 17 % yield.

¹H NMR (400 MHz, DMSO) δ 12.06 (s, 1H), 7.95 (s, 1H), 7.85 (s, 1H), 7.72 (dd, *J* = 8.2, 1.3 Hz, 1H), 7.30 (dd, *J* = 8.4, 2.2 Hz, 2H), 7.14 (t, *J* = 6.0 Hz, 1H), 6.35 (d, *J* = 1.7 Hz, 1H), 6.25 (dd, *J* = 8.6, 1.8 Hz, 1H), 4.23 (d, *J* = 5.7 Hz, 2H), 3.80 (s, 3H), 1.29 (s, 11H). ¹³C NMR (101 MHz, DMSO) δ 162.83 (s), 162.28 (s), 154.41 (s), 140.68 (s), 136.48 (s), 135.73 (s), 135.32 (s), 134.66 (s), 130.40 (s), 119.05 (s), 118.74 (s), 114.92 (s), 105.38 (s), 95.02 (s), 86.46 (s), 84.16 (s), 56.03 (s), 41.86 (s), 25.15 (s).

R_f: 0.4; HRMS (ESI) calcd for C₂₄H₂₆BN₃O₄ [M + H]⁺ 431.30 found 432.2088; M.p. = 262 °C

Synthesis of 4-amino-2-methoxybenzonitrile **32**



2-methoxy-4aminobenzonitrile **30** (2.00 g, 11.23 mmol), NH₄Cl (1.80 g, 33.68 mmol) and zinc powder (2.20 g, 33.68 mmol) were placed in a round bottomed flask equipped with a magnetic stirring bar and dissolved in 1:1 mixture of EtOH:AcOEt (40 mL, 0.28M). The reacting mixture was heated to 40°C and vigorously stirred for two hours, when TLC (Hex:AcOEt 1:1) analysis showed complete consumption of the starting material.

Zinc powder was filtered over a celite pad which was washed with AcOEt while the mother liquor was extracted with water. The two phases were separated and the organic one dried over Na₂SO₄, filtered and concentrated in vacuo to afford the product (1.65 g, 11.13mmol) in quantitative yield without need of further purification.

^1H NMR (400 MHz, DMSO) δ 7.24 (d, J = 8.4 Hz, 1H), 6.27 (d, J = 1.9 Hz, 1H), 6.21 (dd, J = 8.4, 1.9 Hz, 1H), 6.18 (s, 2H), 3.78 (s, 3H). ^{13}C NMR (101 MHz, DMSO) δ 162.90 (s), 155.38 (s), 134.71 (s), 118.90 (s), 106.90 (s), 96.13 (s), 85.94 (s), 55.83 (s).

R_f : 0.38; HRMS (ESI) calcd for $\text{C}_8\text{H}_8\text{N}_2\text{O}$ $[\text{M} + \text{H}]^+$ 148.17 found 149.0709; M.p. = 100 °C

General procedure for the preparation of 6-Halogenated-3-formyl-1- \langle (pivaloyloxy)methyl \rangle quinol-2-one 35d, e, f and 2- \langle (pivaloyloxy)methyl \rangle -6-halogenatedquinoline-3-carbaldehyde 36d, e, f

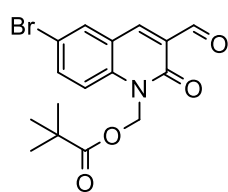
Compounds **21d,e,f** (1 eq.) and anhydrous K_2CO_3 (1.5 eq.) were placed in a round bottomed flask equipped with a magnetic stirring bar, flushed with argon and dissolved in DMF (0.2M). The solution was stirred at 60 °C for 30 minutes, allowed to cool to room temperature before addition of POM-Cl (1.5 eq.) and left under stirring for 2 hours when TLC (Hex:AcOEt 4:1) analysis showed complete consumption of the starting material. The reaction was diluted with ethyl acetate, extracted with water, dried over Na_2SO_4 , filtered and concentrated in vacuo. An aliquot was used to analyze the ratio between the two products while the rest was loaded on silica and purified through column chromatography (Hex: AcOEt 9:1) to afford compounds **35d** and **36d**, as well as **35e** and **36e** and **35f** and **36f** as pale yellow solids.

6-Bromo-3-formyl-1- \langle (pivaloyloxy)methyl \rangle quinol-2-one 35e and 2- \langle (pivaloyloxy)methyl \rangle -6-bromo quinoline-3-carbaldehyde 36e

6-Bromo-3-formyl-quinolone **21e**: 873.2 mg (3.46 mmol)

Yield: 42% total

6-Bromo-3-formyl-1- \langle (pivaloyloxy)methyl \rangle quinol-2-one 35e



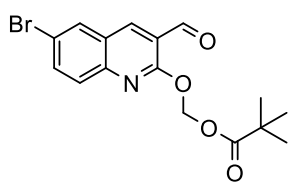
R_f : 0.4

Yield: 16% (207.0 mg, 0.56 mmol)

^1H NMR (400 MHz, CDCl_3) δ 10.46 (s, 1H), 8.32 (s, 1H), 7.90 (d, J = 2.3 Hz, 1H), 7.78 (dd, J = 9.1, 2.3 Hz, 1H), 7.30 (d, J = 9.1 Hz, 2H), 6.36 (s, J = 34.5 Hz, 2H), 1.22 (s, 9H). ^{13}C NMR (101 MHz, CDCl_3) δ 189.09 (s), 177.71 (s), 161.11 (s), 144.18 (d, J = 103.4 Hz), 141.19 (s), 136.64 (s), 133.91 (s), 128.01 – 124.35 (m), 120.83 (s), 116.67 (s), 116.17 (s, J = 50.4 Hz), 65.51 (s), 39.11 (s), 26.98 (s).

HRMS (ESI) calcd for $\text{C}_{16}\text{H}_{16}\text{BrNO}_4$ $[\text{M} + \text{H} + \text{Na}]^+$ 366.22 found 388.0154; M.p. = 166 °C

2-*-(pivaloyloxy)methyl*]-6-bromoquinoline-3-carbaldehyde **36e**



R_f: 0.8

Yield: 26% (329.6 mg, 0.9 mmol)

¹H NMR (400 MHz, CDCl₃) δ 10.44 (s, 1H), 8.53 (s, 1H), 7.99 (d, J = 2.1 Hz, 1H), 7.80 (dd, J = 8.9, 2.2 Hz, 1H), 7.73 (d, J = 9.0 Hz, 1H), 6.33 (s, 2H),

1.22 (s, J = 12.5 Hz, 10H). ¹³C NMR (101 MHz, CDCl₃) δ 188.15 (s), 177.32 (s), 159.06 (s), 146.94 (s), 139.02 (s), 135.95 (s), 131.43 (s), 129.22 (s), 126.07 (s), 120.19 (s), 119.09 (s), 82.29 (s), 38.84 (s), 26.90 (s).

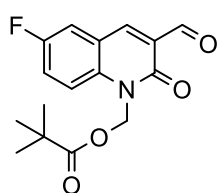
MS (ESI) calcd for C₁₆H₁₆BrNO₄ [M + H]⁺ 366.22 found 399.76 (MeOH adduct); M.p. = 149 °C

6-Fluoro-3-formyl-1-*-(pivaloyloxy)methyl*quinol-2-one **35d** and 2-*-(pivaloyloxy)methyl*]-6-fluoroquinoline-3-carbaldehyde **35d**

6-Fluoro-3-formyl-quinolone **21d**: 226.90 mg (1.18 mmol)

Yield: 73% total

6-Fluoro-3-formyl-1-*-(pivaloyloxy)methyl*quinol-2-one **35d**



R_f: 0.3

Yield: 24% (85 mg, 0.28 mmol)

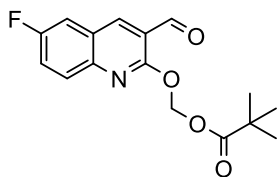
¹H NMR (400 MHz, DMSO) δ 10.22 (s, 1H), 8.52 (s, 1H), 7.89 (dd, J = 8.5, 3.0 Hz, 1H), 7.74 – 7.65 (m, 1H), 7.61 (dd, J = 9.4, 4.4 Hz, 1H), 6.29 (s, 2H), 1.11

(s, J = 6.4 Hz, 10H). ¹⁹F NMR (376 MHz, DMSO) δ -119.47 (s). ¹³C NMR (101 MHz, DMSO) δ 189.65 (s), 177.08 (s), 160.67 (s), 158.08 (d, J = 241.5 Hz), 142.38 (d, J = 3.0 Hz), 137.69 (s), 126.00 (s), 122.38 (d, J = 24.3 Hz), 120.30 (d, J = 9.2 Hz), 117.68 (d, J = 8.3 Hz), 117.00 (d, J = 22.9 Hz).

HRMS (ESI) calcd for C₁₆H₁₆FNO₄ [M + H]⁺ 305.31 found 306.1139

m.p. 114 °C

2-*-(pivaloyloxy)methyl*]-6-fluoroquinoline-3-carbaldehyde **36d**



R_f: 0.7

Yield: 49% (178.75 mg, 0.58 mmol)

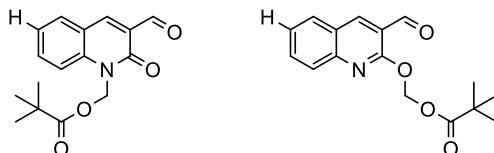
¹H NMR (400 MHz, DMSO) δ 10.27 (s, 1H), 8.75 (s, 1H), 7.90 (dd, J = 9.0, 2.8 Hz, 1H), 7.80 (dt, J = 20.6, 10.3 Hz, 1H), 7.71 (td, J = 8.9, 2.9 Hz, 1H),

6.25 (s, 2H), 1.12 (s, 9H). ¹⁹F NMR (376 MHz, DMSO) δ -114.96 (s). ¹³C NMR (101 MHz, DMSO) δ 188.57 (s), 176.86 (s), 160.63 (s), 158.96 – 156.87 (m), 144.84 (s), 140.83 (d, J = 5.1 Hz), 129.75

(d, J = 8.9 Hz), 125.64 (d, J = 10.6 Hz), 123.15 (d, J = 25.7 Hz), 120.39 (s), 113.66 (d, J = 22.3 Hz), 82.64 (s), 26.92 (s).

HRMS (ESI) calcd for C₁₆H₁₆FNO₄ [M + H]⁺ 305.31 found 338.15 (MeOH adduct); M.p. = 92 °C

(3-formyl-2-oxoquinolin-1(2H)-yl)methyl pivalate **35f** and ((3-formylquinolin-2-yl)oxy)methyl pivalate **36f** were further used as a mixture, without purification.



2-oxo-1,2-dihydroquinoline-3-carbaldehyde **21f**: 200.0 mg (1.15 mmol)

35f R_f: 0.3

36f R_f: 0.8

Yield: 63% total (213.22 mg, 0.74 mmol)

¹H NMR (400 MHz, DMSO) δ 10.31 (s, 1H), 10.25 (s, 1H), 8.87 (s, 1H), 8.60 (s, 1H), 8.19 – 8.15 (m, 1H), 8.05 (dd, J = 7.8, 1.5 Hz, 1H), 7.62 – 7.56 (m, 2H), 7.44 – 7.38 (m, 1H), 6.31 (s, J = 3.3 Hz, 1H), 6.30 (s, 2H), 1.14 (s, 10H), 1.13 (s, J = 4.4 Hz, 7H). ¹³C NMR (101 MHz, DMSO) δ 189.81 (s), 188.87 (s), 177.21 (s), 176.94 (s), 161.01 (s, J = 3.0 Hz), 158.78 (s), 147.89 (s), 143.64 (s), 141.83 (s), 140.98 (s), 134.79 (s), 133.79 (s), 132.73 (s), 130.69 (s), 127.30 (s), 126.37 (s), 125.18 (s), 125.14 (s), 124.18 (s), 120.00 (s), 119.35 (s), 115.40 (s), 82.68 (s), 66.36 (s), 38.91 (s), 38.75 (s), 27.11 (s), 27.00 (s).

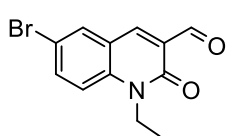
MS (ESI) calcd for C₁₆H₁₇NO₄ [M + H]⁺ 287.32 found 288.41; M.p. = not determined

Synthesis of 6-Bromo-3-formyl-2-(1-ethyl)-quinolone 35g and 6-bromo-2-ethoxyquinoline-3-carbaldehyde 36g was carried out using the general procedure used to introduce the POM protection where POM-Cl was replaced with bromoethane (39 μL, 0.76mmol)

6-Bromo-3-formyl-quinolone **21f**: 87.40 mg (0.35 mmol)

Yield: 86% total

6-Bromo-3-formyl-2-(1-ethyl)-quinolone 35g



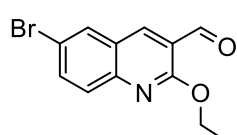
R_f: 0.2

Yield: 28% (25.2 mg, 0.1mmol)

¹H NMR (400 MHz, DMSO) δ 10.27 (s, 1H), 8.47 (s, 1H), 8.28 (d, J = 2.4 Hz, 1H), 7.89 (dd, J = 9.1, 2.4 Hz, 1H), 7.63 (d, J = 9.2 Hz, 1H), 4.32 (q, J = 7.1 Hz, 2H), 1.24 (t, J = 7.1 Hz, 3H). ¹³C NMR (101 MHz, DMSO) δ 190.34 (s), 160.61 (s), 140.37 (d, J = 19.5 Hz), 140.27 (s), 136.65 (s), 134.18 (s), 125.99 (s), 121.24 (s), 117.70 (s), 114.90 (s), 37.46 (s), 13.01 (s).

HRMS (ESI) calcd for C₁₂H₁₀BrNO₂ [M + H]⁺ 280.12 found 279.9969; M.p. = 171 °C

6-Bromo-2-ethoxyquinoline-3-carbaldehyde 36g



R_f: 0.8

Yield: 56% (55.0 mg, 0.20 mmol)

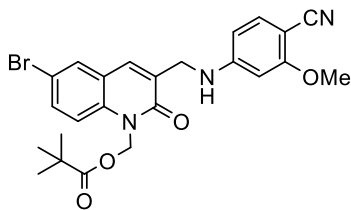
¹H NMR (400 MHz, DMSO) δ 10.33 (s, 1H), 8.69 (s, 1H), 8.35 (d, J = 2.3 Hz, 1H), 7.89 (dd, J = 8.9, 2.3 Hz, 1H), 7.71 (d, J = 8.9 Hz, 1H), 4.57 (q, J = 7.1 Hz, 2H), 1.44 (t, J = 7.1 Hz, 4H). ¹³C NMR (101 MHz, DMSO) δ 189.29 (s), 161.13 (s), 147.24 (s), 139.80 (s), 135.90 (s), 132.26 (s), 129.22 (s), 125.87 (s), 120.82 (s), 117.74 (s), 62.82 (s), 14.72 (s).

HRMS (ESI) calcd for C₁₂H₁₀BrNO₂ [M + H]⁺ 280.12 found 279.9970

M.p. = 112 °C

Synthesis of (6-Bromo-3-(((4-cyano-3-methoxyphenyl)amino)methyl)-2-oxoquinolin-1(2H)-yl)methyl pivalate 37e

6-Bromo-3-formyl-1-(pivaloyloxy)methylquinol-2-one **35e** (207.0 mg, 0.56 mmol) and compound **32** (74.4 mg, 0.51 mmol) were placed in a round bottomed flask equipped with a magnetic stirring bar and flushed with argon before addition of dry DMF (1 mL). The mixture was cooled to 0°C with the aid of an ice bath before addition of TMS-Cl (161 μL, 1.27 mmol) and NaBH₄ (20 mg, 0.51 mmol). After two hours TLC (Hex:AcOEt 6:4) analysis showed complete consumption of the limiting reagent **32**, therefore the mixture was further diluted with AcOEt followed by quench of the excess of trimethylsilyl chloride upon addition of Na₂CO₃ (s.s.). The organic phase was extracted and dried over Na₂SO₄, filtered, concentrated in vacuo and loaded on silica before column chromatography (Hex: AcOEt 6:4) purification to yield compound **37e** as yellow solid in 55% yield (141.4 mg, 0.28 mmol).



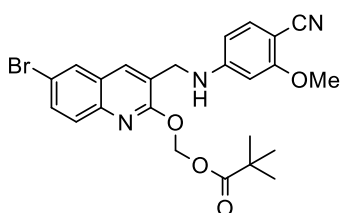
^1H NMR (400 MHz, CDCl_3) δ 7.70 (d, $J = 2.2$ Hz, 1H), 7.65 (dd, $J = 9.0, 2.3$ Hz, 1H), 7.60 (s, 1H), 7.33 (d, $J = 8.5$ Hz, 1H), 7.25 (d, $J = 9.0$ Hz, 1H), 6.35 (s, 2H), 6.24 (dd, $J = 8.5, 2.1$ Hz, 1H), 6.17 (d, $J = 2.0$ Hz, 1H), 4.44 (d, $J = 0.9$ Hz, 2H), 3.86 (s, 3H), 1.21 (s, $J = 13.8$ Hz, 11H). ^{13}C NMR (101 MHz, CDCl_3) δ 177.65 (s), 162.99 (s), 161.28 (s),

152.35 (s), 136.89 (s), 135.54 (s), 134.96 (s), 133.50 (s), 131.16 (s), 130.08 (s), 121.65 (s), 117.81 (s), 116.24 (s), 115.79 (s), 105.15 (s), 95.56 (s), 90.23 (s), 66.02 (s), 55.79 (s), 43.66 (s), 40.97 – 37.24 (m), 26.99 (s).

R_f : 0.4; HRMS (ESI) calcd for $\text{C}_{24}\text{H}_{24}\text{BrN}_3\text{O}_4$ $[\text{M} + \text{H}]^+$ 498.38 found 498.1024; M.p. = 137 °C

Synthesis of ((6-bromo-3-(((4-cyano-3-methoxyphenyl)amino)methyl)quinolin-2-yl)oxy)methyl pivalate 38e

2-((pivaloyloxy)methyl)-6-bromoquinoline-3-carbaldehyde **36e** (329.6 mg, 0.90 mmol) and compound **32** (121.2 mg, 0.81 mmol) were placed in a round bottomed flask equipped with a magnetic stirring bar and flushed with argon before addition of dry DMF (1 mL). The mixture was cooled to 0°C with the aid of an ice bath before addition of TMS-OTf (366 μL , 2.02 mmol) and NaBH_4 (32.2 mg, 0.81 mmol). After 1.15 hours TLC (Hex:AcOEt 6:4) analysis showed complete consumption of the limiting reagent **32**, therefore the mixture was further diluted with AcOEt followed by quench the excess of trimethylsilyl chloride upon addition of Na_2CO_3 (s.s.). The organic phase was extracted and dried over Na_2SO_4 , filtered, concentrated in vacuo and loaded on silica and purified by column chromatography (Hex: AcOEt 7:3) to yield compound **17a** as yellow solid in 48 % yield (192.5 mg, 0.39 mmol).



^1H NMR (400 MHz, CDCl_3) δ 7.86 (s, 1H), 7.83 (d, $J = 1.6$ Hz, 1H), 7.71 (d, $J = 8.9$ Hz, 1H), 7.68 (dd, $J = 8.9, 1.9$ Hz, 1H), 7.27 (d, $J = 8.5$ Hz, 1H), 6.27 (s, 2H), 6.19 (dd, $J = 8.5, 1.8$ Hz, 1H), 6.15 (d, $J = 1.6$ Hz, 1H), 5.13 (t, $J = 5.9$ Hz, 1H), 4.48 (d, $J = 5.8$ Hz, 2H), 3.81 (s, 3H), 1.20 (s, 9H). ^{13}C NMR (101 MHz, CDCl_3) δ 177.83 (s), 162.92 (s), 157.95

(s), 152.77 (s), 143.99 (s), 135.57 (s), 134.82 (s), 132.91 (s), 129.38 (s), 128.97 (s), 126.81 (s), 122.79 (s), 118.37 (s), 118.13 (s), 104.92 (s), 95.20 (s), 89.43 (s), 82.26 (s), 55.67 (s), 42.49 (s), 26.91 (s).

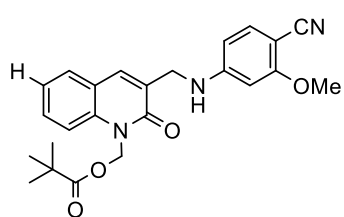
R_f : 0.6; HRMS (ESI) calcd for $\text{C}_{24}\text{H}_{24}\text{BrN}_3\text{O}_4$ $[\text{M} + \text{H}]^+$ 498.38 found 498.1024; M.p. = 152 °C

Synthesis of (3-(((4-cyano-3-methoxyphenyl)amino)methyl)-2-oxoquinolin-1(2H)-yl)methyl pivalate **37f** and ((3-(((4-cyano-3-methoxyphenyl)amino)methyl)quinolin-2-yl)oxy)methyl pivalate **38f** was carried out using the same procedure as for compound **38e** by reacting the mixture of compounds **35f** and **36f**

35f + **36f** : 209.22 mg (0.73 mmol)

Yield: 63% (0.46 mmol)

(3-(((4-cyano-3-methoxyphenyl)amino)methyl)-2-oxoquinolin-1(2H)-yl)methyl pivalate **37f**



R_f: 0.3

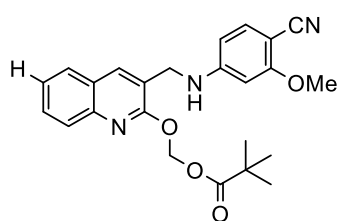
Yield: 35% (110 mg, 0.26 mmol)

¹H NMR (400 MHz, CDCl₃) δ 7.70 (s, 1H), 7.58 – 7.51 (m, 2H), 7.32 (d, J = 8.9 Hz, 1H), 7.27 (m, 2H), 6.35 (s, 2H), 6.23 (dd, J = 8.5, 2.1 Hz, 1H), 6.17 (d, J = 2.0 Hz, 1H), 4.42 (s, 2H), 3.80 (s, 3H), 1.19 (s, 9H).

¹³C NMR (101 MHz, CDCl₃) δ 177.76 (s), 162.96 (s), 161.72 (s), 152.99 (s), 137.96 (s), 136.92 (s), 134.75 (s), 130.76 (s), 129.03 (s), 128.72 (s), 123.35 (s), 120.18 (s), 118.19 (s), 113.98 (s), 105.09 (s), 95.24 (s), 89.20 (s), 66.22 (s), 55.70 (s), 43.36 (s), 26.99 (s), 26.89 (s).

MS (ESI) calcd for C₂₄H₂₅N₃O₄ [M + H]⁺ 419.48 found 420.14; M.p. = oil

((3-(((4-cyano-3-methoxyphenyl)amino)methyl)quinolin-2-yl)oxy)methyl pivalate **38f**



R_f: 0.66

Yield: 27% (85.0 mg, 0.20 mmol)

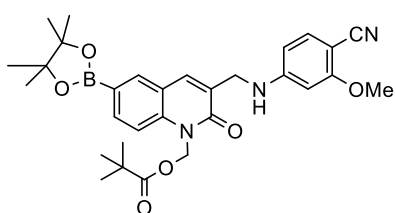
¹H NMR (400 MHz, CDCl₃) δ 7.96 (s, 1H), 7.86 (d, J = 8.4 Hz, 1H), 7.69 (dd, J = 8.1, 1.1 Hz, 1H), 7.63 (ddd, J = 8.4, 7.0, 1.5 Hz, 1H), 7.41 (ddd, J = 8.1, 7.0, 1.2 Hz, 1H), 7.25 (d, J = 8.5 Hz, 1H), 6.31 (s, 2H),

6.21 (dd, J = 8.5, 2.1 Hz, 1H), 6.17 (d, J = 2.0 Hz, 1H), 4.47 (s, 2H), 3.80 (s, 3H), 1.21 (s, 9H). ¹³C NMR (101 MHz, CDCl₃) δ 177.90 (s), 162.91 (s), 157.70 (s), 153.04 (s), 145.33 (s), 136.78 (s), 134.71 (s), 129.65 (s), 127.36 (s), 127.24 (s), 125.66 (s), 125.03 (s), 121.61 (s), 118.30 (s), 105.03 (s), 95.15 (s), 89.04 (s), 82.24 (s), 55.61 (s), 42.54 (s), 38.86 (s), 26.91 (s).

MS (ESI) calcd for C₂₄H₂₅N₃O₄ [M + H]⁺ 419.48 found 420.05; M.p. = oil

Synthesis of *(3-(((4-cyano-3-methoxyphenyl)amino)methyl)-2-oxo-6-(4,4,5,5-tetramethyl-1,3,2-dioxaborolan-2-yl)quinolin-1(2H)-yl)methyl pivalate 39* and *((3-(((4-cyano-3-methoxyphenyl)amino)methyl)-6-(4,4,5,5-tetramethyl-1,3,2-dioxaborolan-2-yl)quinolin-2-yl)oxy)methyl pivalate 40* was carried out with the procedure used to prepare compound **33**.

(3-(((4-cyano-3-methoxyphenyl)amino)methyl)-2-oxo-6-(4,4,5,5-tetramethyl-1,3,2-dioxaborolan-2-yl)quinolin-1(2H)-yl)methyl pivalate 39



Starting material **37e**: 141.40 mg (0.28 mmol)

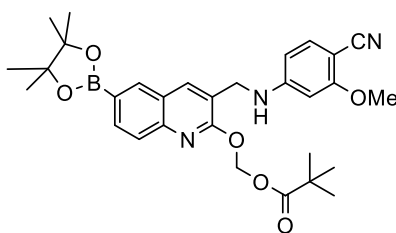
R_f(Hex:AcOEt 6:4): 0.35

Yield: 87% (133.7 mg, 0.25 mmol)

¹H NMR (400 MHz, CDCl₃) δ 7.99 (d, J = 1.2 Hz, 1H), 7.95 (dd, J = 8.5, 1.4 Hz, 1H), 7.68 (s, 1H), 7.30 (d, J = 8.5 Hz, 2H), 6.37 (s, 2H), 6.22 (dd, J = 8.5, 2.0 Hz, 1H), 6.14 (d, J = 2.0 Hz, 1H), 4.42 (s, 2H), 3.84 (s, 3H), 1.19 (s, J = 5.2 Hz, 10H). ¹³C NMR (101 MHz, CDCl₃) δ 177.72 (s), 162.99 (s), 161.79 (s), 152.76 (s), 139.95 (s), 137.05 (s), 136.73 (s), 136.20 (s), 134.87 (s), 128.47 (s), 119.55 (s), 118.01 (s), 113.32 (s), 104.98 (s), 95.19 (s), 89.58 (s), 84.23 (s), 66.12 (s), 55.74 (s), 43.36 (s), 24.88 (s).

HRMS (ESI) calcd for C₃₀H₃₆BN₃O₆ [M + H]⁺ 545.44 found 546.2769; M.p. > 300 °C

((3-(((4-cyano-3-methoxyphenyl)amino)methyl)-6-(4,4,5,5-tetramethyl-1,3,2-dioxaborolan-2-yl)quinolin-2-yl)oxy)methyl pivalate 40



Starting material **38e**: 192.50 mg (0.39 mmol)

R_f(Hex:AcOEt 6:4): 0.63

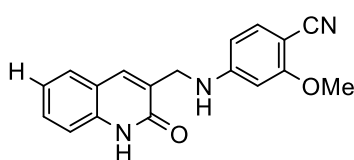
Yield: 80% (166.0 mg, 0.30 mmol)

¹H NMR (400 MHz, CDCl₃) δ 8.22 (s, 1H), 8.03 (dd, J = 8.4, 1.4 Hz, 1H), 7.98 (s, 1H), 7.87 (d, J = 8.4 Hz, 1H), 7.30 (d, J = 8.5 Hz, 1H), 6.31 (s, J = 7.4 Hz, 2H), 6.22 (dd, J = 8.5, 2.1 Hz, 1H), 6.14 (d, J = 2.0 Hz, 1H), 4.49 (s, 2H), 3.85 (s, J = 5.7 Hz, 3H), 1.20 (s, J = 2.1 Hz, 9H). ¹³C NMR (101 MHz, CDCl₃) δ 177.91 (s), 162.96 (s), 158.43 (s), 152.59 (s), 147.02 (s), 137.48 (s), 135.41 (s), 134.90 (s), 134.86 (s), 126.31 (s), 124.96 (s), 121.42 (s), 117.96 (s), 105.04 (s), 95.16 (s), 89.73 (s), 84.13 (s), 82.36 (s), 55.68 (s), 42.73 (s), 38.87 (s), 24.92 (s).

HRMS (ESI) calcd for C₃₀H₃₆BN₃O₆ [M + H]⁺ 545.44 found 546.2769; M.p. > 300 °C

Synthesis of 2-methoxy-4-(((2-oxo-1,2-dihydroquinolin-3-yl)methyl)amino)benzonitrile 30f

Mixture of (3-(((4-cyano-3-methoxyphenyl)amino)methyl)-2-oxoquinolin-1(2H)-yl)methyl pivalate **37f** and ((3-(((4-cyano-3-methoxyphenyl)amino)methyl)quinolin-2-yl)oxy)methyl pivalate **38f** (30.0 mg, 71.5 μmol) were placed in a round bottomed flask equipped with a magnetic stirring bar and MeOH and 2M NaOH solution were added. The starting material was not completely dissolved, therefore the reaction did not reach complete consumption of the starting material as indicated by TLC (Hex:AcOEt 3:2). After 72 hours, HCl was added to quench the excess of base and the mixture was directly loaded on silica and purified by column chromatography (Hex: AcOEt 75:25) to yield compound **10c** as white solid in 37 % yield (8 mg, 26.2 μmol).



^1H NMR (400 MHz, DMSO) δ 11.92 (s, 1H), 7.77 (s, 1H), 7.63 (dd, J = 7.8, 0.9 Hz, 1H), 7.50 – 7.44 (m, 1H), 7.32 (d, J = 8.1 Hz, 1H), 7.30 (d, J = 8.6 Hz, 1H), 7.19 – 7.13 (m, 2H), 6.36 (d, J = 1.8 Hz, 1H), 6.25 (dd, J = 8.6, 1.8 Hz, 1H), 4.25 (d, J = 5.8 Hz, 2H), 3.80 (s, 3H). ^{13}C

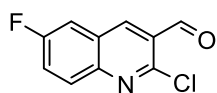
NMR (101 MHz, DMSO) δ 162.86 (s), 162.05 (s), 154.47 (s), 138.44 (s), 136.00 (s), 134.71 (s), 130.45 (s), 130.32 (s), 128.11 (s), 122.38 (s), 119.47 (s), 118.71 (s), 115.36 (s), 105.45 (s), 94.99 (s), 86.50 (s), 56.04 (s), 41.79 (s).

R_f : 0.1; MS (ESI) calcd for $\text{C}_{18}\text{H}_{15}\text{N}_3\text{O}_2$ $[\text{M} + \text{H}]^+$ 305.34 found 306.15; M.p. = 152 $^\circ\text{C}$

General procedure for the preparation of *N*-aryl-(4-halogenated)-3-dimethylamino-3-formylacrylamide 13d, e, f and 6-halogenated-2-chloro-quinoline 14d,e,f using BTC :

Triphosgene (7 eq.) was placed in a flask, previously flushed with argon and equipped with a magnetic stirring bar, and cooled to 0 $^\circ\text{C}$ with the aid of a in ice bath. DMF (7 eq.) was added dropwise with a dropping funnel and followed by addition of the starting para substituted acetanilide (1 eq.). The solid mixture was allowed to reach room temperature and left under stirring for 2 hours followed by heating at 75 $^\circ\text{C}$ for an additional 2 hours. After completion of the reaction, checked by TLC (Hex:AcOEt 3:2) of a quenched aliquot, water was slowly added to the crude mixture while stirring, the precipitate was filtered on a paper filter and washed with water to yield the final product which was used without need of further purification.

6-Fluoro-2-chloro-quinoline **14d**



4-Fluoroacetanilide **6d**: 1.5 g (9.70 mmol)

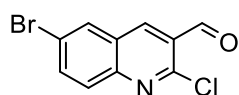
R_f: 0.81

Yield: 41% (834.0 mg, 3.98 mmol)

¹H NMR (400 MHz, CDCl₃) δ 10.59 (s, 1H), 8.73 (s, 1H), 8.11 (dd, J = 9.2, 5.1 Hz, 1H), 7.67 (ddt, J = 10.7, 5.4, 2.7 Hz, 1H), 7.62 (dd, J = 8.1, 2.8 Hz, 1H). ¹⁹F NMR (376 MHz, CDCl₃) δ -109.95 (s). ¹³C NMR (101 MHz, CDCl₃) δ 188.94 (s), 161.06 (d, J = 252.0 Hz), 146.88 (s), 139.50 (d, J = 5.7 Hz), 131.20 (d, J = 9.1 Hz), 127.39 (s), 127.29 (s), 126.90 (s), 123.84 (d, J = 25.9 Hz), 112.66 (d, J = 22.3 Hz).

MS (ESI) calcd for C₁₀H₅ClFNO [M + H]⁺ 209.60 found 209.0040; M.p. = 172 °C

6-Bromo-2-chloro-quinoline **14e**



4-Bromoacetanilide **6e**: 4.14 g (19.34 mmol)

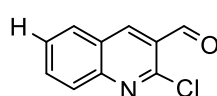
R_f: 0.89

Yield: 40% (2.1 g, 7.77 mmol)

¹H NMR (400 MHz, DMSO-d₆) δ 10.33 (s, 1H), 8.97 (s, 1H), 8.61 (d, J=2.3 Hz, 1H), 8.12 (dd, J=9.0, 2.3 Hz, 1H), 8.00 (d, J=9.0 Hz, 1H). ¹³C NMR (101 MHz, DMSO) δ 189.67 (s), 150.10 (s), 147.65 (s), 140.78 (s), 137.10 (s), 132.46 (s), 130.37 (s), 128.19 (s), 127.56 (s), 121.55 (s).

HRMS (ESI) calcd for C₁₀H₅BrClNO [M + H]⁺ 270.51 found 227.12; M.p. = 164 °C

2-Chloro-3-quinoline carboxaldehyde **14f**



Acetanilide: 1.5 g (11.09 mmol)

R_f: 0.78

Yield: 42% (886.3 mg, 4.62 mmol)

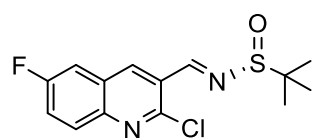
¹H NMR (400 MHz, DMSO) δ 10.38 (s, 1H), 8.98 (s, 1H), 8.30 – 8.25 (m, 1H), 8.04 (ddt, J = 8.5, 1.4, 0.7 Hz, 1H), 7.98 (ddd, J = 10.1, 5.8, 2.4 Hz, 1H), 7.76 (ddd, J = 8.1, 6.7, 1.4 Hz, 1H). ¹³C NMR (101 MHz, DMSO) δ 189.84 (s), 149.45 (s), 149.02 (s), 141.85 (s), 134.35 (s), 130.68 (s), 128.72 (s), 128.24 (s), 126.82 (s), 126.80 (s).

HRMS (ESI) calcd for C₁₀H₆ClNO [M + H]⁺ 191.61 found 191.0132; M.p. = 146 °C

General procedure for the preparation of (*R*)-*N*-((6-Halogenated-2-chloroquinolin-3-yl)methylene)-2-methylpropane-2-sulfinamides **41d-f**

6-Halogenated-2-chloro-quinoline (1 eq.) **14d-f** was placed in a flask with anhydrous CuSO₄ (1.5 eq.), flushed with argon and equipped with a magnetic stirring bar. The starting material was dissolved in DCE (0.5M) and heated to 55°C for 30 minutes before addition of (*R*)-2-methylpropane-2-sulfinamide (1.5 eq.). The reaction was left under vigorous stirring at 55°C until complete consumption of the starting material was indicated by TLC (Hex:AcOEt 3:2). CuSO₄ was then filtered off through a pad of celite and washed with chloroform. The filtrate was dried over Na₂SO₄, concentrated in vacuo, loaded on silica and purified via column chromatography (Hex:AcOEt 95%:5%) to obtain the final compound as a solid.

(R)-*N*-((6-Fluoro-2-chloroquinolin-3-yl)methylene)-2-methylpropane-2-sulfinamide **41d**



6-Fluoro-2-chloro-quinoline **14d**: 712.9 mg (3.40 mmol)

Reaction time: 16h

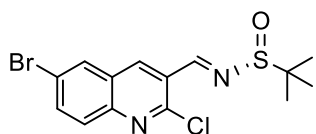
R_f: 0.73

Yield: 75% (799.4 mg, 2.56 mmol)

¹H NMR (400 MHz, DMSO) δ 9.10 (s, 1H), 8.89 (s, *J* = 4.5 Hz, 1H), 8.13 – 8.06 (m, 2H), 7.90 – 7.84 (m, 1H), 1.26 (s, *J* = 20.9 Hz, 11H). ¹⁹F NMR (376 MHz, DMSO) δ -111.08 (s). ¹³C NMR (101 MHz, DMSO) δ 160.74 (d, *J* = 247.8 Hz), 159.01 (s), 148.91 (s), 145.73 (s), 139.54 (d, *J* = 5.6 Hz), 131.18 (d, *J* = 9.5 Hz), 128.05 (d, *J* = 11.1 Hz), 126.24 (s), 123.54 (d, *J* = 26.2 Hz), 113.21 (d, *J* = 22.9 Hz), 58.58 (s), 22.63 (s).

HRMS (ESI) calcd for C₁₄H₁₄ClFN₂OS [M + H]⁺ 312.19 found 313.0570; M.p. = 149 °C

(R)-*N*-((6-Bromo-2-chloroquinolin-3-yl)methylene)-2-methylpropane-2-sulfinamide **41e**



6-Bromo-2-chloro-quinoline **14e**: 1.00 g (3.71 mmol)

Reaction time: 72h

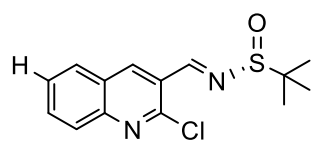
R_f: 0.80

Yield: 50% (693 mg, 1.85 mmol)

¹H NMR (400 MHz, DMSO) δ 12.33 (s, 1H), 8.78 (d, *J* = 2.8 Hz, 1H), 8.63 (d, *J* = 8.9 Hz, 1H), 8.18 (dd, *J* = 10.7, 2.1 Hz, 1H), 7.75 (td, *J* = 8.9, 2.2 Hz, 1H), 7.30 (dd, *J* = 8.8, 5.6 Hz, 1H). ¹³C NMR (101 MHz, DMSO) δ 161.14 (s), 158.34 (s), 139.70 (s), 139.42 (s), 135.49 (s), 132.29 (s), 125.81 (s), 120.74 (s), 117.95 (s), 114.52 (s), 58.19 (d, *J* = 2.1 Hz), 22.59 (s).

HRMS (ESI) calcd for C₁₄H₁₄BrClN₂OS [M + H]⁺ 373.69 found 372.9773; M.p. = 220 °C

(R,S)-*N*-((2-Chloroquinolin-3-yl)methylene)-2-methylpropane-2-sulfonamide **41f**



2-Chloro-3-quinoline carboxaldehyde **14f**: 445.0 mg (2.32 mmol)

Reaction time: 16h

R_f: 0.68

Yield: 80% (545.2 mg, 1.85 mmol)

¹H NMR (400 MHz, CDCl₃) δ 9.13 (s, 1H), 8.86 (s, 1H), 8.08 (dd, *J* = 8.5, 0.8 Hz, 1H), 8.00 – 7.94 (m, 1H), 7.85 (ddd, *J* = 8.5, 7.0, 1.4 Hz, 1H), 7.65 (ddd, *J* = 8.1, 5.3, 1.1 Hz, 1H), 1.34 (s, 10H). ¹³C NMR (101 MHz, CDCl₃) δ 159.25 (s), 150.08 (s), 148.88 (s), 138.84 (s), 132.64 (s), 128.94 (s), 128.60 (s), 127.89 (s), 126.80 (s), 125.76 (s), 58.45 (s), 22.78 (s).

HRMS (ESI) calcd for C₁₄H₁₅ClN₂OS [M + H]⁺ 294.80 found 295.0668; M.p. = 151 °C

General procedure for the preparation of (*R*)-*N*-((*S*)-1-(6-Halogenated-2-chloroquinolin-3-yl)ethyl)-2-methylpropane-2-sulfinamides 42d-f and (*R*)-*N*-((*R*)-1-(6-Halogenated-2-chloroquinolin-3-yl)ethyl)-2-methylpropane-2-sulfinamides 43d-f:

(*R*)-*N*-((6-halogenated-2-chloroquinolin-3-yl)methylene)-2-methylpropane-2-sulfinamide (1 eq.) **41d-f** was placed in a flask previously flushed with argon, dissolved in CH₂Cl₂ (0.15M) and cooled to -60°C for 15 minutes before addition of MeMgBr (3M in diethylether (1.5 eq.)). After 3 hours, the mixture was moved into the freezer at -20°C and left overnight. Next morning, TLC analysis (Hex:AcOEt 3:2) showed almost complete conversion of the starting material therefore the mixture was quenched with NH₄Cl, diluted with chloroform and extracted. The combined organic phases were dried over Na₂SO₄, concentrated in vacuo, loaded on silica and purified via column chromatography (Hex:AcOEt 90%:10%) to obtain the final compounds as a solid.

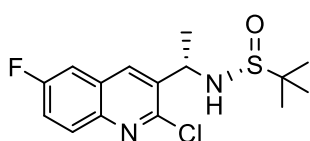
(*R*)-*N*-((*S*)-1-(6-Fluoro-2-chloroquinolin-3-yl)ethyl)-2-methylpropane-2-sulfinamides **42d** and (*R*)-*N*-((*R*)-1-(6-fluoro-2-chloroquinolin-3-yl)ethyl)-2-methylpropane-2-sulfinamides **43d**

(*R*)-*N*-((6-fluoro-2-chloroquinolin-3-yl)methylene)-2-methylpropane-2-sulfinamide **41d**: 790.0 mg (2.53 mmol)

Reaction time: 72h

Yield: 24% total

(*R*)-*N*-((*S*)-1-(6-Fluoro-2-chloroquinoline-3-yl)ethyl)-2-methylpropane-2-sulfinamide **42d**



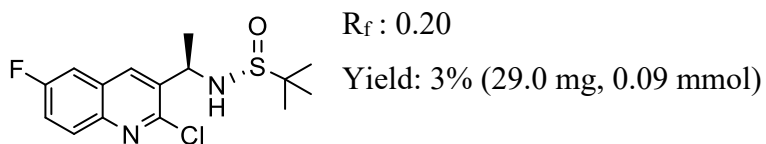
R_f: 0.16

Yield: 21% (175.0 mg, 0.53 mmol)

¹H NMR (400 MHz, DMSO) δ 8.48 (s, 1H), 7.97 (dd, *J* = 9.2, 5.3 Hz, 1H), 7.82 (dd, *J* = 9.2, 2.8 Hz, 1H), 7.65 (td, *J* = 8.9, 2.9 Hz, 1H), 5.64 (d, *J* = 6.4 Hz, 1H), 4.84 (p, *J* = 6.6 Hz, 1H), 1.61 (d, *J* = 6.8 Hz, 3H), 1.11 (s, 9H). ¹⁹F NMR (376 MHz, DMSO) δ -112.21 (s, *J* = 13.8 Hz). ¹³C NMR (101 MHz, DMSO) δ 160.53 (d, *J* = 246.6 Hz), 149.20 (d, *J* = 2.8 Hz), 143.62 (s), 137.28 (s), 136.90 (d, *J* = 5.2 Hz), 130.81 (d, *J* = 9.5 Hz), 128.34 (d, *J* = 10.8 Hz), 120.96 (d, *J* = 26.1 Hz), 111.60 (d, *J* = 22.2 Hz), 55.85 (s), 52.62 (s), 23.29 (s), 23.08 (s).

HRMS (ESI) calcd for C₁₅H₁₈ClFN₂OS [M + H]⁺ 328.83 found 329.0886; M.p. = 114 °C

(R)-*N*-((*R*)-1-(6-Fluoro-2-chloroquinoline-3-yl)ethyl)-2-methylpropane-2-sulfinamide **43d**



^1H NMR (400 MHz, DMSO) δ 8.55 (s, 1H), 8.04 (dd, J = 8.9, 5.3 Hz, 1H), 7.88 (dd, J = 8.9, 1.9 Hz, 1H), 7.73 (t, J = 7.6 Hz, 1H), 6.08 (d, J = 6.8 Hz, 1H), 4.91 – 4.76 (m, 1H), 1.52 (d, J = 6.6 Hz, 3H), 1.12 (s, 9H). ^{19}F NMR (376 MHz, DMSO) δ -112.17 (s). ^{13}C NMR (101 MHz, DMSO) δ 160.59 (d, J = 246.3 Hz), 148.90 (s), 143.71 (s), 137.90 (s), 137.08 (d, J = 5.2 Hz), 130.91 (d, J = 9.5 Hz), 128.37 (d, J = 10.7 Hz), 121.10 (d, J = 26.0 Hz), 111.69 (d, J = 22.4 Hz), 55.87 (s), 51.15 (s), 23.13 (s), 22.98 (s).

MS (ESI) calcd for $\text{C}_{15}\text{H}_{18}\text{ClFN}_2\text{OS}$ $[\text{M} + \text{H}]^+$ 328.83 found 329.18; M.p. = 138 °C

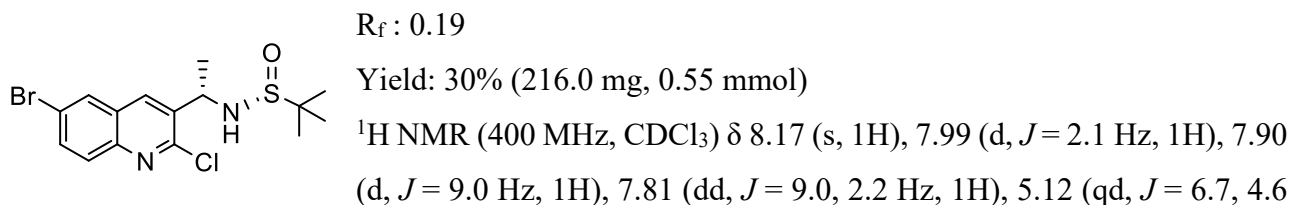
(R)-*N*-((*S*)-1-(6-Bromo-2-chloroquinolin-3-yl)ethyl)-2-methylpropane-2-sulfinamides **42e** and *(R)*-*N*-((*R*)-1-(6-Bromo-2-chloroquinolin-3-yl)ethyl)-2-methylpropane-2-sulfinamides **43e**

(R)-*N*-((6-Bromo-2-chloroquinolin-3-yl)methylene)-2-methylpropane-2-sulfinamide **41d**: 693.0 mg (1.85 mmol)

Reaction time: 72h

Yield: 43% total

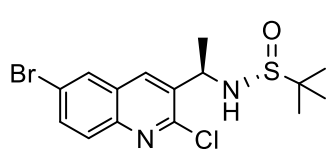
(R)-*N*-((*S*)-1-(6-Bromo-2-chloroquinolin-3-yl)ethyl)-2-methylpropane-2-sulfinamides **42e**



^1H NMR (400 MHz, CDCl_3) δ 8.17 (s, 1H), 7.99 (d, J = 2.1 Hz, 1H), 7.90 (d, J = 9.0 Hz, 1H), 7.81 (dd, J = 9.0, 2.2 Hz, 1H), 5.12 (qd, J = 6.7, 4.6 Hz, 1H), 3.49 (d, J = 4.2 Hz, 1H), 1.71 (d, J = 6.7 Hz, 3H), 1.28 (s, 9H). ^{13}C NMR (101 MHz, CDCl_3) δ 150.30 (s), 145.41 (s), 136.53 (s), 135.17 (s), 133.95 (s), 129.97 (s), 129.58 (s), 128.36 (s), 121.20 (s), 56.12 (s), 51.92 (s), 23.45 (s), 22.62 (s).

HRMS (ESI) calcd for $\text{C}_{14}\text{H}_{14}\text{BrClN}_2\text{OS}$ $[\text{M} + \text{H}]^+$ 373.69 found 389.0085; M.p. = 134 °C

(R)-*N*-((*R*)-1-(6-Bromo-2-chloroquinolin-3-yl)ethyl)-2-methylpropane-2-sulfinamides **43e**



R_f : 0.25

Yield: 13% (92.0 mg, 0.24 mmol)

$^1\text{H NMR}$ (400 MHz, CDCl_3) δ 8.17 (s, 1H), 8.00 (d, $J = 2.1$ Hz, 1H), 7.91 (d, $J = 9.0$ Hz, 1H), 7.81 (dd, $J = 9.0, 2.2$ Hz, 1H), 5.12 (qd, $J = 6.7, 4.5$ Hz, 1H), 3.51 (d, $J = 4.3$ Hz, 1H), 1.71 (d, $J = 6.7$ Hz, 4H), 1.28 (s, 11H). $^{13}\text{C NMR}$ (101 MHz, CDCl_3) δ 150.30 (s), 145.41 (s), 136.52 (s), 135.17 (s), 133.95 (s), 129.96 (s), 129.58 (s), 128.36 (s), 121.20 (s), 56.14 (s), 51.93 (s), 23.44 (s), 22.62 (s).

HRMS (ESI) calcd for $\text{C}_{15}\text{H}_{18}\text{BrClN}_2\text{OS}$ $[\text{M} + \text{H}]^+$ 389.74 found 389.0085

M.p. = 110.5 °C

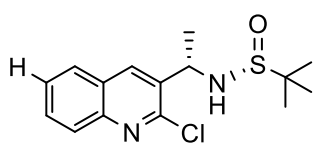
(R)-*N*-((*S*)-1-(2-Chloroquinoline-3-yl)ethyl)-2-methylpropane-2-sulfinamide **42f** and *(R)*-*N*-((*R*)-1-(2-Chloroquinoline-3-yl)ethyl)-2-methylpropane-2-sulfinamide **43f**

(R,E)-*N*-((2-chloroquinolin-3-yl)methylene)-2-methylpropane-2-sulfinamide **41f**: 104 mg (0.35 mmol)

Reaction time: 16h

Yield: 56% total

(R)-*N*-((*S*)-1-(2-Chloroquinoline-3-yl)ethyl)-2-methylpropane-2-sulfinamide **42f**



R_f : 0.12

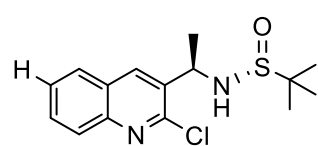
Yield: 36% (39 mg, 0.13 mmol)

$^1\text{H NMR}$ (400 MHz, CDCl_3) δ 8.24 (s, 1H), 8.02 (d, $J = 8.5$ Hz, 1H), 7.81 (d, $J = 8.1$ Hz, 1H), 7.73 (ddd, $J = 8.4, 7.0, 1.3$ Hz, 1H), 7.60 – 7.53 (m, 1H), 5.16 – 5.06 (m, 1H), 3.54 (d, $J = 4.6$ Hz, 1H), 1.71 (d, $J = 6.7$ Hz, 3H), 1.25 (s, 9H).

$^{13}\text{C NMR}$ (101 MHz, CDCl_3) δ 149.87 (s), 146.85 (s), 136.23 (d, $J = 7.4$ Hz), 135.30 (s), 130.52 (d, $J = 5.9$ Hz), 128.26 (s), 127.52 (s), 127.28 (s), 127.24 (s), 56.09 (s), 52.14 (s), 23.46 (s), 22.62 (s, $J = 42.2$ Hz).

HRMS (ESI) calcd for $\text{C}_{15}\text{H}_{19}\text{ClN}_2\text{O}_2\text{S}$ $[\text{M} + \text{H}]^+$ 310.84 found 311.0977; M.p. = oil

(R)-*N*-((*R*)-1-(2-Chloroquinoline-3-yl)ethyl)-2-methylpropane-2-sulfonamide **43f**



R_f: 0.20

Yield: 20% (22 mg, 0.07 mmol)

¹H NMR (400 MHz, CDCl₃) δ 8.25 (s, 1H), 8.04 (dd, *J* = 8.1, 0.5 Hz, 1H), 7.84 (dd, *J* = 8.2, 1.1 Hz, 1H), 7.75 (ddd, *J* = 8.5, 7.0, 1.4 Hz, 1H), 7.59 (ddd, *J* = 8.1, 7.0, 1.2 Hz, 1H), 5.16 – 5.07 (m, 1H), 3.49 (d, *J* = 4.4 Hz, 1H), 1.73 (d, *J* = 6.7 Hz, 4H), 1.27 (s, 9H).

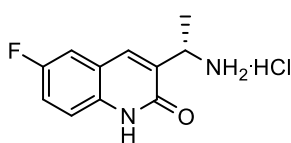
¹³C NMR (101 MHz, CDCl₃) δ 149.90 (s), 146.88 (s), 136.24 (s), 135.30 (s), 130.50 (s), 128.30 (s), 127.52 (s), 127.29 (s, *J* = 4.0 Hz), 127.25 (s), 56.09 (s), 52.17 (s), 23.47 (s), 22.62 (s).

HRMS (ESI) calcd for C₁₅H₁₉ClN₂O₂S [M + H]⁺ 310.84 found 311.0977; M.p. = oil

General procedure for the preparation of (*S*)- and (*R*)-3-(1-Aminoethyl)-6-halogenatedquinoline-2(1*H*)-one hydrochlorides (*S*)- **45d-f and (*R*)-**45d-f**:**

The corresponding sulfonamides (**42d-f** and **43d-f**) were placed in a flask equipped with a magnetic stirring bar, dissolved in a 1:1 mixture of dioxane and 1N HCl (0.2M) and heated to 100°C until complete consumption of the starting material, as indicated by TLC (Hex:AcOEt 3:2). The solvent was then evaporated and the crude mixture was left overnight drying at the oil pump. All products were characterized by mass analysis and used without further purification.

(S)-3-(1-Aminoethyl)-6-fluoroquinoline-2(1*H*)-one hydrochlorides (*S*)- **45d**

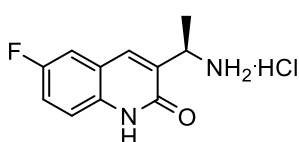


42d: 334.7 mg (1.02 mmol)

Reaction time: 2h

R_f: 0.0; MS (ESI) calcd for C₁₁H₁₂Cl₂FN₂O [M + H]⁺ 242.68 found 207.30

(R)-3-(1-Aminoethyl)-6-fluoroquinoline-2(1*H*)-one hydrochlorides (*R*)-**45d**

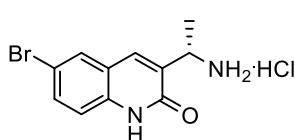


43d: 167.0 mg (0.51 mmol)

Reaction time: 2h

R_f: 0.0; MS (ESI) calcd for C₁₁H₁₂Cl₂FN₂O [M + H]⁺ 224.69 found 207.30

(S)-3-(1-Aminoethyl)-6-bromoquinoline-2(1*H*)-one hydrochlorides (*S*)- **45e**

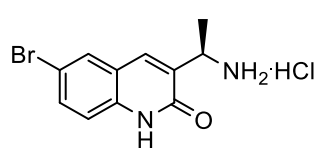


42e: 245.0 mg (0.628 mmol)

Reaction time: 4h

R_f: 0.0; MS (ESI) calcd for C₁₁H₁₂BrClN₂O [M + H]⁺ 303.58 found 268.07

(R)-3-(1-Aminoethyl)-6-fluoroquinoline-2(1H)-one hydrochlorides (**R**)- 45e



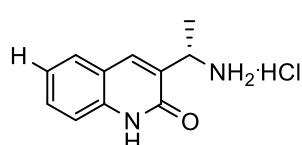
43e: 103.0 mg (0.26 mmol)

Reaction time: 4h

R_f : 0.0; MS (ESI) calcd for C₁₁H₁₂BrClN₂O [M + H]⁺ 303.58 found

268.07

(S)-3-(1-Aminoethyl)-quinoline-2(1H)-one hydrochlorides (**S**)- 45f

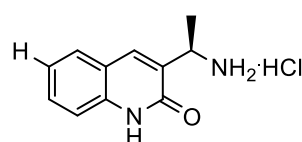


42f: 144 mg (0.46 mmol)

Reaction time: 7h

R_f : 0.0; MS (ESI) calcd for C₁₁H₁₃ClN₂O [M + H]⁺ 224.69 found 189.34

(R)-3-(1-Aminoethyl)-quinoline-2(1H)-one hydrochlorides (**R**)- 45f



43f: 219 mg (0.70 mmol)

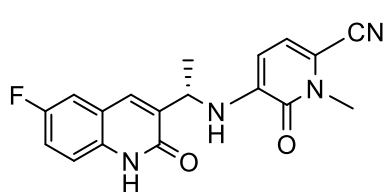
Reaction time: 7h

R_f : 0.0; MS (ESI) calcd for C₁₁H₁₃ClN₂O [M + H]⁺ 224.69 found 189.34

General procedure for the preparation of (*S*)- and (*R*)-5-((1-(6-Halogenated-2-oxo-1,2-dihydroquinolin-3-yl)ethyl)amino)-1-methyl-6-oxo-1,6-dihydropyridine-2-carbonitriles (*S*)- 46d-f and (*R*)-46d-f:

5-Fluoro-1-methyl-6-oxo-1,6-dihydropyridine-2-carbonitrile (1.1 eq.) **55** and the corresponding quinolone hydrochlorides (*(S)*-45d-f and *(R)*-45d-f) were placed in a flask, previously flushed with argon and equipped with a magnetic stirring bar, and dissolved in DMSO (0.1M) before further addition of DIPEA (3 eq.). The reaction mixture was heated to 110°C until complete consumption of the quinolone hydrochlorides, as indicated by TLC (Hex:AcOEt 1:4). The mixture was allowed to reach room temperature, diluted in AcOEt and DIPEA was quenched with water. The organic phase was separated and further washed with brine. The reunited organic phases were dried over Na₂SO₄, filtered, concentrated in vacuo, loaded on silica and purified via column chromatography to obtain the final compounds as solid.

(S)-5-((1-(6-Fluoro-2-oxo-1,2-dihydroquinoline-3-yl)ethyl)amino)-1-methyl-6-oxo-1,6-dihydropyridine-2-carbonitriles (**S**)-46d



(S)-45d: 247.53 mg (1.02 mmol)

Reaction time: 16h

R_f: 0.39

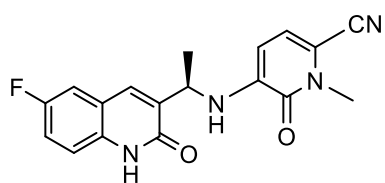
Yield: 20% (72.0 mg, 0.21 mmol)

α_D : +86.6 (0.187 g/100mL)

¹H NMR (400 MHz, CDCl₃) δ 12.70 (s, 1H), 7.65 (s, 1H), 7.47 (dd, J = 9.0, 4.6 Hz, 1H), 7.27 (td, J = 8.5, 2.7 Hz, 1H), 7.20 (dd, J = 8.5, 2.7 Hz, 1H), 6.70 (d, J = 7.8 Hz, 1H), 6.37 (d, J = 6.7 Hz, 1H), 5.95 (d, J = 7.9 Hz, 1H), 4.89 (p, J = 6.6 Hz, 1H), 3.76 (s, 3H), 1.67 (d, J = 6.7 Hz, 3H). ¹⁹F NMR (376 MHz, CDCl₃) δ -119.13 (s). ¹³C NMR (101 MHz, CDCl₃) δ 161.20 (d, J = 365.0 Hz), 156.97 (s), 156.85 (s), 141.29 (s), 134.44 (d, J = 3.3 Hz), 134.36 (s, J = 7.3 Hz), 134.29 (s), 120.40 (d, J = 9.0 Hz), 119.39 (s), 118.82 (d, J = 24.6 Hz), 117.46 (d, J = 8.3 Hz), 114.73 (s), 112.54 (d, J = 22.7 Hz), 105.82 (s), 104.45 (s), 47.82 (s), 34.66 (s), 21.42 (s).

HRMS (ESI) calcd for C₁₈H₁₅ClFN₄O₂ [M + H]⁺ 338.12 found 339.1251; M.p. = 218°C

(R)-5-((1-(6-Fluoro-2-oxo-1,2-dihydroquinoline-3-yl)ethyl)amino)-1-methyl-6-oxo-1,6-dihydropyridine-2-carbonitriles (**R**)-46d



(R)-45d: 123.03 mg (0.51 mmol)

Reaction time: 16h

R_f: 0.39

Yield: 35% (60.2 mg, 0.18 mmol)

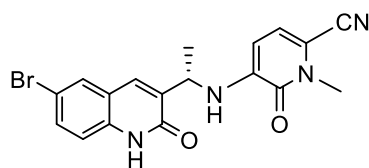
α_D : -63.7 (0.124 g/100mL)

¹H NMR (400 MHz, DMSO) δ 12.00 (s, 1H), 7.77 (s, 1H), 7.50 (dd, J = 9.2, 2.6 Hz, 1H), 7.44 – 7.30 (m, 2H), 6.97 (d, J = 7.8 Hz, 1H), 6.94 (d, J = 7.7 Hz, 1H), 5.97 (d, J = 8.1 Hz, 1H), 4.70 (p, J = 6.7 Hz, 1H), 3.59 (s, 3H), 3.33 (s, J = 8.7 Hz, 3H). ¹⁹F NMR (376 MHz, DMSO) δ -120.87 (s).

¹³C NMR (101 MHz, DMSO) δ 160.01 (d, J = 270.3 Hz), 156.38 (s), 156.30 (s), 141.90 (s), 135.54 (s), 135.14 (s), 134.13 (d, J = 3.1 Hz), 120.15 (d, J = 9.1 Hz), 119.90 (s), 118.52 (d, J = 24.5 Hz), 117.18 (d, J = 8.5 Hz), 115.63 (s), 113.00 (d, J = 22.8 Hz), 105.01 (s), 104.11 (s), 47.83 (s), 34.54 (s), 20.86 (s).

HRMS (ESI) calcd for C₁₈H₁₅ClFN₄O₂ [M + H]⁺ 338.12 found 339.1251; M.p. = 218°C

(S)-5-((1-(6-Bromo-2-oxo-1,2-dihydroquinoline-3-yl)ethyl)amino)-1-methyl-6-oxo-1,6-dihydropyridine-2-carbonitriles (**S**)-46e



(S)-45e: 116.0 mg (0.43 mmol)

Reaction time: 16h

R_f: 0.58

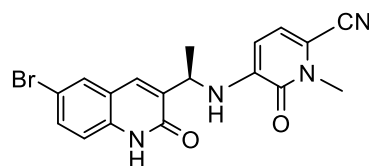
Yield: 56% (96.0 mg, 0.24 mmol)

¹H NMR (400 MHz, CDCl₃) δ 12.53 (s, 1H), 7.61 (d, J = 2.0 Hz, 1H), 7.59 (s, 1H), 7.54 (dd, J = 8.7, 2.0 Hz, 1H), 7.32 (d, J = 8.7 Hz, 1H), 6.67 (d, J = 7.8 Hz, 1H), 6.36 (d, J = 6.6 Hz, 1H), 5.91 (d, J = 7.9 Hz, 1H), 4.84 (p, J = 6.5 Hz, 1H), 3.73 (s, J = 8.4 Hz, 3H), 1.64 (d, J = 6.6 Hz, 3H).

¹³C NMR (101 MHz, CDCl₃) δ 162.90 (s), 156.80 (s), 141.25 (s), 140.61 (s), 136.66 (s), 134.42 (s), 133.95 (s), 133.18 (s), 129.95 (s), 121.16 (s), 119.40 (s), 117.44 (s), 115.25 (s), 114.72 (s), 105.76 (s), 104.50 (s), 47.76 (s), 40.94 (s), 34.65 (s).

MS (ESI) calcd for C₁₅H₁₈BrClN₂OS [M + H]⁺ 399.25 found 399.01; M.p. = oil

(R)-5-((1-(6-Bromo-2-oxo-1,2-dihydroquinoline-3-yl)ethyl)amino)-1-methyl-6-oxo-1,6-dihydropyridine-2-carbonitriles (**R**)-46e



(R)-45e: 85.0 mg (0.32 mmol)

Reaction time: 16h

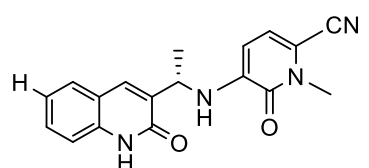
R_f: 0.58

Yield: 50% (64.6 mg, 0.16 mmol)

¹H NMR (400 MHz, CDCl₃) δ 11.94 (s, 1H), 8.24 (d, J = 7.3 Hz, 1H), 7.68 (d, J = 2.1 Hz, 1H), 7.63 – 7.59 (m, 2H), 7.31 (d, J = 8.7 Hz, 1H), 6.93 (d, J = 7.3 Hz, 1H), 6.70 (d, J = 7.8 Hz, 1H), 6.29 (d, J = 6.6 Hz, 1H), 5.93 (d, J = 7.9 Hz, 1H), 4.88 (p, J = 6.6 Hz, 1H), 3.77 (d, J = 6.1 Hz, 3H), 1.68 (d, J = 6.7 Hz, 4H). ¹³C NMR (101 MHz, CDCl₃) δ 162.90 (s), 156.80 (s), 141.25 (s), 136.66 (s), 134.42 (s), 133.18 (s), 129.95 (s), 121.16 (s), 119.40 (s), 117.44 (s), 115.25 (s), 114.72 (s), 113.18 (s), 105.76 (s), 104.50 (s), 47.76 (s), 40.94 (s), 34.65 (s).

MS (ESI) calcd for C₁₅H₁₈BrClN₂OS [M + H]⁺ 399.25 found 399.03; M.p. = oil

(S)-5-((1-(2-Oxo-1,2-dihydroquinoline-3-yl)ethyl)amino)-1-methyl-6-oxo-1,6-dihydropyridine-2-carbonitriles (**S**)-46f



(S)-45f: 105.8 mg (0.47 mmol)

Reaction time: 16h

R_f: 0.57

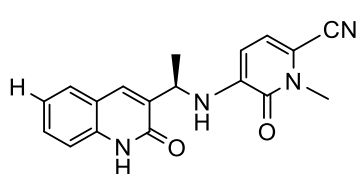
Yield: 26% (40.0 mg, 0.12 mmol)

α_D : not determined

^1H NMR (400 MHz, CDCl_3) δ 12.57 (s, 1H), 7.73 (s, 1H), 7.58 – 7.45 (m, 3H), 7.23 (ddd, $J = 8.1$, 7.0, 1.3 Hz, 1H), 6.70 (d, $J = 7.8$ Hz, 1H), 6.38 (d, $J = 6.7$ Hz, 1H), 5.99 (d, $J = 8.1$ Hz, 1H), 4.94 (p, $J = 6.6$ Hz, 1H), 3.77 (s, 3H), 1.70 (d, $J = 6.7$ Hz, 3H). ^{13}C NMR (101 MHz, CDCl_3) δ 163.37 (s), 156.89 (s), 141.40 (s), 137.76 (s), 135.29 (s), 133.04 (s), 130.48 (s), 127.84 (s), 122.91 (s), 119.83 (s), 119.52 (s), 115.79 (s), 114.81 (s), 105.64 (s), 104.51 (s), 47.68 (s), 34.65 (s), 21.53 (s).

HRMS (ESI) calcd for $\text{C}_{18}\text{H}_{16}\text{N}_4\text{O}_2$ $[\text{M} + \text{H}]^+$ 320.25 found 321.1353; M.p. = oil

(R)-5-((1-(2-Oxo-1,2-dihydroquinoline-3-yl)ethyl)amino)-1-methyl-6-oxo-1,6-dihydropyridine-2-carbonitriles **(R)**-46f



(R)-45f: 123.03 mg (0.51 mmol)

Reaction time: 16h

R_f : 0.57

Yield: 35% (60.2 mg, 0.18 mmol)

α_D : not determined

^1H NMR (400 MHz, CDCl_3) δ 12.57 (s, 1H), 7.73 (s, 1H), 7.58 – 7.45 (m, 3H), 7.23 (ddd, $J = 8.1$, 7.0, 1.3 Hz, 1H), 6.70 (d, $J = 7.8$ Hz, 1H), 6.38 (d, $J = 6.7$ Hz, 1H), 5.99 (d, $J = 8.1$ Hz, 1H), 4.94 (p, $J = 6.6$ Hz, 1H), 3.77 (s, 3H), 1.70 (d, $J = 6.7$ Hz, 3H). ^{13}C NMR (101 MHz, CDCl_3) δ 163.37 (s), 156.89 (s), 141.40 (s), 137.76 (s), 135.29 (s), 133.04 (s), 130.48 (s), 127.84 (s), 122.91 (s), 119.83 (s), 119.52 (s), 115.79 (s), 114.81 (s), 105.64 (s), 104.51 (s), 47.68 (s), 34.65 (s), 21.53 (s).

HRMS (ESI) calcd for $\text{C}_{18}\text{H}_{16}\text{N}_4\text{O}_2$ $[\text{M} + \text{H}]^+$ 320.25 found 321.1353

M.p. = oil

General procedure for the preparation of (S)- and (R)-((6-bromo-3-(1-((6-cyano-1-methyl-2-oxo-1,2-dihydropyridin-3-yl)amino)ethyl)quinolin-2-yl)oxy)methyl pivalate (S)- and (R)-47e and (S)- and (R)-((6-bromo-3-(1-((6-cyano-1-methyl-2-oxo-1,2-dihydropyridin-3-yl)amino)ethyl)-2-oxoquinolin-1(2H)-yl)methyl pivalate (S)- and (R)-48e:

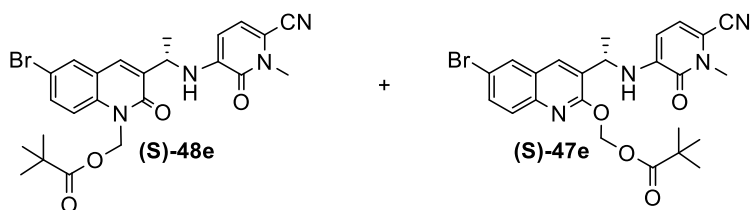
(S)- or (R)-46e (1 eq.) and K_2CO_3 (1.5 eq.) were placed in a flask, previously flushed with argon and equipped with a magnetic stirring bar, dissolved in DMF (0.2 M) and left under vigorous stirring at 60°C for 15 minutes. Afterwards, the mixture was allowed to reach room temperature before addition of POM-Cl (1.5 eq.). TLC (Hex: AcOEt 3:2) analysis after 16 hours showed complete consumption of the starting material and presence of two products. Saturated solution of ammonium chloride was added to the reaction which was then extracted with ethyl acetate until the aqueous phase resulted

product free. The combined organic phase was dried over Na₂SO₄, filtered, concentrated in vacuo and filtered via column chromatography to remove the unreacted starting material and the polar impurities. The combined products were isolated as solids in 85% yield and characterized.

R_fN-protected products **47e**: 0.61

R_fO-protected products **48e**: 0.77

(*S*)-((6-bromo-3-(1-((6-cyano-1-methyl-2-oxo-1,2-dihydropyridin-3-yl)amino)ethyl)quinolin-2-yl)oxy)methyl pivalate (**S**)-**47e** and (*S*)-((6-bromo-3-(1-((6-cyano-1-methyl-2-oxo-1,2-dihydropyridin-3-yl)amino)ethyl)-2-oxoquinolin-1(2*H*)-yl)methyl pivalate (**S**)-**48e**



(S)-**46e**: 203 mg, 0.51 mmol

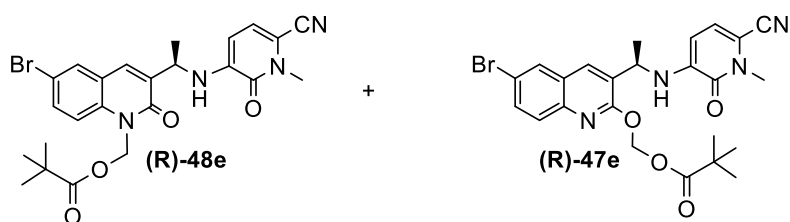
Yield : 84% (221 mg, 0.43 mmol)

¹H NMR (400 MHz, CDCl₃) δ 7.83 (d, *J* = 2.0 Hz, 1H), 7.80 (s, 1H), 7.74

(d, *J* = 8.9 Hz, 1H), 7.70 (dd, *J* = 8.9, 2.1 Hz, 1H), 7.66 (d, *J* = 2.2 Hz, 1H), 7.63 (dd, *J* = 8.9, 2.3 Hz, 1H), 7.51 (s, 1H), 7.22 (d, *J* = 8.9 Hz, 1H), 6.70 (d, *J* = 7.8 Hz, 1H), 6.63 (d, *J* = 7.8 Hz, 1H), 6.34 (dd, *J* = 11.3, 5.3 Hz, 4H), 6.20 (d, *J* = 6.1 Hz, 1H), 6.13 (d, *J* = 6.4 Hz, 1H), 5.90 (d, *J* = 8.0 Hz, 1H), 5.75 (d, *J* = 7.9 Hz, 1H), 4.88 – 4.77 (m, 2H), 3.77 (d, *J* = 1.2 Hz, 6H), 1.63 (d, *J* = 6.6 Hz, 8H), 1.63 (d, *J* = 6.7 Hz, 7H), 1.23 (s, 2H), 1.22 (s, 11H).

HRMS (ESI) calcd for C₂₄H₂₅BrN₄O₄ [M + H]⁺ 513.39 found 513.1135; M.p.: not measured

(*R*)-((6-bromo-3-(1-((6-cyano-1-methyl-2-oxo-1,2-dihydropyridin-3-yl)amino)ethyl)quinolin-2-yl)oxy)methyl pivalate (**R**)-**47e** and (*R*)-((6-bromo-3-(1-((6-cyano-1-methyl-2-oxo-1,2-dihydropyridin-3-yl)amino)ethyl)-2-oxoquinolin-1(2*H*)-yl)methyl pivalate (**R**)-**48e**



(R)-**46e**: 58 mg, 0.14 mmol

Yield: 99% (74 mg, 0.13 mmol)

traces of DMF

¹H NMR (400 MHz, CDCl₃) δ 7.81 (d, *J* = 2.0 Hz, 1H), 7.80 (s, 1H), 7.72

(d, *J* = 8.9 Hz, 1H), 7.68 (dd, *J* = 8.9, 2.1 Hz, 1H), 7.64 (d, *J* = 2.2 Hz, 1H), 7.61 (dd, *J* = 8.9, 2.3 Hz, 1H), 7.51 (s, 1H), 7.21 (d, *J* = 8.9 Hz, 1H), 6.69 (d, *J* = 7.8 Hz, 1H), 6.62 (d, *J* = 7.8 Hz, 1H), 6.33 (dd, *J* = 11.2, 5.3 Hz, 3H), 6.22 (d, *J* = 6.2 Hz, 1H), 6.14 (d, *J* = 7.5 Hz, 1H), 5.90 (d, *J* = 7.9 Hz, 1H), 5.74 (d, *J* = 7.9 Hz, 1H), 4.87 – 4.76 (m, 2H), 3.75 (s, 2H), 3.75 (s, 2H), 1.62 (d, *J* = 6.7 Hz, 6H), 1.21 (s, 9H), 1.21 (s, 5H).

HRMS (ESI) calcd for C₂₄H₂₅BrN₄O₄ [M + H]⁺ 513.39 found 513.1135; M.p.: not measured

General procedure for the preparation of (S)- and (R)-((3-(1-((6-cyano-1-methyl-2-oxo-1,2-dihydropyridin-3-yl)amino)ethyl)-6-(4,4,5,5-tetramethyl-1,3,2-dioxaborolan-2-yl)quinolin-2-yl)oxy)methyl pivalate (S)- and (R)-49 and (S)- and (R)-((3-(1-((6-cyano-1-methyl-2-oxo-1,2-dihydropyridin-3-yl)amino)ethyl)-2-oxo-6-(4,4,5,5-tetramethyl-1,3,2-dioxaborolan-2-yl)quinolin-1(2H)-yl)methyl pivalate (S)- and (R)-50:

Compounds (S)-47e and (S)-48e or (R)-47e and (R)-48e (1 eq.), bis(pinacolato)diboron (1.2 eq.), potassium acetate (7 eq.) and Pd(dppf)Cl₂ (5%) were placed in a round bottomed flask equipped with a magnetic stirring bar and flushed with argon for 5 minutes before being dissolved with dioxane (0.1 M). The mixture was heated at 80°C for 4.5 hours when mass analysis confirmed complete consumption of the starting material. The reaction was diluted with ethyl acetate and extracted with water and brine. The combined organic phase was further dried over Na₂SO₄, filtered and concentrated in vacuo. Finally, the crude product was loaded on silica and purified by column chromatography (Hexane: AcOEt 60%:40%).

Collected fractions yielded the final compounds (S)-49 and (S)-50 or (R)-49 and (R)-50 as white solids.

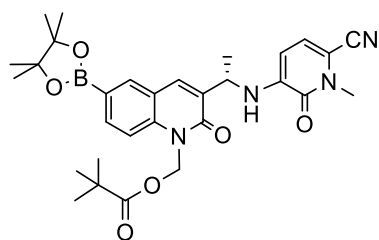
R_fN-protected products (S)-49 and (R)-49: 0.44

R_fO-protected products (S)-50 and (R)-50: 0.63

(S)-47e and (S)-48e: 221 mg, 0.43 mmol

Total yield: 56% (136 mg, 0.23 mmol)

(S)-((3-(1-((6-cyano-1-methyl-2-oxo-1,2-dihydropyridin-3-yl)amino)ethyl)-6-(4,4,5,5-tetramethyl-1,3,2-dioxaborolan-2-yl)quinolin-2-yl)oxy)methyl pivalate (S)-49



Yield: 23% (60 mg, 0.10 mmol)

α_D : -53.7 (0.095 g/100mL)

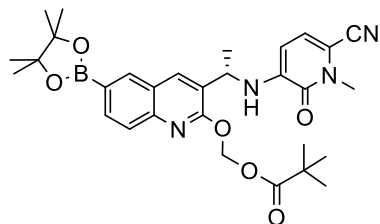
¹H NMR (400 MHz, CDCl₃) δ 7.97 (d, *J* = 1.2 Hz, 1H), 7.94 (dd, *J* = 8.5, 1.4 Hz, 1H), 7.59 (s, 1H), 7.29 (d, *J* = 8.4 Hz, 1H), 6.68 (d, *J* = 7.8 Hz, 1H), 6.43 – 6.33 (m, 2H), 6.13 (d, *J* = 6.5 Hz, 1H), 5.89 (d, *J* = 7.9 Hz, 1H), 4.88 – 4.80 (m, 1H), 3.78 (s, *J* = 2.5 Hz, 3H), 1.64 (d, *J* = 6.6 Hz, 5H), 1.36 (s, 9H), 1.22 (s, 9H).

^{13}C NMR (101 MHz, CDCl_3) δ 177.78 (s), 161.31 (s), 156.75 (s), 141.15 (s), 140.01 (s), 136.66 (s), 136.38 (s), 135.22 (s), 132.42 (s), 119.58 (s), 119.30 (s), 114.74 (s), 113.24 (s), 105.85 (s), 104.61 (s), 84.19 (s), 66.38 (s), 47.88 (s), 34.60 (s), 29.70 (s), 27.02 (s), 24.90 (s), 24.83 (s), 21.28 (s).

HRMS (ESI) calcd for $\text{C}_{30}\text{H}_{37}\text{BN}_4\text{O}_6$ $[\text{M} + \text{H}]^+$ 560.46 found 561.2878 ; M.p. = amorphous solid

(S)-(3-(1-((6-cyano-1-methyl-2-oxo-1,2-dihydropyridin-3-yl)amino)ethyl)-2-oxo-6-(4,4,5,5-tetramethyl-1,3,2-dioxaborolan-2-yl)quinolin-1(2H)-yl)methyl pivalate (**S**)-50

Yield: 30% (76 mg, 0.13 mmol)



α_D : -0.119.8 (0.086 g/100mL)

^1H NMR (400 MHz, CDCl_3) δ 8.18 (d, J = 0.9 Hz, 1H), 8.00 (dt, J = 11.2, 5.6 Hz, 1H), 7.88 (s, 1H), 7.82 (dd, J = 12.9, 5.9 Hz, 1H), 6.60 (d, J = 7.8 Hz, 1H), 6.38 (d, J = 5.3 Hz, 1H), 6.35 (d, J = 5.3 Hz, 1H),

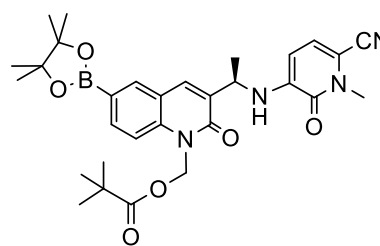
6.21 (d, J = 6.4 Hz, 1H), 5.74 (d, J = 8.0 Hz, 1H), 4.82 (p, J = 6.6 Hz, 1H), 3.78 (s, 3H), 1.63 (d, J = 6.7 Hz, 5H), 1.38 (s, 8H), 1.22 (s, 9H). ^{13}C NMR (101 MHz, CDCl_3) δ 177.56 (s), 157.96 (s), 156.75 (s), 147.06 (s), 141.16 (s), 135.59 (s), 135.20 (s), 134.71 (s), 126.33 (s), 125.53 (s), 125.22 (s), 119.16 (s), 114.71 (s), 105.85 (s), 104.60 (s), 84.06 (s), 81.98 (s), 47.48 (s), 34.60 (s), 26.92 (s), 24.92 (s), 24.87 (s), 21.99 (s).

HRMS (ESI) calcd for $\text{C}_{30}\text{H}_{37}\text{BN}_4\text{O}_6$ $[\text{M} + \text{H}]^+$ 560.46 found 561.2878; M.p. = amorphous solid

(R)-47e and **(R)**-48e: 74 mg, 0.14 mmol

Total yield: 33% (136 mg, 0.23 mmol)

(R)-((3-(1-((6-cyano-1-methyl-2-oxo-1,2-dihydropyridin-3-yl)amino)ethyl)-6-(4,4,5,5-tetramethyl-1,3,2-dioxaborolan-2-yl)quinolin-2-yl)oxy)methyl pivalate (**R**)-49



Yield: 10% (8.1 mg, 14 μmol)

α_D : +33.8 (0.154 g/100mL)

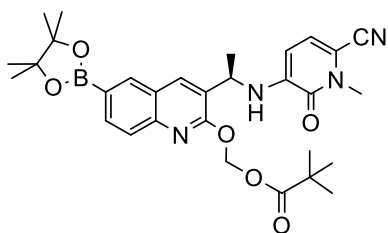
^1H NMR (400 MHz, CDCl_3) δ 7.97 (d, J = 1.1 Hz, 1H), 7.94 (dd, J = 8.5, 1.4 Hz, 1H), 7.59 (s, 1H), 7.29 (d, J = 7.6 Hz, 2H), 6.68 (d, J = 7.8 Hz, 1H), 6.43 – 6.33 (m, 2H), 6.13 (d, J = 6.4 Hz, 1H), 5.89

(d, J = 7.9 Hz, 1H), 4.84 (p, J = 6.4 Hz, 1H), 3.78 (s, 3H), 1.64 (d, J = 6.6 Hz, 4H), 1.36 (s, 11H), 1.22 (s, 8H).

^{13}C NMR (101 MHz, CDCl_3) δ 177.81 (s), 161.32 (s), 156.74 (s), 141.13 (s), 140.00 (s), 136.67 (s), 136.39 (s), 135.23 (s), 132.39 (s), 119.58 (s), 119.34 (s), 114.76 (s), 113.25 (s), 104.64 (s), 84.20 (s), 66.39 (s), 47.88 (s), 34.63 (s), 27.02 (s), 24.91 (s), 24.83 (s), 21.28 (s).

HRMS (ESI) calcd for $\text{C}_{30}\text{H}_{37}\text{BN}_4\text{O}_6$ $[\text{M} + \text{H}]^+$ 560.46 found 561.2878; M.p. = amorphous solid

(R)-(3-(1-((6-cyano-1-methyl-2-oxo-1,2-dihydropyridin-3-yl)amino)ethyl)-2-oxo-6-(4,4,5,5-tetramethyl-1,3,2-dioxaborolan-2-yl)quinolin-1(2H)-yl)methyl pivalate (**R**)-50



Yield: 23% (19 mg, 34 μmol)

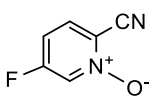
α_D : +76.9 (0.117 g/100mL)

^1H NMR (400 MHz, CDCl_3) δ 8.18 (s, 1H), 8.01 (dd, $J = 8.4, 1.3$ Hz, 1H), 7.88 (s, 1H), 7.84 (d, $J = 8.4$ Hz, 1H), 6.60 (d, $J = 7.8$ Hz, 1H), 6.38 (d, $J = 5.3$ Hz, 1H), 6.34 (d, $J = 5.3$ Hz, 1H), 6.21 (d, $J =$

6.3 Hz, 1H), 5.73 (d, $J = 7.9$ Hz, 1H), 4.82 (p, $J = 6.5$ Hz, 1H), 3.77 (s, 3H), 1.63 (d, $J = 6.7$ Hz, 3H), 1.37 (s, 12H), 1.22 (s, 9H). ^{13}C NMR (101 MHz, CDCl_3) δ 177.57 (s), 157.97 (s), 156.74 (s), 147.05 (s), 141.15 (s), 135.60 (s), 135.21 (s), 134.70 (s), 126.33 (s), 125.53 (s), 125.22 (s), 119.18 (s), 114.73 (s), 105.83 (s), 104.62 (s), 84.06 (s), 81.96 (s), 47.48 (s), 38.85 (s), 34.61 (s), 26.92 (s), 24.90 (d, $J = 5.6$ Hz), 21.99 (s).

HRMS (ESI) calcd for $\text{C}_{30}\text{H}_{37}\text{BN}_4\text{O}_6$ $[\text{M} + \text{H}]^+$ 560.46 found 561.2878; M.p. = amorphous solid

Synthesis of 2-Cyano-5-fluoropyridine 1-oxide 52

 5-fluoropicolinonitrile **51** (4.2 g, 34.5 mmol) and hydrogen peroxide urea UHP (6.5 g, 69 mmol, 2 eq.) were placed in a flask, previously flushed with argon and equipped with a magnetic stirring bar, and dissolved in CH_2Cl_2 (200 mL, 0.17M). The mixture was cooled with the aid of an ice bath before the dropwise addition of trifluoro acetic anhydride (10.5 mL, 72.5 mmol, 2.1 eq.), allowed to reach r.t. and left overnight under vigorous stirring. After 20 hours, TLC (Hex: AcOEt 3:2) analysis showed complete consumption of the starting material. The reacting mixture was cooled to 0°C and 100 mL of aqueous Na_2SO_3 solution (8.7 g, 60 mmol) was added in two portions to quench UHP and stirred for 15 minutes. The layers were then separated and the aqueous layer was extracted with CH_2Cl_2 . The combined organic layers were dried over Na_2SO_4 , filtered and concentrated in vacuo to give the final product without need of further purification (4.02 g, 29.09 mmol, yield = 85%).

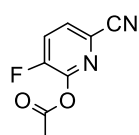
R_f 2-cyano-5-fluoropyridine 1-oxide: 0.66

R_f product: 0.18

¹H NMR (400 MHz, CDCl₃) δ 8.33 – 8.11 (m, 1H), 7.71 (dd, *J* = 9.0, 6.5 Hz, 1H), 7.21 – 7.13 (m, 1H). ¹⁹F NMR (376 MHz, CDCl₃) δ -111.40 (s). ¹³C NMR (101 MHz, CDCl₃) δ 162.18 (d, *J* = 262.5 Hz), 131.45 (d, *J* = 10.5 Hz), 130.84 (d, *J* = 38.4 Hz), 113.46 (d, *J* = 21.4 Hz), 111.06 (s).

HRMS (ESI) calcd for C₆H₃FN₂O [M + H]⁺ 138.10 found 138.0225; M.p. = 145 °C

Synthesis of 6-Cyano-3-fluoropyridin-2-yl acetate **53**



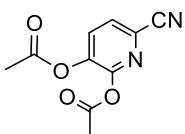
2-Cyano-5-fluoropyridine 1-oxide **52** (4.02 g, 29.09 mmol) was placed in a flask equipped with a magnetic stirring bar, dissolved in acetic anhydride (40 mL) and refluxed 16 hours. TLC (Hex: AcOEt 3:2) analysis didn't show any improvement

between 8 and 16 hours of reflux therefore the mixture was allowed to cool to room temperature before evaporation of the acetic anhydride. The crude product was then dissolved in ethyl acetate, loaded on silica and purified via column chromatography (Hex:AcOEt 90%:10%) to yield the final product (2.07g, 11.5 mmol, yield = 40%).

¹H NMR (400 MHz, CDCl₃) δ 7.74 – 7.62 (m, 1H), 2.39 (d, *J* = 3.1 Hz, 2H). ¹⁹F NMR (376 MHz, CDCl₃) δ -121.37 (s). ¹³C NMR (101 MHz, CDCl₃) δ 167.18 (s), 152.59 (d, *J* = 289.1 Hz), 147.51 (d, *J* = 15.8 Hz), 129.35 (d, *J* = 4.9 Hz), 126.88 (d, *J* = 5.9 Hz), 126.66 (d, *J* = 18.4 Hz), 115.59 (s), 20.42 (s).

R_f: 0. 80; HRMS (ESI) calcd for C₈H₅FN₂O₂ [M + H]⁺ 180.14 found 180.0329; M.p. = 90 °C

6-cyanopyridine-2,3-diyl diacetate was isolated and characterized as side-product **53b**

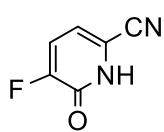


R_f **53b** : 0.54

Yield : 13% (653.49 mg, 2.9 mmol) ¹H NMR (400 MHz, CDCl₃) δ 7.85 (d, *J* = 8.2 Hz, 1H), 7.72 (d, *J* = 8.2 Hz, 1H), 2.39 (s, 3H), 2.36 (s, 3H).

MS (ESI) calcd for C₁₀H₈N₂O₄ [M + H]⁺ 220.18 found 221.18; M.p. = not measured

Synthesis of 5-Fluoro-6-oxo-1,6-dihydropyridine-2-carbonitrile **54**



6-Cyano-3-fluoropyridin-2-yl acetate **53** (2.07 g, 11.05 mmol) and K_2CO_3 (3.18 g, 23 mmol, 2 eq.) were placed in a flask, previously flushed with argon and equipped with a magnetic stirring bar, dissolved in methanol (23 mL, 0.5M) and the mixture was left

under vigorous stirring at room temperature. TLC (Hex: AcOEt 7:3) analysis after 1 hour showed complete consumption of the starting material. Methanol was completely evaporated and the crude mixture was dissolved in water (25 mL), acidified with concentrated HCl (4 mL) and extracted with ethyl acetate (150 mL). The organic phase was dried over Na_2SO_4 , filtered and concentrated in vacuo to yield the final product (1.49 g, 10.8 mmol, yield = 94%).

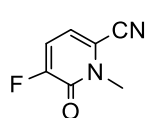
1H NMR (400 MHz, $CDCl_3$) δ 12.28 (s, 6H), 7.28 (t, $J = 2.9$ Hz, 1H), 7.16 (ddd, $J = 10.8, 5.7, 2.8$ Hz, 9H), 6.87 (ddd, $J = 7.6, 6.1, 2.9$ Hz, 9H). ^{19}F NMR (376 MHz, $CDCl_3$) δ -125.55 (s). ^{13}C NMR (101 MHz, $CDCl_3$) δ 155.33 (d, $J = 18.9$ Hz), 152.36 (d, $J = 265.3$ Hz), 122.07 (d, $J = 18.1$ Hz), 118.58 (d, $J = 4.5$ Hz), 114.97 (s).

R_f : 0. 0; HRMS (ESI) calcd for $C_6H_3FN_2O$ $[M + H]^+$ 138.02 found 138.0223; M.p. = 209 °C

Synthesis of 5-Fluoro-1-methyl-6-oxo-1,6-dihydropyridine-2-carbonitrile **55** and 5-fluoro-6-methoxypicolinonitrile **55b**

5-Fluoro-6-oxo-1,6-dihydropyridine-2-carbonitrile **54** (1.49g, 10.8 mmol) and K_2CO_3 (2.99 g, 21.6 mmol, 2 eq.) were placed in a flask, previously flushed with argon and equipped with a magnetic stirring bar, dissolved in DMF (30 mL, 0.35M) and left under vigorous stirring at room temperature for 15 minutes. Afterwards, the mixture was cooled to 0°C with the aid of an ice bath, MeI (740 μ L, 11.9 mmol, 1.1 eq.) was added dropwise and the reaction was allowed to reach room temperature. TLC (Hex: AcOEt 1:1) analysis after 2 hours showed complete consumption of the starting material but presence of two products. 2 mL of 2M NaOH were added to quench excess of MeI, the reaction was diluted with ethyl acetate and extracted until the aqueous phase resulted product free. The combined organic phase was dried over Na_2SO_4 , filtered, concentrated in vacuo and purified via column chromatography (Hex:AcOEt 80%:20%) to yield the final product and the corresponding O-protected analog as pure solids.

5-Fluoro-1-methyl-6-oxo-1,6-dihydropyridine-2-carbonitrile 55



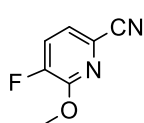
R_f : 0.56

Yield : 40% (670 mg, 4.4 mmol)

¹H NMR (400 MHz, CDCl₃) δ 7.12 (t, *J* = 7.9 Hz, 1H), 6.77 (dd, *J* = 7.7, 4.5 Hz, 1H), 3.78 (s, 3H). ¹⁹F NMR (376 MHz, CDCl₃) δ -116.91 (s). ¹³C NMR (101 MHz, CDCl₃) δ 155.82 (d, *J* = 263.1 Hz), 155.35 (d, *J* = 26.3 Hz), 118.32 (d, *J* = 18.9 Hz), 117.19 (d, *J* = 6.1 Hz), 114.29 (d, *J* = 6.6 Hz), 112.29 (s, *J* = 2.0 Hz), 34.96 (s, *J* = 1.5 Hz).

HRMS (ESI) calcd for C₇H₅FN₂O [M + H]⁺ 152.13 found 152.0381; M.p. = 107 °C

5-fluoro-6-methoxypicolinonitrile 55b



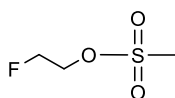
R_f : 0.85

Yield : not determined

¹H NMR (400 MHz, CDCl₃) δ 7.43 (dd, *J* = 9.1, 8.0 Hz, 1H), 7.34 (dd, *J* = 8.0, 3.1 Hz, 1H), 4.06 (s, 3H). ¹⁹F NMR (376 MHz, CDCl₃) δ -129.40 (s). ¹³C NMR (101 MHz, CDCl₃) δ 154.21 (d, *J* = 12.4 Hz), 149.93 (d, *J* = 269.5 Hz), 124.85 (d, *J* = 6.5 Hz), 123.44 (d, *J* = 5.2 Hz), 123.34 (d, *J* = 8.1 Hz), 116.64 (s), 54.65 (s).

MS (ESI) calcd for C₇H₅FN₂O [M + H]⁺ 152.13 found 153.02 ; M.p. = not determined

Synthesis of 2-fluoroethyl methanesulfonate 65



Fluoroethanol (1g, 15.61 mmol, 1 eq.) was placed in a flask, previously flushed with argon and equipped with a magnetic stirring bar, and dissolved in CH₂Cl₂ (15 mL, 0.1 M) before addition of triethylamine (3.30 mL, 23.41 mmol, 1.5 eq.). The mixture was cooled to 0°C before addition of Ms-Cl (1.32 mL, 17.61 mmol, 1.1 eq.), which made the solution turn turbid and yellow. After 3 hours the mixture was diluted with CH₂Cl₂, washed with ice water, 10% HCl solution, saturated solution of NaHCO₃ and brine. The combined organic phases were dried over Na₂SO₄, filtered and concentrated in vacuo to yield the final product as an orange oil (2.10g, 14.77 mmol, yield = 95%).

¹H NMR (400 MHz, DMSO) δ 4.78 – 4.69 (m, 1H), 4.65 – 4.59 (m, 1H), 4.52 – 4.47 (m, 1H), 4.44 – 4.39 (m, 1H), 3.22 (s, 3H). ¹⁹F NMR (376 MHz, DMSO) δ -223.51 (s).

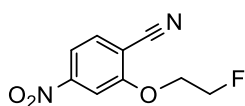
R_f : 0.54 (Hex:AcOEt 3:2)

MS (ESI) calcd for C₃H₇FO₃S [M + H] 142.14 found: not detectable; M.p. = oil

General procedure for the synthesis of 2-(2-fluoroethoxy)-4-nitrobenzonitrile 67d and 2-(2-(benzyloxy)ethoxy)-4-nitrobenzonitrile 67g

2-Hydroxy-4-nitrobenzonitrile (1 eq.) and cesium carbonate (1.3 eq.) were placed in a flask, previously flushed with argon and equipped with a magnetic stirring bar, dissolved in DMF (0.2M) before addition of **65** or **66** (1.3 eq.) The mixture was heated to 60°C and left under vigorous stirring until TLC (Hex: AcOEt 3:2) analysis after 2.5 hours showed complete consumption of the starting material. The DMF was evaporated before dissolving the crude in ethyl acetate and water and proceed with separation of the two phases. The organic phase was dried over Na₂SO₄, filtered, concentrated in vacuo and purified via column chromatography to yield the final products.

2-(2-fluoroethoxy)-4-nitrobenzonitrile 67d



2-fluoroethyl methanesulfonate **65**: 250.00 mg (1.52 mmol)

Reaction time: 2.5h

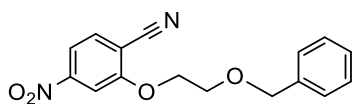
R_f: 0.26

Yield: 100% (319 mg, 1.51 mmol)

¹H NMR (400 MHz, DMSO) δ 8.11 (d, *J* = 8.5 Hz, 1H), 8.04 (d, *J* = 2.0 Hz, 1H), 7.95 (dd, *J* = 8.5, 2.1 Hz, 1H), 4.91 – 4.86 (m, 1H), 4.79 – 4.74 (m, 1H), 4.69 – 4.64 (m, 1H), 4.62 – 4.57 (m, 1H). ¹⁹F NMR (376 MHz, DMSO) δ -222.61 (s, *J* = 19.7 Hz). ¹³C NMR (101 MHz, DMSO) δ 160.85 (s), 151.79 (s), 135.79 (s), 116.59 (s), 115.24 (s), 108.76 (s), 107.12 (s), 82.14 (d, *J* = 167.4 Hz), 69.81 (d, *J* = 18.8 Hz).

MS (ESI) calcd for C₉H₇FN₂O₃ [M + H]⁺ 210.16 found: not detectable; M.p. = oil

2-(2-(benzyloxy)ethoxy)-4-nitrobenzonitrile 67g



(2-chloroethoxy)methyl)benzene **66**: 2.55 g (11.88 mmol)

Reaction time: 2.5h

R_f: 0.23

Yield: 85% (2.95 g, 10.11 mmol)

¹H NMR (400 MHz, DMSO) δ 8.09 (d, *J* = 8.5 Hz, 1H), 8.04 (d, *J* = 2.0 Hz, 1H), 7.92 (dd, *J* = 8.5, 2.1 Hz, 1H), 7.39 – 7.22 (m, 5H), 4.61 (s, 2H), 4.55 – 4.48 (m, 2H), 3.88 – 3.79 (m, 2H). ¹³C NMR (101 MHz, DMSO) δ 161.34 (s), 151.75 (s), 138.69 (s), 135.66 (s), 128.72 (s), 127.88 (s), 127.78 (s), 116.25 (s), 115.41 (s), 108.78 (s), 107.08 (s), 72.48 (s), 70.12 (s), 68.15 (s).

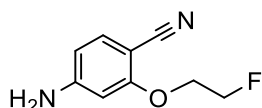
MS (ESI) calcd for C₁₆H₁₄N₂O₄ [M + H]⁺ 298.30 found: not detectable; M.p. > 300

General procedure for the synthesis of 4-amino-2-(2-fluoroethoxy)benzonitrile 68d and 4-amino-2-(2-(benzyloxy)ethoxy)benzonitrile 68g

68d or **68g** (1 eq.), NH₄Cl (10 eq.) and zinc powder (10 eq.) were placed in a round bottomed flask equipped with a magnetic stirring bar and dissolved in ethanol (0.2M). The reaction mixture was left under vigorous stirring at room temperature until mass analysis of an aliquot indicated consumption of the starting material.

Zinc powder was filtered off over a celite pad which was washed with ethanol. The organic phase was dried over Na₂SO₄, filtered, concentrated in vacuo and purified via column chromatography to yield the final products.

4-amino-2-(2-fluoroethoxy)benzonitrile 68d



2-(2-fluoroethoxy)-4-nitrobenzonitrile **67d**: 972 mg (4.62 mmol)

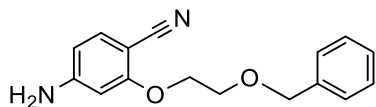
Reaction time: 40h

R_f: 0.38; Yield: 74% (616 mg, 3.42 mmol)

¹H NMR (400 MHz, DMSO) δ 7.26 (d, *J* = 8.4 Hz, 1H), 6.27 – 6.20 (m, 2H), 6.19 (s, 2H), 4.85 – 4.77 (m, 1H), 4.74 – 4.66 (m, 1H), 4.27 (dd, *J* = 4.6, 3.2 Hz, 1H), 4.20 (dd, *J* = 4.6, 3.2 Hz, 1H). ¹⁹F NMR (376 MHz, DMSO) δ -222.25 (s). ¹³C NMR (101 MHz, DMSO) δ 161.75 (s), 155.30 (s), 134.88 (s), 118.66 (s), 107.27 (s), 96.95 (s), 86.22 (s), 82.32 (d, *J* = 167.1 Hz), 67.88 (d, *J* = 19.1 Hz).

MS (ESI) calcd for C₉H₉FN₂O [M + H]⁺ 180.18 found 181.35; M.p. = 133.6°C

4-amino-2-(2-(benzyloxy)ethoxy)benzonitrile 68g



2-(2-(benzyloxy)ethoxy)-4-nitrobenzonitrile **67g** : 2.95 g (10.11 mmol)

Reaction time: 30h

R_f: 0.30; Yield: 60% (1.63 g, 6.07 mmol)

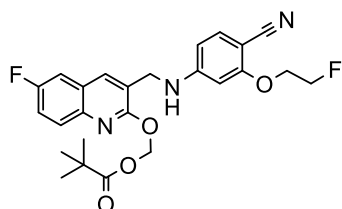
¹H NMR (400 MHz, DMSO) δ 7.40 – 7.27 (m, 5H), 7.25 (d, *J* = 8.4 Hz, 1H), 6.25 (d, *J* = 1.9 Hz, 1H), 6.19 (dd, *J* = 8.4, 1.9 Hz, 1H), 6.16 (s, 2H), 4.61 (s, 2H), 4.14 (dd, *J* = 5.3, 3.8 Hz, 2H), 3.78 (dd, *J* = 5.3, 3.9 Hz, 2H). ¹³C NMR (101 MHz, DMSO) δ 161.96 (s), 157.69 (s), 138.83 (s), 134.47 (s), 128.74 (s), 127.83 (s), 118.29 (s), 105.01 (s), 95.17 (s), 89.34 (s), 72.52 (s), 68.51 (s), 68.18 (s).

HRMS (ESI) calcd for C₁₆H₁₆N₂O₂ [M + H]⁺ 268.32 found 269.1286; M.p. = oil

General procedure for the synthesis of ((3-(((4-cyano-3-(2-fluoroethoxy)phenyl)amino)methyl)-6-fluoroquinolin-2-yl)oxy)methyl pivalate 59d, 2-(2-cyano-5-(((6-fluoro-2-((pivaloyloxy)methoxy)quinolin-3-yl)methyl)amino)phenoxy)ethyl benzoate 59g and 2-(2-cyano-5-(((6-fluoro-2-oxo-1-((pivaloyloxy)methyl)-1,2-dihydroquinolin-3-yl)methyl)amino)phenoxy)ethyl benzoate 60g:

POM protected 6-fluoroquinolones **35d** and/or **36d** (1 eq.) and **68d** or **68e** (1 eq.) were placed in a round bottomed flask equipped with a magnetic stirring bar and flushed with argon before addition of dry DMF (1 M). The mixture was cooled to 0°C with the aid of an ice bath before addition of TMS-OTf (2.5 eq.) and NaBH₄ (1 eq.). When TLC (Hex:AcOEt 3:2) analysis showed complete consumption of the starting materials, the mixture was further diluted with AcOEt followed by addition of Na₂CO₃ (s.s.) to quench of the excess of trimethylsilyl chloride. The organic phase was extracted and dried over Na₂SO₄, filtered, concentrated in vacuo and loaded on silica before purification by column chromatography to yield the desired compounds.

((3-(((4-cyano-3-(2-fluoroethoxy)phenyl)amino)methyl)-6-fluoroquinolin-2-yl)oxy)methyl pivalate 59d



4-amino-2-(2-fluoroethoxy)benzonitrile **68d** : 126.00 mg (0.67 mmol)
 ((6-fluoro-3-formylquinolin-2-yl)oxy)methyl pivalate **36d**: 206.10 mg
 (0.67 mmol)

Reaction time: 1h

R_f : 0.45; Yield: 44% (138.00 mg, 0.29 mmol)

¹H NMR (400 MHz, DMSO) δ 8.12 (s, 1H), 7.82 (dd, *J* = 9.2, 5.3 Hz, 1H), 7.77 (dd, *J* = 9.4, 2.9 Hz, 1H), 7.58 (td, *J* = 8.8, 2.9 Hz, 1H), 7.33 (d, *J* = 8.6 Hz, 1H), 7.26 (t, *J* = 6.0 Hz, 1H), 6.34 (d, *J* = 1.7 Hz, 1H), 6.26 (dd, *J* = 8.7, 1.8 Hz, 1H), 6.24 (s, 2H), 4.79 (dd, *J* = 4.6, 3.1 Hz, 1H), 4.67 (dd, *J* = 4.6, 3.0 Hz, 1H), 4.43 (d, *J* = 5.5 Hz, 2H), 4.32 – 4.28 (m, 1H), 4.25 – 4.21 (m, 1H), 1.13 (s, 9H). ¹⁹F NMR (376 MHz, DMSO) δ -116.13 (s), -222.26 (s). ¹³C NMR (101 MHz, DMSO) δ 177.03 (s), 161.14 (d, *J* = 124.8 Hz), 158.11 (s), 157.84 (d, *J* = 2.1 Hz), 154.22 (s), 141.89 (s), 136.42 (d, *J* = 4.5 Hz), 134.88 (s), 129.47 (d, *J* = 9.0 Hz), 126.47 (d, *J* = 10.3 Hz), 124.06 (s), 119.60 (d, *J* = 25.5 Hz), 118.40 (s), 111.68 (d, *J* = 22.2 Hz), 105.92 (s), 95.87 (s), 87.20 (s), 82.85 (d, *J* = 50.6 Hz), 81.44 (s), 68.09 (d, *J* = 19.1 Hz), 41.40 (s), 26.99 (s).

HRMS (ESI) calcd for C₂₅H₂₅F₂N₃O₄ [M + H]⁺ 469.49 found 470.1889; M.p. = 161.2 °C

2-(2-cyano-5-(((6-fluoro-2-((pivaloyloxy)methoxy)quinolin-3-yl)methyl)amino)phenoxy)ethyl benzoate **59g** and 2-(2-cyano-5-(((6-fluoro-2-oxo-1-((pivaloyloxy)methyl)-1,2-dihydroquinolin-3-yl)methyl)amino)phenoxy)ethyl benzoate **60g**:

2-(2-(benzyloxy)ethoxy)-4-nitrobenzonitrile **68g** : 957.04 mg (3.57 mmol)

(6-fluoro-3-formyl-2-oxoquinolin-1(2H)-yl)methyl pivalate **35d** and ((6-fluoro-3-formylquinolin-2-yl)oxy)methyl pivalate **36d**: 1.09 g (3.57 mmol)

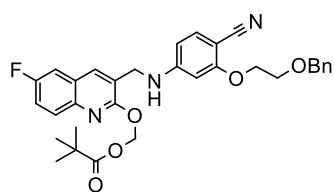
Reaction time: 1h

59g R_f: 0.6

60g R_f: 0.3

Yield: 70% (1.41 g, 2.54 mmol)

2-(2-cyano-5-(((6-fluoro-2-((pivaloyloxy)methoxy)quinolin-3-yl)methyl)amino)phenoxy)ethyl benzoate **59g**



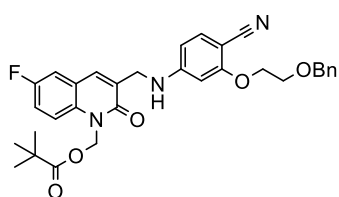
Yield: 44 % (885.20 mg, 1.58 mmol)

¹H NMR (400 MHz, DMSO) δ 8.11 (s, 1H), 7.82 (dd, *J* = 9.2, 5.3 Hz, 1H), 7.75 (dd, *J* = 9.4, 2.9 Hz, 1H), 7.58 (td, *J* = 8.8, 2.9 Hz, 1H), 7.36 – 7.21 (m, 7H), 6.33 (d, *J* = 1.5 Hz, 1H), 6.27 – 6.23 (m, 3H), 4.55 (s, 2H), 4.42 (d, *J* = 5.7 Hz, 2H), 4.16 (dd, *J* = 5.3, 3.7 Hz, 2H), 3.76 – 3.71 (m, 2H), 1.12 (s, 9H). ¹⁹F NMR (376 MHz, DMSO) δ -116.12 (s). ¹³C NMR (101 MHz, DMSO) δ 177.02 (s), 162.17 (s), 160.52 (s), 157.98 (d, *J* = 26.9 Hz), 154.17 (s), 141.88 (s), 138.76 (s), 136.37 (d, *J* = 4.6 Hz), 134.79 (s), 129.47 (d, *J* = 9.1 Hz), 128.71 (s), 127.83 (d, *J* = 2.2 Hz), 126.47 (d, *J* = 10.2 Hz), 124.08 (s), 119.59 (d, *J* = 25.3 Hz), 118.58 (s), 111.67 (d, *J* = 22.1 Hz), 105.77 (s), 95.78 (s), 87.24 (s), 82.59 (s), 72.50 (s), 68.37 (s), 68.15 (s), 41.38 (s), 38.72 (s), 26.99 (s).

HRMS (ESI) calcd for C₃₂H₃₂FN₃O₅ [M + H]⁺ 557.62 found 558.2401

M.p. = oil

2-(2-cyano-5-(((6-fluoro-2-oxo-1-((pivaloyloxy)methyl)-1,2-dihydroquinolin-3-yl)methyl)amino)phenoxy)ethyl benzoate **60g**



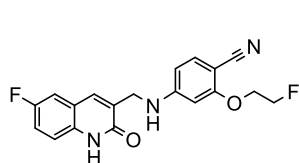
Yield: 27 % (553.10 mg, 0.95 mmol)

¹H NMR (400 MHz, DMSO) δ 7.77 (s, 1H), 7.66 (dd, *J* = 8.6, 2.1 Hz, 1H), 7.54 – 7.47 (m, 2H), 7.36 – 7.24 (m, 7H), 7.19 (t, *J* = 6.1 Hz, 1H), 6.37 – 6.25 (m, 4H), 4.56 (s, 2H), 4.29 (d, *J* = 5.6 Hz, 2H), 4.18 (dd, *J* = 5.3, 3.7 Hz, 2H), 3.75 (dd, *J* = 5.2, 3.8 Hz, 2H), 1.12 (s, 9H). ¹⁹F NMR (376 MHz, DMSO) δ -120.26

(s). ^{13}C NMR (101 MHz, DMSO) δ 177.21 (s), 161.53 (d, $J = 135.6$ Hz), 159.29 (s), 156.90 (s), 154.28 (s), 138.78 (s), 135.47 (d, $J = 2.4$ Hz), 134.75 (s), 131.08 (s), 128.71 (s), 127.82 (d, $J = 1.9$ Hz), 121.31 (d, $J = 9.1$ Hz), 118.64 (s), 118.49 (d, $J = 23.8$ Hz), 116.99 (d, $J = 8.3$ Hz), 114.27 (d, $J = 23.0$ Hz), 105.89 (s), 95.73 (s), 87.09 (s), 72.51 (s), 68.40 (s), 68.19 (s), 67.02 (s), 42.24 (s), 38.89 (s), 27.12 (s).

MS (ESI) calcd for $\text{C}_{32}\text{H}_{32}\text{FN}_3\text{O}_5$ $[\text{M} + \text{H}]^+$ 557.62 found 558.15; M.p. = 196.2 °C

Synthesis of 4-(((6-fluoro-2-oxo-1,2-dihydroquinolin-3-yl)methyl)amino)-2-(2-fluoroethoxy)benzonitrile 58d:



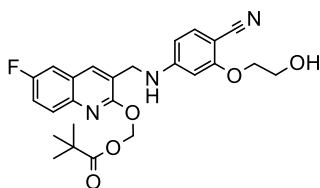
((3-(((4-cyano-3-(2-fluoroethoxy)phenyl)amino)methyl)-6-

fluoroquinolin-2-yl)oxy)methyl pivalate **59d** was suspended in 2 mL of 40% NaOH_{aq} (2 mL) and methanol (2 mL) and left stirring at 50°C. After one hour, a transparent solution was obtained, suggesting full conversion of the insoluble starting material, confirmed by TLC (Hex:AcOEt 3:2) analysis. Methanol was evaporated, the aqueous phase placed at 4°C overnight and filtered to yield the final compound as white crystals (10.65 mg, 0.03 mmol, yield = 10%).

^1H NMR (400 MHz, DMSO) δ 12.02 (d, $J = 16.0$ Hz, 1H), 7.72 (s, 1H), 7.55 (dd, $J = 9.3, 2.5$ Hz, 1H), 7.38 (dd, $J = 8.9, 2.7$ Hz, 1H), 7.33 (d, $J = 8.6$ Hz, 2H), 7.18 (t, $J = 6.0$ Hz, 1H), 6.35 (d, $J = 1.6$ Hz, 1H), 6.28 (dd, $J = 8.6, 1.6$ Hz, 1H), 4.82 – 4.77 (m, 1H), 4.70 – 4.64 (m, 1H), 4.35 – 4.30 (m, 1H), 4.25 (t, $J = 5.9$ Hz, 3H), 3.18 (d, $J = 5.2$ Hz, 2H). ^{19}F NMR (376 MHz, DMSO) δ -121.03 (s), -222.24 (s). ^{13}C NMR (101 MHz, DMSO) δ 161.79 (s), 161.73 (s), 157.49 (d, $J = 237.7$ Hz), 154.38 (s), 135.14 (s), 134.91 (d, $J = 3.0$ Hz), 134.81 (s), 131.92 (s), 120.19 (d, $J = 9.0$ Hz), 118.51 (s), 118.28 (d, $J = 24.4$ Hz), 117.13 (d, $J = 8.5$ Hz), 112.92 (d, $J = 22.9$ Hz), 106.05 (s), 95.70 (s), 86.85 (s), 82.30 (d, $J = 167.1$ Hz), 68.08 (d, $J = 19.0$ Hz), 41.85 (s).

R_f : 0.0; HRMS (ESI) calcd for $\text{C}_{19}\text{H}_{15}\text{F}_2\text{N}_3\text{O}_2$ $[\text{M} + \text{H}]^+$ 355.34 found 356.1206; M.p. >300 °C

Synthesis of ((3-(((4-cyano-3-(2-hydroxyethoxy)phenyl)amino)methyl)-6-fluoroquinolin-2-yl)oxy)methyl pivalate 61g



2-(2-cyano-5-(((6-fluoro-2-((pivaloyloxy)methoxy)quinolin-3-

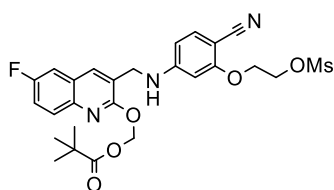
yl)methyl)amino)phenoxy)ethyl benzoate **59g** was placed in a flask with palladium/charcoal (15% mass, 110 mg) and ethanol (15 mL, 0.1 M) was added before the mixture was flushed with hydrogen steam for ten minutes. The flask was closed with a rubber septum and a balloon filled with hydrogen was placed on top. The mixture was left under stirring for 5 hours when an aliquot was taken, the charcoal filtered

and the solution analyzed by TLC (Hex:AcOEt 3:2) to confirm complete consumption of the starting material. The charcoal was filtered off on a celite pad which was washed with ethanol. The organic phase was dried over Na₂SO₄, filtered and concentrated in vacuo to yield the final compound in a pure form as dark solid (718 mg, 1.53 mmol, yield = 97%).

¹H NMR (400 MHz, DMSO) δ 8.12 (s, 1H), 7.82 (dd, *J* = 9.2, 5.3 Hz, 1H), 7.76 (dd, *J* = 9.4, 2.9 Hz, 1H), 7.58 (td, *J* = 8.8, 2.9 Hz, 1H), 7.30 (d, *J* = 8.5 Hz, 1H), 7.22 (t, *J* = 6.0 Hz, 1H), 6.33 (d, *J* = 1.6 Hz, 1H), 6.27 – 6.20 (m, 3H), 4.88 (t, *J* = 5.3 Hz, 1H), 4.42 (d, *J* = 5.7 Hz, 2H), 4.01 (t, *J* = 5.0 Hz, 2H), 3.70 (dd, *J* = 10.2, 5.2 Hz, 2H), 1.13 (s, 9H). ¹⁹F NMR (376 MHz, DMSO) δ -116.12 (s). ¹³C NMR (101 MHz, DMSO) δ 177.02 (s), 162.26 (s), 160.53 (s), 157.98 (d, *J* = 27.1 Hz), 154.17 (s), 141.88 (s), 136.39 (d, *J* = 4.6 Hz), 134.88 (s), 129.47 (d, *J* = 9.1 Hz), 126.47 (d, *J* = 10.2 Hz), 124.11 (s), 119.59 (d, *J* = 25.4 Hz), 118.62 (s), 111.68 (d, *J* = 22.1 Hz), 105.43 (s), 95.92 (s), 87.28 (s), 82.59 (s), 70.46 (s), 59.70 (s), 41.39 (s), 38.73 (s), 27.00 (s).

R_f: 0.15; HRMS (ESI) calcd for C₂₅H₂₆FN₃O₅ [M + H]⁺ 467.50 found 468.1932; M.p. >300

Synthesis of ((3-(((4-cyano-3-(2-((methylsulfonyl)oxy)ethoxy)phenyl)amino)methyl)-6-fluoroquinolin-2-yl)oxy)methyl pivalate **63**



((3-(((4-cyano-3-(2-hydroxyethoxy)phenyl)amino)methyl)-6-fluoroquinolin-2-yl)oxy)methyl pivalate **61g** (718 mg, 1.53 mmol) was placed in a round bottomed flask equipped with a magnetic stirring bar and flushed with argon before addition of dry CH₂Cl₂ (7.5 mL, 0.2 M).

The mixture was cooled to 0°C with the aid of an ice bath before addition of NEt₃ (320 μL, 2.29 mmol, 1.5 eq.) and Ms-Cl (142 μL, 1.83 mmol, 1.2 eq.). After 30 minutes at 0°C, TLC analysis showed presence of remained starting materials, therefore the mixture was left under stirring at room temperature for 2 additional hours. TLC analysis showed no improvement, hence the mixture was diluted with water and extracted. The organic phase was dried over Na₂SO₄, filtered, concentrated in vacuo and loaded on silica before purification by column chromatography (Hex:AcOEt 75%:25%) to yield the desired compound (650 mg, 1.19 mmol, yield = 78%).

¹H NMR (400 MHz, DMSO) δ 8.12 (s, 1H), 7.82 (dd, *J* = 9.1, 5.3 Hz, 1H), 7.76 (dd, *J* = 9.4, 2.9 Hz, 1H), 7.58 (td, *J* = 8.9, 2.9 Hz, 1H), 7.34 (d, *J* = 8.6 Hz, 1H), 7.27 (t, *J* = 5.9 Hz, 1H), 6.36 (d, *J* = 1.2 Hz, 1H), 6.27 (dd, *J* = 8.7, 1.3 Hz, 1H), 6.24 (s, 2H), 4.54 (dd, *J* = 5.2, 3.1 Hz, 2H), 4.44 (d, *J* = 5.6 Hz, 2H), 4.28 (dd, *J* = 5.1, 3.2 Hz, 2H), 3.24 (s, 3H), 1.13 (s, 9H). ¹⁹F NMR (376 MHz, DMSO) δ -116.12 (s). ¹³C NMR (101 MHz, DMSO) δ 177.03 (s), 161.56 (s), 160.53 (s), 157.99 (d, *J* = 26.2 Hz),

154.27 (s), 141.89 (s), 136.41 (d, $J = 4.7$ Hz), 134.88 (s), 129.47 (d, $J = 9.1$ Hz), 126.48 (d, $J = 10.4$ Hz), 124.05 (s), 119.61 (d, $J = 25.2$ Hz), 118.44 (s), 111.69 (d, $J = 22.1$ Hz), 106.01 (s), 95.92 (s), 87.10 (s), 82.60 (s), 68.90 (s), 66.74 (s), 41.40 (s), 38.74 (s), 37.25 (s), 27.00 (s).

R_f : 0.23 (Hex:AcOEt 3:2); HRMS (ESI) calcd for $C_{26}H_{28}FN_3O_7S$ $[M + H]^+$ 545.58 found 546.1704;

M.p. = 129.7 °C

5.3 Radiochemistry

5.3.1 [¹⁸F]Fluoride production

Non-carrier-added [¹⁸F]fluoride was produced daily via the ¹⁸O(p,n) ¹⁸F nuclear reaction through bombardment of enriched water with protons. The irradiation was carried out at the JSW cyclotron BC1710 (INM-5, Forschungszentrum Jülich) with 16.5 MeV beam flow.

5.3.2 Equipment

Aqueous ¹⁸F⁻ was fixed on Sep-Pak® Accell Plus QMA Carbonate Plus Light cartridges (130 mg sorbent, part no. 186004051) previously preconditioned with 1 mL of water. Oasis HLB (30 mg sorbent, part no. WAT094225) cartridges were used for the solid phase extraction before and after isolation of the pure products. Both products were supplied by Waters GmbH (Eschborn, Germany). Dry solvents for radiolabeling were purchased by Merck (Darmstadt, Germany).

All reactions were performed under air conditions in Wheaton v-vials, equipped with PTFE magnetic stirring bars and sealed with silicone septa. The reactors were placed in an aluminum block on the magnetic stirrer, equipped with boreholes matching the reaction vessels.

A glass stirring bar was used for radiofluorinations when the product was prepared to undergo biological evaluation in order to ensure higher molar activities.

5.3.3 Chromatography

The reactions were analyzed with an analytical HPLC system consisting on a Dionex Ultimate 3000 pump and Ultimate 3000 RS variable Wavelength detector (Thermo scientific) coupled in flow with a HERM LB500 radiodetector (Berthold Technologies, Bad Wildbad, Germany). An aliquot was injected in the HPLC Rheodyne 6 port injection valve equipped with a sample loop of 20 μL installed before the chromatographic column. A second aliquot was always injected behind the column in a similar valve and used as internal reference for the total activity. The second injection was not performed for quality controls.

The UV and radioactivity detectors were connected in series, giving a time delay of 0.25 min between the corresponding responses using 1 mL per minute flow rate.

For the analysis of all tracers reported in this work a Synergi Hydro-RP 4 μm (80 Å) 250 × 4.6 mm (Phenomenex, Aschaffenburg, Germany) was used.

For the analysis of the tracers containing a stereocenter, a CHIRALPACK AD column was used.

All tracers were isolated on a semipreparative system consisting of a Knauer K-100 pump, a Knauer K-2501 UV Detector, a Rheodyne 6 port injection valve equipped with a 2 mL injection loop and a custom-made Geiger counter. The column used was a Synergi Hydro RP 10 μ m (80 Å), LC column 250 x 10 mm (Phenomenex, California, USA) with a flow rate of 4.7 mL/min.

Table 13, 14 and 15 indicate the columns, eluent and retention times for the analysis of the produced radiotracers.

Table 13: Analytical HPLC conditions for the synthesized radiotracers using a Synergi Hydro-RP 4 μ m (80 Å) 250 \times 4.6 mm.

Tracer	Analytical HPLC	
	Eluent	t _R (min)
[¹⁸ F]mIDH-138	35% ACN + gradient 35-80%	17.7
[¹⁸ F](S)-olutasidenib	32% ACN + gradient 32-80%	12.3
[¹⁸ F](R)-olutasidenib	32% ACN + gradient 32-80%	12.3
[¹⁸ F]FE-mIDH	40% ACN + 0.1%TFA + gradient 40-90%	12.4

Table 14: Analytical HPLC conditions for [¹⁸F](S)- and [¹⁸F](R)-olutasidenib using a CHIRALPACK AD, 10 μ m (80 Å) 250 \times 4.6 mm.

Tracer	Chiral Analytical HPLC	
	Eluent	t _R (min)
[¹⁸ F](S)-olutasidenib	20% iPrOH in hexane	21.8
[¹⁸ F](R)-olutasidenib	20% iPrOH in hexane	19.4

Table 15: Semi-preparative HPLC conditions for the synthesized radiotracers using a Synergi Hydro RP 10 μ m (80 Å), LC column 250 x 10 mm.

Tracer	Semi-preparative HPLC	
	Eluent	t _R (min)
[¹⁸ F]mIDH-138	30% ACN	42-47
[¹⁸ F](S)-olutasidenib	28% ACN	35-39
[¹⁸ F](R)-olutasidenib	28% ACN	35-39
[¹⁸ F]FE-mIDH	35% ACN + 0.1%TFA	62-68

5.3.4 Important values for the description of the radiolabeled substances

5.3.4.1 Radiochemical conversion (RCC)

The radiochemical conversion defines the amount of fluoride-18 which is incorporated in the precursor to give the desired product and can be calculated through an HPLC analysis of the crude mixture. Two aliquots are injected in the HPLC before and after the column in the same volume of 20 μL . The peaks of the desired labelled compound and of the total activity are integrated and the ratio between the values gives the percentage of conversion.

Injection behind the column is fundamental for a precise analysis. HPLC columns, in particular the Hydro-RP, are designed to absorb most of the $^{18}\text{F}^-$. For this reason, the sum of amount of the unreacted fluoride-18 with the one introduced in the product is always significantly lower than the one actually introduced. The latter can be calculated without attenuation by injecting the crude mixture in a system that bypasses the column and elutes directly to the detectors.

5.3.4.2 Radiochemical purity (RCP)

The radiochemical purity can be calculated with the analytical HPLC and is the ratio of the activity of the desired product and the total activity of product and any present byproduct. Most often the main byproduct is $^{18}\text{F}^-$ itself which, as explained, cannot really be quantified with HPLC. When a defluorination is suspected, or after an HPLC purification, a radio-TLC can be performed to more easily visualise the presence of unreacted fluoride-18.

5.3.4.3 Radiochemical yield (RCY)

Defined as the decay corrected activity of the final purified product divided by the starting activity. The RCY is calculated by simply measuring with a curiemeter the starting and final activities and time. Subsequently the final activity is decay corrected to the starting time and divided by the starting activity to give the RCY in percentage.

5.3.4.3 Activity yield (AY)

The activity yield is the non-decay-corrected RCY. The ratio between the final and starting activity is calculated without adjustments to the total synthesis time. The activity yield is the important

parameter during the radiotracer's production for a delivery synthesis because it allows to easily calculate the required starting activity for the desired amount of product.

5.3.4.4 Molar Activity (A_m)

The molar activity is defined as the ratio between the activity of the radiotracer and the sum of the radioactive compound and the carrier amount (Equation 11). It is expressed in GBq/ μ mol and can be calculated at the end of the synthesis by injecting a known volume of the final tracer (either the HPLC cut or the final formulation) of known activity at a specific time. The peak area of the isotopically stable compound can be integrated and correlated to a certain quantity, expressed in mg, through a calibration curve. For the latter, decreasing known concentrations of reference compound are injected in the HPLC and a linear correlation of the peak area and the compound's concentration can be obtained.

$$A_m = \frac{\text{Activity (GBq)}}{\text{moles of carrier } (\mu\text{mol})} \quad \text{Equation 11}$$

It has to be noted that the values used for the calibration curve refer always to the absorption of a certain compound at a certain wavelength when detected by a certain detector. Therefore, the same HPLC must be used to perform the calibration curve and calculate the molar activity. It is common use to integrate the peaks where the compound has the maximum absorbance and the solvent signals do not interfere (normally 254 nm or 272 nm). Finally, while it is not needed to perform a different calibration curve when a different column is used, it is fundamental to do it when the tracer changes, since its absorption will most likely be different from previous tracers.

5.3.5 Radiosynthesis of [^{18}F]mIDH-138

5.3.5.1 *Radiofluorination of (3-(((4-cyano-3-methoxyphenyl)amino)methyl)-2-oxo-6-(4,4,5,5-tetramethyl-1,3,2-dioxaborolan-2-yl)quinolin-1(2H)-yl)methyl pivalate 39 or ((3-(((4-cyano-3-methoxyphenyl)amino)methyl)-6-(4,4,5,5-tetramethyl-1,3,2-dioxaborolan-2-yl)quinolin-2-yl)oxy)methyl pivalate 40*

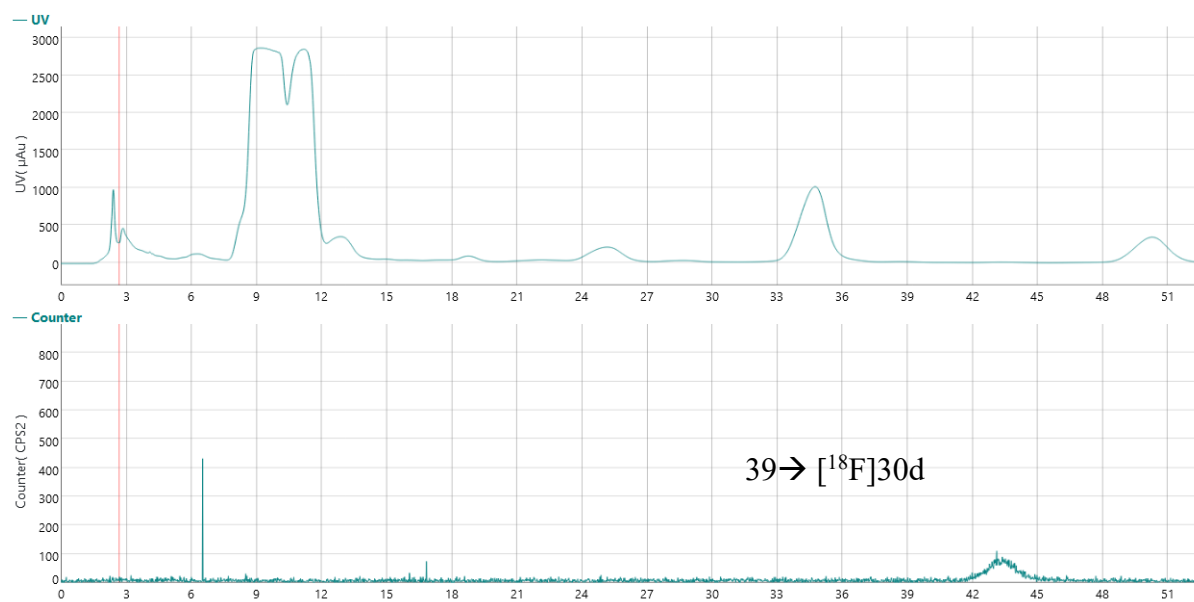
[^{18}F]fluoride was trapped on a QMA cartridge, previously preconditioned with 1 mL of water, and the remaining water was removed by rinsing the QMA from the male side with 1 mL of methanol

and 10 mL of air. The fluoride was then eluted with 1 mL of 1 mg/ mL solution of tetraethylammoniumbicarbonate in methanol which was afterwards evaporated (85°C, 200bar, 5 min) before addition of an equimolar mixture of 10µmol of **39** or **40** (5,45 mg) and (4-PhePy)₄Cu(ClO₄)₂ (9mg) dissolved in 500 µL of DMA. The mixture was left under stirring for 10 minutes at 110°C, then cooled for few minutes before addition of 200 µL of 0.25M NaOH_{aq.} in 50% MeOH at 80°C for 3 min. Finally, 200 µL of 5% TFA in acetonitrile were added to quench the reaction. An aliquot was diluted with acetonitrile and water for HPLC evaluation of the radiochemical conversion.

The crude mixture was then diluted with 2 mL of water and loaded on a HLB cartridge which was afterwards rinsed with 6 mL of water before eluting the product with 1.5 mL of ACN:water mixture (1:2) which was injected in the semi-preparative HPLC column for purification.

The pure collected fraction was diluted with ~40 mL of water and loaded on a HLB cartridge. The final radiotracer was eluted with 1 mL of EtOH and this solution used for the evaluation of the molar activity and radiochemical yield. The solution was afterwards evaporated to dryness with full vacuum at 35°C to allow the formulation with 1% Tween 80 solution in phosphate buffer (200µL) affording [¹⁸F]**30d** ready to inject.

The crude reaction mixtures of [¹⁸F]**30d** from **39** and **40** were purified via preparative HPLC (Figures 38).



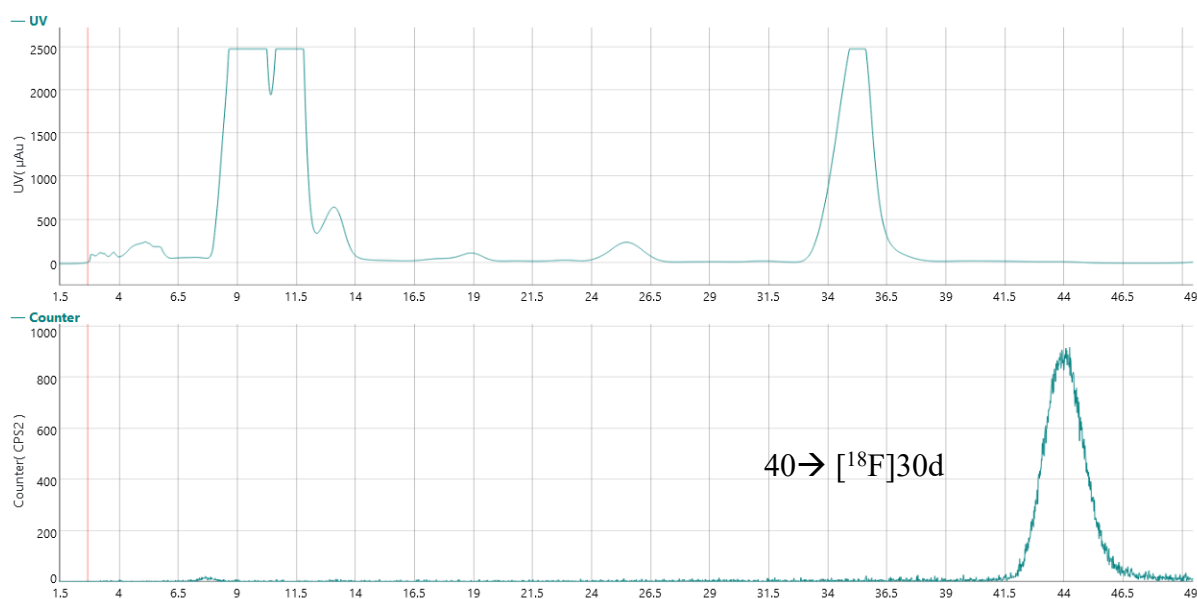


Figure 38: Traces of the purification of $[^{18}\text{F}]\mathbf{30d}$ from precursors $\mathbf{39}$ and $\mathbf{40}$ by semipreparative HPLC (Top: UV chromatogram, 254 nm; bottom: radio chromatogram). Synergi Hydro RP 10 μm (80 Å), LC column 250 x 10 mm. Eluent: 30% ACN in water

The isolated peak was identified as the desired tracer by co-injection with the reference compound, previously characterized.

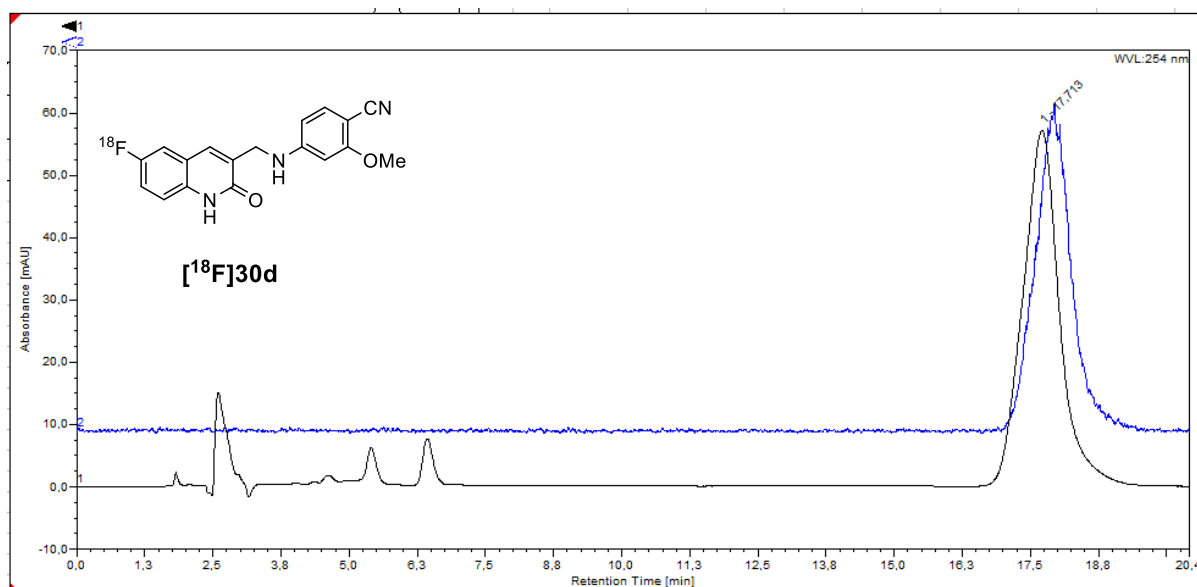


Figure 39: HPLC trace of $[^{18}\text{F}]\mathbf{30d}$ co-injected with the non-radioactive reference compound $\mathbf{30d}$ (95% pure) (Black: UV chromatogram, 254 nm; blue: radio chromatogram). Synergi Hydro-RP 4 μm (80 Å) 250 x 4.6 mm. Eluent: 35% ACN in water, 1 mL/min.

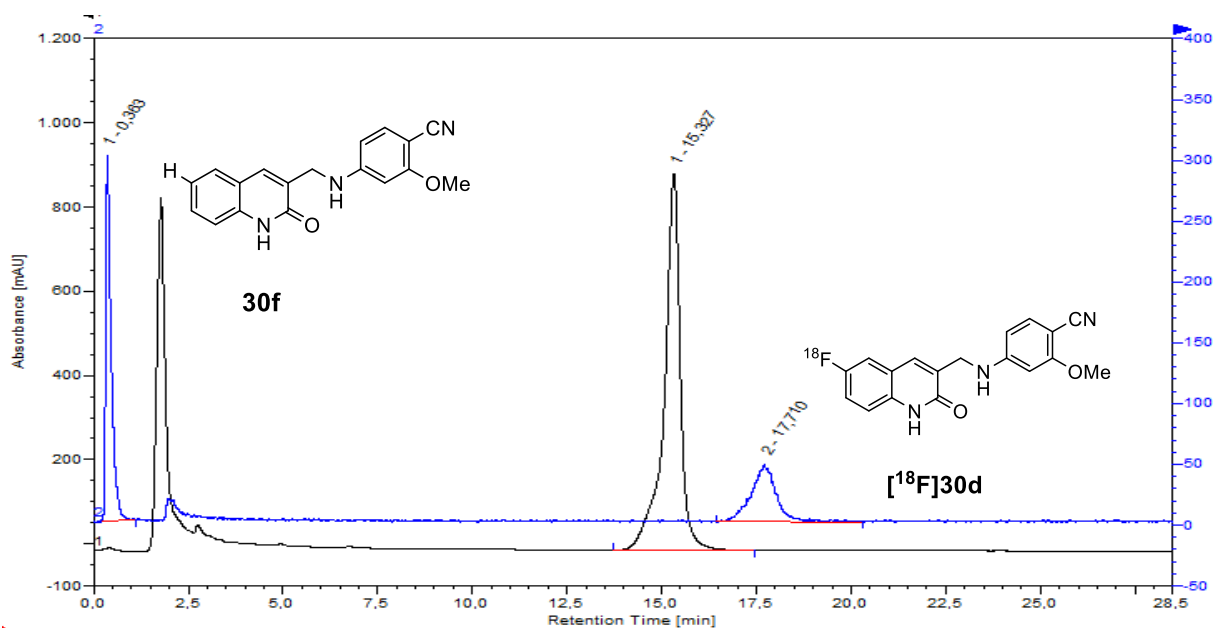
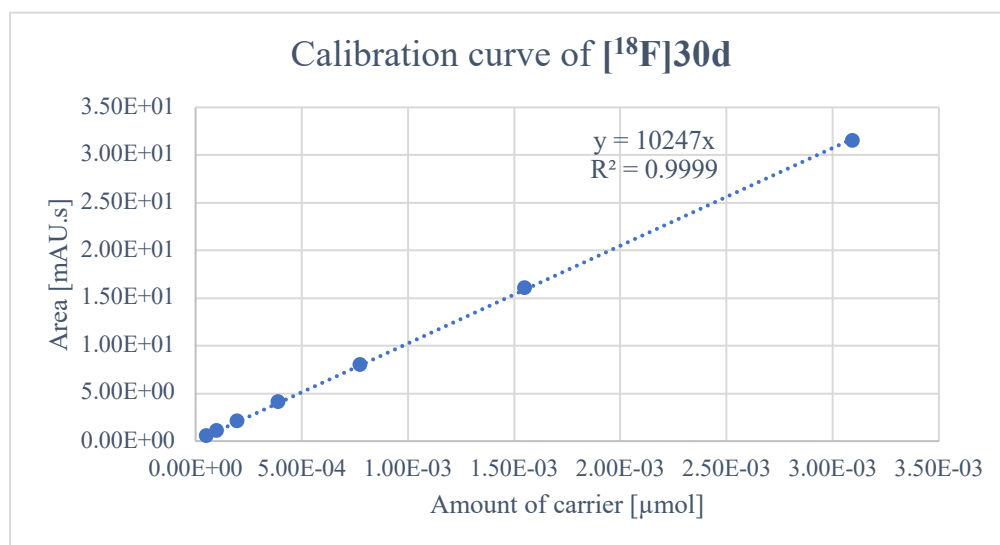


Figure 40: HPLC trace of [¹⁸F]30d co-injected with the protodeboronated impurity **30f** (Black: UV chromatogram, 272 nm; blue: radio chromatogram). Synergi Hydro-RP 4 μm (80 Å) 250 × 4.6 mm. Eluent: 35% ACN in water, 1 mL/min.

The calibration curve for the calculation of the molar activity of [^{18}F]30d was measured at 254 nm (Graph 9) with the data reported in Table 16.



Graph 9. Calibration curve for molar activities determination for the tracer [^{18}F]30d

mg/1 mL	mg/20 μL	g/20 μL	mol (g/323.13 g/mol)	μmol	Average Area
5.00E-02	1.00E-03	1.00E-06	3.09E-09	3.09E-03	3.15E+01
2.50E-02	5.00E-04	5.00E-07	1.55E-09	1.55E-03	1.61E+01
1.25E-02	2.50E-04	2.50E-07	7.73E-10	7.73E-04	8.05E+00
6.25E-03	1.25E-04	1.25E-07	3.87E-10	3.87E-04	4.12E+00
3.13E-03	6.25E-05	6.25E-08	1.93E-10	1.93E-04	2.14E+00

Table 16: Calibration data for the determination of the molar activity of [^{18}F]30d

5.3.5.2 Radiofluorination of 2-methoxy-4-(((2-oxo-6-(4,4,5,5-tetramethyl-1,3,2-dioxaborolan-2-yl)-1,2-dihydroquinolin-3-yl)methyl)amino)benzonitrile **33**

The unprotected precursor **33** was radiofluorinated using the general procedure indicated in 5.3.2.1. An equimolar mixture of 30 μmoles of **33** and copper mediator was dissolved in DMA and added to a reactor containing previously dried $^{18}\text{F}^-$. The mixture was stirred at 110°C for 10 minutes before addition of 200 μL of water to quench the reaction. An aliquot was analyzed *via* HPLC.

5.3.6 Radiosynthesis of 6-¹⁸F]Fluoro-(S)-olutasidenib and 6-¹⁸F]Fluoro-(S)-olutasidenib

5.3.6.1 Copper mediated radiofluorination of (S)- and (R)-3-(1-((6-cyano-1-methyl-2-oxo-1,2-dihydropyridin-3-yl)amino)ethyl)-2-oxo-6-(4,4,5,5-tetramethyl-1,3,2-dioxaborolan-2-yl)quinolin-1(2H)-yl)methyl pivalate (**S**)**49** and (**R**)**49** and (S)-((3-(1-((6-cyano-1-methyl-2-oxo-1,2-dihydropyridin-3-yl)amino)ethyl)-6-(4,4,5,5-tetramethyl-1,3,2-dioxaborolan-2-yl)quinolin-2-yl)oxy)methyl pivalate (**S**)**50** and (**R**)**50**

The procedure applied to precursors **39** and **40**, previously described in 5.3.5.1 was carried out on the O-protected precursors (**S**)**50** and (**R**)**50**. The reaction was carried out at 100°C for 15 minutes and followed by basic cleavage of protecting group and mild acidification prior to injection of analytical and semi-preparative HPLC for analysis of RCC and purification. The volume of the eluate was reduced through a HLB cartridge, eluted with 1mL of ethanol and analyzed to calculate the molar activity. After evaporation, the radiotracers could be formulated in PBS buffer.

The crude reaction mixtures of [¹⁸F](S)- and [¹⁸F](R)-**46d** were purified via preparative HPLC (Figure 41).

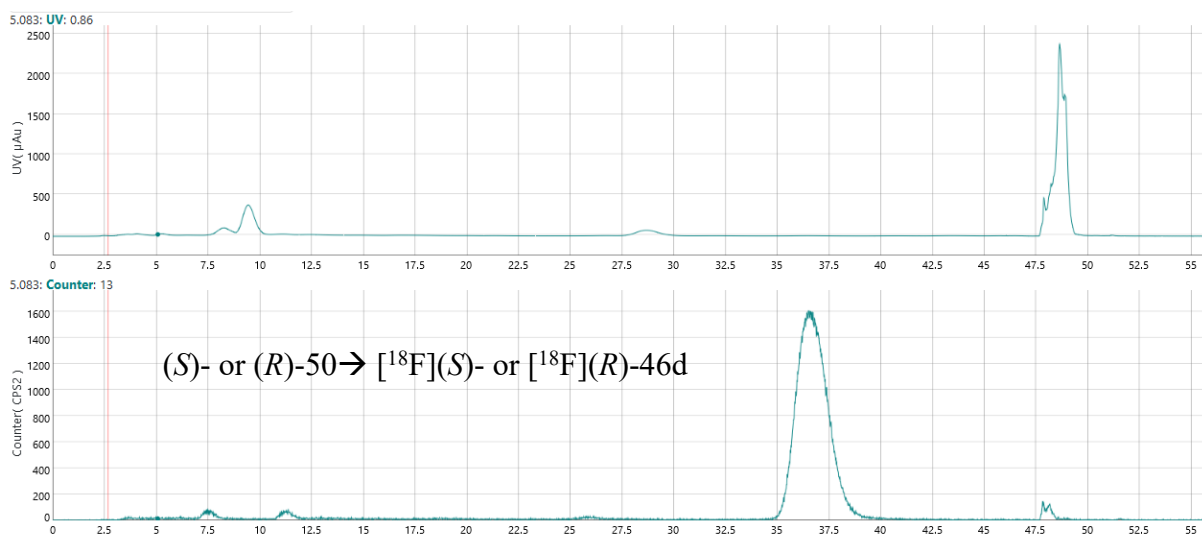


Figure 41: Trace of the purification of [¹⁸F](S)- and [¹⁸F](R)-**46d** from precursors (**S**)**50** and (**R**)**50** by semipreparative HPLC (Top: UV chromatogram, 270 nm; bottom: radiochromatogram). Synergi Hydro RP 10µm (80 Å), LC column 250 x 10 mm. Eluent: 28% ACN in water

The isolated peak was identified as the desired tracer by co-injection with the reference compound, previously characterized.

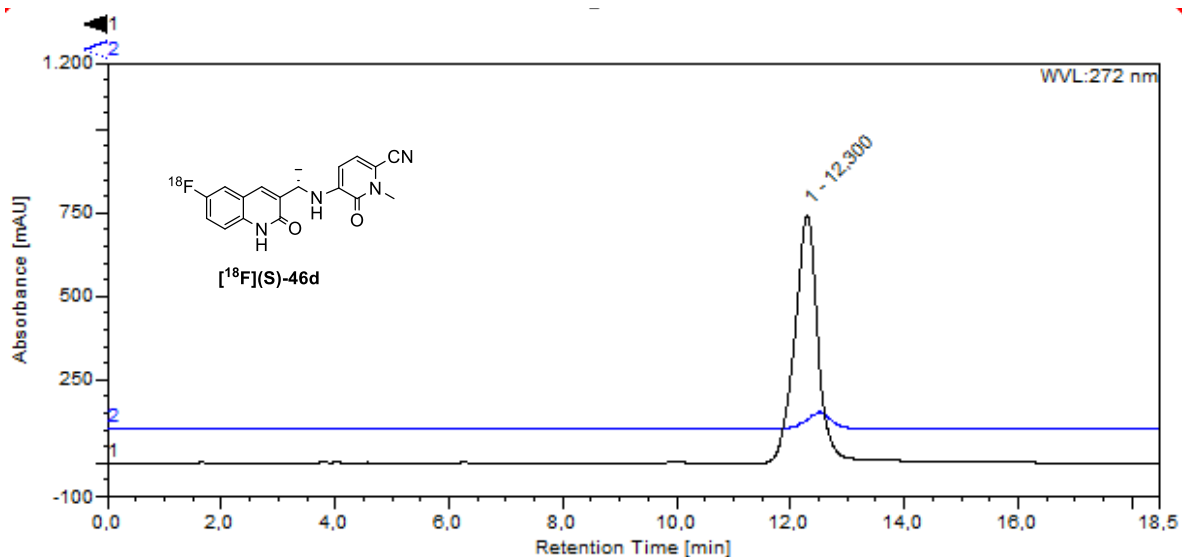


Figure 42: HPLC trace of [^{18}F](S)- or [^{18}F](R)-46d co-injected with the non-radioactive reference compound (S)-46d (99% pure) (Black: UV chromatogram, 272 nm; blue: radio chromatogram). Synergi Hydro-RP 4 μm (80 \AA) 250 \times 4.6 mm. Eluent: 32% ACN in water, 1 mL/min.

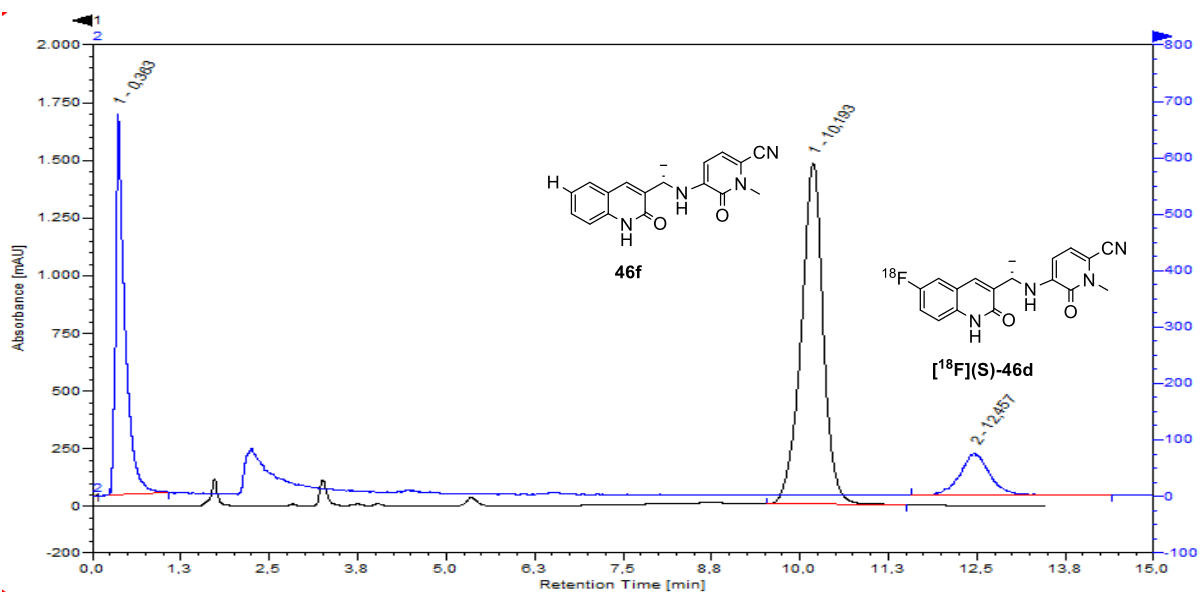
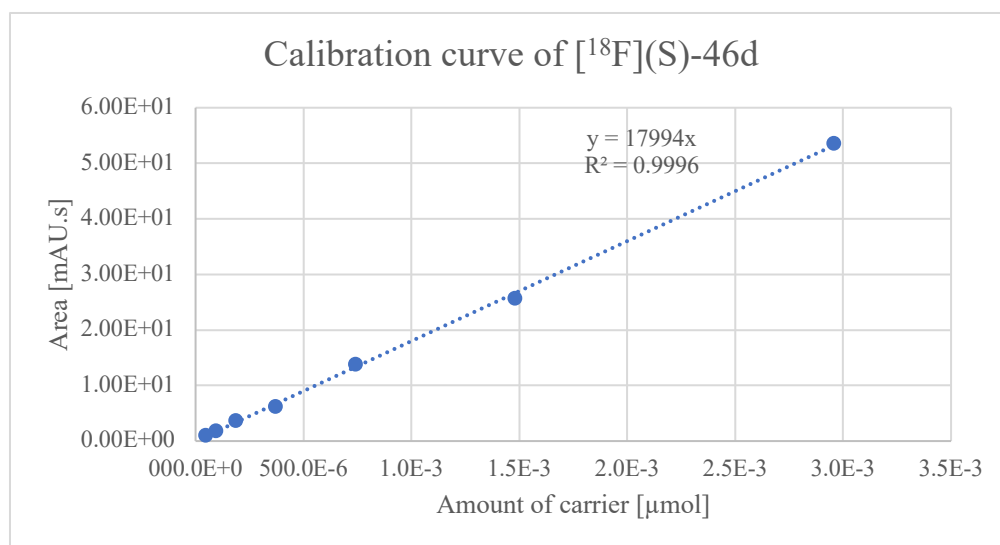


Figure 43: HPLC trace of [^{18}F](S)- or [^{18}F](R)-46d co-injected with the protodeboronated impurity 46f (Black: UV chromatogram, 272 nm; blue: radio chromatogram). Synergi Hydro-RP 4 μm (80 \AA) 250 \times 4.6 mm. Eluent: 32% ACN in water, 1 mL/min.

The calibration curve for the calculation of the molar activity of $[^{18}\text{F}](\text{S})\text{-46d}$ was measured at 272 nm (Graph 10 with the data reported in Table 17).



Graph 10: Calibration curve for molar activities determination for the tracers $[^{18}\text{F}](\text{S})\text{-46d}$ and $[^{18}\text{F}](\text{R})\text{-46d}$

mg/1 mL	mg/20 μL	g/20 μL	mol (g/323.13 g/mol)	μmol	Average Area
5.00E-02	1.00E-03	1.00E-06	2.96E-09	2.69E-03	5.35E+01
2.50E-02	5.00E-04	5.00E-07	1.48E-09	1.48E-03	2.57E+01
1.25E-02	2.50E-04	2.50E-07	7.39E-10	7.39E-04	1.38E+00
6.25E-03	1.25E-04	1.25E-07	3.69E-10	3.69E-04	6.23E+00
3.13E-03	6.25E-05	6.25E-08	1.85E-10	1.85E-04	3.65E+00
1.56 E-03	3.12E-05	3.13E-08	9.24E-11	9.24E-05	1.82E+00
7.81E-04	1.56E-05	1.56E-08	4.62E-11	4.62E-05	1.02E+00

Table 17: Calibration data for the determination of the molar activity of $[^{18}\text{F}](\text{S})\text{-46d}$ and $[^{18}\text{F}](\text{R})\text{-46d}$

5.3.6.2 Determination of enantiomeric excess

The reference compounds (**S**)-**46d**, (**R**)-**46d** and radiofluorination precursors (**S**)-, (**R**)-**49** and (**S**)-, (**R**)-**50** were dissolved in chloroform in ~ 1 mg/mL concentrations and injected in the cell of the polarimeter to be analyzed (Table 18) in terms of optical rotation and specific rotation. Before, a blank measurement of pure chloroform was measured.

Compound	Temperature	N (mg/mL)	Optical rotation	Specific rotation
(<i>S</i>)-46d	20.1 °C	0.187	0.162	86.6
(<i>R</i>)-46d	20.1 °C	0.124	-0.079	-63.7
(<i>S</i>)-49	20.4 °C	0.095	-0.051	-53.7
(<i>R</i>)-49	20.2 °C	0.154	0.052	43.8
(<i>S</i>)-50	20.1 °C	0.086	-0.103	-119.8
(<i>R</i>)-50	20.4 °C	0.116	0.090	79.9

Table 18: Optical rotation of reference compounds and precursors

The isolated radiotracers [^{18}F](**S**)- and [^{18}F](**R**)-**46d** were identified as the desired enantiomers by co-injection in the chiral HPLC column with the corresponding reference compound, previously characterized.

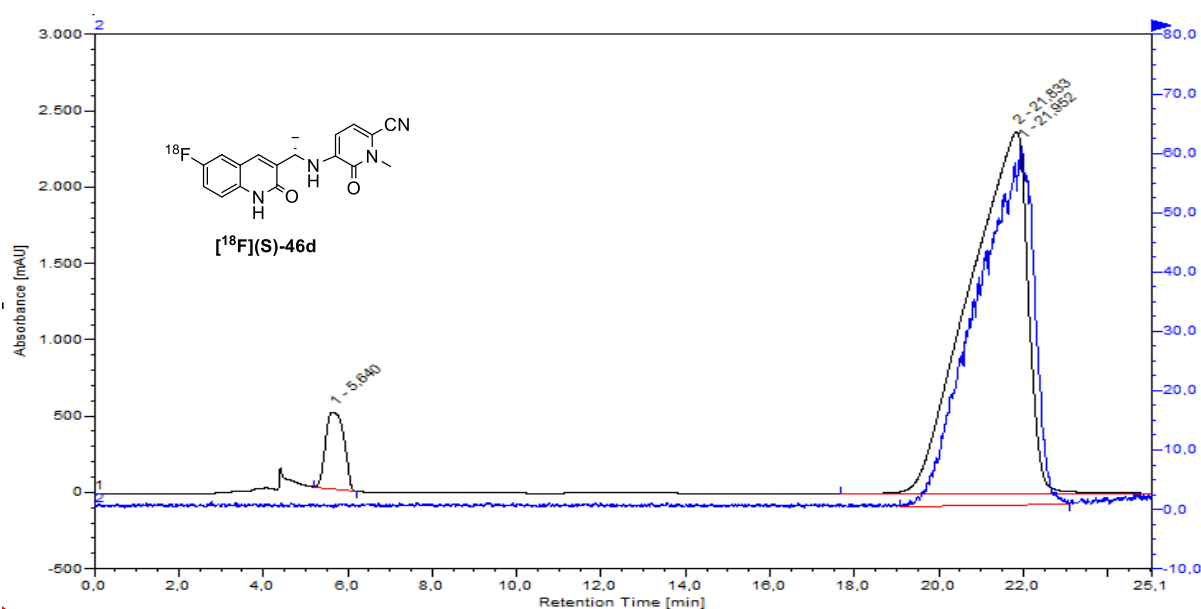


Figure 44: HPLC trace of [^{18}F](**S**)-**46d** co-injected with the non-radioactive reference compound (**S**)-**46d** (>99% pure) (Black: UV chromatogram, 272 nm; blue: radio chromatogram). CHIRALPACK AD, 10 μm (80 \AA) 250 \times 4.6 mm. Eluent: 20% *i*PrOH in hexane, 1 mL/min.

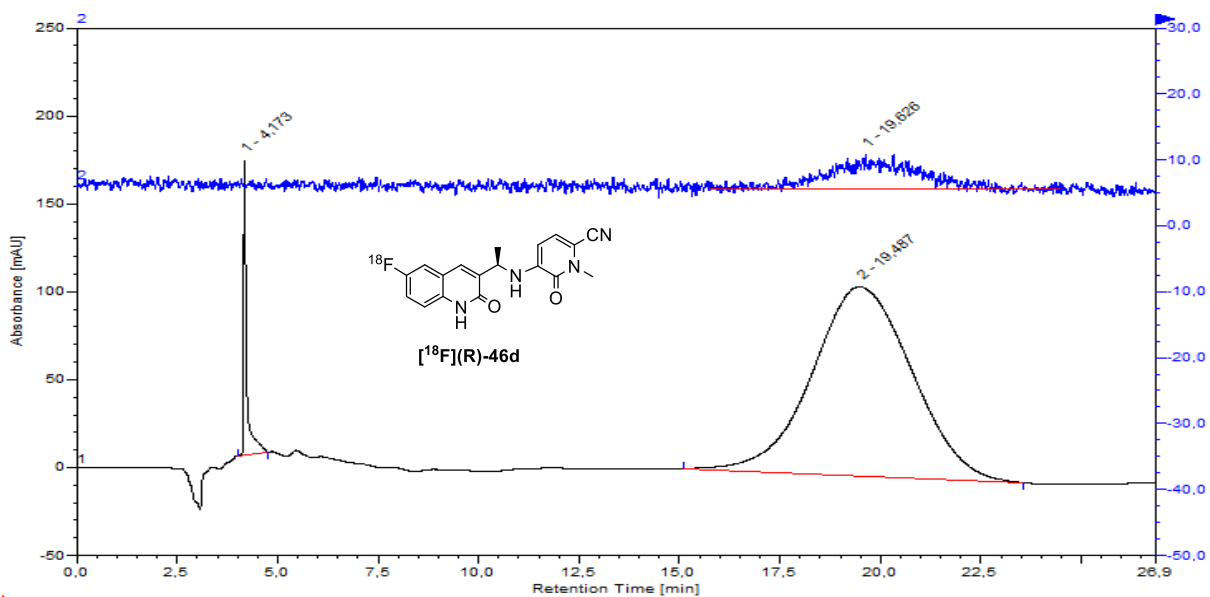


Figure 45: HPLC trace of $[^{18}\text{F}](\text{R})\text{-46d}$ co-injected with the non-radioactive reference compound $(\text{R})\text{-46d}$ (>99% pure) (Black: UV chromatogram, 272 nm; blue: radio chromatogram). CHIRALPACK AD, 10 μm (80 \AA) 250 \times 4.6 mm. Eluent: 20% *i*PrOH in hexane, 1 mL/min.

5.3.7 Radiosynthesis of [^{18}F]FE-mIDH

5.3.7.1 Aliphatic radiofluorination of ((3-(((4-cyano-3-(2-(methylsulfonyl)oxy)ethoxy)phenyl)amino)methyl)-6-fluoroquinolin-2-yl)oxy)methyl pivalate **63**

[^{18}F]Fluoride was trapped on a QMA cartridge, previously preconditioned with 1 mL of water, and the remaining water was removed by rinsing the QMA from the male side with 1 mL of methanol and 10 mL of air. The fluoride was then eluted with 0.5 mL of 1 mg/mL solution of tetramethylammonium triflate in methanol which was afterwards evaporated (85°C, 200bar, 5 min) before addition of 3.5 μmol s of **63** (2 mg) dissolved in 500 μL of ACN. The mixture was left under stirring for 15 minutes at 85°C and cooled to room temperature before addition of 100 μL of 0.1M NaOH_{aq.} in EtOH at 35°C for 10 min. Finally, 400 μL of water were added to quench the reaction. An aliquot was diluted with acetonitrile and water for HPLC evaluation of the radiochemical conversion.

The crude mixture was injected in the semi-preparative HPLC column for purification.

The pure collected fraction was used directly for the biological evaluation in cells.

The crude reaction mixture of [^{18}F]**58d** from **63** was purified via preparative HPLC (Figure 46).

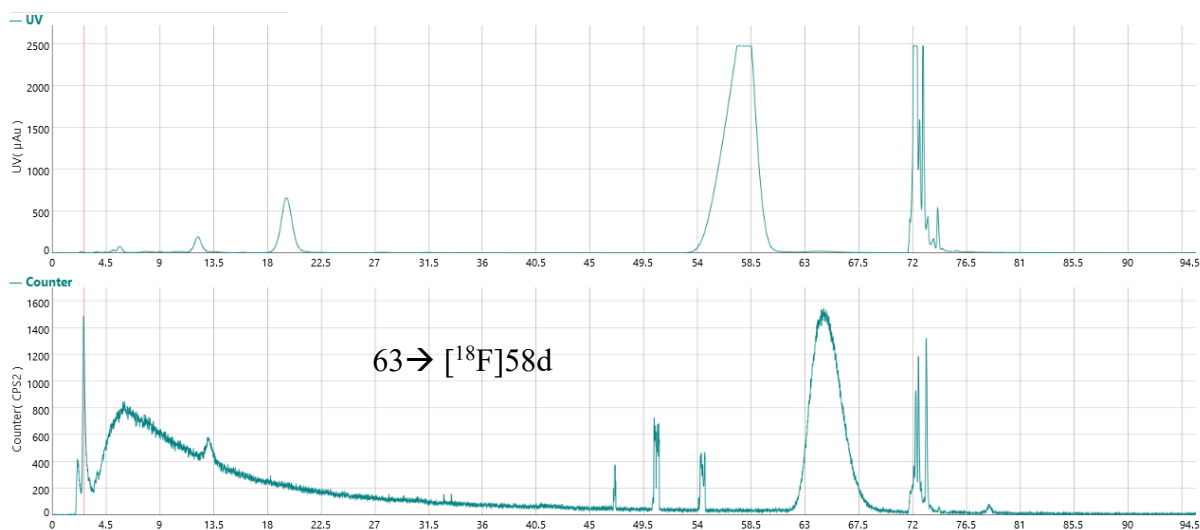


Figure 46: Trace of the purification of [^{18}F]**58d** from precursor **63** by semipreparative HPLC (Top: UV chromatogram, 270 nm; bottom: radio chromatogram). Synergi Hydro RP 10 μm (80 Å), LC column 250 x 10 mm. Eluent: 35% ACN in water + 0.1% TFA

The isolated peak was identified as the desired tracer by co-injection with the reference compound, previously characterized.

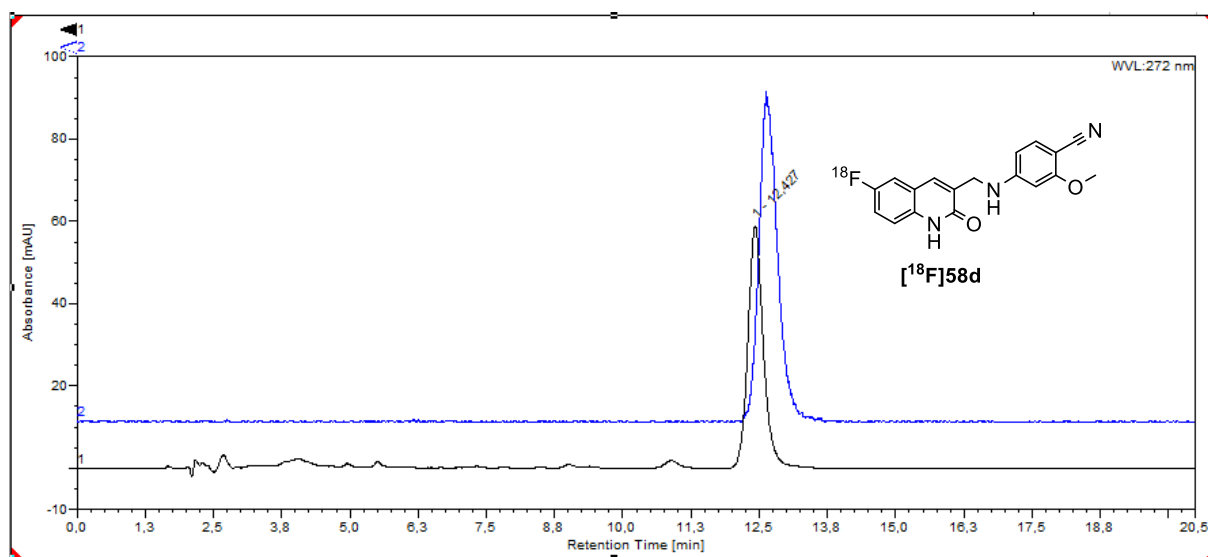


Figure 47: HPLC trace of $[^{18}\text{F}]\mathbf{58d}$ co-injected with the non-radioactive reference compound $\mathbf{58d}$ (96% pure) (Black: UV chromatogram, 272 nm; blue: radio chromatogram). Synergi Hydro-RP 4 μm (80 \AA) 250 \times 4.6 mm. Eluent: 35% ACN in water + 0.1% TFA, 1 mL/min.

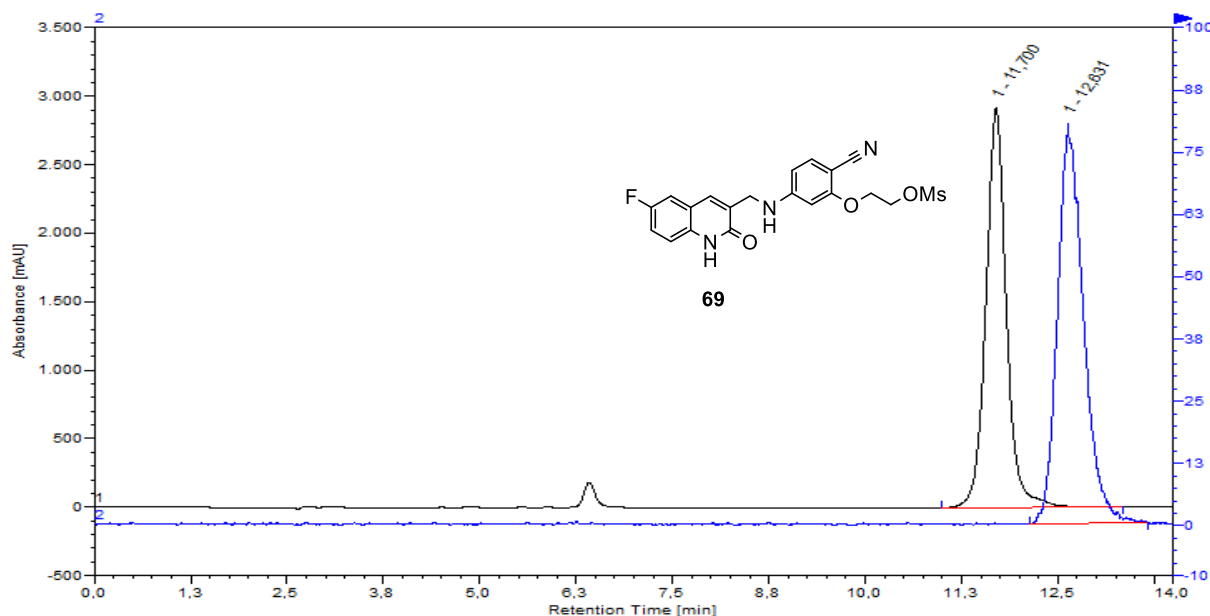


Figure 48: HPLC trace of $[^{18}\text{F}]\mathbf{58d}$ co-injected with the deprotected precursor $\mathbf{69}$ (Black: UV chromatogram, 272 nm; blue: radio chromatogram). Synergi Hydro-RP 4 μm (80 \AA) 250 \times 4.6 mm. Eluent: 35% ACN in water + 0.1% TFA, 1 mL/min.

For the optimization of the radiofluorination condition, the intermediate $[^{18}\text{F}]\mathbf{63}$ was identified via co-injection of the protected reference compound $\mathbf{59d}$.

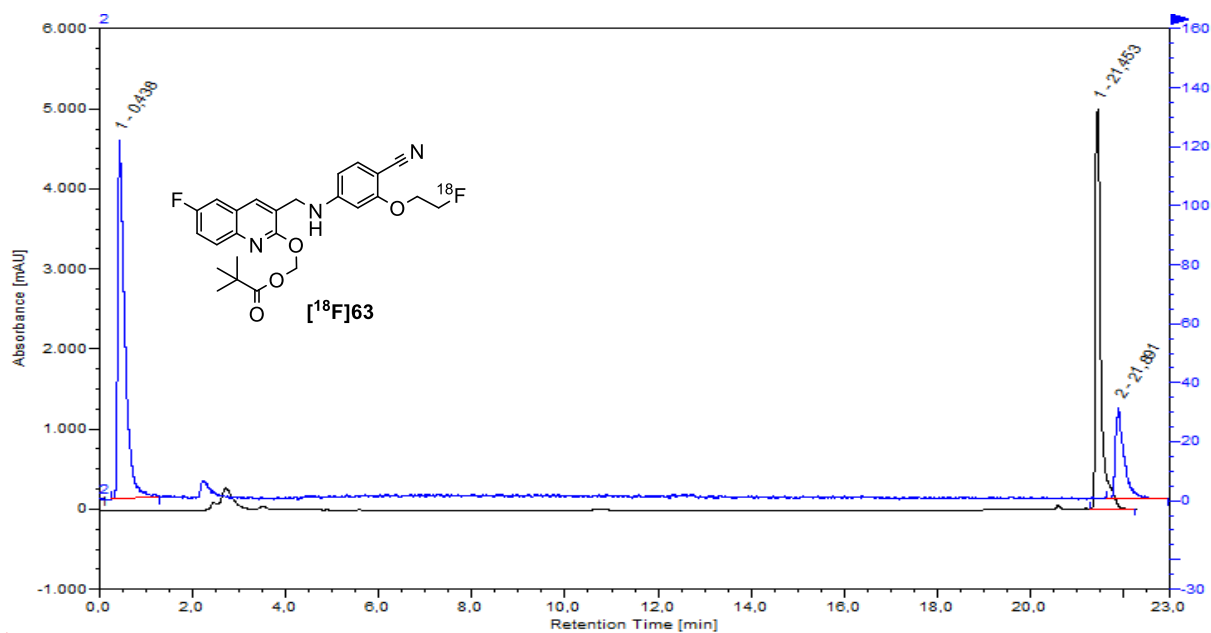
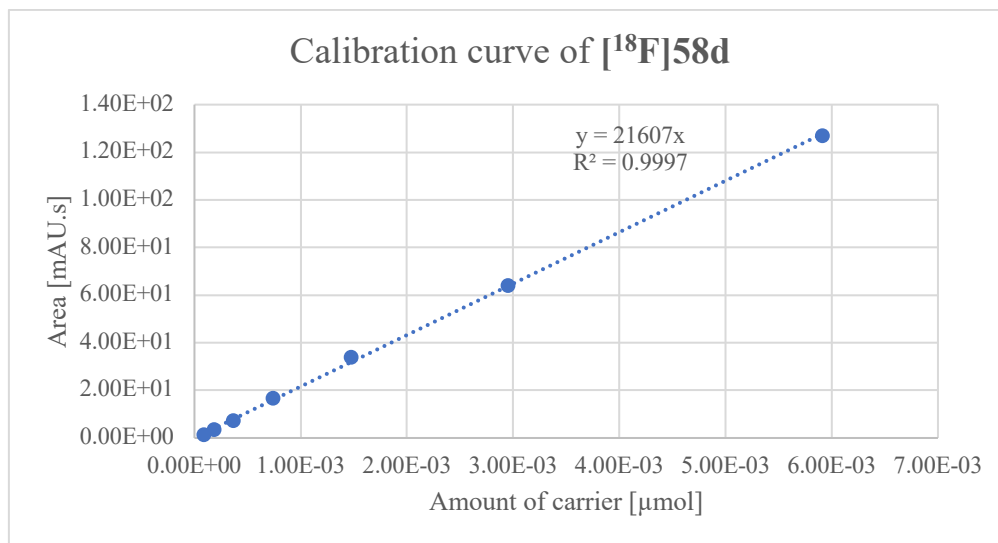


Figure 49: HPLC trace of $[^{18}\text{F}]\mathbf{63}$ co-injected with the precursor $\mathbf{63}$ (Blue: UV chromatogram, 272 nm; black: radio chromatogram). Synergi Hydro-RP $4\ \mu\text{m}$ ($80\ \text{\AA}$) $250 \times 4.6\ \text{mm}$. Eluent: 35% ACN in water + 0.1% TFA, 1 mL/min.

The calibration curve for the calculation of the molar activity of [¹⁸F]58d was measured at 272 nm (Graph 11) with the data reported in Table 19.



Graph 11. Calibration curve for molar activities determination for the tracer [¹⁸F]58d

mg/1 mL	mg/20 μL	g/20 μL	mol (g/323.13 g/mol)	μmol	Average Area
1.00E-01	2.00E-03	2.00E-06	5.91E-09	5.91E-03	1.27E+02
5.00E-02	1.00E-03	1.00E-06	2.96E-09	2.96E-03	6.41E+01
2.50E-02	5.00E-04	5.00E-07	1.48E-09	1.48E-03	3.39E+01
1.25E-02	2.50E-04	2.50E-07	7.39E-10	7.39E-04	1.68E+01
6.25E-03	1.25E-04	1.25E-07	3.69E-10	3.69E-04	7.22E+00
3.13E-03	6.25E-05	6.25E-08	1.85E-10	1.85E-04	3.60E+00
1.56E-03	3.13E-05	3.13E-08	9.24E-11	9.24E-05	1.49E+00
7.81E-04	1.56E-05	1.56E-08	4.62E-11	4.62E-05	9.52E-01

Table 19: Calibration data for the determination of the molar activity of [¹⁸F]58d

5.4 Biological Evaluation

5.4.1 In vitro Stability tests in serum

500 µL of rat serum were placed in a 2 mL vial and prewarmed in a thermoshaker at 37°C for 5 minutes before addition of 0.5 µL of the radiotracer solution (DMSO, approximately 0.5-1 MBq). The mixture was shaken for a total amount of time of one hour while 60 µL aliquotes were removed at 5, 15, 30 and 60 minutes and added to a vial containing 120 µL of acetonitrile. Each time-point was replicated in triplicate. Each vial was vortexed for 2 minutes and further centrifugated for 2 minutes. Afterwards, 2.5 µL of supernatant were spotted on each lane of the radio TLC, together with the reference compound. The plate was developed with different eluents, according to the tracers and baseline, frontline and reference compound, previously detected with the aid of a UV lamp, were spotted with activity to be visualized with a phosphor imager. The TLC plate was scanned at the phosphor imager, all peaks were integrated and the background subtracted. The radiotracers were identified by comparison of the migration distance of the radioactive spots with the non-radioactive reference compounds.

5.4.2 Stability test in solution

All the radiotracers were tested in PBS buffer at room temperature to ensure their stability in sight of *in vitro* and *in vivo* experiments. 500 µL of buffer were placed in a vial and 0.5 µL of organic solution of the radiotracer (approximately 0.5-1 MBq) were added and left at room temperature for up to three hours. At starting point and after 1, 2 and 3 hours, 2.5 µL of solution were taken and spotted on the radio TLC which was air-dried and developed with different eluents, according to the tracers. TLC was scanned at the phosphor imager and all peaks were integrated and the baseline subtracted. The radiotracers were identified by comparison of the migration distance of the radioactive spots with the non-radioactive reference compounds.

In some cases, a complete defluorination of radiotracer was detected at the starting time and after 1 hour but not at the final time, clear sign of silica degradation. In those cases, the aliquots were spotted on separate TLC plates, each with the reference compound, and immediately developed to avoid tracer degradation by silica. In all cases, 100% purity was retained with this procedure.

5.4.3 Calculation of lipophilicity

The radiotracer was dissolved in DMSO and 1 μ L was added to a 1:1 mixture of n-octanol and aqueous solution with a total volume of 1.5 mL. The mixture was then vortexed for 2 minutes and then the two phases were separated with the aid of a centrifuge for another 2 minutes. Finally, 300 μ L were taken from the organic phase and measured at the low gamma counter while the same amount was taken from the water phase with the aid of a syringe and a needle to make a hole in the lower part of the vial in order to avoid contact with the organic phase. The measurement was repeated in triplicate.

The logarithm of the ratio between the activity in the organic and the water phase was calculated to give an average value and the standard deviation between the three values.

When PBS buffer was used as aqueous solution, the final value was referred as $\text{Log}D_{7.4}$ while when water was used, the final value was defined $\text{Log}P$.

5.4.4 Cell uptake experiments

*Experiments performed by Dr. D.Bier, Dr. D.Schneider and A.Schulze

Cellular uptake experiments were performed on the radiotracers with human glioblastoma astrocytoma cell line (U87MG-WT) and the U87MG cell line with a point mutation where arginine is exchanged by histidine at codon 132 (IDH1-R132H), purchased from the American Type Culture Collection (ATCC) and maintained in 10% fetal bovine serum (FBS), Eagle's Minimum Essential Medium (MEM) with antibiotics (penicillin–streptomycin mixed solution, Gibco, Thermofischer). Cells were cultivated in a well-humidified incubator with 5% CO_2 and 95% air at 37 °C. Around 18.5 kBq (0.5 μ Ci) of radiotracer was incubated in cells for 1 h, the supernatant was separated and fractions were measured in a gammacounter to determine radioactivity.

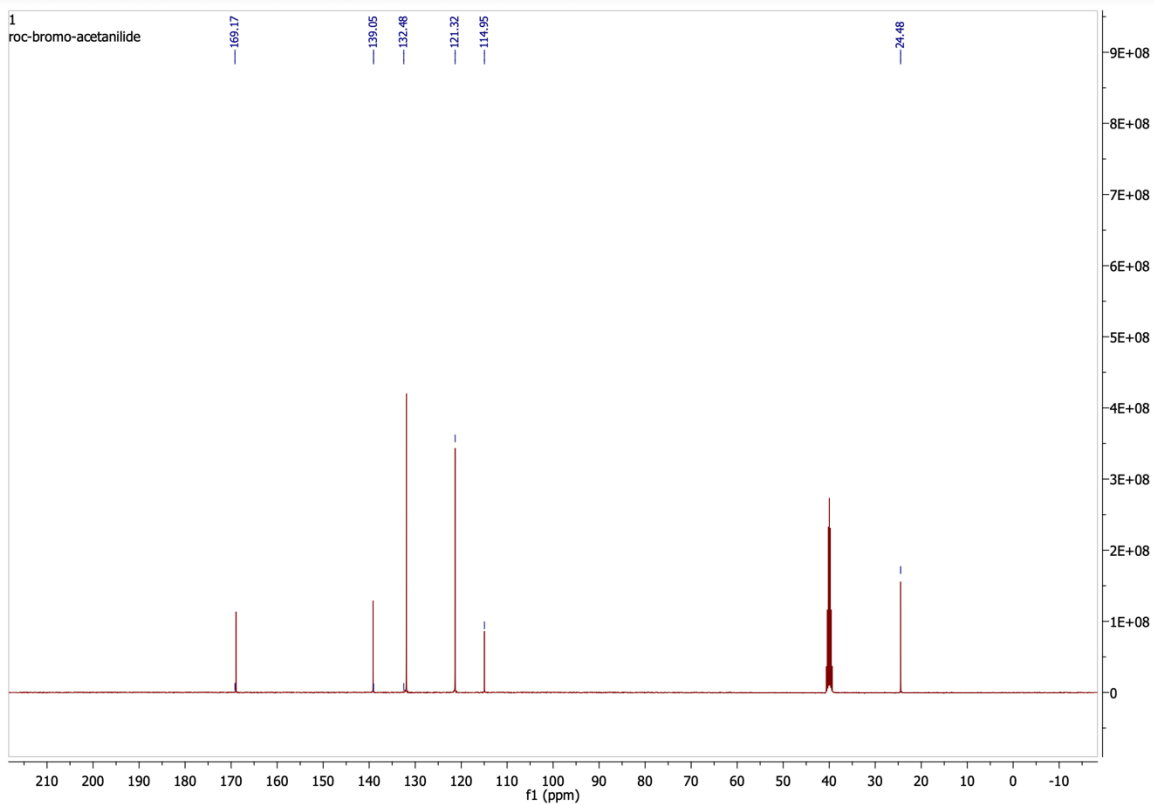
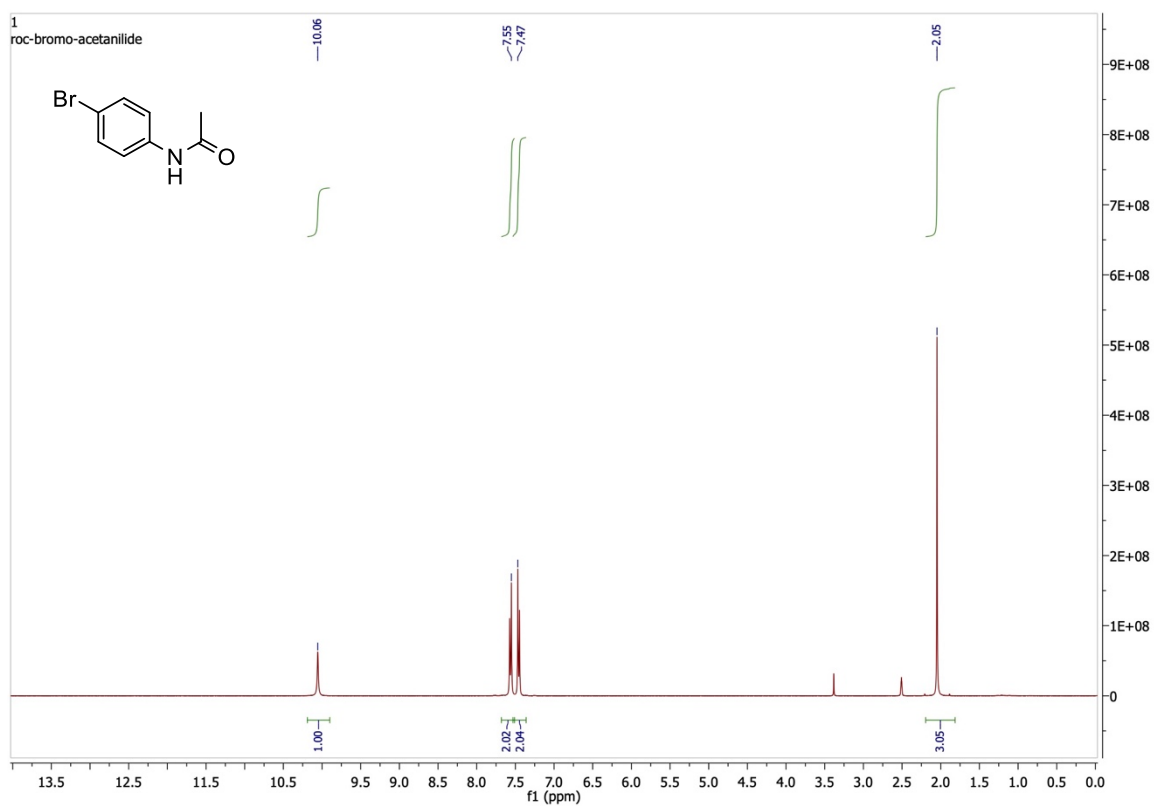
The total protein concentration of the cell lysate was measured by a bicinchoninic acid (BCA) assay and the uptake of radiotracer was calculated as ratio of radioactivity in the cell fraction and the supernatant and normalized by protein content (% uptake/100 μ g protein).

To assess the ability of the radiotracer to cross the cell membrane and enter the intracellular compartment, separate cell fractionation experiments were conducted. Following incubation with radiotracer as described above, the cells were detached with trypsin and dispersed via ultra-turrax (1 min at maximum speed) on ice. After centrifugation (50,000 g at 4°C), the supernatant containing the cell plasma was separated from the pellet which consist mainly of the cell membranes, organelles,

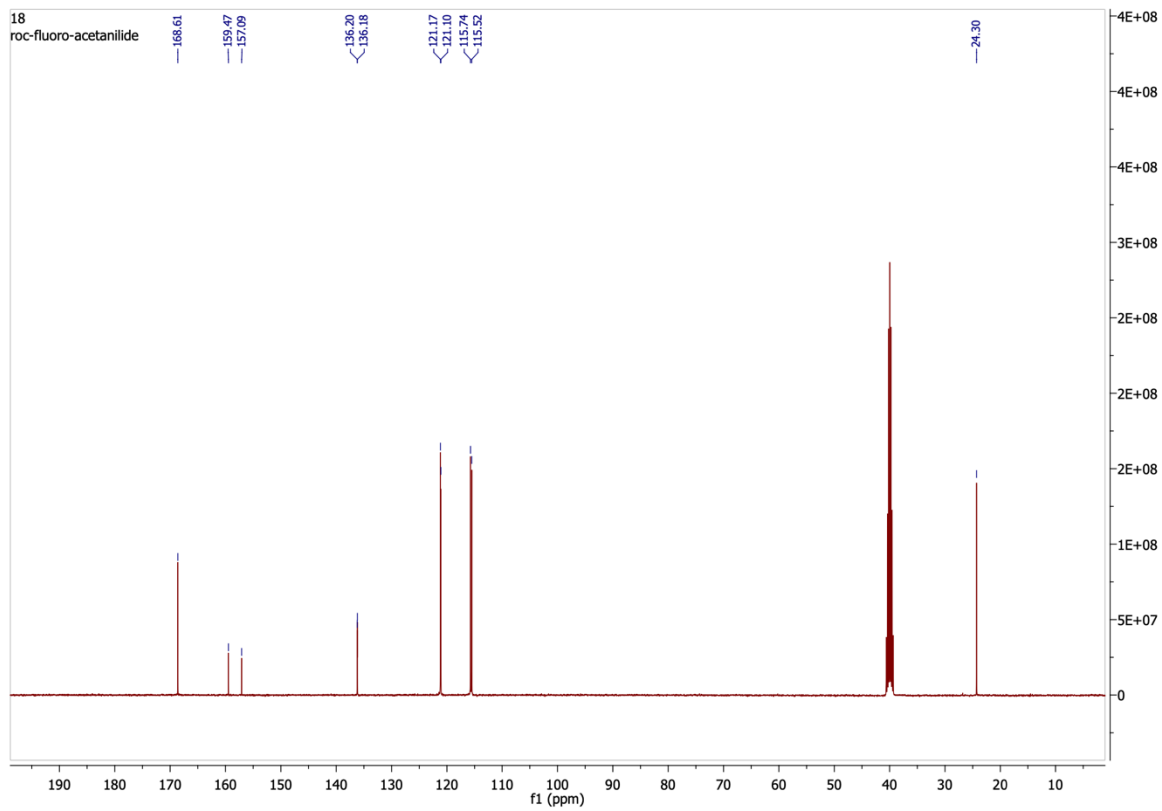
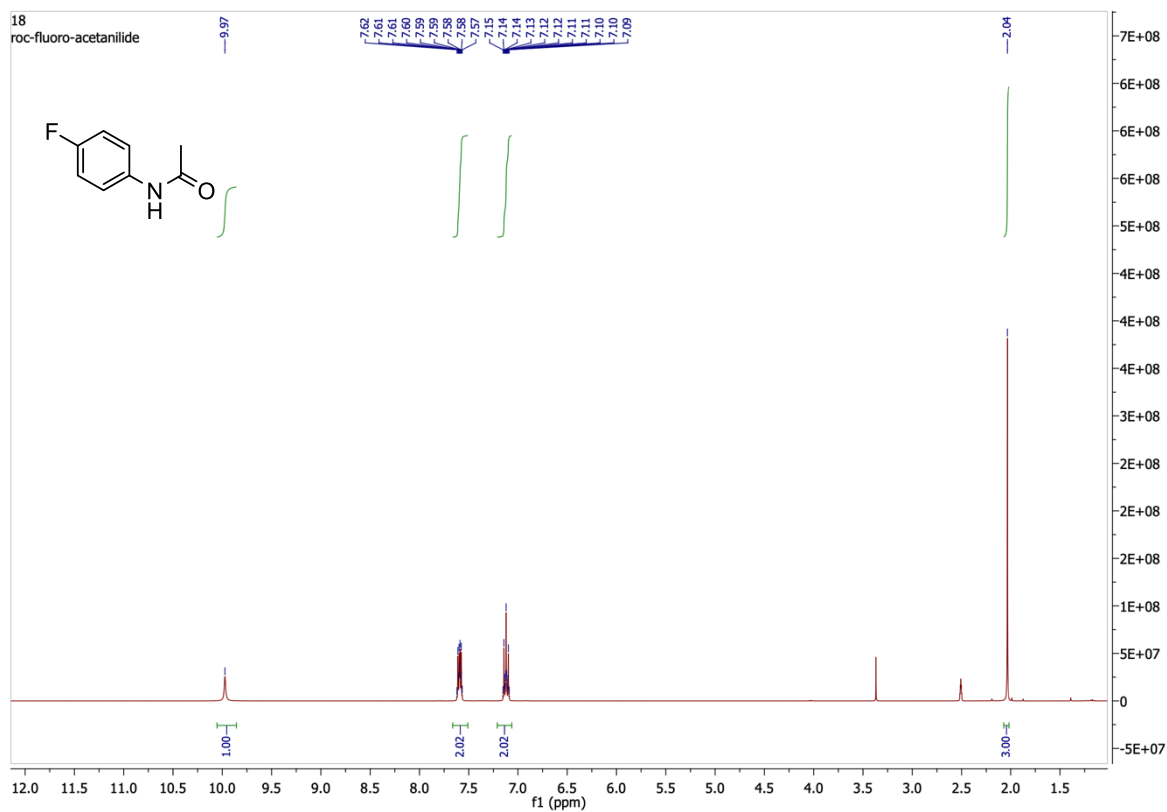
and nuclei. Both fractions were measured in the gammacounter and the percentage of radiotracer present in the cell plasma was calculated from the activity ratio.

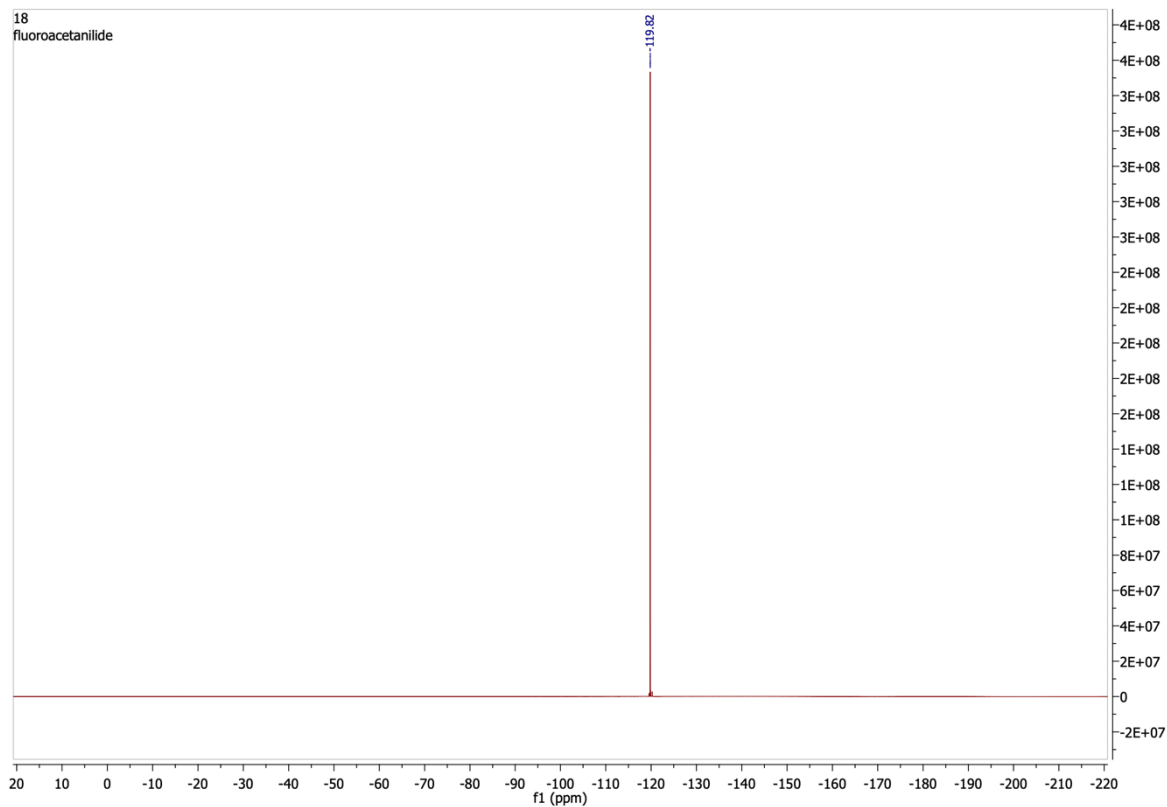
6. NMR

^1H and ^{13}C NMR Spectra of 4-bromoacetanilide **6e**

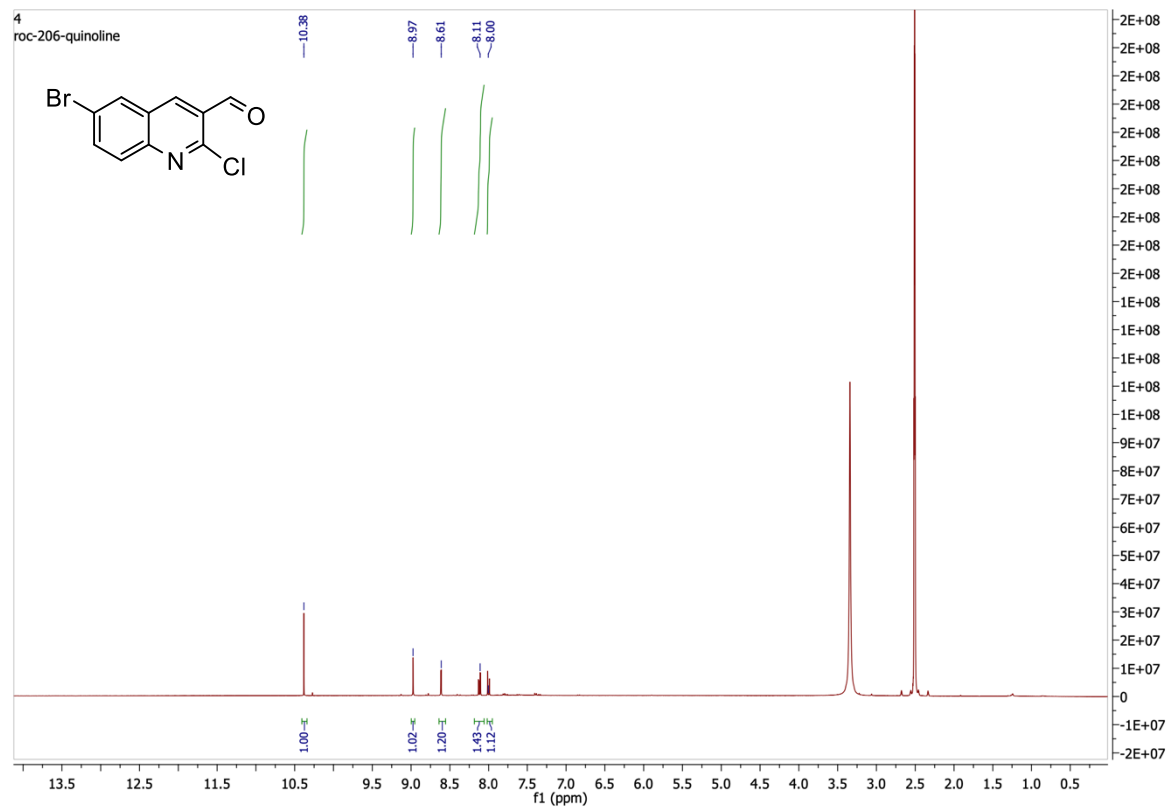


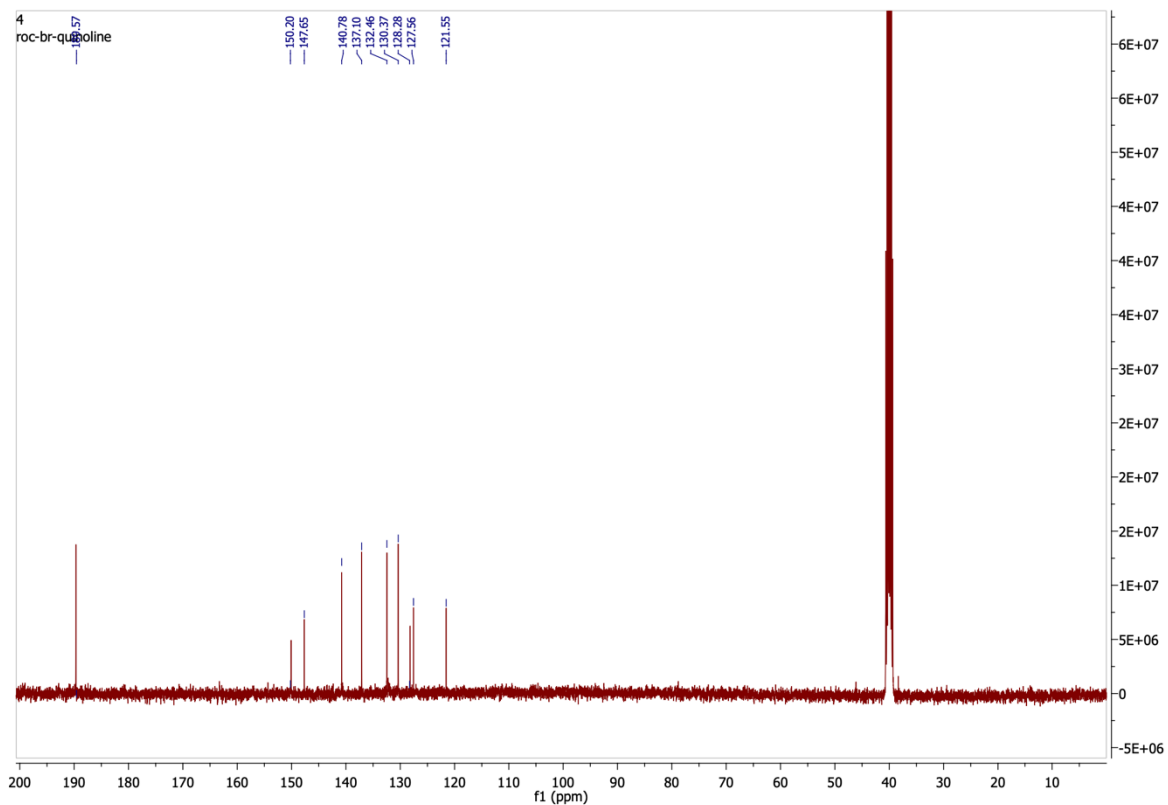
^1H , ^{13}C and ^{19}F NMR Spectra of 4-fluoroacetanilide **6d**



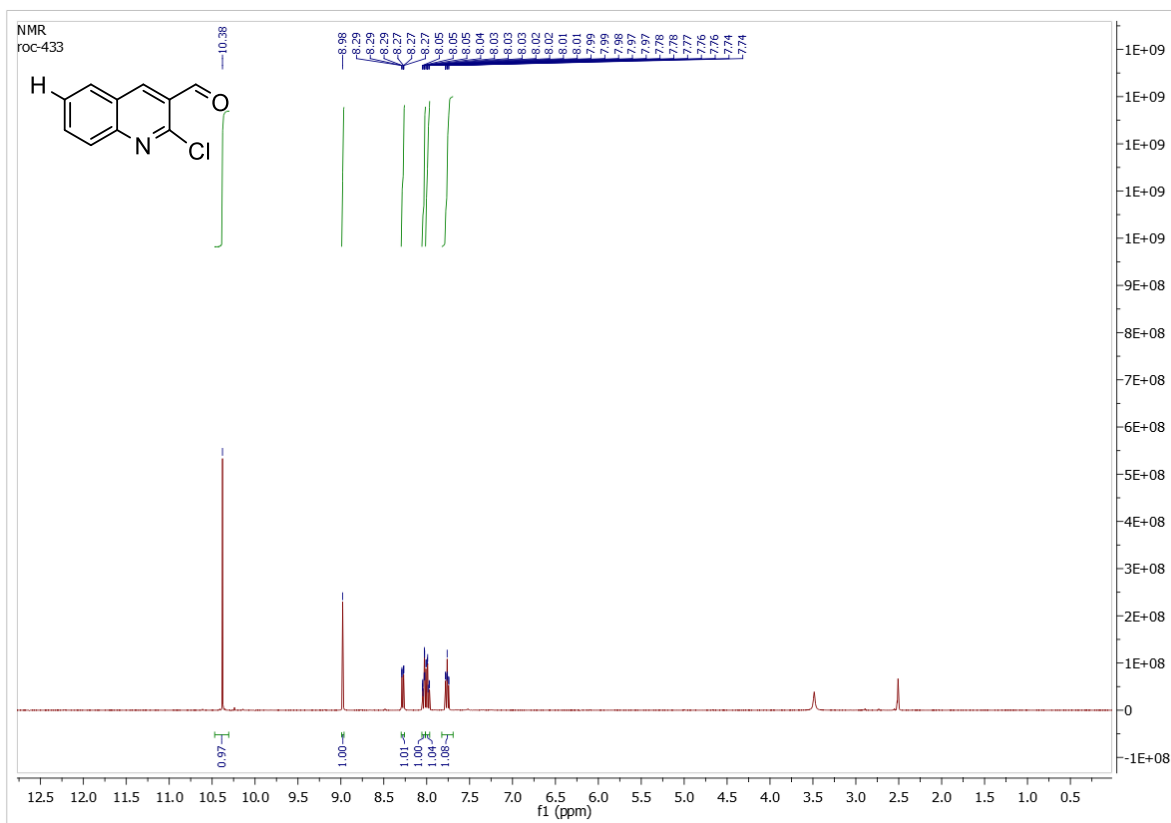


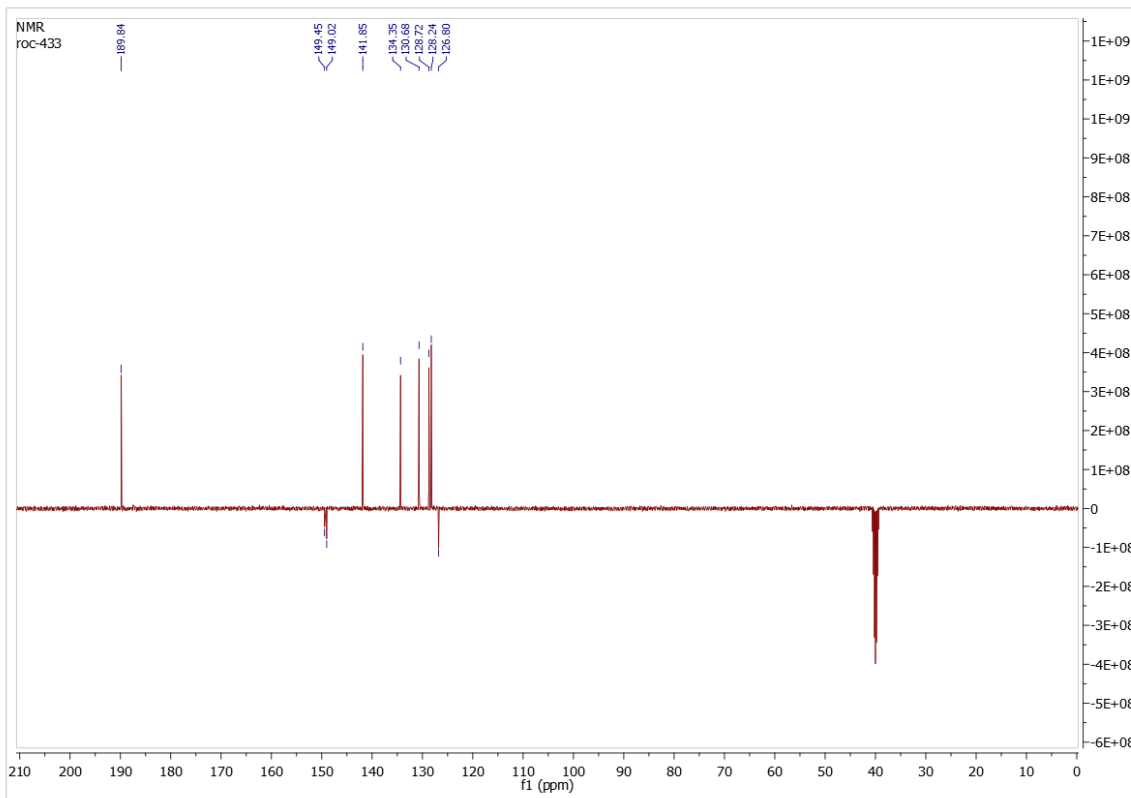
^1H and ^{13}C NMR Spectra of 6-bromo-3-formyl-2-chloro-quinoline **14e**



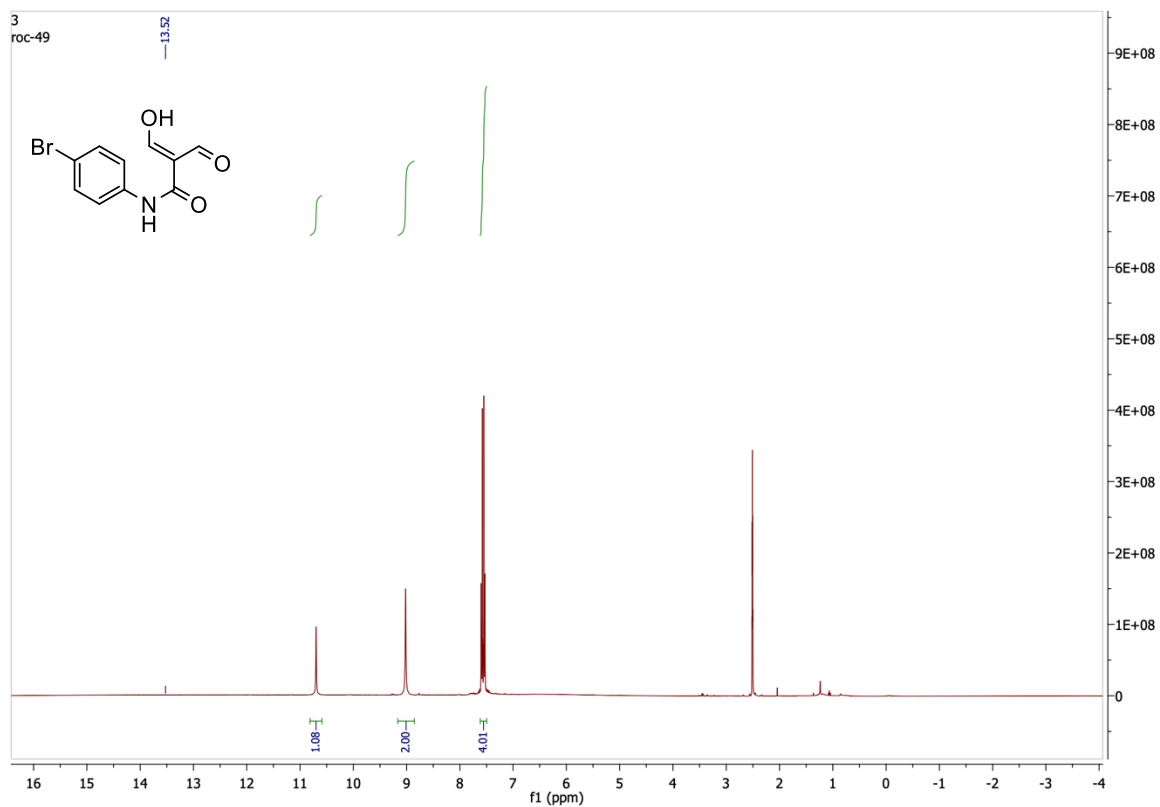


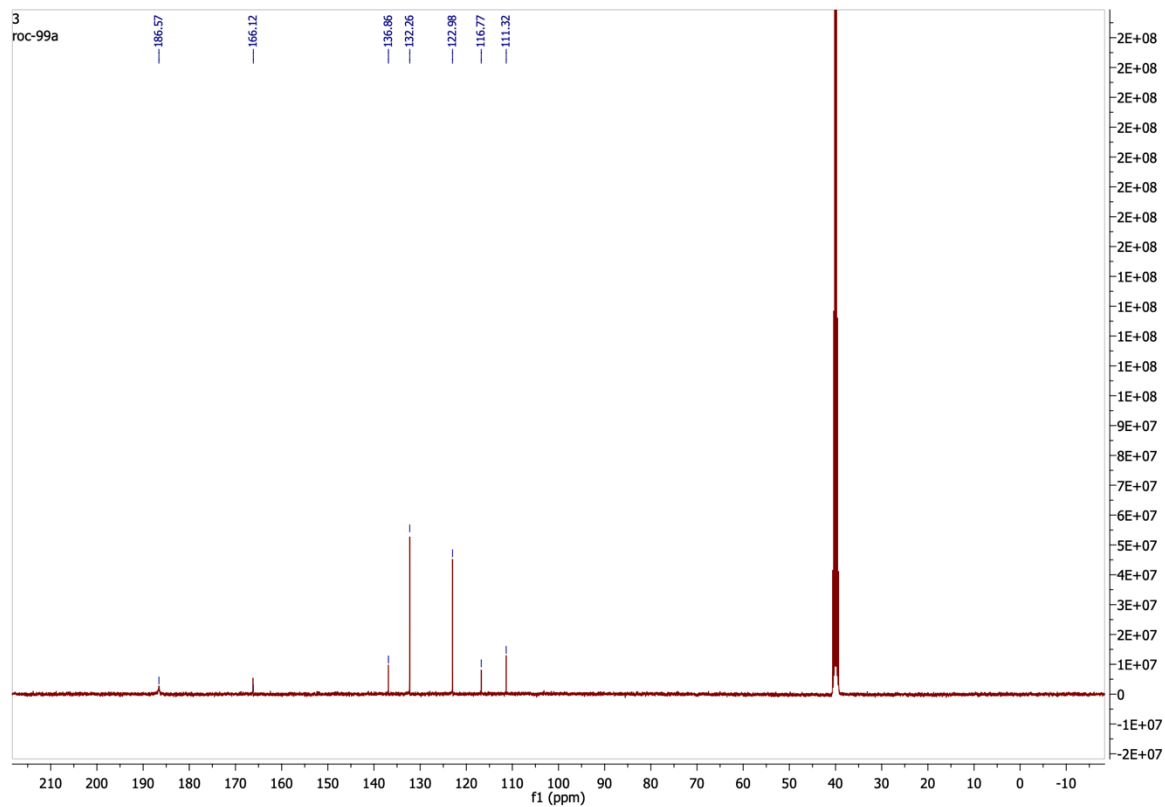
^1H and ^{13}C NMR Spectra of 2-chloro-3-quinoline carboxaldehyde **14f**



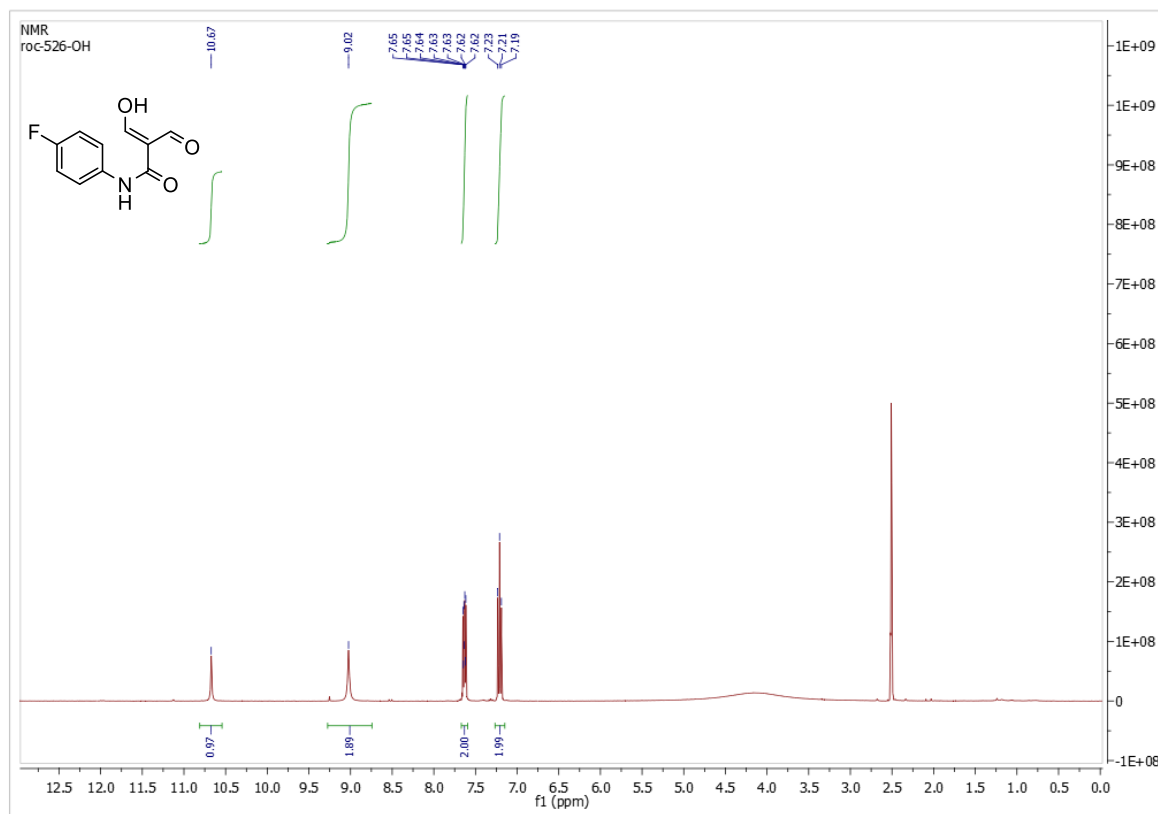


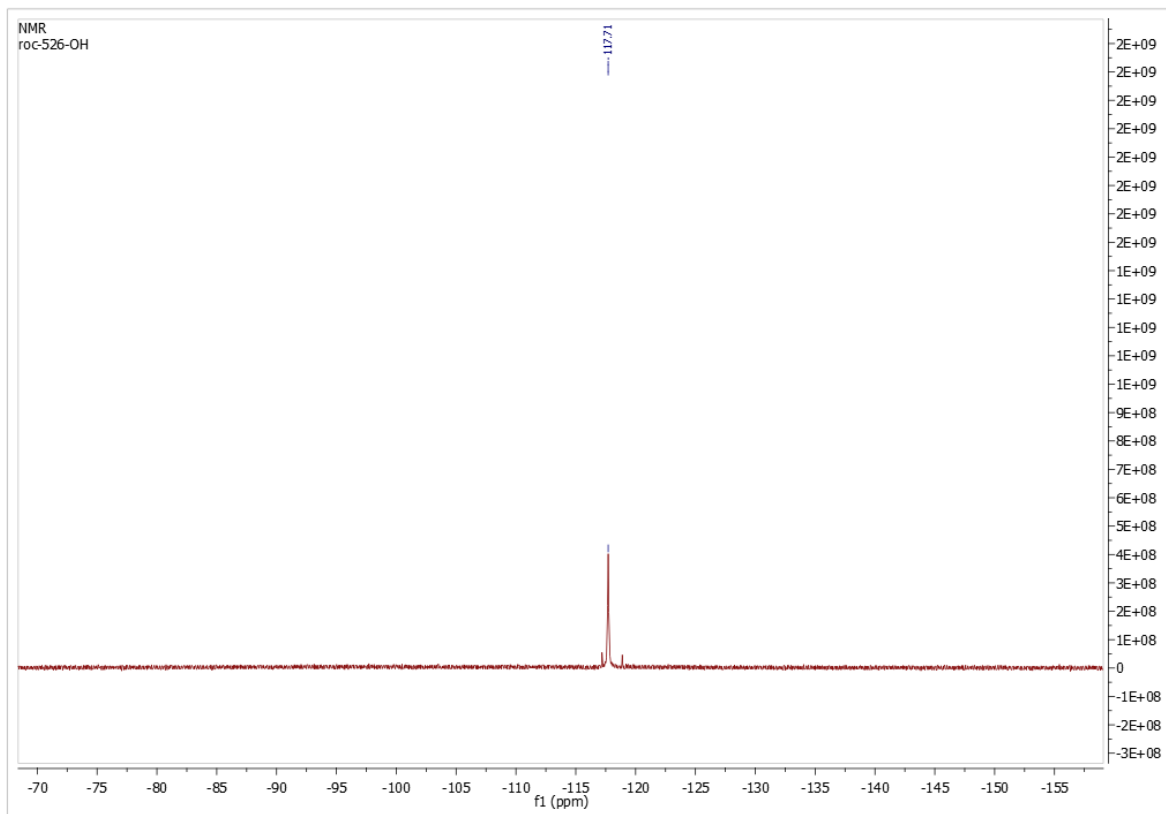
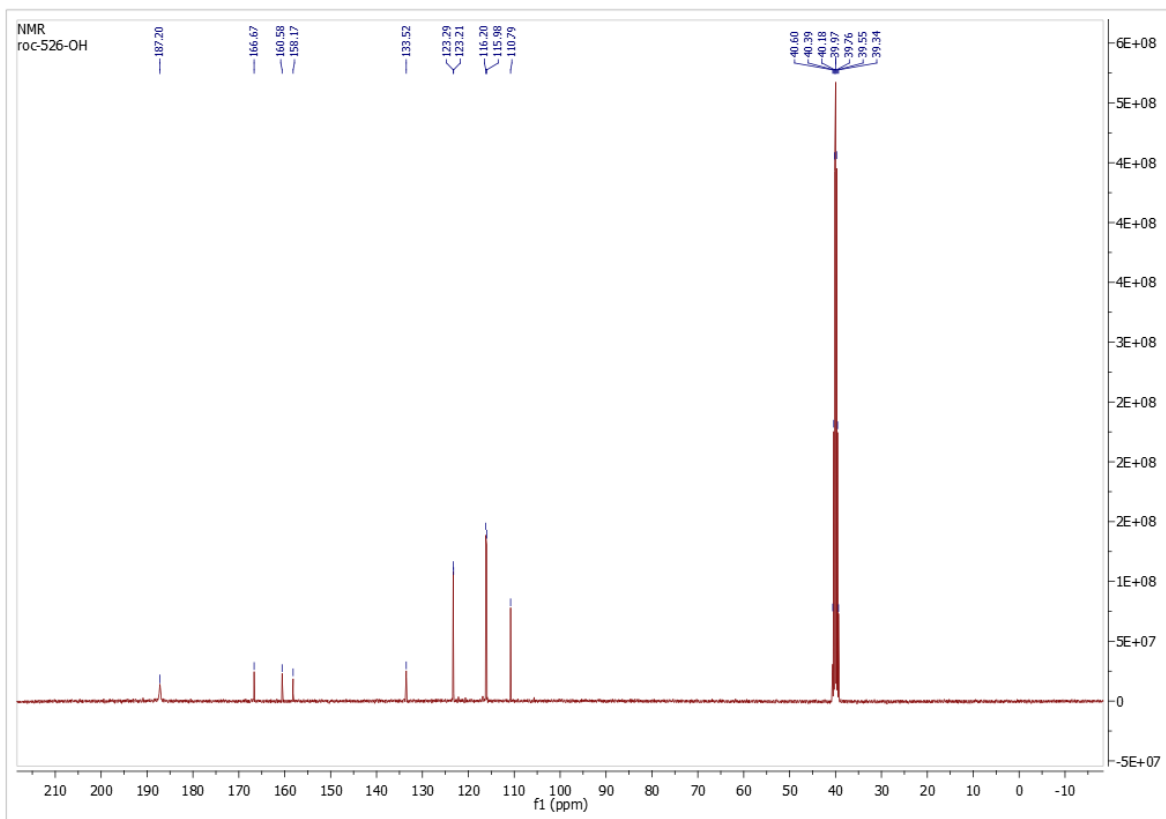
^1H and ^{13}C NMR Spectra of *N*-aryl-(4-bromo)-2-formyl-3-hydroxyacrylamide **20e**



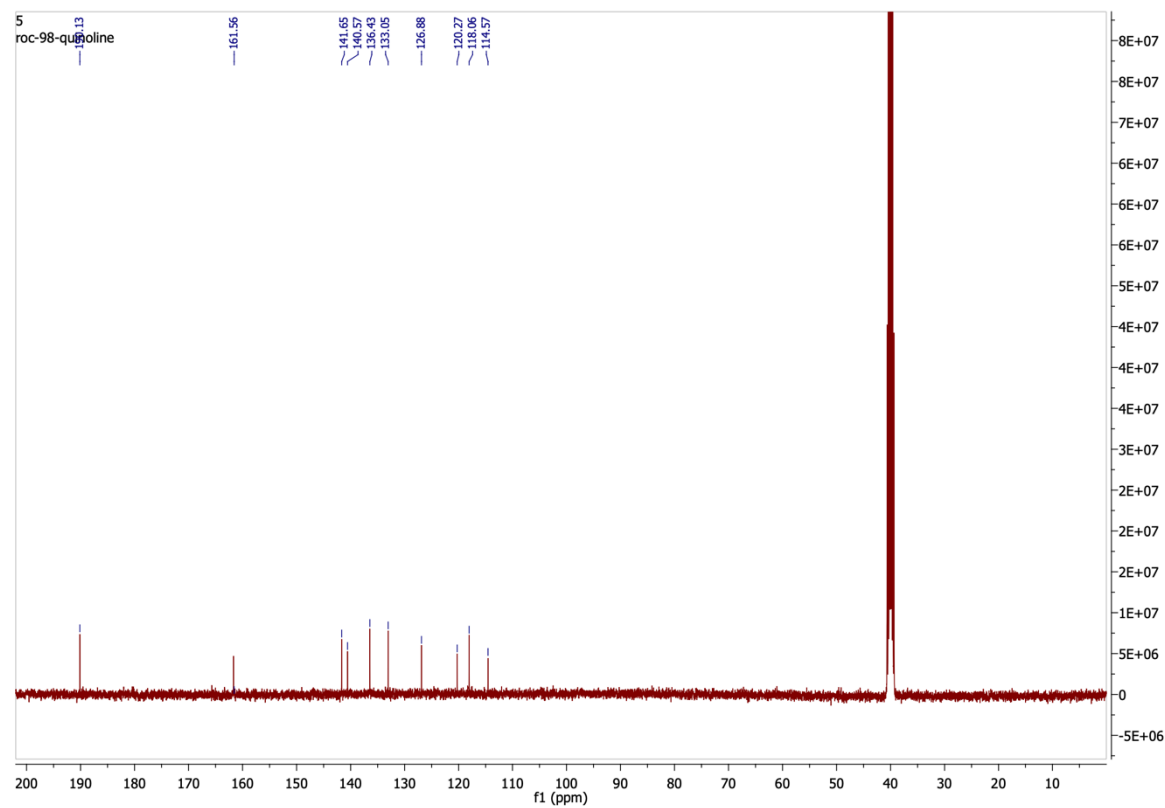
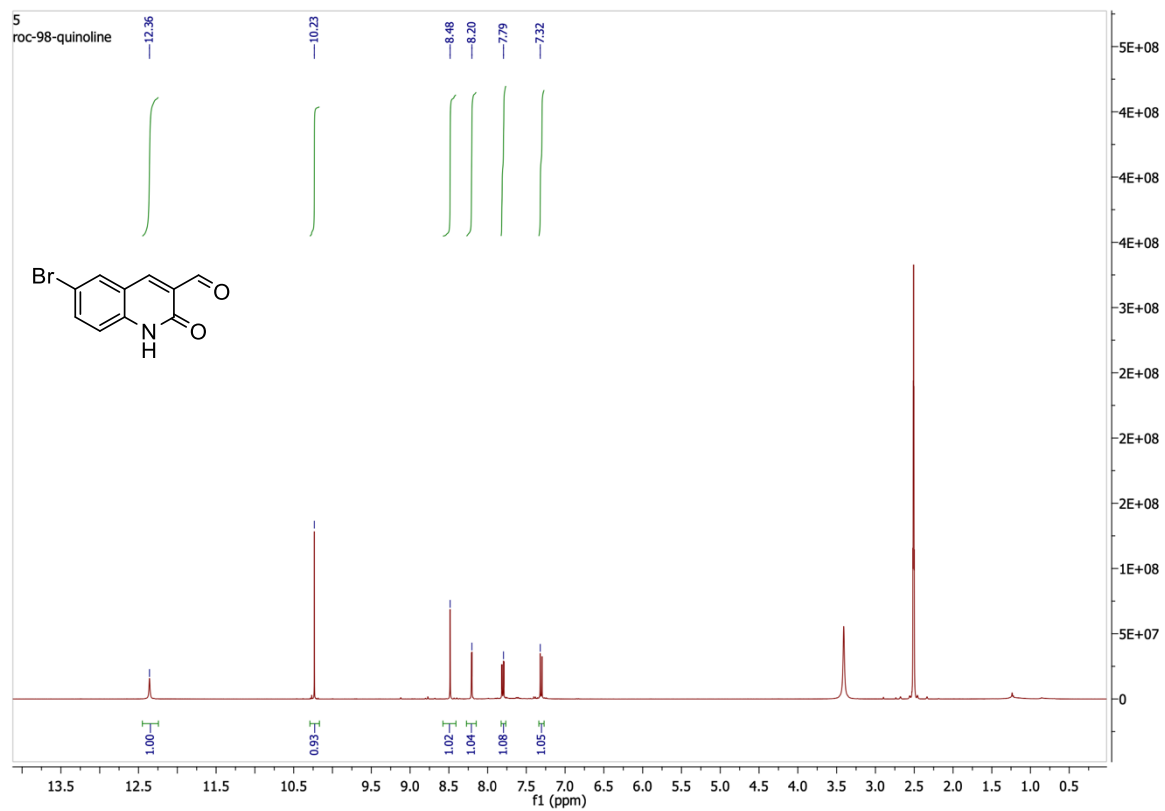


^1H , ^{13}C and ^{19}F NMR Spectra of *N*-aryl-(4-fluoro)-2-formyl-3-hydroxyacrylamide **20d**

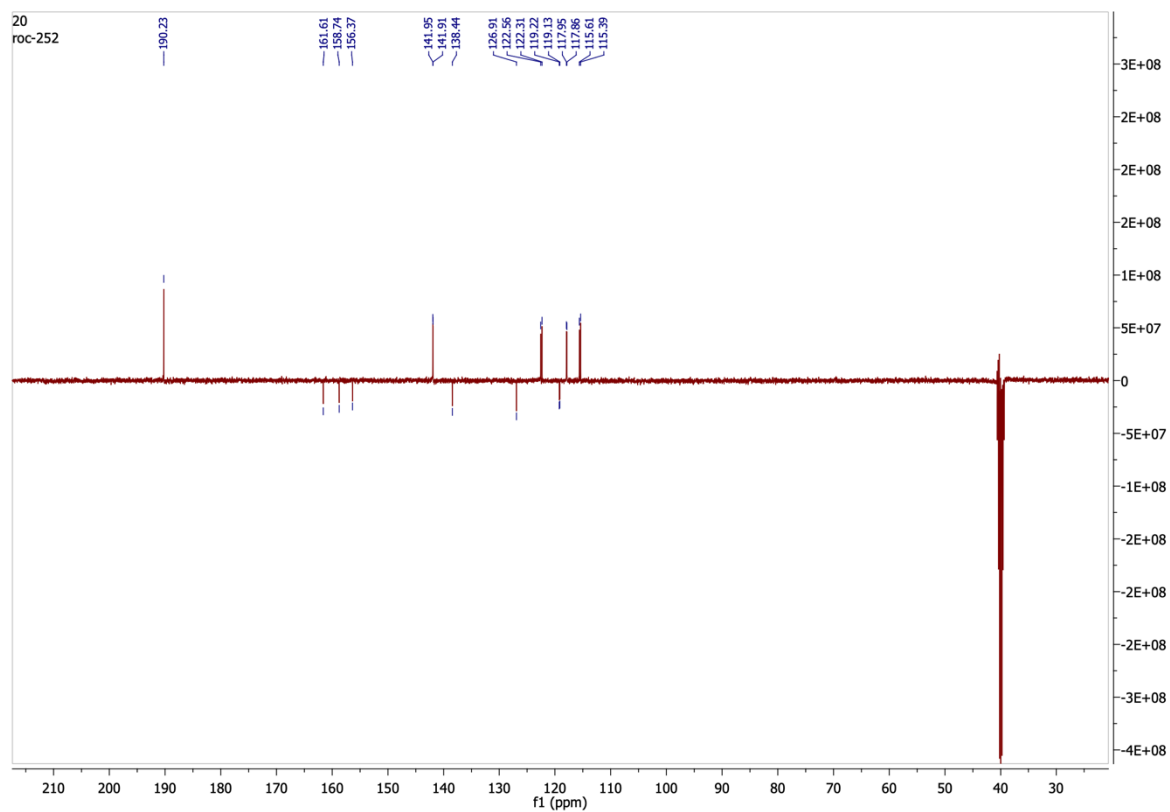
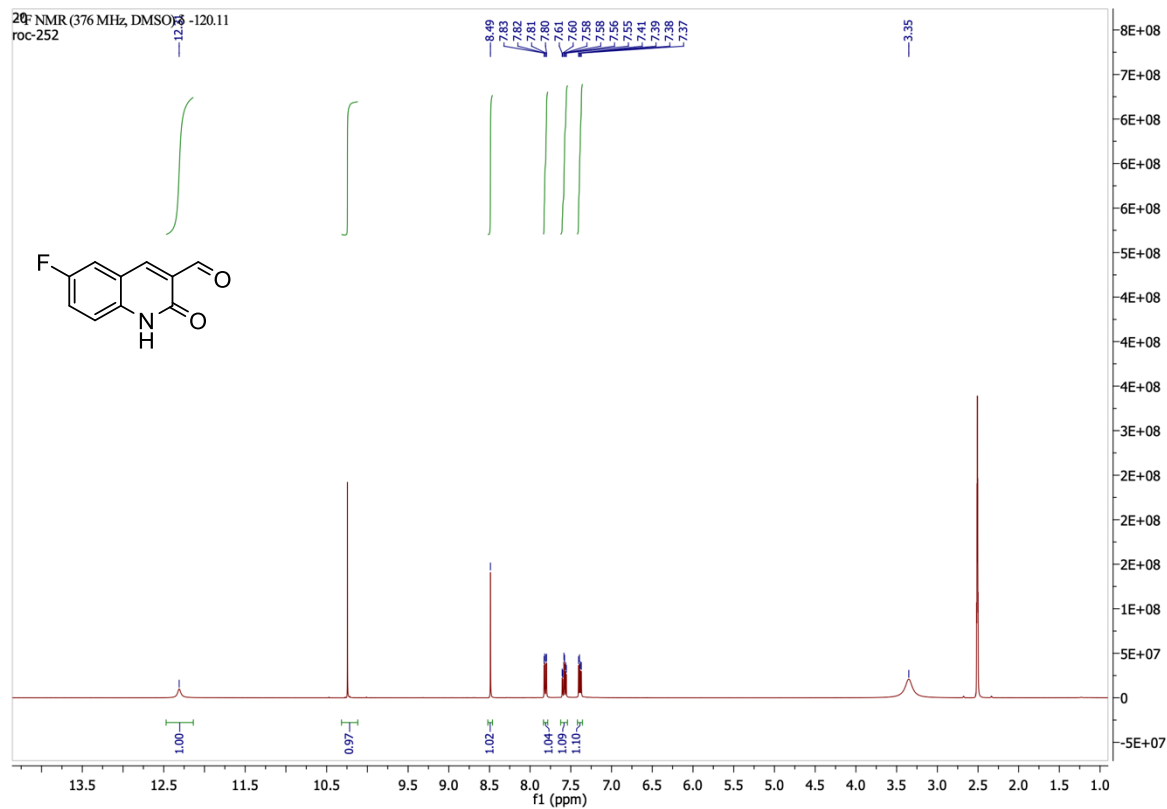


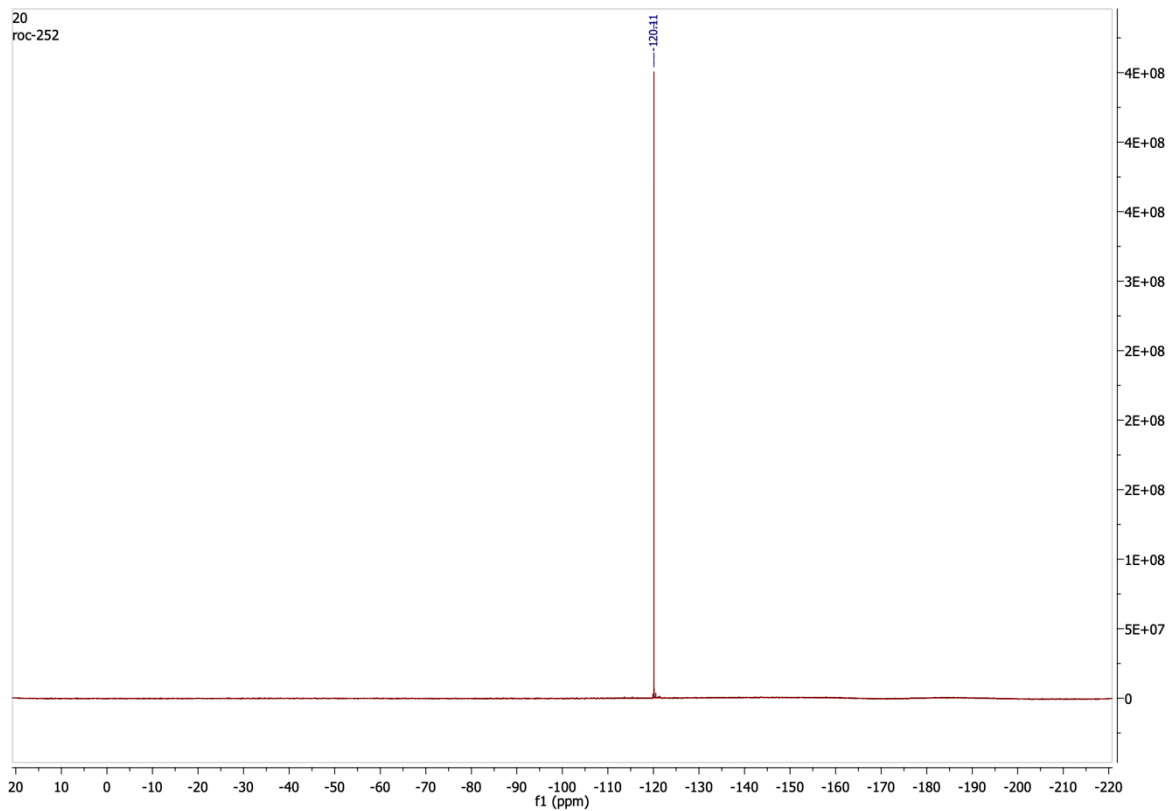


^1H and ^{13}C NMR Spectra of 6-Bromo-3-formyl-2-quinolone **21e**

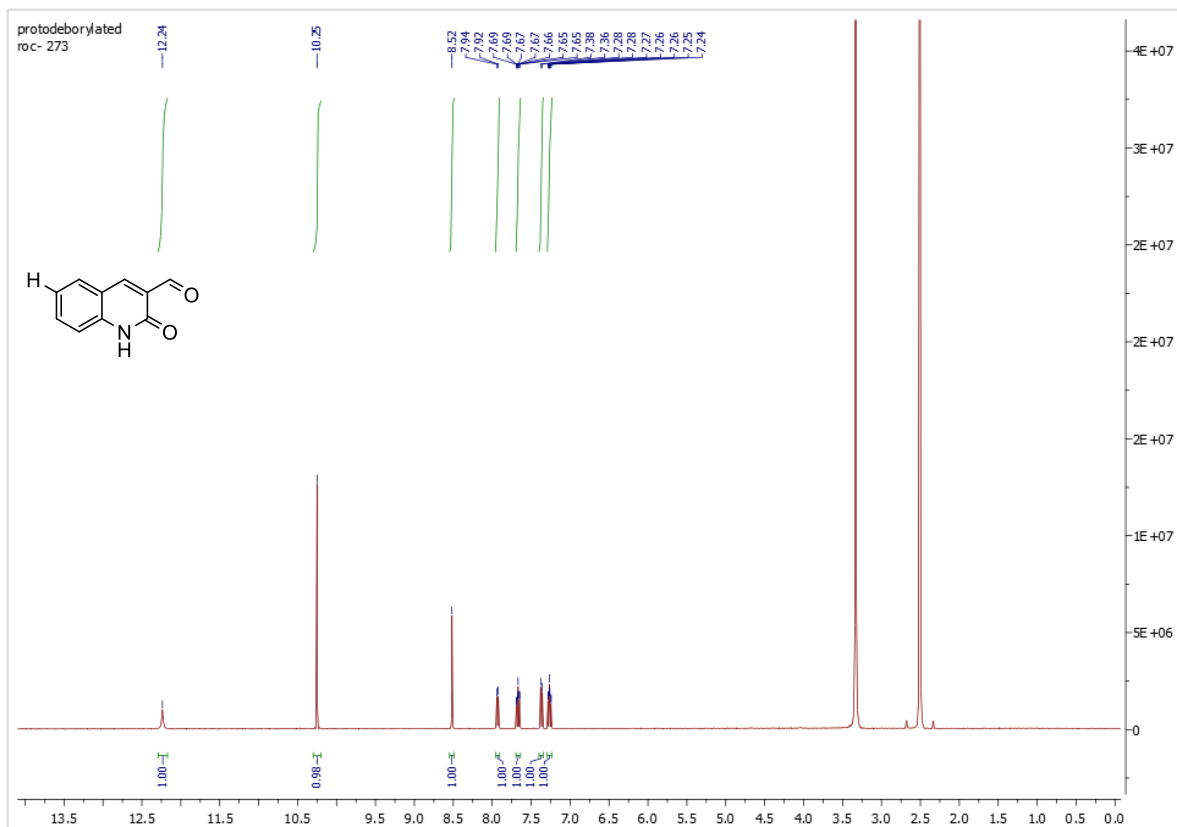


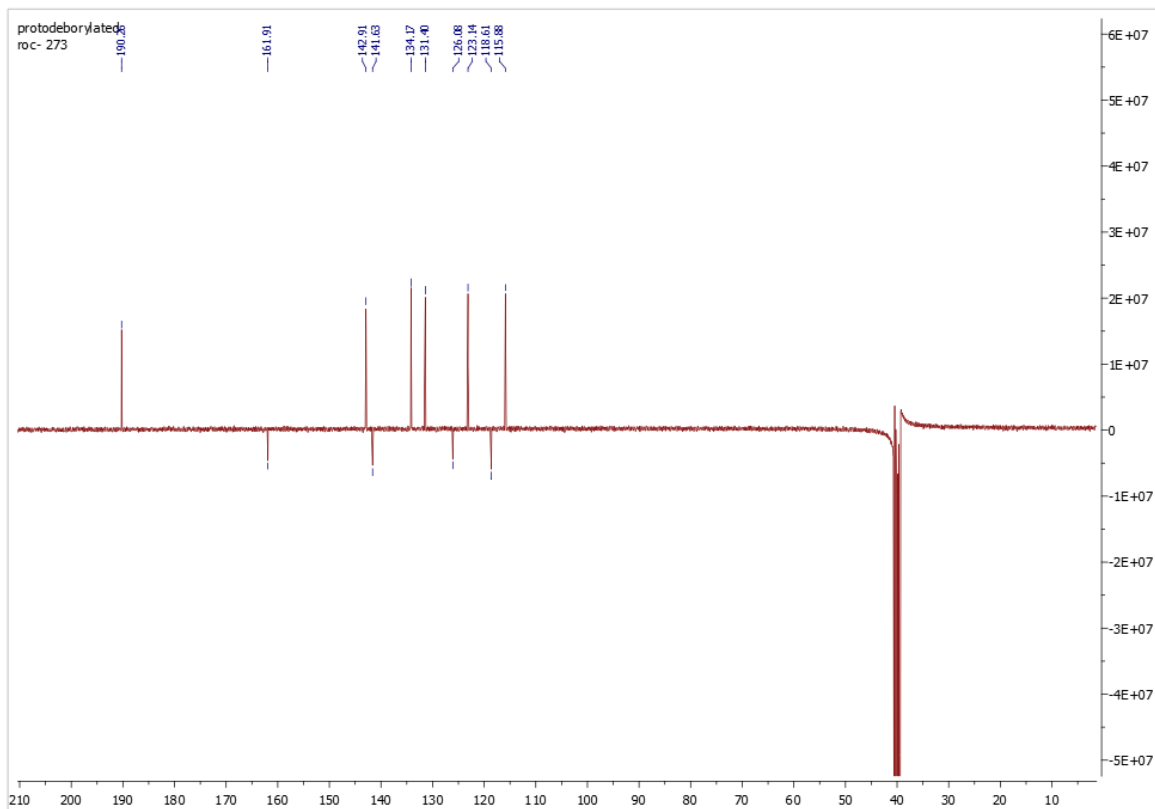
^1H , ^{13}C and ^{19}F NMR Spectra of 6-fluoro-3-formyl-quinolone **21d**



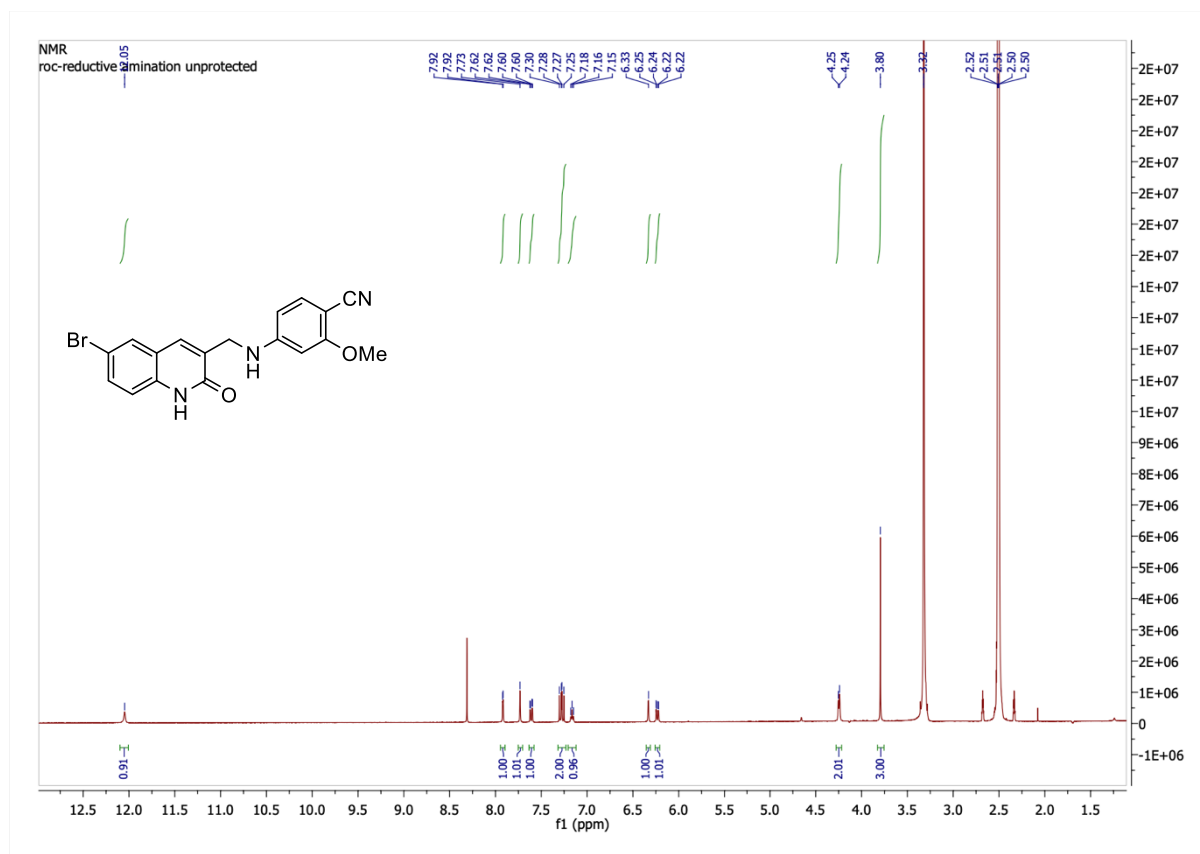


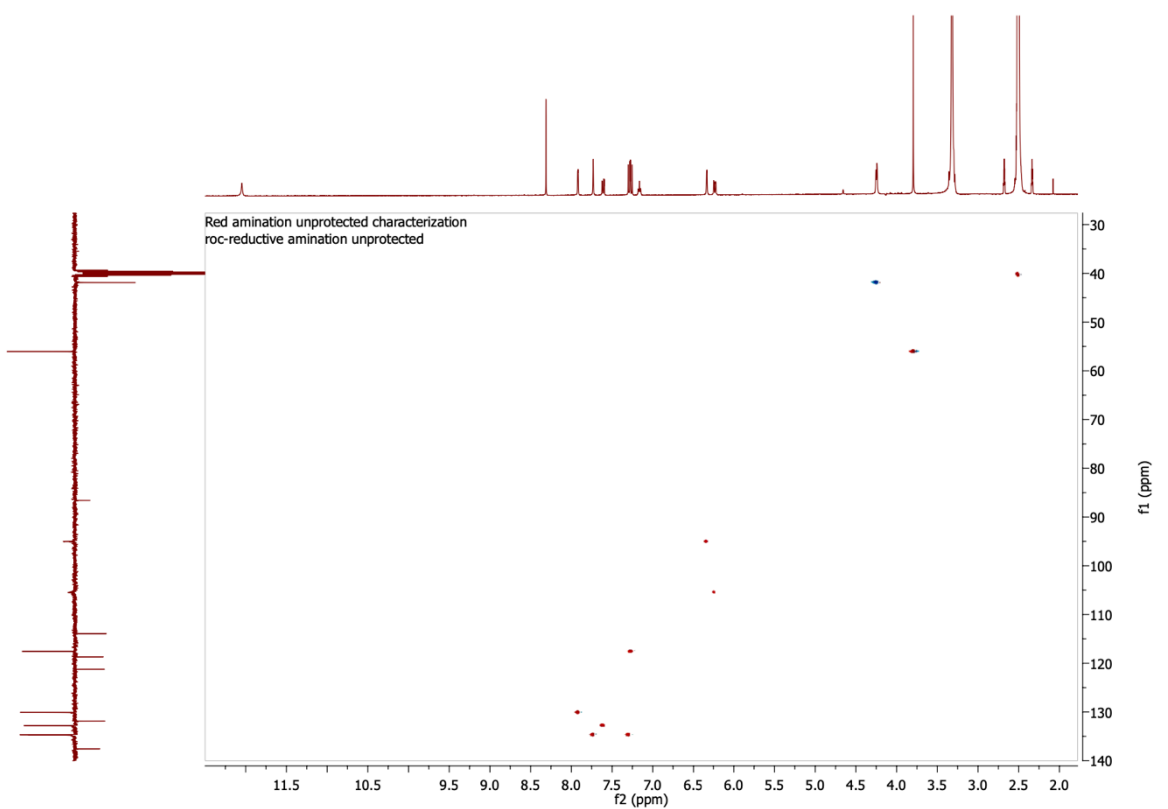
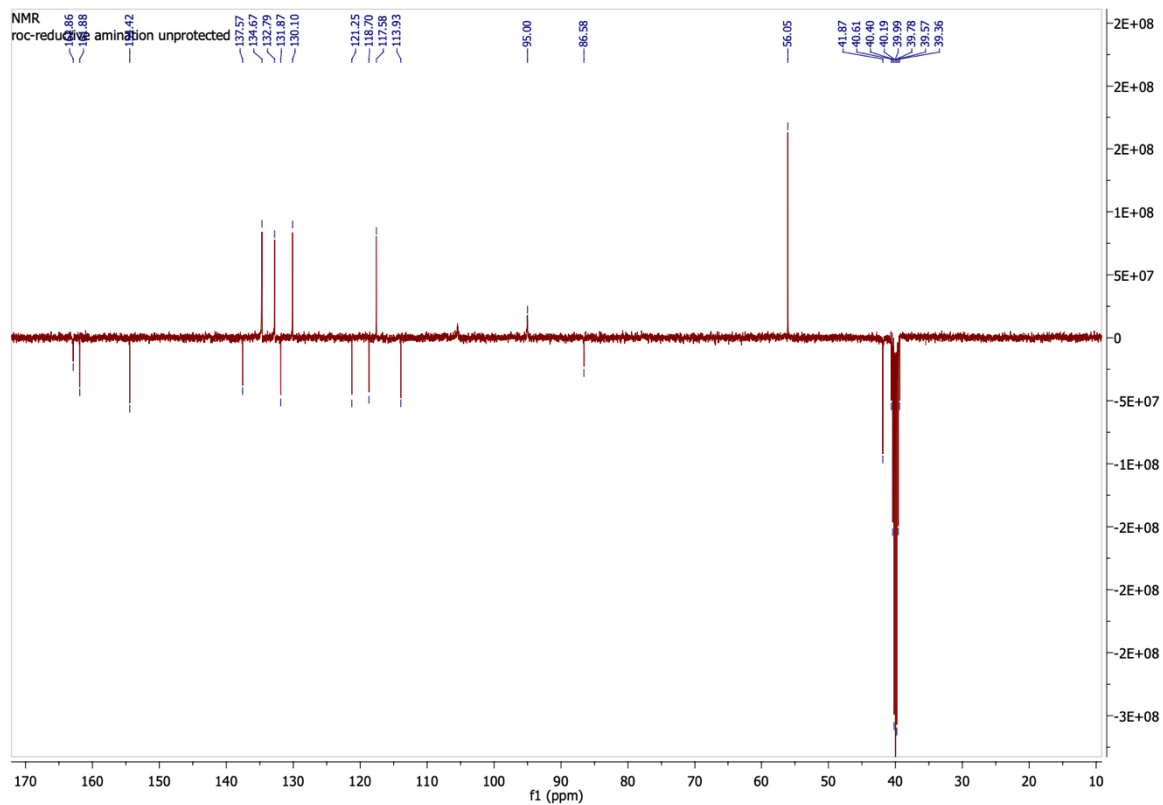
^1H , ^{13}C and ^{19}F NMR Spectra of 3-Formyl-2-quinolone **21f**



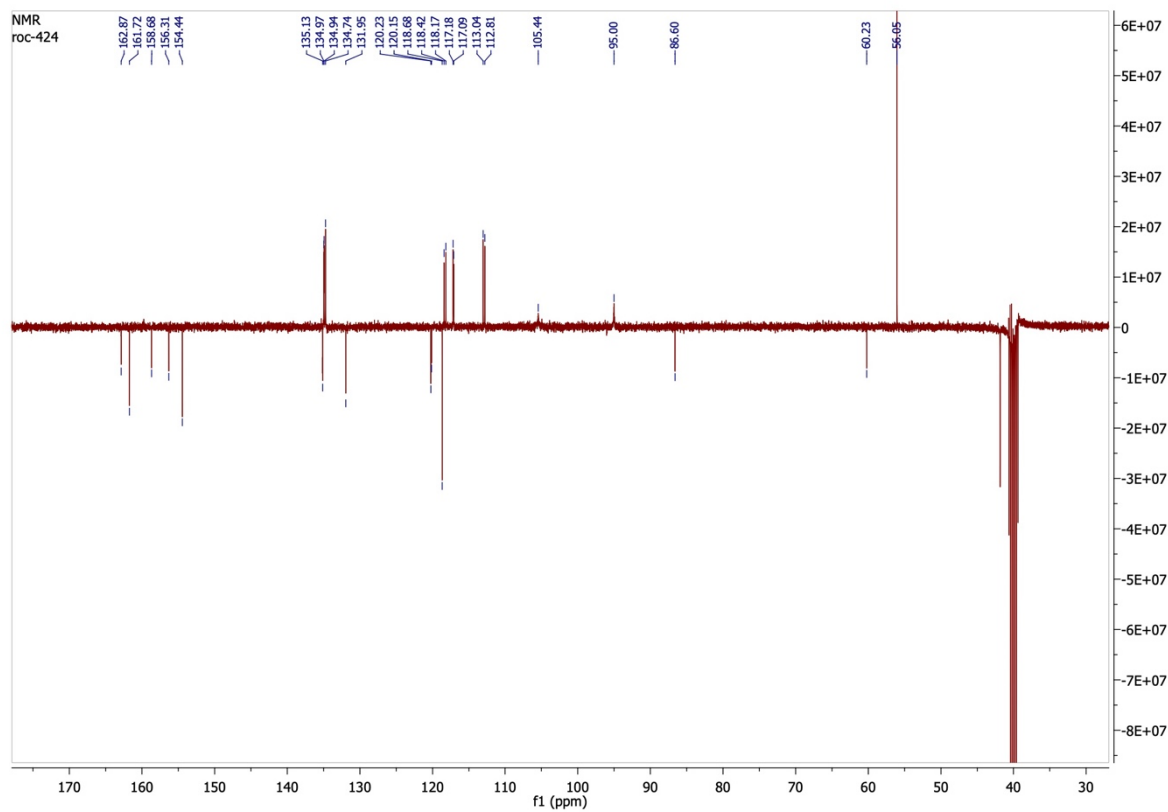
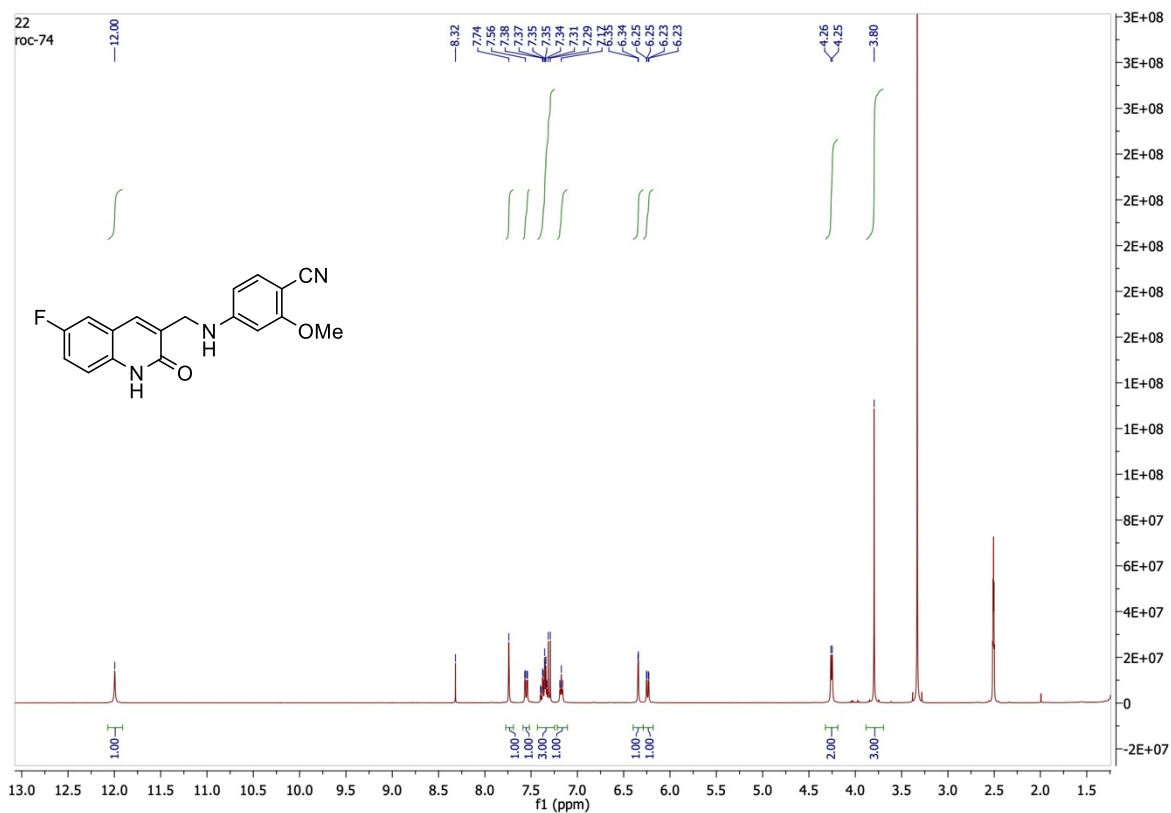


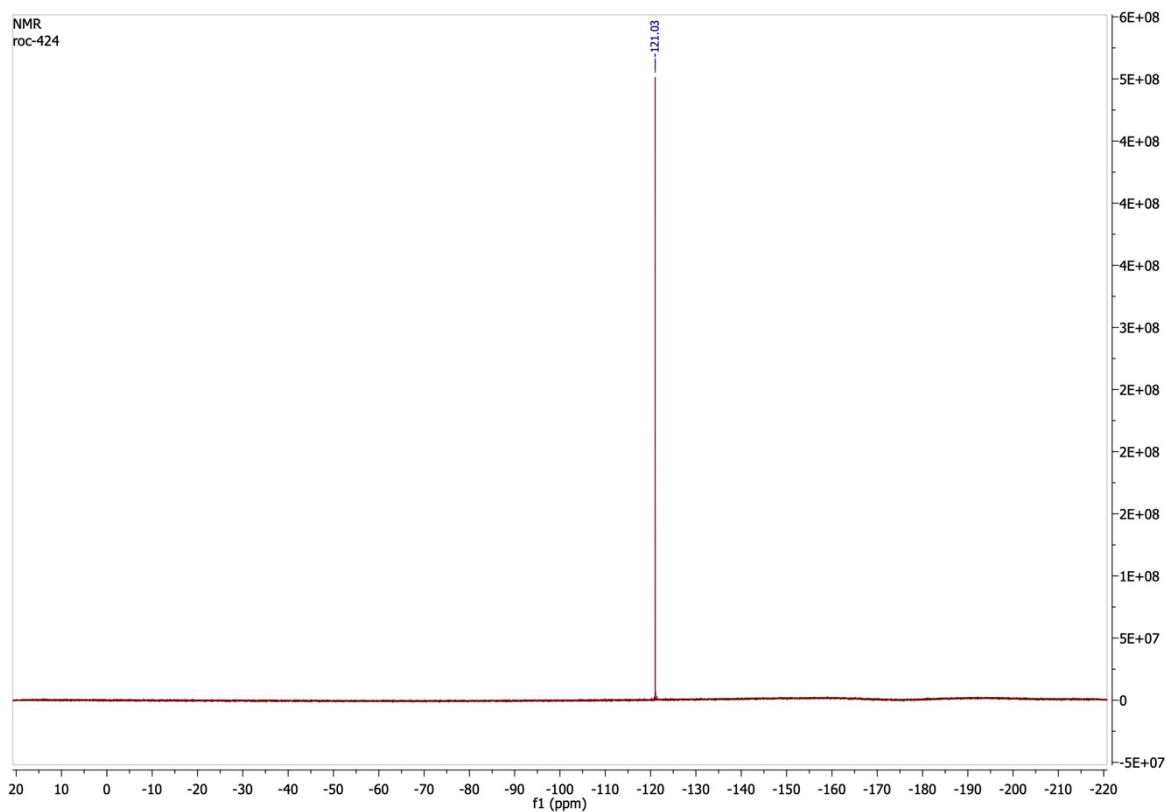
¹H and ¹³C NMR Spectra of 4-[[6-bromo-2-oxo-1,2-dihydroquinolin-3-yl)methyl]amino}-2-methoxybenzonitrile **30e**



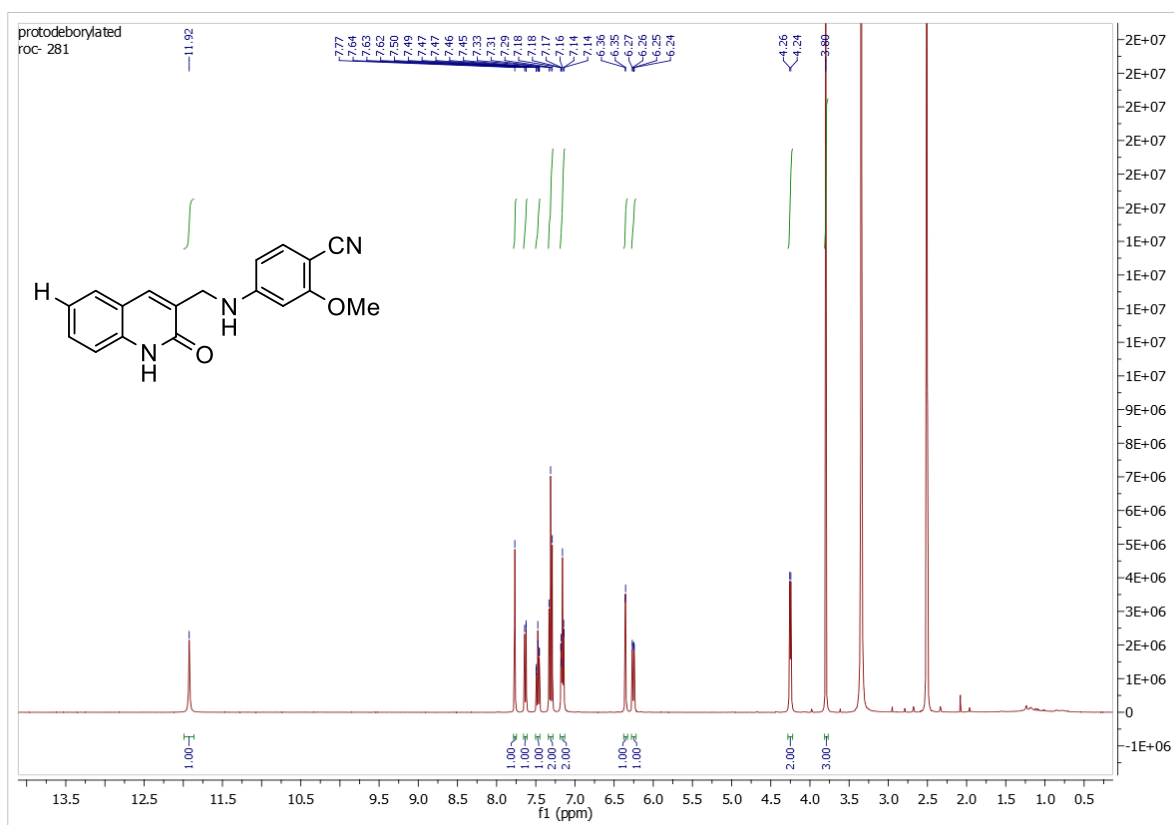


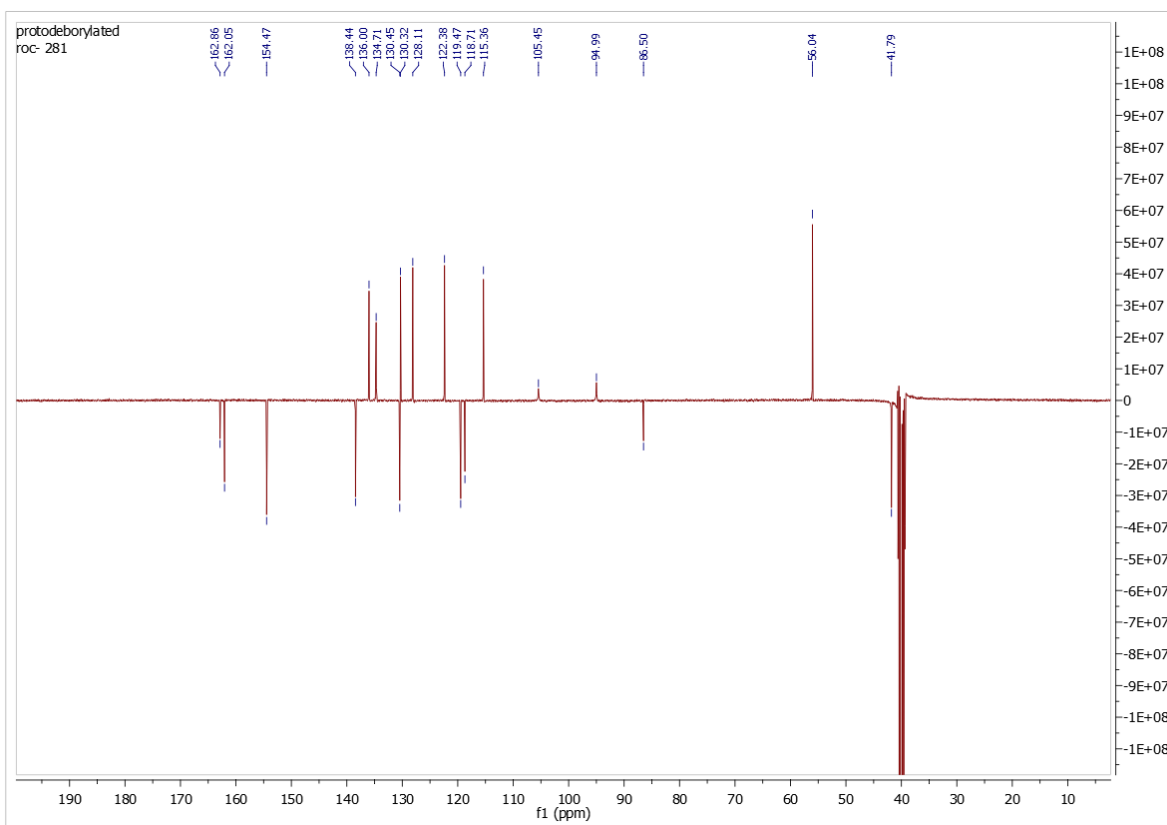
¹H, ¹³C and ¹⁹F NMR Spectra of 4-{[(6-fluoro-2-oxo-1,2-dihydroquinolin-3-yl)methyl]amino}-2-methoxybenzonitrile **30d**



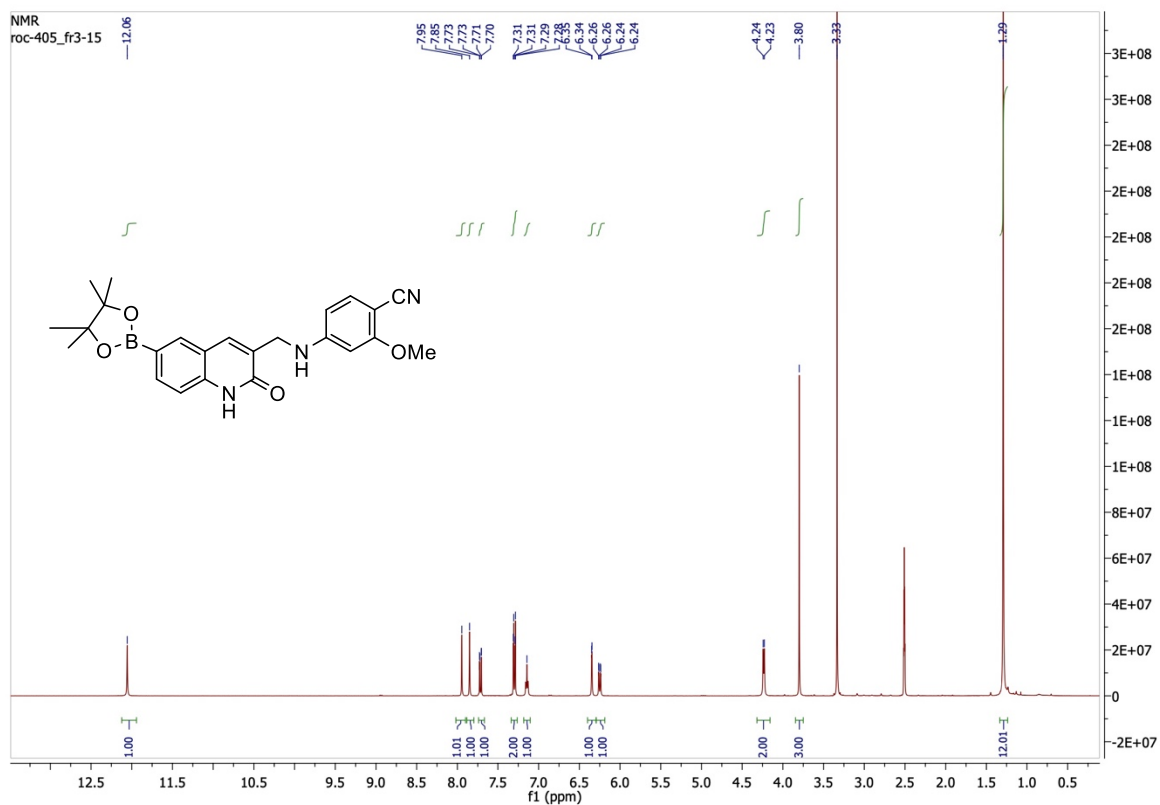


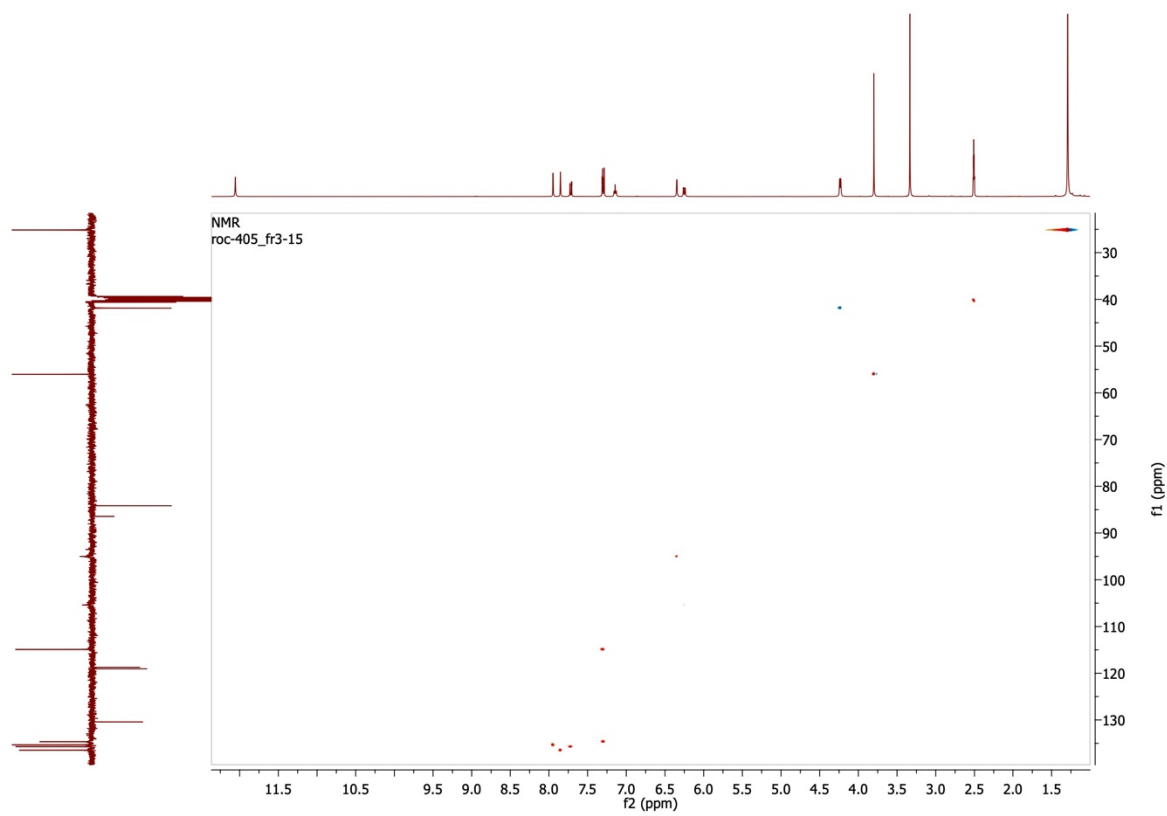
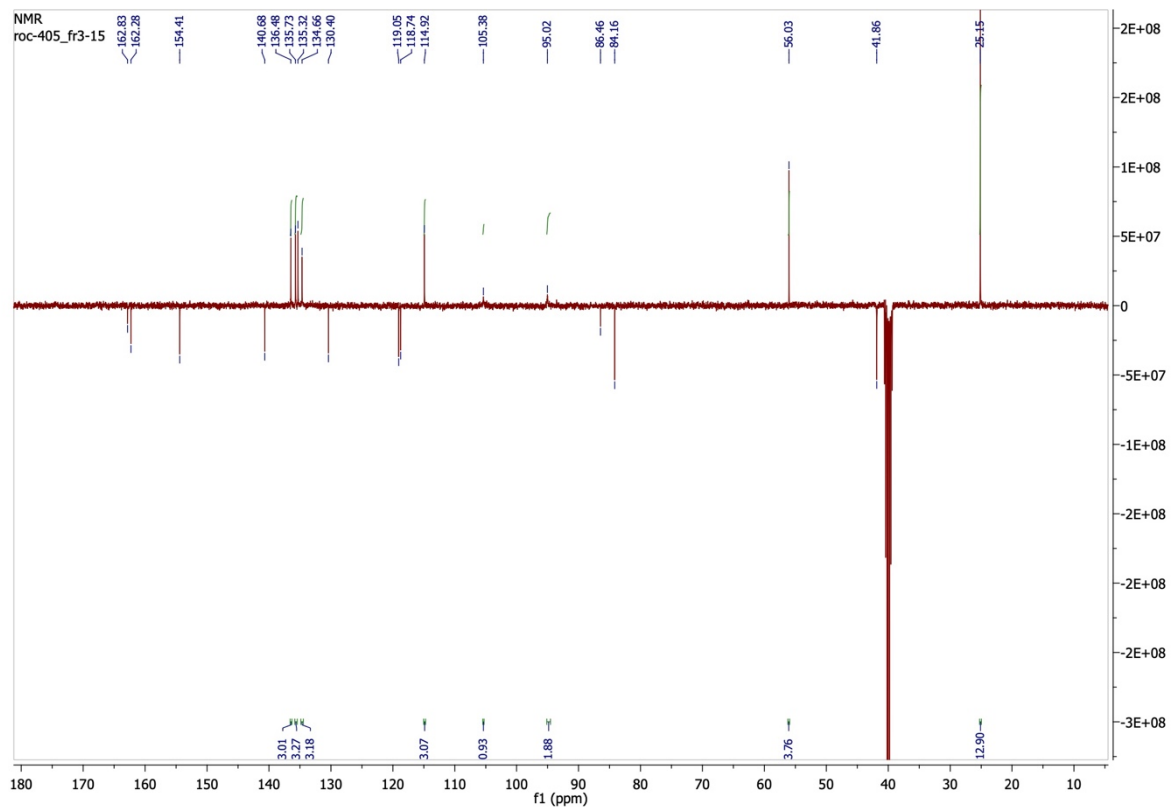
^1H , ^{13}C NMR Spectra of 2-methoxy-4-(((2-oxo-1,2-dihydroquinolin-3-yl)methyl)amino)benzonitrile **30f**



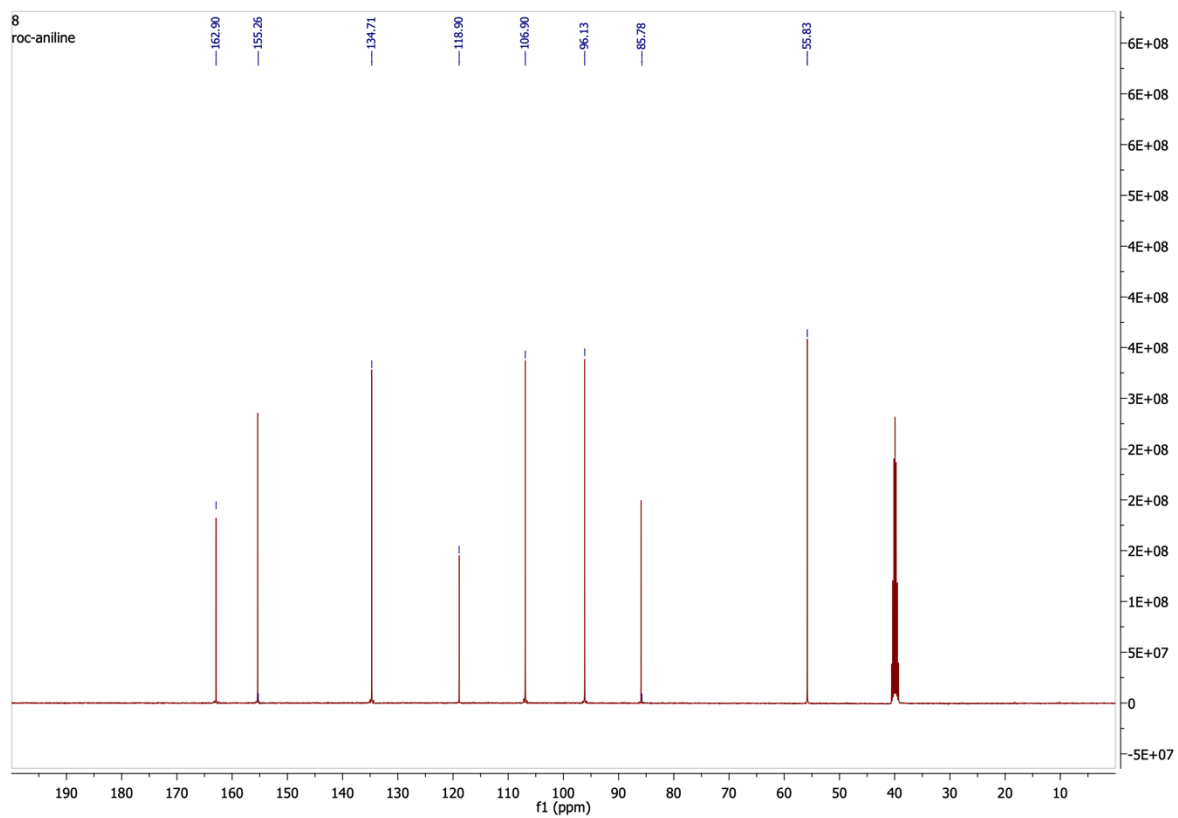
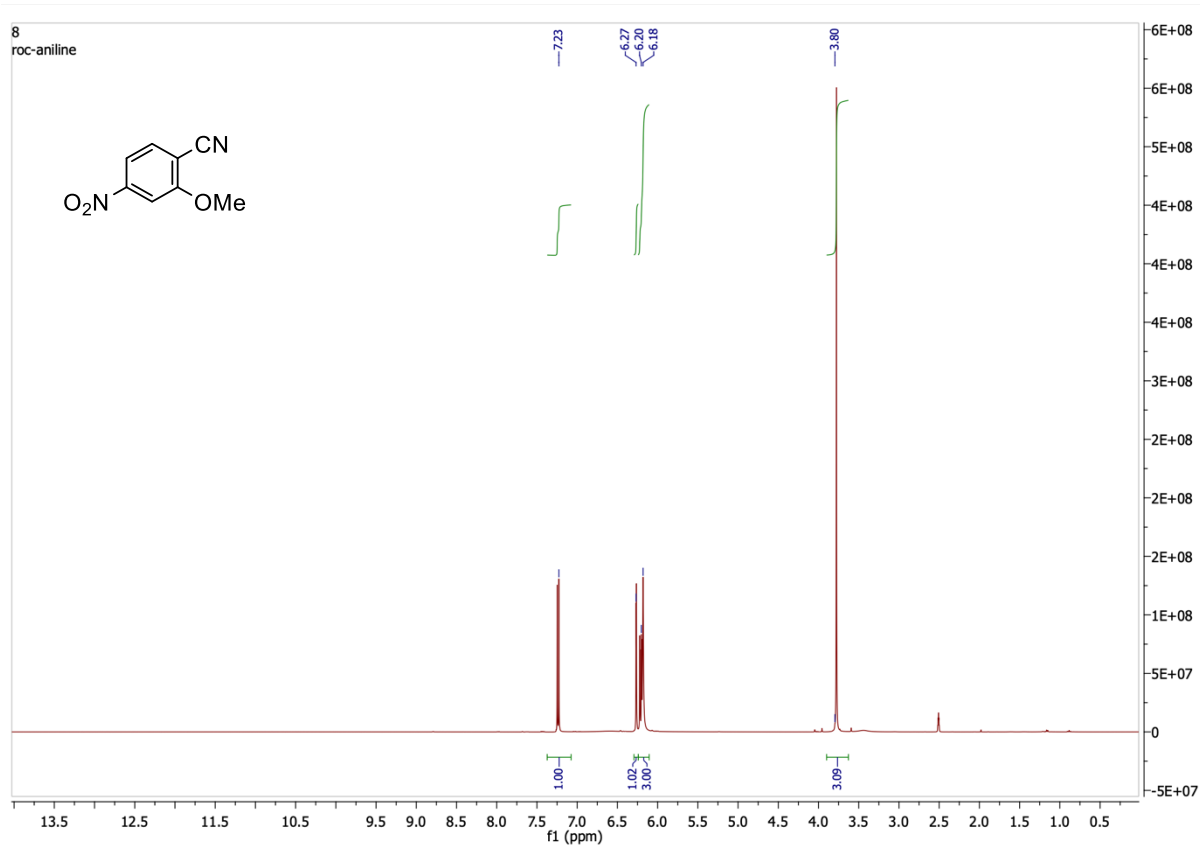


^1H and ^{13}C NMR Spectra of 4- $\{[(6-(4,4,5,5\text{-tetramethyl-1,3,2-dioxaborolan-2-yl)quinolin-1(2H)-one)methyl]amino\}$ -2-methoxybenzonitrile **33**

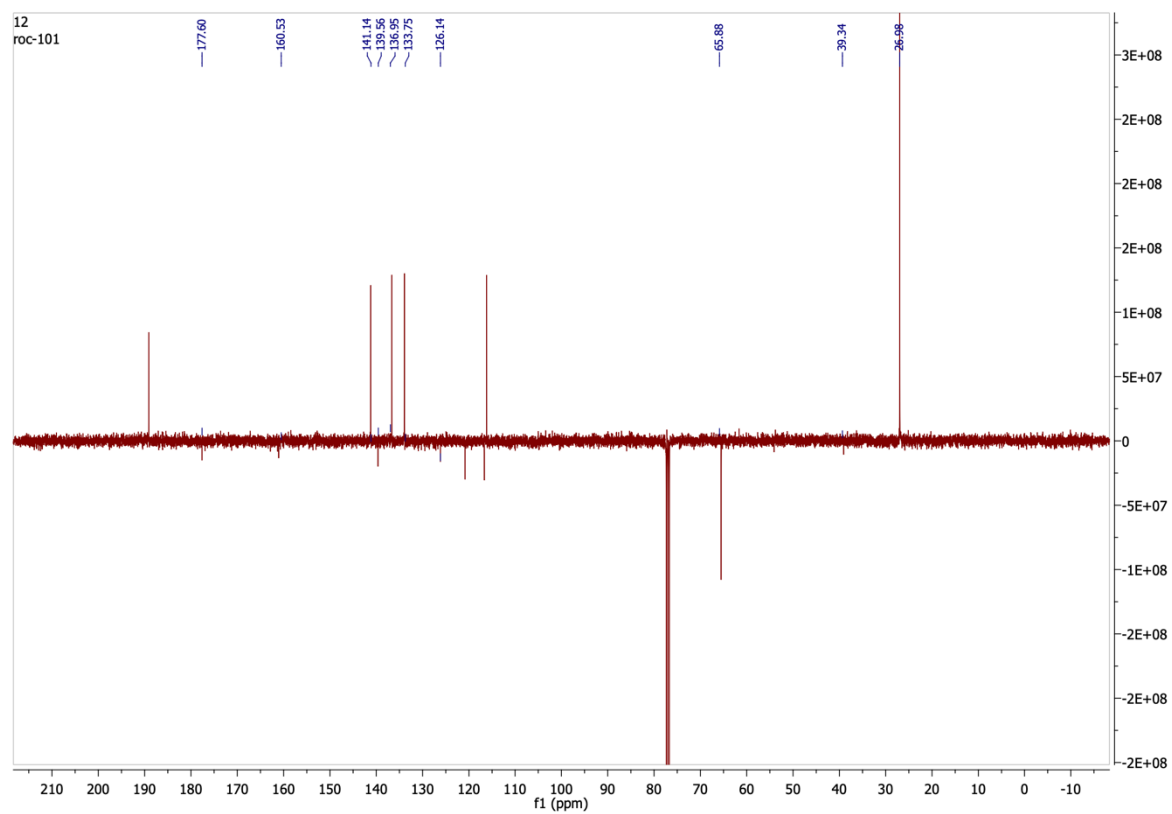
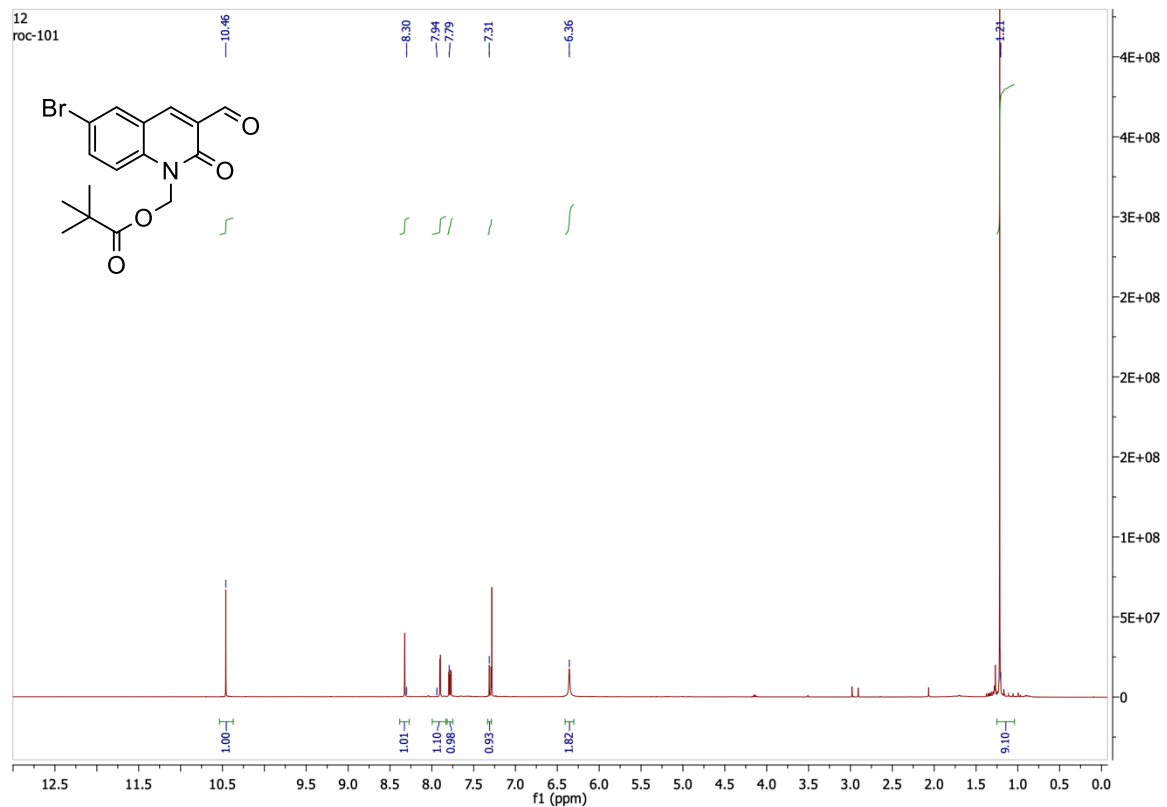




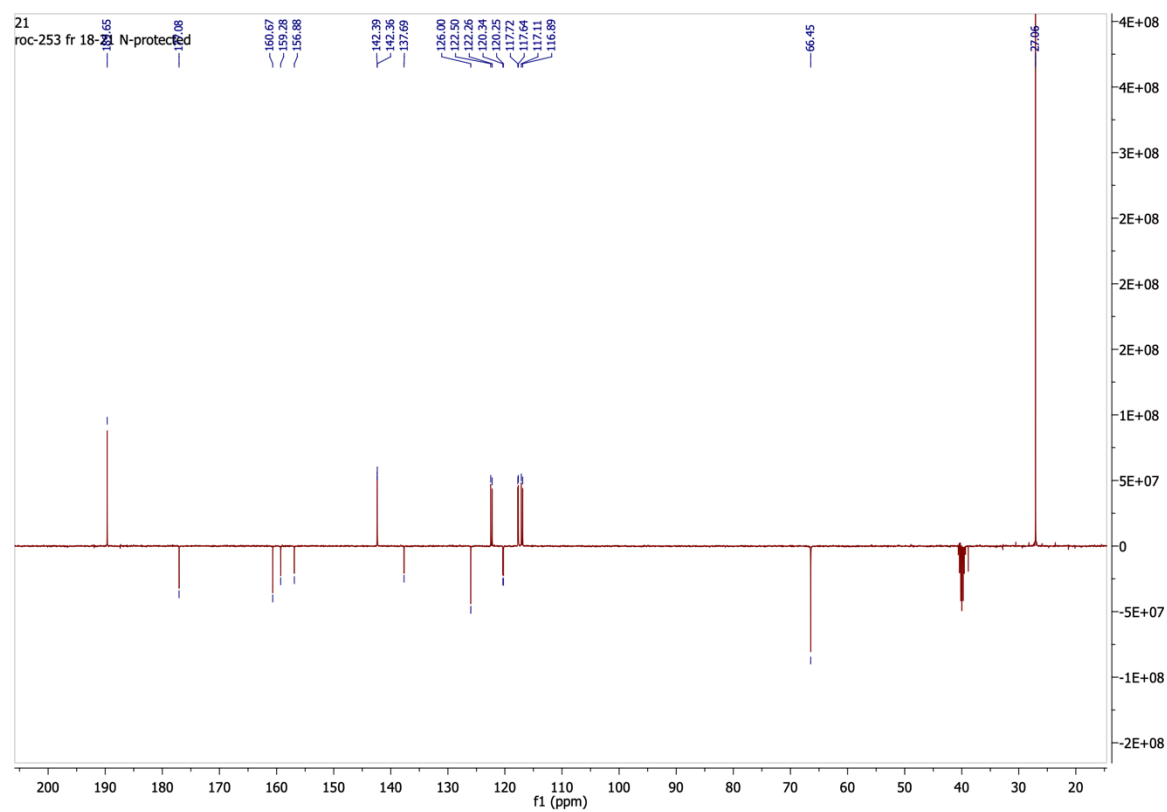
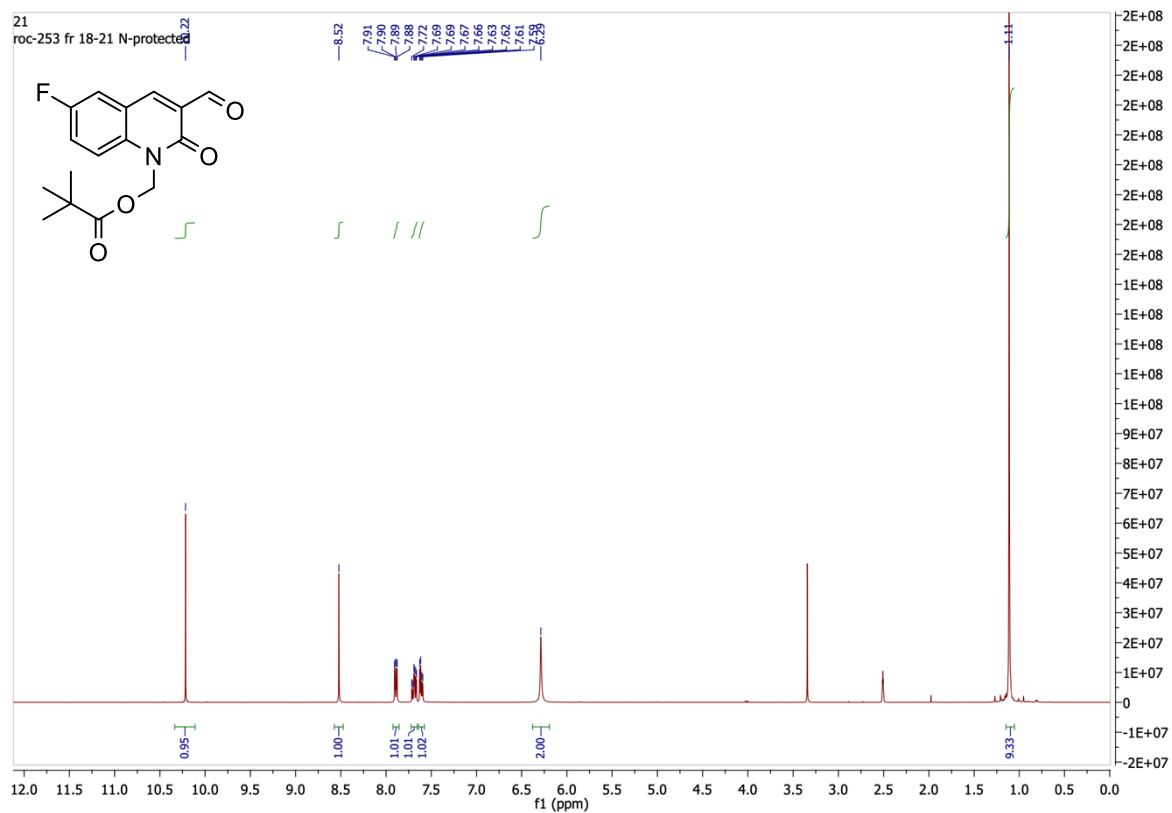
¹H and ¹³C NMR Spectra of 4-amino-2-methoxybenzonitrile 32

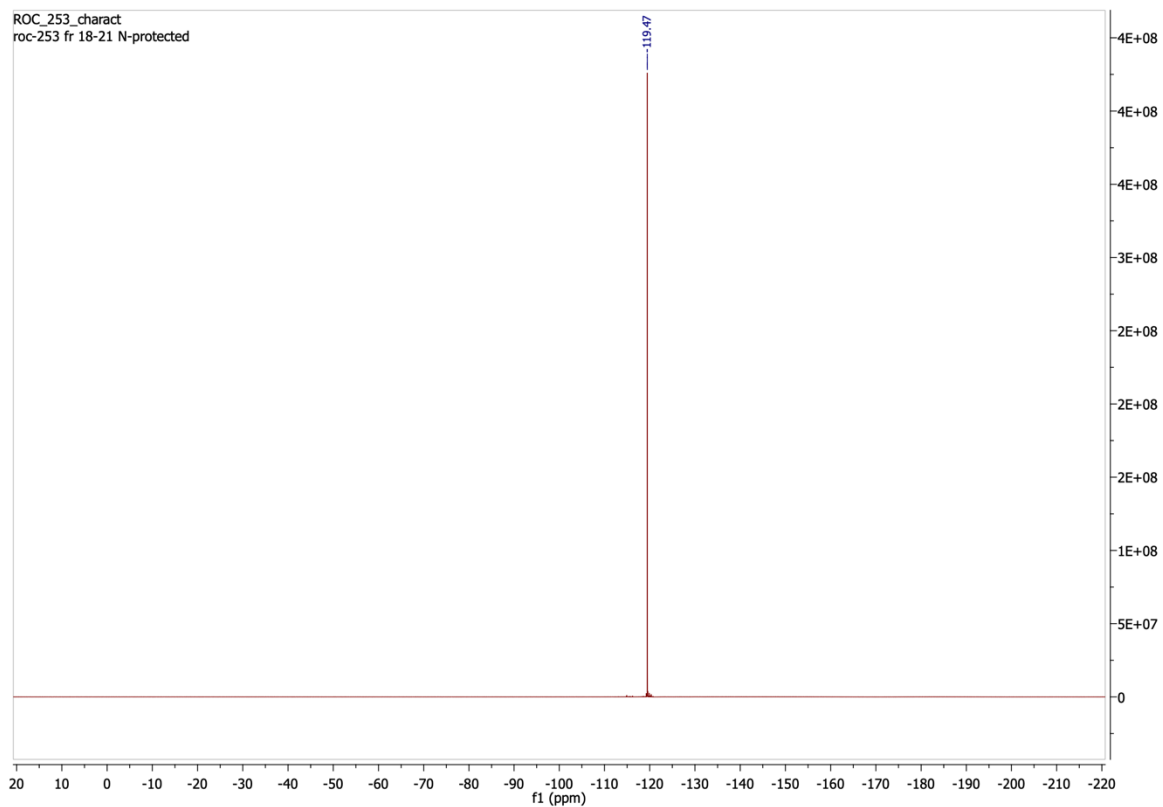


^1H and ^{13}C NMR Spectra of 6-bromo-3-formyl-1-((pivaloyloxy)methyl)quinol-2-one **35e**

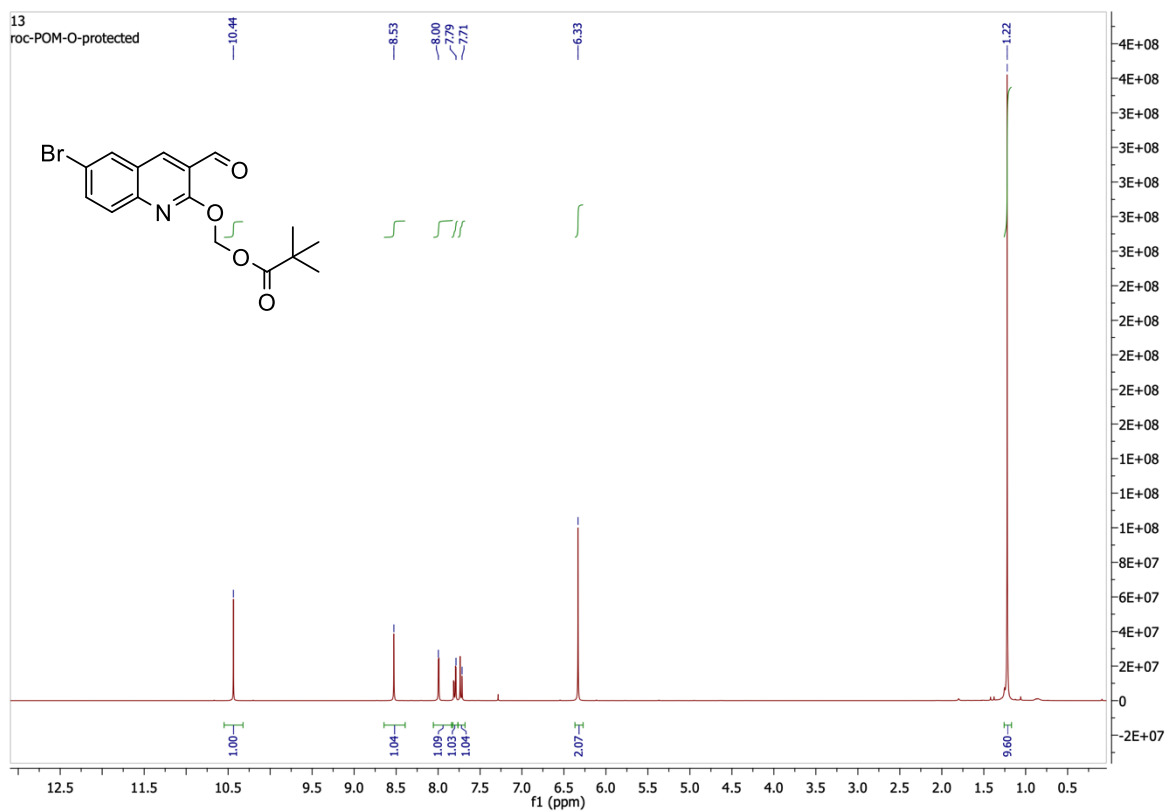


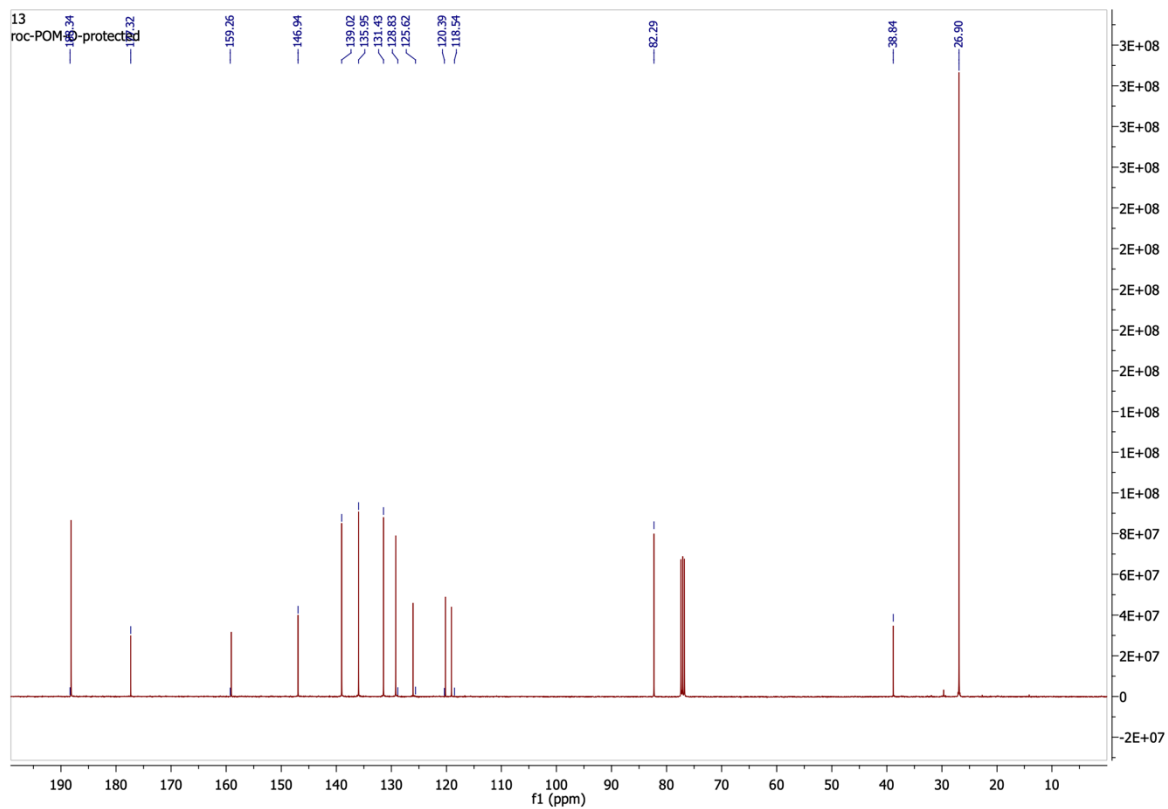
^1H , ^{13}C and ^{19}F NMR Spectra of 6-fluoro-3-formyl-1-((pivaloyloxy)methyl)quinolin-2-one **35d**



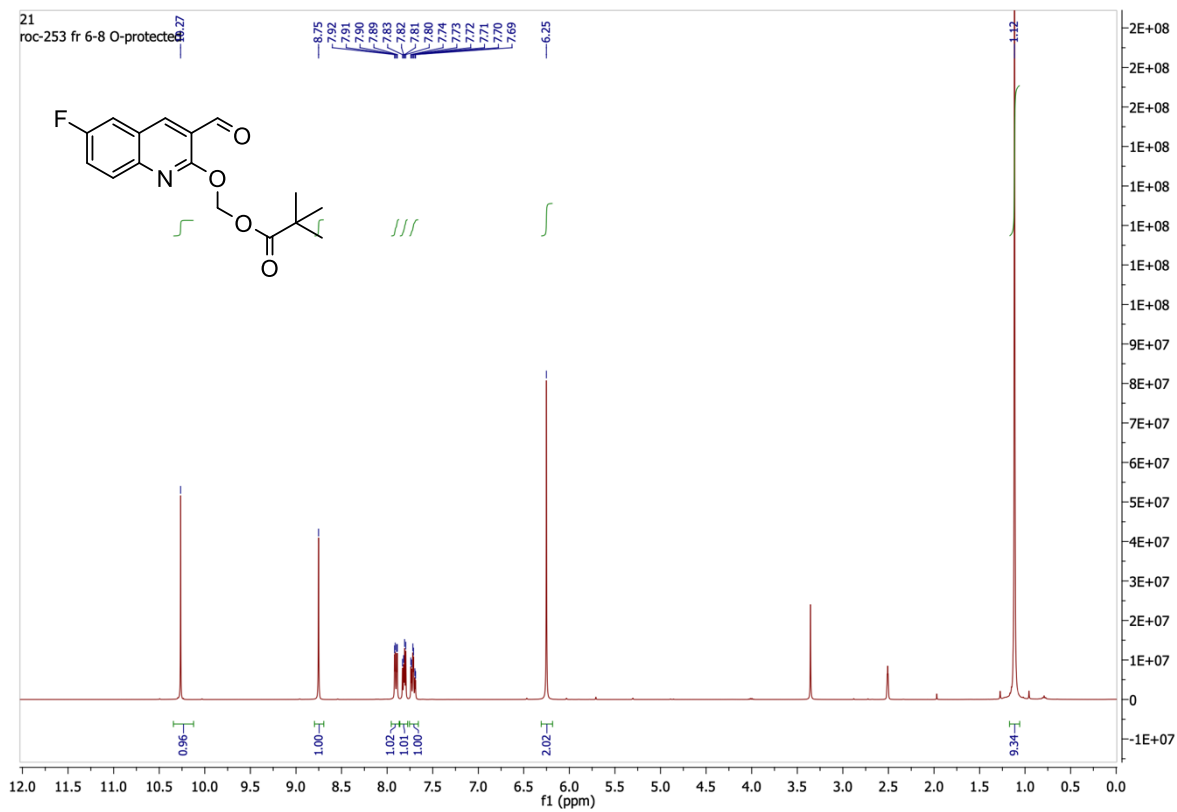


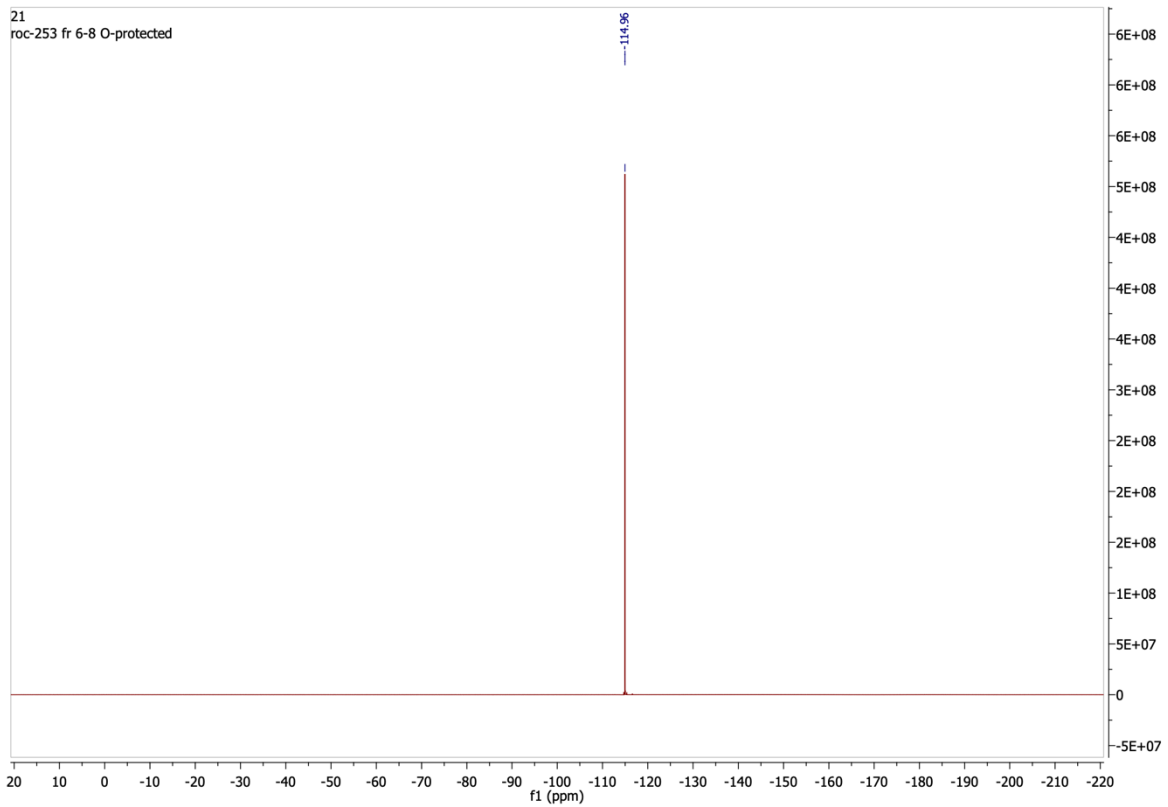
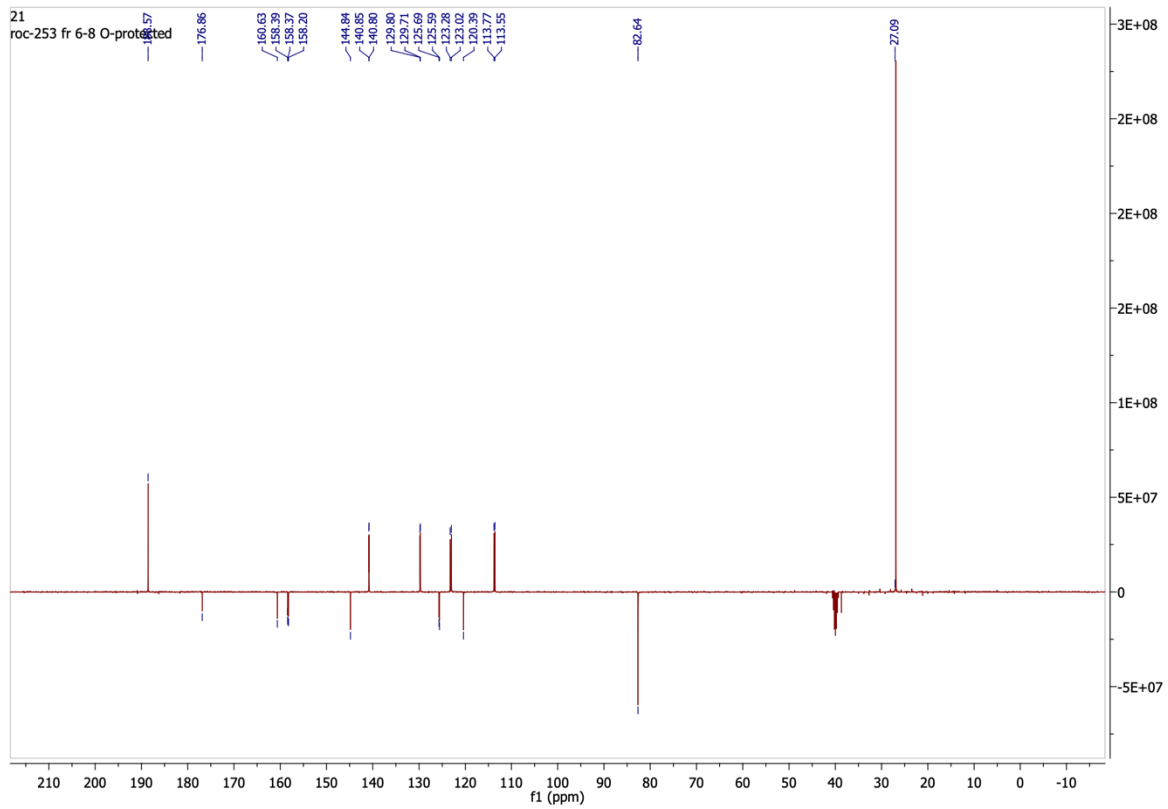
^1H and ^{13}C NMR Spectra of 2-*(pivaloyloxy)methyl*-6-bromoquinoline-3-carbaldehyde **36e**



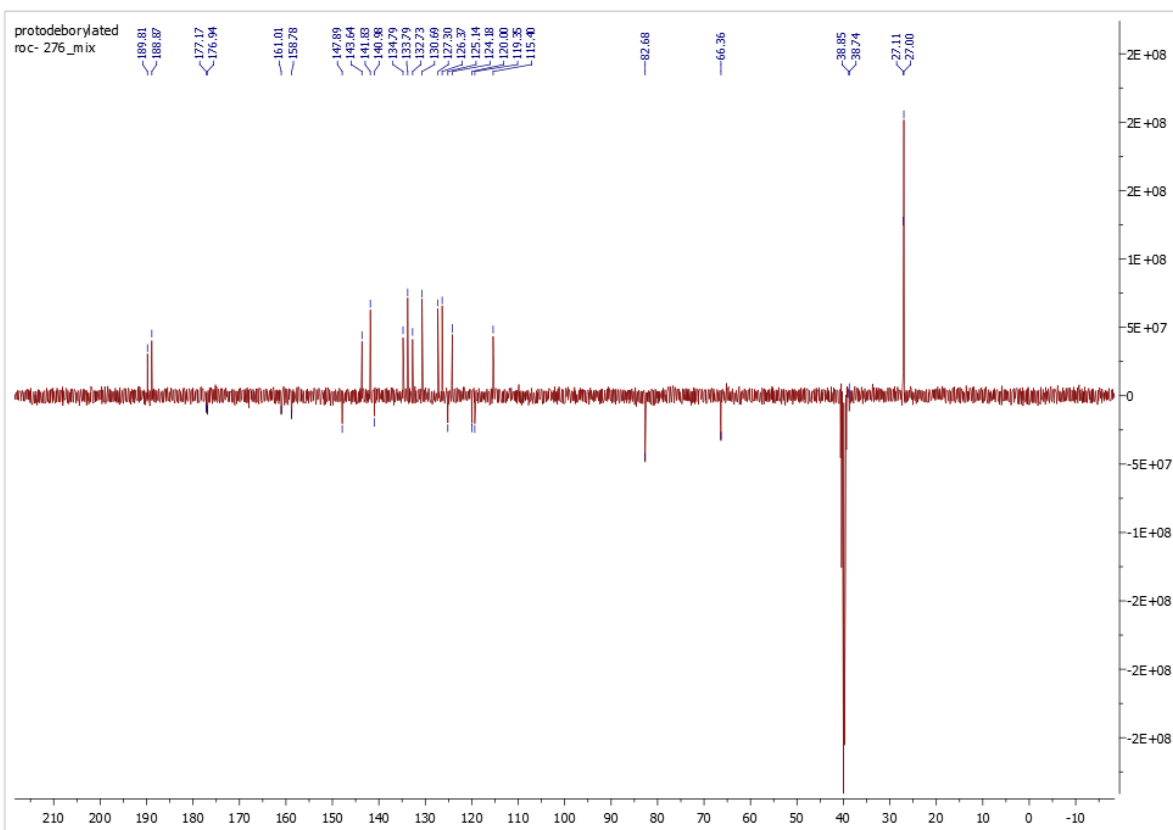
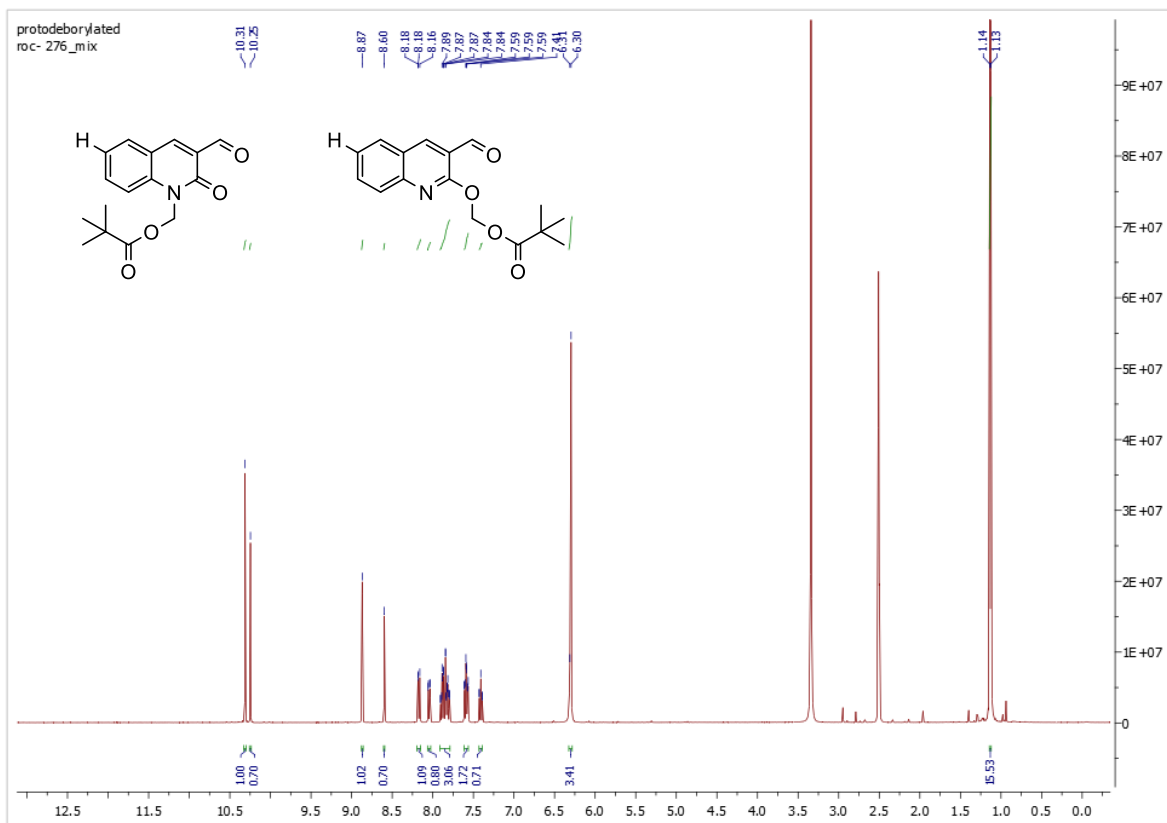


^1H , ^{13}C and ^{19}F NMR Spectra of 2-*(pivaloyloxy)methyl*-6-fluoroquinoline-3-carbaldehyde **36d**

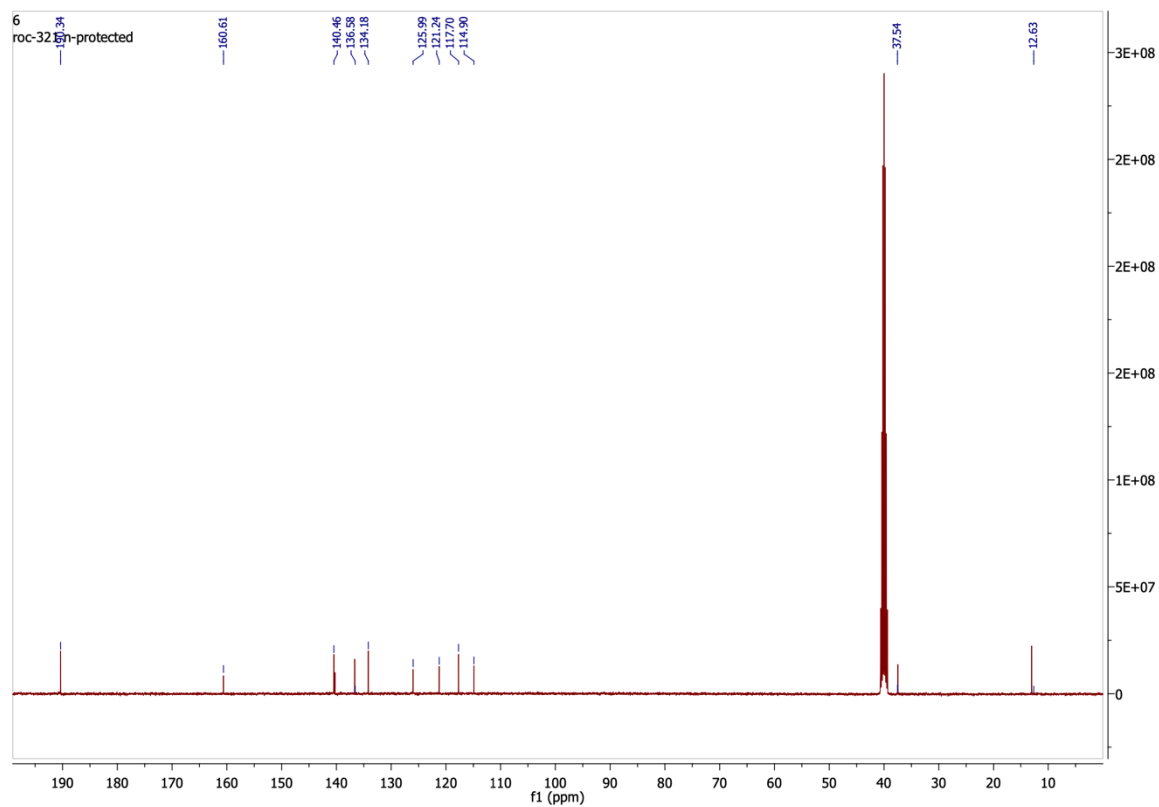
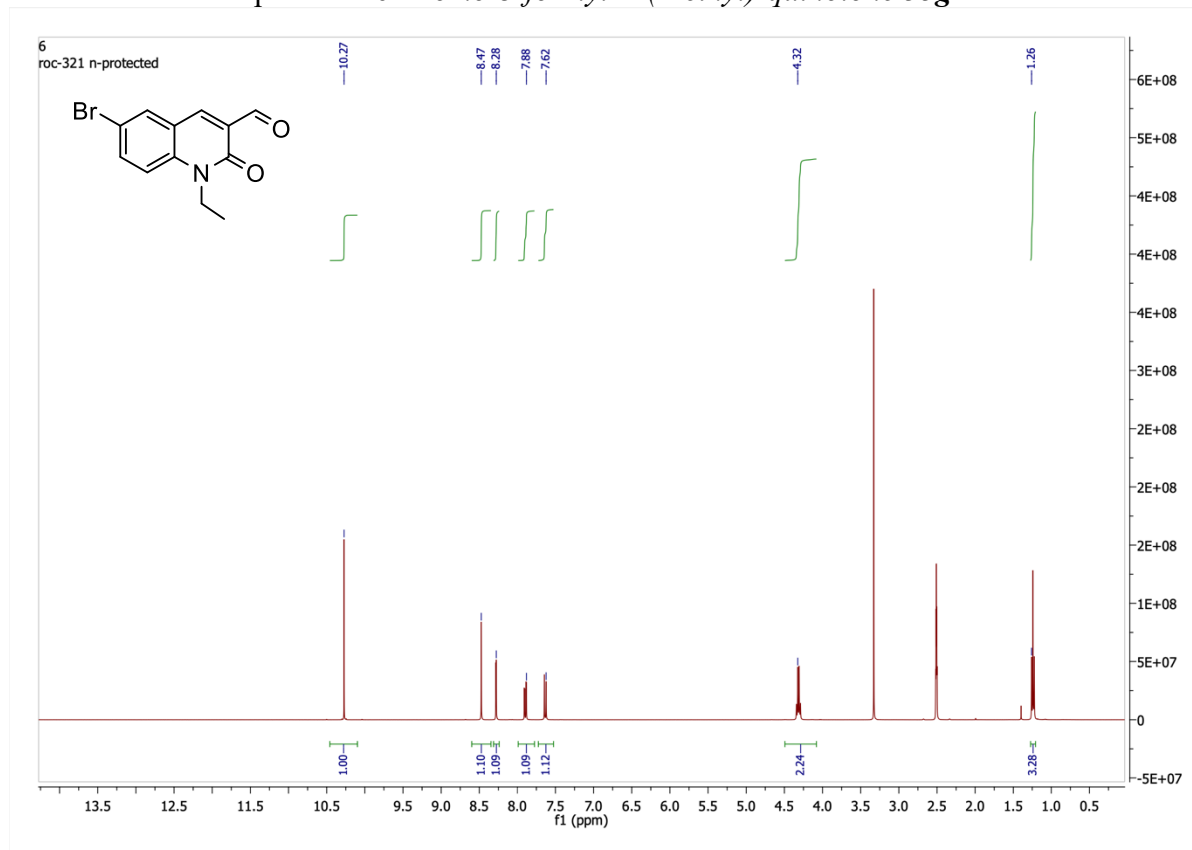




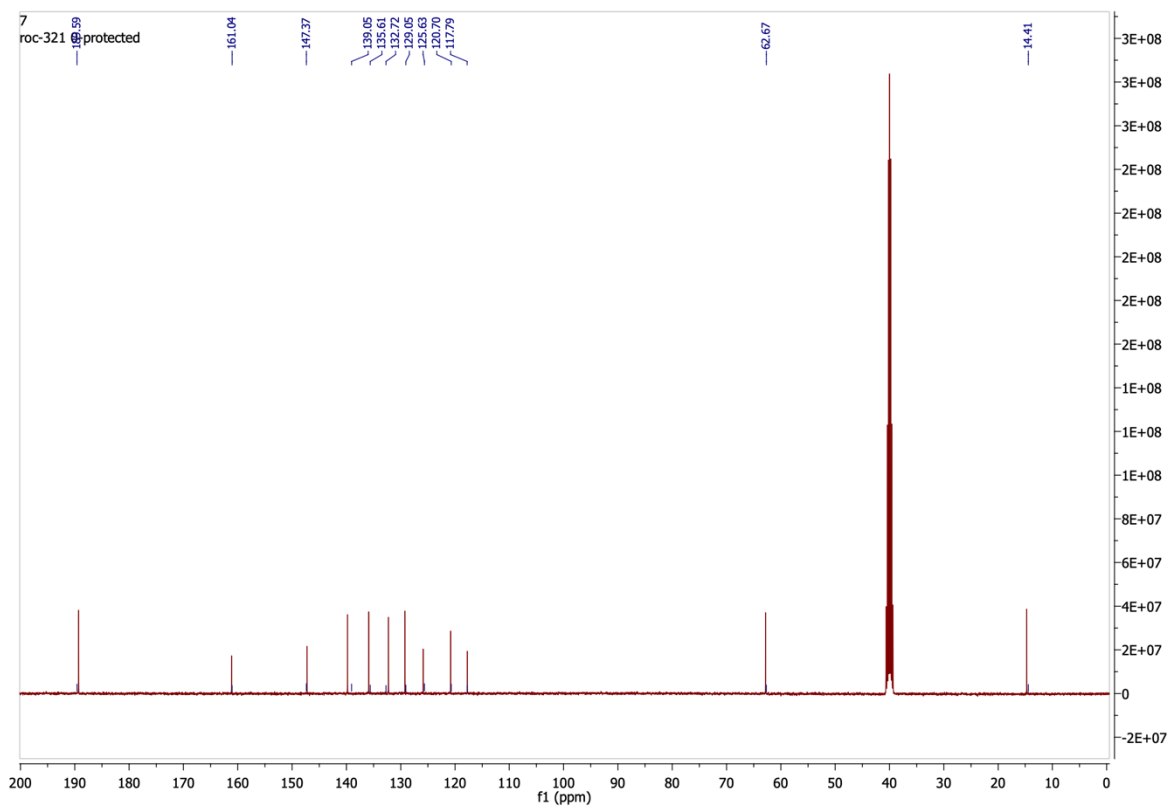
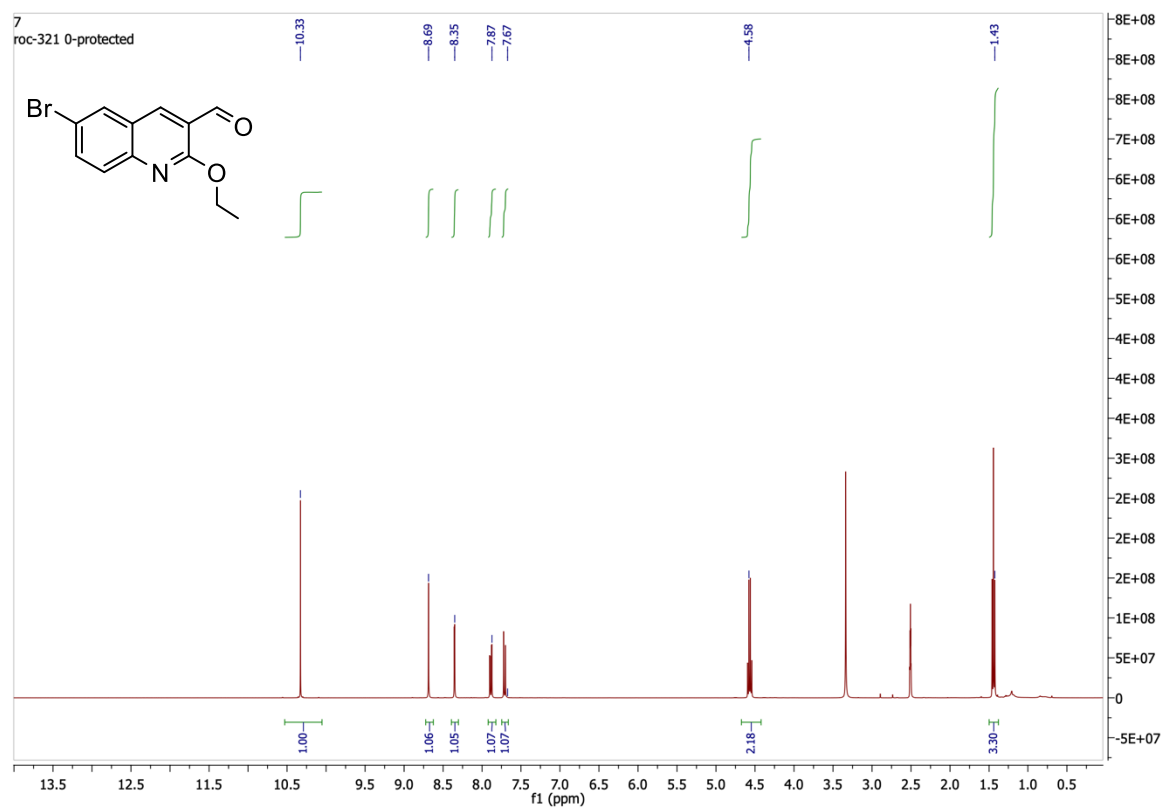
^1H , ^{13}C and ^{19}F NMR Spectra of (3-formyl-2-oxoquinolin-1(2H)-yl)methyl pivalate **35f** and ((3-formylquinolin-2-yl)oxy)methyl pivalate **36f**



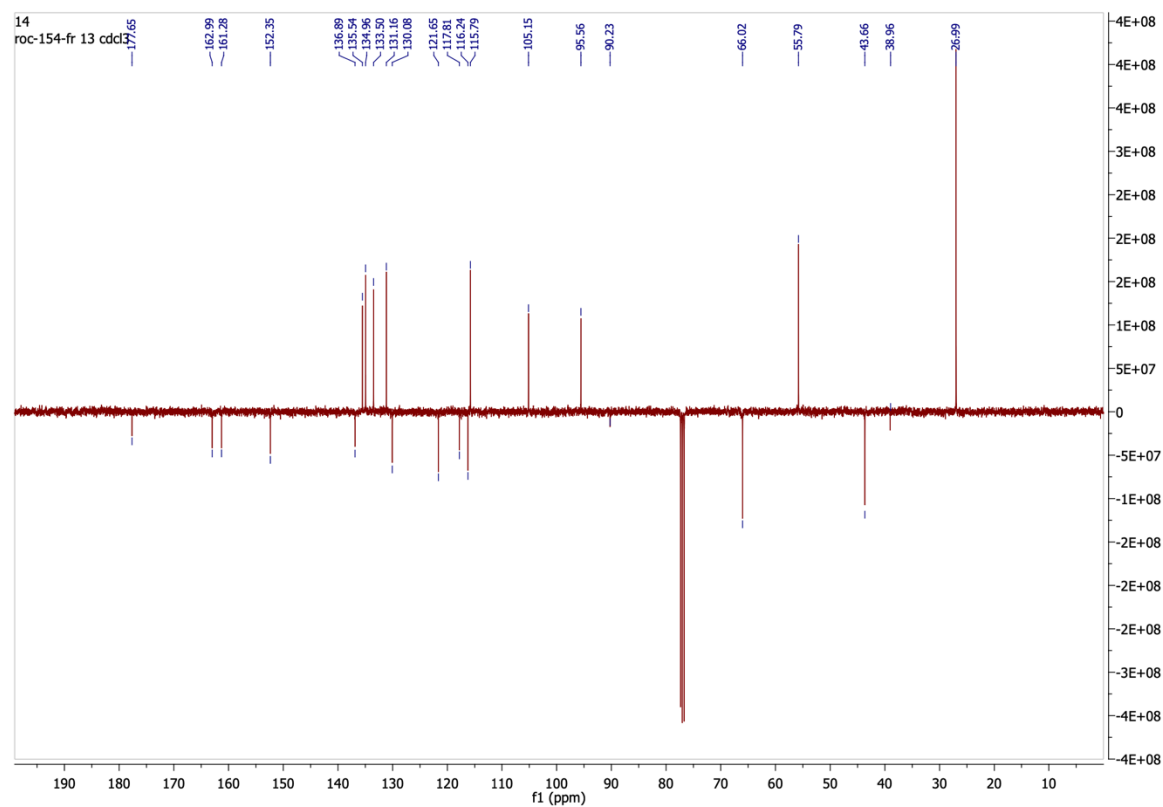
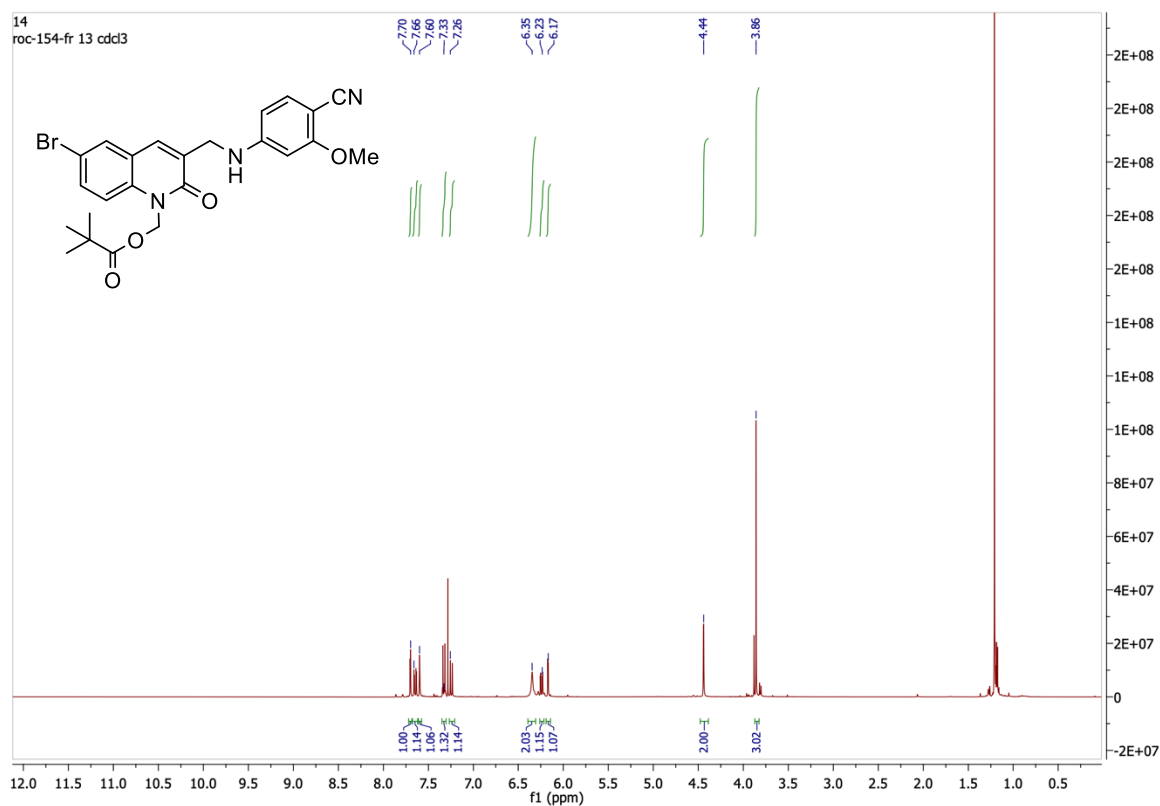
¹H and ¹³C NMR Spectra of 6-Bromo-3-formyl-2-(1-ethyl)-quinolone 35g

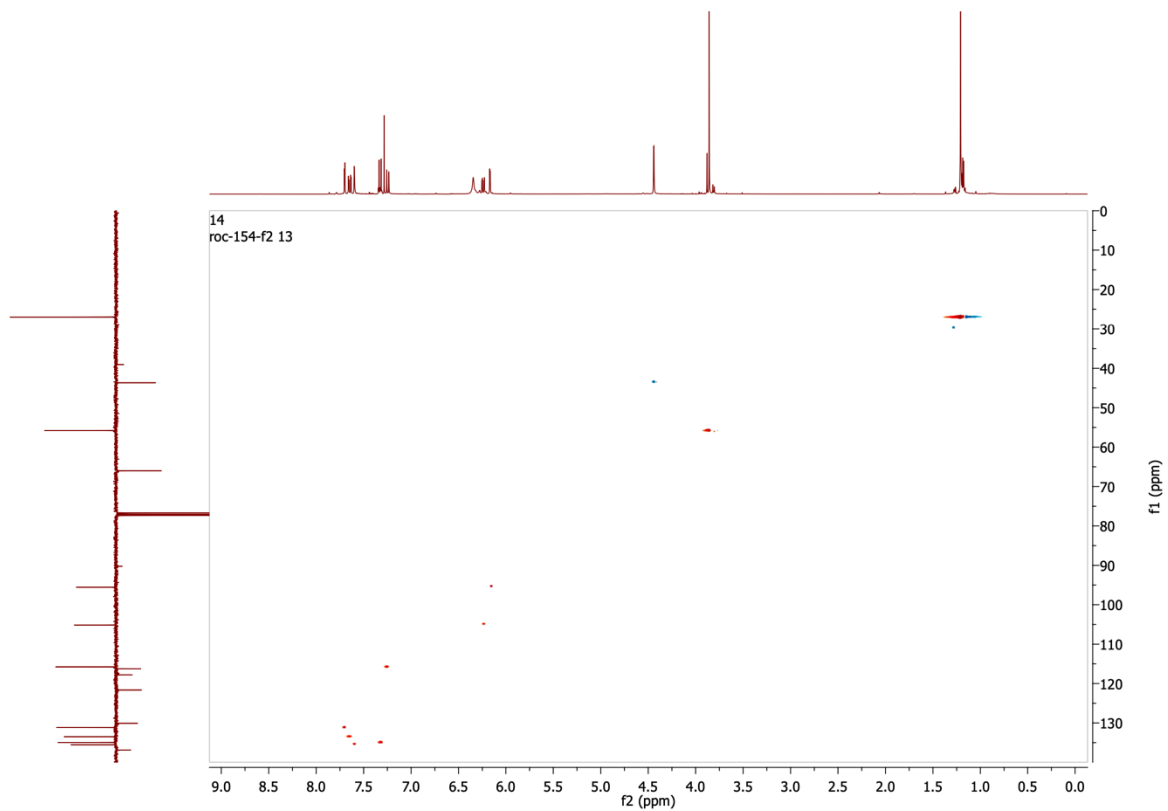


^1H and ^{13}C NMR Spectra of 6-bromo-2-ethoxyquinoline-3-carbaldehyde **36g**

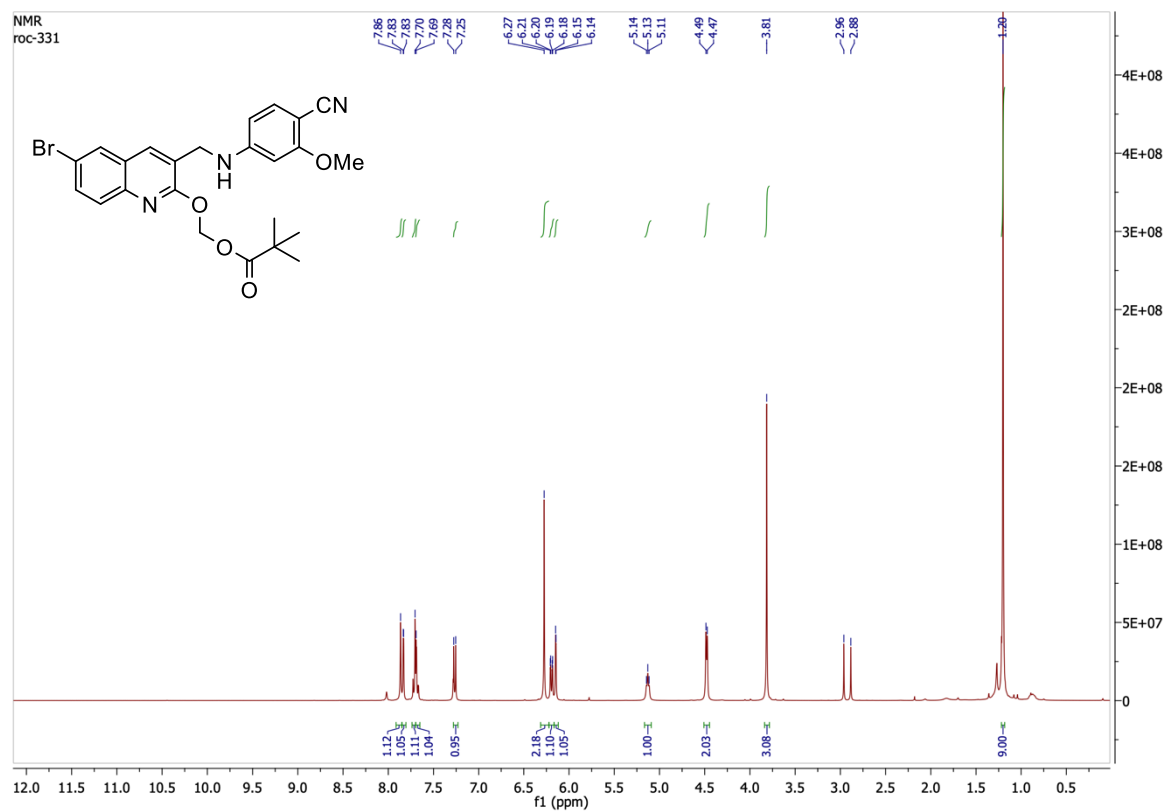


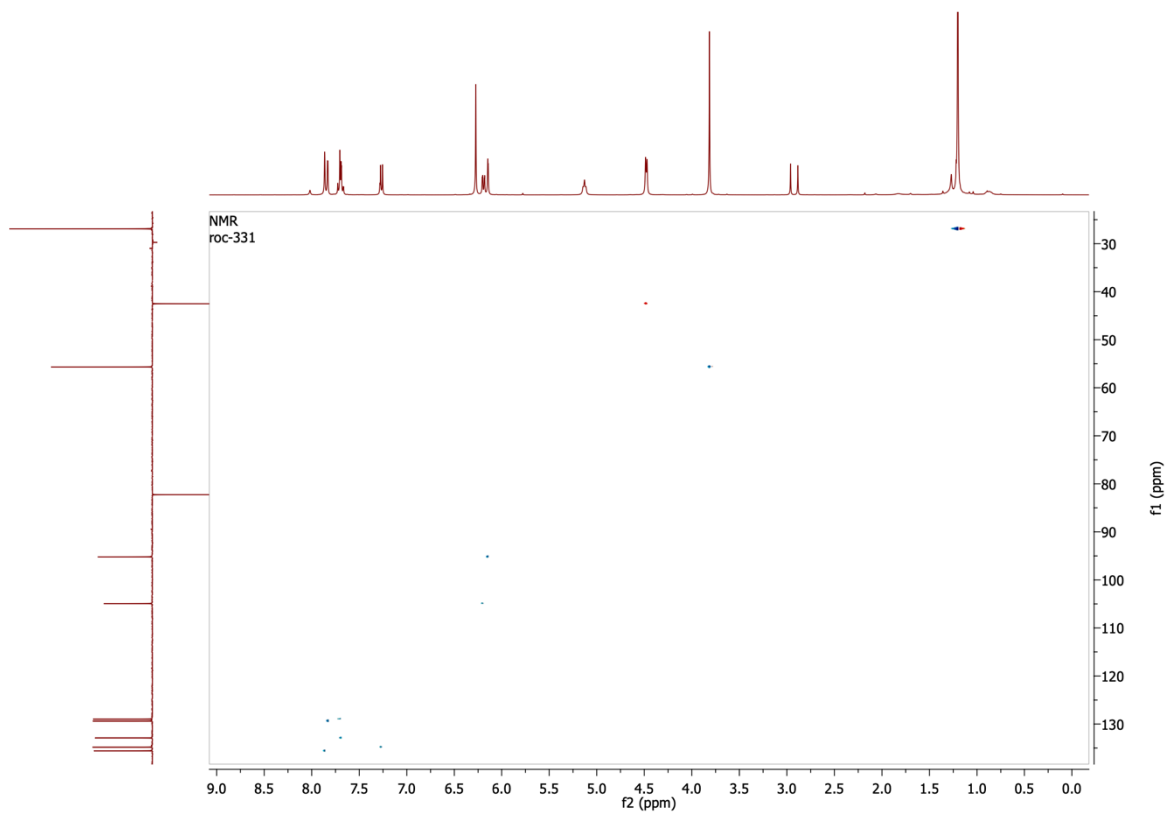
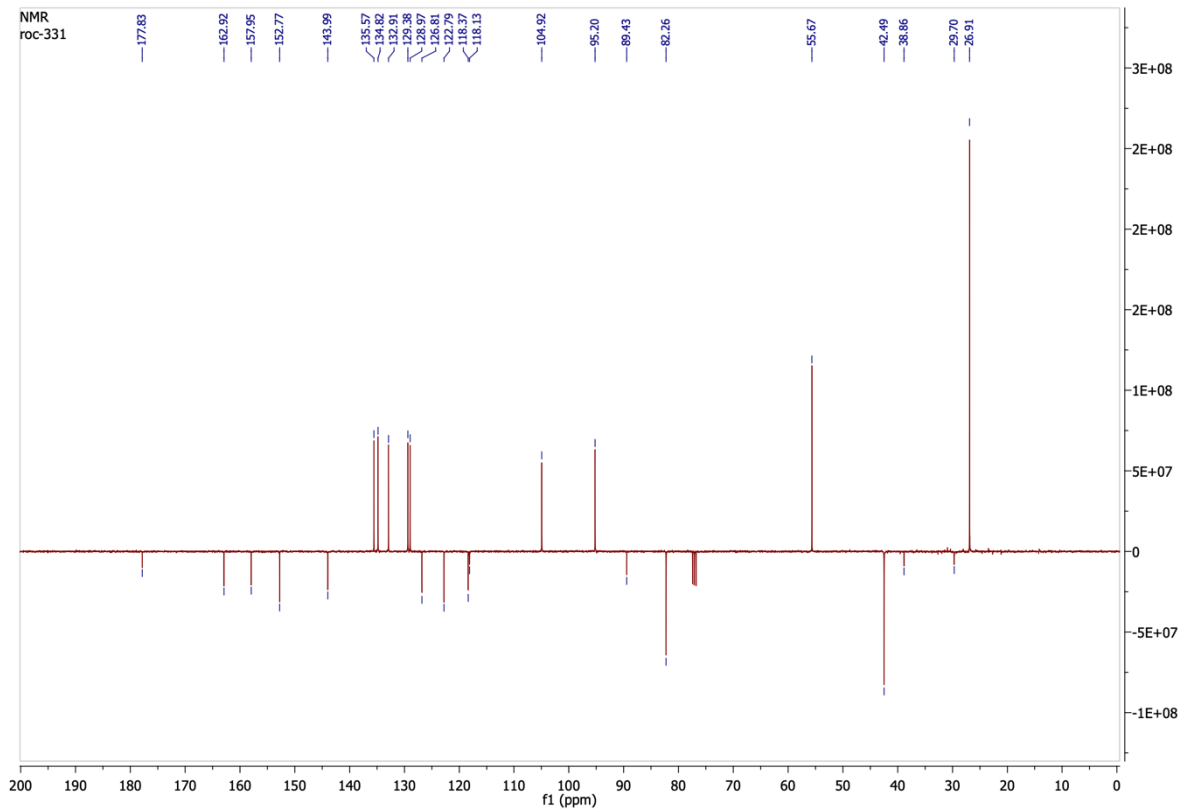
^1H and ^{13}C NMR Spectra of (6-bromo-3-(((4-cyano-3-methoxyphenyl)amino)methyl)-2-oxoquinolin-1(2*H*)-yl)methyl pivalate **37e**



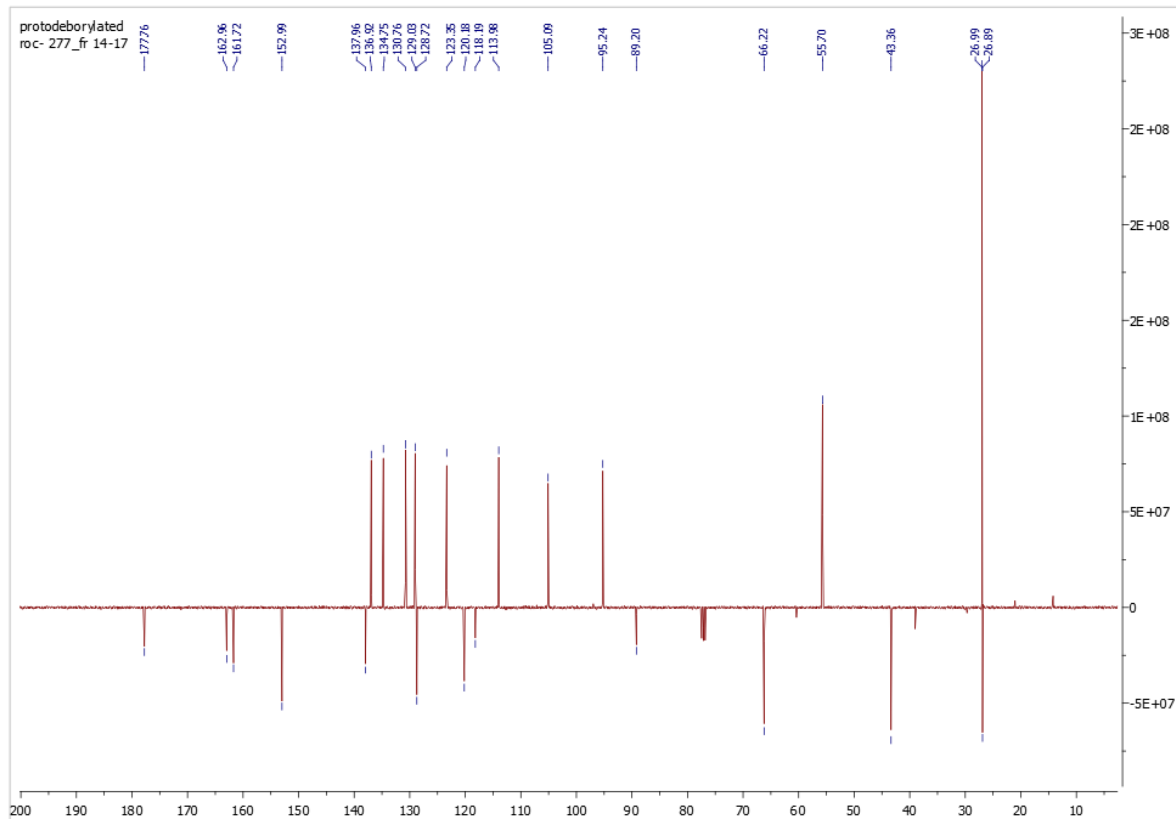
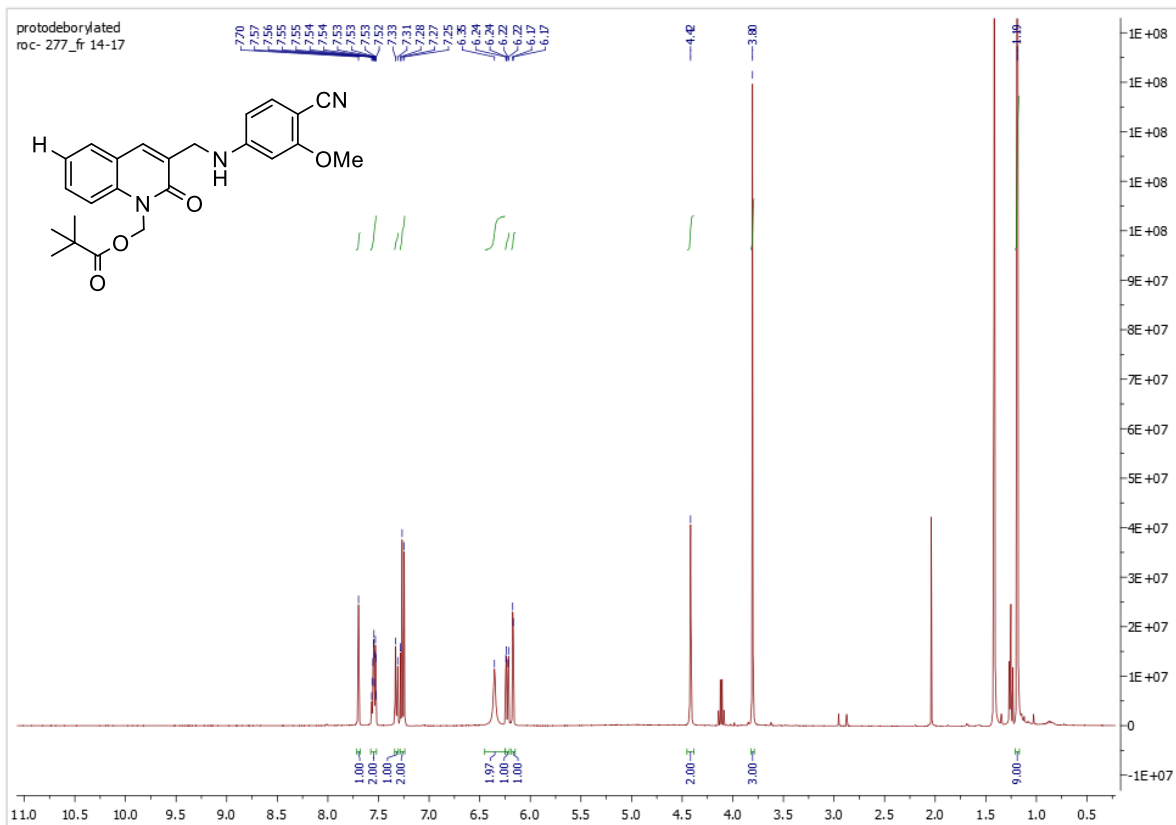


^1H , ^{13}C and HSQC NMR Spectra of ((6-bromo-3-((4-cyano-3-methoxyphenyl)amino)methyl)quinolin-2-yl)oxy)methyl pivalate **38e**

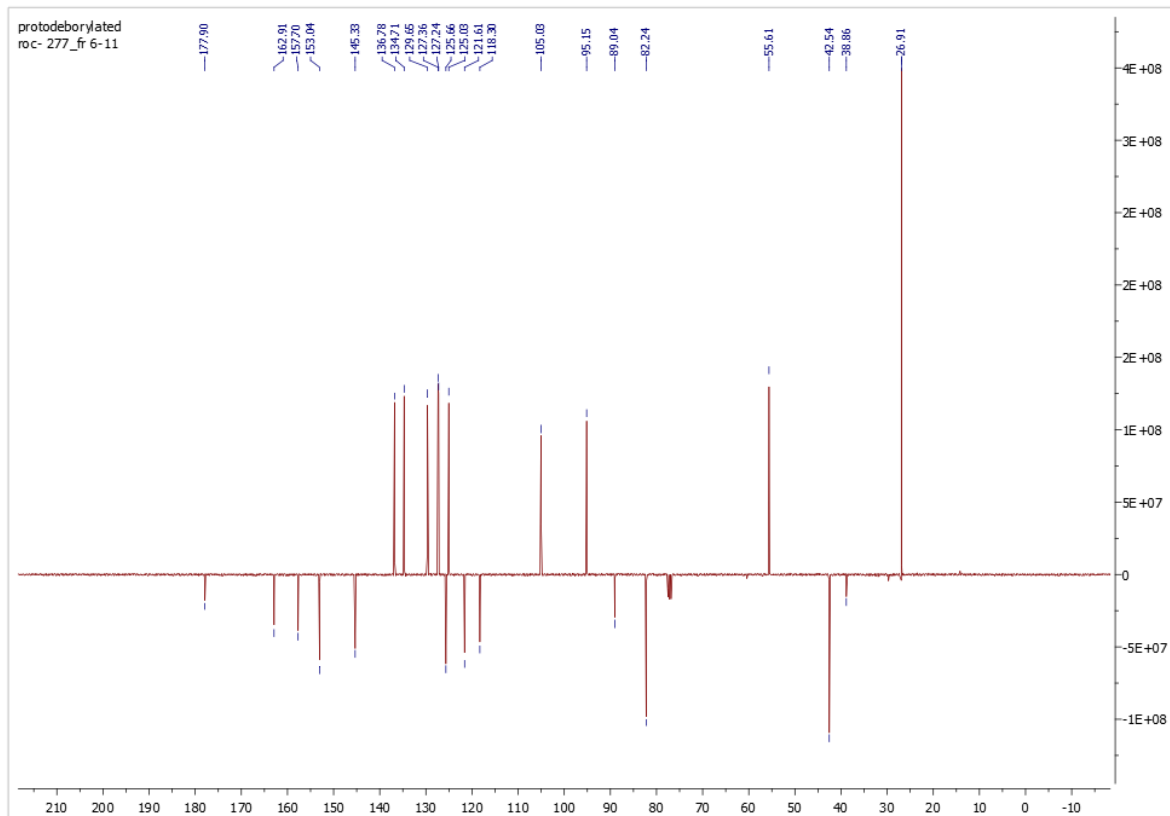
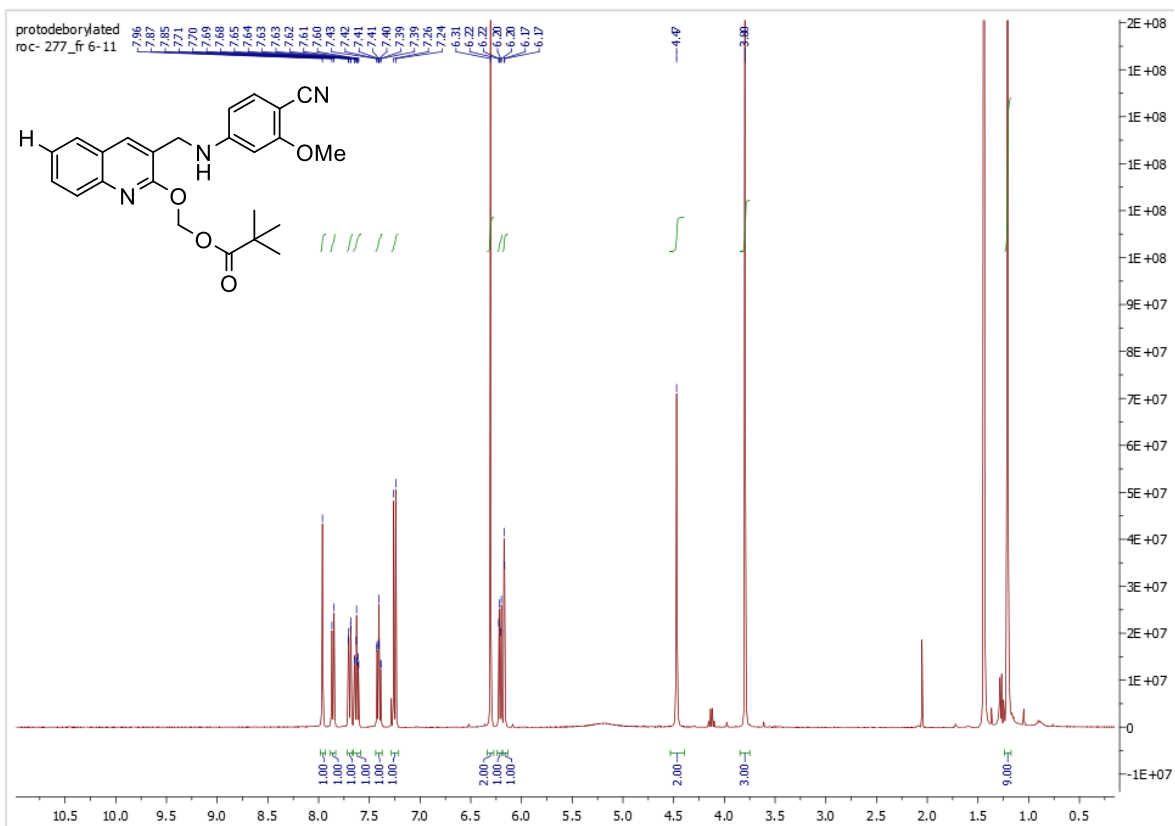




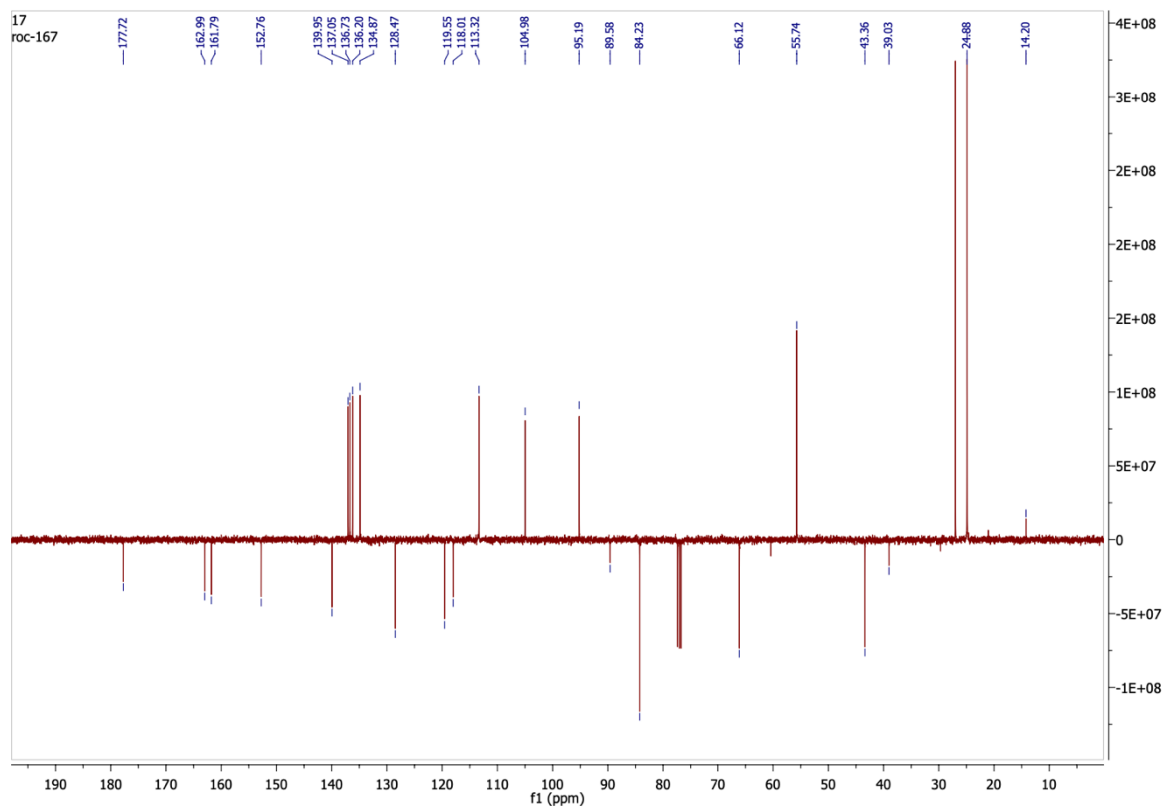
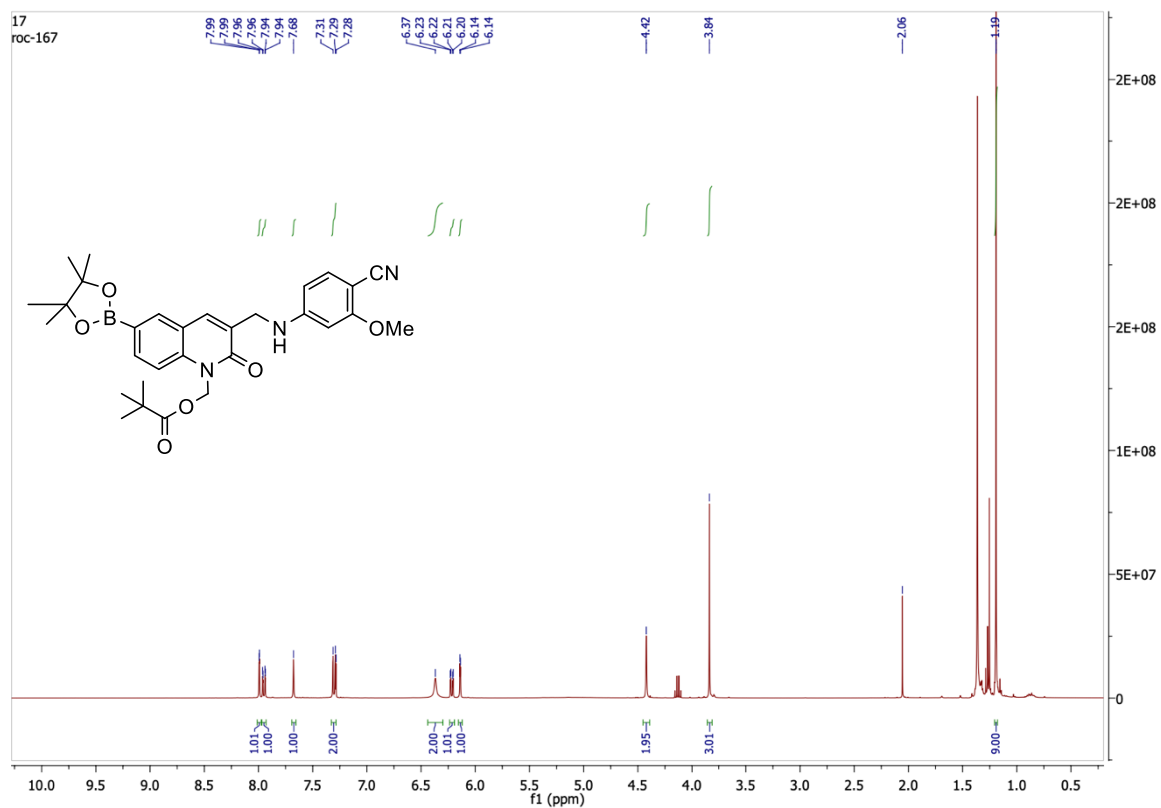
¹H and ¹³C NMR Spectra of (3-(((4-cyano-3-methoxyphenyl)amino)methyl)-2-oxoquinolin-1(2H)-yl)methyl pivalate **37f**



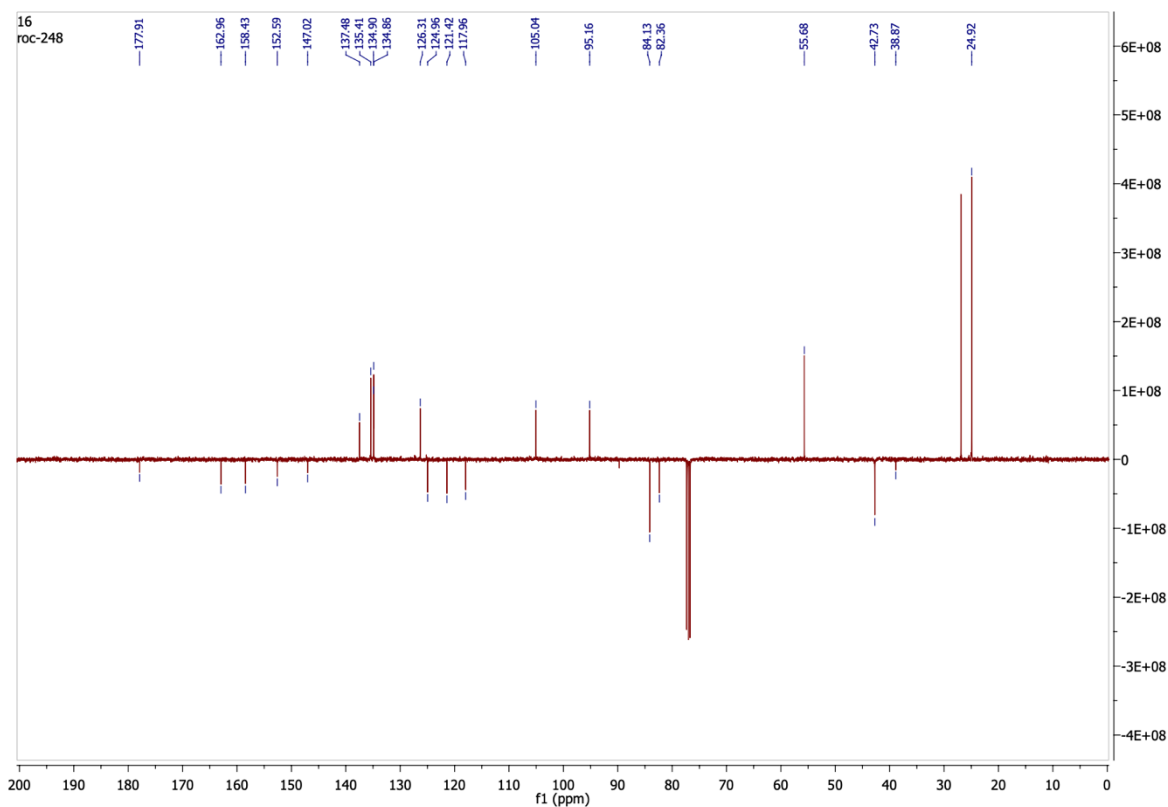
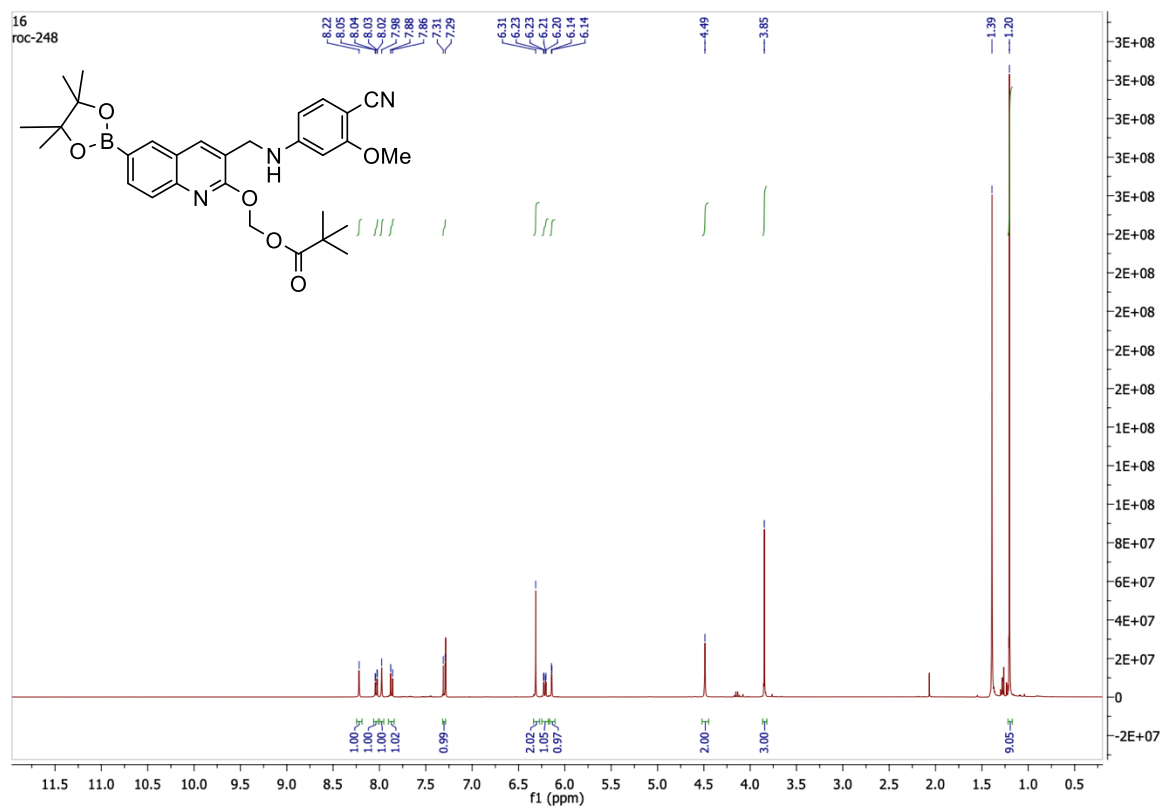
^1H and ^{13}C NMR Spectra of ((3-(((4-cyano-3-methoxyphenyl)amino)methyl)quinolin-2-yl)oxy)methyl pivalate **38f**



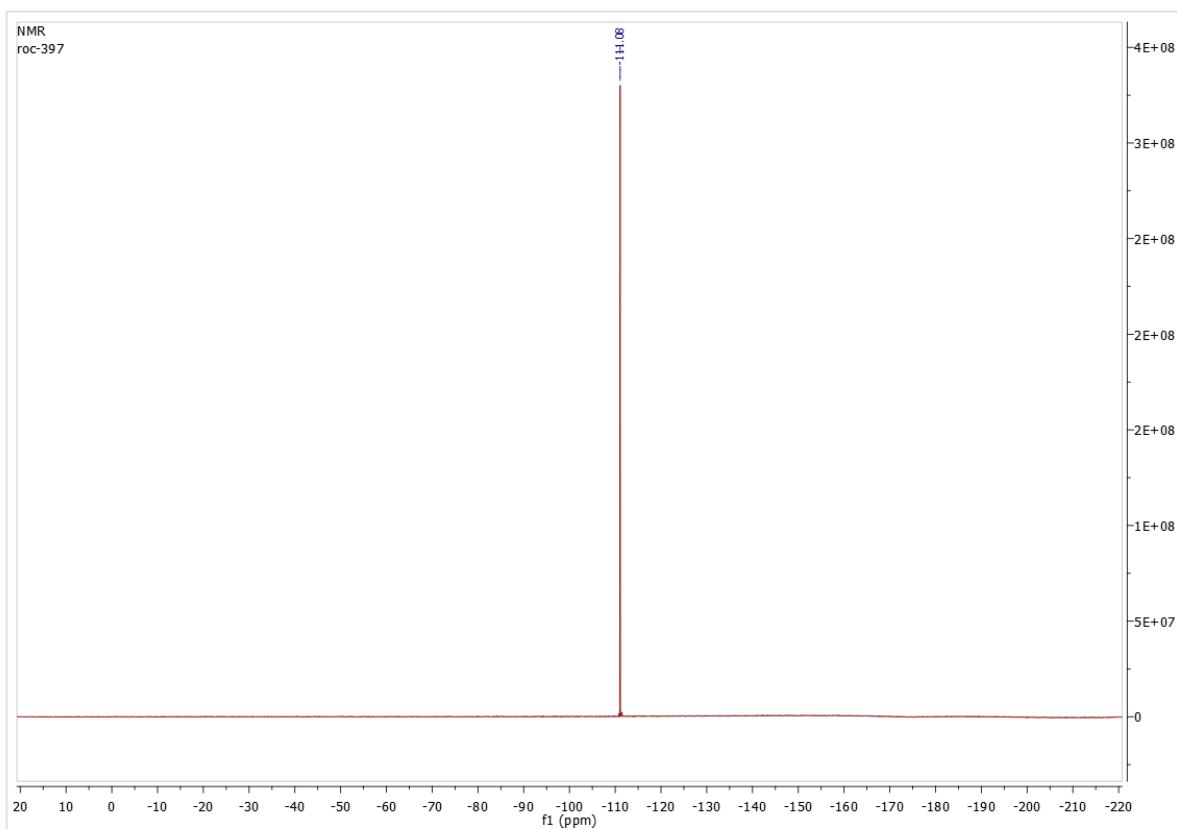
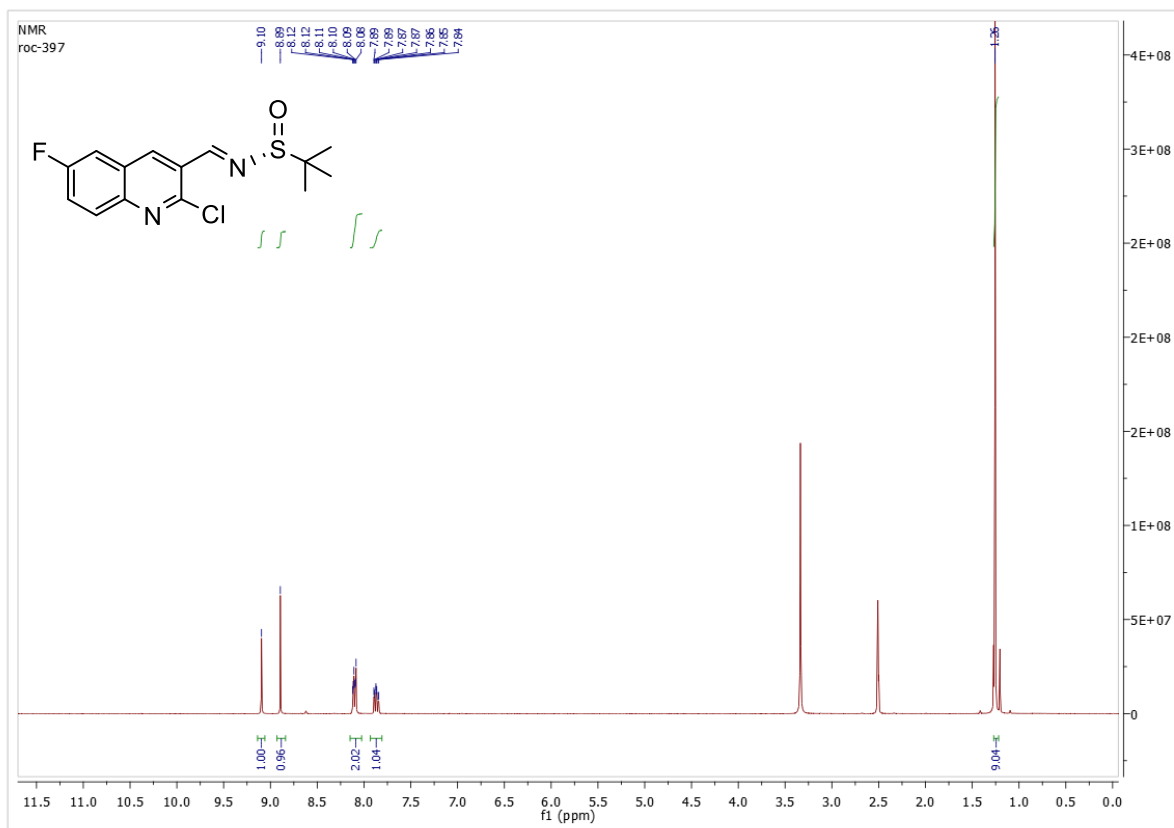
¹H and ¹³C NMR Spectra of (3-(((4-cyano-3-methoxyphenyl)amino)methyl)-2-oxo-6-(4,4,5,5-tetramethyl-1,3,2-dioxaborolan-2-yl)quinolin-1(2H)-yl)methyl pivalate **39**

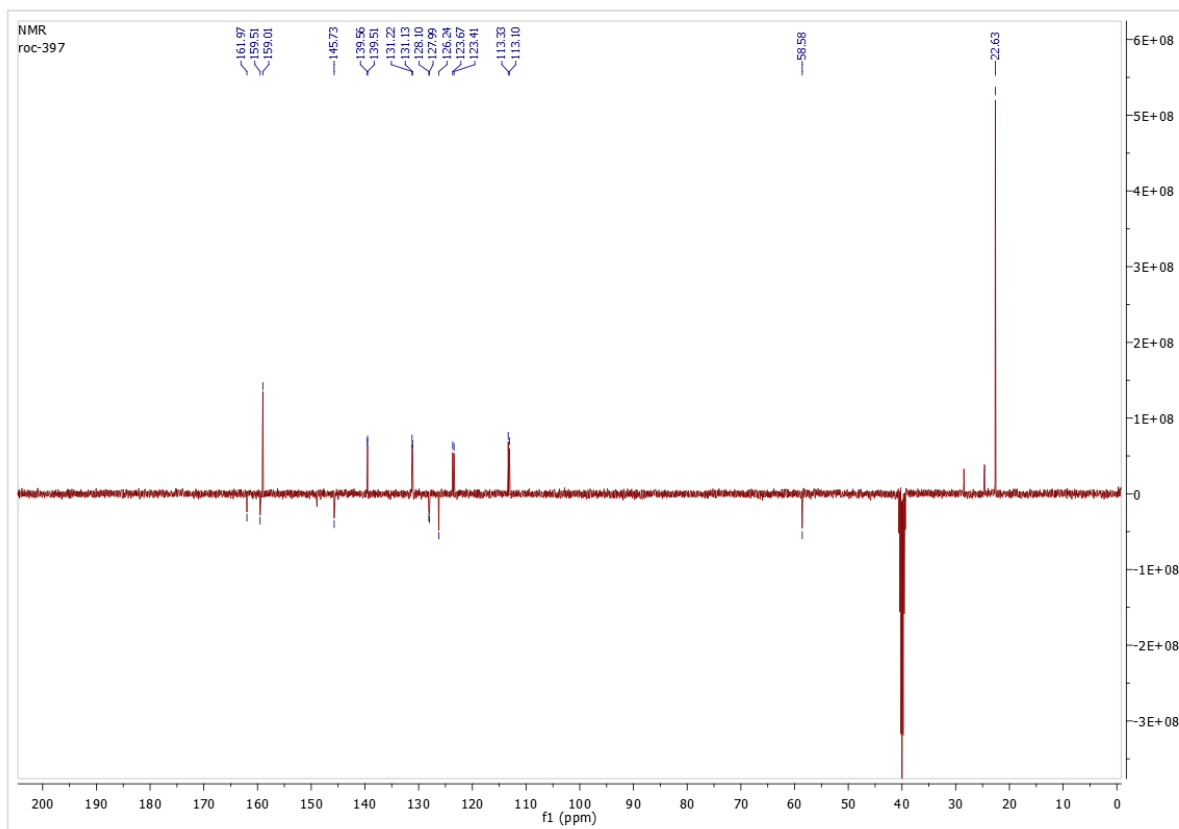


¹H and ¹³C NMR Spectra of ((3-(((4-cyano-3-methoxyphenyl)amino)methyl)-6-(4,4,5,5-tetramethyl-1,3,2-dioxaborolan-2-yl)quinolin-2-yl)oxy)methyl pivalate **40**

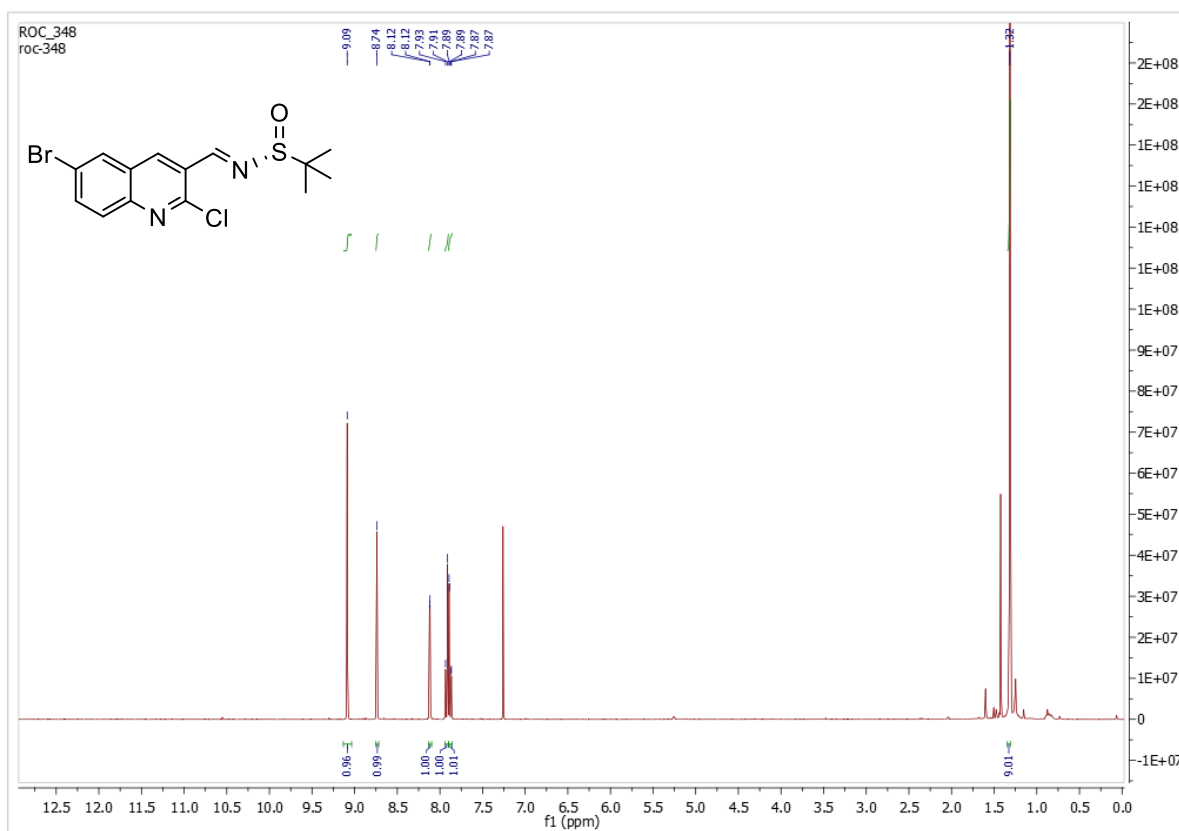


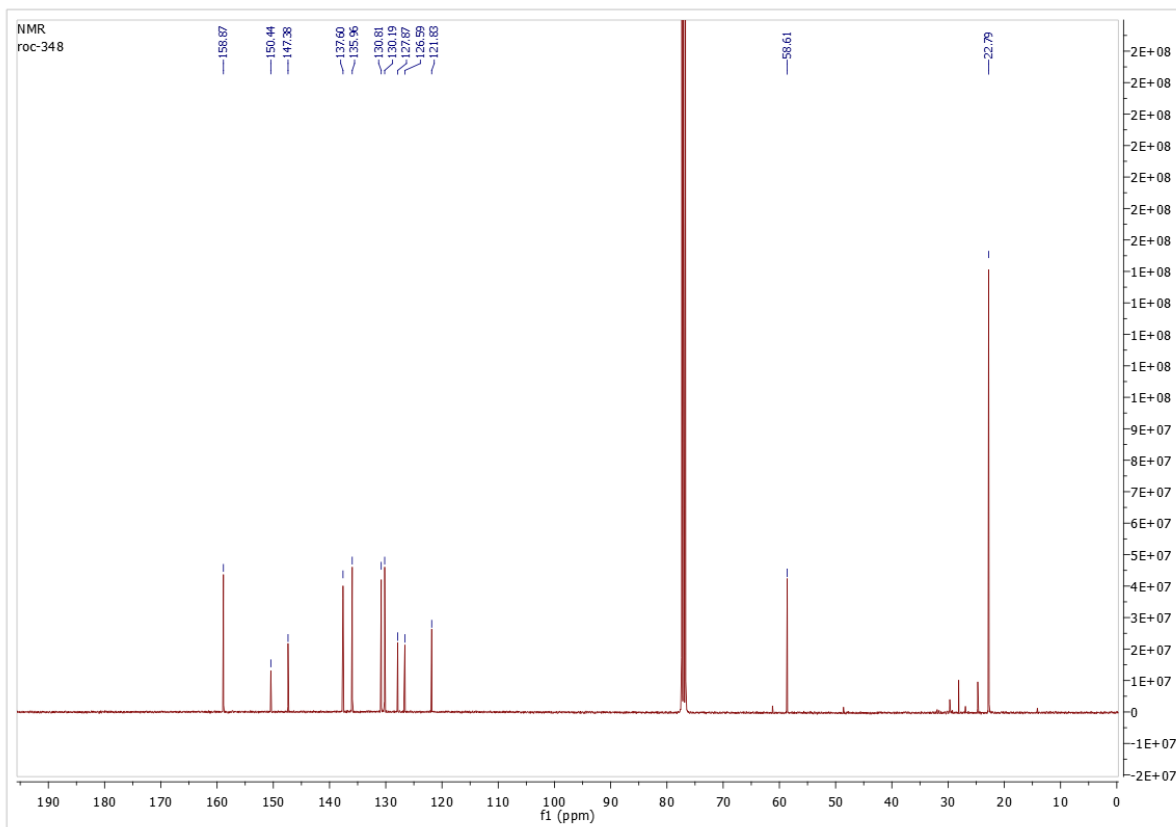
^1H , ^{19}F and ^{13}C NMR Spectra of (*R*)-*N*-((6-Fluoro-2-chloroquinolin-3-yl)methylene)-2-methylpropane-2-sulfinamide **41d**



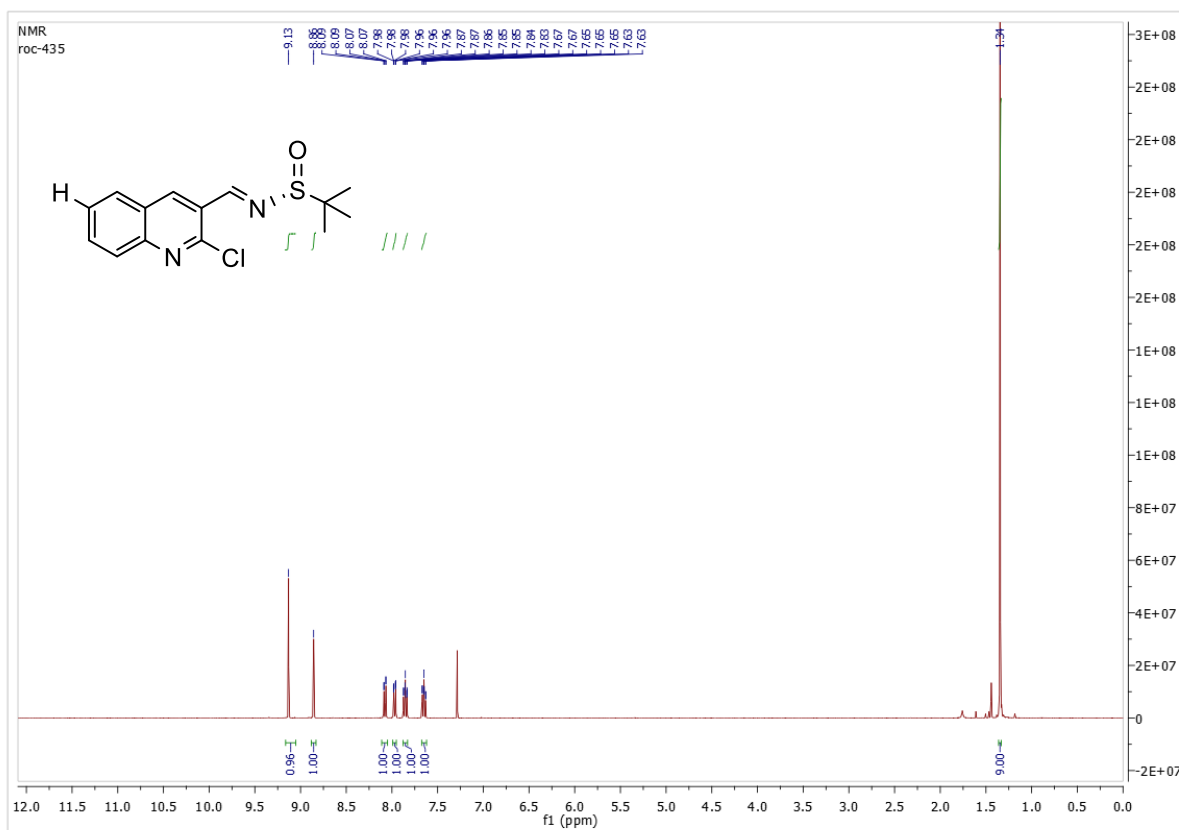


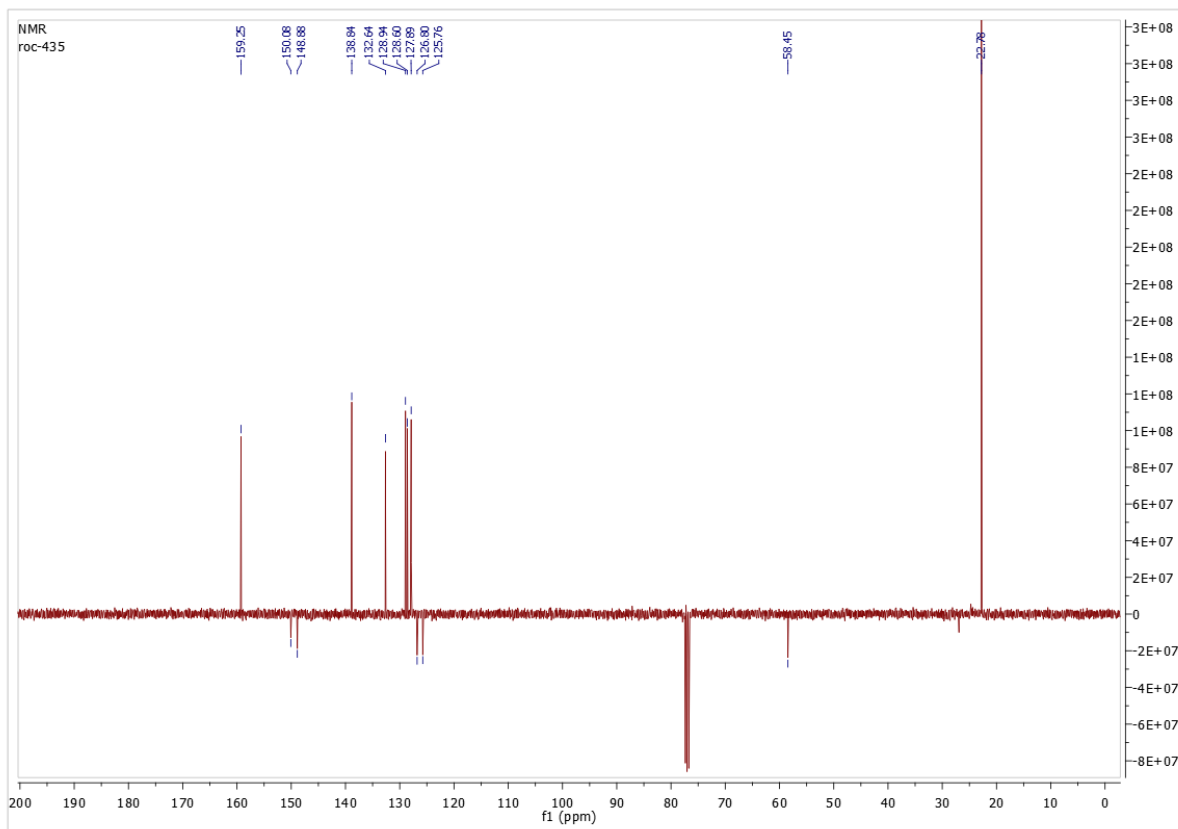
^1H and ^{13}C NMR Spectra of (*R*)-*N*-((6-Bromo-2-chloroquinolin-3-yl)methylene)-2-methylpropane-2-sulfonamide **41e**



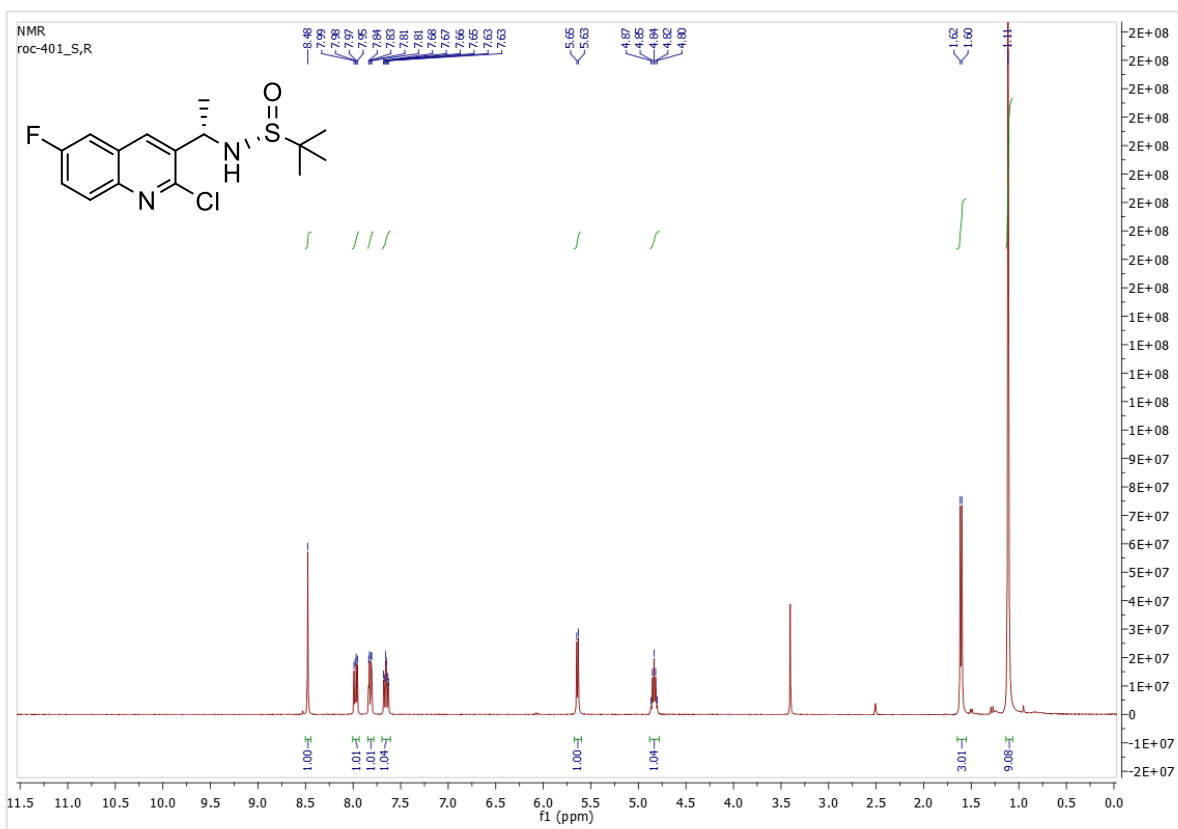


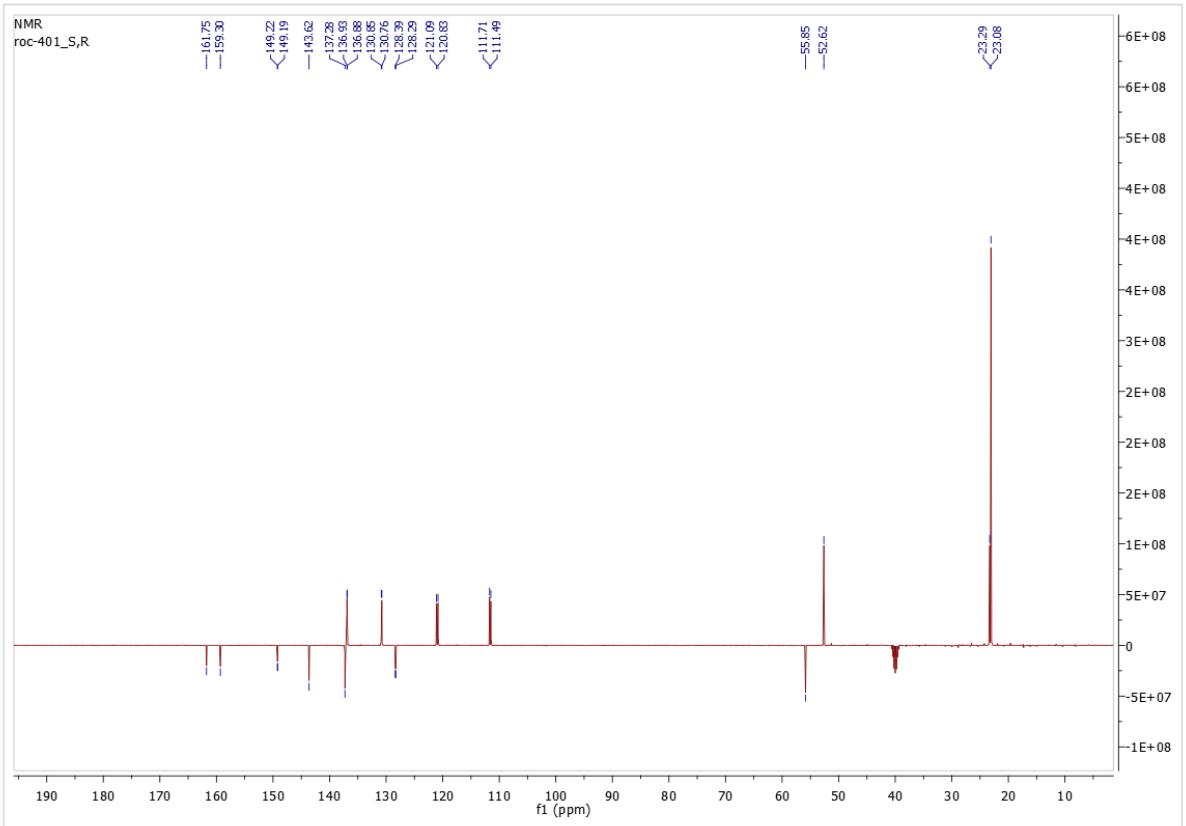
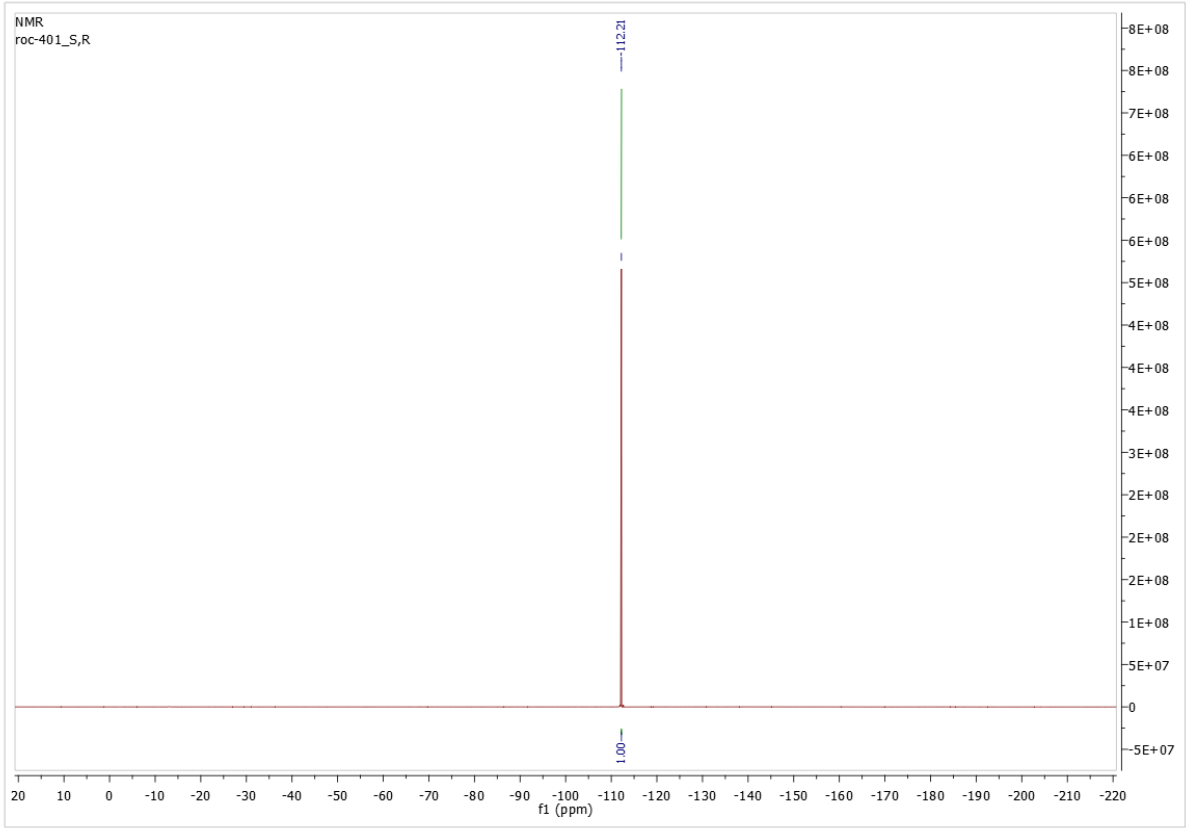
^1H and ^{13}C NMR Spectra of (R,S)-N-((2-Chloroquinolin-3-yl)methylene)-2-methylpropane-2-sulfonamide **41f**



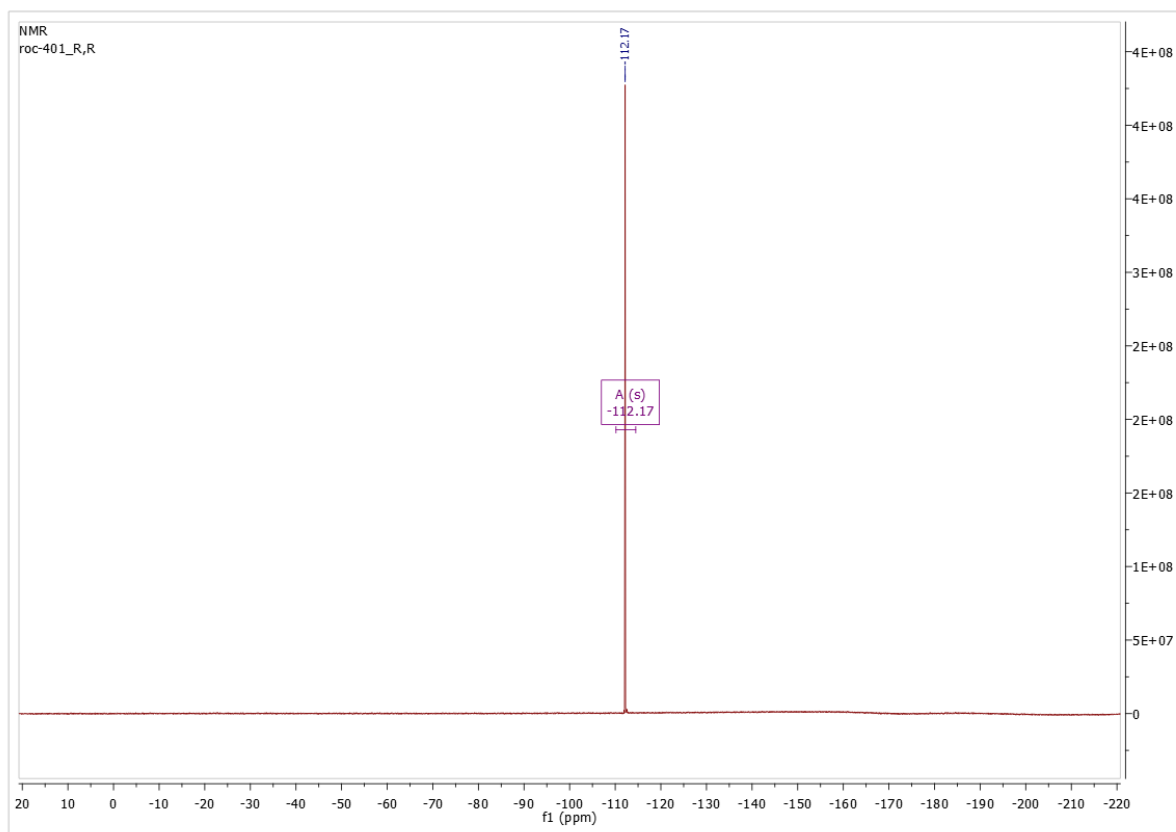
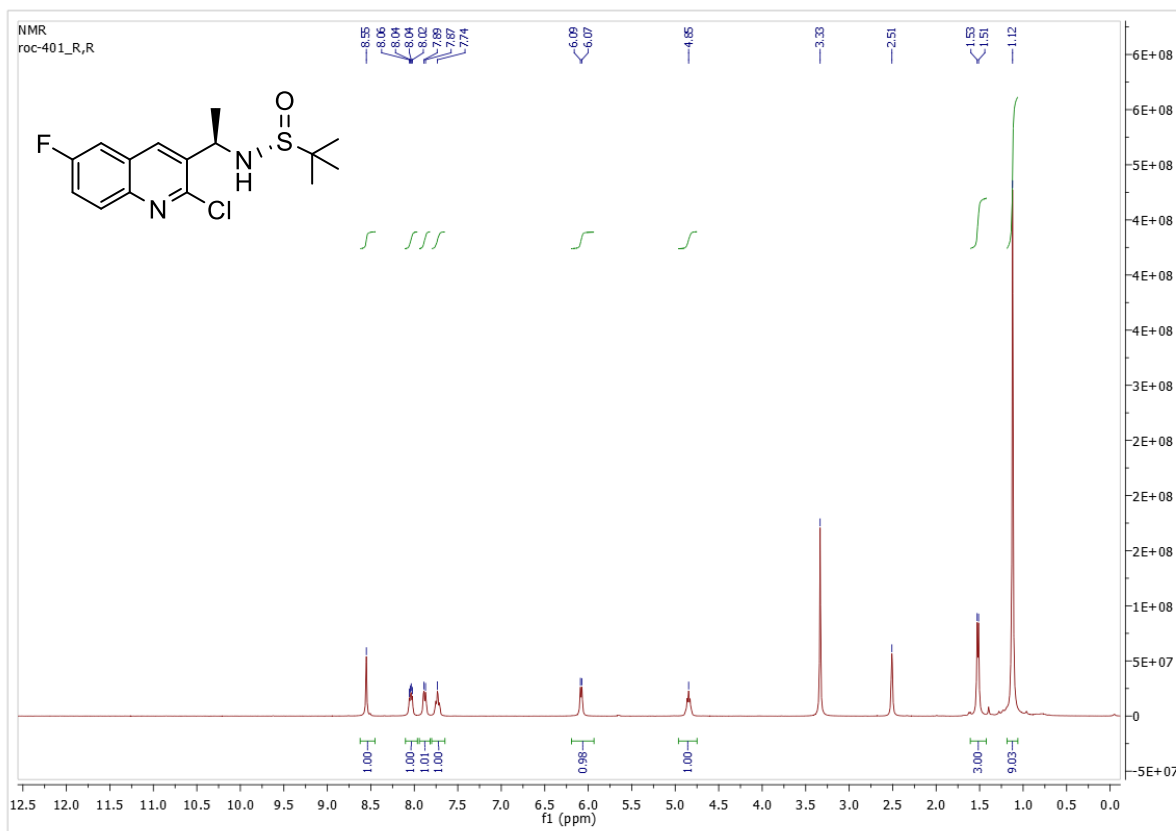


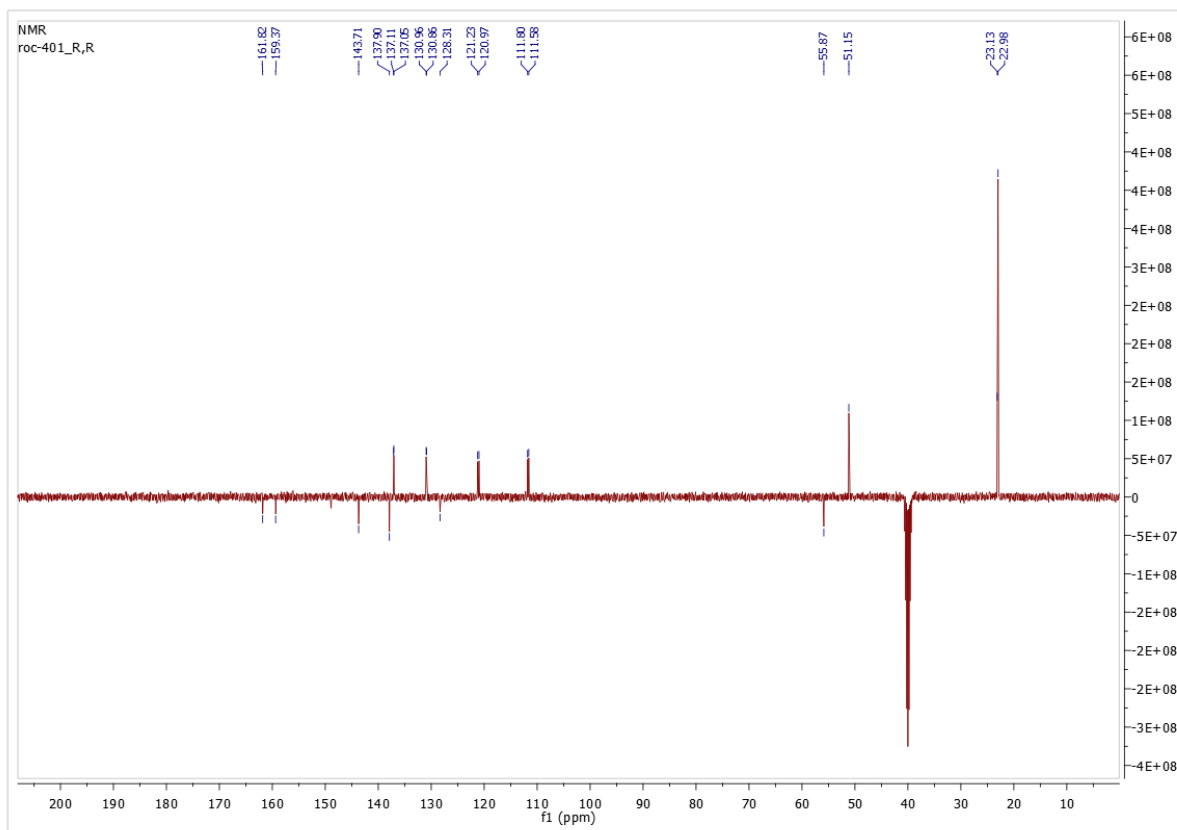
^1H , ^{19}F and ^{13}C NMR Spectra of (*R*)-*N*-((*S*)-1-(6-Fluoro-2-chloroquinoline-3-yl)ethyl)-2-methylpropane-2-sulfinamide **42d**



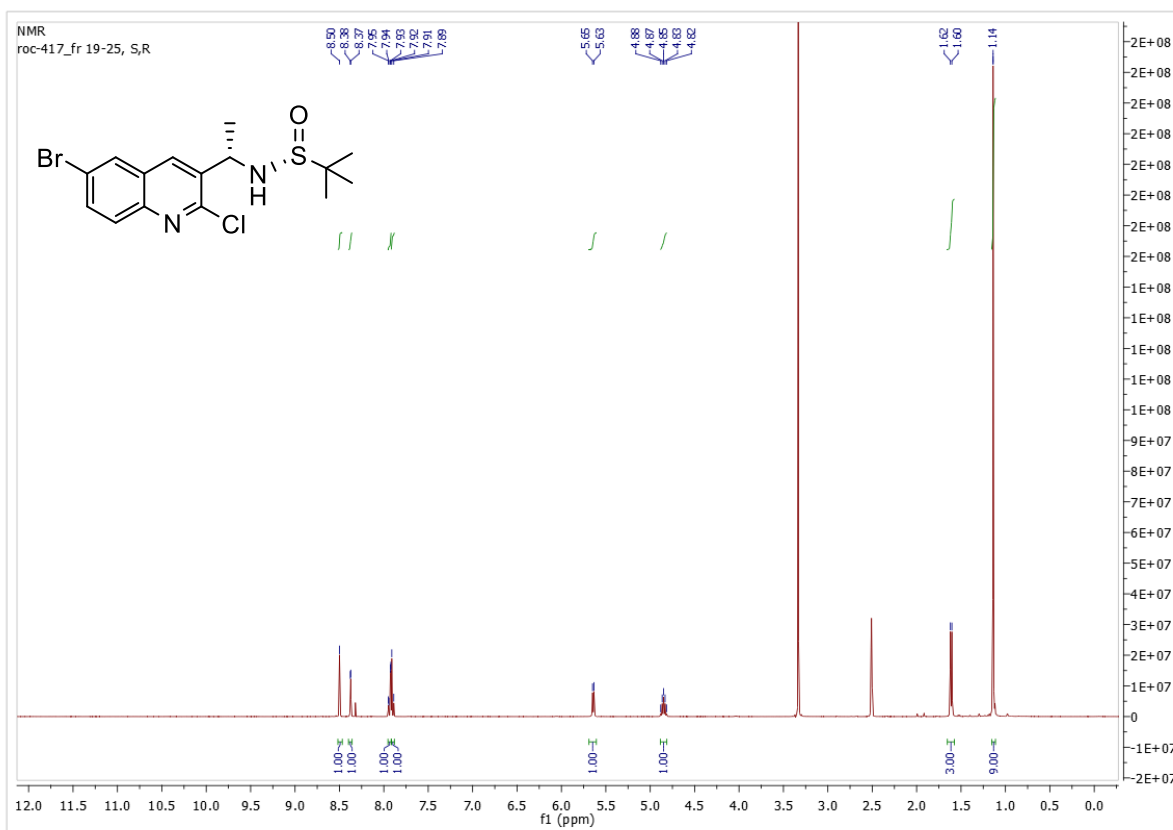


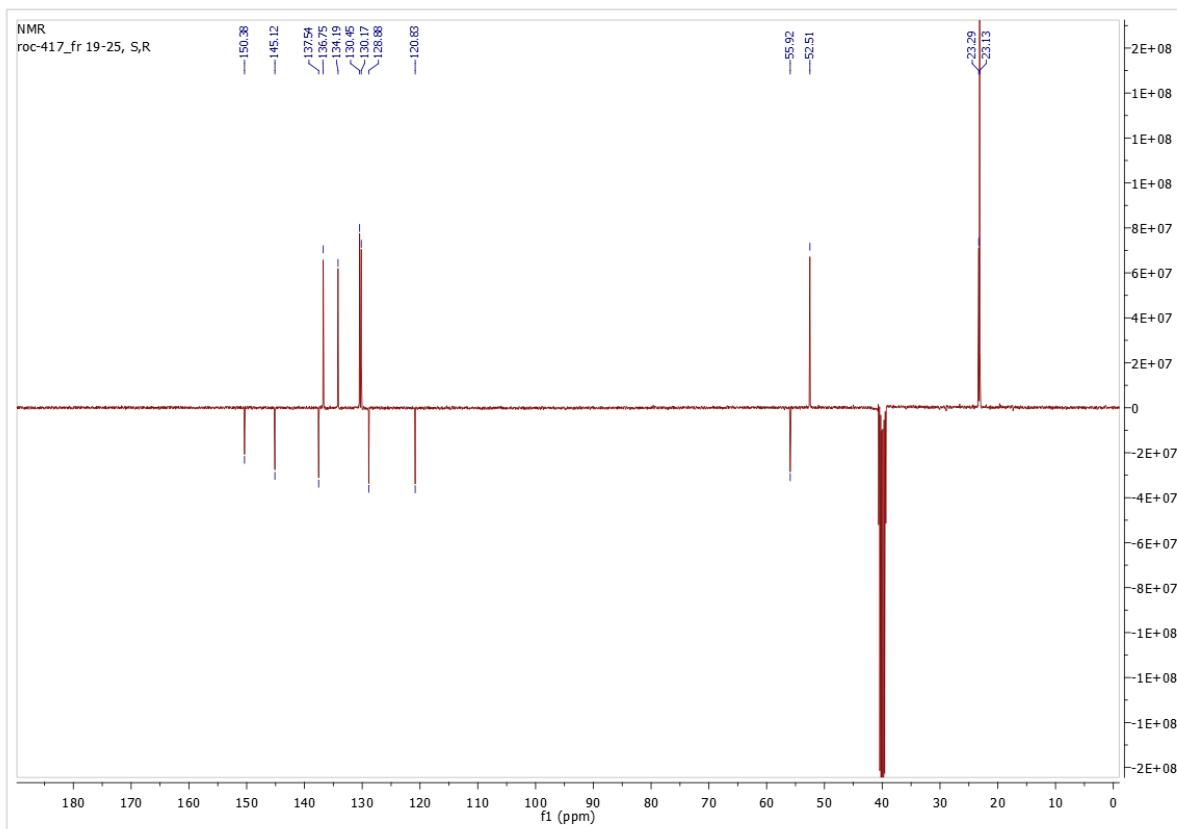
^1H , ^{19}F and ^{13}C NMR Spectra of (*R*)-*N*-((*R*)-1-(6-Fluoro-2-chloroquinoline-3-yl)ethyl)-2-methylpropane-2-sulfonamide **43d**



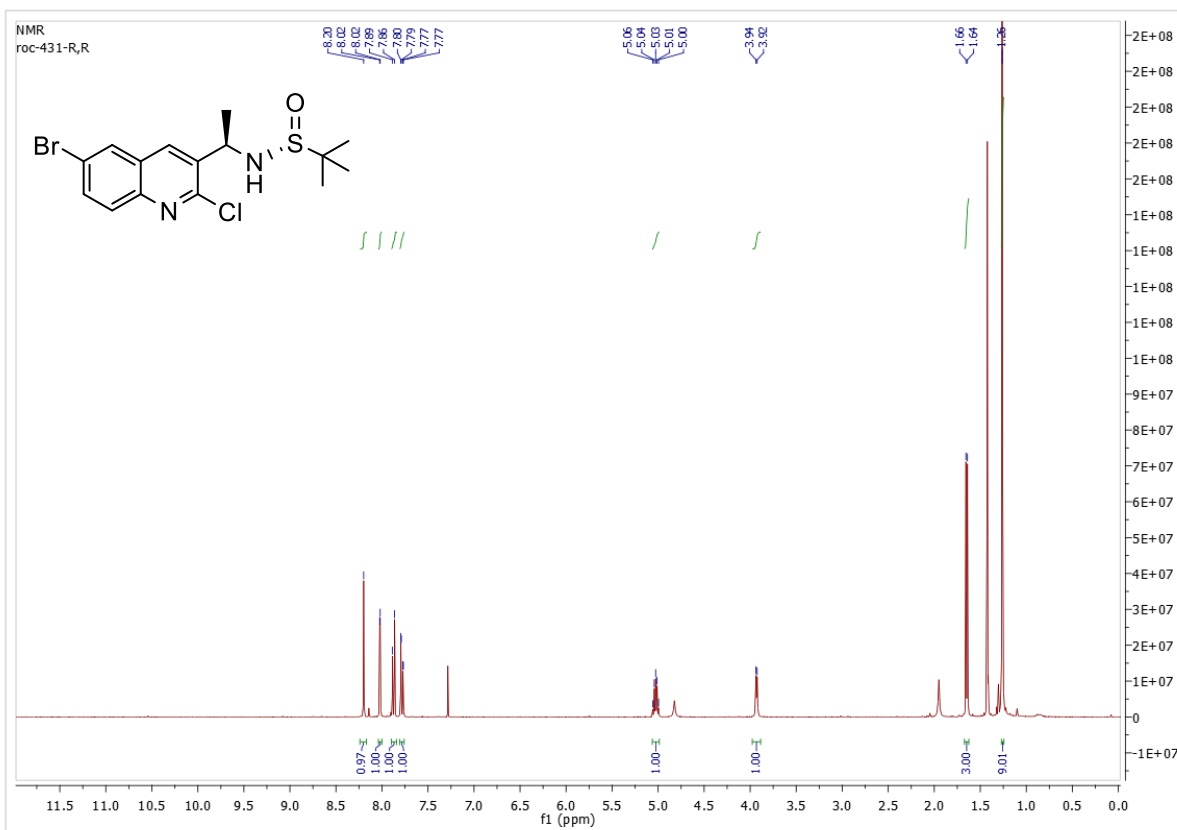


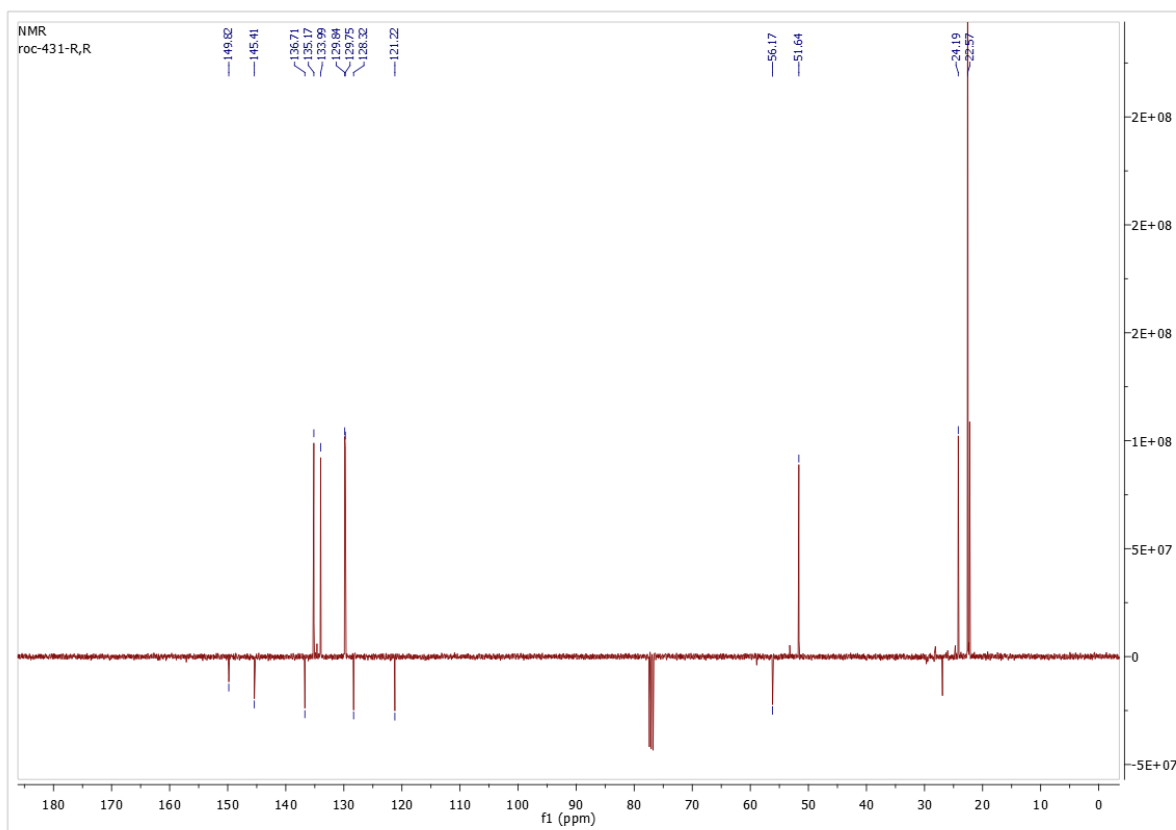
^1H and ^{13}C NMR spectra of (*R*)-*N*-((*S*)-1-(6-Bromo-2-chloroquinolin-3-yl)ethyl)-2-methylpropane-2-sulfonamides **42e**



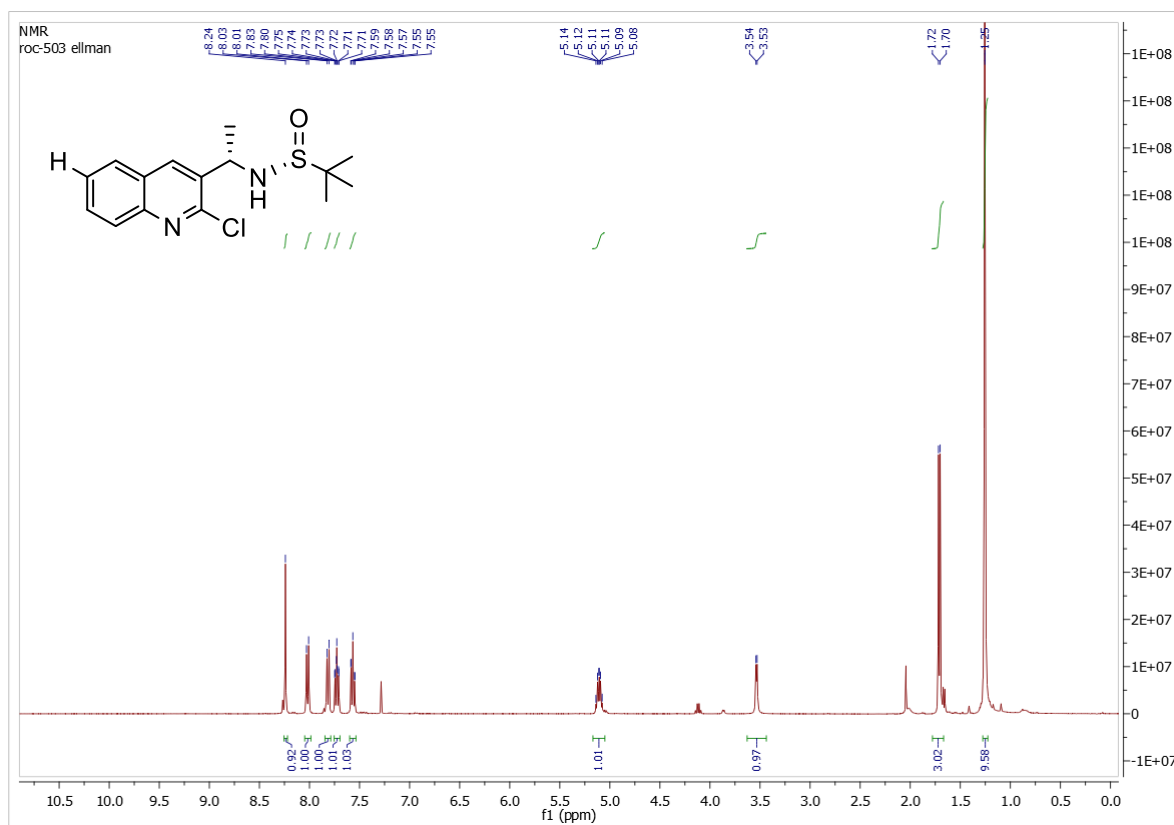


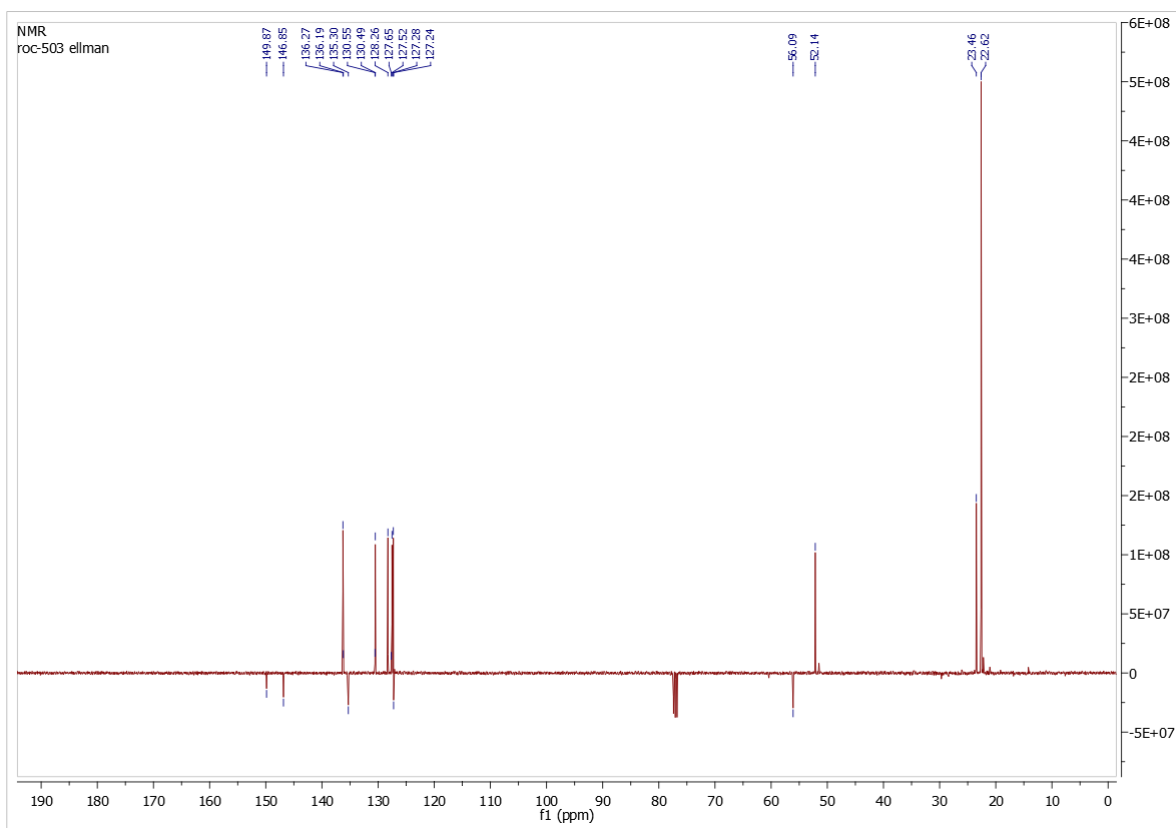
^1H and ^{13}C NMR spectra of (*R*)-*N*-((*R*)-1-(6-bromo-2-chloroquinolin-3-yl)ethyl)-2-methylpropane-2-sulfonamides **43e**



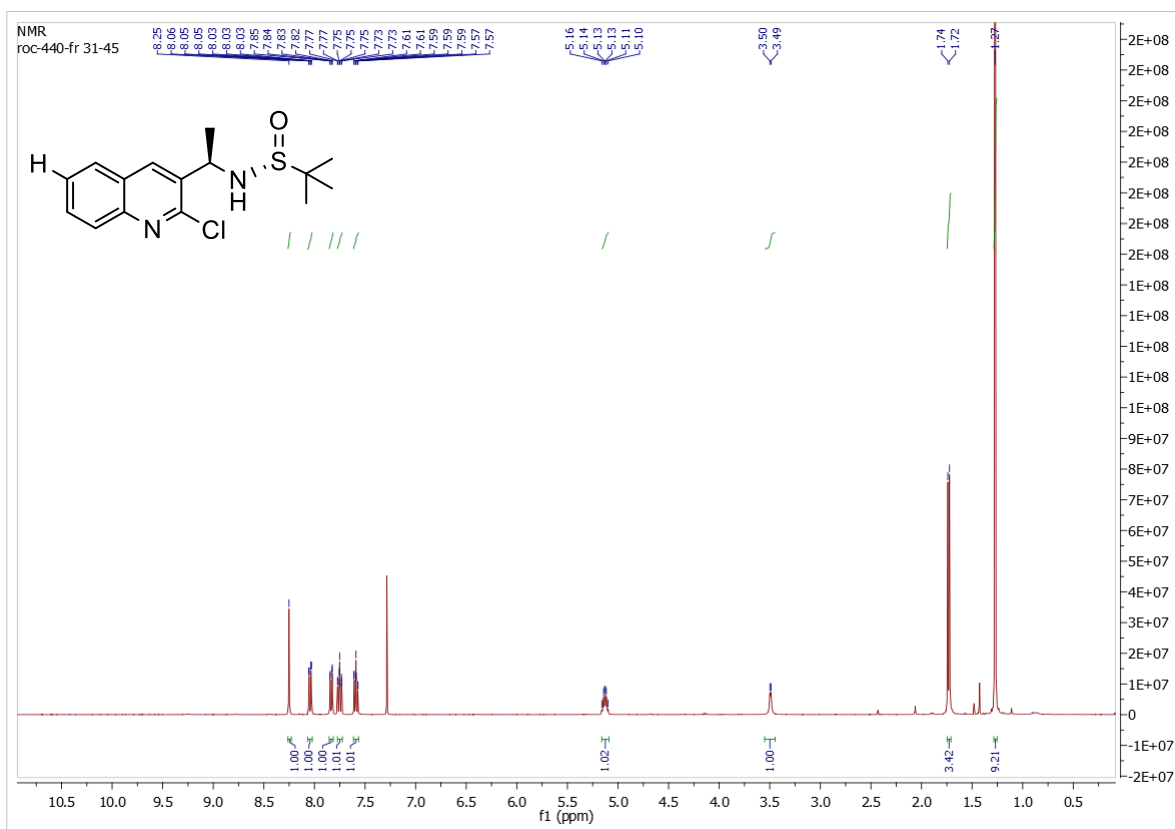


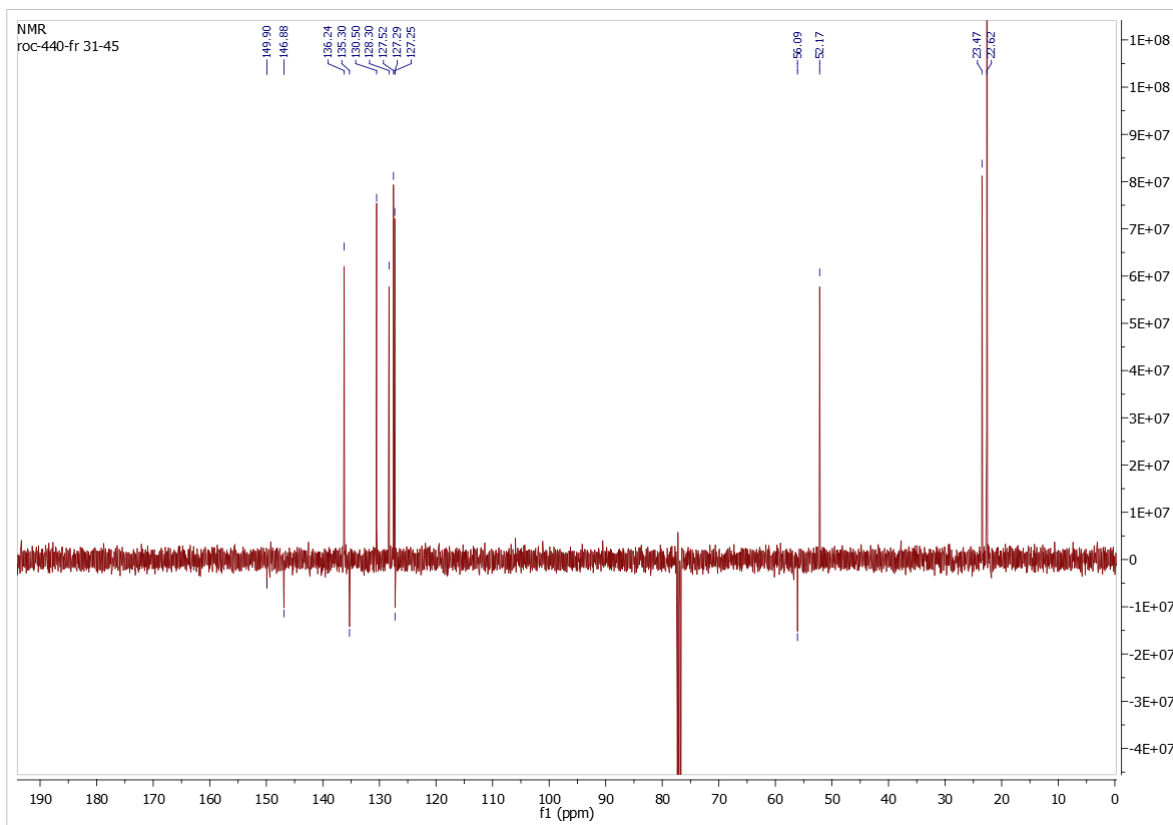
^1H and ^{13}C NMR spectra of (*R*)-*N*-((*S*)-1-(2-chloroquinoline-3-yl)ethyl)-2-methylpropane-2-sulfonamide **42f**



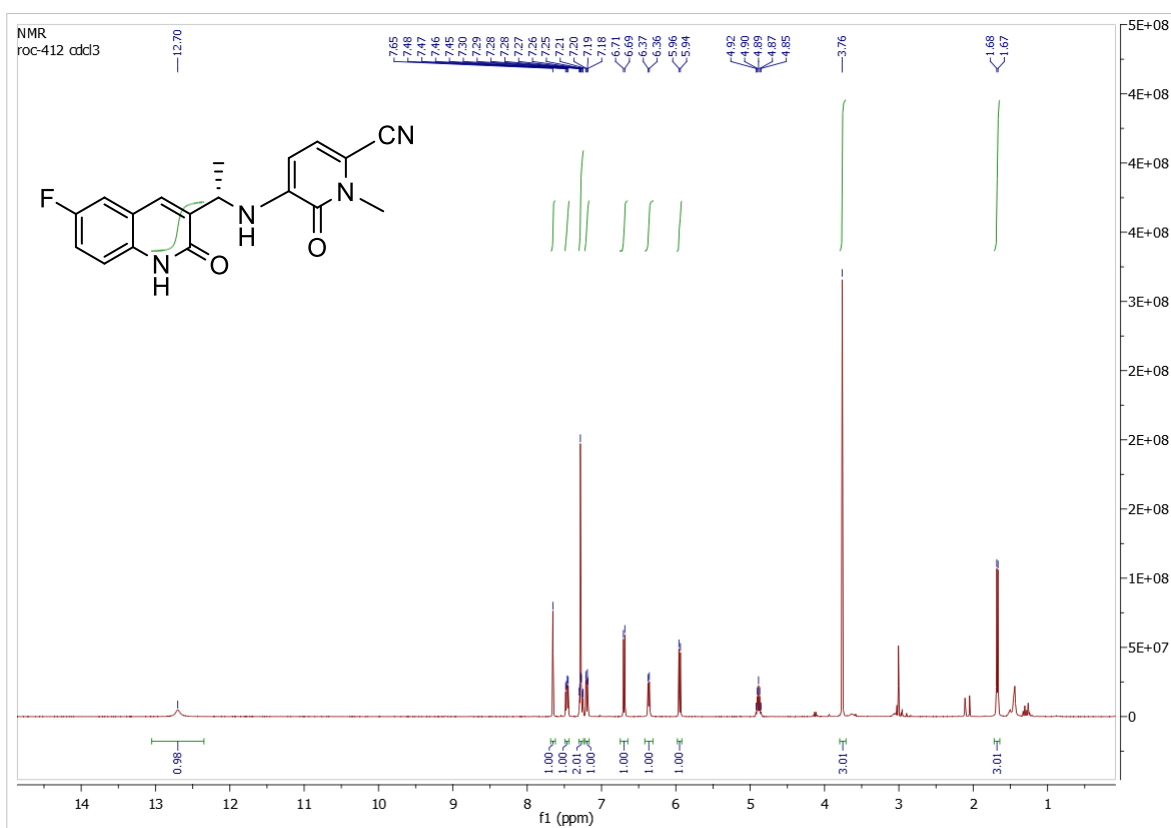


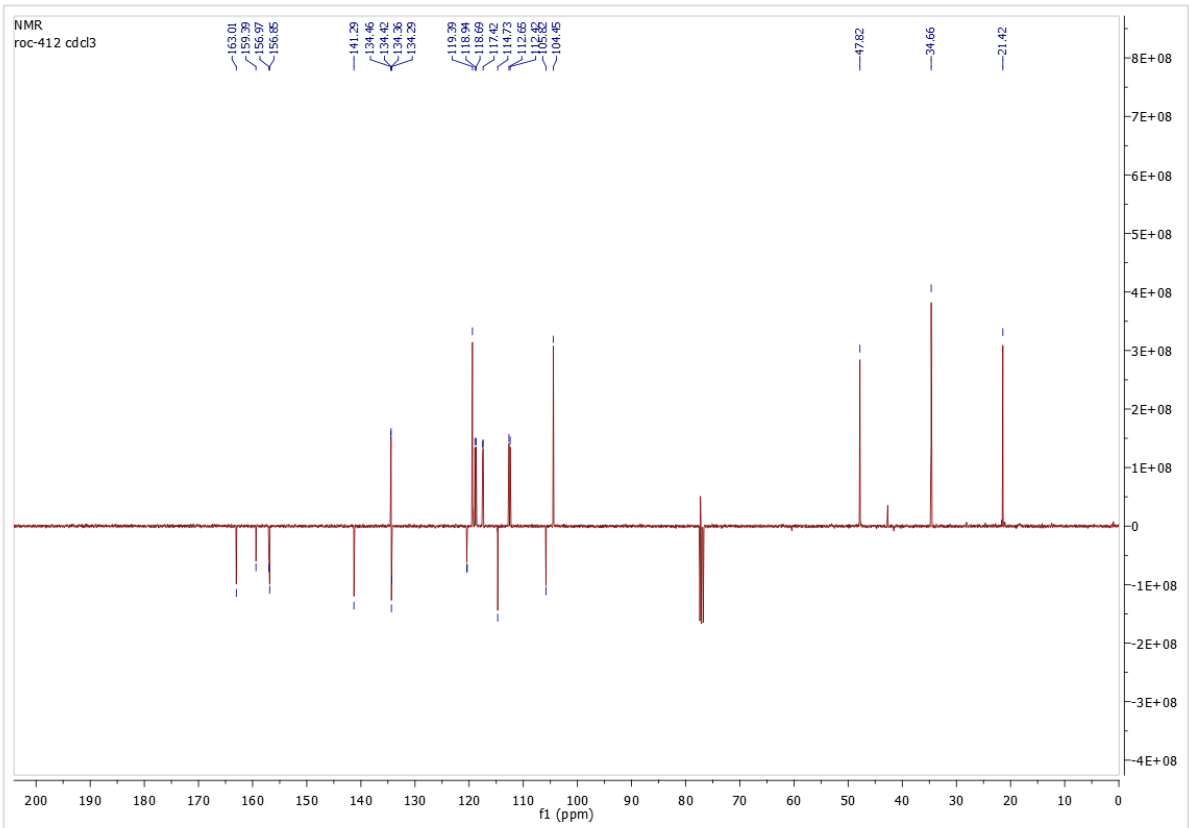
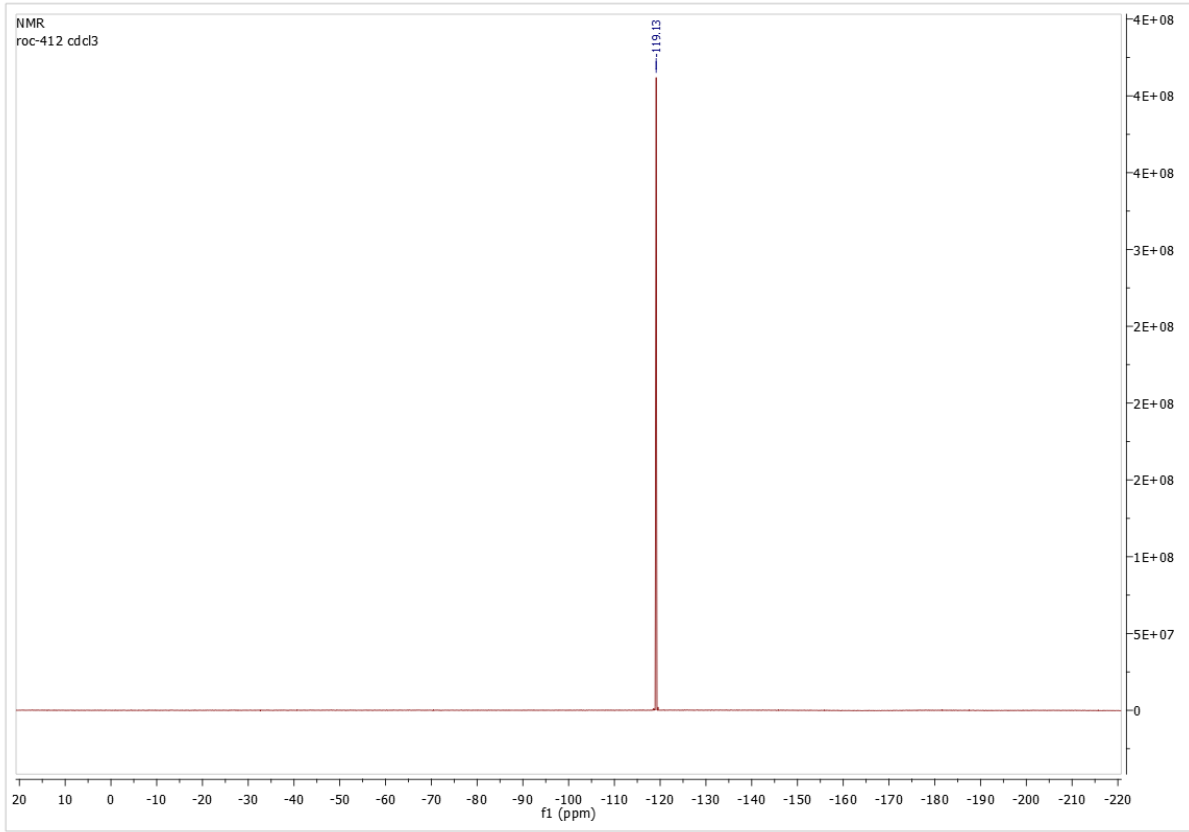
^1H and ^{13}C NMR spectra of (*R*)-*N*-((*R*)-1-(2-Chloroquinoline-3-yl)ethyl)-2-methylpropane-2-sulfonamide **43f**



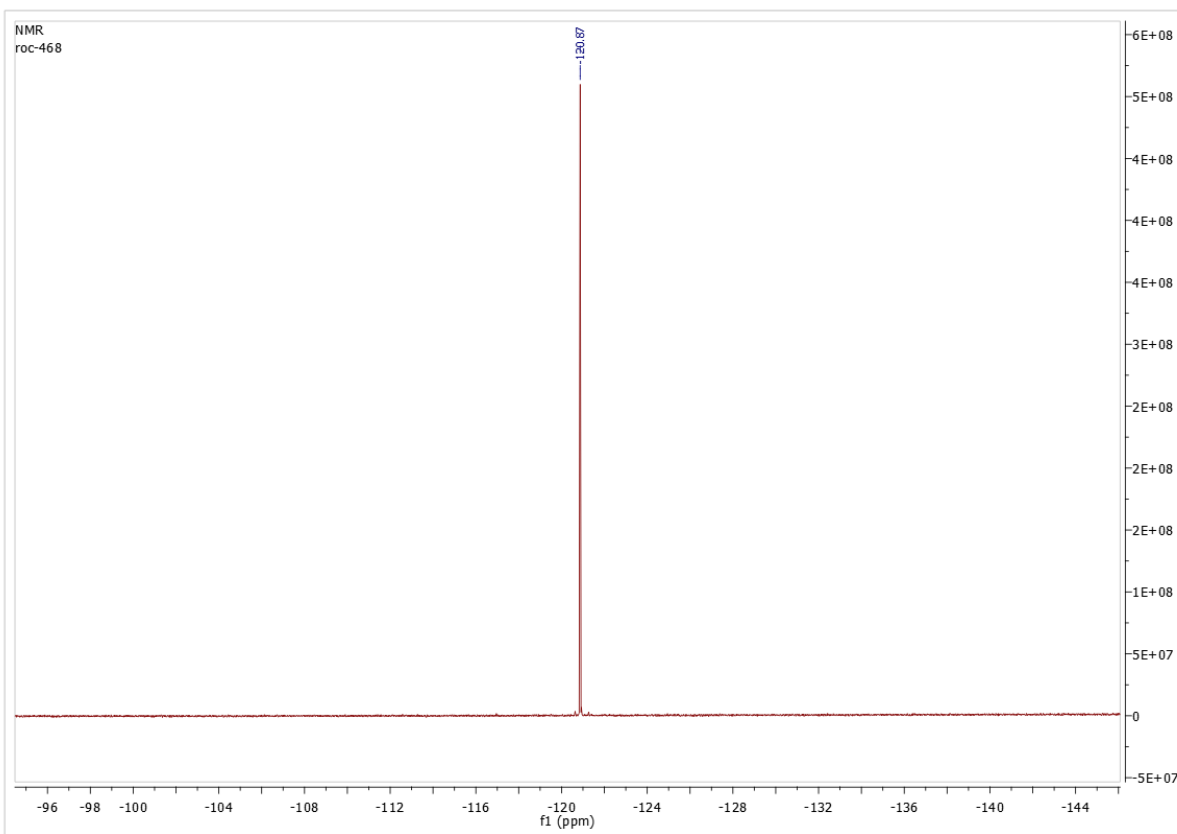
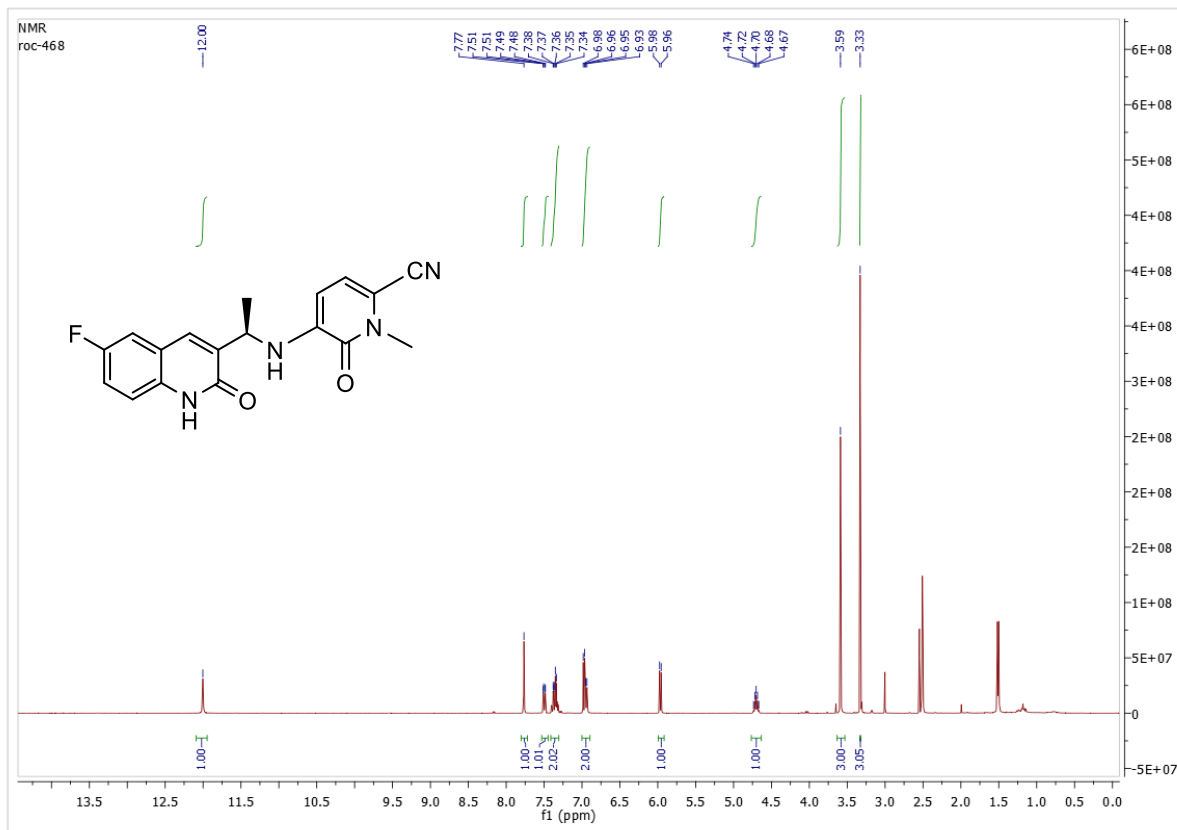


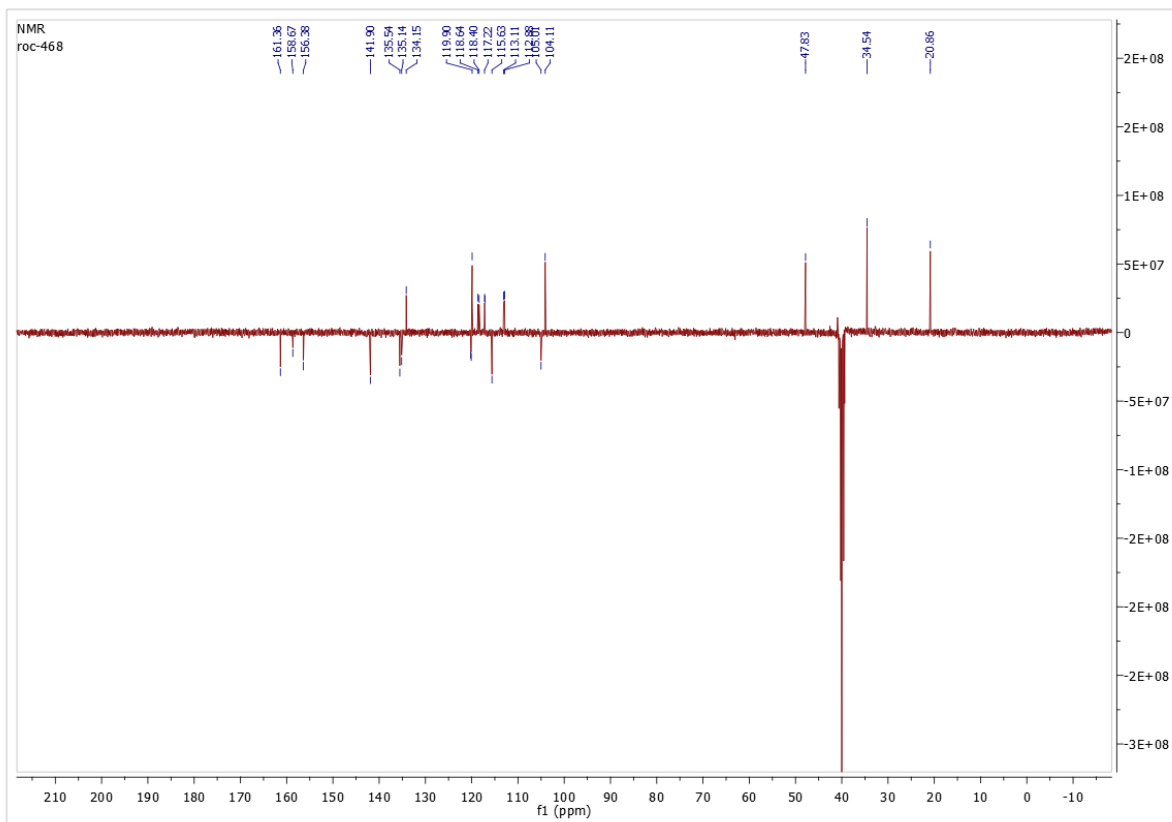
^1H , ^{19}F and ^{13}C NMR Spectra of (*S*)-5-((1-(6-Fluoro-2-oxo-1,2-dihydroquinolin-3-yl)ethyl)amino)-1-methyl-6-oxo-1,6-dihydropyridine-2-carbonitriles (**S**)-46d



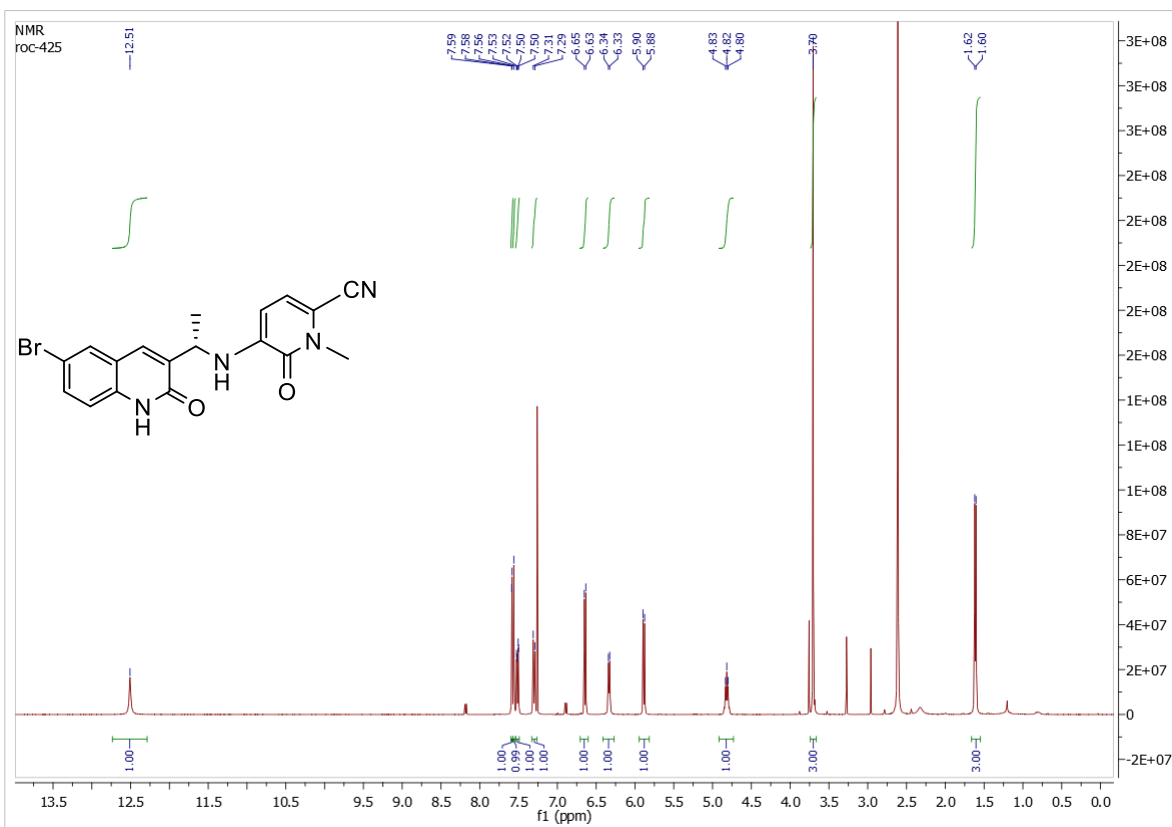


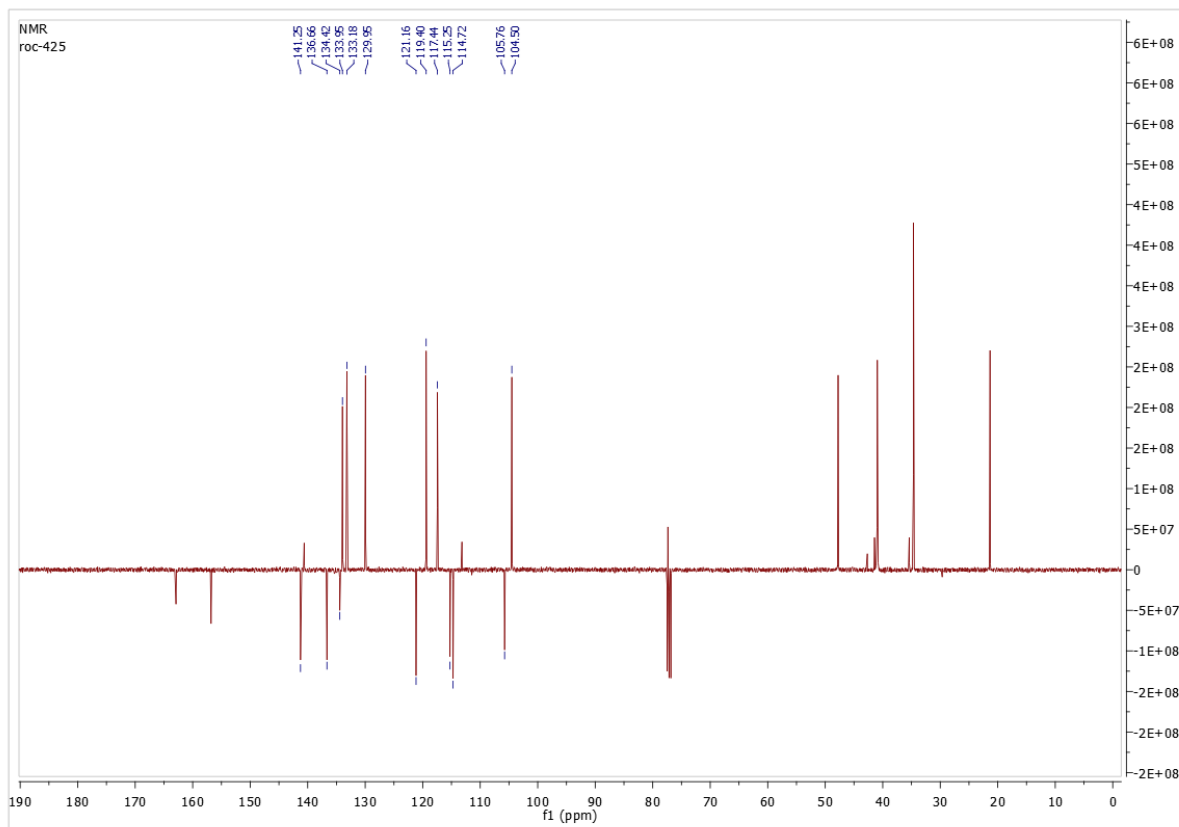
^1H , ^{19}F and ^{13}C NMR Spectra of (*R*)-5-((1-(6-Fluoro-2-oxo-1,2-dihydroquinolin-3-yl)ethyl)amino)-1-methyl-6-oxo-1,6-dihydropyridine-2-carbonitriles (**R**)-46d



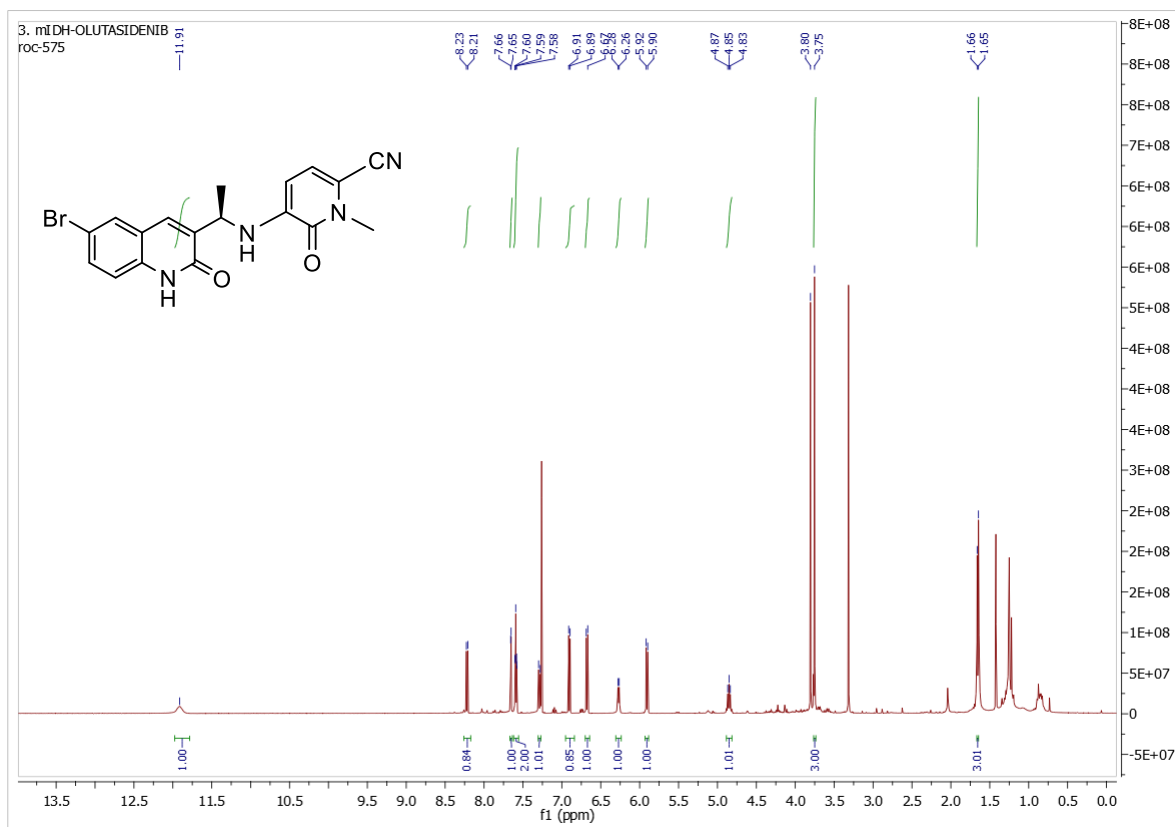


^1H and ^{13}C NMR spectra of (*S*)-5-((1-(6-Bromo-2-oxo-1,2-dihydroquinoline-3-yl)ethyl)amino)-1-methyl-6-oxo-1,6-dihydropyridine-2-carbonitriles (**S**)-46e

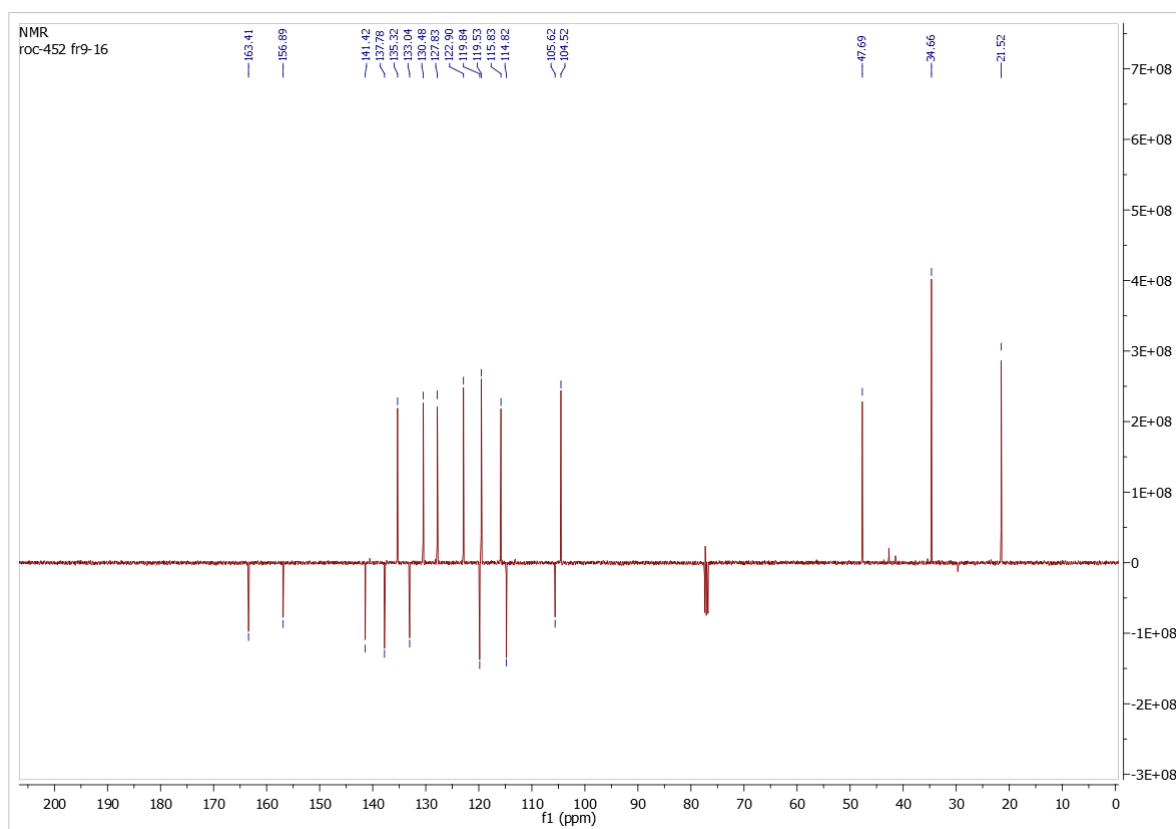
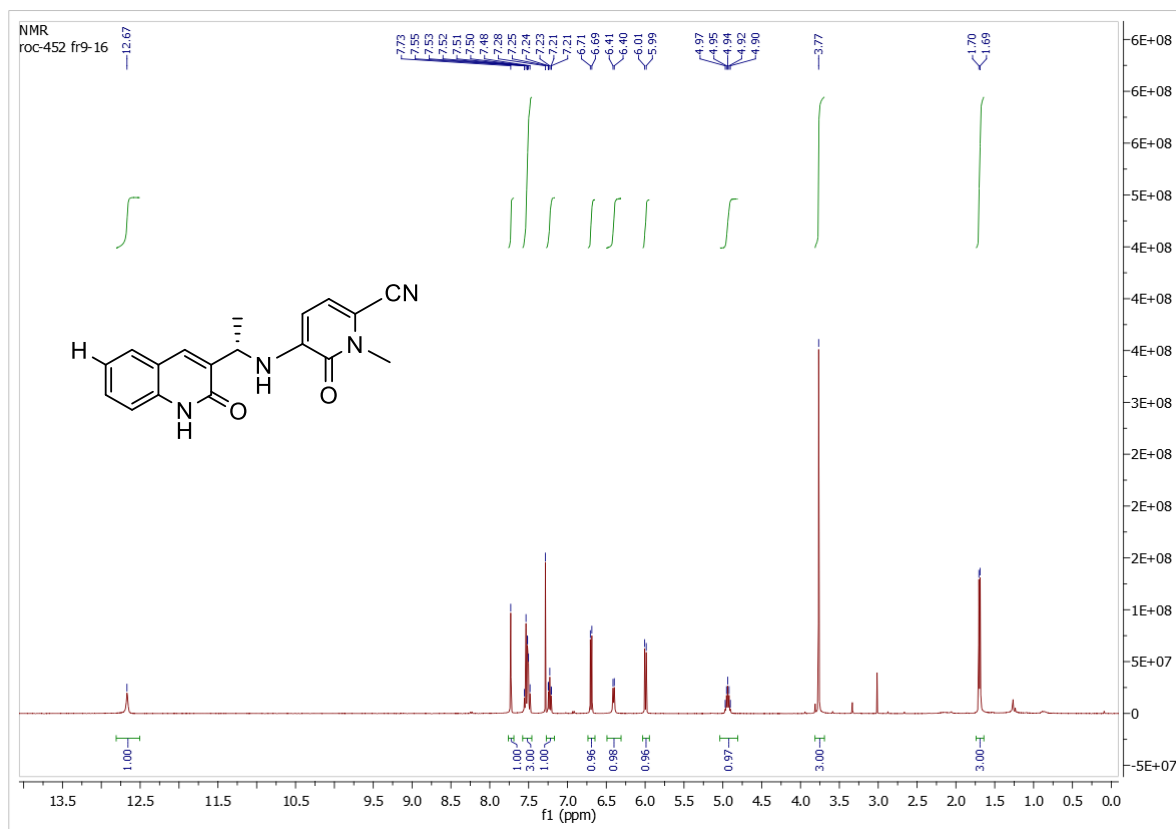




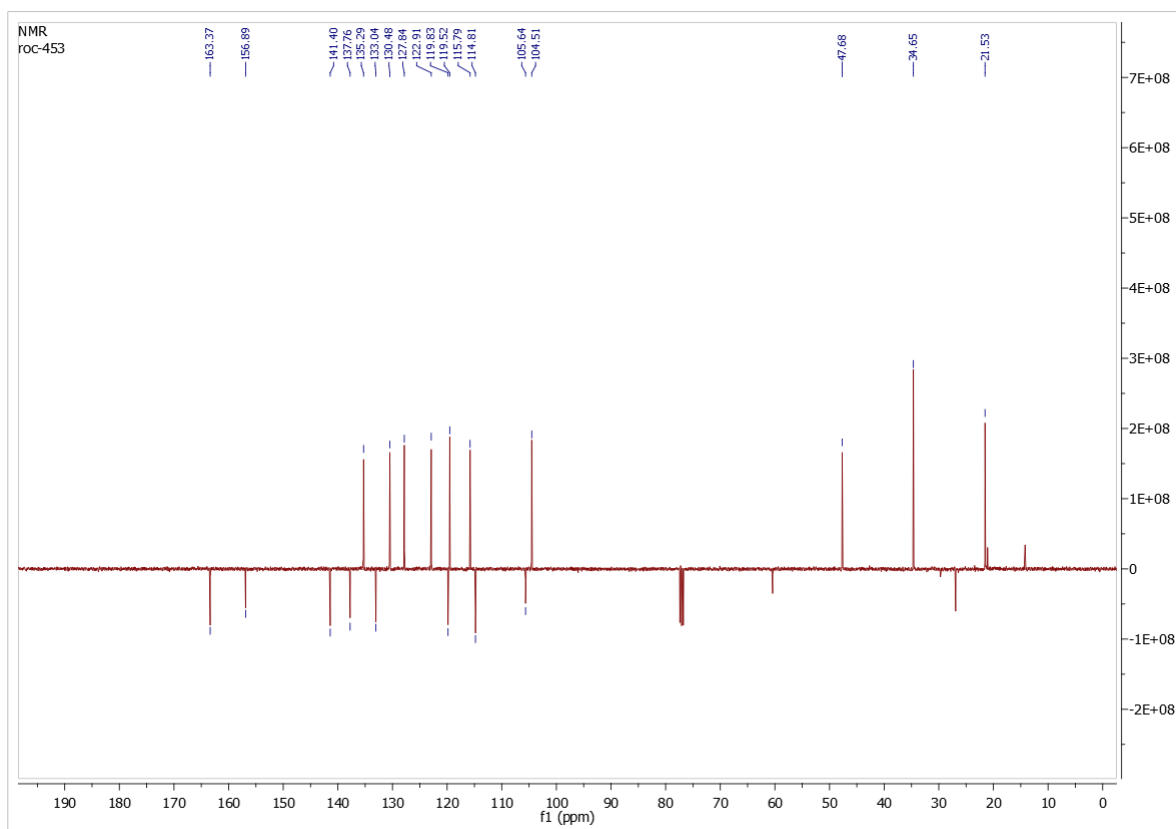
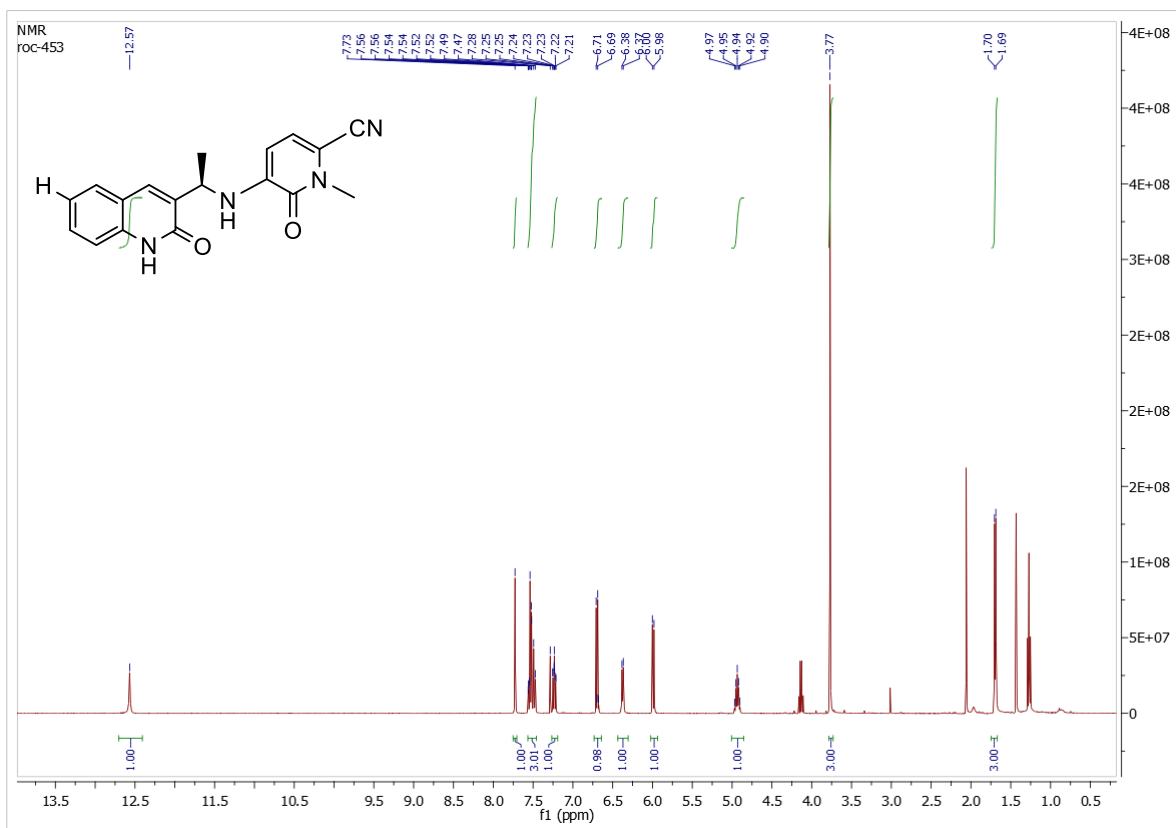
^1H NMR spectra of (*R*)-5-((1-(6-Bromo-2-oxo-1,2-dihydroquinoline-3-yl)ethyl)amino)-1-methyl-6-oxo-1,6-dihydropyridine-2-carbonitriles (**R**)-46



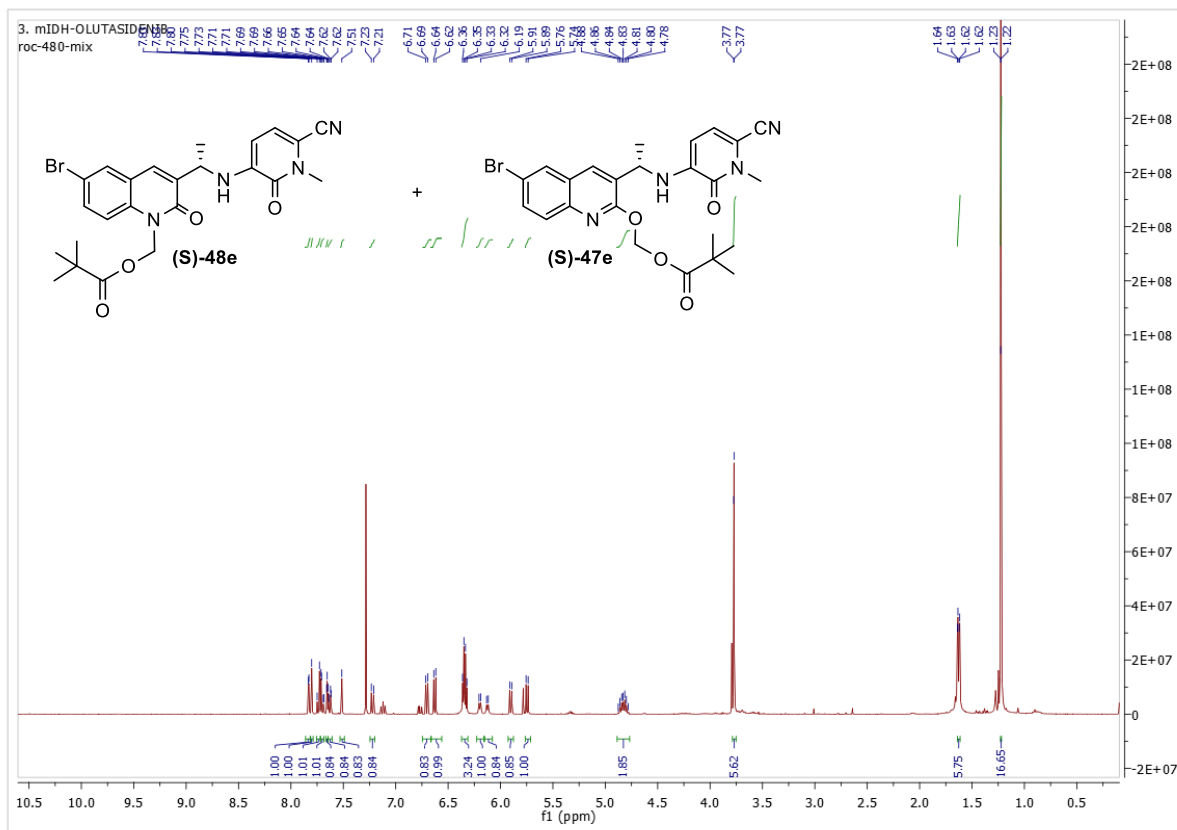
^1H and ^{13}C NMR spectra of (*S*)-5-((1-(2-Oxo-1,2-dihydroquinoline-3-yl)ethyl)amino)-1-methyl-6-oxo-1,6-dihydropyridine-2-carbonitriles (**S**)-46f



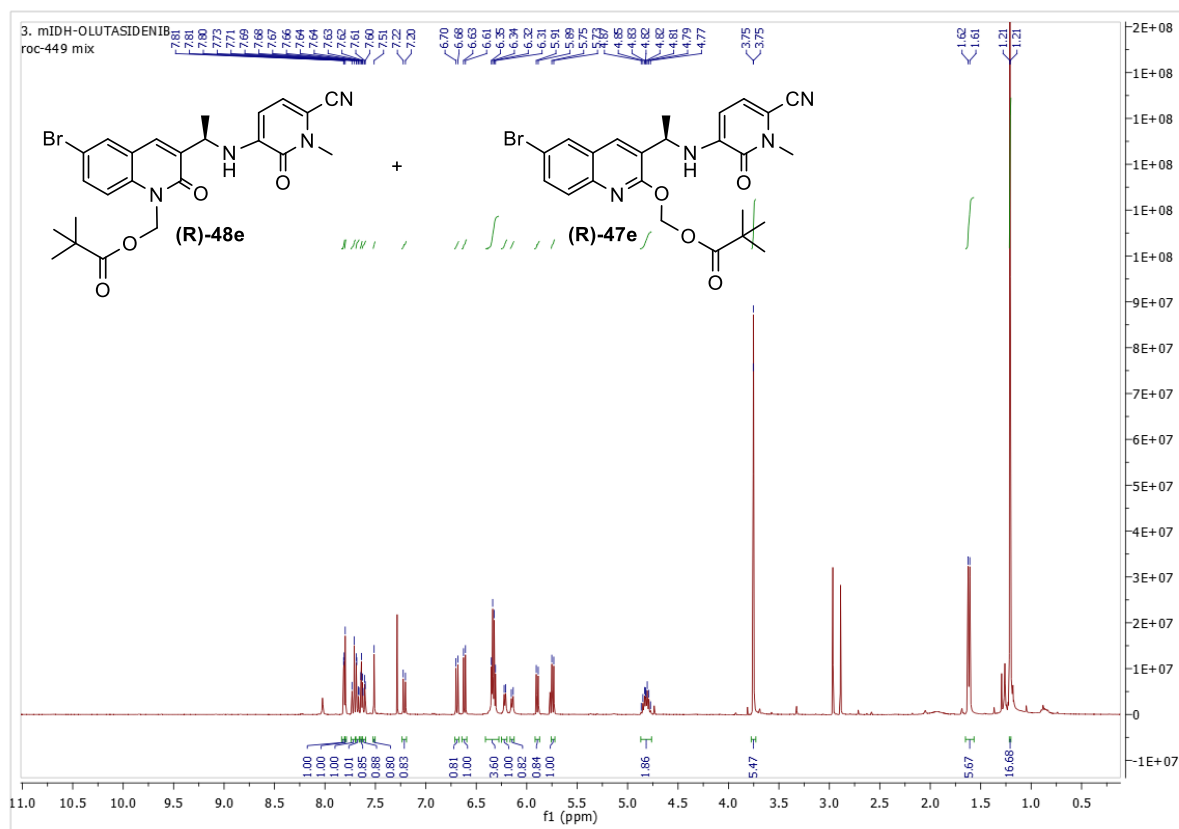
^1H and ^{13}C NMR spectra of (*R*)-5-((1-(2-Oxo-1,2-dihydroquinoline-3-yl)ethyl)amino)-1-methyl-6-oxo-1,6-dihydropyridine-2-carbonitriles (**R**)-46f



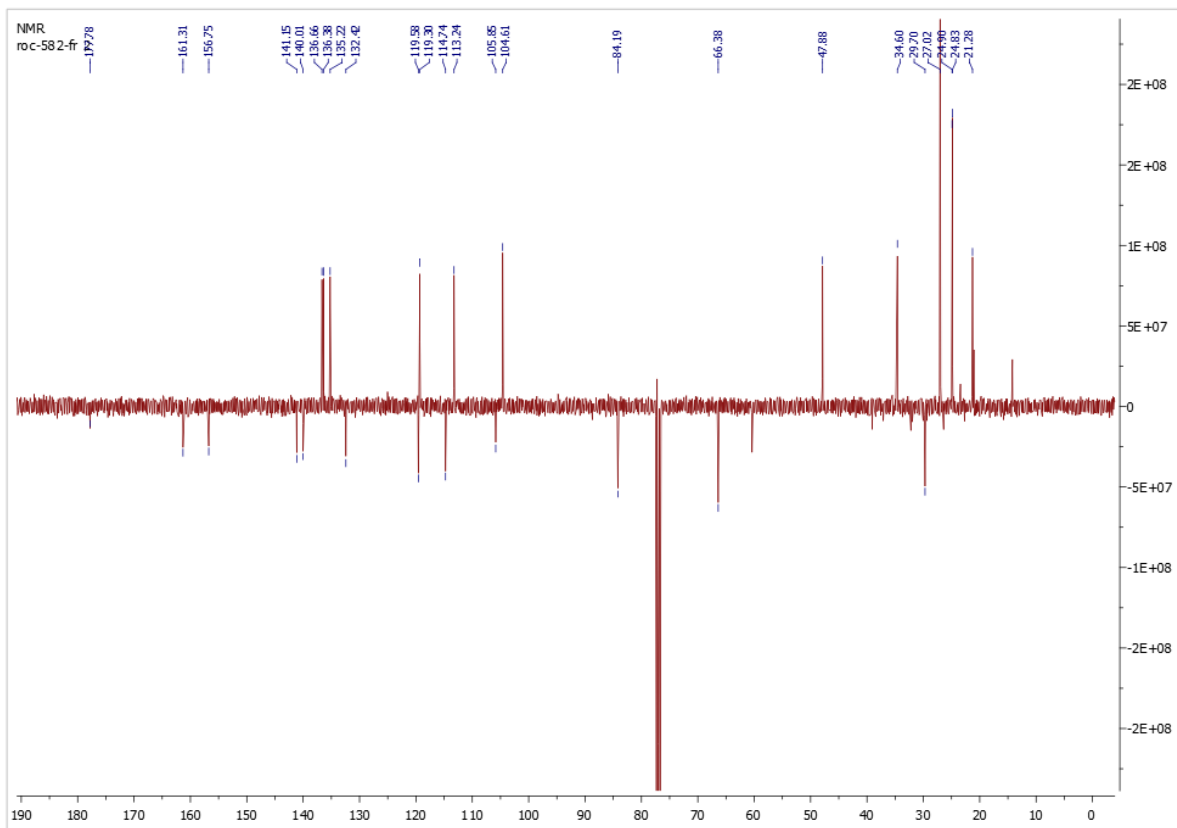
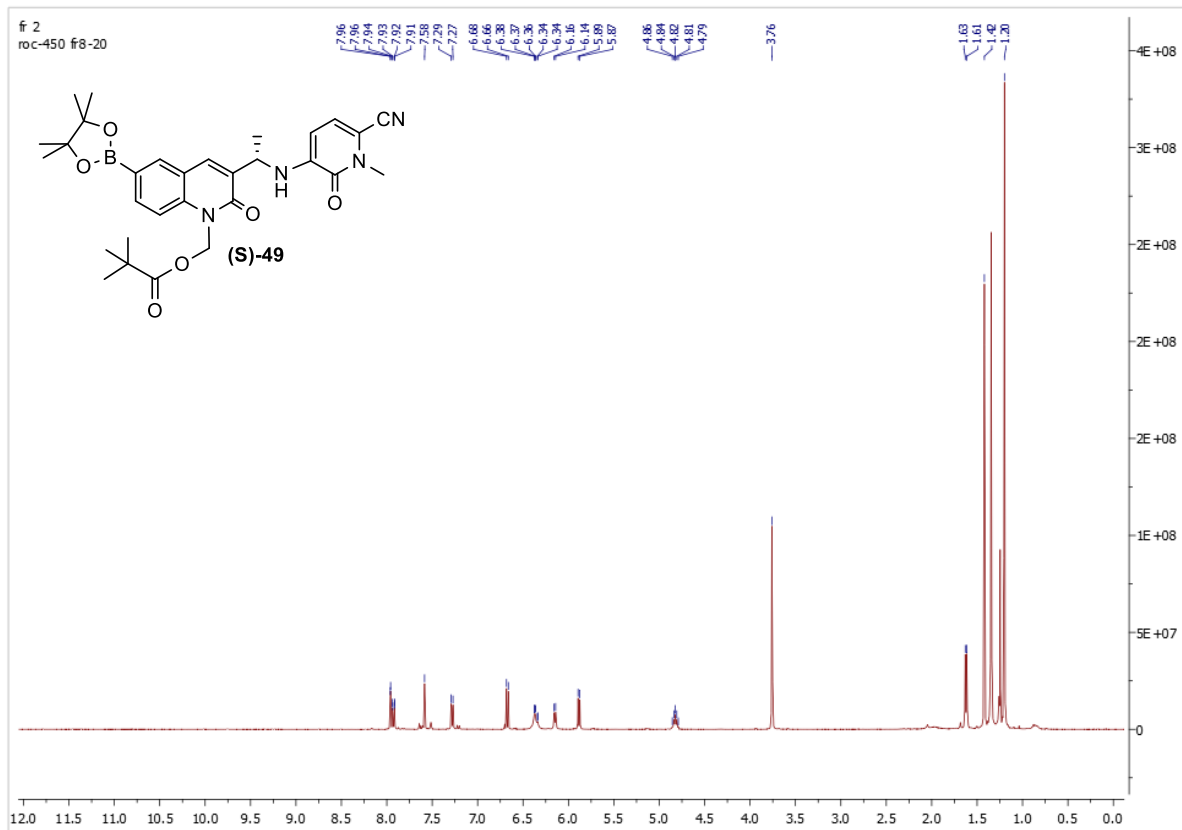
^1H NMR spectra of (*S*)-((6-bromo-3-(1-((6-cyano-1-methyl-2-oxo-1,2-dihydropyridin-3-yl)amino)ethyl)quinolin-2-yl)oxy)methyl pivalate (**S**)-**47e** and (*S*)-(6-bromo-3-(1-((6-cyano-1-methyl-2-oxo-1,2-dihydropyridin-3-yl)amino)ethyl)-2-oxoquinolin-1(2H)-yl)methyl pivalate (**S**)-**48e**



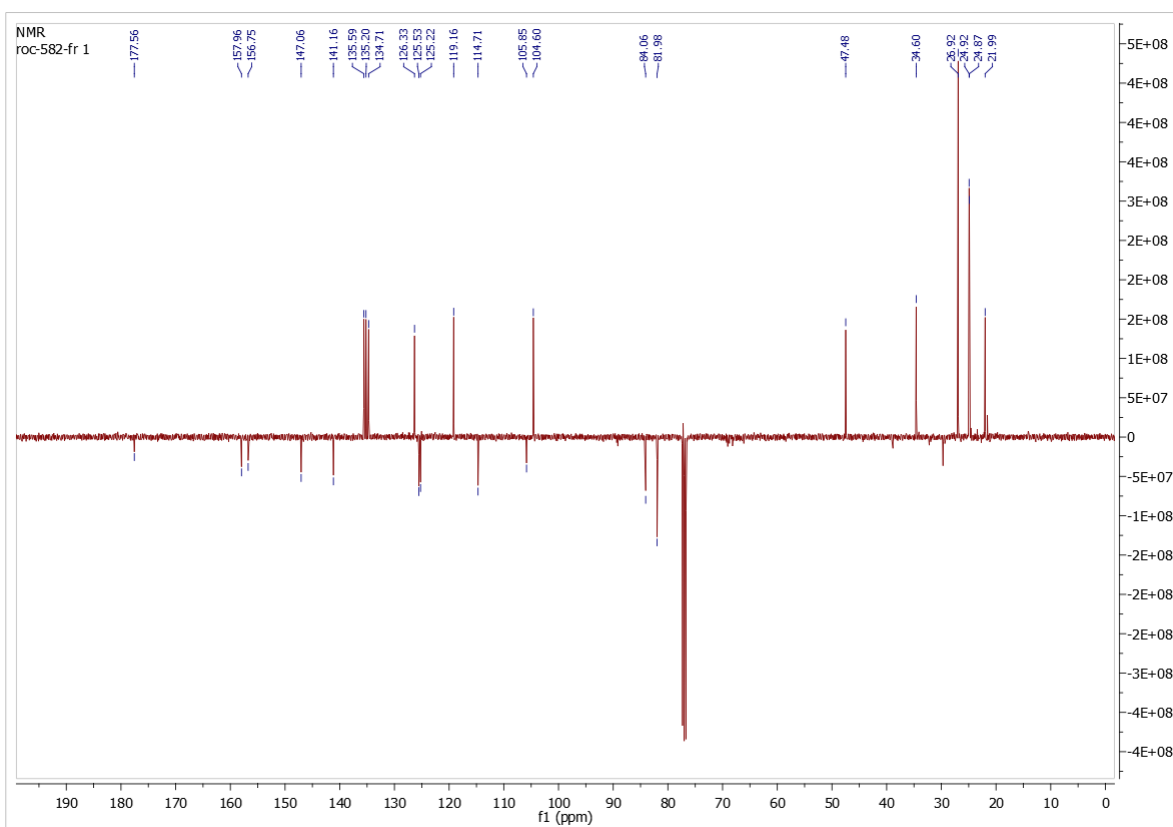
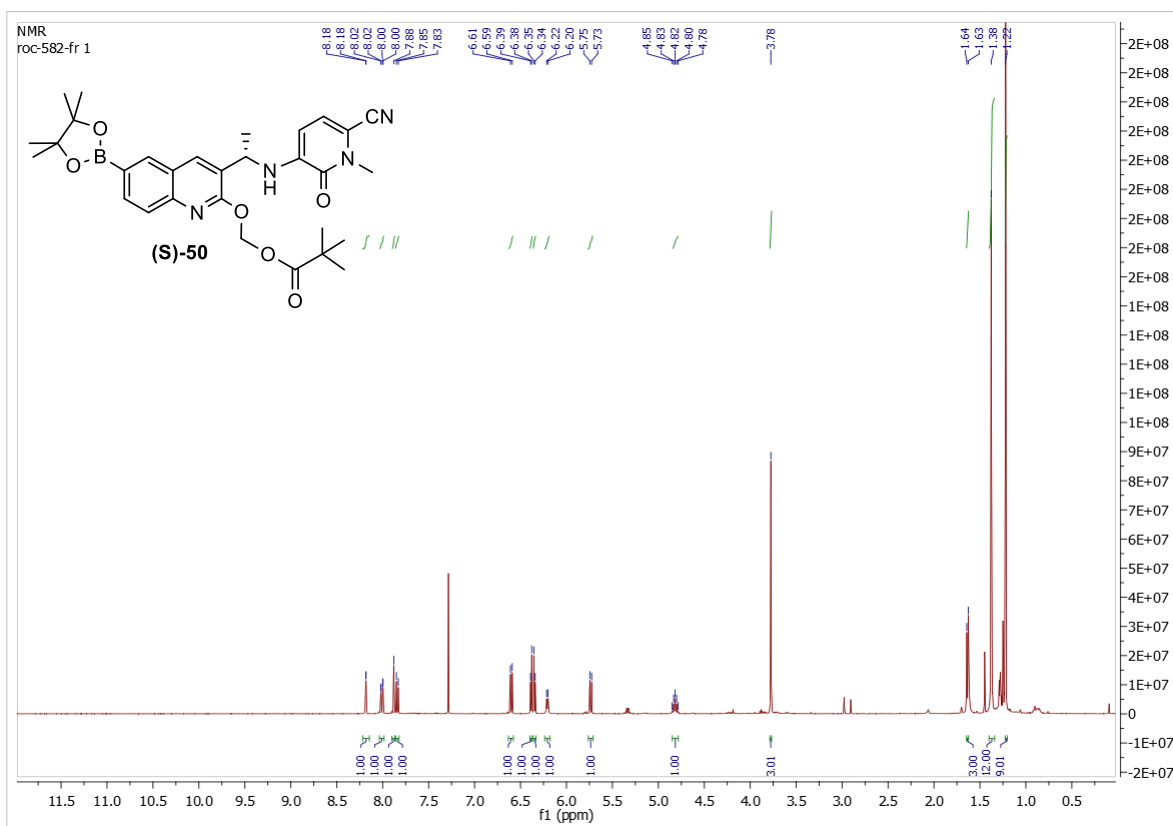
¹H NMR spectra of (R)-((6-bromo-3-(1-((6-cyano-1-methyl-2-oxo-1,2-dihydropyridin-3-yl)amino)ethyl)quinolin-2-yl)oxy)methyl pivalate (**(R)-47e**) and (R)-(6-bromo-3-(1-((6-cyano-1-methyl-2-oxo-1,2-dihydropyridin-3-yl)amino)ethyl)-2-oxoquinolin-1(2H)-yl)methyl pivalate (**(R)-48e**)



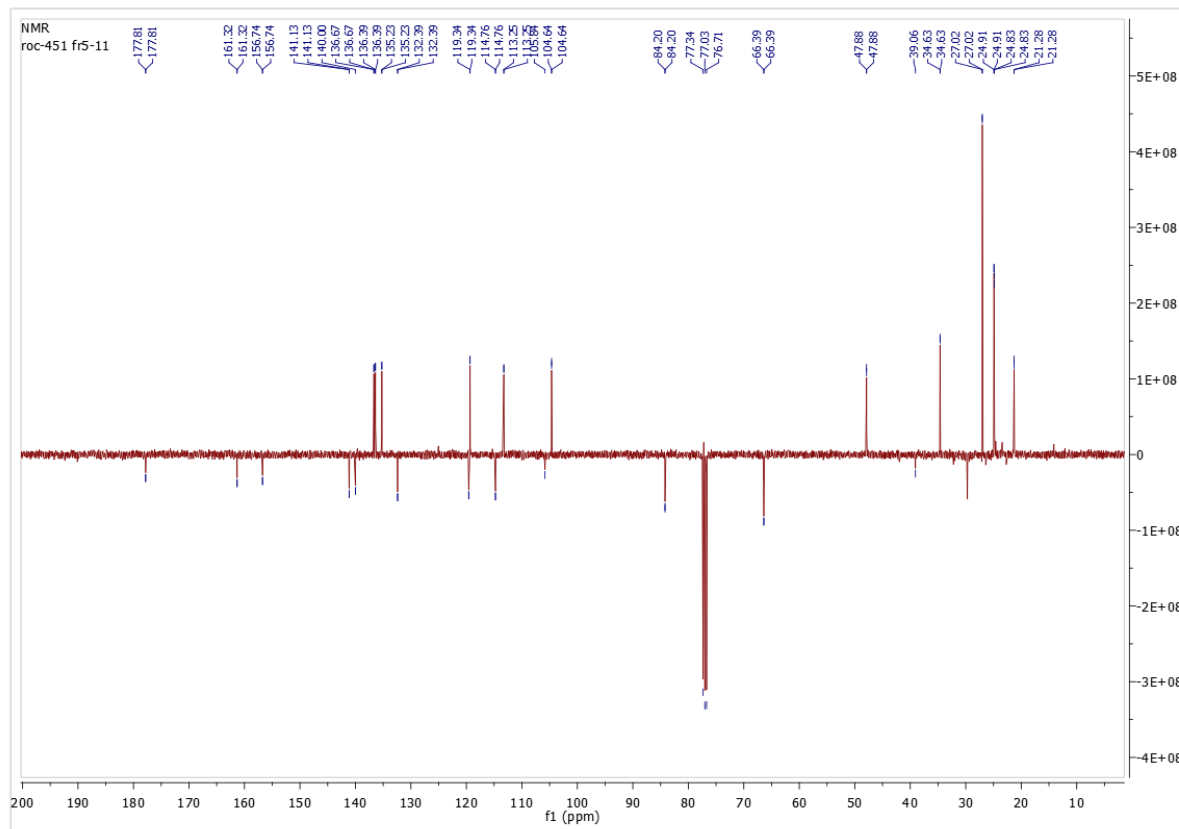
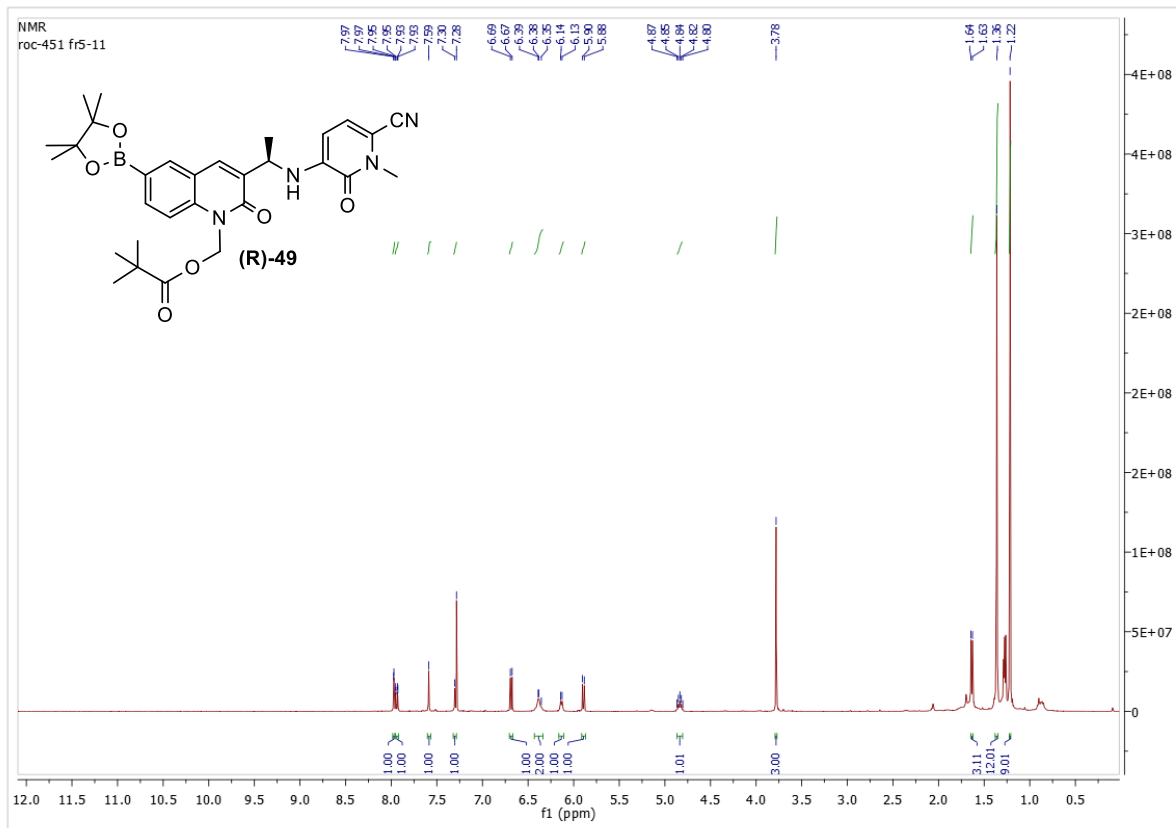
^1H and ^{13}C NMR spectra of (*S*)-((3-(1-((6-cyano-1-methyl-2-oxo-1,2-dihydropyridin-3-yl)amino)ethyl)-6-(4,4,5,5-tetramethyl-1,3,2-dioxaborolan-2-yl)quinolin-2-yl)oxy)methyl pivalate (**S**)-49



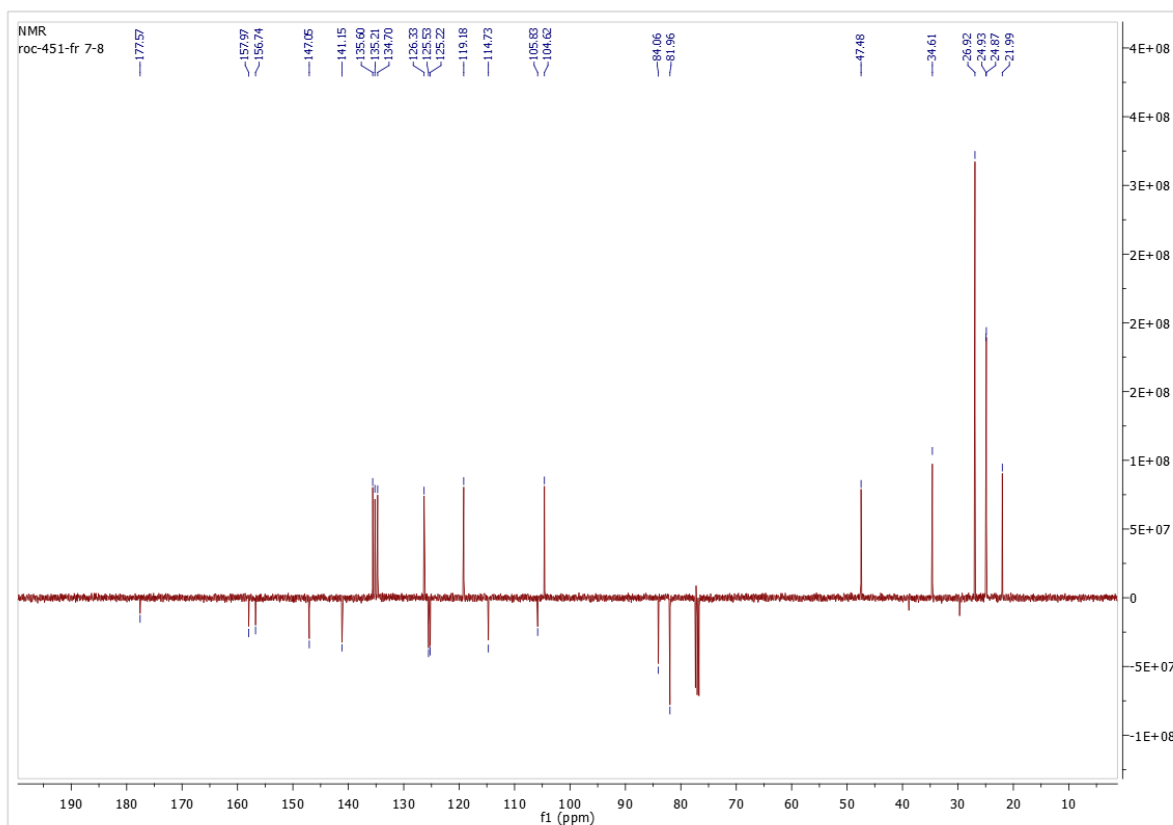
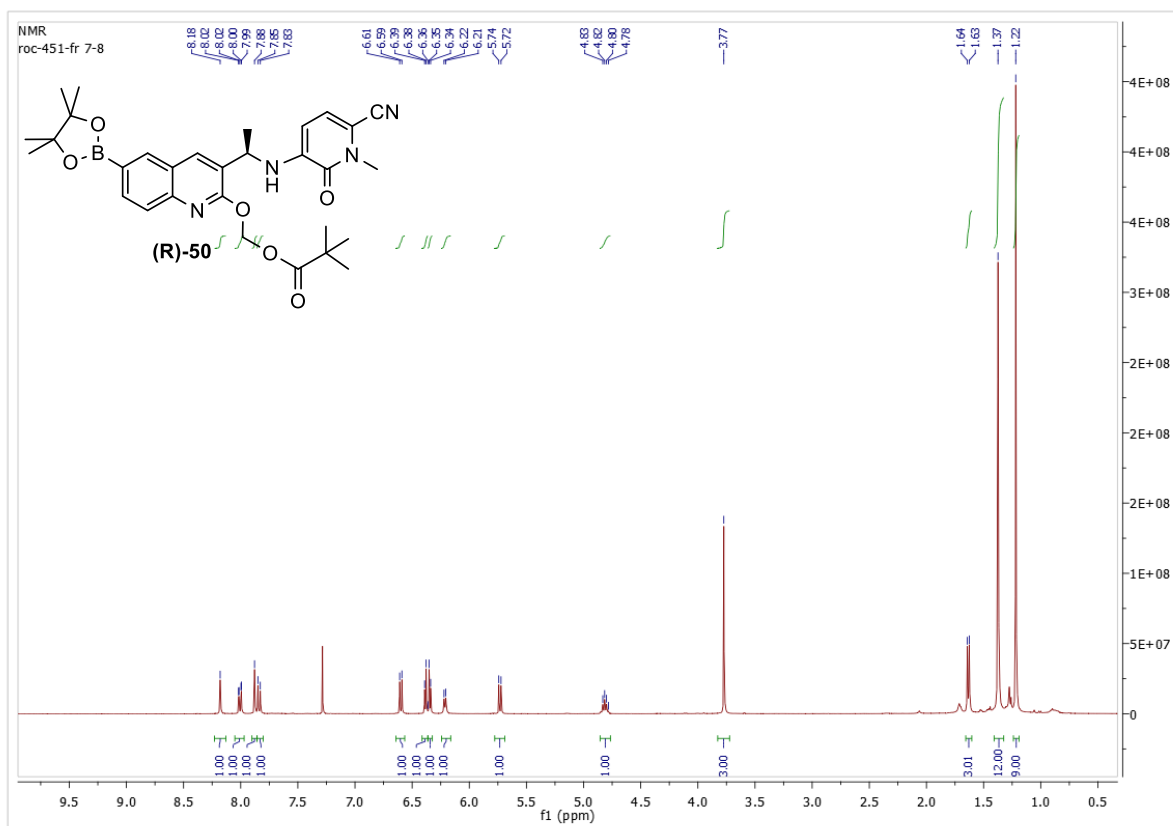
^1H and ^{13}C NMR spectra of (*S*)-3-(1-((6-cyano-1-methyl-2-oxo-1,2-dihydropyridin-3-yl)amino)ethyl)-2-oxo-6-(4,4,5,5-tetramethyl-1,3,2-dioxaborolan-2-yl)quinolin-1(2H)-yl)methyl pivalate (**S**-50)

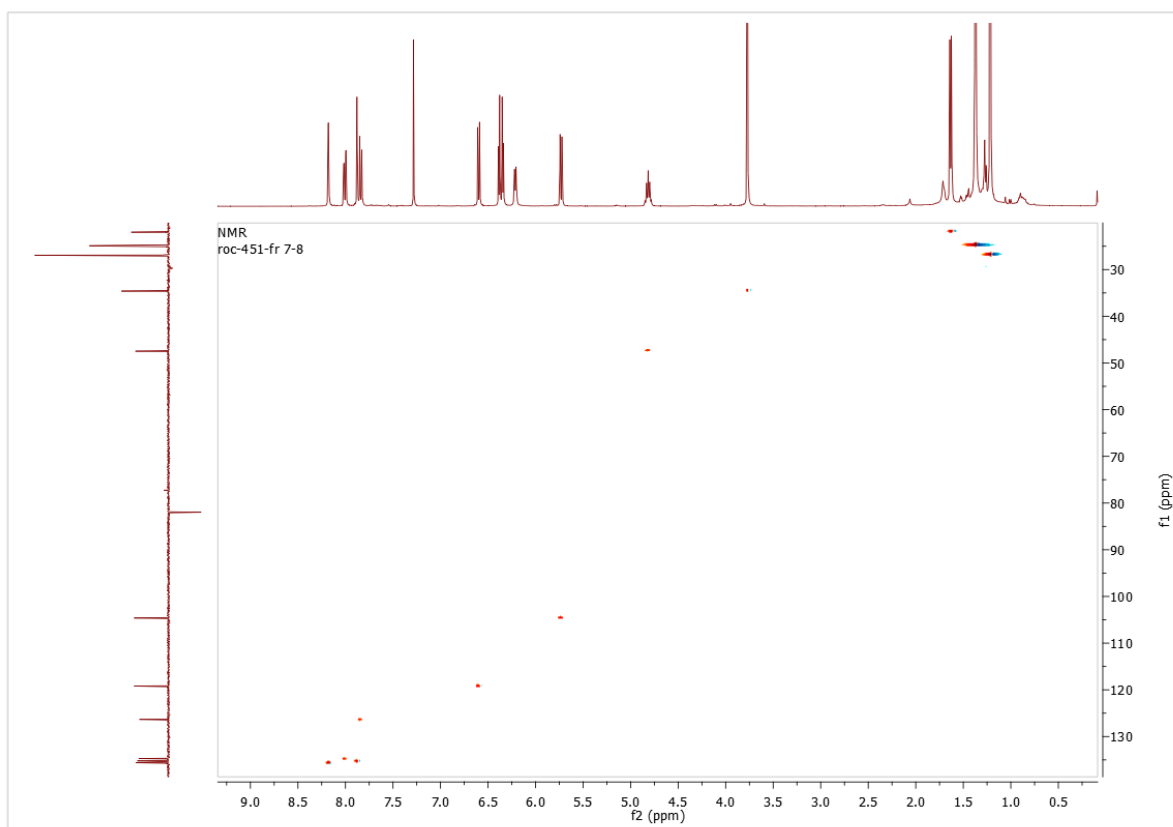


^1H and ^{13}C NMR spectra of (*R*)-((3-(1-((6-cyano-1-methyl-2-oxo-1,2-dihydropyridin-3-yl)amino)ethyl)-6-(4,4,5,5-tetramethyl-1,3,2-dioxaborolan-2-yl)quinolin-2-yl)oxy)methyl pivalate (**R**)-49

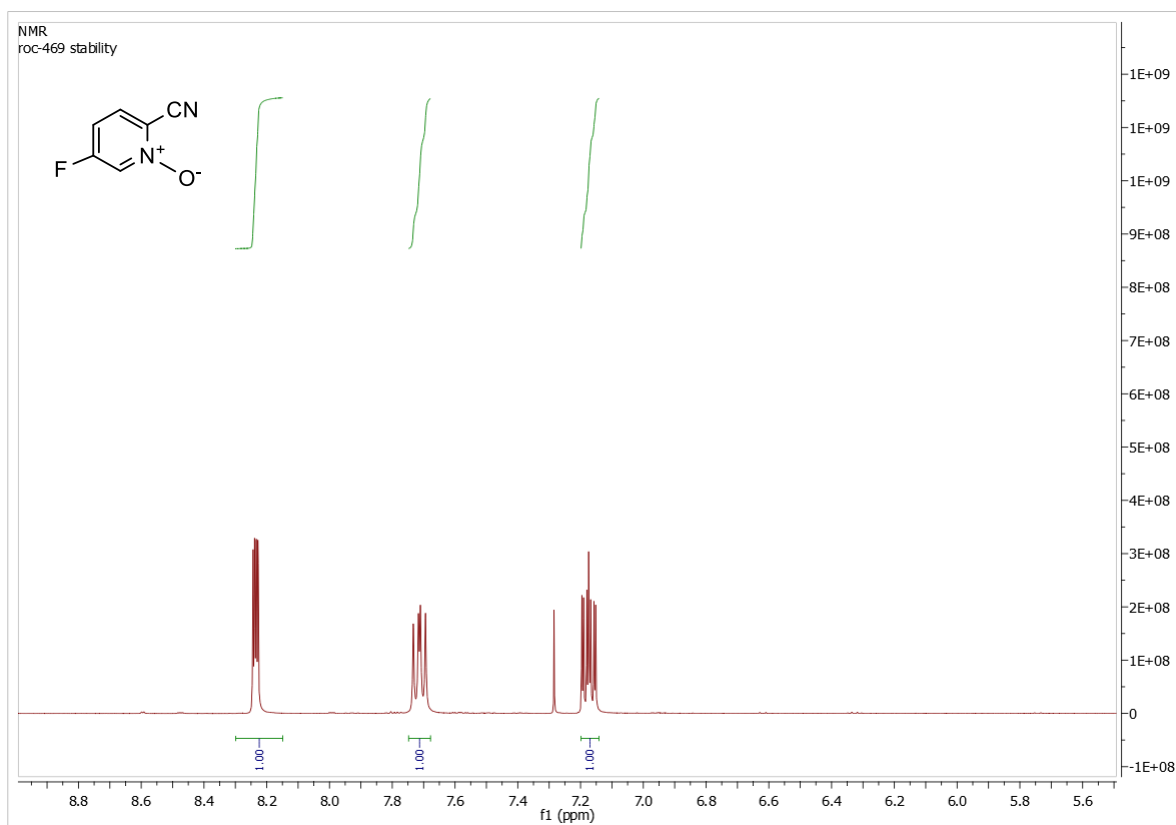


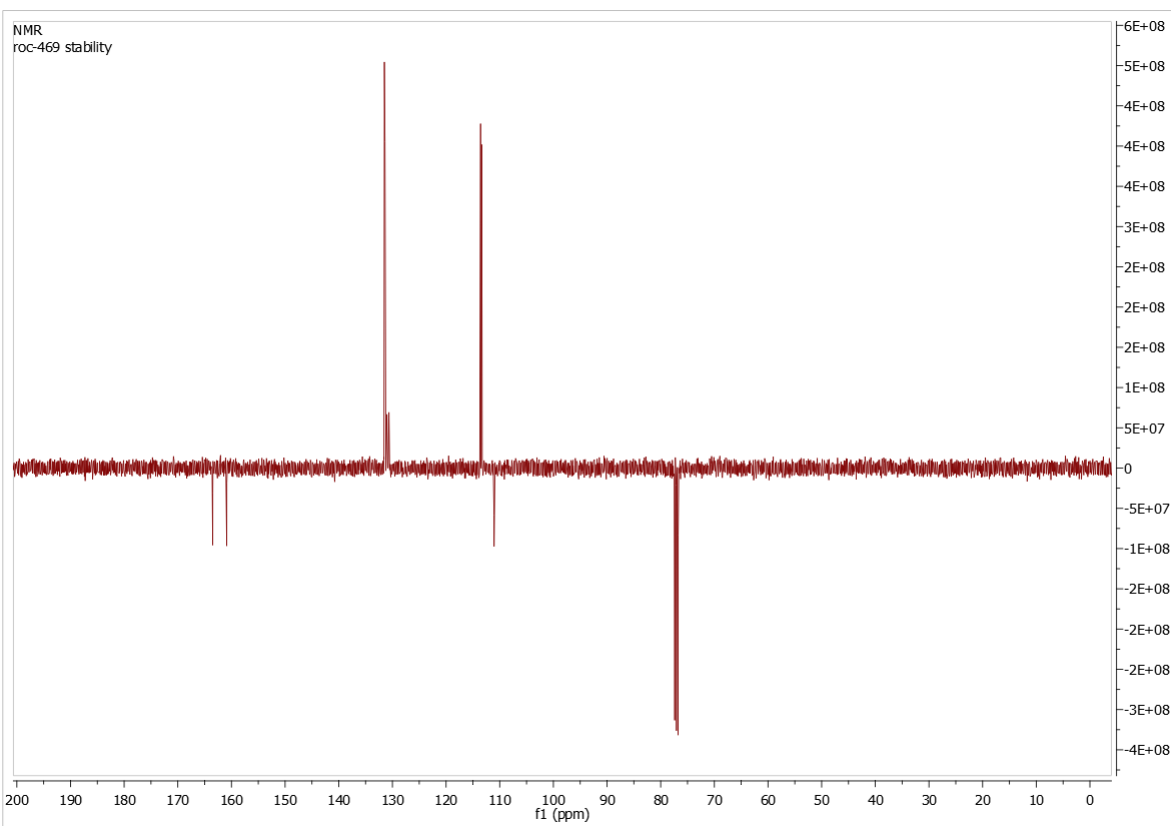
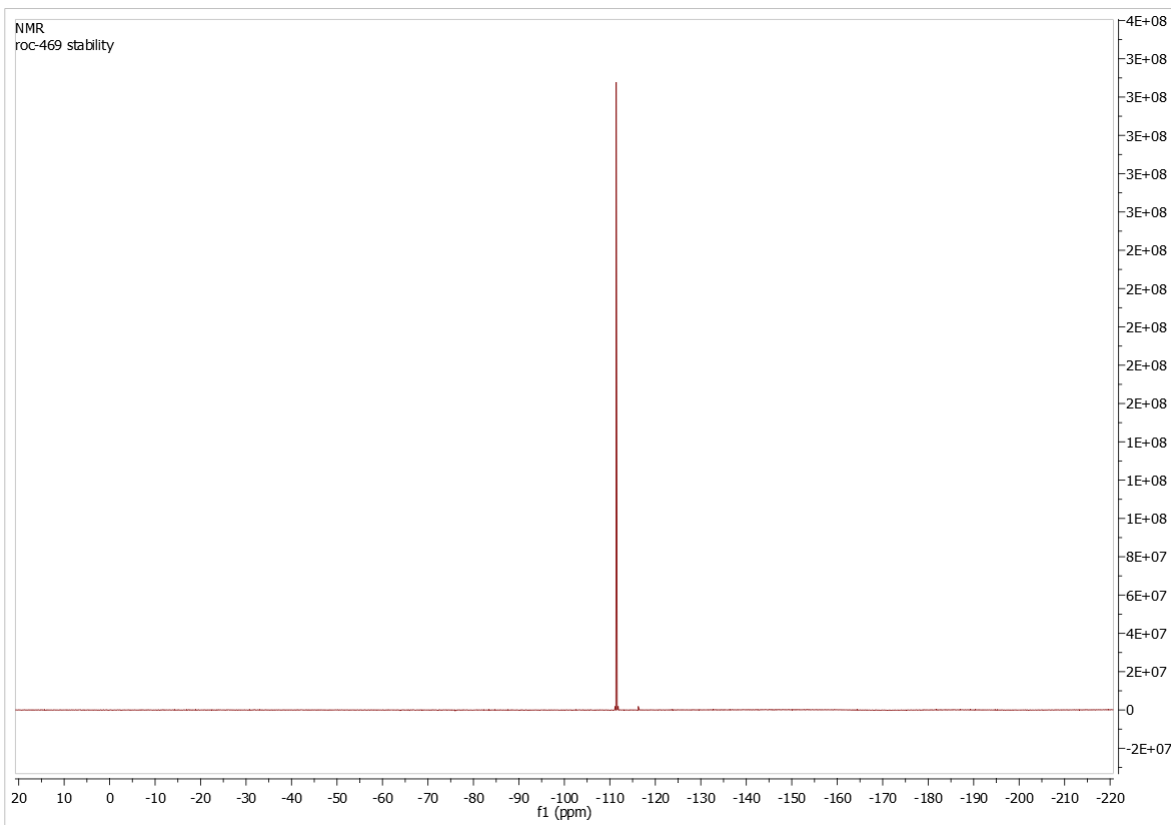
^1H , ^{13}C and HSQC NMR spectra of (*R*)-(3-(1-((6-cyano-1-methyl-2-oxo-1,2-dihydropyridin-3-yl)amino)ethyl)-2-oxo-6-(4,4,5,5-tetramethyl-1,3,2-dioxaborolan-2-yl)quinolin-1(2H)-yl)methyl pivalate (**R**)-50



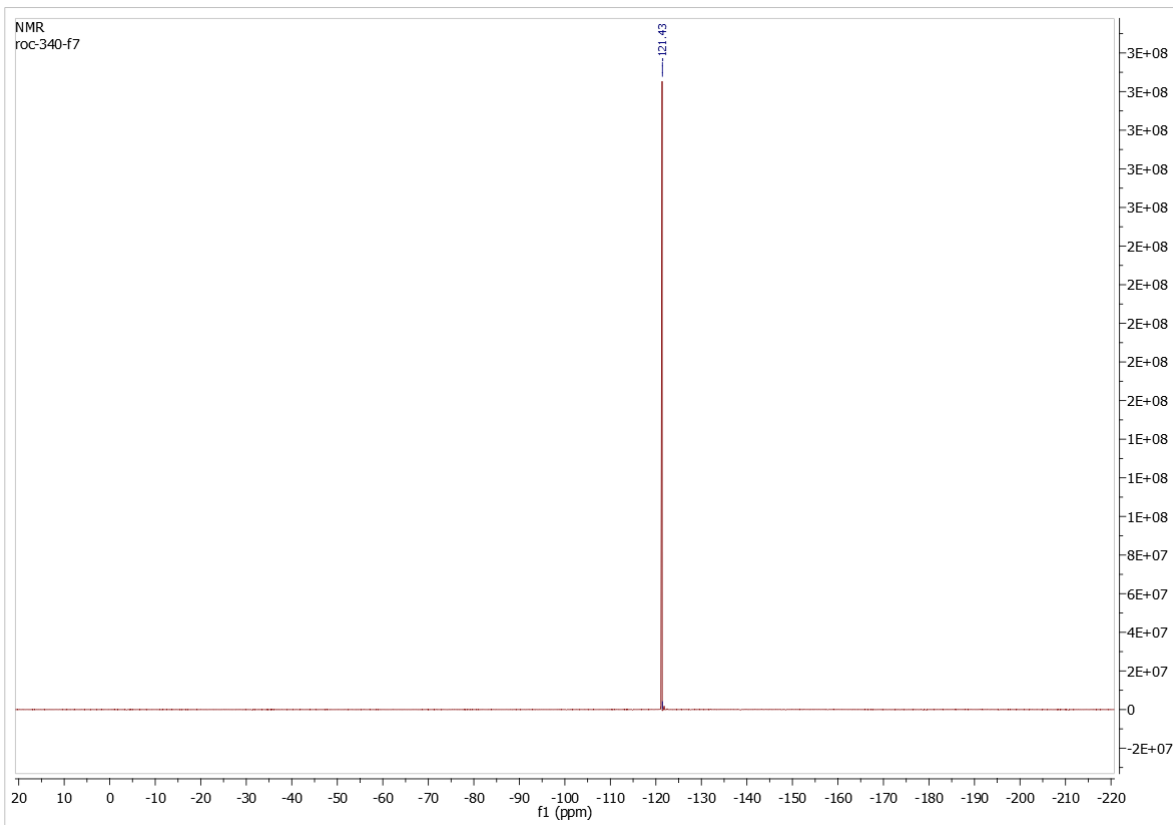
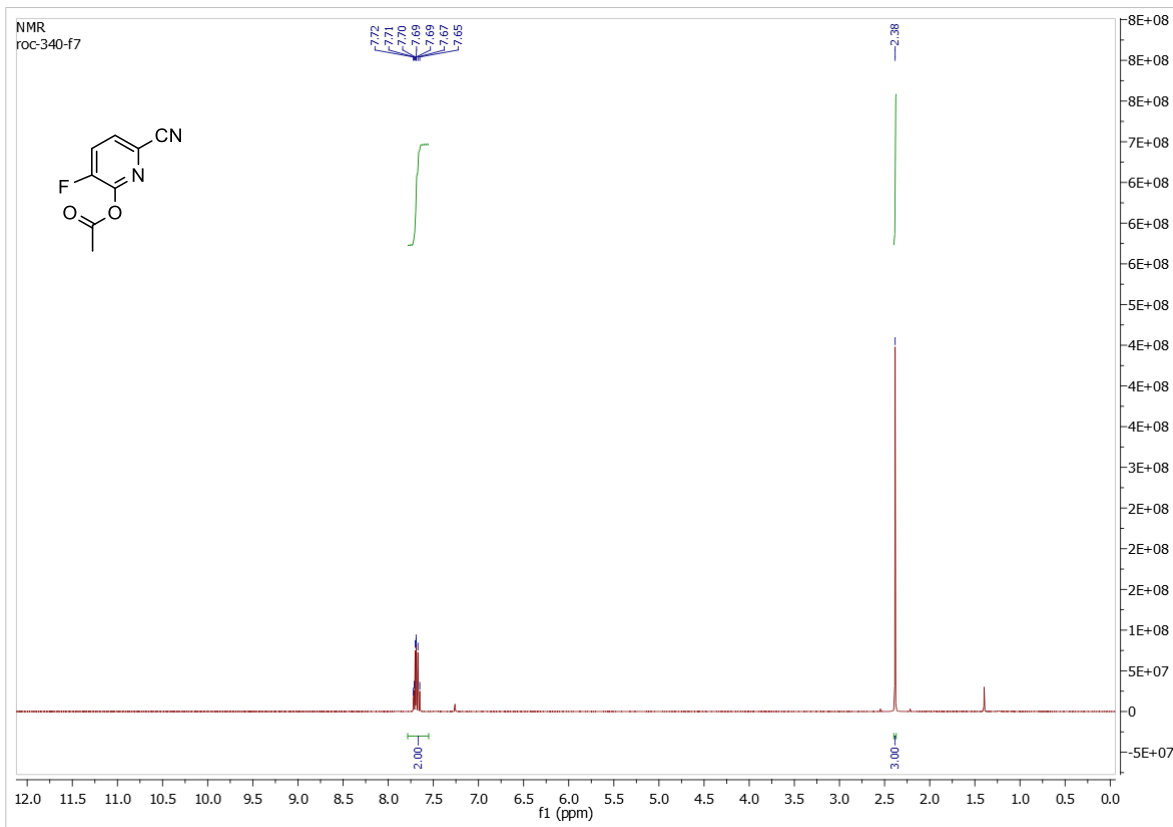


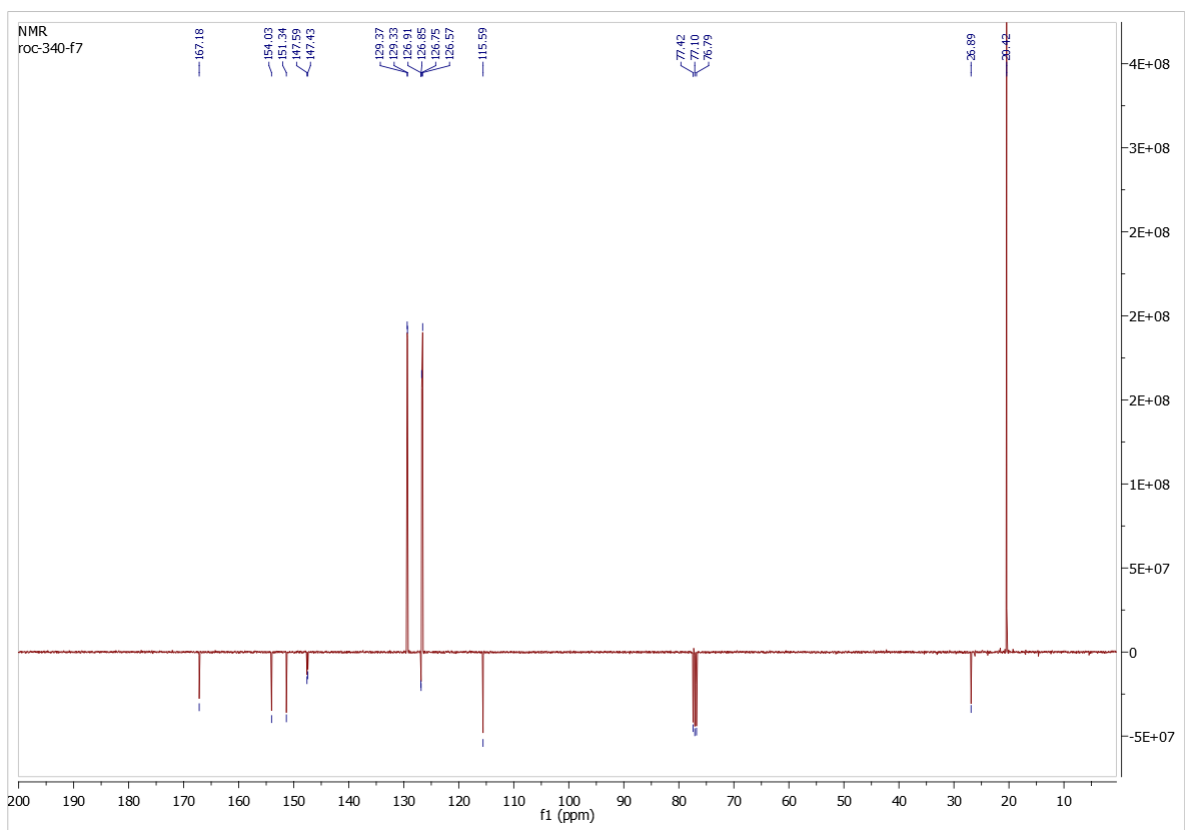
^1H , ^{19}F and ^{13}C NMR spectra of 2-Cyano-5-fluoropyridine 1-oxide **52**



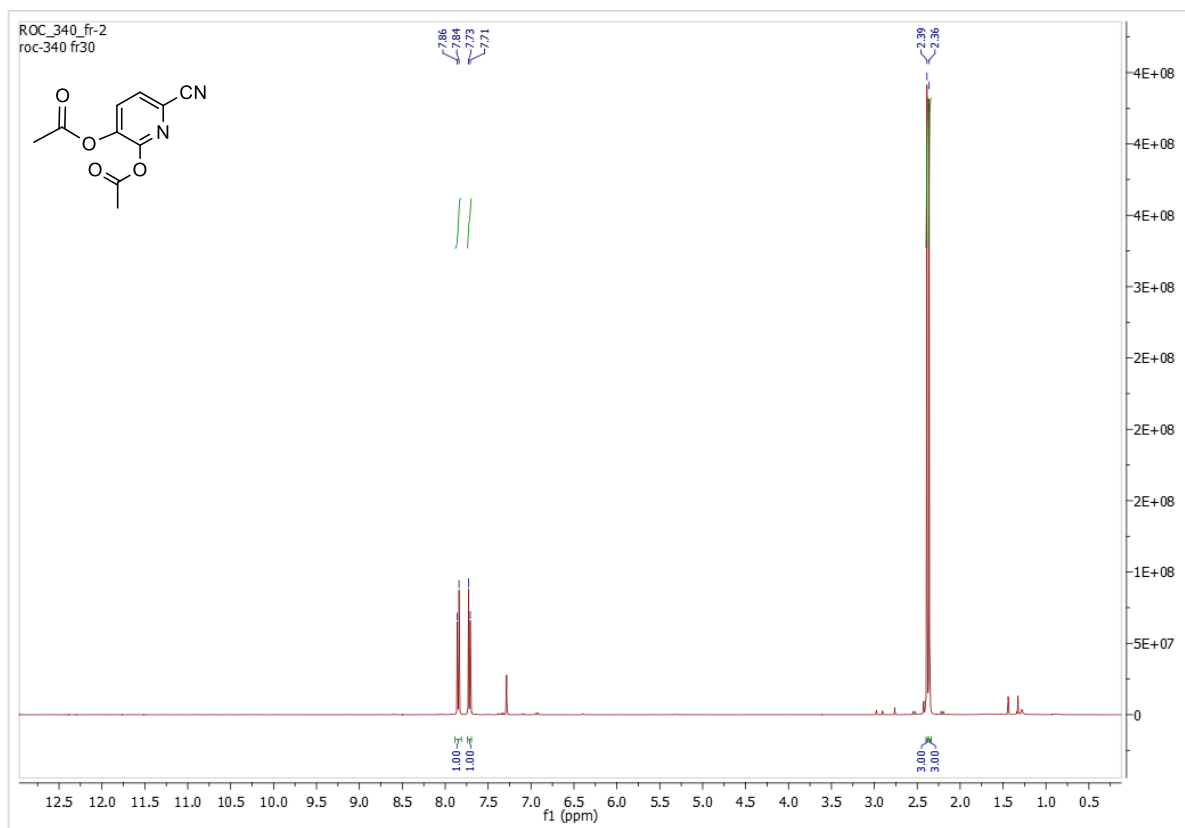


^1H , ^{19}F and ^{13}C NMR spectra of 6-Cyano-3-fluoropyridin-2-yl acetate **53**

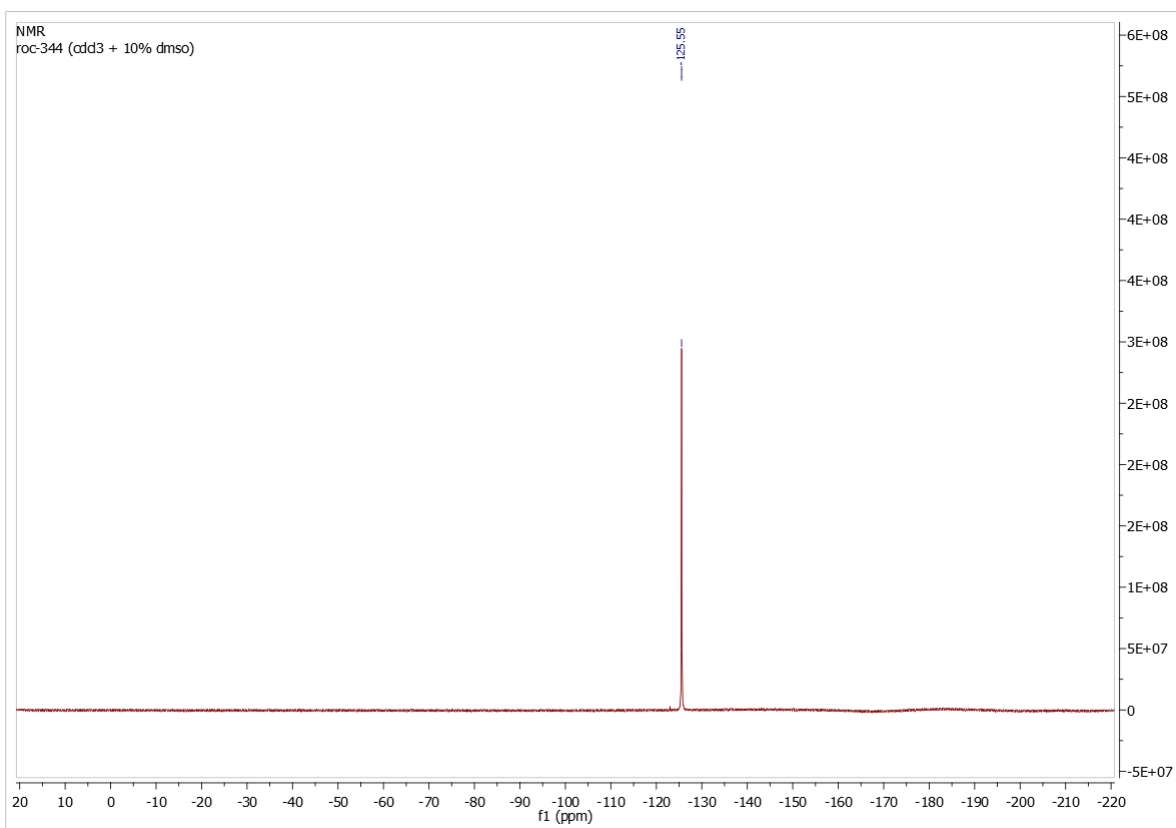
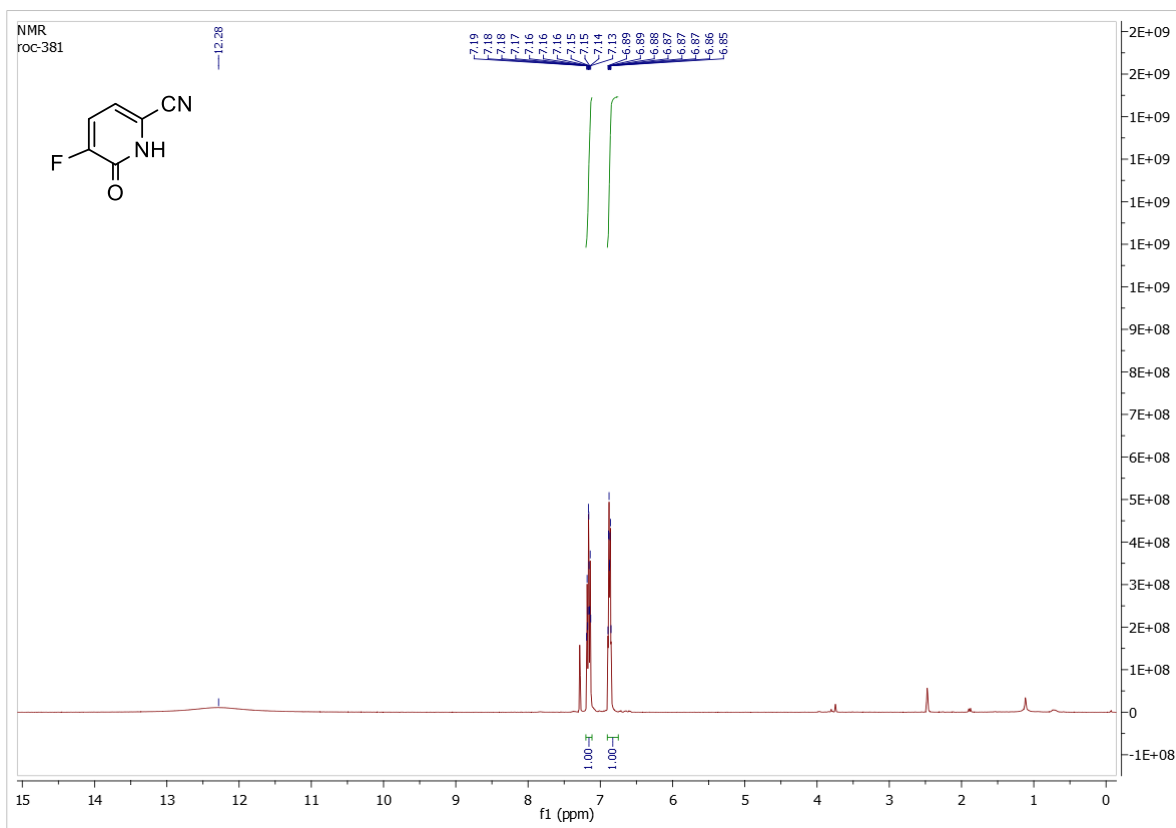


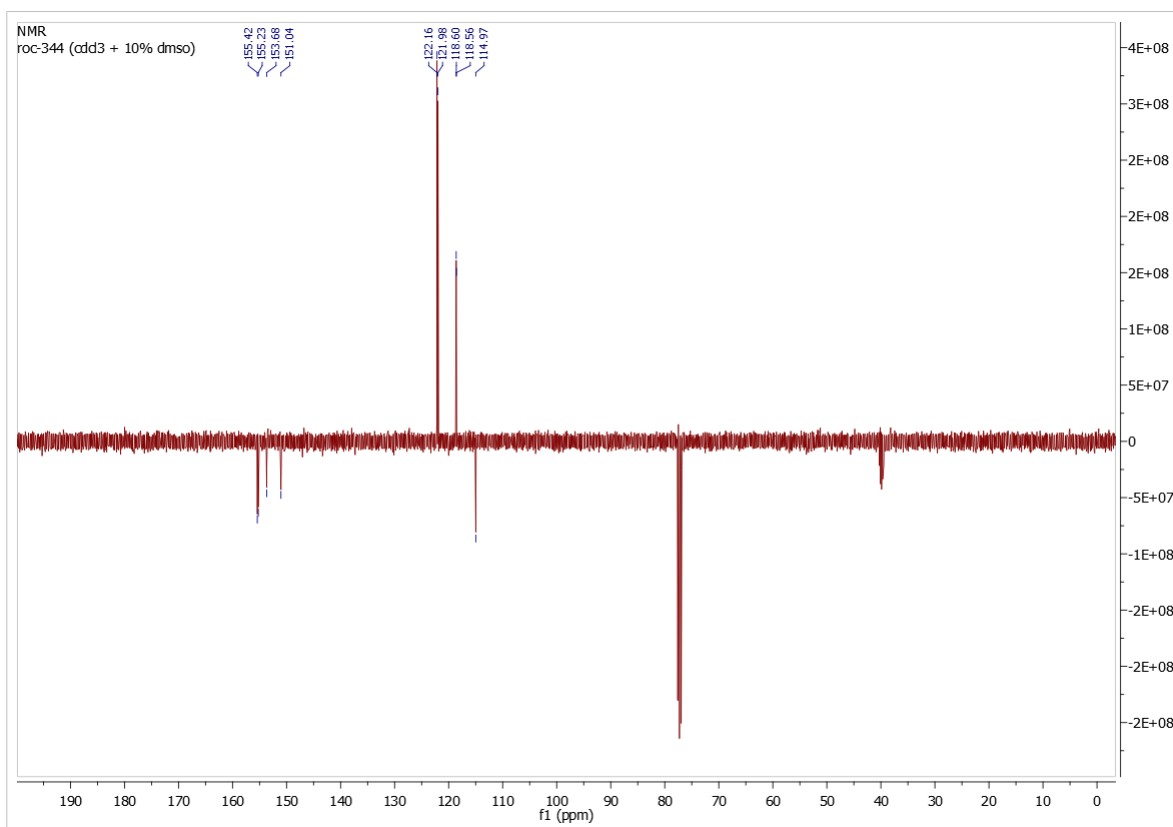


^1H NMR spectra of 6-cyanopyridine-2,3-diyl diacetate **53b**

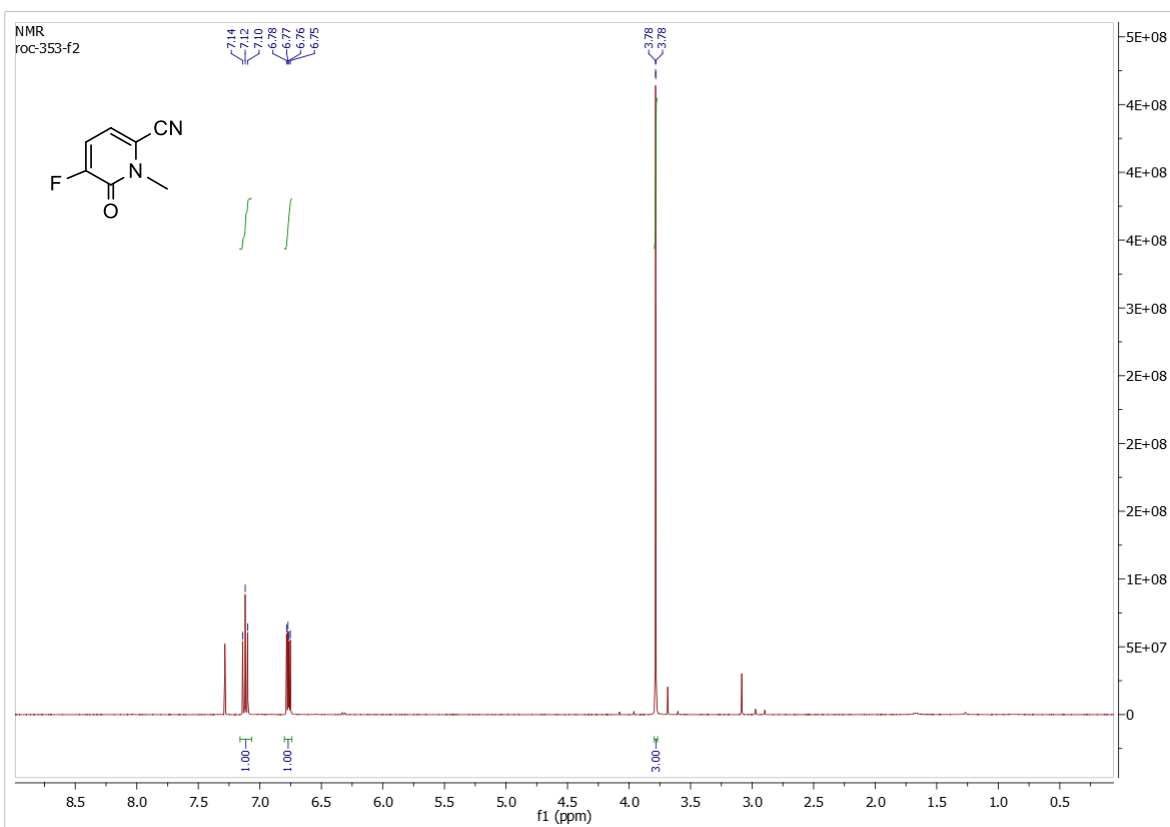


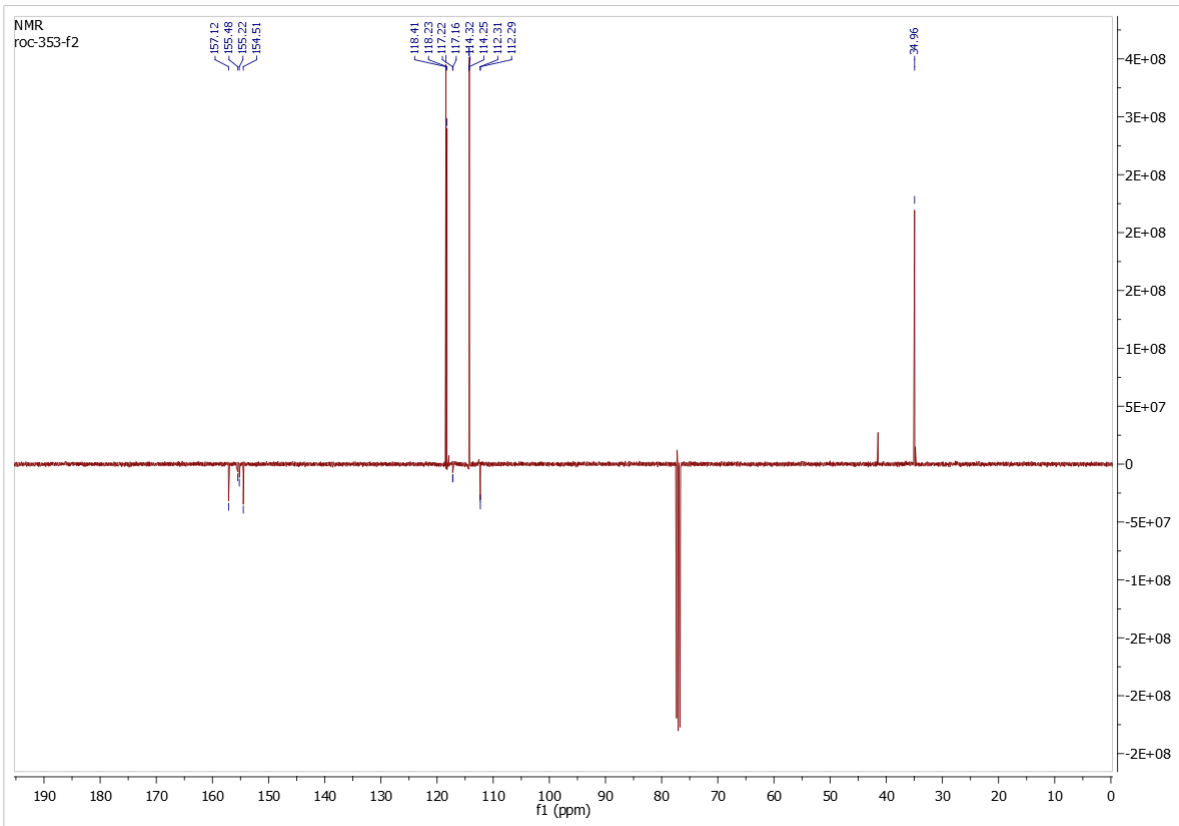
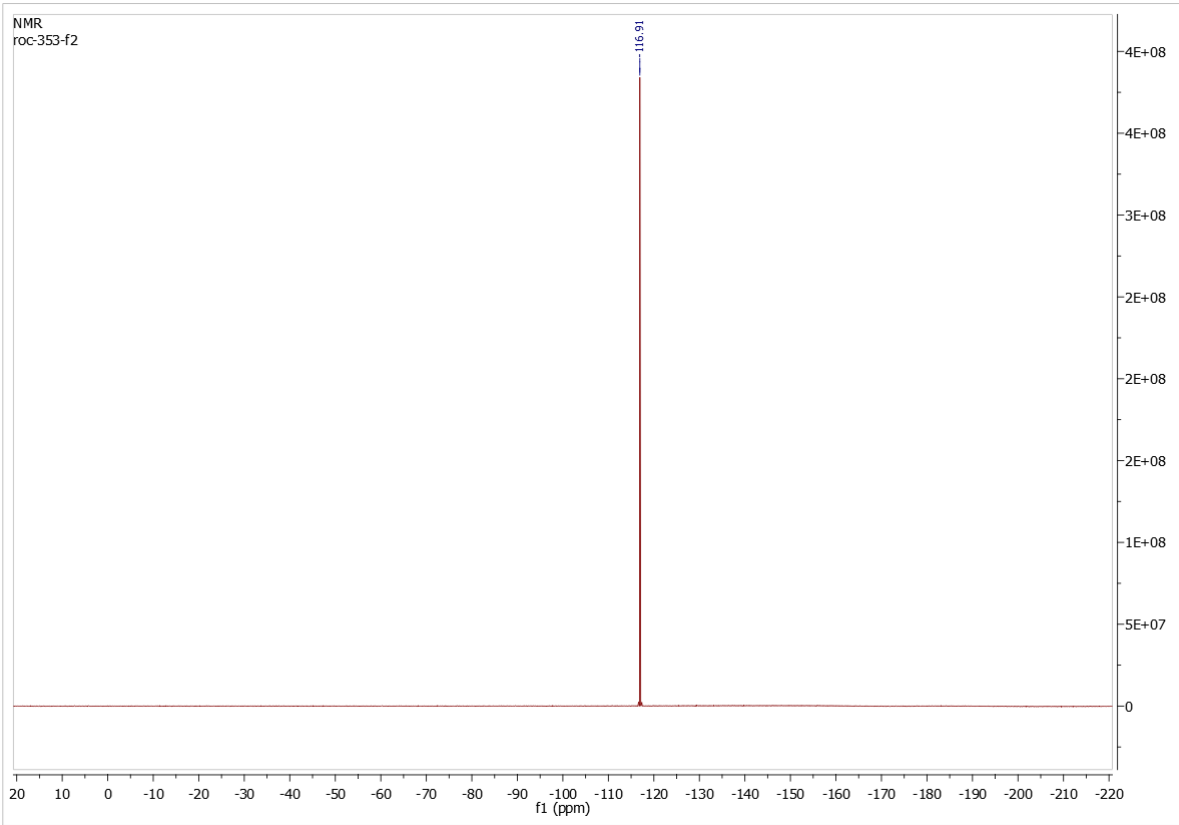
^1H , ^{19}F and ^{13}C NMR spectra of 5-Fluoro-6-oxo-1,6-dihydropyridine-2-carbonitrile **54**



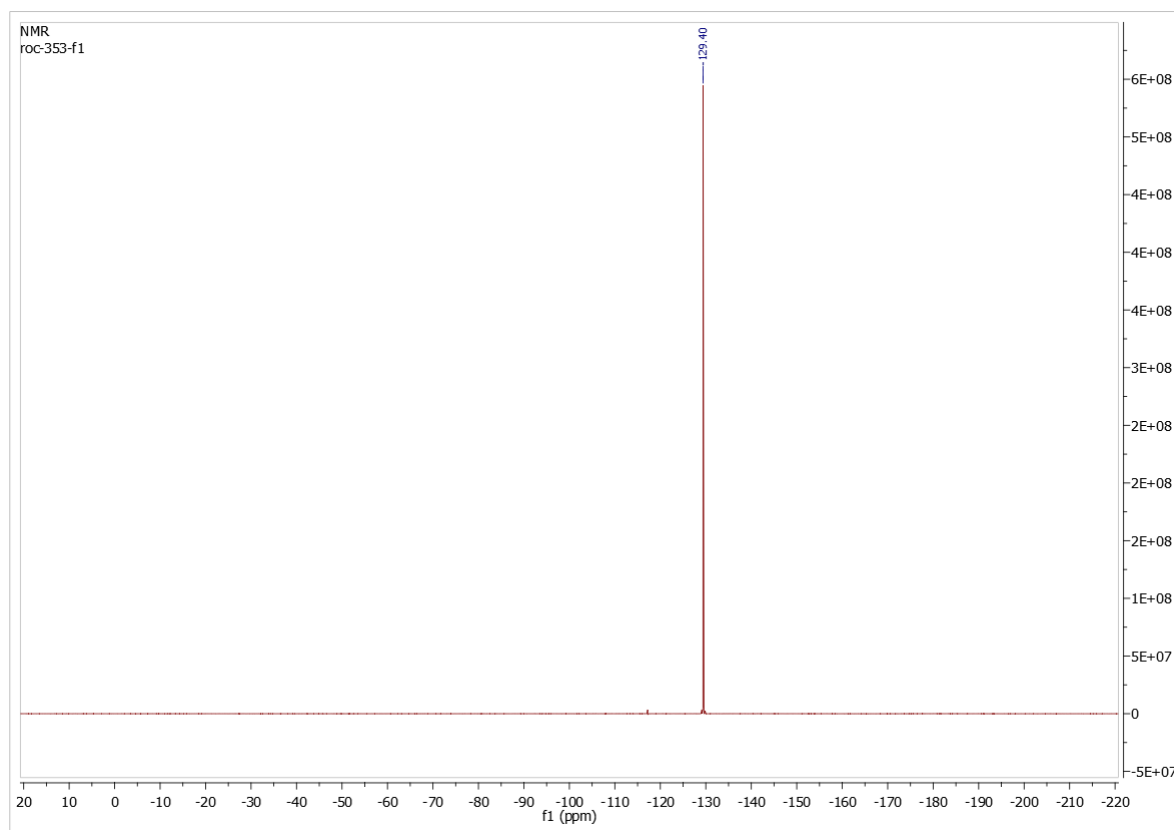
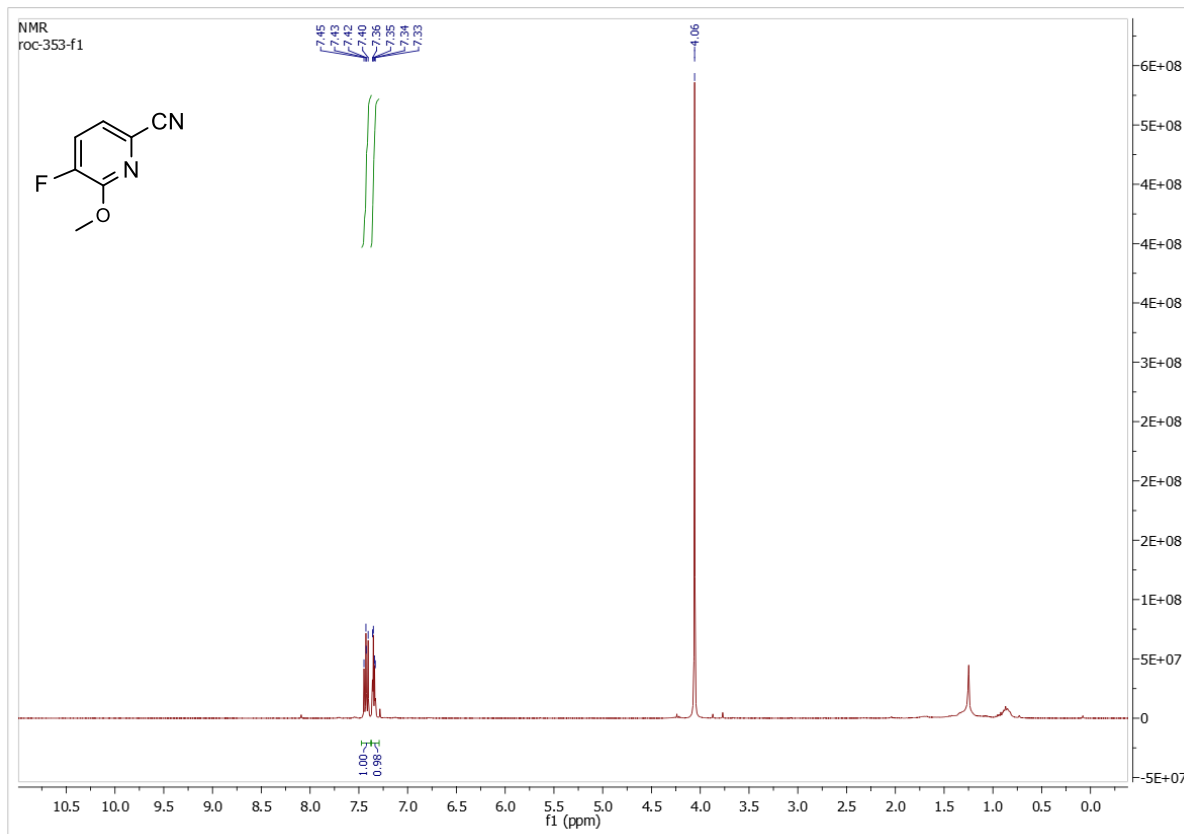


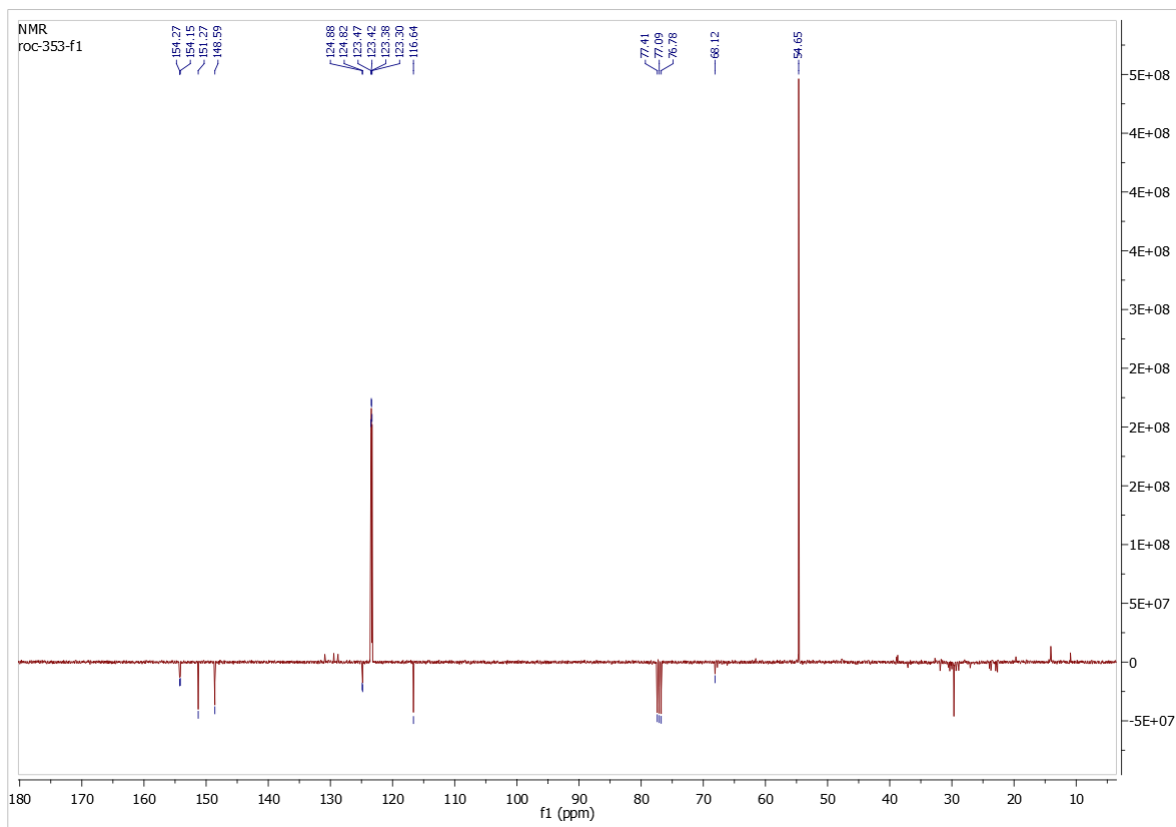
^1H , ^{19}F and ^{13}C NMR spectra of 5-Fluoro-1-methyl-6-oxo-1,6-dihydropyridine-2-carbonitrile **55**



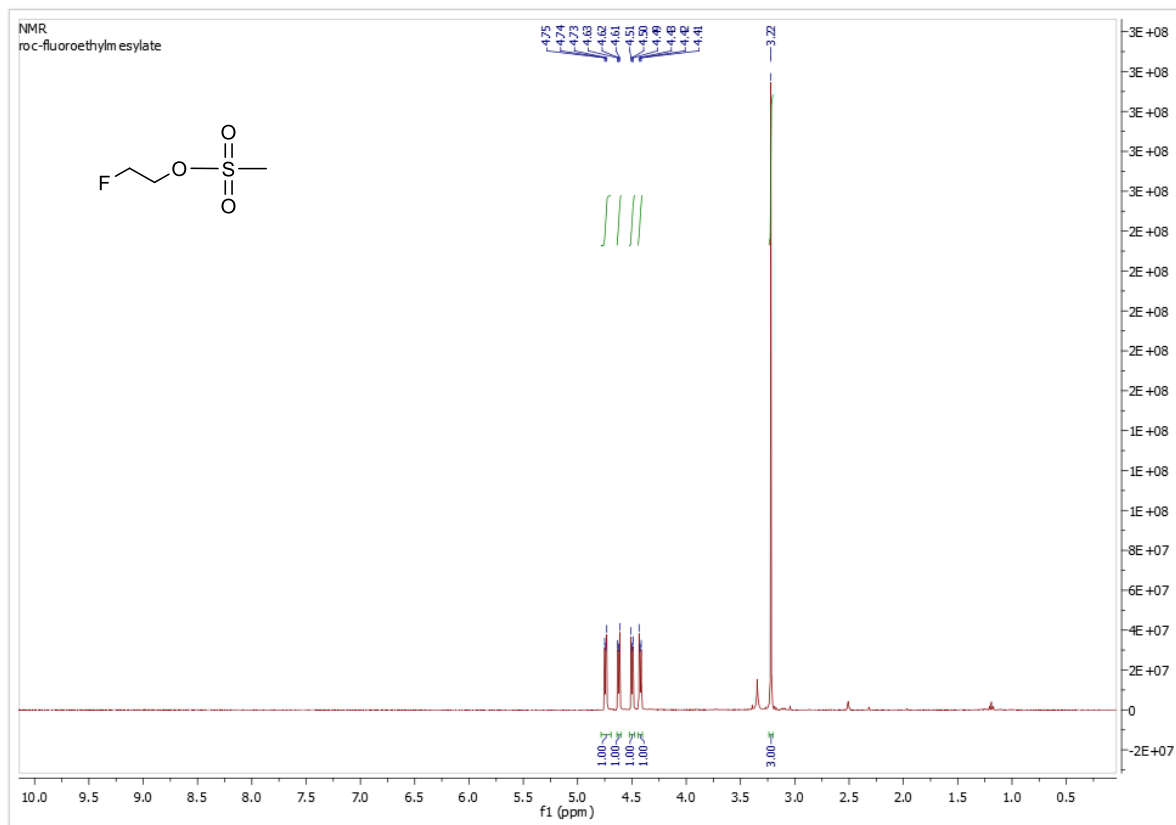


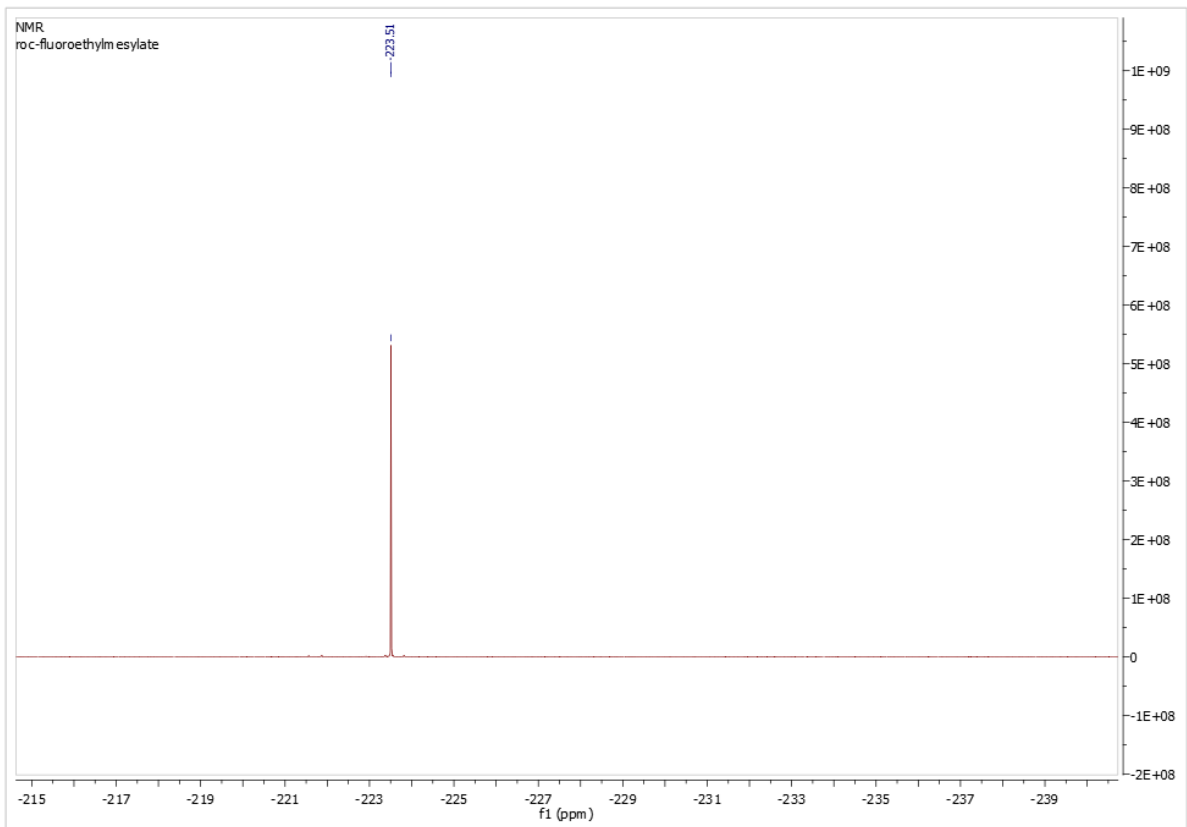
^1H , ^{19}F and ^{13}C NMR spectra of 5-fluoro-6-methoxypicolinonitrile **55b**



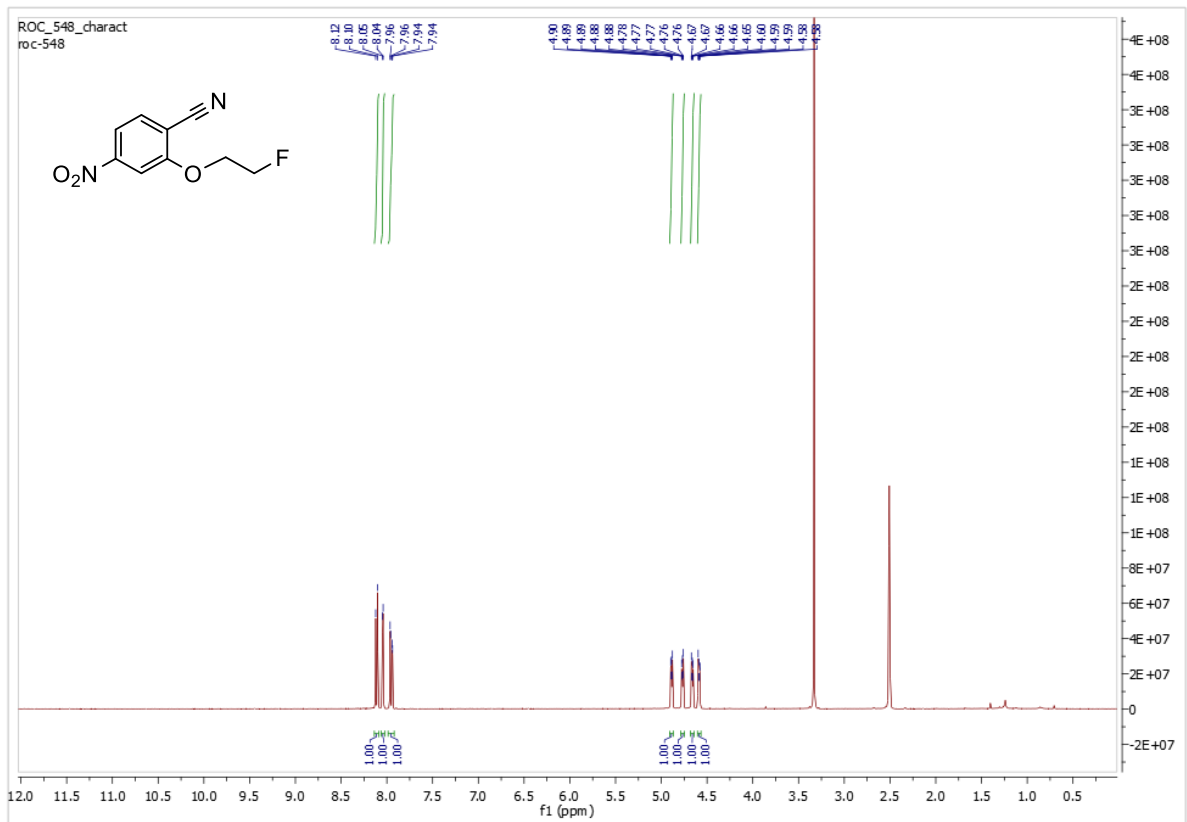


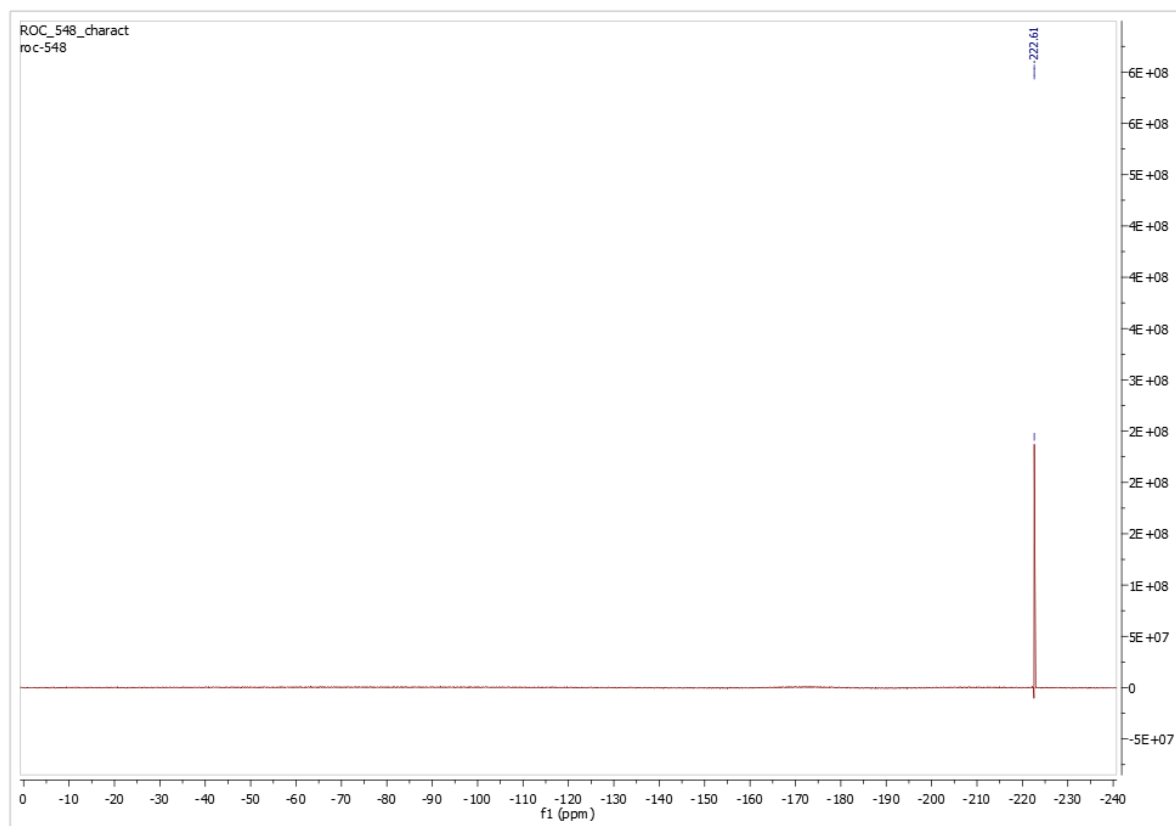
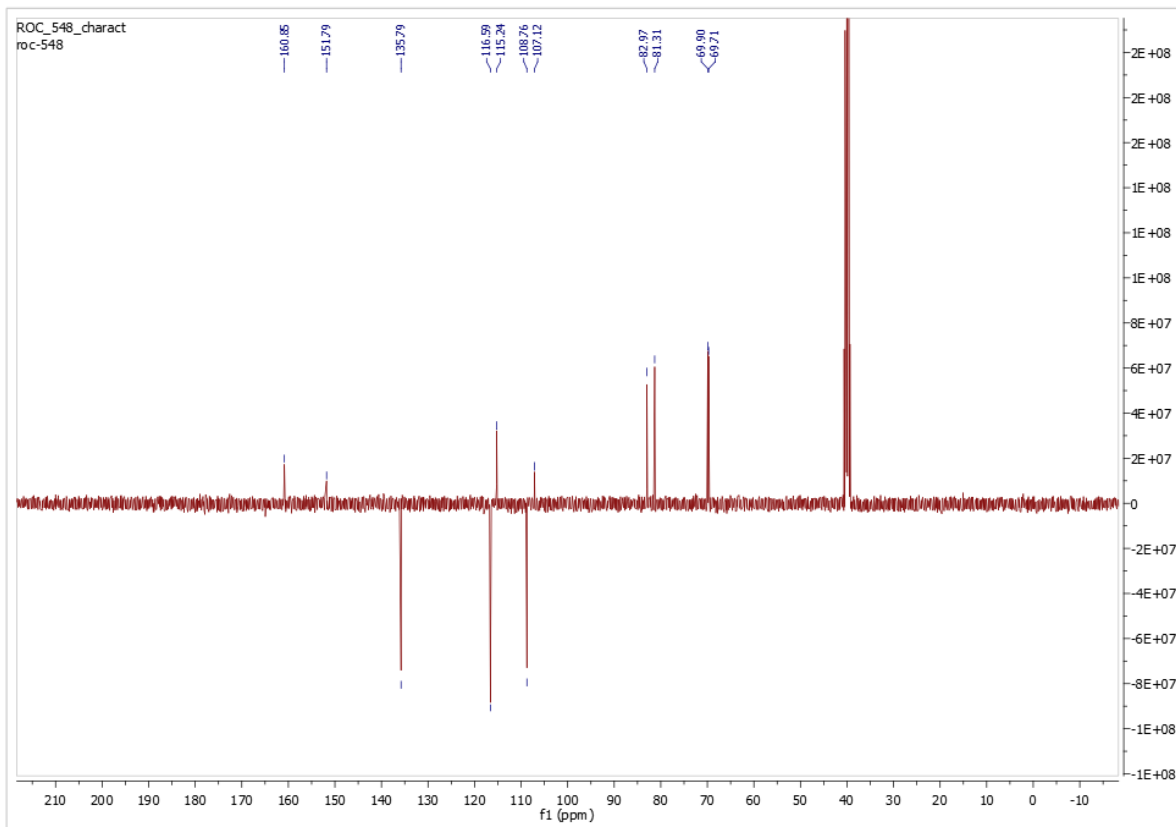
¹H and ¹⁹F NMR Spectra of 2-fluoroethyl methanesulfonate **65**



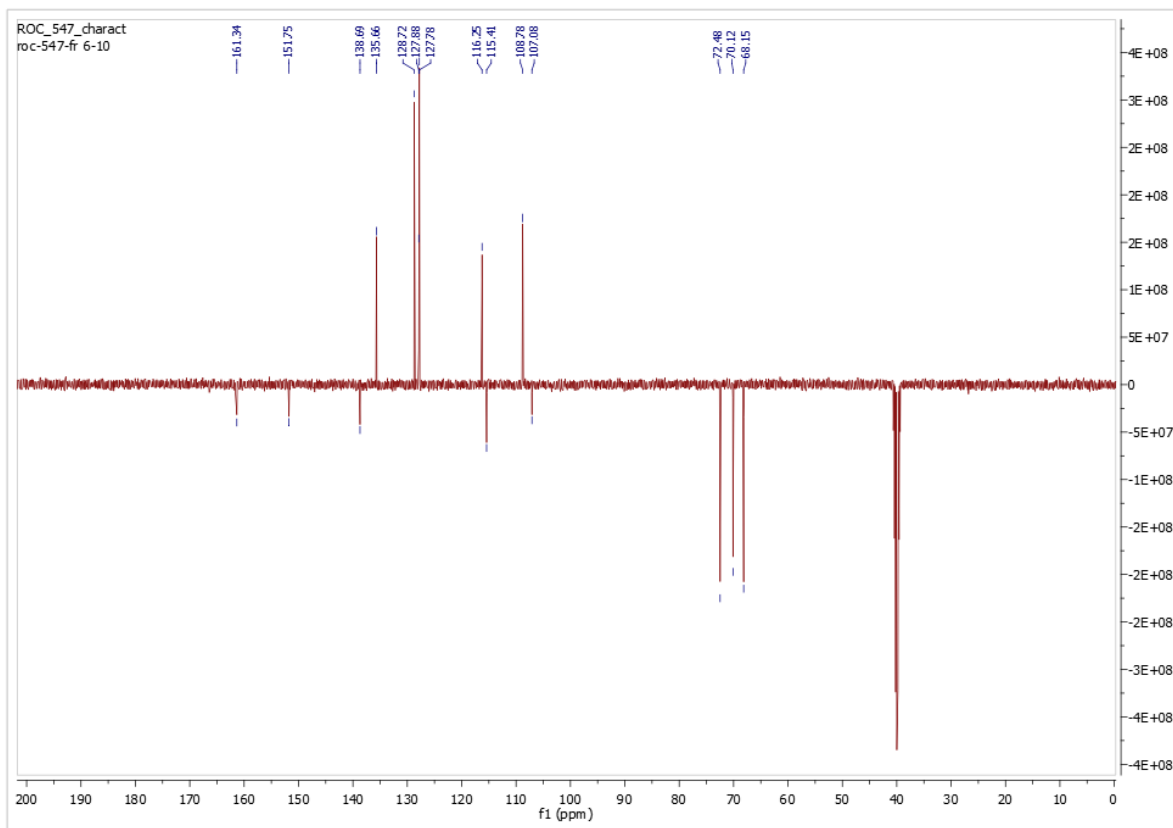
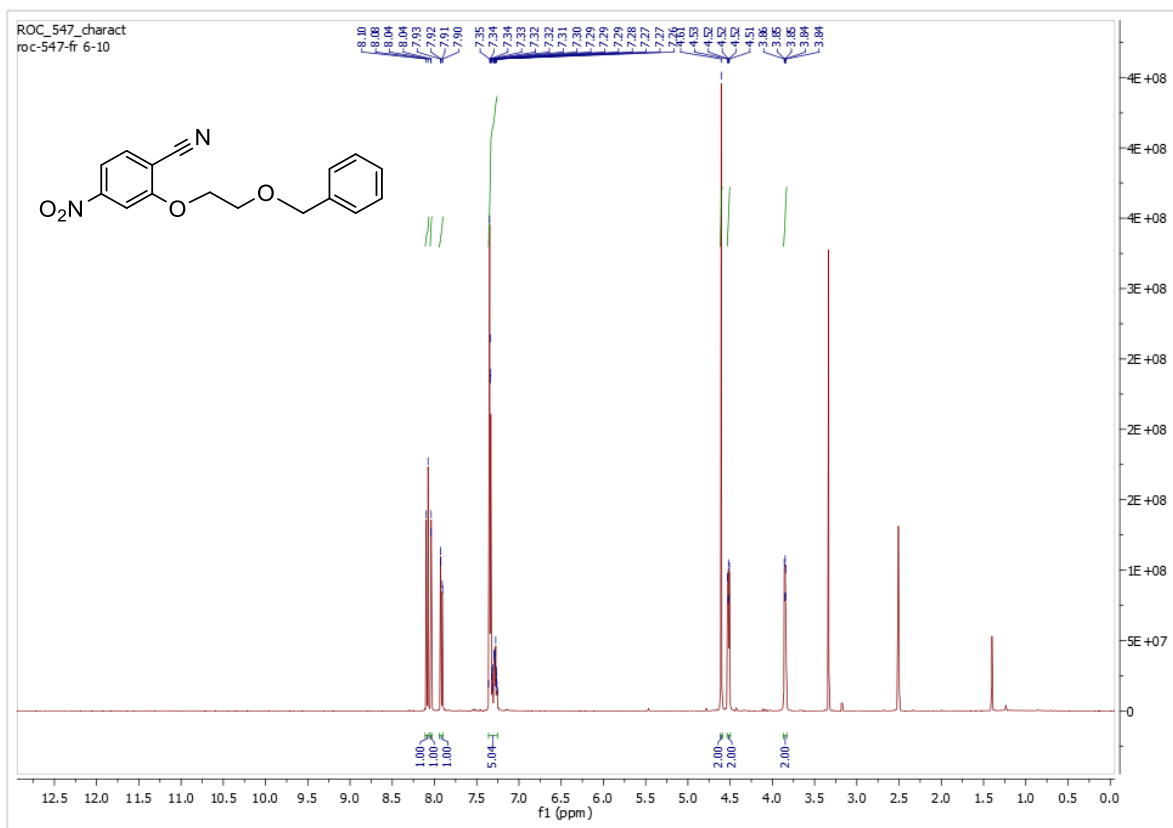


^1H , ^{13}C and ^{19}F NMR Spectra of 2-(2-fluoroethoxy)-4-nitrobenzonitrile **67d**

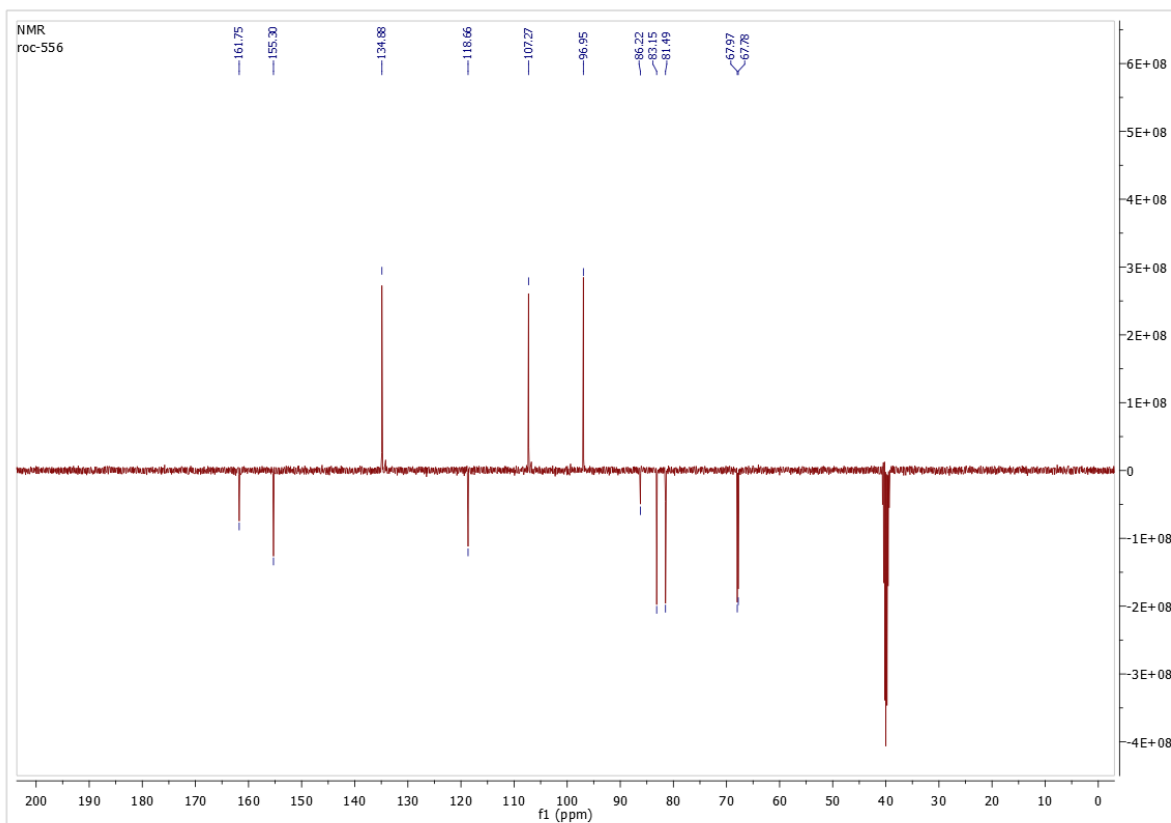
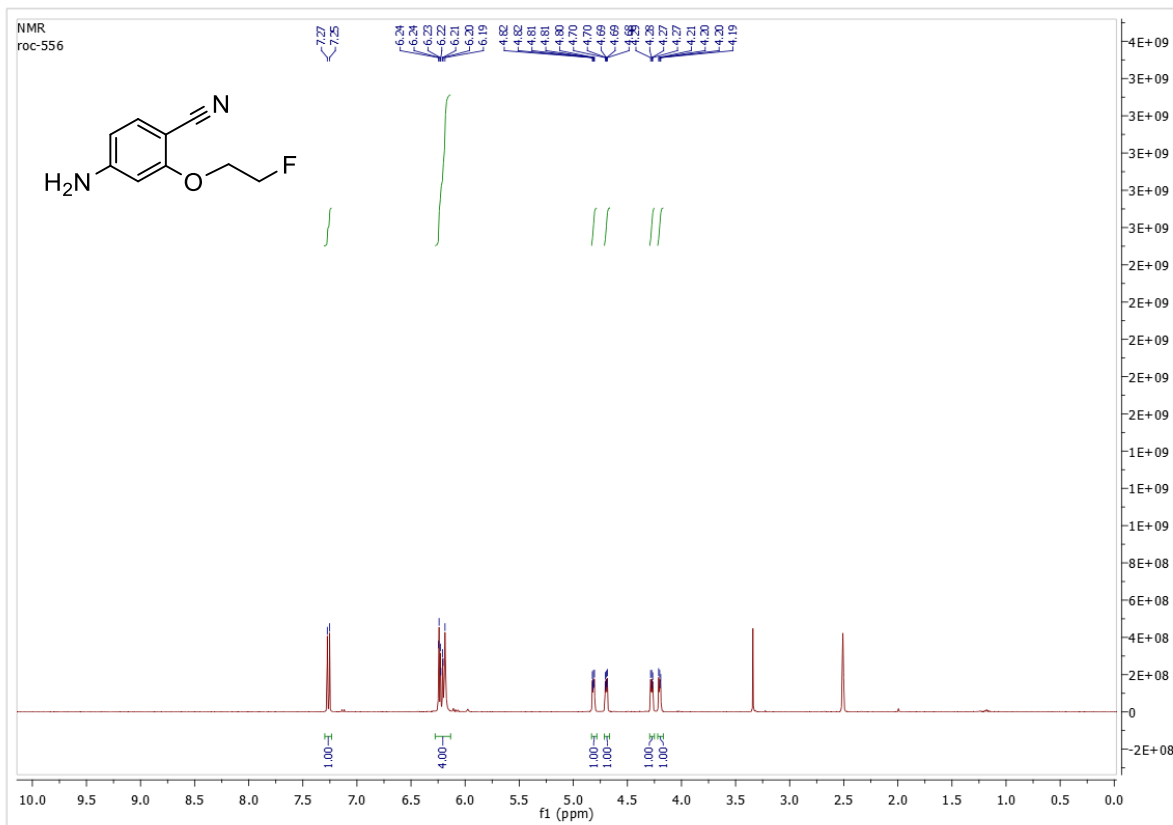


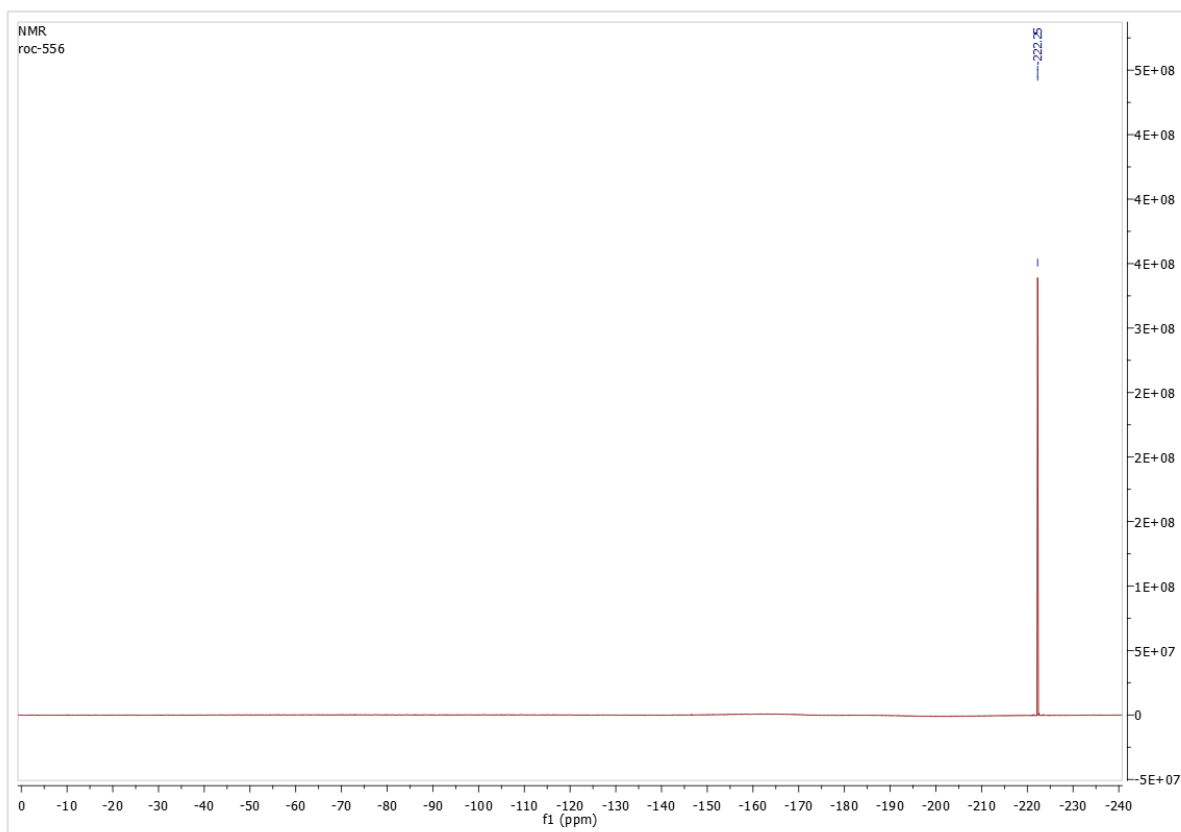


^1H and ^{13}C NMR Spectra of 2-(2-(benzyloxy)ethoxy)-4-nitrobenzonitrile **67g**

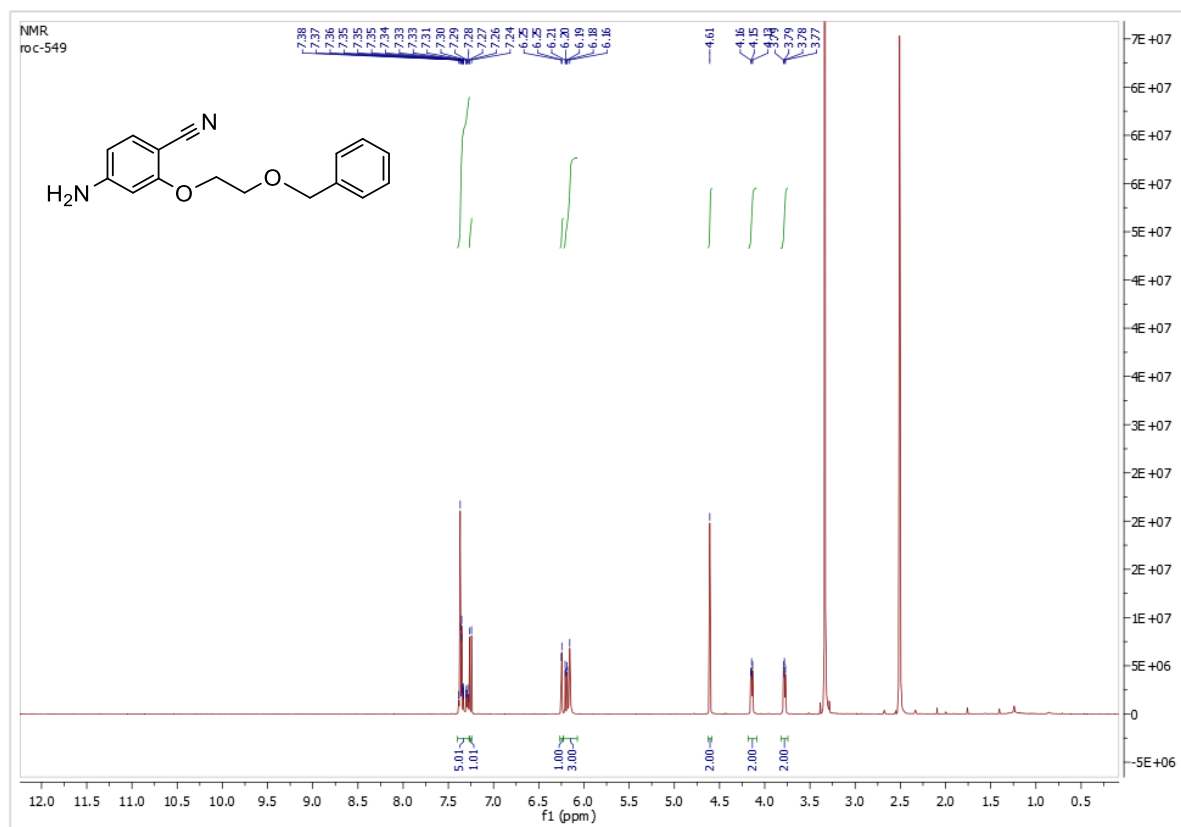


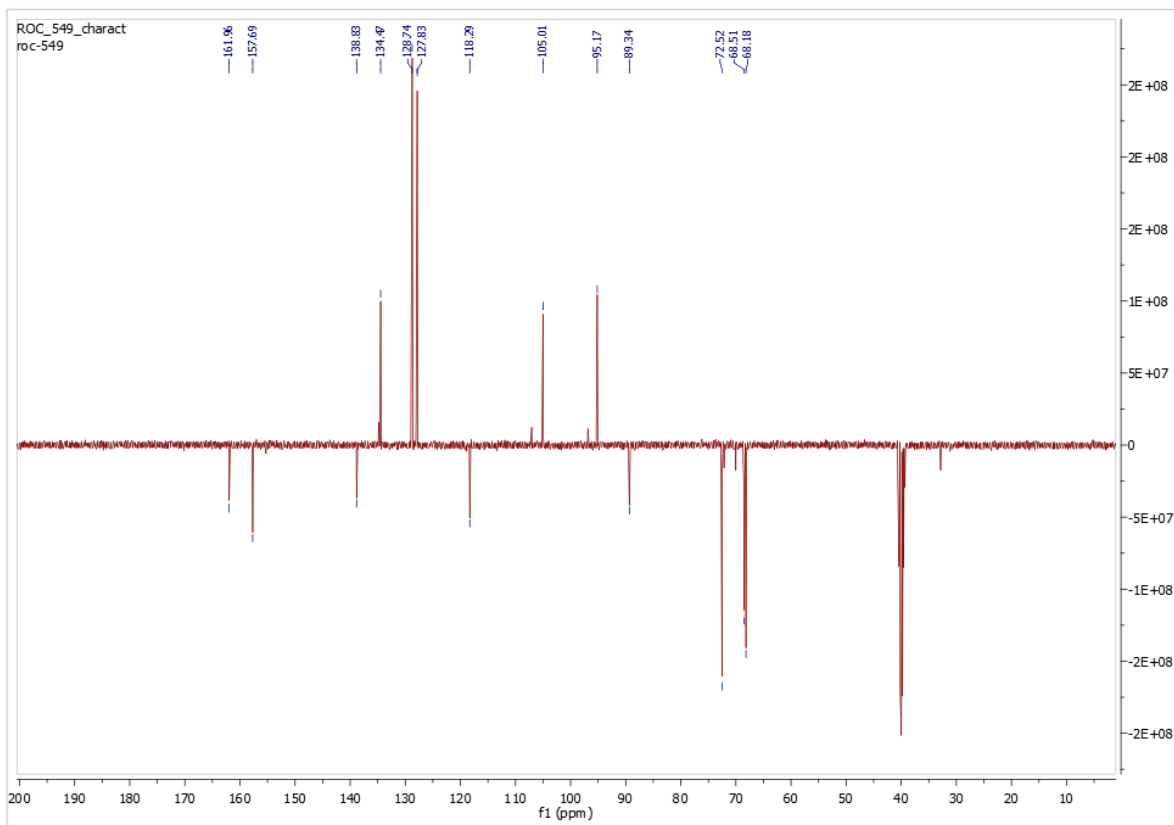
^1H , ^{13}C and ^{19}F NMR Spectra of 4-amino-2-(2-fluoroethoxy)benzonitrile **68d**



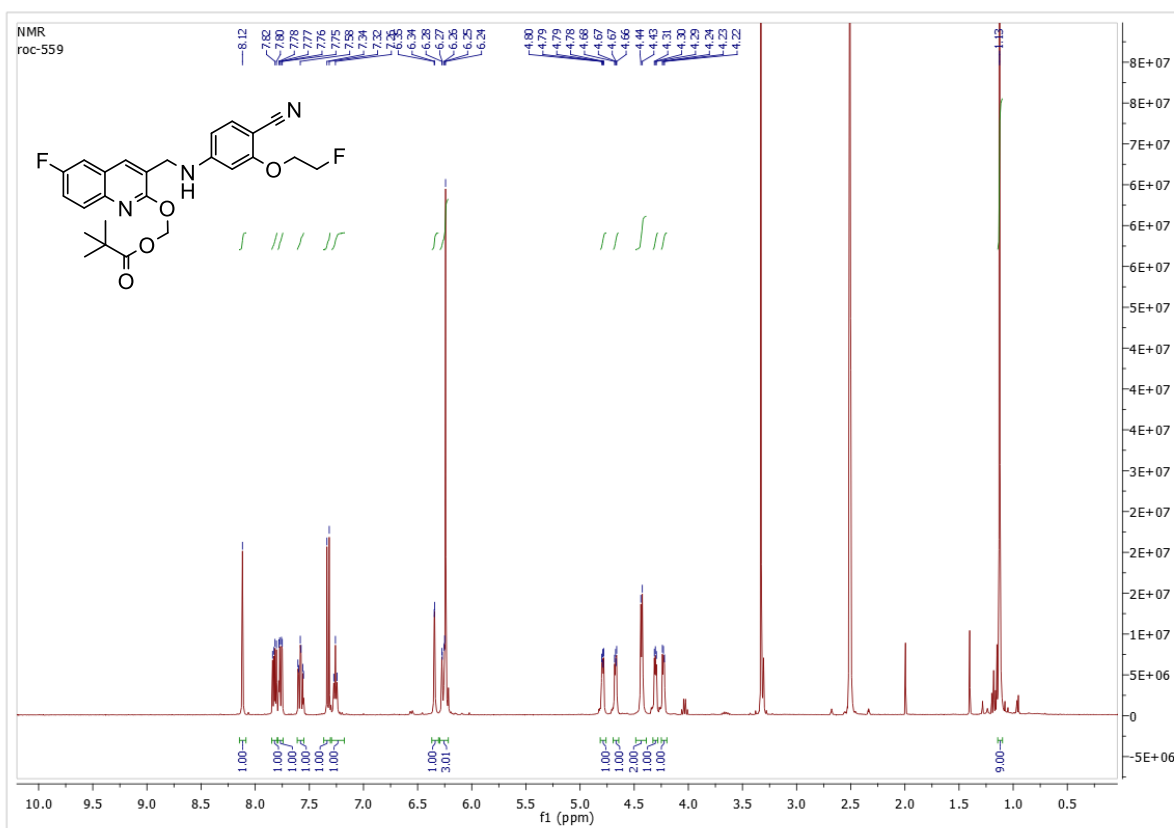


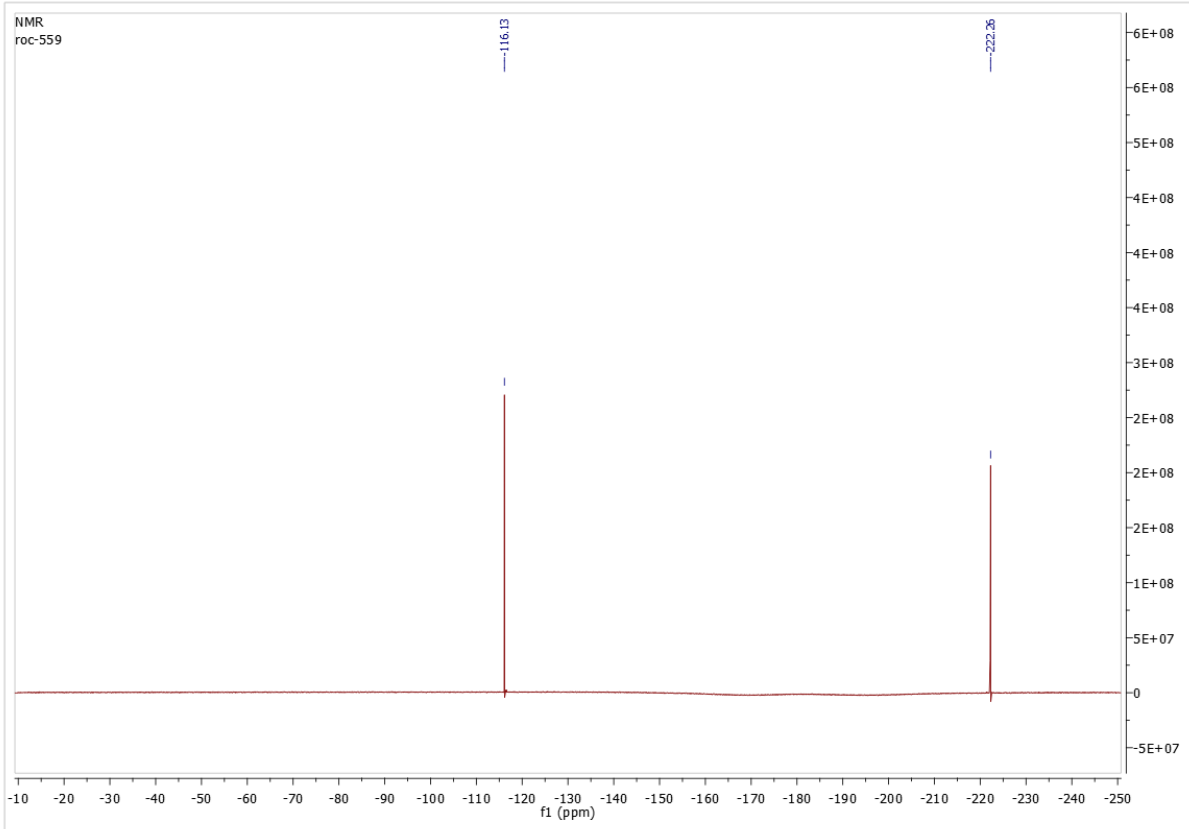
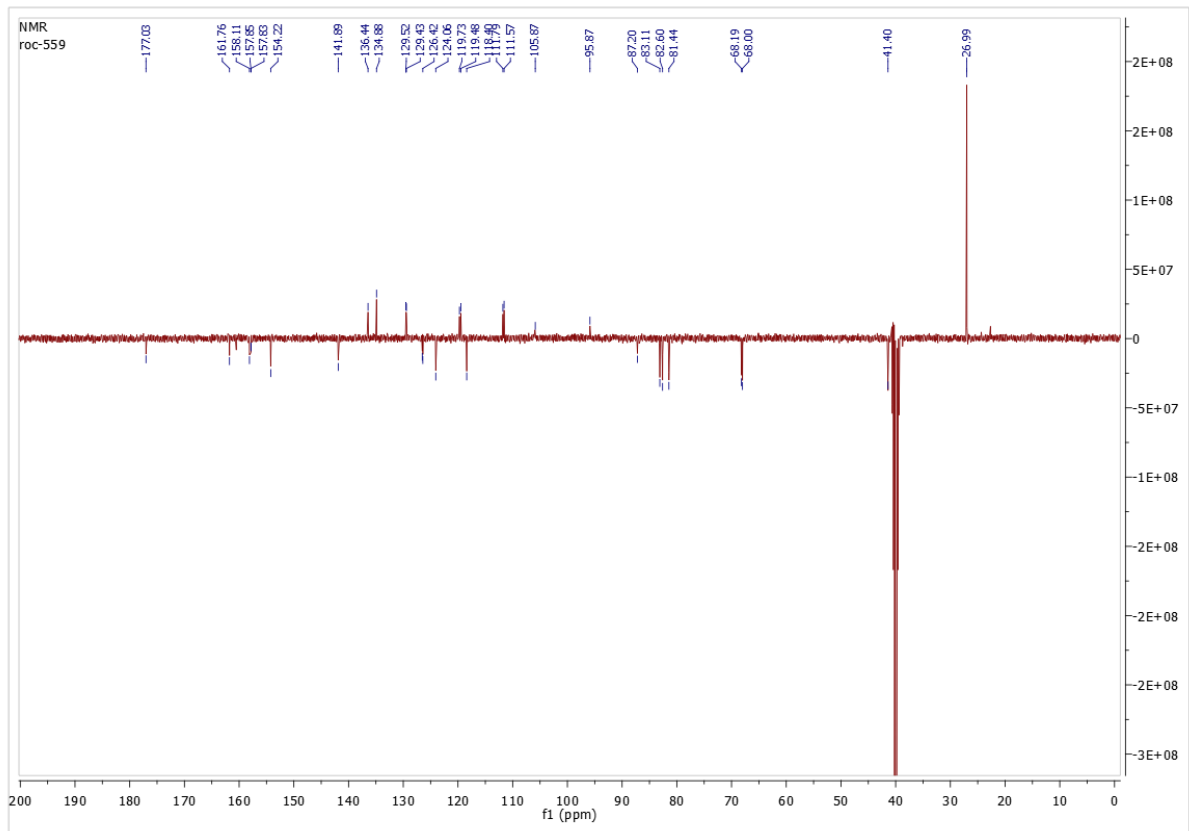
^1H and ^{13}C NMR Spectra of 4-amino-2-(2-(benzyloxy)ethoxy)benzonitrile **68g**



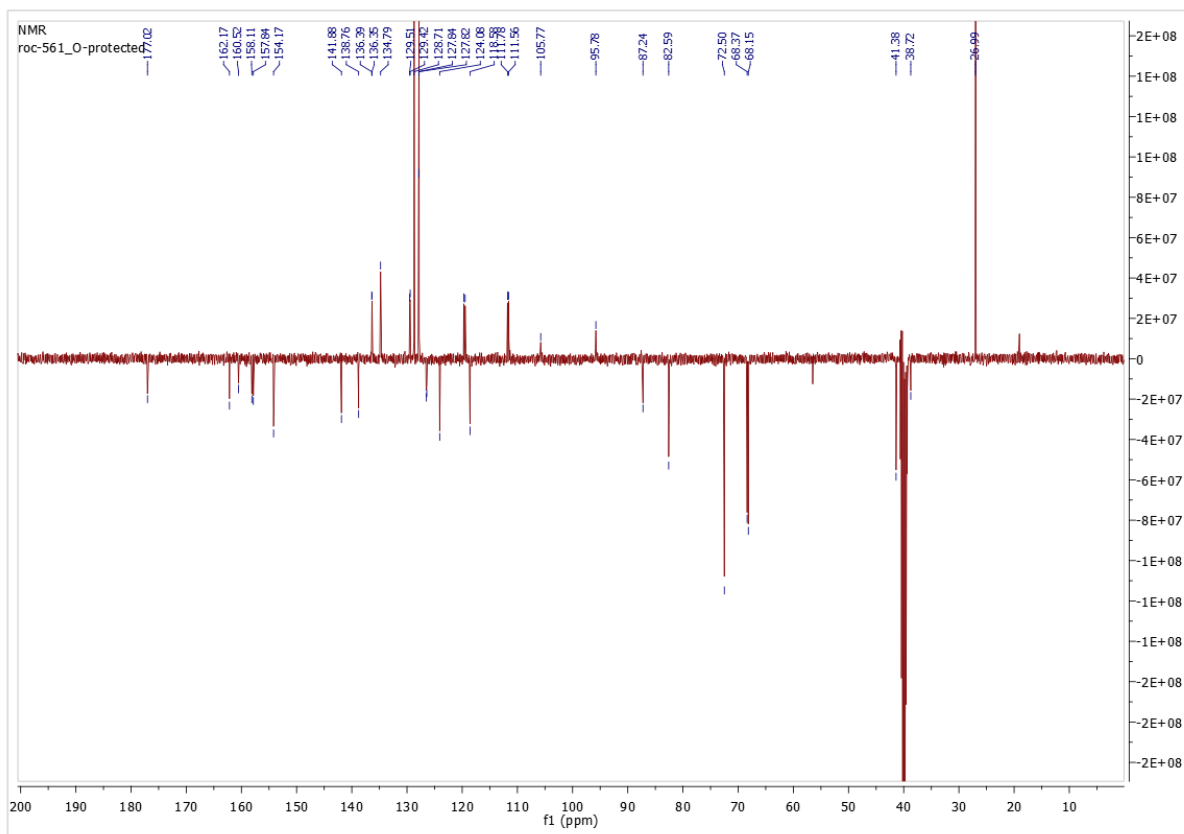
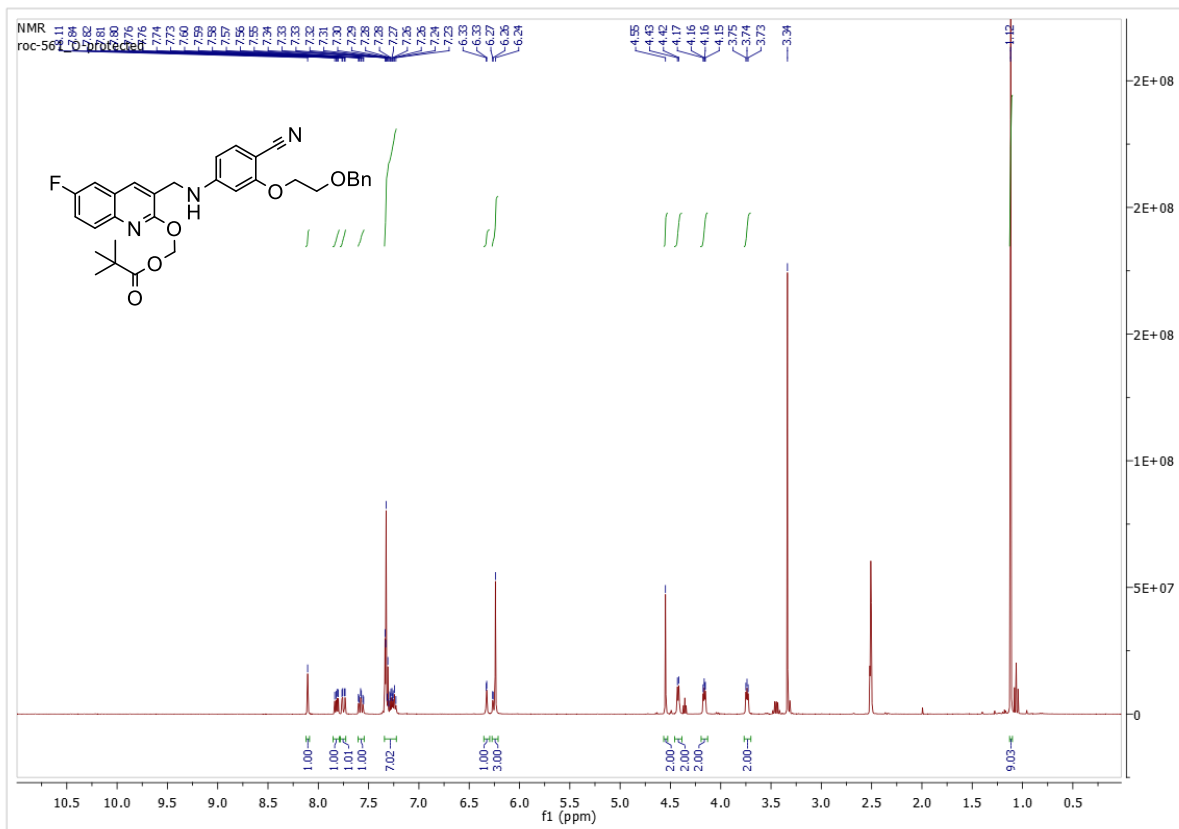


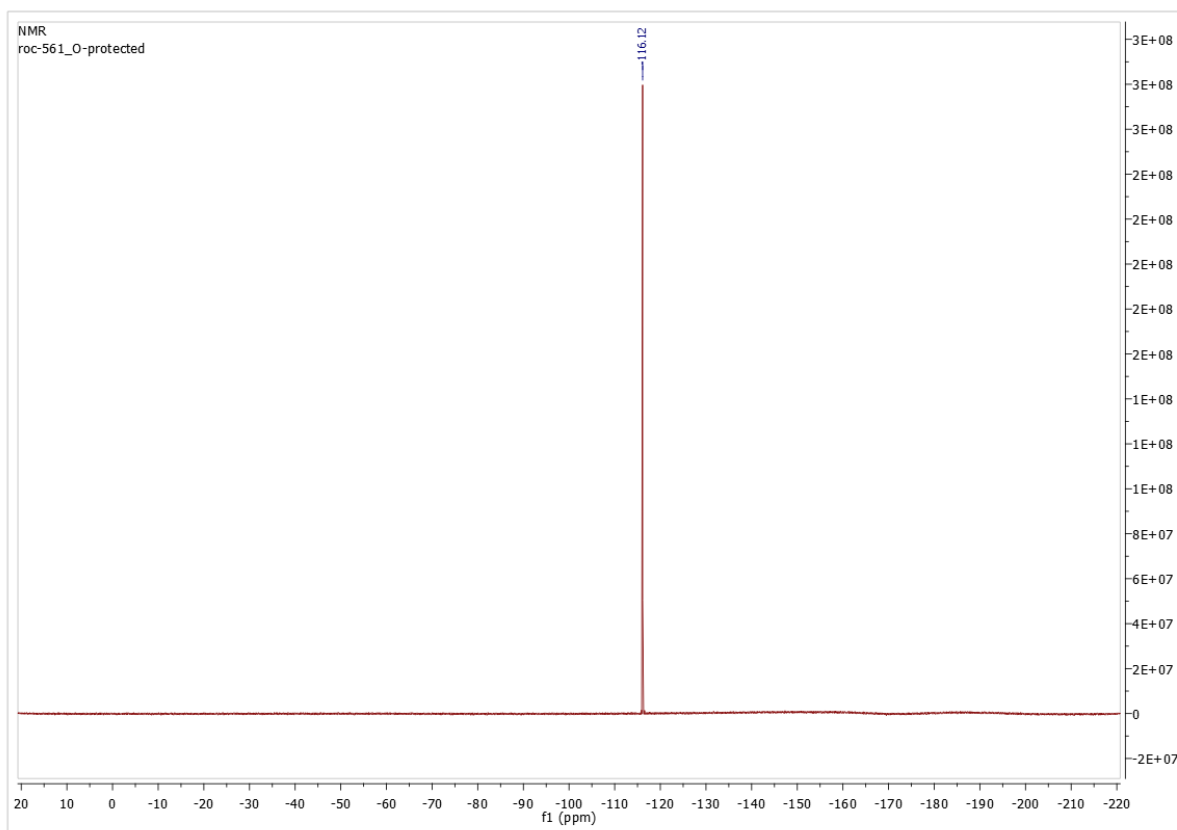
^1H , ^{13}C and ^{19}F NMR Spectra of ((3-(((4-cyano-3-(2-fluoroethoxy)phenyl)amino)methyl)-6-fluoroquinolin-2-yl)oxy)methyl pivalate **59d**



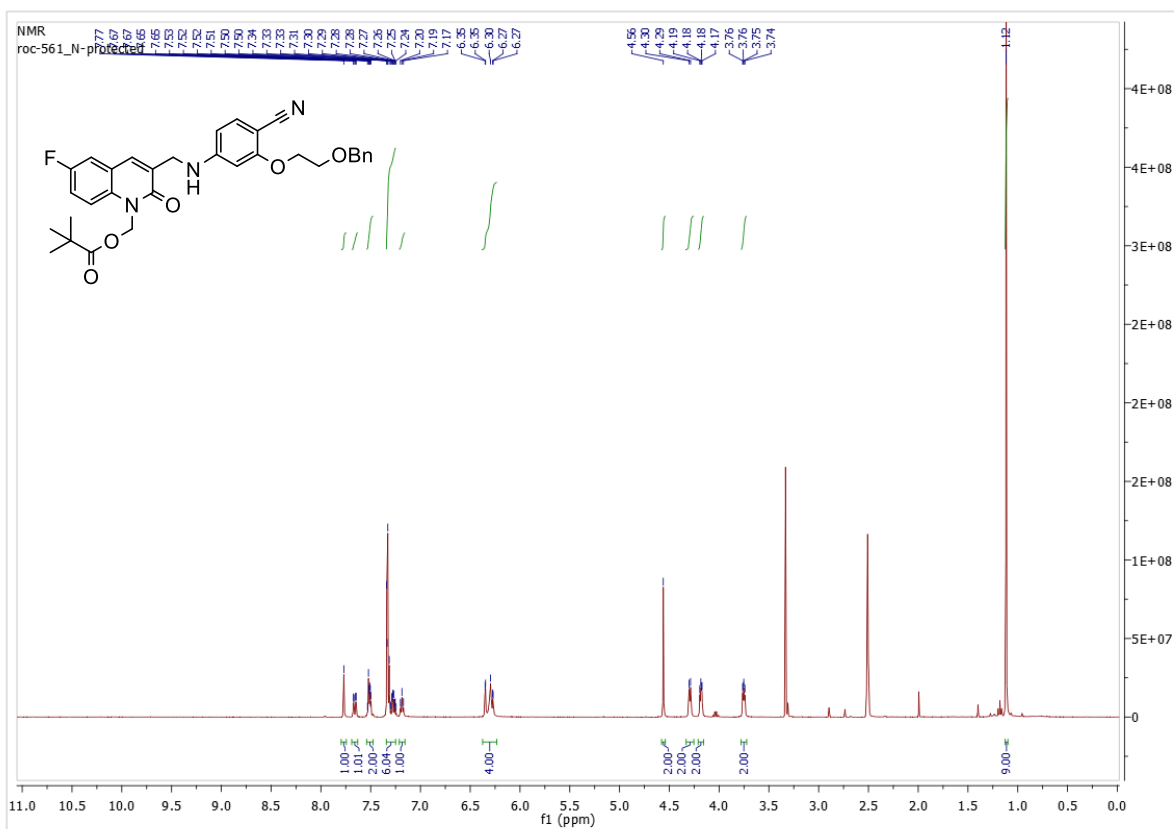


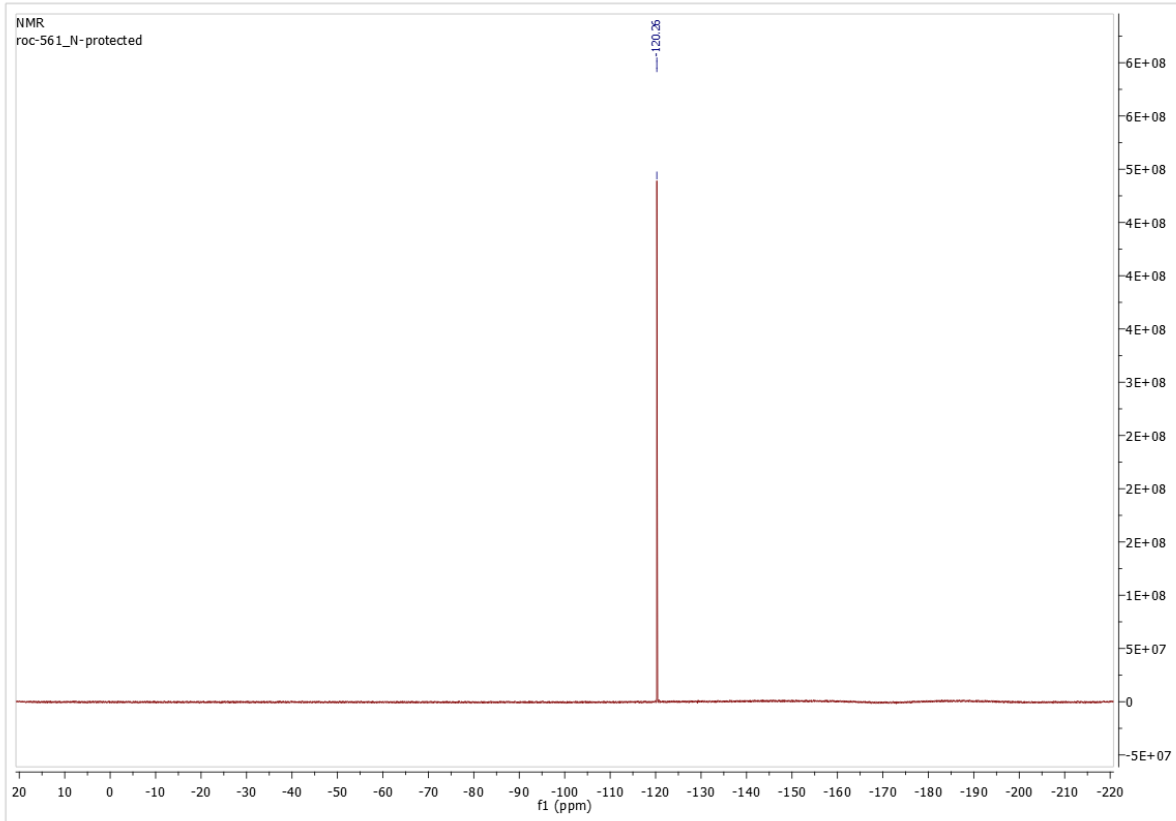
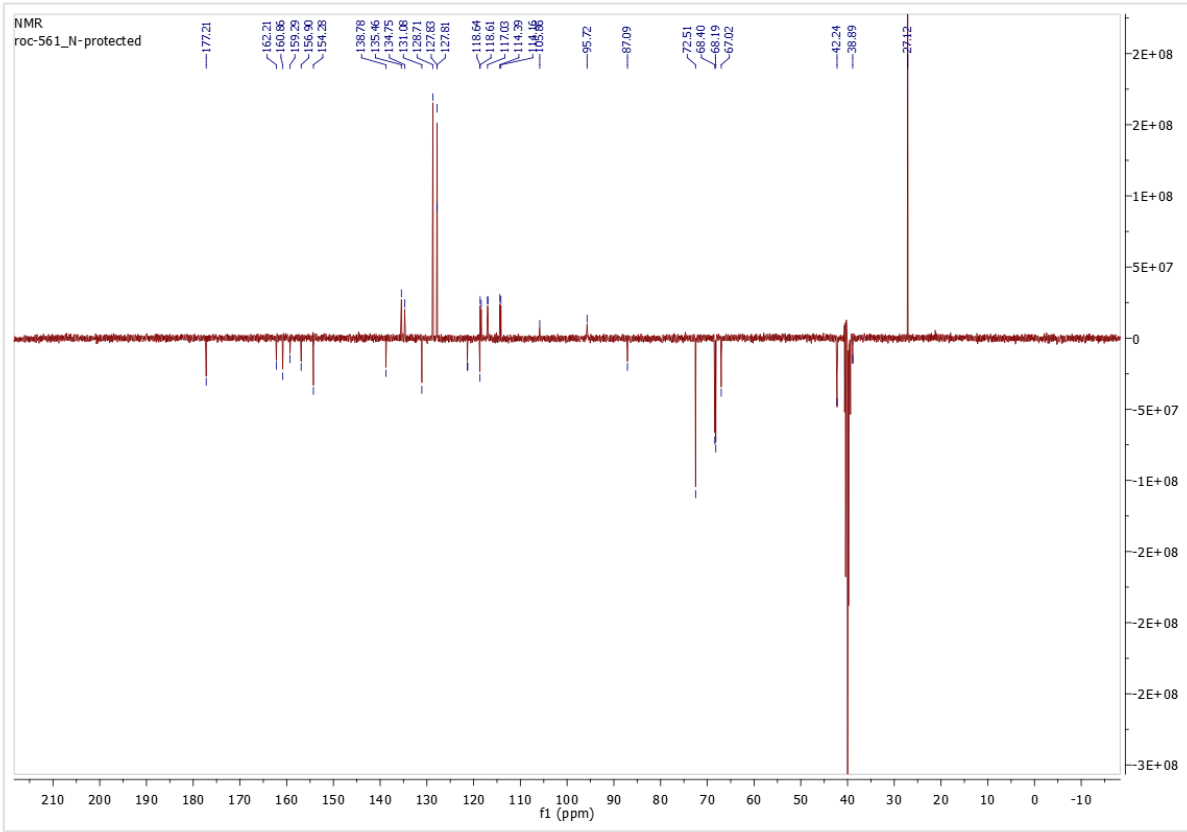
^1H , ^{13}C and ^{19}F NMR Spectra of 2-(2-cyano-5-(((6-fluoro-2-((pivaloyloxy)methoxy)quinolin-3-yl)methyl)amino)phenoxy)ethyl benzoate **59g**

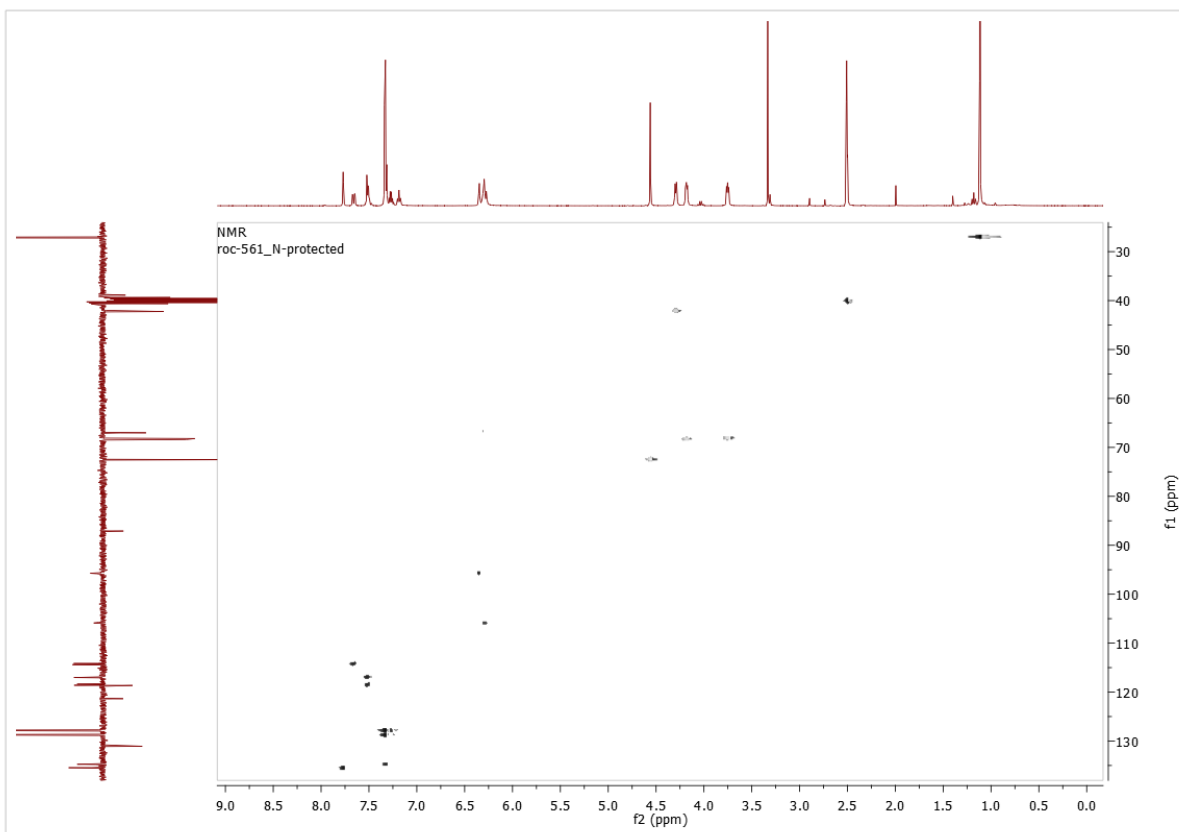




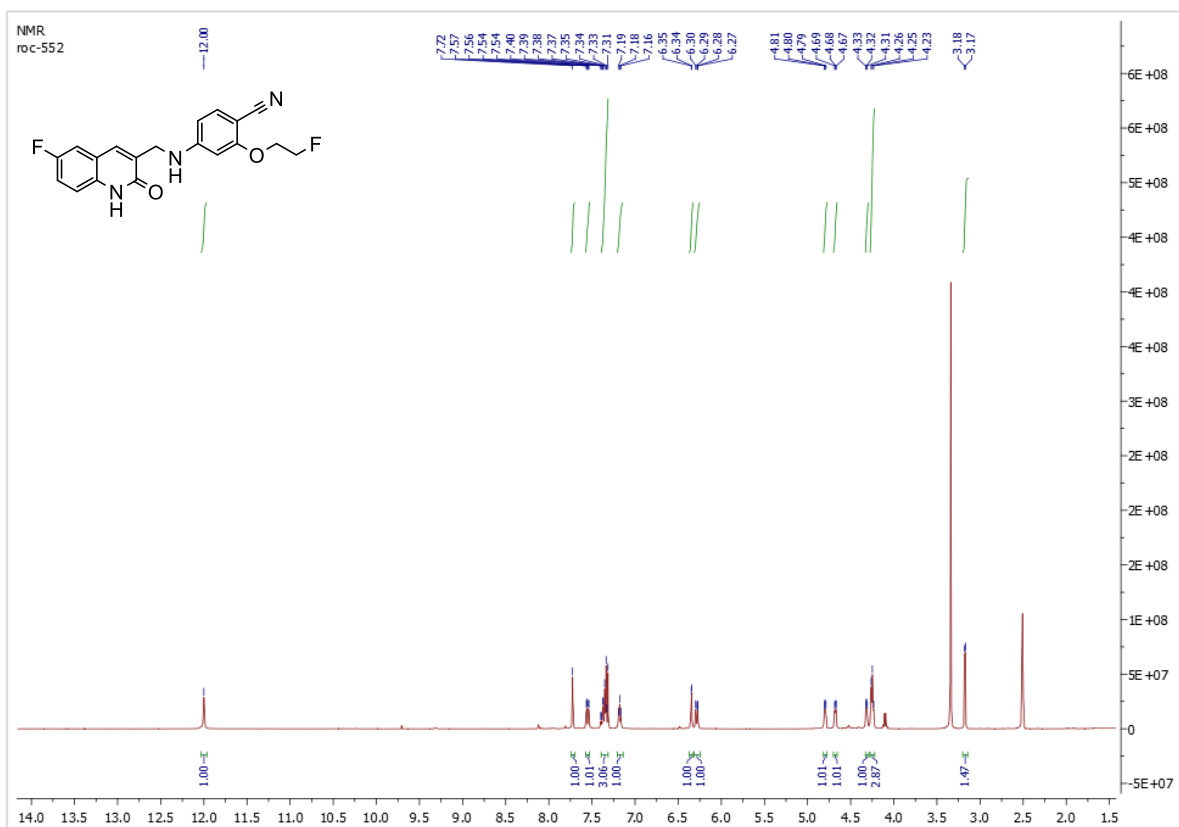
^1H , ^{13}C and ^{19}F NMR Spectra of 2-(2-cyano-5-(((6-fluoro-2-oxo-1-((pivaloyloxy)methyl)-1,2-dihydroquinolin-3-yl)methyl)amino)phenoxy)ethyl benzoate **60g**

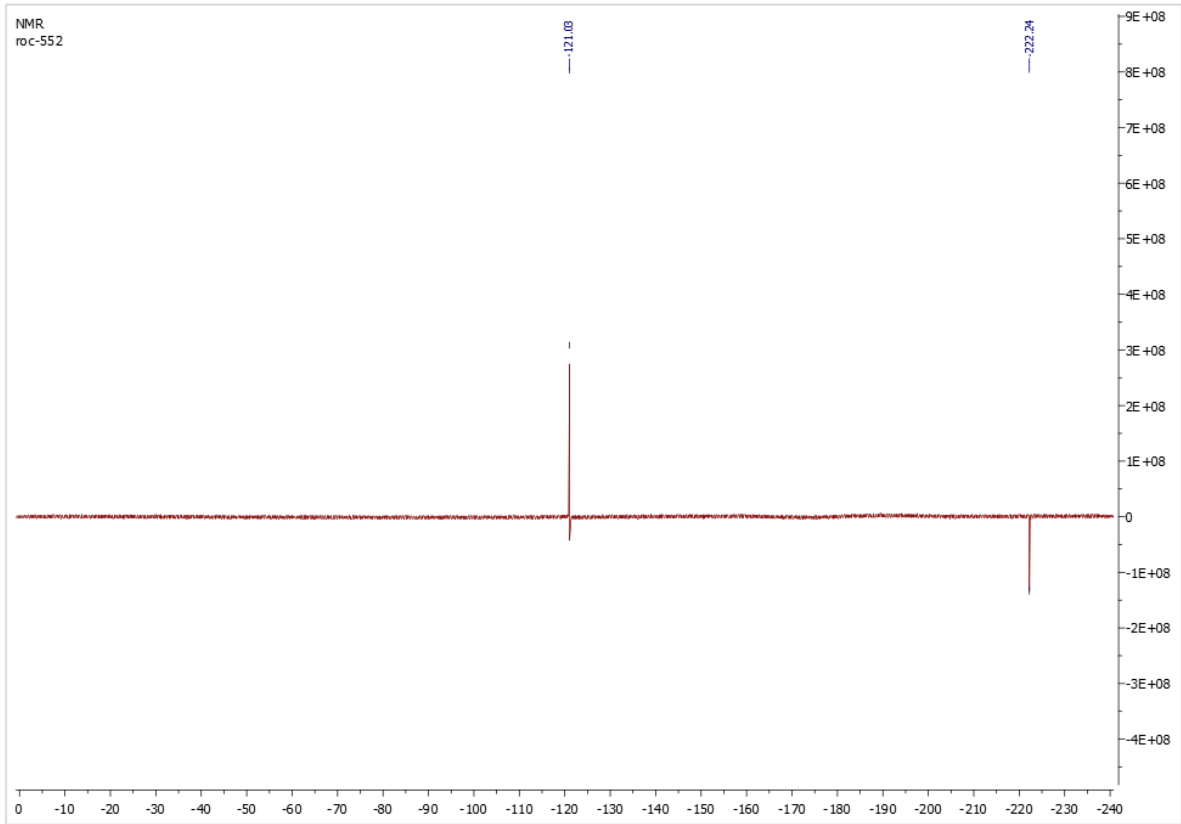
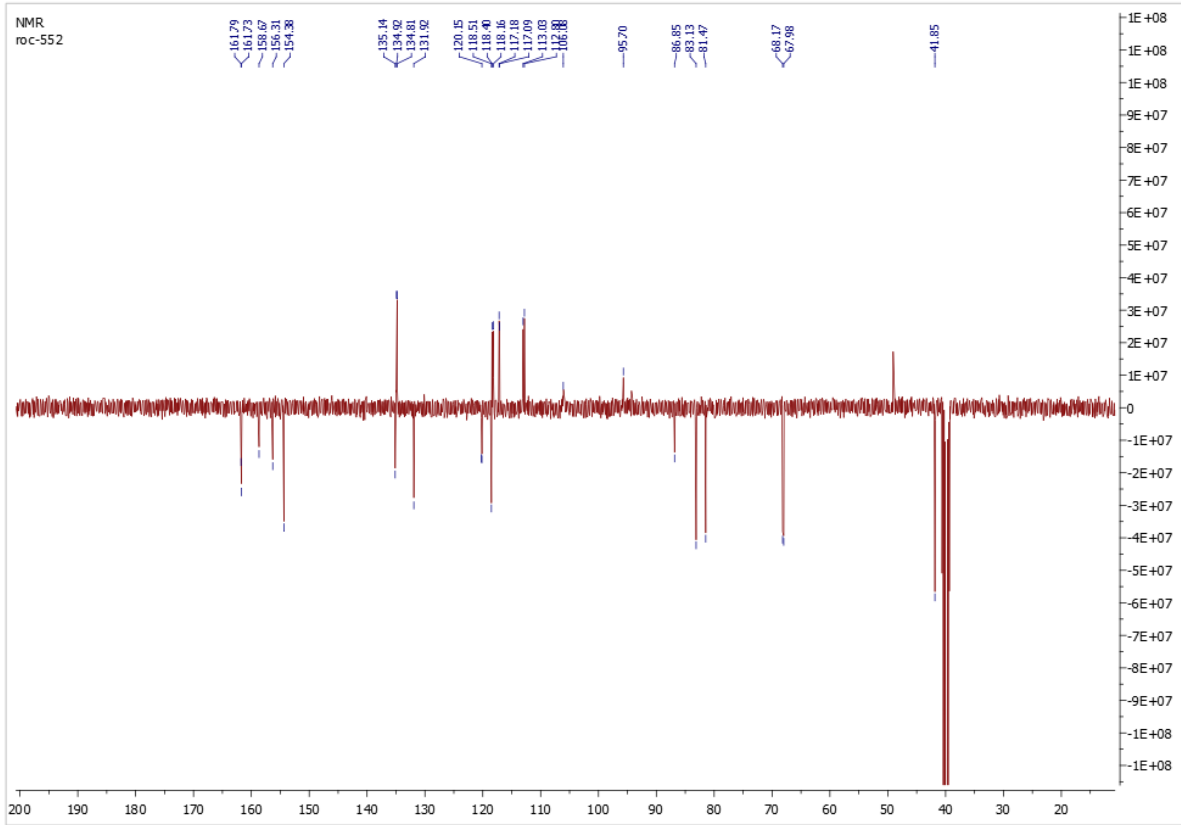




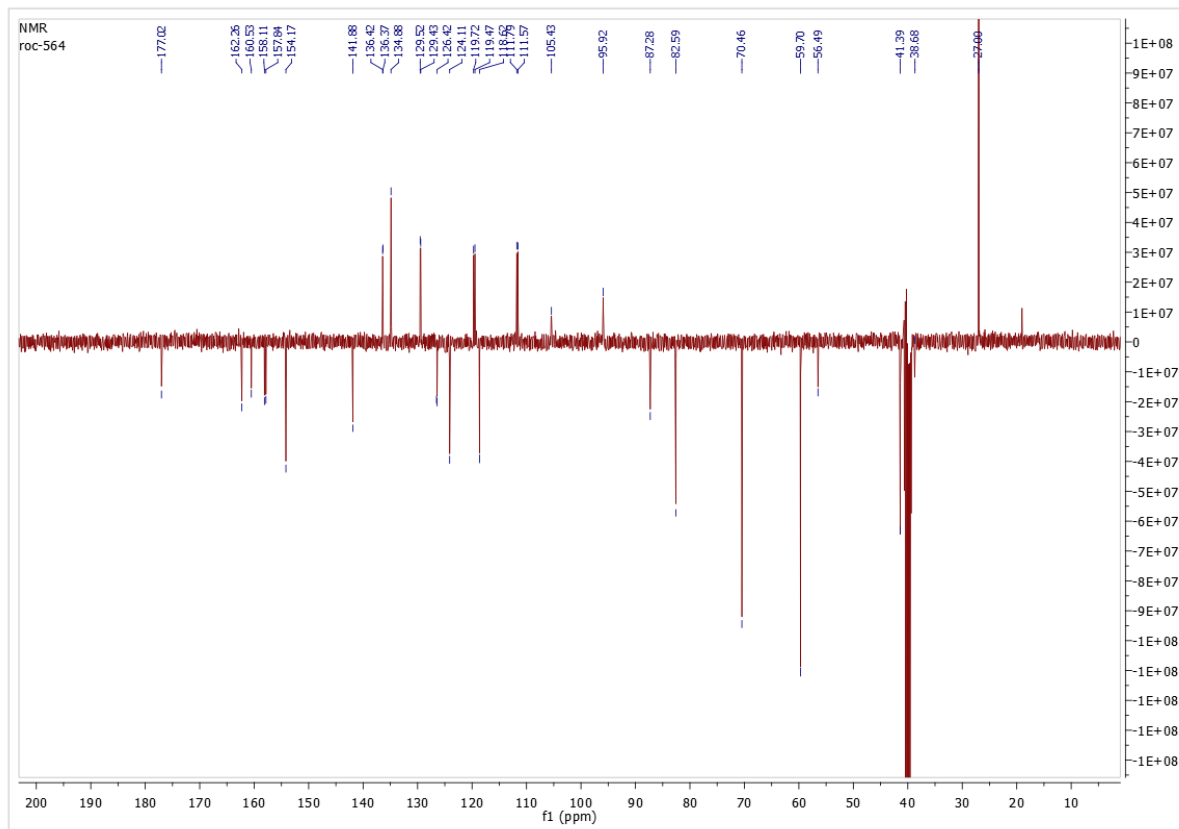
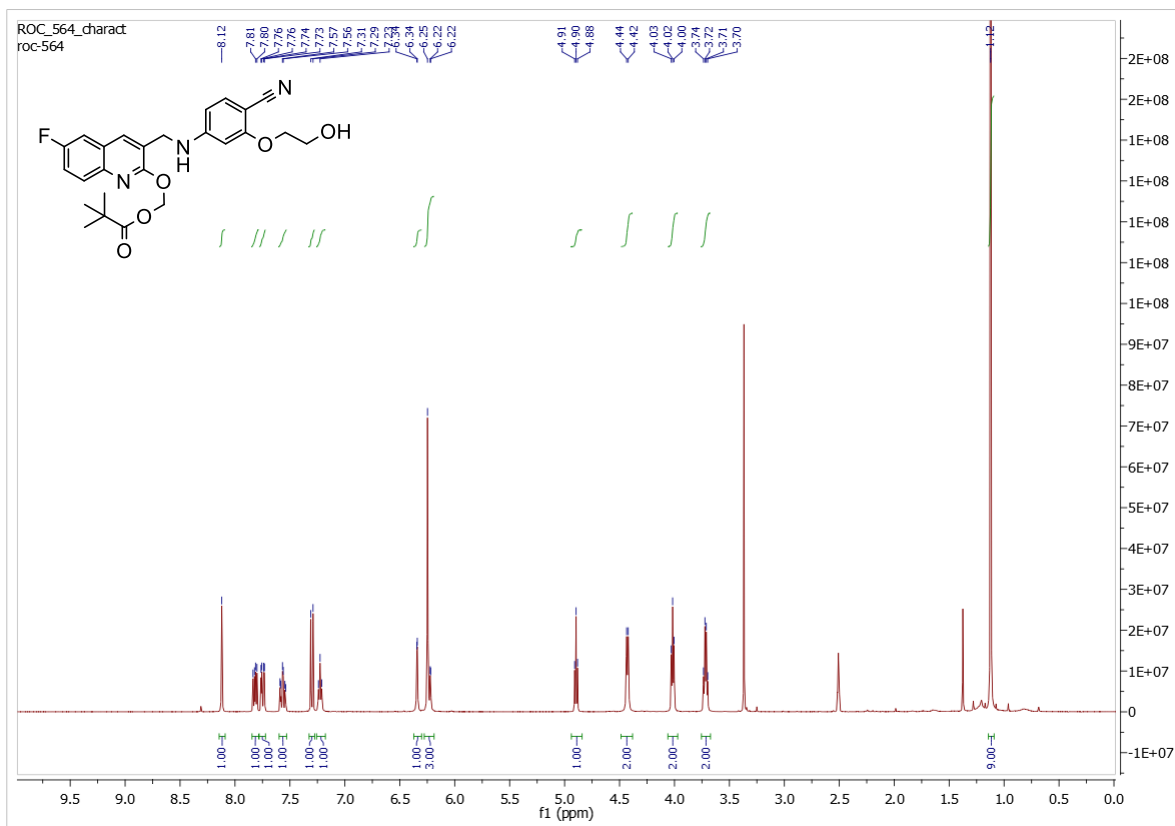


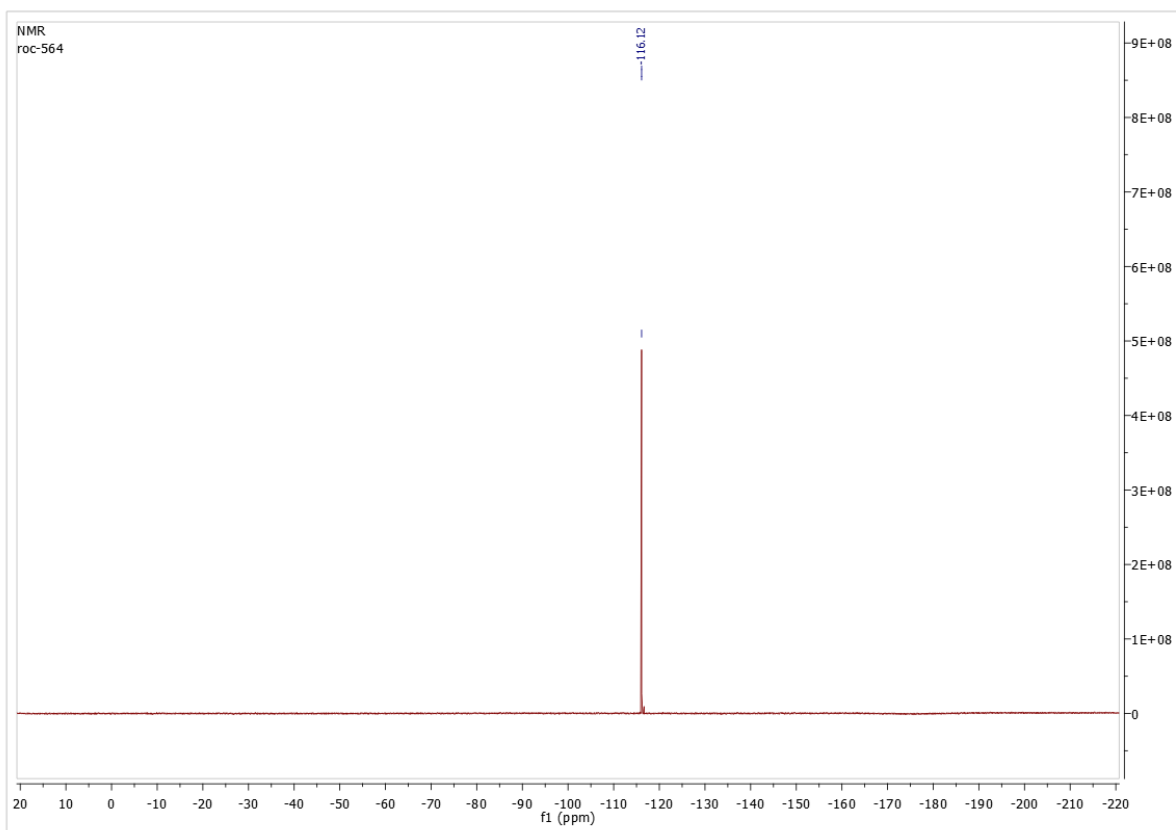
^1H , ^{13}C and ^{19}F NMR Spectra of 4-(((6-fluoro-2-oxo-1,2-dihydroquinolin-3-yl)methyl)amino)-2-(2-fluoroethoxy)benzonitrile **58d**



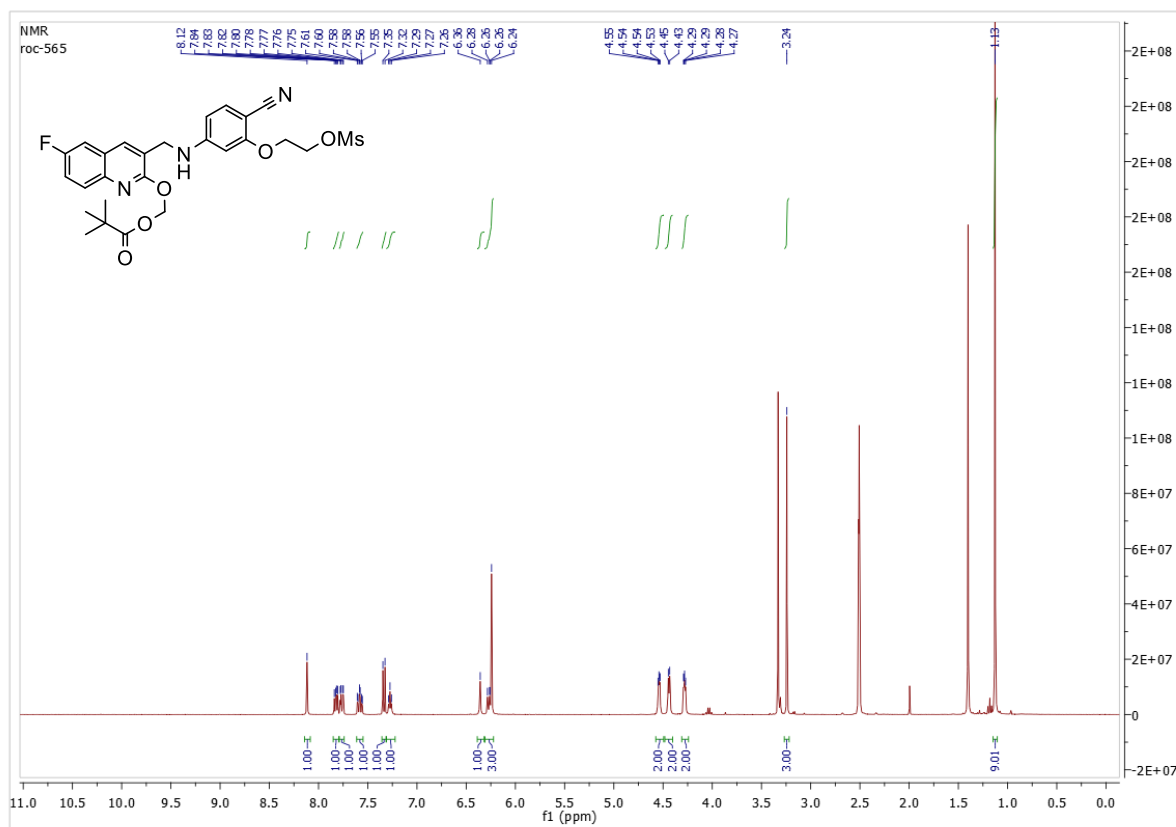


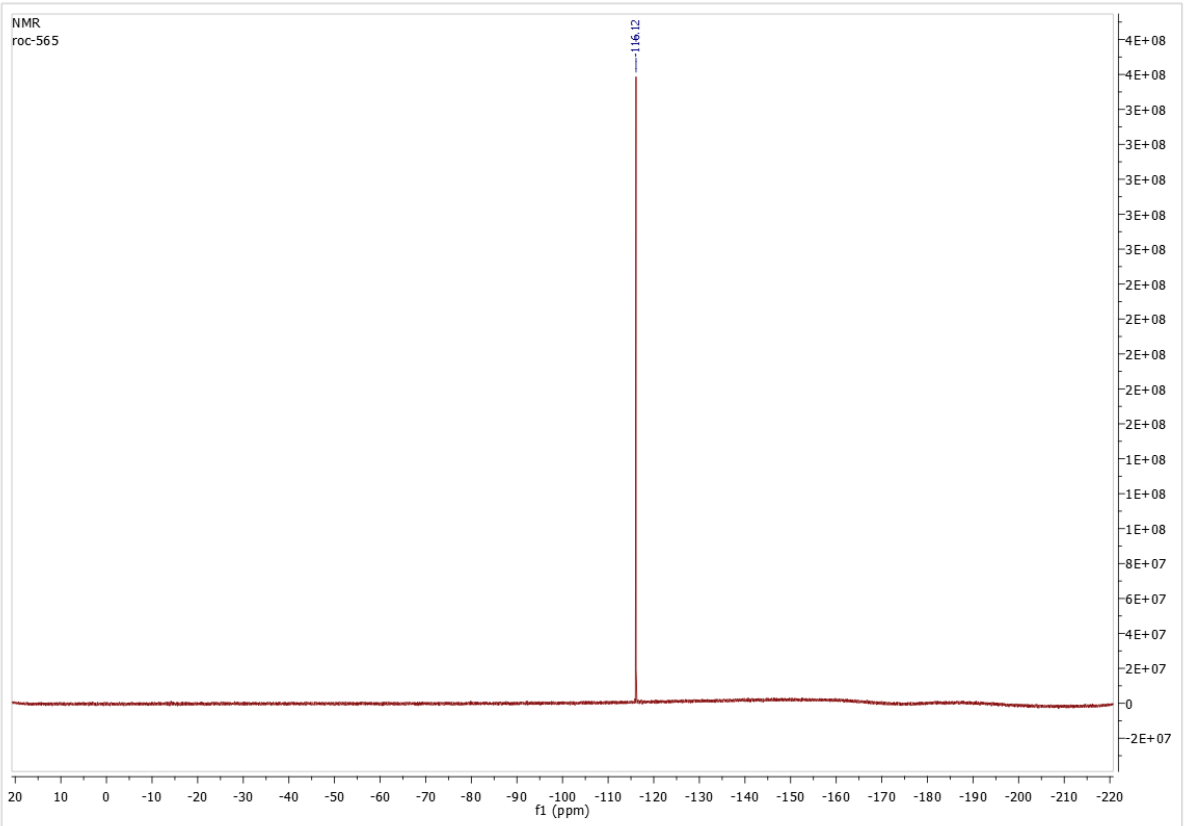
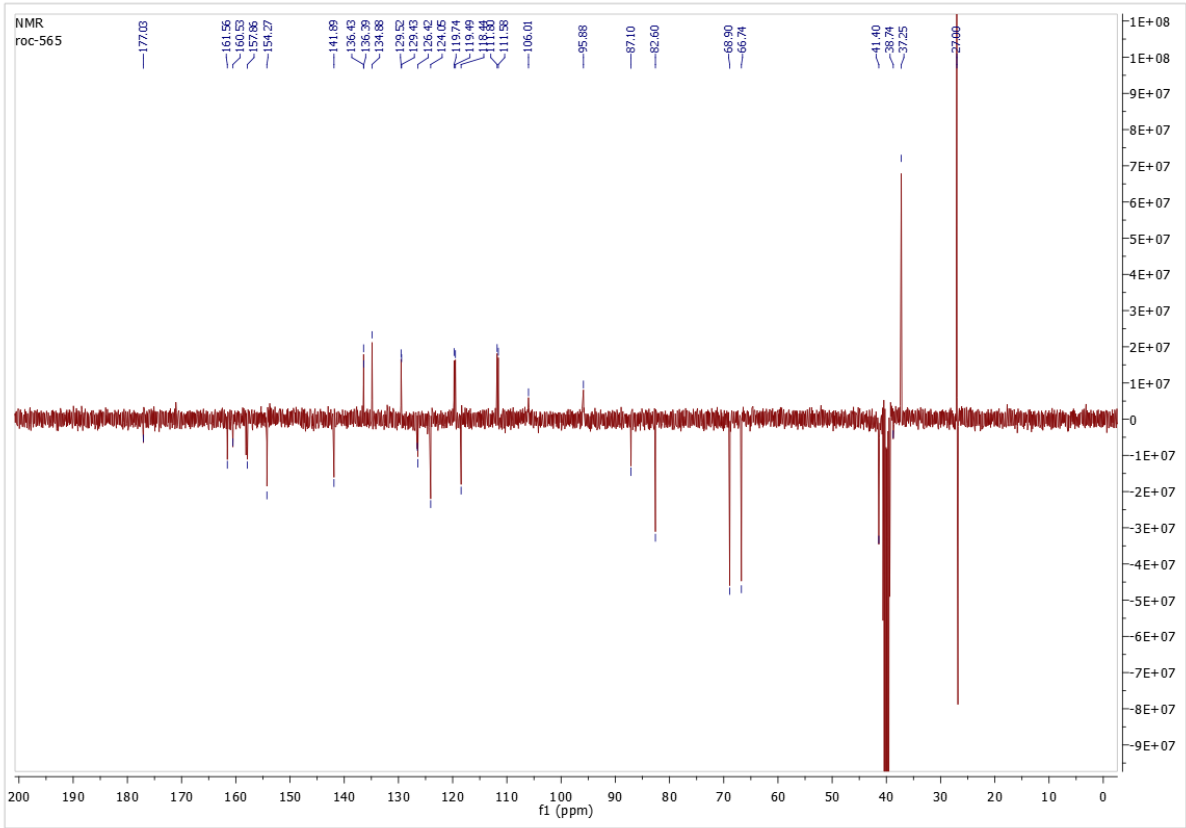
^1H , ^{13}C and ^{19}F NMR Spectra of ((3-(((4-cyano-3-(2-hydroxyethoxy)phenyl)amino)methyl)-6-fluoroquinolin-2-yl)oxy)methyl pivalate **61g**





^1H , ^{13}C and ^{19}F NMR Spectra of ((3-(((4-cyano-3-(2-((methylsulfonyl)oxy)ethoxy)phenyl)amino)methyl)-6-fluoroquinolin-2-yl)oxy)methyl pivalate **63**





7. Abbreviations

Ac	Acetyl
ACN	Acetonitrile
AcOEt	Ethylacetate
AcOH	Acetic acid
AEC	Anion exchange cartridge
Ala or A	Alanine
AML	Acute myeloid leukemia
Aq.	Aqueous
Arg or R	Arginine
A_m	Molar activity
A_s	Specific activity
Asp or D	Aspartic acid
ATCC	American Type Culture Collection
B_{max}	Maximum specific binding
BBB	Blood brain barrier
BCA	Bicinchoninic acid
Bn	Benzyl
Bq	Becquerel
Bpin	Boronic acid pinacol ester
(Bpin) ₂	Bis(pinacolato)diboron
BTC	Triphosgene
β^+	Positron
Calcd	Calculated
CAM	Chorio Allantoic Membrane
Cat	catalytic
[¹¹ C]DOPA	β -[¹¹ C]-L-3,4-dihydroxyphenylalanine
[¹¹ C]MET	L-[methyl- ¹¹ C]methionine
conc.	Concentrated
CNS	Central nervous system
CT	Computed tomography
<i>d</i>	Doublet
d	Days
DBU	1,8-Diazabicyclo[5.4.0]undec-7-ene
DCE	Dichloroethane
DIPEA	N,N-diisopropylethylamine
DMA	Dimethylacetamide
DMAP	4-Dimethylaminopyridine
DMF	Dimethylformamide
DMI	1,3-Dimethyl-2-imidazolidinone

DMSO	Dimethylsulfoxide
E	Enzyme
$E\beta^+$	Positron energy
EDD	Estimated delivery day
ELSD	Evaporation light scattering detector
eq.	Equivalents
ES	Enzyme-substrate complex (Michaelis complex)
ESI	Electron-spray ionization
Et	Ethyl
EtOH	Ethanol
EWG	Electron-withdrawing group
FBS	fetal bovine serum
$[^{18}\text{F}]\text{FDG}$	2-deoxy-2- $[^{18}\text{F}]$ fluoroglucose
Fig	Figure
$[^{18}\text{F}]\text{FET}$	L- $[^{18}\text{F}]$ fluoroethyltyrosine
$[^{18}\text{F}]\text{FMISO}$	$[^{18}\text{F}]$ -fluoromisonidazole
FZJ	Forschungszentrum Jülich (Research center Jülich)
g	Gram
GBq	Gigabecquerel
GBM	Glioblastoma
Glide	Grid-based Ligand Docking with Energetics
Gln or Q	Glutamine
Glu or E	Glutamic acid
h	Hour
Hex	Hexane
2HG	2-(<i>R</i>)-Hydroxyglutarate
HGG	High-grade gliomas
HLB	Hydrophilic-lipophilic balance cartridge
HPLC	High performance liquid chromatography
HRMS	High resolution mass spectrometry
Hys or H	Hystidine
IC_{50}	half maximum inhibitory concentration
ICT	Isocitrate
IDH	Isocitrate dehydrogenase
Ile or I	Isoleucine
INM	Institut für Neurowissenschaften und Medizin (Institute for Neuroscience and Medicine)
J	Coupling constant
J	Joule
k_{Binding}	Association constant
K_{D}	Dissociation equilibrium constant

$k_{\text{Dissociation}}$	Dissociation constant
K_{eq}	Equilibrium constant
keV	kiloelectronvolt
α -KG	α -Ketoglutarate
K_i	Inhibitory constant
K_M	Michaelis constant
K222	Kryptofix [®] 222
k_1	Association constant (enzymes)
k_2	Product formation constant (enzymes)
k_{-1}	Dissociation constant (enzymes)
L	Liter
LAT1	L-type amino acid transporter
Leu or L	Leucine
LG	Leaving group
LGG	low-grade glioma
log	logarithm
logD	Partition coefficient
logP	Octanol-water partition coefficient
m	multiplet
m -	<i>meta</i>
m	milligrams
M	Molar
max	Maximum
MBq	Mega Becquerel
mCPBA	meta-chloroperoxybenzoic acid
MD	Molecular dynamics
Me	Methyl
MEM	Eagle's Minimum Essential Medium
MeOH	Methanol
mIDH	Mutant Isocitrate dehydrogenase
min	Minutes
mol	Mole
M.p.	Melting point
MRI	Magnetic Resonance Imaging
MS	Mass spectrometry
n	neutron
NADP ⁺	Nicotinamide adenine dinucleotide phosphate (oxidized form)
NADPH	Nicotinamide adenine dinucleotide phosphate (reduced form)
NaOH	Sodium hydroxide
n.c.a.	Non carrier added
NMM	N-Methylmorpholine

NMR	Nuclear magnetic resonance spectroscopy
NOTA	1,4,7-triazacyclononane-1,4,7-triacetic acid
<i>o</i> -	<i>ortho</i> -
OMs	Mesylate
OTf	Triflate
OTs	Tosylate
<i>p</i>	quintet
<i>p</i> -	<i>para</i> -
P	Protein
PBS	Phosphate buffer
Pd(dppf)Cl ₂	[1,1'-Bis(diphenylphosphino)ferrocene]dichloropalladium(II)
PET	Positron Emission Tomography
PPA	Polyphosphoric acid
ppm	Parts per million
Pr	Propyl
PSMA	Prostate-specific membrane antigen
PTSE	Polytetrafluoroethylene (Teflon)
<i>q</i>	quartet
QMA	Quaternary methyl ammonium cartridge
R	Receptor
R _f	Relation to front
RCC	Radiochemical conversion
RCY	Radiochemical yield
RMSD	Root Mean Square Deviation
RP	Reversed phase
rt	Room temperature
<i>s</i>	singlet
s	Seconds
S	Substrate
sat	Saturated
S _N 1	Nucleophilic substitution 1
S _N 2	Nucleophilic substitution 2
S _N Ar	Nucleophilic aromatic substitution
sol	Solution
SPE	Solid phase extraction
SPECT	Single photon emission computed tomography
<i>t</i>	triplet
t	Time
t _R	Retention time
t _{1/2}	Half life
TBAB	Tetrabutylammonium bicarbonate

tBuOH	<i>tert</i> -Butanol
TCTA	4,4',4'-Tris(carbazol-9-yl)triphenylamine
TEA	Triethylamine
TEAB	Tetraethylammonium bicarbonate
TET	(2S)-O-(2'-tosyloxyethyl)-N-trityl-tyrosine- <i>tert</i> -butyl ester
TET2	Tet methylcytosine dioxygenase 2
TFA	Trifluoroacetic acid
TFAA	Trifluoroacetic anhydride
THF	Tetrahydrofurane
TLC	Thin layer chromatography
Trp or W	Tryptophan
Tyr or Y	Tyrosine
UHP	Urea hydrogen peroxide
UV	Ultraviolet
U87-MG	Uppsala 87 Malignant Glioma
Val or V	Valine
VHR	Vilsmeier-Haack reagent
v_1	Velocity of association
v_{-1}	Velocity of dissociation
v_2	Velocity of product formation
v_{\max}	Maximum velocity
WHO	World health organization
wtIDH	Wild type IDH
y	Yield
°C	Celsius degrees
Å	Ångström

8. Literature

- ¹ Kratz, J.V., Lieser, K.H. Nuclear and Radiochemistry: Fundamentals and Applications (2013), Chapter 11: Techniques in nuclear chemistry.
- ² Myers WG. Georg Charles de Hevesy: the father of nuclear medicine. *J Nucl Med.* (1979), 20(6), 590-594
- ³ Detected Events in Positron Tomography, European medical.info, last revised 17.05.2023
- ⁴ Halder R., Ritter T., 18F-Fluorination: Challenge and Opportunity for Organic Chemists. *J. Org. Chem.* (2021) 86, 13873-13884.
- ⁵ Fiechter M, Ghadri JR, Gebhard C, Fuchs TA, Pazhenkottil AP, Nkoulou RN, Herzog BA, Wyss CA, Gaemperli O, Kaufmann PA. Diagnostic value of ¹³N-ammonia myocardial perfusion PET: added value of myocardial flow reserve. *J Nucl Med.* (2012),1230-4.
- ⁶ Maaniitty T, Knuuti J, Saraste A. ¹⁵O-Water PET MPI: Current Status and Future Perspectives. *Semin. Nucl. Med.* (2020), 50(3):238-247.
- ⁷ Kołodziej M, Bober B, Saracyn M, Kamiński G. The role of PET/CT with ¹¹C-Methionine in contemporary nuclear medicine. *Wiad Lek.* (2020), 73(9), 2076-2079.
- ⁸ Meanwell N.A. Fluorine and Fluorinated Motifs in the Design and Application of Bioisosteres for Drug Design. *J Med Chem.* (2018) 61, 5822-5880.
- ⁹ Swallow S. Fluorine in medicinal chemistry. *Prog Med Chem.* (2015), 54, 65-133.
- ¹⁰ Banerjee S.R., Pomper MG. Clinical applications of Gallium-68. *Appl Radiat Isot.* (2013), 76, 2-13.
- ¹¹ Policroniades R., Moreno E., Varela A., Murillo G., Huerta A., Ortiz M.E., Chávez E., F-18 production by means of ²⁰Ne(d,4He) reaction at ININ, *Revista mexicana de Fisica* (2008) 54, 46-49.
- ¹² de Goeij, J. J. M.; Bonardi, M. L. How do we define the concepts specific activity, radioactive concentration, carrier, carrier-free and no- carrier-added? *J. Radioanal. Nucl. Chem.* (2005) 263, 13–18.
- ¹³ Fowler J.S., Ido T., Initial and subsequent approach for the synthesis of 18FDG. *Semin Nucl Med* (2002) 32, 6-12.
- ¹⁴ Preshlock S., Tredwell M., Gouverneur V., 18F-Labeling of Arenes and Heteroarenes for Applications in Positron Emission Tomography. *Chem. Rev.* (2016) 116, 719-766.
- ¹⁵ Hess E., Blessing G., Coenen H.H., Quaim S.M., Improved Target System for Production of High Purity [¹⁸F]Fluorine via the ¹⁸O(p,n)¹⁸F Reaction. *Appl.Radiat. Isot.* (2000) 52, 1431-1440.
- ¹⁶ Kambali I, Parwanto, Suryanto H., Huda N, Listiawadi F.D., Astarina H, Ismuha R.R., Kardinah, Dependence of 18F Production Yield and Radioactive Impurities on Proton Irradiation Dose, *Physics Research International* (2017), 2124383.
- ¹⁷ Füchtner, F.; Preusche, S.; Mading, P.; Zessin, J.; Steinbach, J. Factors affecting the specific activity of [¹⁸F]fluoride from a [¹⁸O]water target. *Nuklearmedizin* (2008) 47, 116–119.
- ¹⁸ Richarz, R., Krapf, P., Zarrad, F., Urusova, E., Neumaier B., Neumaier B., Neither azeotropic drying, nor base nor other additives: a minimalist approach to 18F-labeling, *Org. Biomol. Chem.* (2014) 12, 8094-8099.
- ¹⁹ Brodack, J.W., Kilbourn M.R., Welch M.J., Katzenellenbogen J.A. NCA 16 alpha-[¹⁸F]fluoroestradiol-17 beta: the effect of reaction vessel on fluorine-18 resolubilization, product yield, and effective specific activity. *Int J Rad Appl Instrum A.* (1986), 37, 217-221.
- ²⁰ Ermert, J., Neumiaer, B., *The Radiopharmaceutical Chemistry of Fluorine-18: Nucleophilic Fluorinations* edited by Lewis, J.S., Windhorst, A.D. and Zeglis, B.M., Springer International Publishing Cham (2019), Chapt 15.

-
- ²¹ Zlatopolsky, B.D., Zischler, J., Krapf, P., Zarrad, F., Urusova, E., Kordys, E., Endepols, H., Neumaier B., Copper-Mediated Aromatic Radiofluorination Revisited: Efficient Production of PET Tracers on a Preparative Scale, *Chem.Eur.J.* (2015) ,21, 5972–5979.
- ²² Mochizuki S., Ishigure N., Ogata Y., Kobayashi T. Analysis of induced radionuclides in replacement parts and liquid wastes in a medical cyclotron solely used for production of ¹⁸F for [¹⁸F]FDG. *Appl. Radiat. Isot.* (2013) 74, 137–143.
- ²³ Hamacher K., Coenen H.H. and Stocklin G., Efficient Stereospecific Synthesis of No-Carrier-Added 2-[¹⁸F]-Fluoro-2-Deoxy-D-Glucose Using Aminopolyether Supported Nucleophilic Substitution (1986), 27, 235-238.
- ²⁴ Yu S., Review of ¹⁸F-FDG Synthesis and Quality Control. *Biomedical Imaging and Intervention Journal* (2006) 2, e57.
- ²⁵ Gallagher B.M., Fowler J.S., Gutterson N.I., MacGregor R.R., Wan C., Wolf A.P., Metabolic Trapping as a principle of Radiopharmaceutical Design: Some Factors Responsible for the Biodistribution of [¹⁸F]2-Deoxy-2-Fluoro-D-Glucose. *J. nucl. Med.* (1978) 19, 1154.1161.
- ²⁶ Liberti M.V., Locasale J.W. The Warburg Effect: How Does it Benefit Cancer Cells? *Trends Biochem Sci.* (2016) 3, 211-218..
- ²⁷ Ortega Pijeira M.S., Nascimento dos Santos S., Araujo Y.B., Lapolli A.L., Nardelli Wandermuren M. et al. A closer look at the synthesis of 2-[¹⁸F] fluoroethyl tosylate to minimize the formation of volatile side-products, *EJMMI Radiopharmacy and Chemistry* (2022) 7-26.
- ²⁸ Lee, S.J., Oh,S.J. Chi, D.Y., Moon, D.H. and Ryu, J.S., High Yielding [¹⁸F]Fluorination Method by Fine Control of the Base *Bull., Korean Chem. Soc.* (2012), 33, 2177-2180.
- ²⁹ Orlovskaya, V., Fedorova, O., Nadporojkii, M., Krasikova, R., A fully automated azeotropic drying free synthesis of O-(2-[¹⁸F]fluoroethyl)- -tyrosine ([¹⁸F]FET) using tetrabutylammonium tosylate, *Appl. Radiat. Isot.* (2019), 152, 135–139.
- ³⁰ Orlovskaya, V., Antuganov, D., Fedorova, O., Timofeev, V., Krasikova, R., Tetrabutylammonium tosylate as inert phase-transfer catalyst: The key to high efficiency SN2 radiofluorinations, *Applied Radiation and Isotopes* (2020), 163, 109195.
- ³¹ Jacobson O., Kiesewetter D.O., Chen X., Fluorine-18 radiochemistry, labeling strategies and synthetic routes. *Bioconjug. Chem.* (2015) 26, 1-18.
- ³² V. V. Grushin, T. P. Tolstaya and I. N. Lisichkina, *Bull. Acad. Sci. USSR, Div. Chem. Sci.* (1983) 33, 1957.
- ³³ Pike VW, Aigbirhio FI. Reactions of cyclotron-produced [¹⁸F] fluoride with diaryliodonium salts—a novel single-step route to no-carrier-added [¹⁸] fluoroarenes. *J. Chem. Soc., Chem. Commun.* (1995) 2215-2216.
- ³⁴ Ross TL, Ermert J, Hocke C et al. Nucleophilic ¹⁸F-fluorination of heteroaromatic iodonium salts with no-carrier-added [¹⁸F] fluoride. *J. Am. Chem. Soc.* (2007) 129, 8018–8025.
- ³⁵ Zhdankin V.V., Stang P.J. Chemistry of Polyvalent Iodine. *Chem. Rev.* (2008) 108, 5299– 5358.
- ³⁶ Rotstein B.H., Stephenson N.A., Vasdev N., Liang S.H., Spirocyclic Hypervalent Iodine(III)- Mediated Radiofluorination of Non-Activated and Hindered Aromatics. *Nat. Commun.* (2014) 5:4365.
- ³⁷ Lee E., Kamlet A.S., Powers D.C. et al. A fluoride-derived electrophilic late-stage fluorination reagent for PET imaging. *Science* (2011), 334, 639-642.
- ³⁸ Mazzotti A.R., Campbell M.G., Tang P., Murphy J.M., Ritter T. Palladium(III)-catalyzed fluorination of arylboronic acid derivatives. *J. Am. Chem. Soc.* (2013) 135, 14012-14015.

-
- ³⁹ Lee E., Hooker J.M., Ritter T. Nickel-mediated oxidative fluorination for PET with aqueous [¹⁸F] fluoride. *J. Am. Chem. Soc.* (2012), 134, 17456–17458.
- ⁴⁰ Ichiishi N., Brooks A.F., Topczewski J.J., Rodnick M.E., Sandfor M.S., Scott P.J.H. Copper-catalyzed [¹⁸F] fluorination of (mesityl)(aryl) iodonium salts. *Org. Lett.* (2014), 16, 3224–3227.
- ⁴¹ Ichiishi N., Canty A.J., Yates B.F., Sanford M.S., Mechanistic Investigations of Cu-Catalyzed Fluorination of Diaryliodonium Salts: Elaborating the CuI/CuIII Manifold in Copper Catalysis. *Organometallics* (2014) 33, 5525–5534.
- ⁴² Tredwell M., Preshlock S.M., Taylor N.J. et al. A general copper-mediated nucleophilic ¹⁸F fluorination of arenes. *Angew. Chem.* (2014), 53, 7751–7755.
- ⁴³ Zlatopolskiy B.D., Zischler J., Krapf P., Zarrad F., Urusova E.A., Kordys E., Endepols, H., Neumaier, B. Copper Mediated Aromatic Radiofluorination Revisited: Efficient Production of PET Tracers on a Preparative Scale. *Chem. A. Eur. J.* (2015) 21, 5972–5979.
- ⁴⁴ Mossine A.V., Brooks A.F., Makaravage K.J. et al. Synthesis of [¹⁸F] arenes via the copper-mediated [¹⁸F] fluorination of boronic acids. *Org. Lett.* (2015), 17, 5780–5783.
- ⁴⁵ Makaravage K.J., Brooks A.F., Mossine A.V. et al. Copper-mediated radiofluorination of arylstannanes with [¹⁸F] KF. *Org. Lett.* (2016), 18, 5440–5443.
- ⁴⁶ Preshlock S., Calderwood S., Verhoog S., Tredwell M., Huiban M., Hienzsch A., Gruber S., Wilson T.C. et al. Enhanced copper-mediated (¹⁸F)-fluorination of aryl boronic esters provides eight radiotracers for PET applications. *Chem Commun (Camb)*. (2016) 52, 8361–8364.
- ⁴⁷ Lee, S., Makaravage K.S., Brooks, A.F., Scott, P. J. H., Sanford, M. S. Copper-Mediated Aminoquinoline-Directed Radiofluorination of Aromatic C–H Bonds with K¹⁸F, *Angew. Chem. Int. Ed.* (2019), 58, 3119–3122.
- ⁴⁸ Zischler J., Kolks N., Modemann D., Neumaier B., Zlatopolskiy B.D. Alcohol-Enhanced Cu-Mediated Radiofluorination, *Chemistry* (2017), 23, 3251–3256.
- ⁴⁹ Kim D.W., Jeong Lim, S.T., Sohn M.H., Katzenellenbogen J.A., Chi D.Y. Facile Nucleophilic Fluorination Reactions Using tert-Alcohols as a Reaction Medium: Significantly Enhanced Reactivity of Alkali Metal Fluorides and Improved Selectivity. *J. Org. Chem.* (2008) 73, 957–962.
- ⁵⁰ Zarrad F., Zlatopolskiy B.D., Krapf P., Zischler J., Neumaier B. A Practical Method for the Preparation of ¹⁸F-Labeled Aromatic Amino Acids from Nucleophilic [¹⁸F]Fluoride and Stannyl Precursors for Electrophilic Radiohalogenation. *Molecules* (2017) 22, 2231.
- ⁵¹ Lahdenpohja S.O., Rajala N.A., Rajander J. et al. Fast and efficient copper-mediated ¹⁸F-fluorination of arylstannanes, aryl boronic acids, and aryl boronic esters without azeotropic drying. *EJNMMI radiopharm. chem.* (2019) 28.
- ⁵² Antuganov, D., Zykov, M., Timofeev, V., Timofeeva, K., Antuganova, Y., Orlovskaya, V., Fedorova, O. Krasikova, R., Copper-Mediated Radiofluorination of Aryl Pinacolboronate Esters: A Straightforward Protocol by Using Pyridinium Sulfonates, *Eur. J. Org. Chem.* (2019), 918–922.
- ⁵³ Orlovskaya, V., Fedorova, O., Kuznetsova, K., Krasikova, R., Cu-Mediated Radiofluorination of Aryl Pinacolboronate Esters: Alcohols as Solvents with Application to 6-L-[¹⁸F]FDOPA Synthesis, *Eur. J. Med. Chem.* (2020), 45, 7079–7086
- ⁵⁴ Hoffmann C., Kolks N., Smets D., Haseloer A., Gröner B., Urusova E.A., Endepols H., Neumaier F., Ruschewitz U., Klein A., Neumaier B., Zlatopolskiy B.D. Next Generation Copper Mediators for the Efficient Production of ¹⁸F-Labeled Aromatics, *Chemistry* (2023), 29, e202202965.
- ⁵⁵ Burke BP, Clemente GS, Archibald SJ. Boron–¹⁸F containing positron emission tomography radiotracers: advances and opportunities. *Contrast Media Mol. Imaging* (2015) 10, 96–110.

-
- ⁵⁶ Rosenthal M, Bosch A, Nickles R et al. Synthesis and some characteristics of no-carrier added [¹⁸F] fluorotrimethylsilane. *Appl. Radiat. Isot.* (1985) 36, 318-319.
- ⁵⁷ Schirmmayer R, Bradtmöller G, Schirmmayer E et al. ¹⁸F-labeling of peptides by means of an organosilicon-based fluoride acceptor. *Angew. Chem. Int. Ed.* (2006) 45, 6047-6050.
- ⁵⁸ Ting R., Adam M.J., Ruth T.J., Perrin D.M. Arylfluoroborates and Alkylfluorosilicates as Potential PET Imaging Agents: High-Yielding Aqueous Biomolecular ¹⁸F-Labeling. *J. Am. Chem. Soc.* (2005) 127, 13094–13095.
- ⁵⁹ Li Y., Ting R., Harwig C.W., auf dKU, Bellac C.L., Lange P.F., Inkster J.A.H., Schaffer P., Adam M.J., et al. Towards kit-like ¹⁸F-labeling of marimastat, a noncovalent inhibitor drug for in vivo PET imaging cancer associated matrix metalloproteases. *Med. Chem. Commun.* (2011) 2, 942–949.
- ⁶⁰ Liu Z., Li Y., Lozada J., Pan J., Lin K.S., Schaffer P., Perrin D.M. Rapid, one-step, high yielding ¹⁸F-labeling of an aryltrifluoroborate bioconjugate by isotope exchange at very high specific activity. *J. Labelled Compd. Radiopharm.* (2012) 55, 491–496.
- ⁶¹ Liu Z., Hundal-Jabal N., Wong M., Yapp D., Lin K.S., Benard F., Perrin D.M. A new ¹⁸F-heteroaryltrifluoroborate radio-prosthetic with greatly enhanced stability that is labelled by ¹⁸F–¹⁹F-isotope exchange in good yield at high specific activity. *Med. Chem. Commun.* (2014) 5, 171–179.
- ⁶² Chansaenpak K., Wang M., Wu Z., Zaman R., Li Z., Gabbai F.P. [(¹⁸F)]-NHC-BF₃ adducts as water stable radio-prosthetic groups for PET imaging. *Chem Commun (Camb).* (2015) 51, 12439-12442.
- ⁶³ Wade C.R., Zhao H., Gabbai F.P. Stabilization of zwitterionic aryltrifluoroborates against hydrolysis. *Chem. Commun.* (2010) 46, 6380–6381.
- ⁶⁴ Li Z., Chansaenpak K., Liu S., Wade C.R., Zhao H., Conti P.S., Gabbai F.P. Harvesting ¹⁸F-fluoride ions in water via direct ¹⁸F–¹⁹F isotopic exchange: radiofluorination of zwitterionic aryltrifluoroborates and in vivo stability studies. *Med. Chem. Commun.* (2012) 3, 1305–1308.
- ⁶⁵ Liu Z., Pourghiasian M., Radtke M.A., Lau J., Pan J., Dias G.M., Yapp D., Lin K.S., Bénard F., Perrin D.M. An Organotrifluoroborate for Broadly Applicable One-Step ¹⁸F-Labeling. *Angew. Chem., Int. Ed.* (2014) 53, 11876–11880.
- ⁶⁶ McBride W.J., Sharkey R.M., Karacay H., D'Souza C.A., Rossi E.A., Laverman P., Chang C.H. et al. A Novel Method of ¹⁸F Radiolabeling for PET. *J. Nucl. Med.* (2009) 50, 991-998.
- ⁶⁷ Zheng Q., Xu H., Wang H., Du W.G.H., Wang N., Xiong H., Gu Y., Noodleman L., Sharpless K.B., Yang G., Wu P. Sulfur [¹⁸F]Fluoride Exchange Click Chemistry Enabled Ultrafast Late-Stage Radiosynthesis. *J. Am. Chem. Soc.* (2021) 143, 3753–3763.
- ⁶⁸ Walter N., Bertram J., Drewes B., Bahutski V., Timmer M., Schütz M.B., Krämer F., Neumaier F., et al. Convenient PET-tracer production via SuFEx ¹⁸F-fluorination of nanomolar precursor amounts. *Eur J Med Chem.* (2022) 237, 114383.
- ⁶⁹ Kuchar M., Pretze M., Knies T. et al. Site-selective radiolabeling of peptides by ¹⁸F-fluorobenzoylation with [¹⁸F] SFB in solution and on solid phase: a comparative study. *Amino acids* (2012) 43, 1431-1443.
- ⁷⁰ De Bruin B., Kuhnast B., Hinnen F., Yaouancq L., Amessou M., Johannes L., Samson A., Boisgard R. et al. 1-[3-(2-[¹⁸F]Fluoropyridin-3-yloxy)propyl]pyrrole-2,5-dione: Design, Synthesis, and Radiosynthesis of a New [¹⁸F]Fluoropyridine-Based Maleimide Reagent for the Labeling of Peptides and Proteins Bioconjug. Chem., (2005) 15, 406-420.
- ⁷¹ Kettenbach K., Schieferstein H., Ross T.L. ¹⁸F-labeling using click cycloadditions. *Biomed. Res Int.* (2014), 361329.
- ⁷² V. Bouvet, M. Wuest, F. Wuest, Copper-free click chemistry with the short-lived positron emitter fluorine-18. *Org. Biomol. Chem.* (2011) 9, 7393-7399.

-
- ⁷³ Van de Bittner G.C., Ricq E.L., Hooker J.M., A philosophy for CNS radiotracer design. *Acc. Chem. Res.* (2014), 47, 3127-34.
- ⁷⁴ Farwell M.D., Pryma D.A., Mankoff D.A., PET/CT imaging in cancer: Current applications and future directions, *Cancer* (2014), 120, 3433-3445.
- ⁷⁵ Boellaard R., Delgado-Bolton R., Oyen W.J., Giammarile F., Tatsch K., Eschner W. et al., FDG PET/CT: EANM procedure guidelines for tumour imaging: version 2.0, *Eur. J. Nucl. Med. Mol. Imaging.* (2015), 42, 328–354.
- ⁷⁶ Carles M., Fechter T., Grosu A.L., Sörensen A., Thomann B., Stoian R.G., Wiedenmann N., Rühle A., Zamboglou C., Ruf J., Martí-Bonmatí L., Baltas D., Mix M., Nicolay N.H. ¹⁸F-FMISO-PET Hypoxia Monitoring for Head-and-Neck Cancer Patients: Radiomics Analyses Predict the Outcome of Chemo-Radiotherapy, *Cancers* (2021), 13, 3449.
- ⁷⁷ Samuel, J., Franklin, C. (2008). Hypoxemia and Hypoxia. In: Myers, J.A., Millikan, K.W., Saclarides, T.J. (eds) *Common Surgical Diseases*. Springer, New York, NY.
- ⁷⁸ Langen K.J., Hamacher K., Weckesser M., Floeth F., Stoffels G., Bauer D., et al, O-(2-[¹⁸F]fluoroethyl)-L-tyrosine: uptake mechanisms and clinical applications. *Nucl. Med. Biol.* (2006), 33, 287–94.
- ⁷⁹ Wright G.L., Haley C., Beckett M.L., Schellhammer P.F., Expression of Prostate-Specific Membrane Antigen in Normal, Benign, and Malignant Prostate Tissues. *Urol. Oncol.* (1995), 1,18–28.
- ⁸⁰ Zlokovic B.V., The blood–brain barrier in health and chronic neurodegenerative disorders, *Neuron* (2008),57, 178–201.
- ⁸¹ Gupta S., Dhanda S., Sandhir R., Anatomy and physiology of blood–brain barrier, *Brain Targeted Drug Delivery System* (2019), 7–31.
- ⁸² Pike V.W. Considerations in the development of reversibly binding PET radioligands for brain imaging, *Curr. Med. Chem.* (2016), 23, 1818–69.
- ⁸³ Hitchcock S.A. Structural modifications that alter the Pglycoprotein efflux properties of compounds. *J. Med. Chem.* (2012), 55,4877–95.
- ⁸⁴ Pike V.W. Considerations in the development of reversibly binding PET radioligands for brain imaging. *Curr. Med. Chem.* (2016), 23, 1818–69.
- ⁸⁵ Herman T.F., Santos C., First Pass Effect, *StatPearls* [internet] (2022), 3186914.
- ⁸⁶ Sharma R., Aboagye E., Development of radiotracers for oncology--the interface with pharmacology, *Br. J. Pharmacol.* (2011), 8, 1565-85.
- ⁸⁷ Ghosh, K.K., Padmanabhan, P., Yang, CT. et al. Dealing with PET radiometabolites. *EJNMMI Res* (2020) 10, 109.
- ⁸⁸ Mishina M., Ishiwata K., Adenosine receptor PET imaging in human brain. *Int. Rev. Neurobiol* (2014) 119, 51–69.
- ⁸⁹ Gerhard F.E., Rasmus P.C., Harald H.S., Raimund M., Gerd F., Helmut B., *Transporters as Drug Targets* (2008) ISBN: 978-3-527-33384-4
- ⁹⁰ Zhang L., Hu K., Shao T., Hou L., Zhang S., Ye W., Josephson L., Meyer J.H., Zhang M.R., Vasdev N., Wang J., Xu H., Wang L., Liang S.H., Recent developments on PET radiotracers for TSPO and their applications in neuroimaging. *Acta Pharm. Sin. B.* (2021), 11, 373-393.
- ⁹¹ Neumaier F., Zlatopolskiy B.D., Neumaier B. Mutated Isocitrate Dehydrogenase (mIDH) as Target for PET Imaging in Gliomas. *Molecules.* (2023), 28, 2890.
- ⁹² Vlassenko A.G., Benzinger T.L., Morris J.C. PET amyloid-beta imaging in preclinical Alzheimer's disease. *Biochim. Biophys Acta.* (2012), 22, 370-379.
- ⁹³ Cassinelli Petersen G., Roytman M., Chiang G.C., Li Y., Gordon M.L., Franceschi A.M. Overview of tau PET molecular imaging. *Curr. Opin. Neurol.* (2022), 35, 230-239.

-
- ⁹⁴ Salomone S. and Waeber C., Selectivity and specificity of sphingosine-1-phosphate receptor ligands: caveats and critical thinking in characterizing receptor-mediated effects., *Front. Pharmacol.* (2011) 2-9.
- ⁹⁵ Pollard T.D., A Guide to Simple and Informative Binding Assays, *Molecular Biology of the Cell* (2010) 21, 4061–4067.
- ⁹⁶ Bylund D.B., Teows M.L. Radioligand binding methods - practical guide and tips. *Am. J. Physiol.* (1993) 265, 421–429.
- ⁹⁷ Cai L., Innis R.B., Pike V.W. Radioligand development for PET imaging of β -amyloid (A β) - current status. *Curr. Med. Chem.* (2007) 14, 19–52.
- ⁹⁸ Keen, M. *Methods in Molecular Biology*, Humana Press; Totowa, NJ, (1999), 106.
- ⁹⁹ Clark, A.J., *The Mode of Action of Drugs on Cells*, (1933) 163–168. London: Arnold and Co.
- ¹⁰⁰ Cheng Y., Prusoff W.H. Relationship between the inhibition constant (K₁) and the concentration of inhibitor which causes 50 per cent inhibition (I₅₀) of an enzymatic reaction. *Biochem Pharmacol.* (1973), 22, 3099-108.
- ¹⁰¹ Rempel B.P., Price E.W., Phenix C.P. Molecular Imaging of Hydrolytic Enzymes Using PET and SPECT. *Molecular Imaging.* (2017) 16.
- ¹⁰² Hardy J.A., Wells J.A. Searching for new allosteric sites in enzymes. *Curr. Opin. Struct. Biol.* (2004) 14, 706–715.
- ¹⁰³ Cumming P., Vasdev N. The assay of enzyme activity by positron emission tomography, in Grunder G, ed. *Molecular Imaging in the Clinical Neurosciences*. New York, NY: Humana Press; (2012) 111–135.
- ¹⁰⁴ Fowler J.S., Logan J., Volkow N.D., Wang G.J., MacGregor R.R., Ding Y.S. Monoamine oxidase: radiotracer development and human studies. *Methods.* (2002) 27, 263–277.
- ¹⁰⁵ Michaelis L. and Menten M.L. Die Kinetik der Invertinwirkung. *Biochem. Z.* (1913) 49, 333-369.
- ¹⁰⁶ Cornish-Bowden A. *Fundamentals of Enzyme Kinetics*. 4th ed. Weinheim, Germany: Wiley-Blackwell (2012) 134–40.
- ¹⁰⁷ Ouertani, Awatef, et al., Effectiveness of enzyme inhibitors in biomedicine and pharmacotherapy, *Adv. Tissue Eng. Regen. Med.* (2019) 5, 85-90.
- ¹⁰⁸ Bhagavan N., Chung-Eun Ha. *Enzyme and enzyme regulation in Essentials of Medical Biochemistry*, Academic Press; second edition (2015) 752.
- ¹⁰⁹ Lain G, Dougall, John Unitt. Evaluation of the biological activity of compounds in the practice of medicinal chemistry. Academic Press; Fourth edition. (2015) 902.
- ¹¹⁰ Copeland R.A., Anderson P.S. *Enzymes and Enzyme Inhibitors in Textbook of Drug Design and Discovery*. 3rd edn. In: P Krogsgaard-Larsen, Liljefors T, Madsen U, editors. New York: Taylor and Francis (2001) 328–363.
- ¹¹¹ R. H. Garret e C. M. Grisham, *Principi di Biochimica*, Padova, Piccin Nuova Libreria, 2004, ISBN 88-299-1693-5.
- ¹¹² Leighton F., Poole B., Lazarov P.W., De Duve C., The synthesis and turnover of rat liver peroxisomes I. fractionation of peroxisome proteins, *J. Cell. Biol.* (1969) 41, 521-535.
- ¹¹³ Cairns, R.A., Mak, T.W. Oncogenic isocitrate dehydrogenase mutations: mechanisms, models, and clinical opportunities. *Cancer Discovery* (2013) 3, 730–741.
- ¹¹⁴ Kim J., Kim K. Y., Jang H.S., Yoshida T., Tsuchiya K., Nitta K., Park J.W., Bonventre J.V., Park K.M. Role of cytosolic NADP⁺-dependent isocitrate dehydrogenase in ischemia-reperfusion injury in mouse kidney. *Am. J. Physiol. Renal. Physiol.* (2009) 296, 622-633.

-
- ¹¹⁵ Xu X., Zhao J., Xu Z., Peng B., Huang Q., Arnold E., Ding J. Structures of human cytosolic NADP-dependent isocitrate dehydrogenase reveal a novel self-regulatory mechanism of activity. *J. Biol. Chem.* (2004) 279, 33946-33957.
- ¹¹⁶ Ward P.S., Cross J.R., Lu C., Weigert O., Abel-Wahab O., Levine R.L., Weinstock D.M. et al. Identification of additional IDH mutations associated with oncometabolite R(-)-2-hydroxyglutarate production. *Oncogene* (2012), 31, 2491-2498.
- ¹¹⁷ Waitkus M.S., Diplas B.H., Yan H., biological role and therapeutical potential of IDH mutations in cancer, *Cancer cell* (2018) 34, 186-195.
- ¹¹⁸ Andronesi O.C., Kim G.S., Gerstner E., Batchelor T., Tzika A.A., Fantin V.R., Vander Heiden M.G, Sorensen A.G. Detection of 2-hydroxyglutarate in IDH-mutated glioma patients by in vivo spectral-editing and 2D correlation magnetic resonance spectroscopy. *Sci. Transl. Med.* (2012), 4, 116ra4.
- ¹¹⁹ Figueroa M.E., Abdel-Wahab O., Lu C., Ward P.S., Patel J., Shih A., Li Y., Bhagwat N., Vasanthakumar A. et al. Leukemic IDH1 and IDH2 mutations result in a hypermethylation phenotype, disrupt TET2 function, and impair hematopoietic differentiation. *Cancer Cell.* (2010) 18, 553-567.
- ¹²⁰ Sasaki M., Knobbe C.B., Itsumi M., Elia A.J., Harris I.S., Chio I.I.C., Cairns R.A., McCracken S. et al. D-2-hydroxyglutarate produced by mutant IDH1 perturbs collagen maturation and basement membrane function. *Genes Dev.* (2012) 26, 2038– 2049.
- ¹²¹ Chowdhury R., Yeoh K.K., Tian Y.M., Hillringhaus L., Bagg E.A., Rose N.R., Leung I.K., Li X.S., et al. The oncometabolite 2-hydroxyglutarate inhibits histone lysine demethylases. *EMBO Rep.* (2011) 12, 463-469.
- ¹²² Yan H., Parsons D.W., Jin G., et al. IDH1 and IDH2 mutations in gliomas. *N. Engl. J. Med.* (2009) 360, 765–773.
- ¹²³ Watanabe, T., Nobusawa, S., Kleihues, P. & Ohgaki, H. IDH1 mutations are early events in the development of astrocytomas and oligodendrogliomas. *Am. J. Pathol.* (2009) 174, 1149–1153.
- ¹²⁴ Parsons D.W., Jones S., Zhanf X., Lin J.C. et al, An integrated genomic analysis of human glioblastoma multiforme. *Science* (2008), 321, 1807-1812.
- ¹²⁵ DiNardo C.D. et al. Characteristics, clinical outcome, and prognostic significance of IDH mutations in AML. *Am. J. Hematol.* (2015) 90, 732–736.
- ¹²⁶ Molenaar R.J. et al. Clinical and biological implications of ancestral and non-ancestral IDH1 and IDH2 mutations in myeloid neoplasms. *Leukemia* (2015) 29, 2134–2142.
- ¹²⁷ Yan H., Parsons D.W., Jin G. et al IDH1 and IDH2 mutations in gliomas. *N. Engl. J. Med.* (2009) 360, 765–773.
- ¹²⁸ Reitman Z.J., Parsons D.W., Yan H. IDH1 and IDH2: not your typical oncogenes. *Cancer Cell* (2010) 17, 215–216.
- ¹²⁹ Balss J., Meyer J., Mueller W. et al Analysis of the IDH1 codon 132 mutation in brain tumors. *Acta Neuropathol.* (2008) 116, 597–602.
- ¹³⁰ Parsons D.W., Jones S., Zhang X. et al An integrated genomic analysis of human glioblastoma multiforme. *Science* (2008) 321, 1807–1812.
- ¹³¹ Han S., Liu Y., Cai S.J., Qian M., et al. IDH mutation in glioma: molecular mechanisms and potential therapeutic targets, *British Journal of Cancer* (2020) 122,1580–1589.
- ¹³² Dang L., White D.W., Gross S., Bennett, B.D., Bittinger M.A., Driggers, E.M., Fantin, V.R. et al., Cancer-associated IDH1 mutations produce 2-hydroxyglutarate. *Nature* (2009) 462, 739 –744.
- ¹³³ Lin D., Wang M., Chen Y., Gong J., Chen L., Shi X., Lan F., Chen Z., Xiong T., Sun H., Wan S. Trends in Intracranial Glioma Incidence and Mortality in the United States, 1975-2018. *Front Oncol.* (2021) 11, 748061.

-
- ¹³⁴ Mahaley M.S. Jr, Mettlin C., Natarajan N., Laws E.R. Jr., Peace B.B. National survey of patterns of care for brain tumor patients. *J. Neurosurg.* (1989) 71, 826–836.
- ¹³⁵ Ostrom Q.T., Cioffi G., Gittleman H., Patil N., Waite K., Kruchko C., et al.. CBTRUS Statistical Report: Primary Brain and Other Central Nervous System Tumors Diagnosed in the United States in 2012-2016. *Neuro Oncol* (2019) 21, 1–100.
- ¹³⁶ Ostrom Q.T. et al. CBTRUS statistical report: primary brain and other central nervous system tumors diagnosed in the United States in 2012-2016. *Neuro-Oncology* (2019) 21, v1–v100.
- ¹³⁷ Leighton C., Fisher B., Bauman G., et al. Supratentorial low-grade glioma in adults: an analysis of prognostic factors and timing of radiation. *J. Clin. Oncol.* (1997) 15, 1294–1301.
- ¹³⁸ Van den Bent M.J., Afra D., De Witte O., et al. Long-term efficacy of early versus delayed radiotherapy for low-grade astrocytoma and oligodendroglioma in adults: the EORTC 22845 randomized trial. *Lancet.* (2005) 366, 985–990.
- ¹³⁹ Keles G.E., Aldape K., Berger M.S. Low-grade gliomas: astrocytoma, oligodendroglioma, and mixed gliomas. In: Winn HR, ed.: *Houmans Neurological Surgery*. 5th ed. Philadelphia, PA: W.B. Saunders Co.; (2004), 950–968.
- ¹⁴⁰ Metellus P., Coulibaly B., Colin C. *et al* Absence of IDH mutation identifies a novel radiologic and molecular subtype of WHO grade II gliomas with dismal prognosis. *Acta Neuropathol* (2011) 120, 719–729.
- ¹⁴¹ Houillier C., Wang X., Kaloshi G. *et al* IDH1 or IDH2 mutations predict longer survival and response to temozolomide in low-grade gliomas. *Neurology* (2010) 75, 1560–1566.
- ¹⁴² Feifenberger G., Kros J.M., Burger P.C. Oligodendrogliomas. In: Kleihues P, Cavenee WK, eds. *World Health Organization Classification of Tumours: Pathology and Genetics—Tumours of the Nervous System*. New York, NY: Oxford University Press, (2000), 56–61.
- ¹⁴³ Gupta R., Webb-Myers R., Flanagan S. *et al* Isocitrate dehydrogenase mutations in diffuse gliomas: clinical and aetiological implications. *J. Clin. Pathol.* (2011) 64, 835–844.
- ¹⁴⁴ Louis D.N., Perry A., Reifenberger G., von Deimling A., Figarella-Branger D., Cavenee W.K. et al. The 2016 World Health Organization Classification of Tumors of the Central Nervous System: a summary. *Acta Neuropathol.* (2016) 131, 803-820.
- ¹⁴⁵ Louis D.N., Perry A., Wesseling P., Brat D.J., Cree I.A., Figarella-Branger D., Hawkins C., Ng H.K. et al. The 2021 WHO Classification of Tumors of the Central Nervous System: a summary. *Neuro Oncol.* (2021), 23, 1231-1251.
- ¹⁴⁶ Upadhyay N., Waldman A.D. Conventional MRI evaluation of gliomas. *Br. J. Radiol.* (2011) Spec. Iss 2, 107-111.
- ¹⁴⁷ Asari S., Makabe T., Katayama S., Itoh T., Tsuchida S., Ohmoto T. Assessment of the pathological grade of astrocytic gliomas using an MRI score. *Neuroradiology* (1994) 36, 308–310.
- ¹⁴⁸ Tanaka Y., Nariai T., Momose T. et al. Glioma surgery using a multimodal navigation system with integrated metabolic images. *J. Neurosurg.* (2009) 110 163–172.
- ¹⁴⁹ Ewelt C., Floeth F.W., Felsberg J. et al. Finding the anaplastic focus in diffuse gliomas: the value of Gd-DTPA enhanced MRI, FET-PET, and intraoperative, ALA-derived tissue fluorescence. *Clin. Neurol. Neurosurg.* (2011) 113, 541–547.
- ¹⁵⁰ Brandsma D., Stalpers L., Taal W. et al. Clinical features, mechanisms, and management of pseudoprogression in malignant gliomas. *Lancet Oncol.* (2008) 9, 453–461.
- ¹⁵¹ Radbruch A., Fladt J., Kickingereider P. et al. Pseudoprogression in patients with glioblastoma: clinical relevance despite low incidence. *Neuro Oncol.* (2015) 17, 151–159.
- ¹⁵² Mansoor N.M., Thust S., Militano V., Fraioli F., PET imaging in glioma: techniques and current evidence. *Nuclear Medicine Communications* (2018) 13, 1064-1080.

-
- ¹⁵³ Meng C., Zorrilla-Veloz R.I., Hu J., Guan B., Ma X. Diagnostic Accuracy of PET for Differentiating True Glioma Progression From Post Treatment-Related Changes: A Systematic Review and Meta-Analysis, *Front. Neurol.* (2021) 12.
- ¹⁵⁴ Laudicella, R. Bauckneht M., Cuppari L. et al. Emerging applications of imaging in glioma: focus on PET/MRI and radiomics. *Clin Transl Imaging* (2021) 9, 609–623.
- ¹⁵⁵ Wei Chen, Clinical Applications of PET in Brain Tumors, *J. Nuc. Med.* (2007) 48, 1468-1481
- ¹⁵⁶ Dunet V., Pomoni A., Hottinger A. et al.. Performance of 18F-FET versus 18F-FDG-PET for the diagnosis and grading of brain tumors: systematic review and meta-analysis. *Neuro Oncol.* (2016) 18, 426–434.
- ¹⁵⁷ Prieto E., Marti-Climent J.M., Dominguez-Prado I. et al. Voxel-based analysis of dual-time-point 18F-FDG PET images for brain tumor identification and delineation. *J. Nucl. Med.* (2011) 52, 865–872.
- ¹⁵⁸ Kubota K., Ogawa M., Ji B., Watabe T., Zhang M.R., Suzuki H., Sawada M., Nishi K., Kudo T. Basic Science of PET Imaging for Inflammatory Diseases. *PET/CT for Inflammatory Diseases.* (2019), 1–42.
- ¹⁵⁹ Chung J.K., Kim Y.K., Kim S.K. et al.. Usefulness of 11C-methionine PET in the evaluation of brain lesions that are hypo- or isometabolic on 18F-FDG PET. *Eur J Nucl Med Mol Imaging.* (2002) 29, 176–182.
- ¹⁶⁰ Rapp M., Heinzl A., Galldiks N. et al. Diagnostic performance of 18F-FET PET in newly diagnosed cerebral lesions suggestive of glioma. *J. Nucl. Med.* (2013) 54, 229–235.
- ¹⁶¹ Becherer A., Karanikas G., Szabo M. et al. Brain tumour imaging with PET: a comparison between [18F]fluorodopa and [11C]methionine. *Eur. J. Nucl. Med. Mol. Imaging.* (2003) 30, 1561–1567.
- ¹⁶² Hutterer M., Nowosielski M., Putzer D. et al. [18F]-fluoro-ethyl-L-tyrosine PET: a valuable diagnostic tool in neuro-oncology, but not all that glitters is glioma. *Neuro Oncol.* (2013) 15, 341–351.
- ¹⁶³ Jansen N.L., Graute V., Armbruster L. et al. MRI-suspected low-grade glioma: is there a need to perform dynamic FET PET? *Eur. J. Nucl. Med. Mol. Imaging.* (2012) 39, 1021–1029.
- ¹⁶⁴ Pöpperl G., Kreth F.W., Mehrkens J.H., Herms J., Seelos K., Koch W., Gildehaus F.W., et al. FET PET for the evaluation of untreated gliomas: correlation of FET uptake and uptake kinetics with tumour grading *Eur. J. Nucl. Med. Mol. Imaging* (2007) 34, 1933–1942.
- ¹⁶⁵ Miyagawa T., Oku T., Uehara H., Desai R., Beattie B., Tjuvajev J., et al. “Facilitated” amino acid transport is upregulated in brain tumors. *J. Cereb. Blood Flow Metab.* (1998) 18, 500–9.
- ¹⁶⁶ Popperl G., Kreth F.W., Herms J., Koch W., Mehrkens J.H., Gildehaus F.J., et al. Analysis of 18F-FET PET for grading of recurrent gliomas: is evaluation of uptake kinetics superior to standard methods? *J. Nucl. Med.* (2006) 47, 393–403.
- ¹⁶⁷ Arbizu J., Tejada S., Marti-Climent J.M. et al. Quantitative volumetric analysis of gliomas with sequential MRI and (11C)-methionine PET assessment: patterns of integration in therapy planning. *Eur. J. Nucl. Med. Mol. Imaging.* (2012) 39, 771–781.
- ¹⁶⁸ Ewelt C., Floeth F.W., Felsberg J. et al. Finding the anaplastic focus in diffuse gliomas: the value of Gd-DTPA enhanced MRI, FET-PET, and intraoperative, ALA-derived tissue fluorescence. *Clin. Neurol. Neurosurg.* (2011) 113, 541–547.
- ¹⁶⁹ Kunz M., Thon N., Eigenbrod S. et al. Hot spots in dynamic (18)F-FET-PET delineate malignant tumor parts within suspected WHO grade II gliomas. *Neuro Oncol.* (2011) 13, 307–316.
- ¹⁷⁰ Tanaka Y., Nariai T., Momose T. et al. Glioma surgery using a multimodal navigation system with integrated metabolic images. *J. Neurosurg.* (2009) 110, 163–172.
- ¹⁷¹ Galldiks N., Langen K., Holy R. et al. Assessment of treatment response in patients with glioblastoma using [18F]fluoroethyl-L-tyrosine PET in comparison to MRI. *J. Nucl. Med.* (2012) 53, 1048–1057.

-
- ¹⁷² Choi C., Ganji S.K., DeBerardinis R.J., Hatanpaa K.J., Rakheja D., Kovacs, Z., Yang, X.L. et al. 2-Hydroxyglutarate Detection by Magnetic Resonance Spectroscopy in IDH-Mutated Patients with Gliomas. *Nat. Med.* (2012) 18, 624–629.
- ¹⁷³ Lohmann P., Lerche C., Bauer E.K., Steger J., Stoffels G., Blau T., Dunkl, V. et al. Predicting IDH Genotype in Gliomas Using FET PET Radiomics. *Sci. Rep.* (2018) 8, 13328.
- ¹⁷⁴ Unterrainer M., Winkelmann I., Suchorska B., Giese A., Wenter V., Kreth F.W., et al. Biological Tumour Volumes of Gliomas in Early and Standard 20–40 Min 18F-FET PET Images Differ According to IDH Mutation Status. *Eur. J. Nucl. Med. Mol. Imaging* (2018) 45, 1242–1249.
- ¹⁷⁵ Verger A., Stoffels G., Bauer E.K., Lohmann P., Blau T., Fink G.R., Neumaier B., Shah N.J., et al. N. Static and Dynamic 18F-FET PET for the Characterization of Gliomas Defined by IDH and 1p/19q Status. *Eur. J. Nucl. Med. Mol. Imaging* (2018) 45, 443–451.
- ¹⁷⁶ Zheng B., Yao Y., Liu, Z., Deng L., Anglin J.L., Jiang H., Prasad B.V., Song, Y. Crystallographic investigation and selective inhibition of mutant isocitrate dehydrogenase. *ACS Med. Chem. Lett.* (2013) 4, 542–546.
- ¹⁷⁷ Liu Z., Yao Y., Kogiso M., Zheng B., Deng L., Qiu J.J., Dong S., Lv H., Gallo J.M., Li X.N., Song, Y. Inhibition of cancer-associated mutant isocitrate dehydrogenases: synthesis, structure-activity relationship, and selective antitumor activity. *J. Med. Chem.* (2014) 57, 8307–8318.
- ¹⁷⁸ Wu F., Jiang H., Zheng B., Kogiso M., Yao Y., Zhou C., Li X.N., Song Y. Inhibition of cancer-associated mutant isocitrate dehydrogenases by 2-thiohydantoin compounds. *J. Med. Chem.* (2015) 58, 6899–6908.
- ¹⁷⁹ Davis M., Pragani R., Popovici-Muller J., Gross S., Thorne N., Salituro F. et al. ML309: A Potent Inhibitor of R132H Mutant IDH1 Capable of Reducing 2-Hydroxyglutarate Production in U87 MG Glioblastoma Cells. *Probe Reports from the NIH Molecular Libraries Program: Bethesda, USA* (2013).
- ¹⁸⁰ Popovici-Muller J., Saunders J.O., Salituro F.G., Travins J.M., Yan S., Zhao F., Gross S., et al. Discovery of the First Potent Inhibitors of Mutant IDH1 That Lower Tumor 2-HG in Vivo. *ACS Med Chem Lett.* (2012) 3, 850-5.
- ¹⁸¹ Rohle D., Popovici-Muller J., Palaskas N., Turcan S., Grommes C., Campos C., et al. An inhibitor of mutant IDH1 delays growth and promotes differentiation of glioma cells. *Science* (2013) 340, 626–630.
- ¹⁸² Dowdy T., Zhang L., Celiku O., Movva S., Lita A., Ruiz-Rodado V., et al. Sphingolipid pathway as a source of vulnerability in IDH1mut glioma. *Cancers* (2020) 12, E2910.
- ¹⁸³ Popovici-Muller J., Lemieux R.M., Artin E., Saunders J.O., Salituro F.G., Travins J., Cianchetta G., et al. Discovery of AG-120 (Ivosidenib): A First-in-Class Mutant IDH1 Inhibitor for the Treatment of IDH1 Mutant Cancers. *ACS Med. Chem. Lett.* (2018) 9, 300-305.
- ¹⁸⁴ Norsworthy K. J., Luo L., Hsu V., Gudi R., Dorff S. E., Przepioraka D., et al. FDA approval summary: Ivosidenib for relapsed or refractory acute myeloid leukemia with an isocitrate dehydrogenase-1 mutation. *Clin. Cancer Res.* (2019) 25, 3205–3209.
- ¹⁸⁵ Levell J.R., Caferro T., Chenail G., Dix I., Dooley J., Firestone B., et al. Optimization of 3-Pyrimidin-4-yl-oxazolidin-2-ones as allosteric and mutant specific inhibitors of IDH1. *ACS Med. Chem. Lett.* (2017) 8, 151–156.
- ¹⁸⁶ Cho Y.S., Levell J.R., Liu G., Caferro T., Sutton J., Shafer C.M., et al. Discovery and evaluation of clinical candidate IDH305, a brain penetrant mutant IDH1 inhibitor. *ACS Med. Chem. Lett.* (2017) 8, 1116–1121.
- ¹⁸⁷ Zhao Q., Manning J.R., Sutton J., Costales A., Sendzik M., Shafer C.M., et al. Optimization of 3-Pyrimidin-4-yl-oxazolidin-2-ones as orally bioavailable and brain penetrant mutant IDH1 inhibitors. *ACS Med. Chem. Lett.* (2018) 9, 746–751.
- ¹⁸⁸ Konteatis Z., Artin E., Nicolay B., Straley K., Padyana A. K., Jin L., et al. Vorasidenib (AG-881): A first-in-class, brain-penetrant dual inhibitor of mutant IDH1 and 2 for treatment of glioma. *ACS Med. Chem. Lett.* (2020) 11, 101–107.

-
- ¹⁸⁹ Caravella J.A., Lin J., Diebold R.B., Campbell A.M., Ericsson A., Gustafson G., et al. Structure-based design and identification of FT-2102 (olutasidenib), a potent mutant-selective IDH1 inhibitor. *J. Med. Chem.* (2020) 63, 1612–1623.
- ¹⁹⁰ Lin J., Lu W., Caravella J.A., Campbell A.M., Diebold R.B., Ericsson A., et al. Discovery and optimization of quinolinone derivatives as potent, selective, and orally bioavailable mutant isocitrate dehydrogenase 1 (mIDH1) inhibitors. *J. Med. Chem.* (2019) 62, 6575–6596.
- ¹⁹¹ Megías-Vericat J.E., Ballesta-López O., Barragán E., Montesinos P. IDH1-mutated relapsed or refractory AML: Current challenges and future prospects. *Blood Lymphat. Cancer* (2019) 9, 19–32.
- ¹⁹² Chitneni S.K., Yan H., Zalutsky M.R. Synthesis and Evaluation of a ¹⁸F-Labeled Triazinediamine Analogue for Imaging Mutant IDH1 Expression in Gliomas by PET. *ACS Med Chem Lett.* (2018) 9, 606-611.
- ¹⁹³ Yen K., Travins J., Wang F., David M.D., Artin E., Straley K., Padyana A., Gross S., et al. AG-221, a First-in-Class Therapy Targeting Acute Myeloid Leukemia Harboring Oncogenic IDH2 Mutations. *Cancer Discov.* (2017) 7, 478-493.
- ¹⁹⁴ Wang T., Lin Q., Zhang Y., Xu Z., Shi D., Cheng Y., Fu Z., Tan H., Cheng D., Shi H. Synthesis and Biological Evaluation of Novel PET Tracers [¹⁸F]AG120 & [¹⁸F]AG135 for Imaging Mutant Isocitrate Dehydrogenase 1 Expression. *Bioorg. Med. Chem.* (2022) 53, 116525.
- ¹⁹⁵ Weber V., Arnaud L., Dukic-Stefanovic S., Wenzel B., Roux V., Chezal J.M., Lai T.H., Teodoro R., et al. A Novel Radioiodinated and Radiofluorinated Analogues of FT-2102 for SPECT or PET Imaging of mIDH1 Mutant Tumours. *Molecules.* (2022) 27, 3766.
- ¹⁹⁶ W. Patrick Walters and Renxiao Wang, *New Trends in Virtual Screening*, *J. Chem. Inf. Model.* (2020) 60, 4109–4111.
- ¹⁹⁷ Morris G.M., Lim-Wilby M. Molecular Docking. In: Kukol, A., *Molecular Modeling of Proteins. Methods Molecular Biology™*, vol 443. Humana Press.(2008)
- ¹⁹⁸ Glide, Schrödinger, LLC, New York, NY, 2023
- ¹⁹⁹ Friesner, R. A.; Murphy, R. B.; Repasky, M. P.; Frye, L. L.; Greenwood, J. R.; Halgren, T. A.; Sanschagrin, P. C.; Mainz, D. T., "Extra Precision Glide: Docking and Scoring Incorporating a Model of Hydrophobic Enclosure for Protein-Ligand Complexes," *J. Med. Chem.*, (2006) 49, 6177–6196.
- ²⁰⁰ Salifu E.Y., Agoni C., Soliman M.E.S. Highlighting the mechanistic role of Olutasidenib (FT-2102) in the selective inhibition of mutated isocitrate dehydrogenase 1 (mIDH1) in cancer therapy. *Informatics in Medicine Unlocked* (2022) 28, 100829.
- ²⁰¹ Kowsari E., Mallakmohammadi M. Ultrasound promoted synthesis of quinolines using basic ionic liquids in aqueous media as a green procedure. *Ultrason Sonochem.* (2011) 1, 447-454.
- ²⁰² Pham T.D.M., Ziora Z.M., Blaskovich M.A.T. Quinolone antibiotics. *Med. Chem. Comm.* (2019) 10,1719-1739.
- ²⁰³ Charris J.; Lobo G., Camacho J., Ferrer R., Barazarte A., Dominguez J., Gamboa N., Rodrigues J., Angel J. Synthesis and Antimalarial Activity of (E) 2-(2-Chloro-3-Quinolinylmethylidene)-5,7-Dimethoxyindanones *Letters in Drug Design & Discovery* (2007) 4, 49–54.
- ²⁰⁴ Abdel-Aal M.A.A., Abdel-Aziz S.A., Shaykoon M.S.A., Abuo-Rahma G.E.A. Towards anticancer fluoroquinolones: A review article. *Arch Pharm (Weinheim).* (2019) 352, e1800376.
- ²⁰⁵ Zimmermann G.S., Neurohr C., Villena-Hermoza H. et al. Anti-inflammatory effects of antibacterials on human bronchial epithelial cells. *Respir. Res.* (2009) 10, 89.
- ²⁰⁶ Eilingsfeld H., Seefelder M., Weidinger H., Amidchloride und Carbamidchloride, *Angew. Chem.* (1960) 72, 836–845.
- ²⁰⁷ Ulrich H., *The chemistry of imidoyl halides* (1968)

- ²⁰⁸ Vilsmeier A.; Haack A., Über die Einwirkung von Halogenphosphor auf Alkyl-formanilide. Eine neue Methode zur Darstellung sekundärer und tertiärer p-Alkylamino-benzaldehyde, Ber., (1927) 60, 119.
- ²⁰⁹ Ulrich H., The Chemistry of Imidoyl Halides, Plenum Press, New York, (1968) p. 87.
- ²¹⁰ Alonso M.A., Úbeda J.I., Avendaño C., Menéndez J.C., Villacampa M., New findings on the Vilsmeier-Haack approach to quinoline derivatives. Tetrahedron (1993) 49, 10997-11008.
- ²¹¹ Metten B., Smet M., Boens N., Dehaen W. Synthesis of APTRA Derivatives as Building Blocks for Low-Affinity Fluorescent Ca²⁺ Indicators, Synthesis (2005) 11, 1838-1844.
- ²¹² Srihari E., Kumar G.S., Kumar, Chebolu N.S.S.P., Seth R.K., Biswas S.S., Balasubramanian S. et al. Synthesis and antimalarial activity of Baylis-Hillman adducts from substituted 2-chloroquinoline-3-carboxaldehydes, Heterocyclic Comm. (2011) 17, 111-119.
- ²¹³ Das S., Trubnikov A.V., Novoselov A.M., Kurkin A.V., Beld J., Altieri A., Kortagere S., Design and Characterization of Novel Small Molecule Activators of Excitatory Amino Acid Transporter 2, ACS Med. Chem. Lett. (2022) 13, 10, 1628-1633.
- ²¹⁴ Roche Holding AG - WO2013/64465, 2013, A1
- ²¹⁵ Murugavel S., Jacob Prasanna C.S., Subashini R., Raveendranatha Reddy H., Ananthkrishnan D., Journal of Molecular Structure (2016) 1122, 134 – 145.
- ²¹⁶ Hazeldine S.T., Polin L., Kushner J., White K., Bougeois N.M., Crantz B., Palomino E. et al. Synthesis and Biological Evaluation of Some Bioisosteres and Congeners of the Antitumor Agent, 2-{4-[(7-Chloro-2-quinoxalinyloxy)phenoxy]propionic Acid (XK469), J. Med. Chem. (2002) 45, 3130-3137
- ²¹⁷ Alan E. Moormann, Reductive Amination of Piperidines with Aldehydes Using Borane-Pyridine, Syn. Comm. (1993) 23, 789-795.
- ²¹⁸ Ahmed F., A Review on the Use of Sodium Triacetoxyborohydride in the Reductive Amination of Ketones and Aldehydes, Organic Process Research & Development (2006) 10, 971-1031.
- ²¹⁹ Ishiyama T., Murata M., Miyaura N., Palladium(0)-Catalyzed Cross-Coupling Reaction of Alkoxydiboron with Haloarenes: A Direct Procedure for Arylboronic Esters, J. Org. Chem. (1995) 23, 7508-7510.
- ²²⁰ Kohno Y., Heterocyclic Biaryl derivative and PDE inhibitor comprising same as active ingredient (2011) US2011/0178041A1
- ²²¹ A) Cai L., Lu S., Pike V.W. Chemistry with [¹⁸F]Fluoride Ion. Eur J Org Chem (2008) 2853-2873.; b) Coenen H.H., Fluorine-18 radiopharmaceuticals beyond [¹⁸F]FDG for use in oncology and neurosciences, Nucl. Med. Biol. (2010) 37, 727-740; c) Ermert J., ¹⁸F-labelling innovations and their potential for clinical application, Clin. Transl. Imaging (2018) 6, 169-193.
- ²²² Schäfer D., Weiß P., Ermert J., Castillo Meleán J., Zarrad F. and Bernd Neumaier. Preparation of No-Carrier-Added 6-[¹⁸F]Fluoro-l-tryptophan via Cu-Mediated Radiofluorination. Eur. J. Org. Chem. (2016) 27, 4621-4628.
- ²²³ Abonia R., Gutiérrez L.F., Insuasty B., Quiroga J., Laali K.K., Zhao C., Borosky G.L., Horwitz S.M., Catalyst-free assembly of giant tris(heteroaryl)methanes: synthesis of novel pharmacophoric triads and model sterically crowded tris(heteroaryl/aryl)methyl cation salts. Beilstein J Org Chem. (2019) 15, 642-654.
- ²²⁴ Morales S., Guijarro F.G., García Ruano J.L., Cid M.B., A General Aminocatalytic Method for the Synthesis of Aldimines J. Am. Chem. Soc. (2014) 136 1082-1089.
- ²²⁵ Pletz J., Berg B., Breinbauer R., A General and Direct Reductive Amination of Aldehydes and Ketones with Electron-Deficient Anilines, Synthesis (2016) 48, 1301-1317.
- ²²⁶ Kundeková B., Máčajová M., Meta M., Čavarga I., Bilčík B. Chorioallantoic Membrane Models of Various Avian Species: Differences and Applications. Biology (2021) 10, 301.

-
- ²²⁷ Nowak-Sliwinska P., Segura T., Iruela-Arispe M.L. The chicken chorioallantoic membrane model in biology, medicine and bioengineering. *Angiogenesis*. (2014) 4, 779-804.
- ²²⁸ Ribatti D. The Chick Embryo Chorioallantoic Membrane (CAM). A Multifaceted Experimental Model. *Mech. Dev.* (2016) 141, 70–77.
- ²²⁹ Cimpean A.M., Ribatti D., Raica M. The Chick Embryo Chorioallantoic Membrane as a Model to Study Tumor Metastasis. *Angiogenesis*. (2008) 11, 311–319.
- ²³⁰ National Institute of Health The Public Health Service Responds to Commonly Asked Questions. *ILAR J.* (1991) 33, 68–70.
- ²³¹ Dünker N., Jendrossek V. Implementation of the Chick Chorioallantoic Membrane (CAM) Model in Radiation Biology and Experimental Radiation Oncology Research. *Cancers*. (2019) 11, 1499.
- ²³² Dupertuis Y.M., Delie F., Cohen M., Pichard C. In Ovo Method for Evaluating the Effect of Nutritional Therapies on Tumor Development, Growth and Vascularization. *Clin. Nutr. Exp.* (2015) 2, 9–17.
- ²³³ FDA approves olutasidenib for relapsed or refractory acute myeloid leukemia with a susceptible IDH1 mutation. News release. FDA. December 1, 2022. Accessed December 1, 2022.
- ²³⁴ Kwak S.H., Shin S., Lee J.H., Shim J.K., Kim M., Lee S.D., Lee A., Bae J., Park J.H., Abdelrahman A., et al. Synthesis and structure-activity relationships of quinolinone and quinoline-based P2X7 receptor antagonists and their anti-sphere formation activities in glioblastoma cells. *Eur. J. Med. Chem.* (2018) 151, 462-481.
- ²³⁵ Arnott E.A., Chan L.C., Cox B.G., Meyrick B., Philips A., POCl₃ Chlorination of 4-Quinazolones. *J. Org. Chem.* (2011) 76, 1653–1661.
- ²³⁶ Venkanna P., Rajanna K.C., Kumar M.S., Ansari M.B., Ali M.M. 2,4,6-Trichloro-1,3,5-triazine and N,N'-dimethylformamide as an effective Vilsmeier–Haack reagent for the synthesis of 2-chloro-3-formyl quinolines from acetanilides. *Tetr. Lett.* (2015) 56, 5164-5167.
- ²³⁷ BTC7DMF FOR QUINOLINES
- ²³⁸ Davis F.A., Reddy R.E., Szewczyk J.M., Reddy G.V., Portonovo P.S., Zhang H., Fanelli D., Reddy R.T. et al. Asymmetric Synthesis and Properties of Sulfinimines (Thiooxime S-Oxides). *J. Org. Chem.* (1997) 62, 2555–2563.
- ²³⁹ Liu G., Cogan D.A., Ellman J.A., Catalytic Asymmetric Synthesis of tert-Butanesulfinamide. Application to the Asymmetric Synthesis of Amines. *J. Am. Chem. Soc.* (1997) 119, 9913–9914.
- ²⁴⁰ Davis A.F., Friedman A.J. Kluger E.W. Chemistry of the sulfur-nitrogen bond. VIII. N-Alkylidenesulfinamides *J. Am. Chem. Soc.* (1974) 96, 5000.
- ²⁴¹ Burger K., Albanbauer J., Kafig F., Penninger S., *Liebigs Ann. Chem.*, 1977, 624
- ²⁴² T. Yoshida, S. Naruto, H. Uno and H. Nishimura, *Chem. Pharm. Bull.*, 1982, 30, 2820
- ²⁴³ Davis A.F. Zhou P., Chen B.C., Asymmetric synthesis of amino acids using sulfinimines (thiooxime S-oxides), *Chem. Soc. Rev.* (1998) 27, 13-18.
- ²⁴⁴ Cogan D.A., Ellman J.A., Asymmetric Synthesis of α,α -Dibranched Amines by the Trimethylaluminum-Mediated 1,2-Addition of Organolithiums to tert-Butanesulfinyl Ketimines. *J. Am. Chem. Soc.* (1999) 121, 268–269.
- ²⁴⁵ Moreau P., Essiz M., Merour J., Bouzard D., Stereoselective addition reactions to chiral N-benzylidene-p-toluenesulfinamides. Application to the synthesis of optically active 1,2-diphenylethylamines. *Tetraedron* (1997) 8, 591-598.
- ²⁴⁶ Solladié G. and Girardin A., Improved Preparation of Optically Active Methyl p-Tolyl Sulfoxide, *Synthesis* (1987) 2, 173.

-
- ²⁴⁷ Han Z., Krishnamurthy D., Grover P., Wilkinson H.S., Fang Q.K., Su X., Lu Z.H., Magiera D., Senanayake C.H. Practical and highly stereoselective technology for preparation of enantiopure sulfoxides and sulfinamides utilizing activated and functionally differentiated N-sulfonyl-1,2,3-oxathiazolidine-2-oxide derivatives *Tetrahedron* (2005) 61, 6386-6480.
- ²⁴⁸ Caron S., Do N.M., Sieser J.E. A practical, efficient, and rapid method for the oxidation of electron deficient pyridines using trifluoroacetic anhydride and hydrogen peroxide–urea complex, *Tetr. Lett.* (2000) 41, 2299-2302.
- ²⁴⁹ Emmons W.D. Peroxytrifluoroacetic Acid. I. The Oxidation of Nitrosamines to Nitramines, *J. Am. Chem. Soc.* (1954) 76, 3470–3472.
- ²⁵⁰ Jung M.E. and Lyster M.A., Quantitative Dealkylation of Alkyl Ethers via Treatment with Trimethylsilyl Iodide. A New Method for Ether Hydrolysis. *J.Org.Chem.* (1977) 42, 3761-3764.
- ²⁵¹ Olah G.A., Narang S.C., Gupta B.G.B., Malhotra R., *Synthetic Methods and Reactions*. 62.' Transformations with Chlorotrimethylsilane/Sodium Iodide, a Convenient in Situ Iodotrimethylsilane Reagent. *J. Org. Chem.* (1979) 44, 1247-1251.
- ²⁵² Ortega Pijeira M.S., Nascimento dos Santos S., Araujo Y.B., Lapolli A.L., Nardelli Wandermuren M. et al. A closer look at the synthesis of 2-[¹⁸F] fluoroethyl tosylate to minimize the formation of volatile side-products, *EJMMI Radiopharmacy and Chemistry* (2022) 7:26.
- ²⁵³ Liu S., Abboud M., Mikhailov V., Liu X., Reinbold R., Schofield C.J., Differentiating Inhibition Selectivity and Binding Affinity of Isocitrate Dehydrogenase 1 Variant Inhibitors. *J. Med. Chem.* (2023) 66, 5279–5288.
- ²⁵⁴ Popovici-Muller J., Lemieux R.M., Artin E., Saunders J.O., Salituro F.G., Travins J., Cianchetta G., et al. Discovery of AG-120 (Ivosidenib): A First-in-Class Mutant IDH1 Inhibitor for the Treatment of IDH1 Mutant Cancers. *ACS Med. Chem. Lett.* (2018) 9, 300-305